CRANFIELD UNIVERSITY

KIRSTY WALLIS

Design of experiment studies for the fabrication processes involved in the micro-texturing of surfaces for fluid control

School of Applied Sciences

PhD Thesis
Academic Years: 2009 - 2013

Supervisor: Dr Jeffrey R. Alcock
November 2013

CRANFIELD UNIVERSITY

SCHOOL OF APPLIED SCIENCES

PhD Thesis

Academic Years 2009 - 2013

KIRSTY WALLIS

Design of experiment studies for the fabrication processes involved in the micro-texturing of surfaces for fluid control

Supervisor: Dr Jeffrey R. Alcock
November 2013

ABSTRACT

This thesis focuses on the use of a design of experiment approach to examine the significance of process factors and interactions on the fabrication of micro-textured surfaces. The micro-textured surfaces examined contain pillar and hole features ranging from 80 – 2 μm in diameter. The processes examined are the deep reactive ion etching of silicon wafers for the production of silicon mould inserts and the micro-injection moulding of polypropylene, high density polyethylene and 316LS stainless steel replicate samples of the silicon mould insert.

During the deep reactive ion etching of the silicon wafers the design of experiment approach was used to determine the significant of platen power, C_4F_8 gas flow and switching times to the presence of pillar undercut of 10 x 10, 5 x 5 and 2 x 2 μm pillars. Undercuts occur when the pillar base has a smaller cross-section than the apex of the pillar. Switching times was found to be the only statistically significant parameter for both 10 x 10 and 5 x 5 μm pillars.

The design of experiment approach is used in the micro-injection moulding of polypropylene, high density polyethylene and 316LS stainless steel replicates to examine the significance of mould temperature, cooling time, holding pressure and injection speed on the part and buffer mass of the produce samples, the height and width of pillar on the replicate surfaces and the variation of the replicated pillars height and width from the original silicon mould insert. Examination of the high density polyethylene replicates found that mould temperature was the most significant factor regarding pillar dimensions (and variation from the silicon mould insert) across the range of pillar sizes. Upon examination of the polypropylene replicates it was found that the factor of most significance on pillar dimensions varied across the different pillar sizes. Holding pressure was identified as the most significant factor with regards to the 53 x 29 and 19 x 80 μm pillars. Injection speed was found to be most significant for the 25 x 25 and 19 x 29 μm pillars. Cooling time was found to be most significant with regards to the 30 x 10, 25 x 10, 20 x 10 and 15 x 10 μm pillars. While

mould temperature was found to be most significant for the 20 x 20, 15 x 15 and 10 x 30 μm pillars. The interaction between mould temperature and injection speed was also found to be the most significant factor with regards to the 43 x 29 and 25 x 30 μm pillars. Examination of the 316LS replicates found that mould temperature was the most significant factor regarding pillar dimensions for 80 x 80 and 19 x 80 μm pillars. While holding pressure was found to be most significant to the 29 x 29 μm pillars and injection speed was identified as most significant to the 53 x 80 μm pillars.

The samples produced during the design of experiment investigations were then used to examine the effect of surface texturing on droplet behaviour. Droplet contact angles were examined on polypropylene, high density polyethylene and silicon samples structured with 10 – 2 μm pillar. Initial droplet contact angles were found to be higher on the polypropylene samples than the high density polyethylene or silicon samples. With the lowest initial contact angles being found for the silicon inserts. Droplet 'channelling' and evaporation were examined on silicon, polypropylene, high density polyethylene and 316LS samples structured with micro-channel surface pillars and holes ranging from 80 – 2 μm in diameter. Contact pinning of the droplet to the surface via the three-phase contact-line was noted during observations of droplet 'channelling'. This pinning effect was observed at all sample tilt angles (30 - 90 ^{o}). With regards to droplet evaporation, the droplets were noted to evaporate evenly (with no or limited contact pinning) on all unstructured surfaces and the surfaces structured with hole features. On the surfaces structured with pillar features, the droplets appeared too evaporated along the surface gradient from the smallest pillars to the largest.

Keywords:

Design of experiment, deep reactive ion etching, polymer micro-injection moulding, metal powder injection moulding, droplet behaviour, contact angles, evaporation

ACKNOWLEDGEMENTS

I would like to extend my thanks to my supervisor Dr Jeffrey Alcock. I really appreciate all the guidance, help and support he has provided me with during my time at Cranfield.

My thanks also go to Usama Attia, for all of his help in conducting my experiments, I couldn't have done it without his help and guidance.

Many thanks to Heather Almond, my subject advisor, for her support and listening to me when I felt lost.

My thanks to all the people who have assisted me with my lab work: Mark Craig, Chris Shaw, Jeff Rao, Andrew Dyer and Christine Kimpton.

To all my friends I have made throughout my time here: the old skool, the new skool, my office mates, CSA peeps and my fellow Sugar ole divas. I thank you for being there for me when I needed you – parties, meals or just a simple tea break, I appreciate every single one.

My deepest thanks to my family for supporting me and encouraging me all these year. Their strength gives me strength, and hope that I have made them proud.

A special thanks to Emma Cowham, Sam Grover and Lucy Hancock for giving me a place of comfort to escape to when I needed time away from the 'Cranfield bubble' (and to Ellie for showing me how much a person can grow in the time it's taken me to complete this work). You guys are like a second family to me and words can't begin to describe how much you mean to me.

Finally, I'd like to thank mon cœur. It's been rough, but you've supported me through the hard times and I can't even begin to tell you how thankful I am xx

And now, on with the next great adventure…

TABLE OF CONTENTS

LIST OF FIGURES

LIST OF TABLES

LIST OF EQUATIONS

Terminology

Term	Definition
ABS	Acrylonitrile butadiene styrene
Ag-Pd	Gold-Palladium
ANOVA	Analysis of variance
COC	Cyclic olefin copolymer
CVD	Chemical vapour deposition
DC	Direct Current
DMCS	Dimethylchlorosilane
DMDCS	Dimethyldichlorosilane
DOE	Design of experiment
DRIE	Deep reactive ion etching
FDDCS	Heptadecafluoro-1,1,2,2-tetrahydroecyldimethylchlorosilane
HDPE	High density polyethylene
HMDS	Hexamethyl disilazane
NaOH	Sodium Hydroxide
OTS	Octadecyltrichlorosilane
PC	Polycarbonate
PCR	Polymerase chain reaction
PMMA	Polymethyl methacrylate
POM	Polyoxymethylene
PP	Polypropylene
PPFC	C_4F_8
PS	Polystyrene
PTFE	Poly(tetrafluoroethylene)
PZT	Lead zirconate titanate
SEM	Scanning electron microscope
±Si	Variation of the replicate samples features from silicon mould insert features
S/N	Signal-to-noise-ratio
SA/V	Surface area/volume ratio

Notation

Symbol	Description	Symbol	Description
nm	Nanometer	Θ_A	Advancing contact angle
μm	Micrometer	Θ_R	Receding contact angle
μL	Microliter	Θ_H	Contact angle hysteresis
mm^2/s	Millimetre squared per second	r_b	Droplet contact radius
Θ_c	Contact angle	R_s	Radius of sphere forming the spherical cap
Θ_y	Youngs contact angle	V_o	Initial droplet volume
γ	Interfacial tension	V	Droplet volume at time of measurement
h	Height	K	constant
b	Width	$L_{(y)}$	Loss function
a	Gap length	y_o	Target value of the quality characteristics
Ø	Surface area fraction	W_1	Width at apex of pillar
Θ_w	Wenzel contact angle	W_2	Width at base of pillar
R	Roughness ratio	U	Undercut
Θ_{CB}	Cassie-Baxter contact angle	$Si_{(v)}$	Dimension of silicon insert features
Θ_F	Fakir contact angle	$Rep_{(v)}$	Dimension of replicate features
(1-Ø)	Surface area fraction of the liquid-vapour interface	Sccm	Standard cubic centimetre per minute
V_i	Injection speed	P_h	Holding pressure
T_b	Melt temperature	T_m	Mould Temperature
μIM	Micro-injection moulding	PIM	Powder injection moulding
μPIM	Micro powder-injection moulding	LPIM	Low-pressure injection moulding
μ-SPiMIM	Micro-sacrificial plastic mould insert micro-injection moulding	2C-PIM	Co-powder injection moulding
nPIM	Nano-powder injection moulding		

1 Introduction

This chapter presents a brief introduction to the research undertaken within this thesis '*Design of experiment studies for the fabrication processes involved in the micro-texturing of surfaces for fluid control*'. An introduction to the importance of surface texturing is outlines in section *1.1 Surface texturing.* The use of experimental design is discussed in section *1.3 Experimental design.* A brief introduction to droplet behaviour is presented in section *1.4 Droplet behaviour*. The aims and objectives of this thesis are discussed in section *1.5 Research aim and objectives*. Finally the structure of this thesis is outlined in section *1.6 Thesis structure*.

1.1 Surface texturing

Surface texturing is the physical/topographical alteration of a given surface from the planar position. Unlike chemical alterations, via surface coatings, the incorporation of textured features does not require an additional step after surface fabrication. This reduces production costs and streamlines sample fabrication.

At the micro-scale these topographical alterations can significantly affect the properties of a surface and have been widely used in a variety of applications.

The use of surface texturing in tribological interfaces, in applications such as face seals, thrust bearings and piston rings, has been noted to reduce friction, decrease surface damage and increase load bearing capacity and part service life[78]. The use of micro-scale surface texturing has also been found to improve adhesion reduction and enhance lubrication[120] within the tribological part interface.

Micro-texturing has also been utilised in the production of solar cell technologies to reduce energy loss caused by the reflection of incoming light[122].

Surface topography is also an important consideration in the production of biomaterials (tissue regeneration and wound healing) for biomedical applications, due to its effect on cellular adhesion, spreading, polarisation and mobility[36].

An increase in surface roughness, by topographical means, can improve the hydrophobicity of a surface making it more water repellent. Micro-texturing can be utilised for this trait to improve droplet movement in a variety of applications such as self-cleaning surfaces[221] and droplet-based lab-on-a-chip applications[100; 179]. The use of surface texturing to facilitate droplet movement uphill has also been documented[31].

The use and application of surface texturing is widespread within a multitude of sectors. As such it is important and beneficial to all that a thorough understanding is obtained regarding the fabrication processes used in the production of micro-scale surface textures.

1.2 Point-of-care testing and microfluidic devices

Point-of-care testing is the *in situ* medical testing at or near the site of patient care. Such devices include glucose meters, home pregnancy tests, blood pressure cuff and rapid HIV testing i.e. OraQuick. The development of these portable diagnostic devices opens doors to the possibility of reliable medical diagnostics in hard to reach areas such as third world countries and places where medical help is required but access to laboratory facilities is difficult, time consuming or expensive.

Through the development of point-of-care testing devices utilisation of lab-on-a-chip technologies has emerged. The use of lab-on-a-chip technologies offers up several advantages in the field of point-of-care testing for health monitoring. Portability [34; 119], integration of components [34; 71; 119], miniaturisation [29; 115], low sample and reagent consumption [29; 34; 115; 119], speed [34; 119] and disposability [119] are but a few of the advantages lab-on-a-chip devices could offer.

One technique used in the development of lab-on-a-chip systems is the manipulation of micro-scale volumes of samples and reagents. This technique is known as microfluidics, the manipulation and control of micro-litre volumes of fluid.

Microfluidic diagnostic devices have been developed for many biological testing applications such as breast cancer diagnosis [102], albumin detection in urine [119], digital polymerase chain reactions (PCR) [115; 185], protein crystallisation [115; 157; 185] and virus detection [157].

One key aspect of these lab-on-a-chip point-of-care devices is that they be user friendly and, due to their disposable nature, easy and cost effective to fabricate [118].

The early fabrication of microfluidic lab-on-a-chip systems used lithographic techniques to structure glass or silicon substrates [34; 41]. More recently the production of microfluidic systems has focused on the use of polymers due to the decrease in cost and the availability of mass replication techniques such as injection moulding [34; 41].

The main obstacle facing the commercial use of these devices is ultimately cost and the ability to commercially mass produce the devices. The incorporation of separately fabricated components into the final device will increases the complexity of the device fabrication and in turn increases the cost of production [71]. One such component is an additional external source of agitation i.e. a pump, which moves the sample and reagents from A to B.

The removal of an external/additional pump and the incorporation of surface textured features which could be fabricated directing onto the polymer would reduce the production time and thereby reduce the cost of the overall device manufacture.

1.3 Experimental design

When using any experimental process it is important to understand how the process factors can influence the final outcome. Traditional methods have involved the alteration of each factor individually to determine its effect on the final product. This method however has two key drawbacks: it is time consuming and does not provide information about how interactions between the factors influence the final product. In relation to the mass production of products it is important to understand the significance and effects of factors and interactions so that any issues discovered during fabrication can be addressed quickly and efficiently so as not to increase the cost of production. In response to the shortcomings of the individual factor analysis method statistical experimental design can be used to examine both individual factors and their interactions simultaneously. Thereby, reducing the number of experiments required.

The importance of understanding how various process factors affect the fabrication of micro-textures surfaces is crucial to the development of surfaces for spontaneous droplet movement. In enhancing the production of these surfaces the prospect of low-cost, high-output micro-textured surfaces for a variety of portable applications comes one step closer.

1.4 Droplet behaviour

As previously mentioned surface texturing can be used to control and manipulate the behaviour of fluid droplets on a given surface. At the micro-scale water droplets no longer automatically fill surface cavities as they would on macro-scale features. Instead the droplet can achieve a high contact angle on the micro surface features without filling the surface cavities. The three-phase contact line of the droplet on the surface (solid surface, water and vapour in the cavity) also becomes more influential at this micro-scale, as the contact line can become pinned to the micro-textured features. This increase in contact angle,

and the influence of the three-phase-contact line, can also result in the spontaneous movement of the droplets across the surface. When this occurs micro-texturing can be used to ensure the movement of a droplet in a specific direction across the surface, which can be beneficial in applications such as self-cleaning surfaces[221] and medical diagnostic devices[100].

1.5 Research aim and objectives

This thesis focuses on the statistical analysis of the fabrication processes used in the production of micro-textured surfaces. Which can be integrated into the design of micro-fluidic lab-on-a-chip devices for the transport of fluid droplets. A statistical experimental design will be used to determine the factors and interactions of significance within the deep reactive ion etching and micro-injection moulding processes. The effect of the produced surface texturing will then be examined for its effect on the behaviour of micro-litre droplets.

1.5.1 Research aim

The aim of this research is to identify the effects of process factors on the fabrication of micro-textured surfaces and the effect of such surfaces on droplet behaviour.

1.5.2 Research objectives

The research objectives of this thesis are:

1. To understand the state-of-the-art in the statistical experimental analysis of micro-scale pillar fabrication.
2. To identify the effect of process factors on the design and fabrication of silicon and nickel mould inserts.

3. To identify the effect of process factors on the micro-moulding of polymer and metal powder feedstocks.
4. Examine the effect of surface texturing on droplet behaviour

1.6 Thesis structure

The following summarises the content of this thesis:

Chapter 2: Literature review

This chapter presents a review of the literature regarding the fabrication of micro-textured surfaces and the behaviour of droplets on micro-textured surfaces. The aim of this chapter is to identify and present the gaps in knowledge with the current literature which will be filled through the course of this research.

Chapter 3: Methodology

This chapter details the methodological approaches used during the course of this research. The various statistical experimental designs available are also outlined in this chapter and the reasons for the selection of the approach used and reviewed.

Chapter 4: Mould design and fabrication results

This chapter presents the results gathered during the fabrication of removable mould inserts for use in micro-injection moulding. The results of the statistical analysis of the deep reactive ion etching process, for use in the production of silicon mould inserts, are also presented.

Chapter 5: Polymer micro-injection moulding results

This chapter details the results gathered during the statistical analysis of polymer micro-injection moulding. Examining the effect of process factors on replicate part mass, pillar height and width and the variation of the replicate features from the original mould insert. The variation in the physical appearance of fabricated the samples produced during the statistical experimental analysis is also presented

Chapter 6: Metal injection moulding results

This chapter presents the results gathered during the statistical analysis of metal powder injection moulding. Examining the physical appearance of fabricated samples and the effect of process factors on part mass, pillar height and width and the variation of the replicate features from the original mould insert.

Chapter 7: Droplet behaviour results

This chapter outlines the results obtained through the examination of droplet behaviour, with regards to contact angle, 'channelling' and evaporation, on silicon, polymer and metal powder micro-structured surfaces.

Chapter 8: Discussion

This chapter presents the main findings and discusses the observations made of the processes and samples fabricated during this research.

Chapter 9: Conclusion

This chapter details the conclusion draw from the information obtained and outline within this thesis and presents the contributions to knowledge achieved during the course of this research.

Chapter 10: Future work

This chapter puts forward suggested future research to be undertaken to further fill the remaining gaps in knowledge identified during the course of this research.

2 Literature review

To understand how the aims and objectives of this research can be realised a review of the literature has been undertaken. This chapter encompasses a review of the state-of-the-art with regards to the fabrication of micro-textured surfaces (*2.3*) and droplet behaviour on micro-textured surfaces (*2.4*). Through this review the identification of gaps within the current knowledge are to be identified and recommendation made for the filling of these gaps.

2.1 Polymer injection moulding

Injection moulding is a low-cost, high throughput, cyclic manufacturing technique used in the mass production of complex polymer parts (Figure 2.1). Polymer heated above its glass transition temperature (Tg) is forced into a mould cavity under high pressure where it solidifies and takes on the shape of the mould cavity along with any surface features from the mould insert/master [13]. The newly produced polymer replicate is then ejected from the mould and the replication cycle starts again. The time taken for each replication cycles ranges from a few seconds to a few minutes [13].

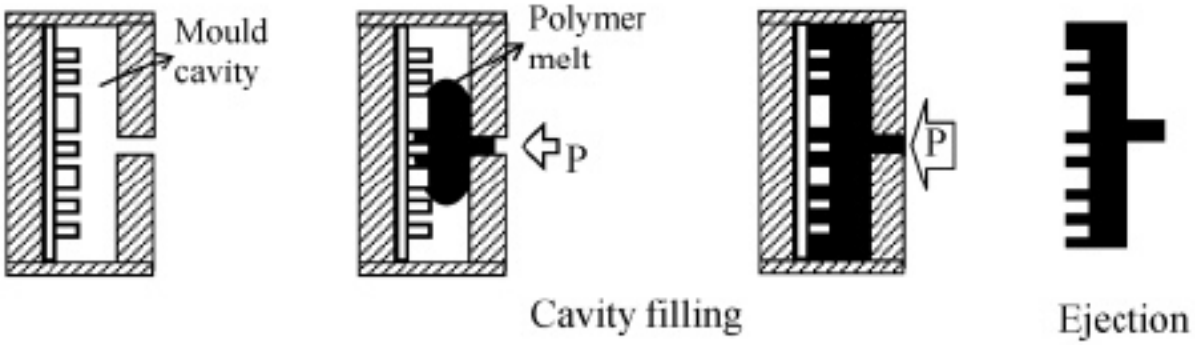

Figure 2.1 Injection moulding [38]

The injection mould which replicates the surface features is known as a mould insert or master. The mould insert is manufactured prior to polymer replication via several possible methods i.e. e-beam writing and lithography [13]. Mould inserts are generally made from silicon, however silicon is brittle and is liable to break during repetitive replication cycles when replicating high-aspect-ratio structures [60]. When replicating surfaces which contain high-aspect-ratio features electroforming can be used to produce a metal shim which can then be used as a mould insert in multiple replication cycles in the place of the silicon mould insert. There are a variety of advantages to the use of injection moulding: Low-cost, high-throughput, can be used with a range of thermoplastics, short cycle times and low equipment maintenance costs compared to lithographic methods [13]. However, like all processes there are disadvantages to injection moulding: polymer shrinkage, warpage [13] and incomplete filling of high-aspect-ratio structures due to the solidification of polymer at mould surface [32; 103; 140; 213]. These issues can be controlled by altering the process parameters, which include: injection speed (V_i), holding pressure (P_h), air evacuation of the cavity, cooling time, melt temperature (T_b) and mould temperature (T_m).

Injection speed is only a parameter during the filling of the mould cavity [177]. A high injection speed increases shear rates of the polymer and decreases the melt viscosity thereby improving filling of the features of the cavity [80; 177].

Holding pressure is used during the holding stage to prevent the polymer melt from flowing back out of the mould and to compensate for shrinkage of the polymer [177]. However increasing holding pressure can also increase stress on the part [13] which could cause issues during demoulding.

Evacuating air from the mould cavity can improve filling of mould features and also the quality of the finished part. However it can also lead to a decrease in mould surface temperature which can affect filling of mould features [177].

Cooling time is the time a replicate is held in the mould between injection and demoulding. This cooling period allows the replicate to reach a uniform ambient temperature prior to demoulding thereby reduction shrinkage [85] and warpage [13].

Melt temperature can be used to improve filling of mould cavities. An increase in melt temperature can cause the viscosity of the melt and the shear stress to decrease thereby making it easier to fill high aspect ratio structures [80; 177]. However, this is not the case for all polymers as in some cases the shear rate increases at higher melt temperatures [80]. Melt temperature can be considered one of the more important parameters when observing high aspect ratio feature replication [140].

Mould temperature is an important parameter to be considered before replication can occur. The temperature difference between the melt temperature and mould temperature can cause premature solidification of the polymer at the entrance to high aspect ratio features [13; 103; 140; 213]. Increasing mould temperature to above the Tg of the polymer can decrease melt viscosity and improve filling of high aspect ratio feature by reducing or preventing the solidification of the polymer melt [80; 177; 210]. Resulting parts are of better quality with improved optical properties, dimensional accuracy, stability and have reduced residual stress [210]. However, an increased mould temperature also leads to an increase in the replication cycle time as the mould temperature must be decreased prior to demoulding. It should be noted that increasing mould temperature does not always improve cavity filling as different polymers react differently to the increased temperature [177].

2.1.1 Polymer micro-injection moulding

The micro-injection moulding process is similar to that of conventional injection moulding. However, replicate features are focused on the micro- range, which are characterised by high surface area/volume ratio (SA/V) features[163]. Compared to conventional injection moulding the micro injection moulding process uses higher injection rates, shorter cycle times and rapid cooling of the polymer melt[163]. However, the rapid cooling of the polymer melt can lead to the premature freezing of the polymer melt at the entrance to the high SA/V features[13; 76; 140; 186; 199]. Process factors must therefore be adjusted within the micro-injection moulding process, such as increasing melt and mould

temperatures, to allow for the complete filling of the high SA/V features[20; 75; 140; 186]. Review papers of polymer micro-injection moulding (μIM) published over the last five years (since 2009) were examined to establish the state-of-the-art in polymer micro-injection moulding[13; 219; 225]. Parts fabricated via micro-injection moulding have been used for numerous applications[225] include: cosmetic and pharmaceutical packaging, biomedical devices (microneedles and scaffolds), micro-optical applications (gratings and lenses), micro-mechanical application (micro-springs and gears), sensors, acutators, micro-pumps (for drug delivery systems) and microfluidic medical diagnostic devices[10; 219]. There is also evidence of polymer micro-injection being utilised in the production of specific dosage drug delivery systems instead of the more common dip-moulding technique. However, the production of these specific dosage drug delivery systems using polymer micro-injection moulding is limited by the thermal stability of the drugs in question[219].

2.2 Powder injection moulding

Review papers of powder injection moulding (PIM) published over the last five years (since 2009) were examined to determine the state-of-the-art in powder injection moulding[9; 166; 172]. Five types of powder injection moulding were identified.

2.2.1 Micro-powder injection moulding

Components produced via micro-powder injection moulding (μPIM) can be categorised into one or more of three categories[9; 166]:

(1) Micro-part: maximum feature size 10 mm

(2) Micro-structured part: dimensions between several mm and several cm. 3D microstructures on surface

(3) Micro-precision parts: tolerance in micro-range but some sections can be of unlimited size

The feedstocks used in μPIM can be metals (carbonyl iron, stainless steel, nickel-iron alloy, copper or tungsten-copper alloy) or ceramics (aluminium oxide, zirconium oxide, yttris-stabilised zirconia or lead zirconate titanate[9]). Feedstocks also contain polymer binders and additives to enhance processability[9]. The process of μPIM involved four main steps: feedstock preparation, injection moulding, debinding and sintering (Figure 2.2).

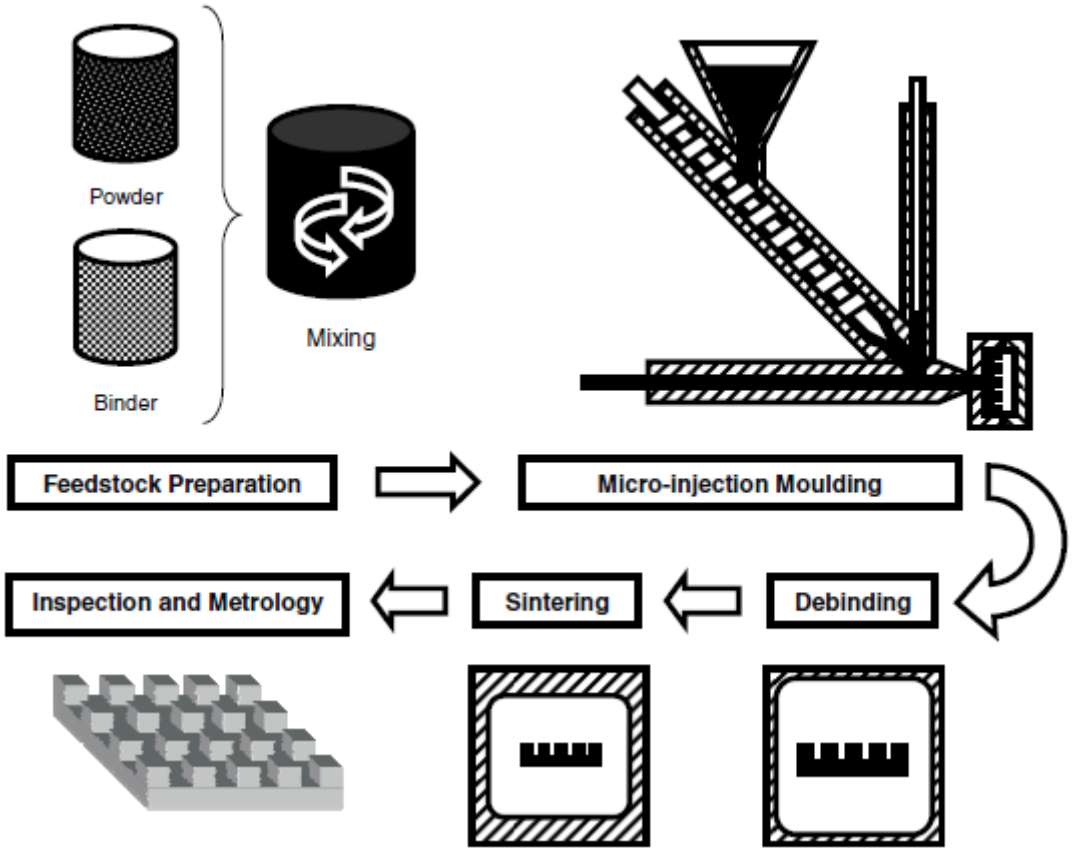

Figure 2.2 Micro-powder injection moulding process[9]

2.2.2 Low-pressure injection moulding

Low-pressure injection moulding (LPIM) is a low cost manufacturing technique which results in less wear of the mould insert. It is an alternative to the more expensive μPIM during product development, when production numbers are small. However, due to the low pressure used this technique is only suitable for powder-melts with low-viscosity binders[166].

2.2.3 Nano-powder injection moulding

Nano-powder injection moulding (nPIM) can be utilised for the mass production of electrodes and micro-gears. However, the mould insert must be lubricated prior to injection to aid in demoulding[166].

2.2.4 Micro-sacrificial plastic mould insert micro-injection moulding

The micro-sacrificial plastic mould insert micro-injection moulding technique (μ-SPiMIM) was developed to improve the filling of narrow cavities, demoulding and handling of fragile replicates during debinding and sintering[166]. The μ-SPiMIM process can be simplified into three steps: (1) manufacture of sacraficial mould insert, (2) injection of feedstock and ejection of mould insert and replicate as one component, (3) removal of sacraficial mould insert and polymer binder, followed by sintering[166].

2.2.5 Co-powder injection moulding

The co-powder injection moulding (2C-PIM) technique can be used to produce fixed multi-component parts i.e. components comprising of soft and hard materials or magnetic and non-magnetic materials. Or movable multi-component parts[172]. Two injection units are used to inject the feedstocks into the moulds either simultaneously or successively[172]. Both metal (17-4PH,

carbonyl iron, 316L, titanium and tungsten) and ceramics (zirconia, alumina, silicon carbide and silicon nitride) can be used[172].

2.3 The fabrication of micro 'textured' surfaces

The surface chemistry of a sample is an important factor to be taken into account when manufacturing surface sensitive devices as the chemical composition of a sample determines the free energy of the surface, which in turn influences the wettability of the surface [195]. The wettability of a surface can however, be adjusted and controlled by making alterations to the surface chemistry either chemically or topographically.

Chemical alterations are used to increase and decrease the wettability of a sample surface by making it more or less hydrophobic than the bulk of the sample [31; 61; 158; 227]. Topographical alterations to a surface are used to increase the surface roughness, thereby increasing the hydrophobicity of a surface. The increased roughness of the surface causes an increase in the contact angle of droplets on that surface, making it easier for the droplet to freely move across the surface due to the increased hydrophobicity [48; 49; 62; 142; 143; 179]. However, the droplet must be suspended on top of the topographical features with air trapped below it, forming a composite structure, in order for the droplet to move freely across the surface [42]. A combination of both chemical and topographical surface alterations can also be used to achieve desired surface wetting properties [33; 100; 139; 208; 215; 226].

Chemically altering the surface chemistry of a sample involves the application of a coating to the sample surface. These coatings effectively alter the chemical composition of the surface whilst leaving the bulk of the sample unchanged [158]. There are a variety of methods used to coat sample surfaces depending on the coating selected. Yang [208] used spin-coating to deposit Teflon onto the surface of selected samples and plasma-enhanced chemical vapour deposition to deposit PPFC (C_4F_8) onto separate samples in order to increase the

hydrophobicity of the surfaces. Zhu [227] used chemical vapour deposition (CVD) of dodecyltrichlorosilane to create a chemical gradient on a sample surface. Gao [65] deposited dimethylchlorosilane (DMCS) onto structured silicon wafers using a vapour-phase reaction lasting 3 days at ~ 70 ^{o}C. Öner [153] also used vapour-phase reactions to deposit organosilanes such as: dimethyldichlorosilane (DMDCS), n-octoyldimethluchlorosilance ODMCS) and heptadecafluoro-1,1,2,2-tetrahydrodecyldimethylchlorosiane (FDDCS) onto silicon samples, each reaction lasting 3 days at 65 - 70 ^{o}C. Youngblood [217] used a combination of etching and sputter-coating to coat a sample in poly(tetrafluoroethylene) (PTFE). In their paper on perfectly hydrophobic surfaces Gao and McCarthy [64] coated silicon wafers in a toluene solution at room temperature by submerging the silicon wafer in the solution. Also in their 2006 paper on 'artificial lotus leaves' Gao and McCarthy coated two textile samples by dipping them into a toluene solution of 4 wt% methylsilicane [61]. As well as chemically coating samples self-assembles monolayes can also be used to chemically alter a samples surface composition. Both Yeh [211] and Bico [22] grafted self-assembled fluorosilianted monolayer's onto sample surfaces in order to alter the surface wettability. Zhu [226] also used grafting of self-assembled monolayer's to alter the wettability of sample surfaces however, the monolayer in this case was octadecyltrichlorosilane (OTS, $C_8H_{37}Cl_3Si$).

Topographically altering the surface chemistry of a sample involves the physical structuring of a sample surface, by removing areas of the sample surface or by moulding a sample to create a 3D structured surface. Altering the topography of a sample is also known as altering a samples surface roughness which is an important feature in determining the hydrophobicity of a surface [33]. To date there have been many studies using and examining surfaces which are topographically structured with pillars [2; 24; 33; 39; 42; 62; 63; 106; 132; 143; 153; 161; 179; 207; 209; 211; 212; 215; 226]. Pillar structures are the topographical feature of choice when constructing a surface which is hydrophobic enough for a droplet to move freely across the surface [33; 62; 179; 208; 212; 215; 226], this is mainly due to the increased

surface roughness created by high-aspect-ratio pillars compared to other topographical structures such as channels and ridges.

2.3.1 Design effects of specimen and mould

The choice and design of mould inserts used during micro-moulding is of great importance as it must be able to withstand the strain of the repetitive moulding process.

Due to the high pressures exerted during injection moulding silicon inserts can fracture during the replication of high-aspect-ratio features. Therefore, when performing multiple replications of high-aspect-ratio features it is more suitable to use a metal insert

There are several journal papers that demonstrate the use of nickel inserts in micro-injection moulding for the replication of structures in the nano range [60; 86; 88; 89; 99; 101; 107; 108; 131; 140; 152; 160; 164; 180; 196; 213]. The use of a nickel insert in micro-injection moulding allows for more replication cycles as nickel is more durable than silicon which is liable to break during repetitive replication cycles especially when replicating high-aspect-ratio structures [60].

The features on structured silicon inserts can be transferred to a nickel shim via the application of a conductive seed-layer followed by electroplating [60; 101; 131; 140; 164]. The conductive seed layer increases the rate of metal deposition and improves adhesion of metal particles to the silicon insert as interactions between silicon and deposited metal particles are very weak [151]. The conductive seed-layer can be applied either by electroless-deposition or sputter-coating.

Alternatively the surface features can be structured directly on the nickel substrate via techniques such as deep reactive ion etching or micro-milling.

2.3.2 Statistical experimental analysis

Statistical experimental design is a technique used to optimise processes by examining the effect of altering factor levels on a selected response. Statistical analysis of the data gathered can determine which factors have a significant upon the process, making it easier to identify factors of interest. During an examination of the available literature it was noted that the use of statistical design to examine the fabrication of polymer and metal powder pillar features via micro-injection moulding was rather sparse. The use of statistical experimental design to examine the deep reactive ion etching process was also examined and also found to be minimally covered within the literature.

2.3.2.1 Polymer micro-injection moulding

Many people have used statistical experimental design, both design of experiment and Taguchi, to examine the effect of process factors on the micro-injection moulding of polymers. Features examined range from tensile bars [155; 189] and gears [89; 176] to micro-channels [187; 188] have been identified within the literature.

Ming-Shyan Huang & Hong-Hua Ku [88] used the Taguchi approach to optimise the mould temperature, melt temperature, holding pressure and injection speed relating to the production of pyramid structures in polymethyl methacrylate (PMMA).

Griffiths et al [79] et al also used the Taguchi approach. They examined the effect of barrel temperature, mould temperature, cooling time and ejection time of the demoulding behaviour of acrylonitrile butadiene styrene (ABS) and polycarbonate (PC) microfluidic platforms containing pin features.

Of the many literature sources examined only Sha et al [176] were found to use the design of experiment approach to examine the fabrication of micro-scale pillar arrays. They examined the effect of barrel temperature, mould temperature, injection speed and distance between micro features on the cavity

filling. The circular pillars, 100 μm and 150 μm in diameter, using polypropylene (PP), polyoxymethylene (POM) and acrylonitrile butadiene styrene (ABS) feedstocks.

Others have also examined the fabrication of pillars in the micro and nano range using polymer micro-injection moulding though not using statistical experimental analysis.

I Saarikoski et al [173; 174] fabricated pillars 18 – 60 μm and 16 – 21 μm in diameter using polycarbonate (PC) and thermoplastic elastomers TPE1 and TPE2. S.G. Li et al [117] fabricated polyacetal pillars 100 μm in diameter. Y.E. Yoo et al [213] produced non-uniform nano-pillars 200 nm in diameter using PP and PC feedstocks. N. Lee et al [110] used polycarbonate (PC) to produce nano-pillars 35 nm in height. H Pranov et al [164] fabricated nano-pillars 310 – 3100 nm in diameter using polystyrene (PS) and polycarbonate (PC) feedstocks. D MaCintyre et al [125] also used polystyrene (PS) and polycarbonate (PC) feedstocks to fabricate pillars 150 nm in diameter.

From this review of the literature it would appear that there is a gap in the current literature relating to the statistical analysis of polymer pillar feature arrays via a design of experiment approach.

The fabrication of sub-micron pillars has already been displayed in the literature however, statistical analysis of pillar features below 100 μm has not been identified.

2.3.2.2 Metal powder micro-injection moulding

With regards to the use of statistical experimental design in the fabrication of metal powder replicates via micro-injection moulding there are several cases in which the Taguchi approach has been utilised.

H. P. Li [113] and M.H.I. Ibrahim et al [90] examined the effect of injection pressure, injection temperature, injection time, powder loading, mould temperature and

holding time on the fabrication of micro dumb-bell and dog bone features in 316L stainless steel.

S. W. Lee et al [111] demonstrated the effect of filling time, feedstock melt temperature, mould temperature and the percentage of the cavity volume filled on pressure, temperature and velocity-related outputs. The moulded feature in question was a tensile bar and the feedstock's examined were 316LS, 60LS %, Alumina and 56LS % with a wax binder.

K Lee et al [109] produced hook-shaped parts using polypropylene (PP) and 316L stainless steel with a wax polymer binder. They examined the effect of melt temperature, shot size, gas delay time and gas pressure on the gas penetration and residual wall thickness of the moulded parts produced.

K.R. Jamaludin et al [93] moulded tensile bars using 316L stainless steel. They examined green defects, strength and density of the tensile bars and how they were effected by mould and holding pressure, mould and melt temperature, cooling time, moulding rate and holding time.

R Urval et al [192] fabricated plates using a 316L stainless steel with a wax binder feedstock. They examined filling time, melt temperature, mould temperature and switchover position on the injection pressure, clamping force, melt front temperature difference and the maximum shear rate.

It was noted that the material of the mould inserts used in these papers was not mentioned.

The production of pillar arrays using metal powder feedstock was also found within the literature though in a lesser quantity than other parts and features.

G. Fu et al [57] fabricated 316LS micro-pillars 60 μm and 40 μm in diameter using a silicon mould insert. G. Fu et al [56] also fabricated 316LS circular column arrays comprising of columns 100 μm and 60 μm in diameter once again using a silicon mould insert.

Z.Y. Liu et al [123] fabricated both square and circular pillar arrays using a silicon mould insert. They examined the fabrication of such features using Alumina, Lead zirconate titanate (PZT) and 316LS feedstocks.

From this review of the available literature it would appear that the examination of pillar arrays using statistical experimental design represents a gap in the literature. The production of metal pillars below 40 μm in diameter is also identified as a gap in the current literature.

2.3.2.3 Deep reactive ion etching

From the examination of the literature it was found that the use of the design of experiment approach relating to the deep reactive ion etching process was not very wide-spread. Three of the papers [19; 137; 150] found examined the effect of given factors on the angle of the feature sidewall. However, the measurement of feature undercut as a response was not found within the literature. Only one paper was found to discuss the examination of pillar arrays.

G. J. O'Brien et al [150] examined trench features etched into silicon and how the trench depth, lateral trench etch, trench sidewall angle and aspect ratio dependent etch were affected. They found that the most significant factors common for all four of the responses were etch cycle time, passivation cycle time and RF coil power.

G. M . Beheim et al [19] also examined trenches 100 – 150 μm in depth etched into single-crystal silicon carbide. The effect of the temperature of the wafer chuck, chamber pressure and concentration of O_2 and Ar gas on the trench depth, slope of the sidewalls, surface roughness and etch rate of the deep reactive ion etching process. They determined that a high pressure within the chamber was required for more vertical sidewalls and a higher concentration of O_2 and Ar is required for a smoother surface.

A.Baram et al [17] used the process pressure and bias power to examine their effects on the etch rate of Pyrex cavities 47 μm in depth. The factor levels used were based on the capabilities of the equipment used. It was determined that the process pressure had little effect on the etch rate while the etch rate was linearly proportional to the bias power.

The fabrication of Fresnel lenses in silicon was examined by T. Nachmias et al [145]. They examined how the chamber pressure, electrode power and CF_4 : O_2 gas flow affected the selectivity of the etch. They determined that the electrode power has less of an effect on selectivity than either chamber pressure or CF_4 : O_2 gas flow.

Only K. Miller et al [137] were found to have examined the effect of factors on the etching of micro-pillar arrays. They examined the effect of etch and passivation cycle time, platen power and coil power on the feature profile angle, scallop depth and scallop peak-to-peak distance. They determined that the profile angle decrease when the platen power was increased. However when then platen power was kept constant and the cycle times were increased the profile angle also increased.

2.4 Behaviour of droplets on micro-textured surfaces

Surface wetting is a key function and has been explored in a vast array of technologies from self-cleaning coatings [42; 70; 96; 169] to droplet transport [70; 96; 191]. In many of these areas the development of a superhydrophobic surface is desirable as it allows for the free movement of droplets, known as the lotus-effect.

The lotus-effect is a term used to describe a superhydrophobic surface on which a droplet can move freely. Many plants and insects are partially if not completely water-repellent [27] and none have been studied more so than the lotus leaf [21; 61; 62; 146; 194].

The lotus leaf has gained much attention in the academic world due to its self-cleaning properties [42; 169; 194] and it is considered to be the archetype of natural water-repellency [27]. The lotus leaf is highly water-repellent due to its two hierarchical surface structures which consist of 10 μm bumps covered in submicron microfibers [27] (Figure 2.3). The surface combines features on the micro- and nanoscale [42] to form a highly rough surface on which a droplet will sit with high contact angles (Figure 2.4) these high contact angles result in a low contact angle hysteresis which in turn allows the droplet to move freely across the surface.

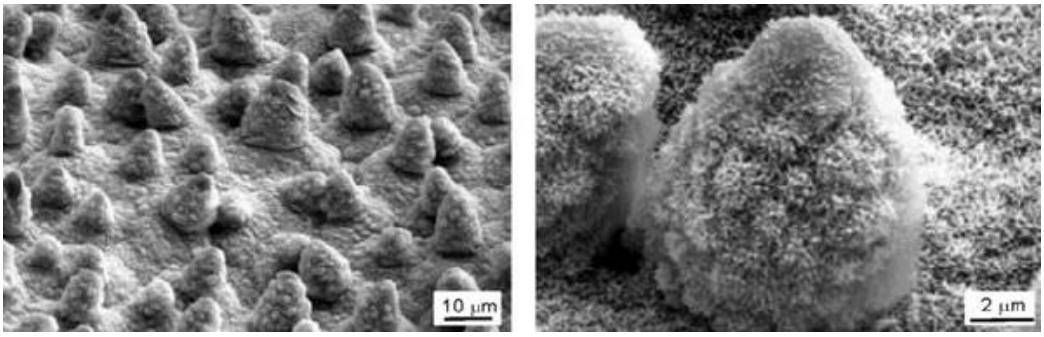

Figure 2.3 SEM images of a lotus leaf surface [21]

Figure 2.4 Water droplet on a lotus leaf [21]

The lotus leaf effect and the concept of increasing surface roughness to improve the hydrophobicity of a surface is now common place within the literature [42; 48; 49; 61; 62; 148; 169; 179; 208; 226].

2.4.1.1 Measurement of surface wettability

The characterisation of surface wettability is determined by examination of the contact angle (θ_c) of a droplet on the surface of interest. The contact angle of a droplet increases as a surface becomes more hydrophobic. Therefore by examining the droplet contact angle on a surface the surface can be characterised and the surface wettability identified [22; 33; 39].

A surface can be categorised according to the contact angles observed. A contact angles below 90 ^{o} indicates a hydrophilic surface whereas a contact angle of above 90 ^{o} indicates a hydrophobic surface [23]. Also droplets on a hydrophobic surface which display contact angles of 150 ^{o} and above can be categorised as superhydrophobic [49; 148; 161; 169; 207; 211]

The contact angle of a droplet is obtained through the measurement of the angle between the solid-liquid and liquid-vapour interfaces (Figure 2.5).

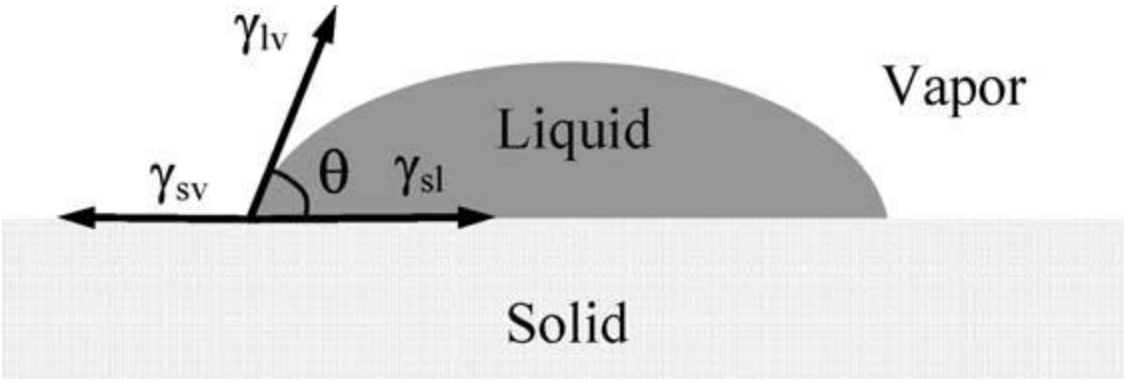

Figure 2.5 Schematic of droplet contact angle and interfacial tensions on a sessile droplet [184]

Measurement of contact angles is one of the key methods of characterising surface wetting. Thomas Young [216] stated:

"For each combination of a solid and a fluid, there is an appropriate angle of contact between the surfaces of the fluid, exposed to the air, and to the solid"

Assuming an ideal flat surface a droplets surface contact angle (θ_y) can be determined by the Young's equation [22; 70; 148],

Equation 1 $\cos\theta_y = \gamma_{SV} - \gamma_{SL} / \gamma_{LV}$

γ_{SL}, γ_{LV} and γ_{SV} being the interfacial tensions of the solid-liquid, liquid-vapour and solid-vapour interfaces (Figure 2.5).

However, the young's equation does not apply on rough surfaces such as a flat surface structured with uniform pillars of controlled geometry (Figure 2.6). The pillar geometry for these surfaces is determined by the pillar width (a), the spacing between pillars (b) and the pillar height (h) (Figure 2.7).

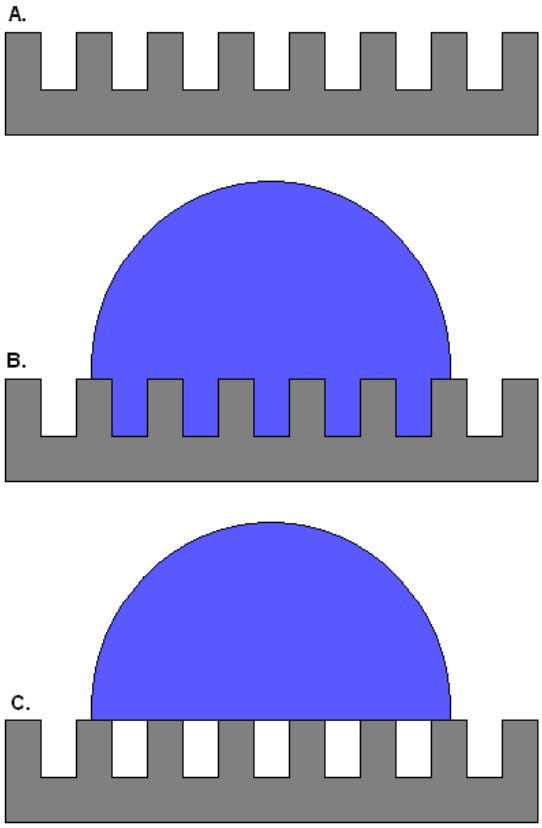

Figure 2.6 a) Smooth surface structured with pillars, b) Droplet in Wenzel state, c) Droplet in Cassie-Baxter state [161; 169; 207; 226]

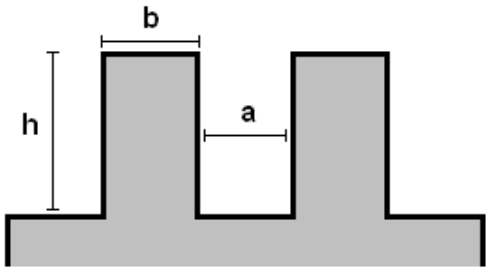

Figure 2.7 (a) gap length, (b) pillar size, (h) pillar height [179; 207]

These dimensions can also be used to calculate the roughness ratio (r) of a surface (Equation 2) and also the surface area fraction (Ø) of the pillars [179] (Equation 3).

Equation 2 $r = 4bh + (a+b)^2 / (a+b)^2$

Equation 3 $Ø = b^2 / (a+b)^2$

When determining the contact angle of a droplet on a rough surface there are two states the droplet can conform to. These are the Wenzel state, identified by Wenzel in 1936 [198], and the Cassie-Baxter state, identified by Cassie and Baxter in 1944 [28].

In the Wenzel state the surface undergoes complete filling of the spaces between pillars by the droplet, known as homogeneous wetting [2] (Figure 2.6). The apparent contact angle (θ_W) for this surface can be determined using the Wenzel equation [65; 169; 179; 195] (Equation 4).

Equation 4 $\cos \theta w = r \cos \theta y$

Alternatively the droplet may conform to the Cassie-Baxter state in which the droplet is in contact with a composite surface, known as heterogeneous wetting [2]. The apparent contact angle for the droplet in this state (θ_{CB}) can be determined using the Cassie-Baxter equation [65; 161; 169; 179] (Equation 5 and Equation 6).

Equation 5 $\cos \theta CB = Ø1 \cos \theta y1 + Ø2 \cos \theta y2$

Equation 6 $\varnothing 1 = \varnothing 2 = 1$

When considering a “Fakir” droplet on a composite surface consisting of solid pillars and vapour (Figure 2.6), the Cassie-Baxter equation can be simplified [179] (Equation 7).

Equation 7 $\cos \theta_F = \varnothing (\cos \theta_y + 1) - 1$

The contact angle of a droplet on this surface is obtained from the surface area fraction of the solid surface (Ø) which has a contact angle (θ_y) calculated from the young’s equation and the surface area fraction of the liquid-vapour interface (1-Ø) [179]. As the liquid-vapour interface is freely suspended between the pillars it is assumed to obtain a contact angle of 180 ° [179]

The contact angle of a droplet can be measured using either the sessile droplet or dynamic droplet technique. The sessile droplet technique uses a goniometer in conjunction with a microscope and some form of image capturing equipment i.e. digital camera, to measure and record the contact angle of a static sessile droplet [39; 217]. Alternatively the contact angle can be measured by using video recording equipment incorporated with digital analysis software [64; 211].

The dynamic droplet technique [42] uses the same equipment for measuring a droplets contact angle as that used in the sessile droplet technique. However, rather than simply recording a value for the droplets static contact angle the droplets volume is increased and decreased in order the find the advancing and receding droplet contact angles. The advancing contact angle is the largest contact angle obtainable before the solid-liquid interface of the droplet increases due to increase droplet volume [149]. The receding contact angle is the smallest contact angle value before the solid-liquid interface decreases due to a

decrease in droplet volume [149]. The difference between the advancing and receding contact angles measurements can then be used to determine the contact angle hysteresis of a droplet, the lower the contact angle hysteresis the more hydrophobic the surface.

Equation 8 $\theta_A - \theta_R = \theta_H$

A low hysteresis value also indicates that a droplet will move more freely across the sample surface than a droplet with a high hysteresis value [33].

2.4.1.2 Wenzel & Cassie-Baxter debate

In recent years there has been much debate concerning the validity of the Wenzel and Cassie-Baxter equations. In 2007 Gao & McCarthy [65] outlined concerns over the validity of these equations, it was proposed that the contact angle behaviour of a droplet is determined by liquid-solid interactions at the three-phase line (Figure 2.8) rather than the surface area beneath the droplet. Gao and McCarthy's subsequently [65; 67-69] outlined experimental data which indicated that the area under a droplet does not affect the contact angle.

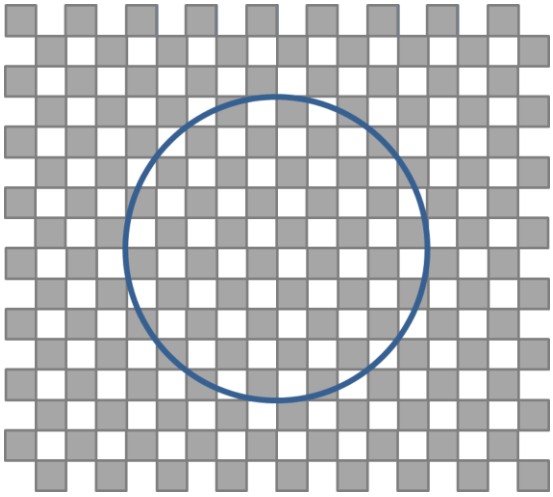

Figure 2.8 Schematic of three-phase contact line

Gao and McCarthy [65; 69] examined the behaviour of a purified water droplet on three two component surfaces. The first surface (a) was a hydrophilic spot in a hydrophobic field, the second surface (b) was a rough spot in smooth field and the third surface (c) was a smooth spot in rough field (Figure 2.9).

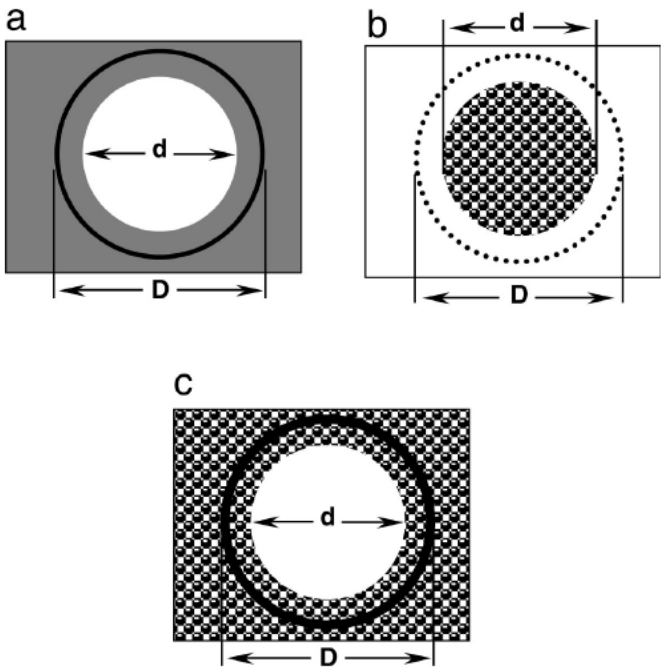

Figure 2.9 (a) hydrophilic spot in a hydrophobic field, (b) rough spot in smooth field, (c) smooth spot in rough field [65; 69]

When examining surface b Gao and McCarthy found that the droplet possessed a high contact angle (θ_A ~ 168 ^{o}) when on the rough spot however, when the droplet expanded past the rough spot and began to spread onto the smooth field the contact angle decreased. When the droplet surface area incorporated both the rough spot and the smooth field the contact angle was found to have decreased to θ_A ~ 117 ^{o}. For surface C the reverse was observed, when the droplet was placed on the smooth spot a low contact angle of θ_A ~ 117 ^{o} was observed. As the droplet was advanced to the edge of the spot the droplet became pinned to the rough perimeter and a contact angle of θ_A ~ 168 ^{o} was observed.

Gao and McCarthy [68; 69] also examined droplet wetting on trough features structured into a high density polyethylene block. The base of the troughs was coated with varying amounts of a hydrophilic monolayer and covered with water

until the coated areas were covered (Figure 2.10). When the high density polyethylene block was tilted the water was observed to move along the troughs.

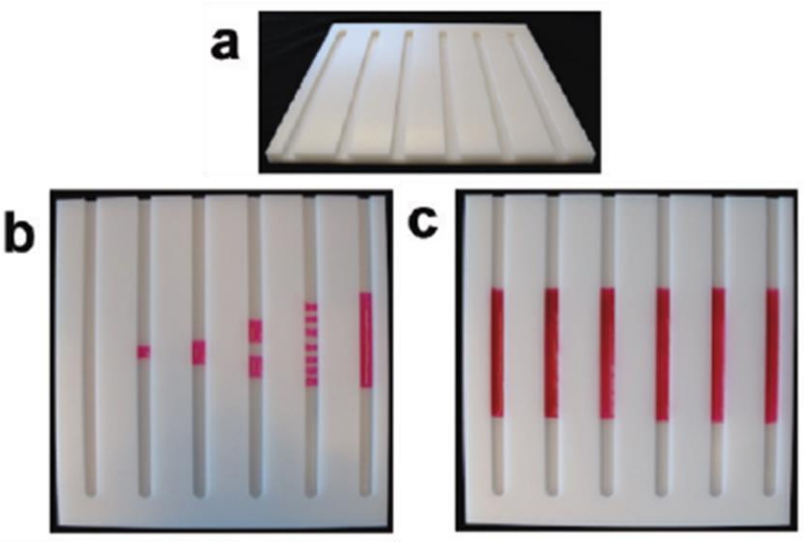

Figure 2.10 (a) parallel troughs milled into a high density polyethylene block, (b) hydrophilic monolayer stripes adsorbed onto base of troughs, (c) hydrophilic Stripes covered with water [68; 69]

Gao and McCarthy's work suggests that the advancing and receding contact angles and the contact angle hysteresis of a droplet are independent of the surface structure under the droplet. Rather it is the structure of the surface at the three-phase line which determines the contact angles of the droplet.

Following the publication of Gao and McCarthy's controversial paper there have been several publications in response to the questioned validity of the Wenzel and Cassie-Baxter equations [24; 129; 132; 156; 212]. McHale [132], Panchagnula [156], and Marmur [129] each determined that the Wenzel and Cassie-Baxter equations were found to be invalid by Goa and McCarthy due to the surfaces used during the experimental investigation. Mamur stated that for the Wenzel and Cassie-Baxter

equations to apply the droplet must be sufficiently larger than the surface roughness and in the case of the surfaces observed by Gao and McCarthy the droplet size is too small [129]. A key assumption, highlighted by McHale, in the use of the Wenzel and Cassie-Baxter equations is that both the surface roughness and surface area fraction must be constant across the entire surface for these equations to apply. Therefore the Wenzel and Cassie-Baxter equations should not be used on the surfaces reported by Gao and McCarthy as the surface roughness features are located in isolated areas of the surface and do not represent the surface as a whole [132]. Panchagnula was of the opinion that Goa and McCarthy's calculations were incorrect due to the incorrect choice of surface area fractions [156]. It would appear that the common theme which can be drawn from these papers is that the Wenzel and Cassie-Baxter equations are valid as long as certain assumptions are considered i.e. uniform roughness across the whole surface [132] and the droplet is larger than the surface roughness [129].

As well as those who disagree with Gao and McCarthy's analysis of the Wenzel and Cassie-Baxter equations, their paper also prompted others to look at the equations in more detail to determine the accuracies and variations between the calculated values and those obtained experimentally. Y. Erbil [212] evaluated the difference between the theoretical (calculated) and experimental contact angles of 166 patterned surfaces containing either cylindrical or square posts (pillars) to determine the validity of the Wenzel or Cassie-Baxter equations. It was determined that of the 166 surfaces evaluated the theoretical Wenzel equation was found to be incorrect for 74 % of the cylindrical post surfaces and 58 % of the square post surfaces [212]. Concerning the Cassie-Baxter equation, it was determined that the equation was still valid although it should be applied with caution as the droplet does not always take on a perfectly 'Fakir' state and can instead sit at an intermediate position between the Wenzel and 'Fakir' state in which the droplet partially fills the cavities between the posts (Figure 2.6).

Currently, despite this debate as to the validity of the Wenzel and Cassie-Baxter equations the use of these equations has yet to disappear from the current

literature on superhydrophobic surfaces. However, there are those out there who make the point of avoiding the use of these equations due to the uncertainty concerning the validity [207].

Due to the continuing debate concerning the Wenzel and Cassie-Baxter equations it has been decided that these equations will not be used to determine the hydrophobicity of the surfaces developed during this research.

2.4.1.3 Droplet Movement on a surface

The movement of a droplet across a surface is an important feature in many applications from self-cleaning coatings to microfluidic devices. When observing droplet movement a probe fluid is generally used, with the most common probe fluid used being deionised water, although other probe fluids such as ethylene glycol [227] can also be used.

Droplet movement on a surface can be due too many factors. External factors like vibration and sample tilting can be used to force movement on a droplet [179], if the sample itself has conductive properties electro-wetting can be applied to move and spread droplets across the surface [66; 106]. Chemical or topographical alteration to the surface can also be used to influence the ease at which a droplet can freely move across a surface. However, for the droplet to move at all on a surface it must first possess a low contact angle hysteresis [66] (Equation 8).

Chaudhury and Whitesides [31] developed a surface with a chemical gradient which caused a gradient in the surface free energy of the sample making it possible for a water droplet to move uphill. The gradient surface was deposited onto a silicon wafer by a vapour-phase reaction with decyltrichlorosilane ($Cl_3Si(CH_2)_9CH_3$). Although the chemical gradient itself is not enough to make a droplet move, the surface must also have a low contact angle hysteresis and be free from defects which could cause pinning of the droplet to the surface. During this study Chaudhury and Whitesides observed droplets moving up an incline of

~ 15 º from the horizontal plane, it was also noted that the droplet moved more rapidly when at the start of the gradient than at the end.

Shastry [179] used a regular array of 2D square pillars to create a rough surface and examined how vibrational energy can be used to overcome pinning of droplets to allow them to move across the surface. The surfaces were structured using photolithography and deep reactive ion etching to from pillars with dimensions for gap length and pillar width ranging from 4 – 8 mm, these formed a textured gradient surface with uniform linear changes along the length. A speaker diaphragm was used to create the vibrations and it was found that droplet pinning could be overcome by subjecting the sample to the external vibrational energy. Shastry also noted that droplets of different volumes came to a stop at different positions along the surface gradient.

Gao and McCarthy [62] compared a droplets ability to move across surfaces structured with rhombus posts (Figure 2.11). The surfaces were subjected to either vapour-phase deposition with dimethyldichlorosilane (DMDCS) to produce rhombus posts with smooth chemically modified surfaces (surface a) or a solution reaction with methyltrichlorosilane which created a nanoscopic second length scale topography on the post tops resulting in a surface with two length scales of topography (surface b). It was found that water droplets did not come to a rest on surface b, but instead rolled freely around the surface.

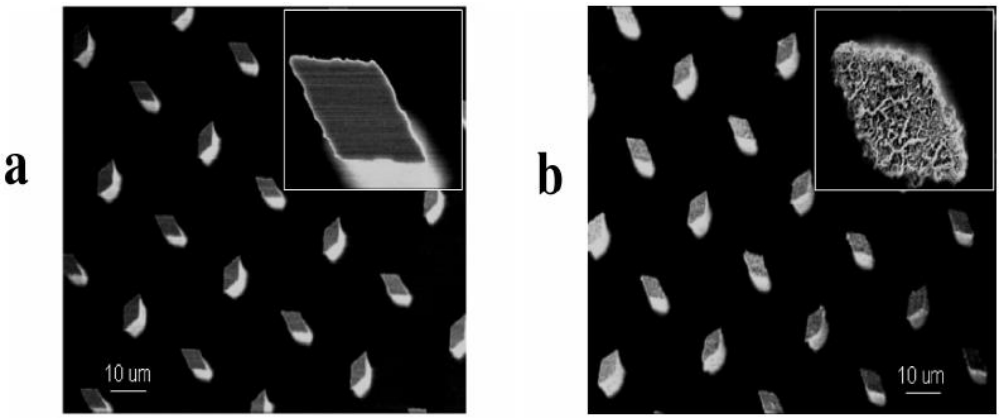

Figure 2.11 (a) rhombus post with chemically modified tops, (b) rhombus posts with second length scale topography [62]

Zhu [227] used silicon wafers with surface energy gradients created using chemical vapour deposition (CVD) with dodecyltrichlorosilane to demonstrate how droplets will move along a surface from a hydrophobic region to a hydrophilic region. It was noted that droplets moved along surfaces from hydrophobic to hydrophilic regions due to the varying surface energies between the regions. A droplet will preferably wet an area with a high surface energy thereby forming a droplet with a low contact angle. Therefore the droplet will move from the hydrophobic to hydrophobic regions on the gradient surface so that it may wet the surface with the highest surface energy.

Fang [48] proposed a design of surface geometry for microfluidic channels which spontaneously moves droplets across a surface (Figure 2.12). Using computer simulations it was found that small pillar width and spacing values were required to obtain a surface roughness structure with low free energy barriers which results in a small hysteresis, thereby allowing droplets to move across the surface.

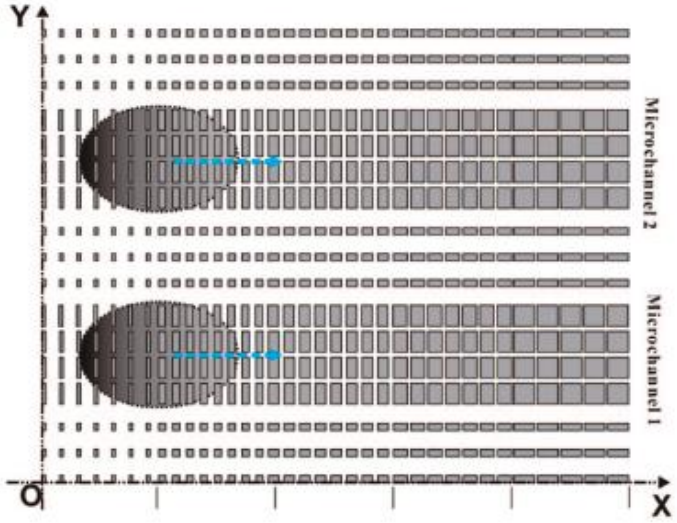

Figure 2.12 Schematic of Fang's proposed surface geometry [48]

Moradi [143] also used computer simulations to design a surface on which droplets would move spontaneously. It was found that the arrangement of pillars on the surface significantly influenced the dynamics of the droplet. Two surface deigns were constructed, each with a different arrangement of pillars but the same pillar density. Surface A contained pillars of two different dimensions arranges in a uniform pattern, surface B also contained pillars of two dimensions but arranged in a 'chessboard' pattern (Figure 2.13). It was found that the droplet moved further on surface B.

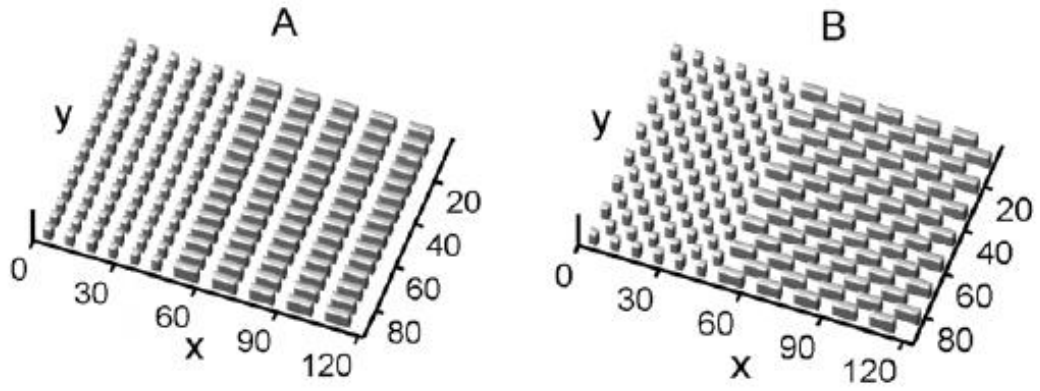

Figure 2.13 (A) pillars in uniform pattern, (B) pillars in 'chessboard' pattern [143]

Droplet movement on a surface can be captured and observed using a high-speed CCD camera connected to a computer through which the footage can be analysed [158; 179; 227]; the camera can also be connected to a goniometer [139; 158] so that the droplets contact angle can be recorded before and after its movement.

2.4.1.4 Droplet evaporation

A natural process which every liquid droplet undertakes is evaporation. Evaporation occurs when the atmosphere directly surrounding the droplet is not saturated with the evaporating substance [44] and liquid from the droplet surface is released as vapour into the surrounding atmosphere.

Once the size of a droplet is decrease to the micro-range the effect of surface tension and gravity on the droplet shape begins to change. In the case of microliter droplets the effects of the droplet surface tension is greater than that of gravity resulting in the formation of a droplet with a spherical cap shape[44]. These spherically caped droplets can be characterised by four factors: droplet

height (h), droplet contact radius (r_b), contact angle (ɵ) and the radius of the sphere forming the spherical cap (R_s) [44] (Figure 2.14).

The evaporation kinetics of a droplet are measured by analysing the change in droplet profiles of these four factors [205].

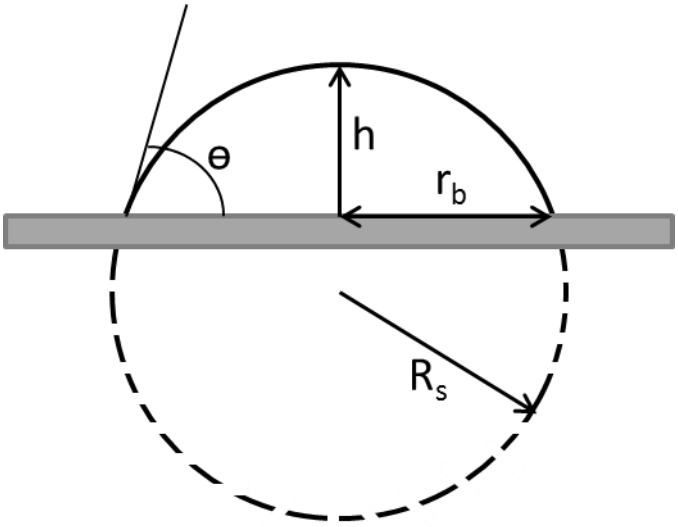

Figure 2.14 Factors characterising a spherical cap droplet on a substrate, droplet height (h), droplet contact radius (r_b), contact angle (ɵ), radius of the sphere forming the spherical cap (R_s) [44]

A spherical cap droplet can be characterised by any two of these factors [44].The relationship between the two radii, contact angle and the volume of the droplet (Vsph) at a particular moment in time can be defined by (Equation 9 - Equation 11)[44].

Equation 9 $R_b = R_s \sin ɵ$

Equation 10 $Rs = (3 V_{sph} / \pi \beta)$

Equation 11 $B = (1 - \cos\theta)^2 (2 + \cos\theta) = 2 – 3\cos\theta + \cos^3\theta$

The height of the spherical cap droplet is related to the two radii and contact angle by (Equation 12 and Equation 13) [44].

Equation 12 $h = R_s (1-\cos\theta)$

Equation 13 $h = r_b \tan(\theta/2)$

Droplets have been observed to exhibit three phases during evaporation on a smooth planar surface. Phase I is the initial pinning of the droplet with a constant contact area (base diameter). In phase II the droplet recedes with a constant contact angle. Phase III is the simultaneous decrease in the droplet contact angle and the droplet base diameter [45; 73; 133; 147; 204-206].

When examining the evaporation of a droplet on a patterned surface, or a droplet containing nanoparticles, phase I is noted to last longer than when observed on a smooth surfaces [147; 204-206]. A second pinning phase is also observed, prior to phase III, in which the droplet changes state from Cassie-Baxter to Wenzel, penetrating and wetting the surface features [204-206]. During this phase the contact area between the droplet and the surface increases as the droplet fills the feature cavities (Figure 2.15). The resulting pinning slows the receding of the droplets three phase line making the process of evaporation last longer than when observed on a smooth surface.

Surface features can also affect the direction of droplet evaporation by causing different areas of the three phase contact line to recede more easily than others due to contact pinning [220]

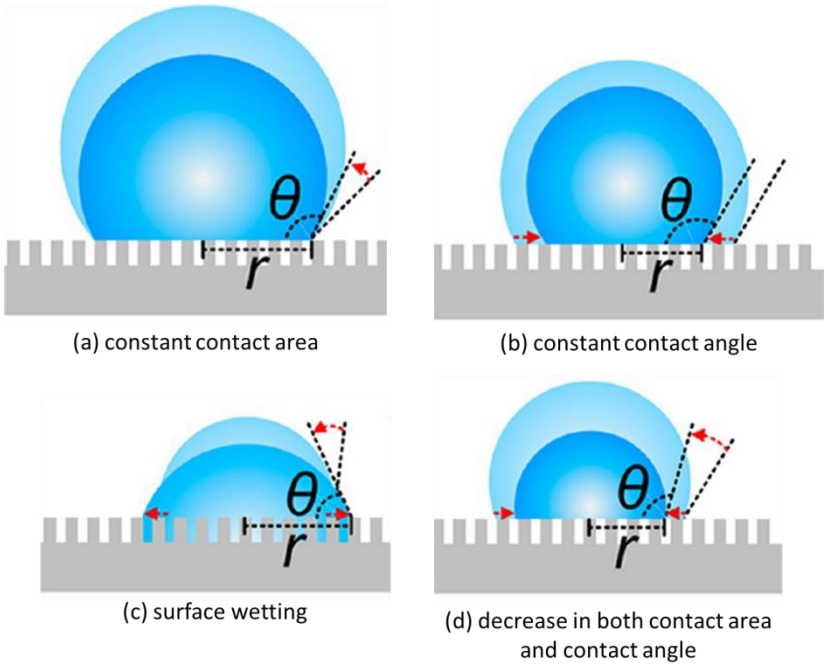

Figure 2.15 Schematic of evaporation phases of a sessile droplet on a patterned surface (a) constant contact area, (b) constant contact angle, (c) surface wetting – droplet changes from Cassie-Baxter to Wenzel state, (d) decrease in both droplet contact angle and contact area [206]

The rate of droplet evaporation can be determined by examining the volume ($V^{2/3}$) of the droplet in question at a given time [205]. V_o is the initial volume of the droplet in microliters and K is the evaporation constant in mm ^{2} / s. It should be noted that the value of K will decrease for the second pinning phase [205] (Equation 14).

Equation 14 $V^{2/3} = V_o^{2/3} - K_t$

The process of evaporation has also been used to deposit particles onto surface features. Dufaur [43] noted that when a droplet evaporates a minute

amount of the liquid is left on the receding top edge of the surface features (Figure 2.16).

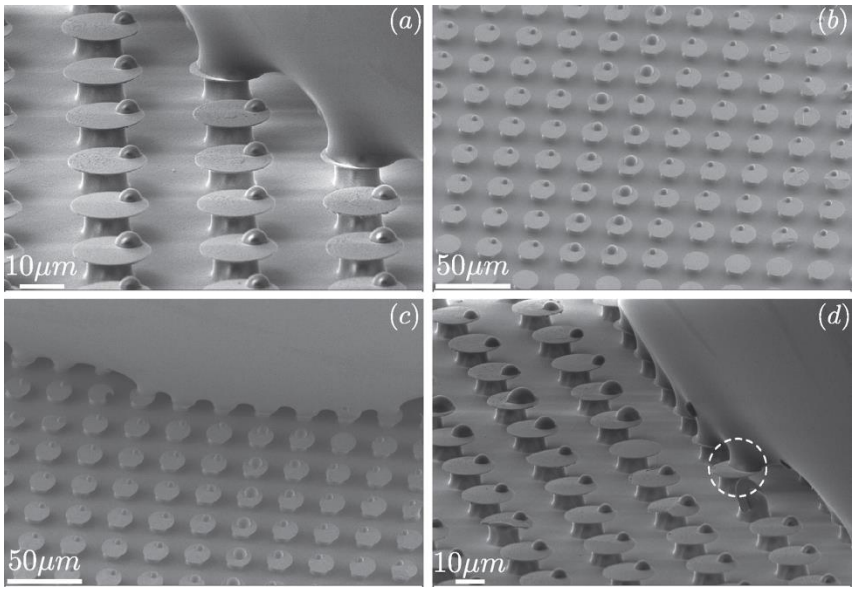

Figure 2.16 Liquid left on top of posts as droplet recedes during evaporation [43]

The high concentration of nanoparticles at the three phase line of an evaporating droplet and the residue left on surface features during evaporation, can allow for the deposition of nanoparticles on surface features [43; 147]. This ability to deposit residue on sample surface using droplet evaporation, known as 'evaporative colloidal lithography', could be used in high-throughput analysis in lab-on-a-chip systems [43].

2.5 Knowledge gap

Micro-fluidic lab-on-a-chip devices are leading the way in the miniaturisation and portability of medical diagnostic devices. The use of incorporated surface texturing to manipulate and direct micro-amounts of fluid are bringing the mass productions of cost effective handheld diagnostic devices one step closer.

As such, it is important that a thorough understanding be gained of the fabrication processes involved and the effect these various micro-structures have on droplet behaviour.

The use of techniques such as deep reactive ion etching and micro-injection moulding in the fabrication of the micro-scale features, which would be required for droplet movement, have been widely discussed. However, the further examination and optimisation of these processes for the fabrication of high aspect ratio features, such as pillars, using statistical experimental analysis is still limited to a handful of papers.

Within those papers there is also a divide between the uses of two approaches to statistical experimental analysis: the Taguchi and the design of experiment approach.

The fabrication and statistical analysis of sub - 100 μm pillars via polymer micro-injection moulding and sub - 40 μm pillars via metal powder micro-injection moulding do not appear within the literature. It was also noted that among the publications examined there were no examples of statistical experimental analysis being used to examine the fabrication of surfaces which contain a wide variety of pillar feature dimensions. Rather, the focus often seems to be on pillar features of the same or a similar size.

The effect of process factors on the fabrication of micro-structured surfaces, particularly sub – 100 μm pillars and surfaces with a mixture of pillar sizes, is an area which needs to be addressed in order to more fully understand the fabrication processes. For example, the process factors of significance in the fabrication of surfaces structured for droplet movement, discussed in section

2.4.1.3 Droplet movement on a surface, do not appear to have been examined. But through the use of statistical analysis the effect of the process factors can be determined and the fabrication process optimised.

Due to the limited information available within the literature regarding the use of statistical experimental design in the fabrication of sub - 100 μm pillar features, an investigation into its use with the deep reactive ion etching and micro-injection moulding processes is recommended. This investigation should focus on determining the effect of process factors on the fabrication of sub – 100 μm pillars arranged to facilitate the manipulation of fluid droplets. With specific attention to the dimensions of the fabricated features and their effects on droplet behaviour.

The use of surface texturing to manipulate fluid droplets could eventually reduce the need for additional pumps within micro-fluidic diagnostic devices. The design of the surface texturing and the accuracy of the features all contribute to the behaviour of the fluid. From altering the hydrophobicity of the surface to ensuring a droplet will move in a specific direction, surface texturing can alter the way in which a droplet will react to external stimuli i.e. vibration. The use of micro-channels in the directional movement of water droplets has been documented. Though the effect of such micro-channelled features on the evaporation of droplets is less widely discussed.

To summaries, through a review of the available literature three gaps in knowledge were identified:

1. The fabrication and statistical analysis of sub – 100 μm polymer pillar features fabricated via micro-injection moulding.
2. The fabrication and statistical analysis of sub – 40 μm metal powder pillar features fabricated my micro-injection moulding.
3. The fabrication and statistical analysis of surfaces containing a wide variety of pillar feature dimensions, rather than just one.

These three areas will therefore be addressed during the course of this thesis to ultimately provide a contribution to knowledge regarding the micro-injection moulding of polymers and metal powders.

3 Methodology

The following chapter outlines the experimental methods used in the process of examining the micro-texturing of surfaces of fluid control. Section *3.1 Overview of experimental design* discusses the use of experimental design as a statistical technique used to identify factors of significance and optimise processes. Section *3.2 Mould design and fabrication* discusses the development, design and fabrication of removable mould inserts to be used in the micro-injection moulding process. The use of experimental design in examining the effect of factor levels in the fabrication process is also discussed. Section *3.3 Micro-moulding* discusses the use of experimental design in examining factors in the micro-injection mould of polymer and metal powder replicates. Section *3.4 Metrology and Optical Analysis* discusses the optical and metrological techniques used throughout the course of this research including contact angle analysis, droplet channelling and droplet evaporation analysis.

3.1 Overview of experimental design

Experimental design is a statistical technique used to optimise a process in question. Unlike the traditional single-factor approach multiple process factors are examined simultaneously. Experimentally designed investigations examine factors at multiple levels and process all possible factor combination in order to gain an understanding of the effect of individual factors and the interactions between factors [141] on a given response.

3.1.1 Single-factor approach

The single-factor approach to experimental design (DOE) involves the alteration of one factor per experiment. When there are several factors of interest this approach can result in a larger number of experiments to be performed in order to obtain the same level of precision compared to factorial designs. It is also not

possible to examine the interactions between factors and their level when altering only a single factor per experiment [141].

3.1.2 Design of experiment

The design of experiment technique enables the determination of significant individual factors and/or interactions between many factors that may affect the response output in a process or design. Factors of interest from a process are selected and varied across a pre-determined range in a randomised order. The gathered response results are then statistically analysed to determine the main effect and/or interaction effect within the process.

3.1.2.1 Response selection

Prior to the construction of the experimental design a response, which is to be measured, must be selected. Once analysed the response will indicate which of the factors examined, if any, are statistically significant to the process. Part mass, feature dimensions, viscosity and strength are examples of possible responses [141].

3.1.2.2 Factor selection

Factors are variables which can influence a process by a variation in its levels. This stage initially requires familiarisation of the experimental process and screening of the factors involved. This is to determine the factors which are the most dominant/relevant and the range at which the various factors function. Once the factors of interest and their ranges have been identified levels can be selected. It is these levels at which the factors will be examined during the design of experiment process [141].

The selected factors can be either quantative or qualitative. A quantative factor has levels which are selected from a range, for example a temperature range of 50 – 80 ^{o}C. Whereas a qualitative factor has levels which are not from a range, for example a light switch is on or off [46].

As well as variable factors there are also uncontrollable factors within a process. These factors also have an influence on the process response however, they are hard to regulate. They should also be monitored during the experimental process despite their uncontrollable nature.

3.1.2.3 Types of design of experiment

The choice of experimental design will be very much dependent upon the factors and levels selected. The basic principles of experimental design and the choice of factorial design must be considered during the development of the experimental design [141].

3.1.2.3.1 The basic principles of experimental design

There are three basic principles of experimental design to be considered: randomisation, replication and blocking.

Randomisation is a procedure used to reduce variability and bias from uncontrollable factors, both known and unknown [141]. Statistical analysis software, such as Minitab®15, can be used to construct and randomise experimental designs using a random number generator.

During the performance of the design of experiment process each factor combination should be repeated several times. This process of replication provides the production of several identical samples, produced under identical conditions, which can be compared to identify any random variation which may need to be explored [46; 141].

When a factor which is not of direct interest in the design of experiment process may have an effect on the response (a nuisance factor) a technique known as blocking can be used. Blocking is a design technique used to reduce variability from nuisance factors to improve precision of the measured response [46; 50; 141].

3.1.2.3.2 Full and fractional factorial designs

The key difference between a full and a fractional factorial design is that a full factorial design can be used to investigate all possible factor level combinations available. Whereas, a fractional factorial design will examine a small fraction of the overall number of factor level combinations available.

The most common full factorial designs are 2^k and 3^k factorial designs. The most common fractional factorial designs as 2^{-k} and 3^{-k}. where k represents the number of factors examined and the number (in this case 2 or 3) represents the number of levels examined for each factor [46; 141]. The possible factor combinations for these factorial designs are often displayed in geometrical representations such as those in Figure 3.1, Figure 3.2 and Figure 3.3. However, once the number of factors exceeded 3 these geographical representations become more difficult to display.

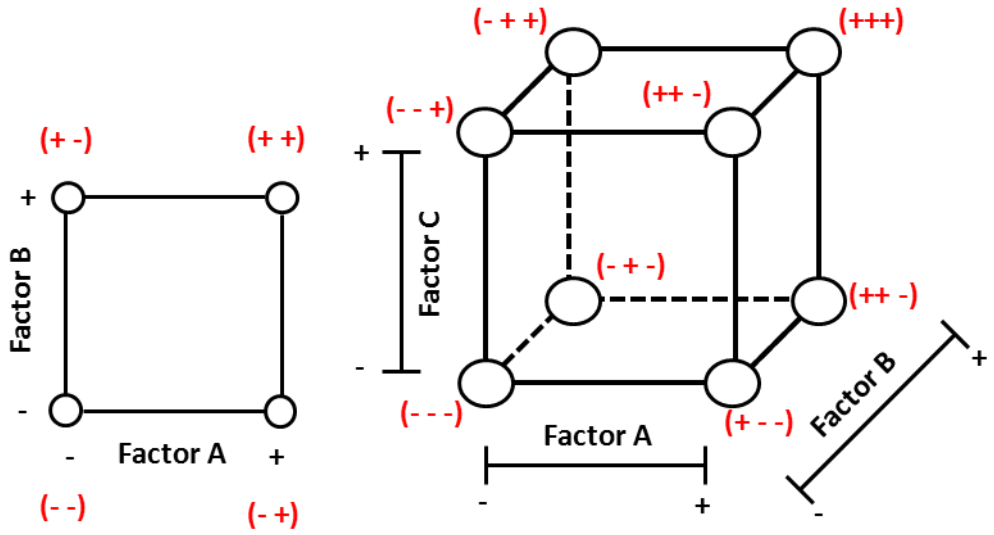

Figure 3.1 Factor combinations for, 2^2 full factorial design (Left) 2^3 full factorial design [141]

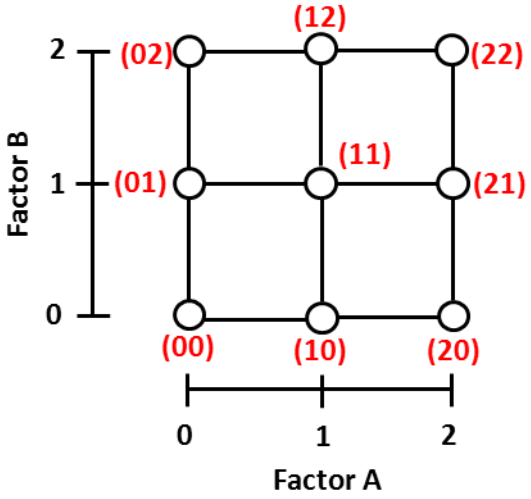

Figure 3.2 Factor combinations for a 3^2 full factorial design [141]

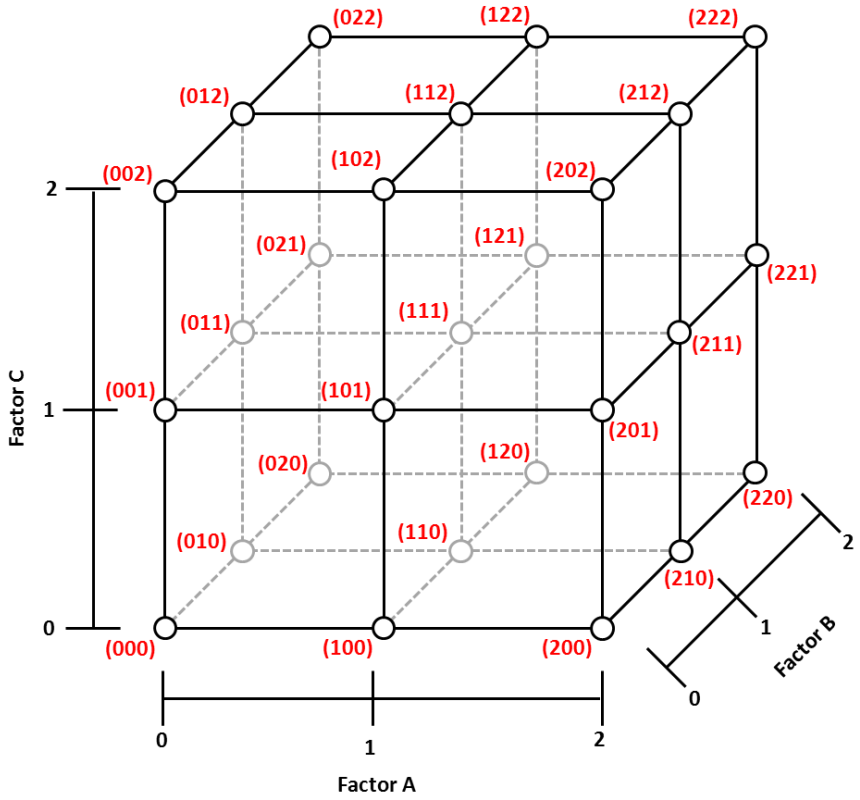

Figure 3.3 Factor combinations for a 3^3 full factorial design [141]

The number of combinations which will be examined during a full and fractional factorial design will vary depending on the number of levels to be examined for each factor (Table 3.1 and

Table 3.2).

Table 3.1 The number of experimental runs required for 2^k and 2^{k-1} factorial designs [138]

Nº Factors (k)	Nº Runs – Full Factorial	Nº Runs – Fractional Factorial
2	4	2
3	8	4
4	16	8
5	32	16
6	64	32
7	128	64
8	256	128
9	512	256
10	1024	512

Table 3.2 The number of experimental runs required for 3^k and 3^{k-1} factorial designs [138]

Nº Factors (k)	Nº Runs – Full Factorial	Nº Runs – Fractional Factorial
2	9	3
3	27	9
4	81	27
5	243	81
6	729	243
7	2187	729
8	6561	2187
9	19683	6561
10	59049	19683

3.1.2.4 Statistical analysis of data

Design of experiment software, such as Minitab15®, allow for the automatic construction of data plots from the raw data gathered. Main effects plots, Pareto charts, interaction plots and normal effects plots can be generated and used to determine the statistical significance of examined factors with regards to a given response.

3.1.3 The Taguchi approach

The Taguchi approach was designed by Dr Genechi Taguchi, a Japanese scientist specialising in improvements to the quality of manufactured products. Taguchi developed a modified form of design of experiment for reducing variability and improving quality in manufacturing processes. He believed that quality should be designed into a product throughout the various manufacturing stages and that quality is best achieved by reducing variation around a desired target. The Taguchi approach defines quality as

"The total loss imparted to the society from the time a product is shipped to the customer" [171]

The higher the quality of the product the lower the loss. The loss is measured in monetary terms and includes all costs associated with the production of the ideal product as well as additional costs incurred by the customer such as repairs.

There are three stages in the Taguchi approach: planning, experimentation and analysis [170]. Taguchi approach uses orthogonal arrays to determine the experimental runs to be processed (Table 3.3). However, unlike factorial design of experiment designs which can examine either full or fractional factorial

designs the Taguchi approach only examines a fraction of the possible available experimental runs.

Table 3.3 Taguchi orthogonal arrays [138]

Orthogonal Array	Factorial Notation	Nº Runs	Nº Factors			
			2 Levels	3 Levels	4 Levels	5 Levels
L4	2^3	4	3			
L8	2^7	8	7			
L9	3^4	9		4		
L12	2^{11}	12	11			
L16	2^{15}	16	15			
L'16	4^5	16			5	
L18	2^1, 3^7	18	1	7		
L25	5^6	25				6
L27	3^{13}	27		13		
L32	2^{31}	32	31			
L'32	2^1, 4^9	32	1			
L36	2^{11}, 3^{12}	36	11	12		
L'36	2^3, 3^{13}	36	3	13		
L50	2^1, 5^{11}	50	1			11
L54	2^1, 3^{25}	54	1	25		
L64	2^{63}	64	63			
L'64	4^{21}	64			21	
L81	3^{40}	81		40		

During the selection of factors the Taguchi approach distinguishes between design and noise factors. Design factors are factors which are easy to control, whereas noise factors are factors which are hard to control [46].

Each orthogonal array is constructed of inner and outer arrays. The inner array is constructed using design factors and the outer arrays is constructed using noise factors (Figure 3.4).

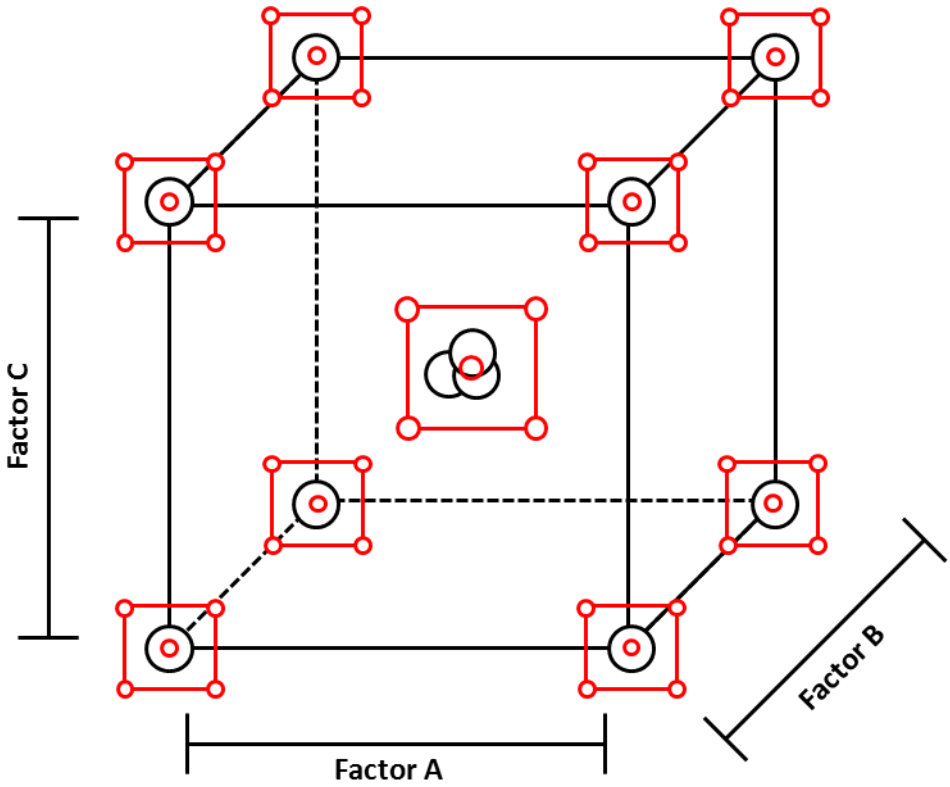

Figure 3.4 Taguchi inner and outer orthogonal arrays [46]

The Taguchi approach is not concerned with the influence of factor interactions, as it is assumed that these interactions are not expected prior to experimentation [50].

Analysis using the Taguchi approach most commonly uses analysis of variance, signal-to-noise-ratio and loss function.

Analysis of Variance (ANOVA) is a statistical method used to determine the contribution of each factor. Analysing the results of a Taguchi orthogonal array enables the identification of which of the factors examined require control and which do not [26].

Signal-to-noise-ratio (S/N), is used to determine the most robust operating conditions. The S/N expresses the results variation around a given target i.e. required dimensions. The larger the ratios value the small the variation from the target [171] .

The 'Loss Function' is used to determine the magnitude of the process tolerances, based upon quality as perceived by the customer (Equation 15 [171]).

Equation 15 $L(y) = k(y-y_o)^2$

L(y) is the loss function, y is the quality characteristic measured i.e. dimensions, y_o is the target value of the quality characteristic and k is a constant dependent on the cost structured of the manufacturing process [171].

3.1.4 Choice of experimental design

There are key differences between the design of experiment and Taguchi approach and the selection of one over the other will depend on the type of experiment being conducted and the conditions involved. The design of experiment approach would be preferred when the influences and interactions between factors is of interest. The design of experiment approach also allows for full and fractional factorial designs to be examined.

The Taguchi approach is used when the aim of the statistical design is to determine the process robustness to 'noise' factors. The Taguchi approach doesn't examine all possible experimental runs but rather runs the statistical

analysis with a fraction of the overall possible runs. Unlike the design of experiment approach which allows for all possible factor combinations to be examined.

As the effect of individual factors and the interactions between factors was of interest within this research and not the robustness of the process. It was decided that a design of experiment approach would be used. The selection of a design of experiment approach also allowed for the examination of all possible factor combinations though the use of a full factorial design.

3.2 Mould insert design and fabrication

The following section outlines the design and fabrication of silicon and nickel inserts for use as removable moulds in the micro-injection moulding process. Section *3.2.1 Silicon mould insert fabrication* and its related subsections outlines the design of surface features and the fabrication methods used to produce the structured silicon mould inserts including photolithography and deep reactive ion etching. Section *3.2.2 Nickel mould insert fabrication* and its related subsections discuss the fabrication of nickel mould inserts by the deposition of a conductive seed layer via sputter-coating and electroless coating. Followed by the construction of a nickel electroform via electroplating to produce the nickel mould insert.

3.2.1 Silicon mould insert fabrication

A silicon wafer was structured using photolithography and deep reactive ion etching (DRIE) to produce eight silicon inserts which can be used in micro-injection moulding or in the fabrication of a nickel electroformed mould insert for use in micro-injection moulding.

3.2.1.1 Photolithography

Photolithography, also known as optical lithography, is a microfabrication technique which uses light and chemical treatments to selectively remove areas of a surface. A silicon wafer, with an oxidised silicon layer, is coated with a photosensitive film known as a photoresist (Figure 3.5) [127]. A photomask is then aligned and placed on the wafer. The photomask is a stencil which can be repeatedly used to produce a selected pattern on the resist coated wafers. Once the photomask has been aligned on the wafer surface the sample is exposed with UV light, this will have a different effect on the resist depending on whether a positive or negative resist was used. The exposed areas of a positive resist will become more soluble while the exposed areas of a negative resist will become insoluble in the developer [54]. Once the sample has been exposed the photomask is removed and the wafer is placed in a developer bath to remove the selected areas of the resist. The sample then undergoes etching to transfer the pattern left by the resist to the wafer surface. After which the remaining resist is removed leaving a newly structured silicon wafer which can then be used as an insert in micro-moulding techniques or undergo further microfabrication. Photolithography has been used in the patterning of surfaces in many studies [63; 153; 179; 211; 212; 226] due to its ability to pattern high-aspect-ratio structures.

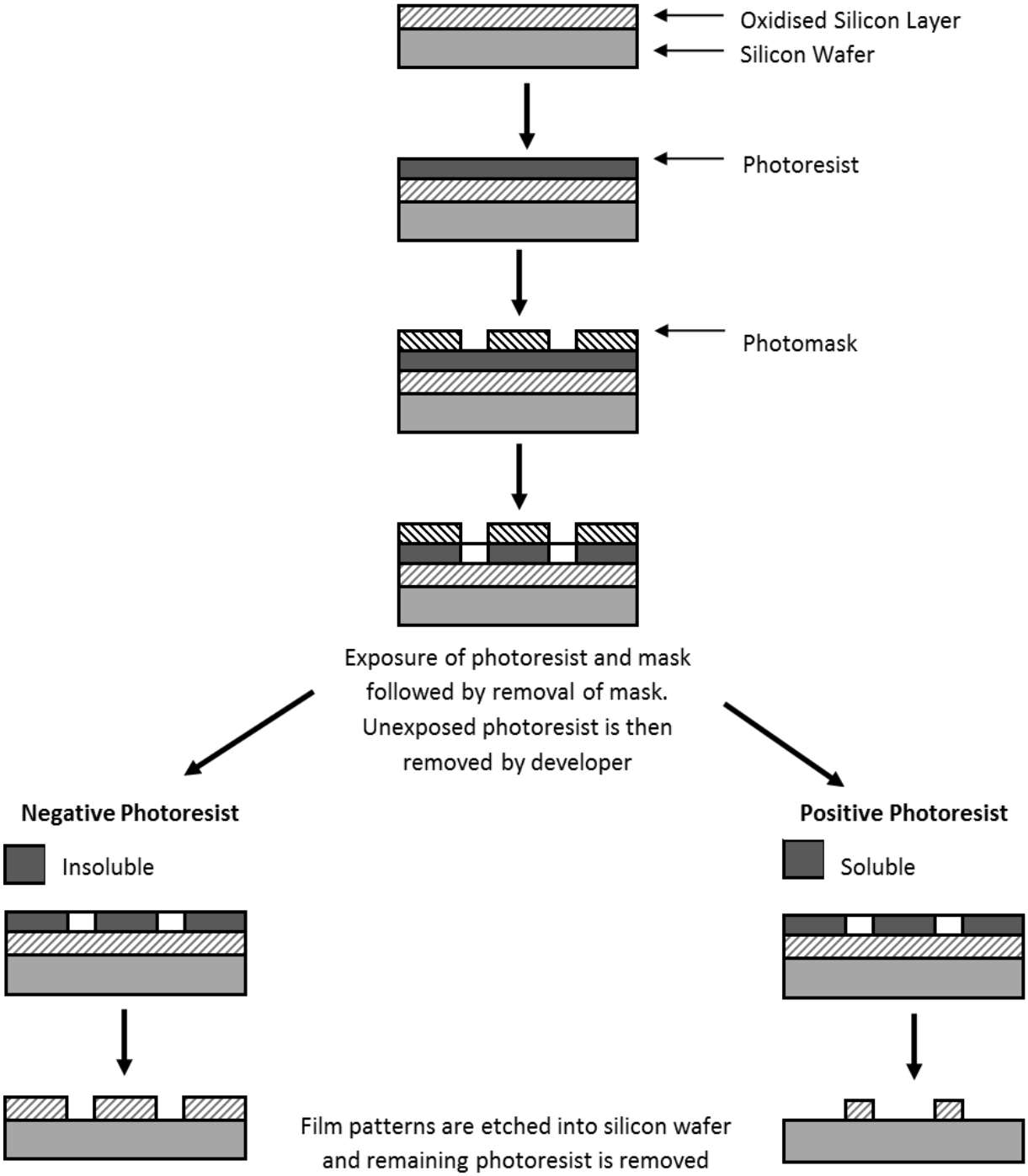

Figure 3.5 Photolithography using positive or negative photoresist [127]

3.2.1.1.1 Photoresist

A photoresist is a light sensitive coating used to protect selected areas of a surface from etching. Photoresists can be either positive or negative. A positive photoresist will become soluble once exposed to ultra-violet light whereas a negative photoresist will become insoluble when exposed. During the deep reactive ion etching (DRIE) process areas of the silicon wafer coated with the photoresist will be protected from etching. The photoresist used during the following photolithography process (s1818) was positive.

3.2.1.1.2 Design of photomask

A photomask is an opaque plate or film patterned with transparencies which allow light to shine through to the underlying sample in a pre-designed pattern. Commonly used in photolithographic processes, photomasks can be made from Soda Lime glass, Fused Silica (Quartz) and polyester films. The pattern represented by the transparencies in this research was designed using AutoCAD software and sent to an external company (JD Photo-Tools) to produce the photomask.

3.2.1.1.3 Photomask

A photomask is an opaque plate patterned with transparencies that acts as a stencil. Photomasks can be repeatedly used to produce a selected pattern onto the photoresist coated silicon wafer by allowing ultra-violet light to shine through the transparencies to the underlying sample.

Photomasks can be either hard or soft contact. Hard contact photomasks are placed in contact with the sample surface during exposure whereas soft contact photomasks are raised 10 – 20 μm above the sample surface [127].

When ordering a photomask it can be defined as either Darkfield or Clearfield. This will define which areas of the photomask will be transparent and which will

be opaque. Features on a Darkfield photomask will appear as transparencies and the background will be opaque. A Clearfield photomask is the opposite of Darkfield on which features will appear as opaque areas and the background will be transparent [95].

In the following photolithography process two Darkfield photomasks were used. The first was a polymer-on-emulsion photomask and the second was chrome-on-glass.

AutoCAD was used to design the photomask layout. As it was intended to use a Darkfield photomask the surface design was constructed so that features would appear as transparencies in the photomask. These features would then be etched into the silicon wafer.

Only closed geometries could be used when designing the photomask transparencies. This was a requirement of the external company who produced the photomask. In this case a closed geometry means that a shape cannot be placed within another, an example of this would be to take a doughnut shape (Figure 3.6). If a circle was merely placed within another it would not be interpreted correctly thus the shape must be designed so that one shape is not enclosed within another.

Due to this requirement for closed geometries the transparencies intended to produce pillars on the silicon surface were designed as a series of rectangles to produce the spacing between the pillars (Figure 3.7). The white areas displayed in Figure 3.7 represent closed geometries which will result in transparencies in the photomask. While the black areas represent the areas which will be opaque on the photomask thus preventing exposure of the surface below.

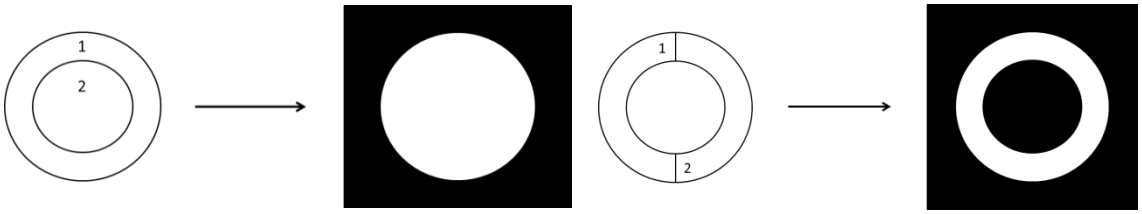

Figure 3.6 Open and closed geometries

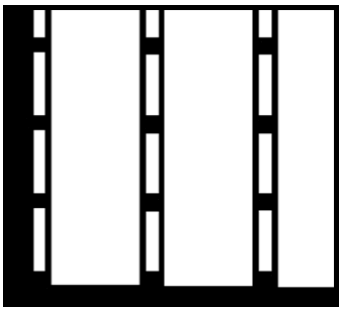

Figure 3.7 Photomask design – white areas represent transparencies in the photomask and black areas represent the opaque areas.

The two photomasks used during the course of this research each contained different surface features which will be discussed in the following sections.

3.2.1.1.4 Micro-channel silicon mould insert design

A pre-existing emulsion-on-polymer photomask, designed by Morel [144], was used to pattern the silicon wafers with pillar and hole features ranging from 80 x 80 μm to 5 x 5 μm. The photomask was designed for a 4 inch wafer, on which eight 12 x 26 mm inserts could be produced (Figure 3.8). The specification of the silicon wafers used is given in Table 3.4. Each of the eight inserts were

designed to contain twelve square areas (Figure 3.9) in which the pillar and hole features are contained.

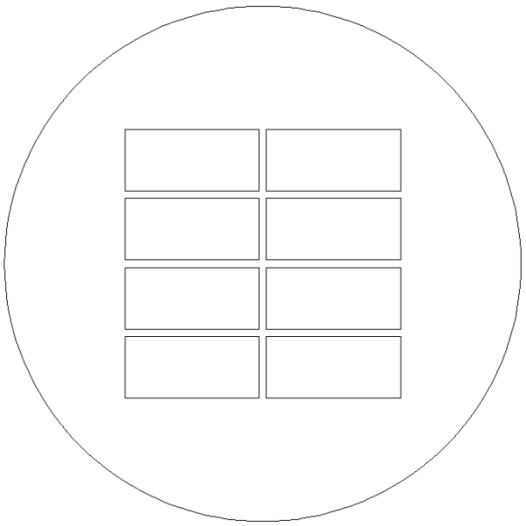

Figure 3.8 Location of inserts on silicon wafer

Table 3.4 Silicon insert specification

Specification	Value
Diameter (mm)	100
Type / Dopant	P / Boron
Orientation	< 100 >
Growth Method	C2
Resistivity (Ωcm)	10 - 30
Thickness (μm)	475 - 525 ± 25
Front Surface	Polished
Back Surface	Etched

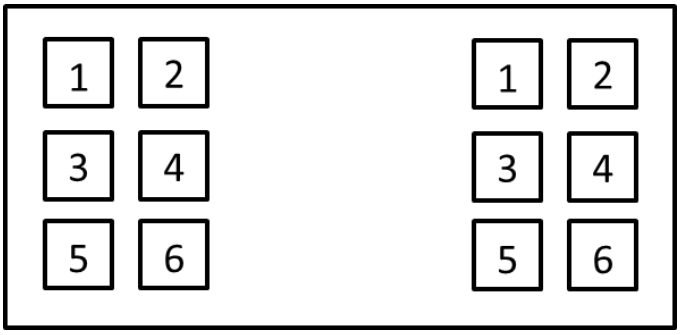

Figure 3.9 Schematic of micro-channel silicon inserts

The feature designs included on the inserts were taken and adapted from the literature to examine how texturing of a surface by varying pillar size and spacing can affect the movement of water droplets on the sample surface.

The surface feature design used to produce the features in squares 3 and 4 (Figure 3.9) were adapted from the work of Fang et al [48] to produce micro-channels of varying pillar size and spacing across the sample surface to produce a wettability gradient.

Fang et al [48] used computer modelling to examine the effect of wettability gradients on droplet motion. By simultaneously decreasing the pillar width and spacing across a surface the free-energy barriers of the advancing and receding contact angles were decreased so that a droplet would move along the roughness gradient. Fang et al [48] also used “virtual walls” to channel the movement of the droplet in a desired direction. These “virtual walls” are made up of pillars with high free-energy barriers thus keeping the droplet on the path of least resistance which is the pillars with the low free-energy barriers (Figure 3.10).

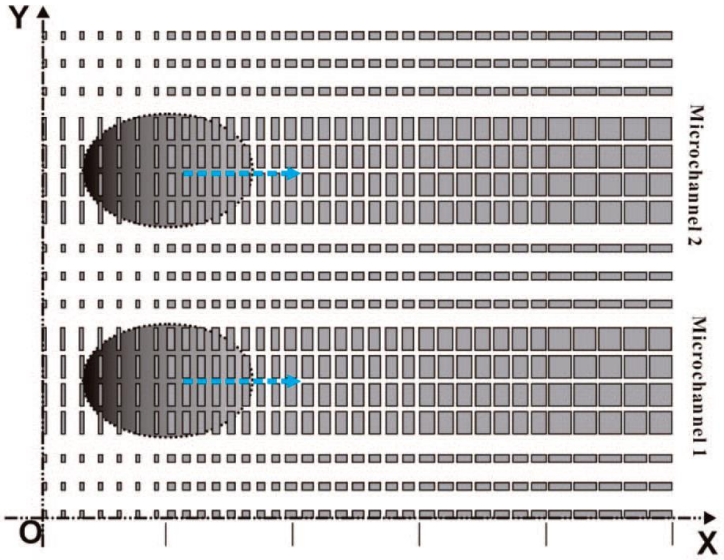

Figure 3.10 Schematic of structured wettability gradient and "virtual walls" proposed by Fang et al [48]

The work of Shastry et al [179] was used as reference to design surface features consisting of pillars of varying gradients in squares 5 and 6 (Figure 3.9).

Shastry et al [179] used the variation of pillar width and gap length to produce a superhydrophobic surface with a surface-energy gradient. Droplets were observed to move down the surface-energy gradient when mechanical vibration was applied to the sample.

The surface features which make up squares 1 and 2 were designed by combining the design patterns proposed by Shastry et al [179] and Fang et al [48]. The presence of microchannels was adapted from the work of Fang et al [48] and the pillar gradient used by Shastry et al [179].

The aim was to experimentally test the validity of these designs as well as to adapt the design principles explored to fabricate a new combination-design for exploring the movement of droplets on a structured surface.

The features in squares 1, 3 and 5 will result in hole features on the etched silicon insert. Whereas features in squares 2, 4 and 6 will result in pillar features on the etched silicon insert. AutoCAD images of the various features are displayed in Figure 3.11, Figure 3.12 and Figure 3.13. The scale bar at the base of each image represents 1mm.

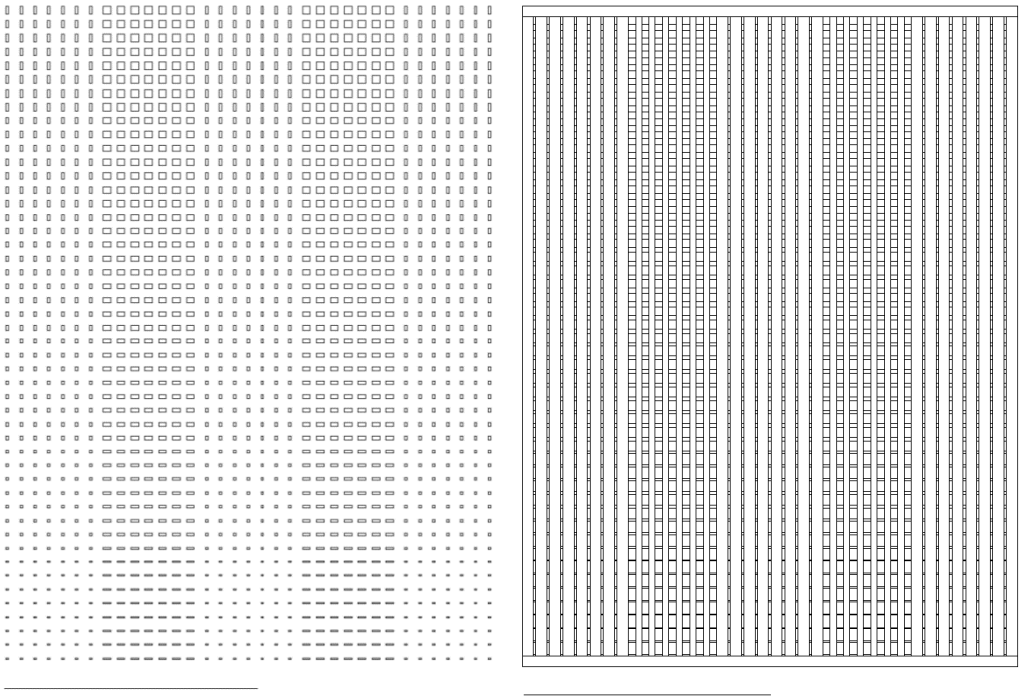

Figure 3.11 AutoCAD image of features in square 1 (left) features in square 2 (right) [144]

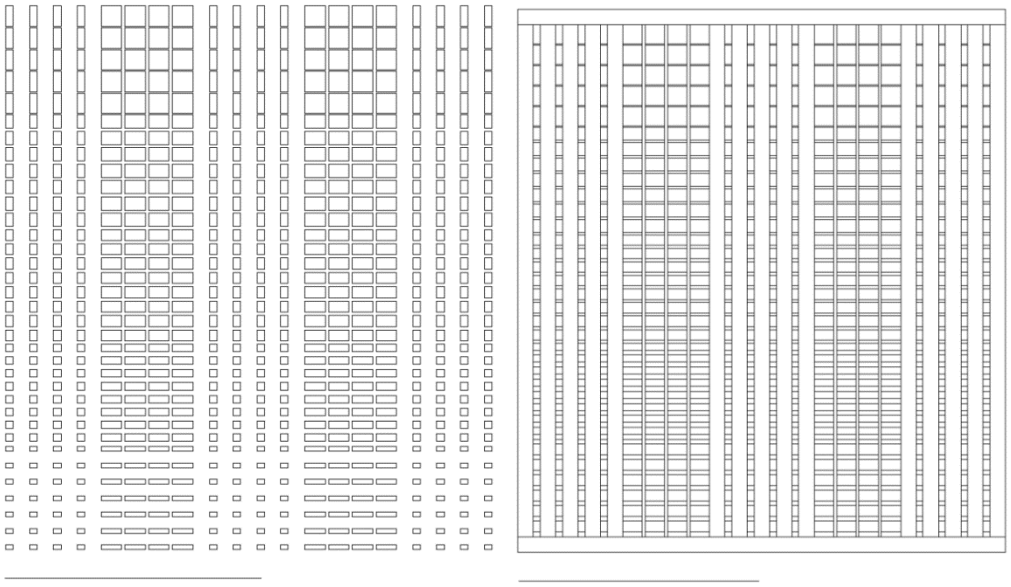

Figure 3.12 AutoCAD image of features in square 3 (left) features in square 4 (right) [144]

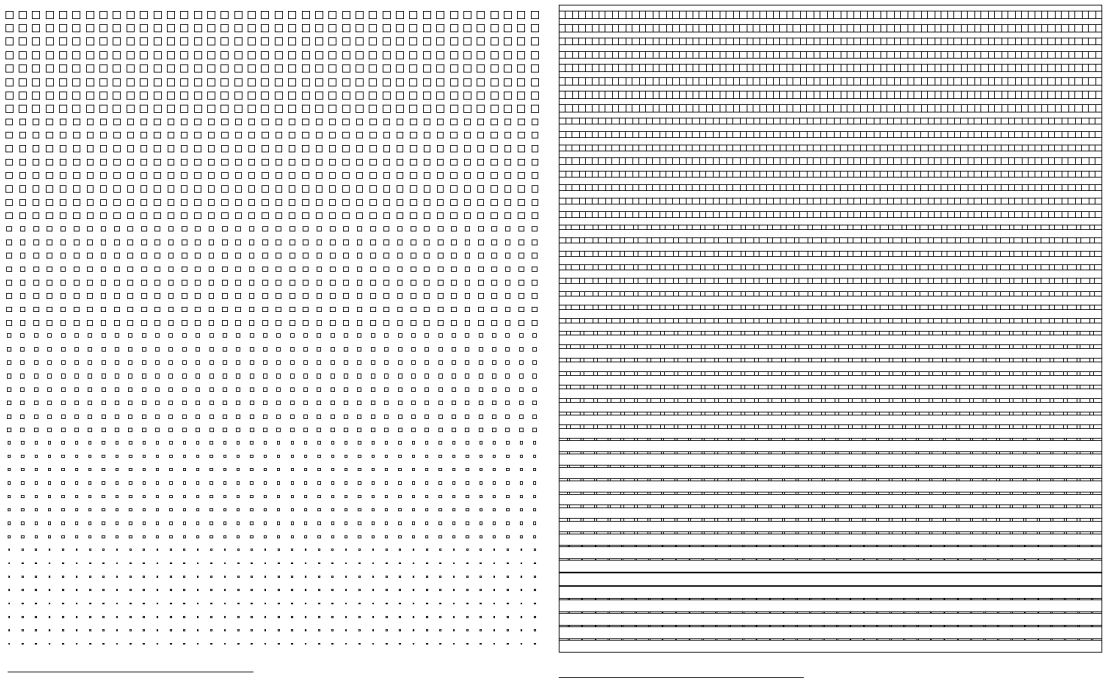

Figure 3.13 AutoCAD image of features in square 5 (left) features in square 6 (right) [144]

As previously mentioned (and displayed in Figure 3.11 and Figure 3.12) the designs in squares 1, 2, 3 and 4 contained micro-channels. Two different micro-channels with varying feature dimensions were used in each square (Table 3.5).

Table 3.5 Feature dimensions in micro-channels

Square	Micro-channel 1 (μm)	Micro-channel 2 (μm)
1 & 2	30 x 30	30 x 10
	25 x 30	25 x 10
	20 x 30	20 x 10
	15 x 30	15 x 10
	10 x 30	10 x 10
	5 x 30	5 x 10
3 & 4	80 x 80	80 x 29
	53 x 80	53 x 29
	43 x 80	43 x 29
	29 x 80	29 x 29
	19 x 80	19 x 29
5 & 6	30 x 30	
	25 x 25	
	20 x 20	
	15 x 15	
	10 x 10	
	5 x 5	

The surface area, feature volume and surface area/volume ratio of the micro-channel features (SA/V) is displayed in Table 3.6, in ascending order.

Table 3.6 Surface area, feature volume and surface area/volume ratio of micro-channel features

Pillar dimensions (μm)	Surface area (μm^2)	Volume (μm^2)	SA/V Ratio
80 x 80	25600	256000	0.100
53 x 80	19120	169600	0.113
43 x 80	16720	137600	0.122
80 x 29	13360	92800	0.144
53 x 29	9634	61480	0.157
43 x 29	8254	49880	0.165
30 x 30	6600	36000	0.183
30 x 10	3800	12000	0.317
29 x 80	13360	92800	0.144
29 x 29	6322	33640	0.188
25 x 30	5900	30000	0.197
25 x 10	3300	10000	0.330
25 x 25	5250	25000	0.210
20 x 30	5200	24000	0.217
20 x 20	4000	16000	0.250
20 x 10	2800	8000	0.350
19 x 80	10960	60800	0.180
19 x 29	4942	22040	0.224
15 x 30	4500	18000	0.250
15 x 10	2300	6000	0.383
15 x 15	2850	9000	0.317
10 x 30	3800	12000	0.317
10 x 10	1800	4000	0.450
5 x 30	3100	6000	0.517
5 x 10	1300	2000	0.650
5 x 5	850	1000	0.850

3.2.1.1.5 10 – 2 μm silicon mould insert design

A chrome-on-glass photomask was used to pattern the silicon wafers with features ranging from 10 - 2 μm. The chrome-on-glass mask was used instead of the cheaper emulsion-on-polymer mask as it produces features below 10 μm with greater accuracy than the emulsion-on-polymer mask [95].

The photomask was designed using AutoCAD. The basic outer dimensions of each insert were kept consistent with those of the micro-channel insert, as the mould used to house the insert during injection moulding would be the same. The dimensions of the features within the insert were altered from those found on the micro-channel inserts (Figure 3.14).

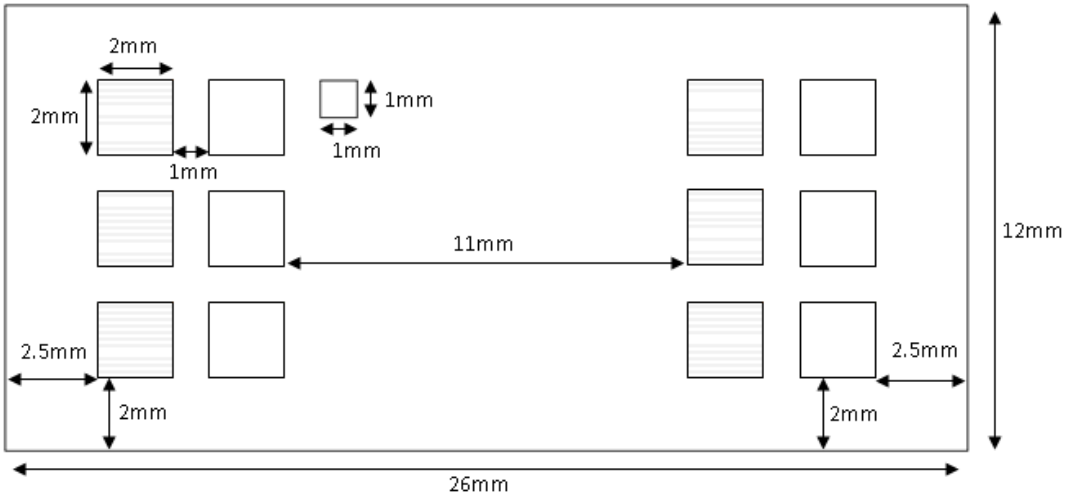

Figure 3.14 Schematic of 10 - 2 μm inserts

The 10 - 2 μm inserts contained twelve 2 x 2 mm squares, in-which the micro-scale features were contained, and one 1 x 1 mm reference point. This would allow the easy identification of the various areas of the insert during metrological analysis. The micro-scale features contained within the mask were 10 x 10 μm, 5 x 5 μm and 2 x 2 μm pillars and holes. The 10 x 10 μm features

were located in squares 1 and 2. The 5 x 5 μm features were located in squares 3 and 4 and the 2 x 2 μm features were located in squares 5 and 6 (Figure 3.15).

These features were chosen as the dimensions are in the lower limitation range of both the photomask and DRIE process i.e. the smallest feature size which can be included on a chrome-on-glass mask is 2 x 2 μm [95].

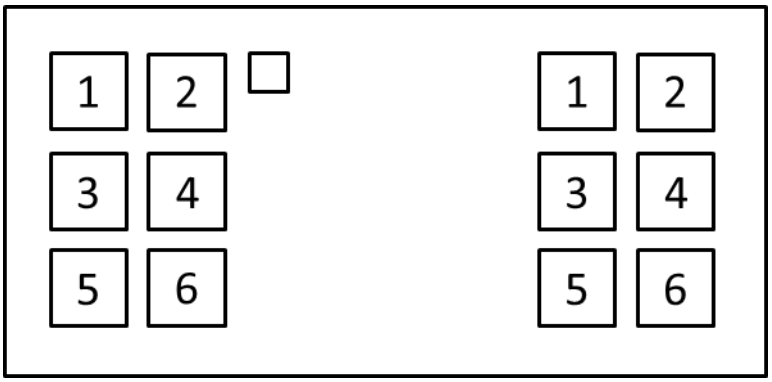

Figure 3.15 Schematic of 10 - 2 μm silicon inserts

The features in squares 1, 3 and 5 will result in hole features on the etched silicon insert. Whereas features in squares 2, 4 and 6 will result in pillar features on the etched silicon insert. AutoCAD images of the various features are displayed in Figure 3.16, Figure 3.17, Figure 3.18 and Figure 3.19.

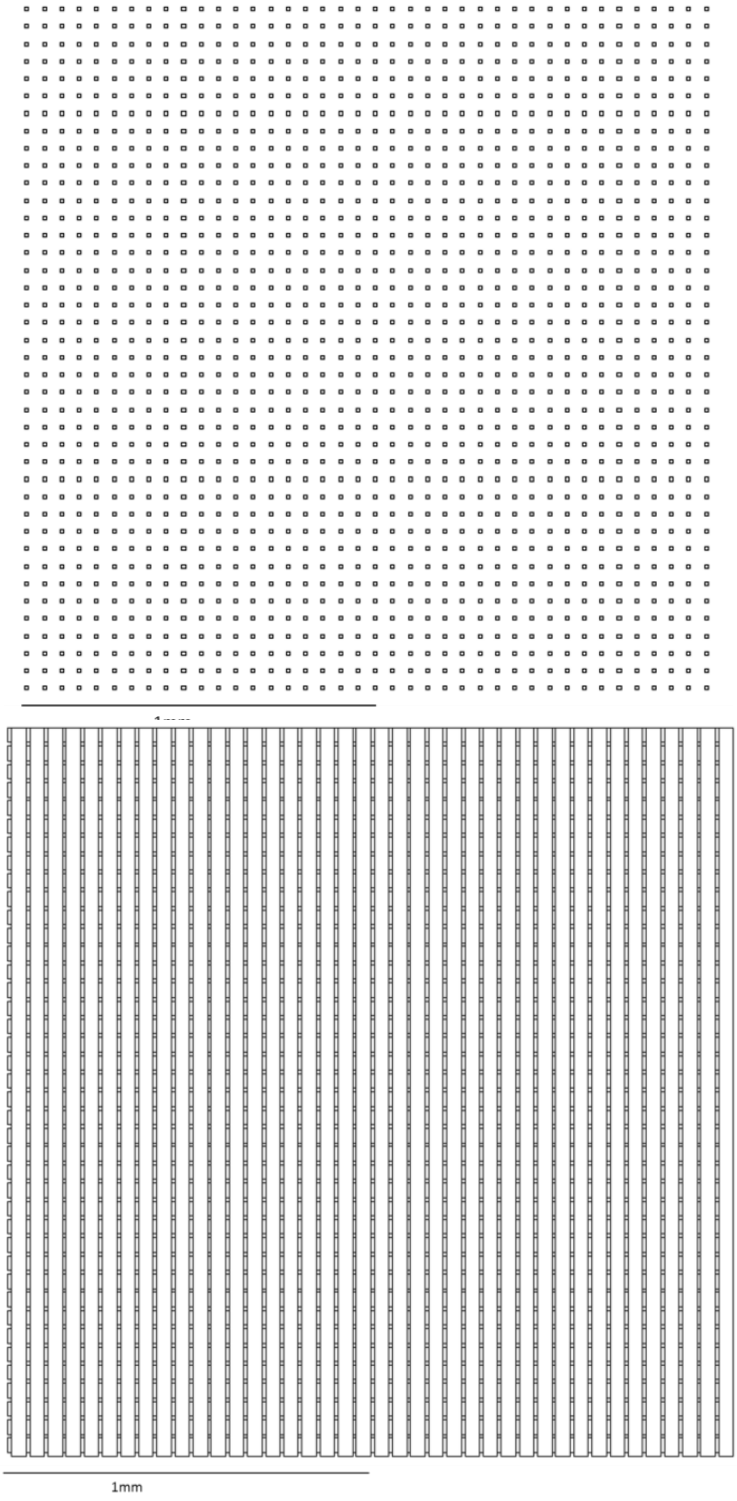

Figure 3.16 AutoCAD image of features in square 1 (top) features in square 2 (bottom)

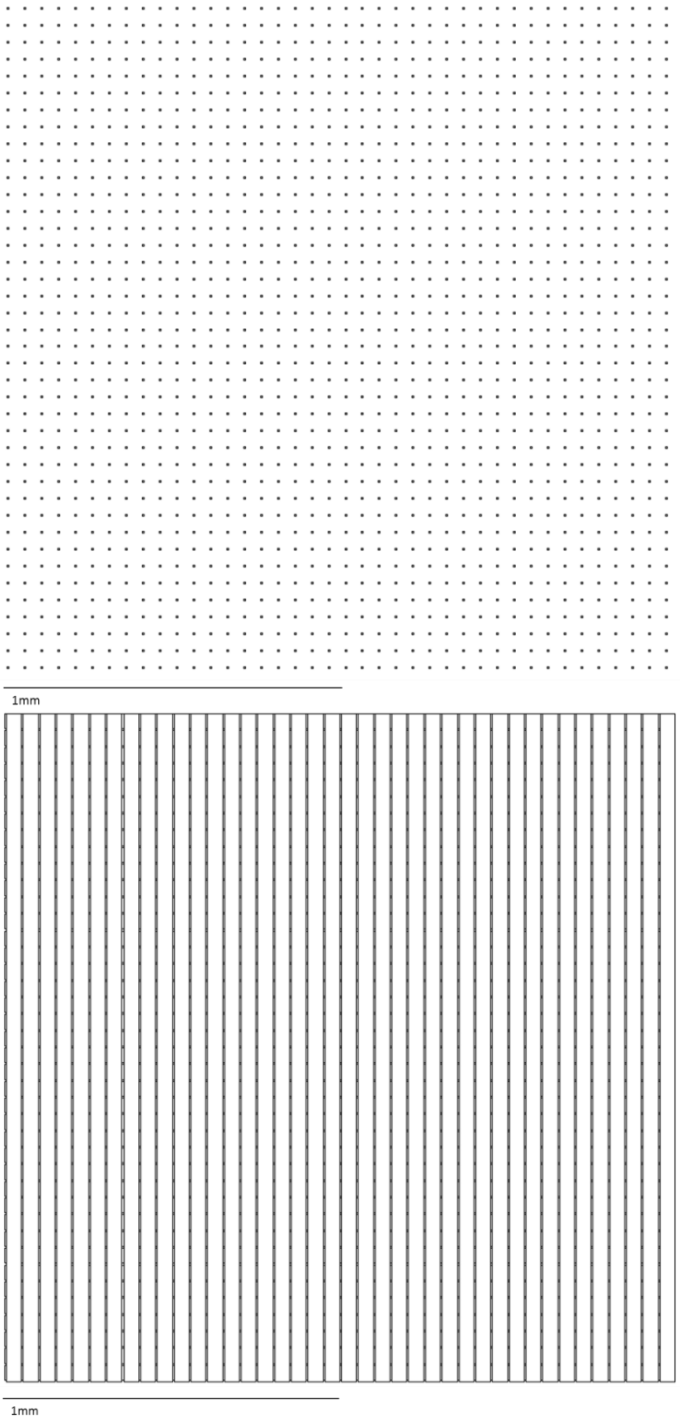

Figure 3.17 AutoCAD image of features in square 3 (top) features in square 4 (bottom)

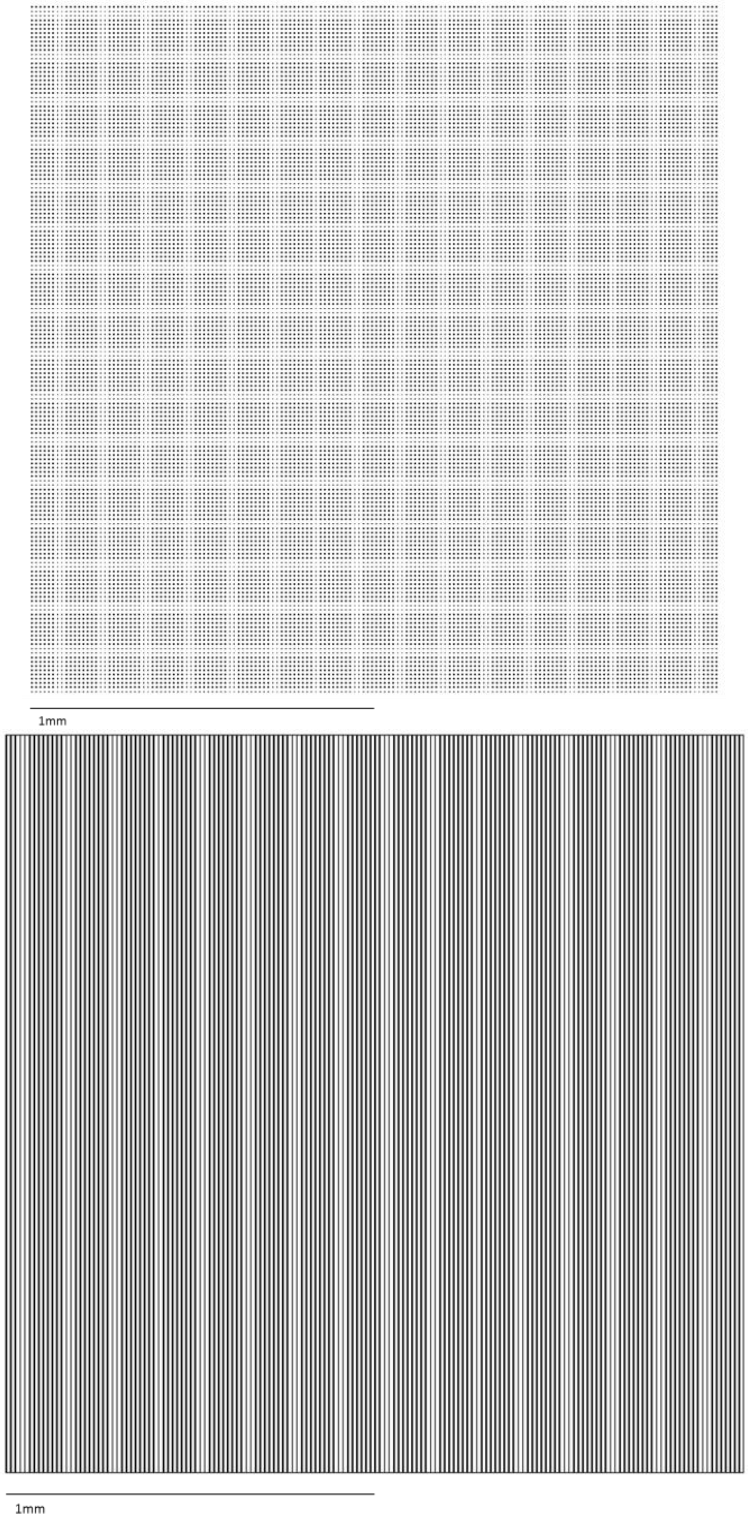

Figure 3.18 AutoCAD image of features in square 5 (top) features in square 6 (bottom)

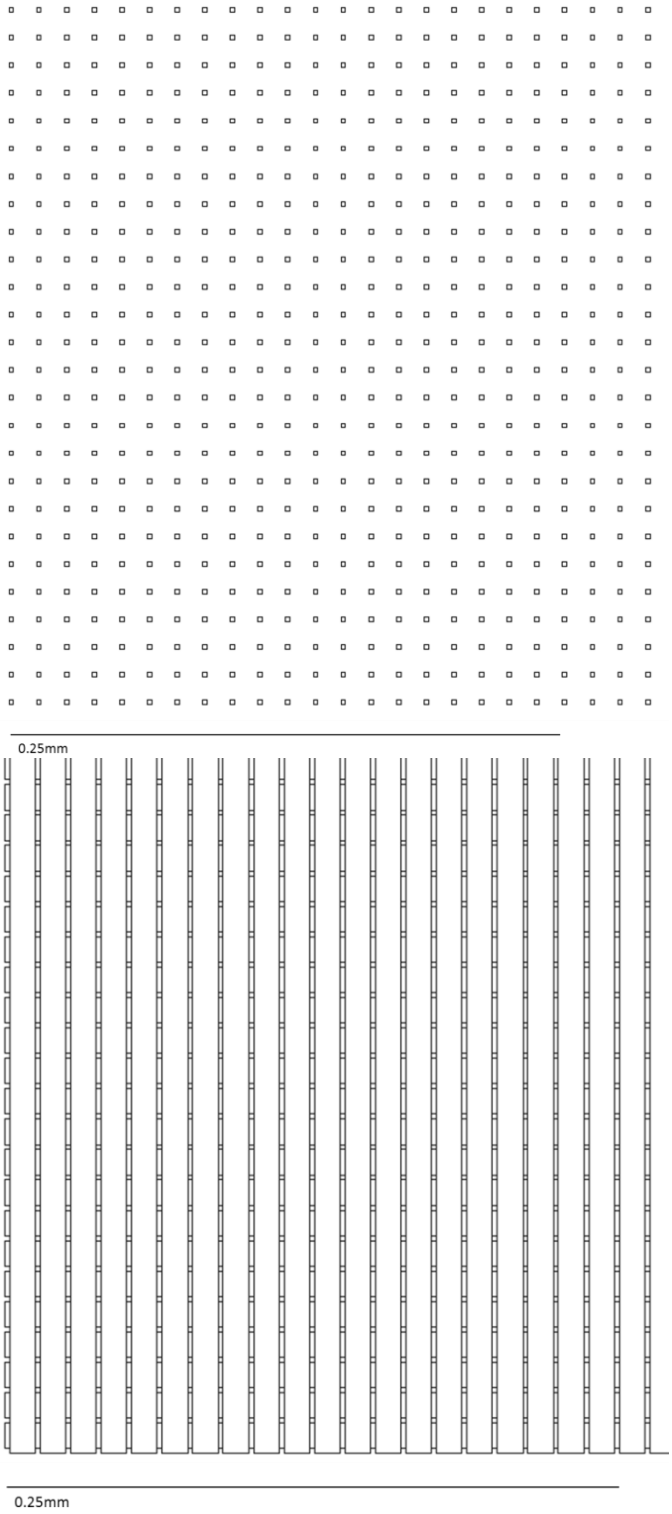

Figure 3.19 Close-up of AutoCAD image of features in square 5 (top) features in square 6 (bottom)

3.2.1.2 Photolithography experimental procedure

The photolithography process was conducted within a clean room environment. The silicon wafer was first placed in a plasma barrel etcher for 2 minutes at 2 mbar to clean the surface prior to photoresist coating. The wafer was then heated on a hot plate set at 115 ^{o}C for 90 seconds to remove any moisture. This improves adhesion of the photoresist to the wafer.

The wafer was placed into a sealed container in-which a cap of Hexamethyl disilazane (HMDS) had been placed. The wafer was then left in the HMDS environment for 15 minutes.

The wafer was then placed on a spin-coater and secured to it by a vacuum. The chosen photoresist was s1818, a positive photoresist which becomes soluble in resist developer once exposed to UV light. The areas on the photoresist not covered by the photomask would be dissolved during the development phase leaving the silicon unprotected and therefore easily etched during deep reactive ion etching. The s1818 resist was poured onto the wafer until it was two thirds covered. The wafer was then spun at a rotational speed of 4000 rpm for a duration of 60 seconds.

Once the spin programme was complete the wafer was returned to the hot plate for a further 90 seconds. The wafer was then placed in a mask aligner and exposed by a UV lamp. Once exposure was complete the wafer was placed in a developer bath and agitated for a specified period. The wafer was then rinsed once with deionised water and once with distilled water (Table 3.7). The wafer was then placed back into the plasma barrel etcher for 2 minutes at 2 mbar prior to etching.

Table 3.7 UV exposure time and developer for silicon inserts

Surface feature design	UV exposure time (sec)	Developer
Micro-channel inserts	28	MF319
10 - 2 µm inserts	25	MF319
10 - 2 µm inserts*	25	AZ 726MF

3.2.1.3 Deep reactive ion etching

Deep reactive ion etching (DRIE) is an anisotropic etching process used to fabricate surface features with vertical sidewalls in silicon. It uses a time-multiplexed etching process [16; 47] in which a combination of etching and the deposition of a protective passivation layer is used so that vertical etching of a sample can be controlled.

This process is known as the Bosch process, in which the wafer is subjected to alternate etching and passivation phases so the silicon surface can be etched with micro-scale features with vertical sidewalls. The Bosch process produces these vertical sidewalls by continuously alternating between an etching phase and a passivation phase, resulting in an anisotropic etch pattern (Figure 3.20).

* 10 - 2 µm inserts for use in micro-injection moulding deign of experiment investigations

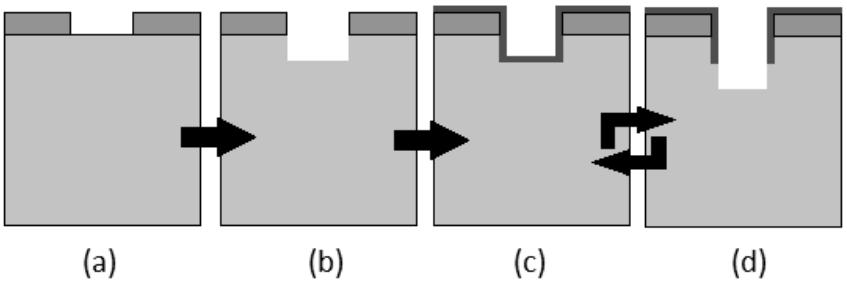

Figure 3.20 Deep reactive ion etching Bosch process (a) silicon wafer with photoresist, (b) anisotropic etching phase, (c) passivation phase, (d) second anisotropic etching phase [136]

During the etching phase the silicon wafer is etched by directional bombardment with plasma ions. Sulfur hexafluoride (SF_6) gas is most commonly used when etching silicon. For the passivation phase the etched silicon is coated in a chemically inert layer. Octafluorocyclobutane (C_4F_8) gas is used to produce this inert layer when etching silicon, which protects the surface from further etching.

During the subsequent etching phase, due to the directional bombardment of plasma ions, the passivation layer at the base of the etched features is sputtered away and further etching of the silicon will continue in an vertical direction [52]. Only the passivation layer at the base of the etched features is removed, the sidewalls of the feature remain coated in the protective layer, which results in highly anisotropic sidewalls. Each phase lasts only a few seconds and the alternation between the two continues for a pre-set period of time until the desired etch depth is reached.

The literature suggests that several parameters can affect the production of undercuts to surface features during DRIE notably: Pressure [19; 47; 145; 197], platen power [47; 84], gas flow [84; 87; 145], switching times [87; 145] and mask size [87]. After examination of this literature and of manufactures guidelines[183] three

parameters were selected for experimental testing: platen power, C_4F_8 gas flow in the passivation phase and switching times between phases. Platen power has a large influence on etch rate [47; 84]. According to Evans & Beheim [47] when a high platen power is combines with high pressure during the etching phase the anisotropic nature of the profile is improved.

Altering the switching times (the ratio between the etching and passivation phases) has been found to have a major effect on the etch profile and presence of undercuts. As shown in Figure 3.21, the proposed mechanism is that by increasing the etch time the likelihood of a negative etch profile, and therefore undercuts, is increased. Whereas if the passivation rate is increased the thickness of the passivation layer is also increased resulting in a reduced etch rate and a more positive etch profile [47] (Figure 3.21).

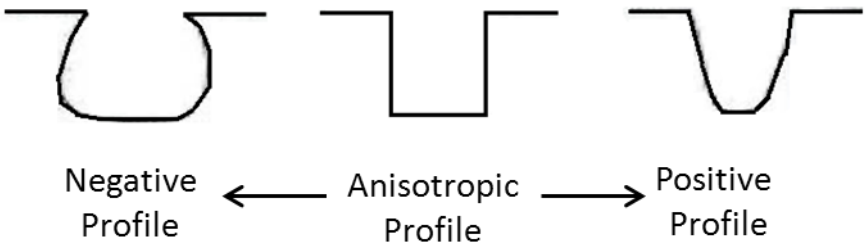

Figure 3.21 Schematic of etch profiles

Alterations to the C_4F_8 gas flow in the passivation phase have been found to effect the production of a more positive etch profile [183] due to the increased thickness of the passivation layer.

During the course of this research, pillar and hole features ranging from 80 x 80 μm to 5 x 5 μm were etched into silicon wafers. A design of experiment

approach was used to examine the effect of platen power, C_4F_8 gas flow in the passivation stage and etching:passivation switching time on the DRIE process.

3.2.1.3.1 Micro-channel insert experimental procedure

The wafer was loaded into the chamber of the DRIE equipment and etched using a time multiplexed deep etching technique (Table 3.8) [16].

Table 3.8 Deep reactive ion ethching time multiplexed recipe settings

Factors	Value
Platen power (W)	12
Coil power (W)	600
SF_6 Gas flow (sccm)	130
C_4F_8 Gas flow (sccm)	85
O2 Gas Flow in etching phase (sccm)	13
Etching pressure (mTorr)	23
Passivation pressure (mTorr)	13
Etching stage duration (sec)	7
Passivation stage duration (sec)	5
Whole process duration (min)	20
Total number of cycles	100

Once the etching process was completed the wafer remained in the DRIE chamber and underwent oxygen plasma cleaning to remove the remaining photoresist (Table 3.9).

The wafer was then removed from the DRIE chamber and rinsed in acetone, then dried with a nitrogen gas flow.

Table 3.9 Oxygen plasma cleaning programme settings

Factors	Value
Duration (min)	3
Coil power (W)	800
Pressure (Torr)	10^{-7}

3.2.1.3.2 Design of experiment of 10 - 2 µm inserts experimental design

The deep reactive ion etching process was investigated using a design of experiment approach. The factor levels used for this DOE are displayed in Table 3.10. The criteria for the selection of these levels are explained in Table 3.11.

Table 3.10 Factor examined; high and low levels

Factor	Low level	High level
Platen power (W)	10	18
C_4F_8 Gas flow in passivation Stage (sccm)†	70	100
Switching times – etching : passivation (s : s)	5:5	9:5

† sccm: standard cubic centimetre per minute

Table 3.11 Reasons for design of experiment levels selected

Factors	Low level	High level
Platen power (W)	The minimum value at which ion directionality could be controlled for the scale of the features examined – taking into account equipment limitations	The maximum value at which ions directionality could be controlled for the scale of the features examined – taking into account equipment limitations
C_4F_8 Gas flow in passivation Stage (sccm)	The minimum value for obtaining a sufficient passivation layer after consideration of the passivation layer required and system pressure – taking into account equipment limitations	The maximum value at which deposited passivation layer would not hinder etching of features after consideration of the passivation layer required and system pressure – taking into account equipment limitations
Switching times – etching : passivation (s : s)	The minimum level chosen due to feature dimensions and passivation layer thickness (if the etching time is too short, in comparison to the passivation time, it will not completely remove the passivation layer and the likelihood of the uneven etching increases)	The maximum level chosen after taking into account the dimensions of the features and the effect on the passivation layer (if the etching time is too long, in comparison to the passivation time, it will quickly remove the passivation layer and begin to isotropically etch the silicon)

The design of experiment scheme used was devised using a full factorial 8 run design generated using Minitab®15. The order of the design of experiment runs (Table 3.12) was generated using a built-in randomizer function in Minitab.

Table 3.12 Randomised 8 run full factorial design of experiment sequence

Run	Platen power (W)	C_4F_8 Gas flow in passivation Stage (sccm)	Switching times – etching : passivation (s : s)
1	-	+	-
2	+	+	-
3	-	+	+
4	-	-	+
5	+	-	+
6	+	+	+
7	+	-	-
8	-	-	-

3.2.1.3.3 10 - 2 µm mould inserts experimental procedure

A deep reactive ion etcher was used to process the experimental runs. Each run consisted of 100 cycles, and due to the various switching times not all runs took the same amount of time (Table 3.13).

Table 3.13 Duration of deep reactive ion etching runs

Run	Sample name	Switching time (s : s)	Total run duration (min)
1	DOE 1	5:5	16:45
2	DOE 2	5:5	16:45
3	DOE 3	9:5	23:29
4	DOE 4	9:5	23:29
5	DOE 5	9:5	23:29
6	DOE 6	9:5	23:29
7	DOE 7	5:5	16:45
8	DOE 8	5:5	16:45

The surface of each wafer was imaged, post etch, using an optical microscope. Wafers then underwent oxygen plasma cleaning (Table 3.14) to remove any remaining photoresist, in order that the features could be examined in an SFEG-Scanning Electron Microscope (SEM).

Wafers were then re-examined using an optical microscope so a comparison of the features, pre and post oxygen plasma cleaning, could be made. Upon comparison it was noted that the surface features were the same on the pre and post oxygen plasma cleaned samples. Demonstrating that the cleaning process had no effect on the etched features.

Table 3.14 O_2 plasma cleaning factor settings

Factor	Value
Pressure (mTorr)	45.0
O_2 Gas flow (sccm)	45
Coil power (W)	800
Platen power (W)	0
Cycle time (min)	5

The pillar features on the wafer surfaces were imaged and examined using an SFEG-SEM. The width at the base and the apex of the pillars were measured using the measurement tool available with the SFEG-SEM software. Each measurement was taken 5 times and an average calculated. The average measurements were then compared to those of the pre-etched features to determine the degree of undercut of the features obtained in each design of experiment run (Section *3.4 Metrology and Optical Analysis*).

3.2.1.4 Wafer dicing

The silicon wafers were taken to Irisys, an external company specialising in advanced infrared technologies, for cutting. The wafer was mounted on an adhesive plastic film to avoid movement of the wafer and cut using a LoadPoint MicroAce 3. The wafer cutting took place in a clean room in which gloves, protective coats, hats and over shoes must be worn. Once the wafer was cut the insert were removed from the adhesive film.

The edges of the inserts were then sanded down using silicon carbide abrasive paper P2500 to remove any rough edges produced during dicing. Leaving the inserts ready for further processing.

3.2.1.5 Mould design

The mould insert casing used during the micro-injection moulding process was utilised from the work undertaken by Morel [144]. The silicon insert is housed in a cavity in the mould casing and secured by two moveable aluminium parts so that the insert remains in place during the injection process (Figure 3.22).

Due to the use of a pre-existing mould casing all silicon inserts fabricated were made to the pre-designed specifications. The ejector pins were located either side of the mould and the gate was located in the centre of the mould (Figure 3.23).

(a)

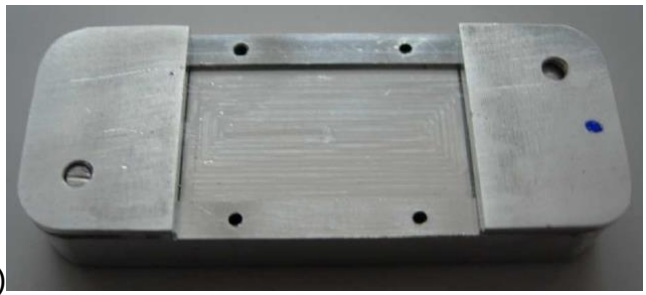

(b)

(c)

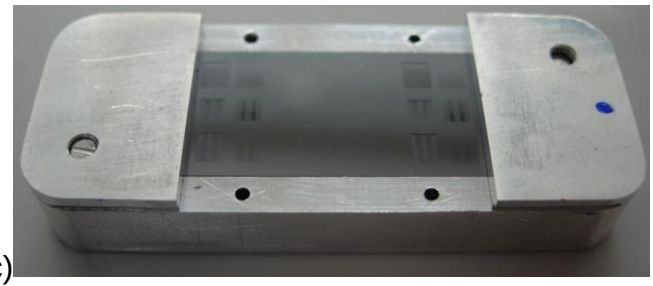

Figure 3.22 (a) pre-made mould, (b) open aluminium parts to allow insertion of silicon insert, (c) closed aluminium parts to secure silicon insert in mould

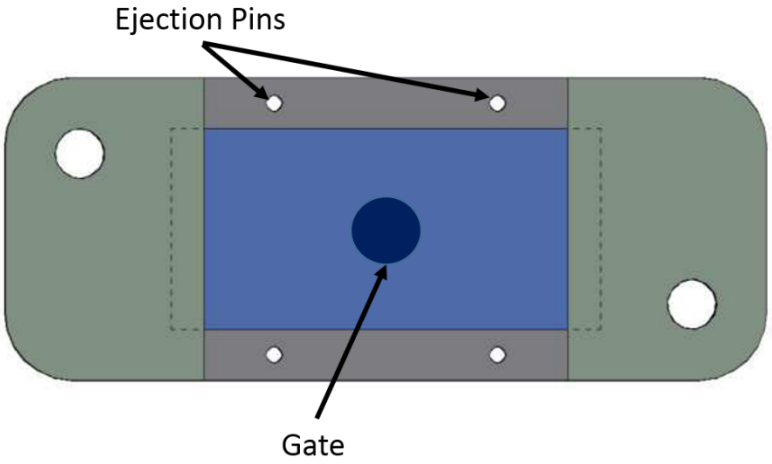

Figure 3.23 Position of ejector pins and gate

3.2.1.6 Fabrication of silicon mould inserts for use in the micro-injection moulding process

Micro-channel silicon inserts were used in the familiarisation of the micro-injection moulding equipment and for design of experiment investigations to produce high density polyethylene (HDPE), polypropylene (PP) and 316LS stainless steel replicates. 10 – 2 μm silicon inserts were used in design of experiment investigations to produce HDPE and PP replicates.

3.2.1.6.1 Etching of 10 - 2 μm silicon mould inserts for micro-injection moulding design of experiment

Silicon wafers were etched with 10 - 2 μm insert features using the process parameters from DOE run 7 (*3.2.1.3.2 Design of experiment of 10 - 2 μm inserts experimental design)*. The process parameters from DOE run 7 were selected as they produced features with the smallest degree of undercut.

Each wafer was individually loaded into the chamber of the DRIE equipment and etched using the parameters displayed in Table 3.15 and Table 3.16. The DRIE process was made-up of 100 cycles

Table 3.15 Etching phase factors

Factor	Value
Platen power (W)	18
Coil power (W)	600
SF_6 Gas flow (sccm)	130
O_2 Gas flow (Sccm)	13
Duration (sec)	5

Table 3.16 Passivation phase factors

Factor	Value
Platen power (W)	0
Coil power (W)	600
C_4F_8 Gas flow (sccm)	70
Duration (sec)	5

The wafers then underwent Oxygen plasma cleaning to remove any remaining photoresist, in order that the features could be examined in an SFEG-SEM. The conditions of cleaning are shown in Table 3.14.

3.2.2 Nickel mould insert fabrication

The nickel mould inserts were constructed using one of two processes: sputter-coating and electroplating or electroless and electroplating. The sputter-coating/electroless process was used to deposit a conductive nickel seed layer onto the surface of the silicon insert so that it became conductive enough for nickel electroplating to take place. The electroplating process results in the production of a nickel electroform which must then be separated from the silicon insert before it can be used in micro-injection moulding.

3.2.2.1 Sputter-coating

Sputter-coating is a deposition process which is used to coat samples in a thin conductive layer prior to electroplating or surface analysis via microscopy i.e. SFEG-SEM. Sputter-coating deposits a thin film of metal onto a substrate surface by bombarding a target, situated at the cathode, made of the metal to be deposited with positive ions from an inert gas, most commonly Argon [105; 128]. The positive ions are produced in a glow discharge plasma and collide with the target surface causing the release of metal atoms which are then deposited onto the sample surface, which is situated at the anode [53; 105; 128]. Sputter-coating results in superior film adhesion than other deposition techniques as the released target atom can penetrate a substrate surface up to 1 - 2 atomic layers [128]. There are several types of sputter-coating systems: DC diode, rf diode, magnetron and ion-beam sputtering [105]. DC diode sputtering is commonly used to deposit thin films using a single target however, sputtering directly from a metal target can cause the build-up of an insulating layer on the target which will lead to charge accumulation and make the system unstable [105]. This charge build-up can be avoided by using a twin target set-up in which the targets alternate between anode and cathode, thereby preventing charge build-up without affecting the deposition rate [105].

3.2.2.1.1 Sputter-coating experimental procedure

A magnetron sputtering set-up was used in the sputter-coating process. The insert was placed in the sputtering chamber which was then placed under vacuum and left to pump-down over night. A pulsed DC power supply was used and the voltage, current and power of the plasma were monitored during the sputtering process (Table 3.17). The insert was sputtered with nickel particles from a target positioned above the samples.

Table 3.17 Parameters of sputtering process

Factor	Value
Frequency (K)	240
Pulse width (nanosec)	16
Voltage (V)	395
Current (A)	0.5
Power (W)	200
Gas flow (sccm)	22

3.2.2.2 Electroless

Electroless-deposition is performed in aqueous solution containing metal salts and reducing agent [53]. In the case of nickel electroless-deposition reduction and oxidation reactions, Equation 16, Equation 17 and Equation 18 [126], take place in order to deposit a nickel layer on the silicon insert:

Equation 16 Reduction: $Ni^{+2} + 2^{e-} \rightarrow Ni$

Equation 17 Oxidation: $H_2PO_2^- + H_2O \rightarrow H_2PO_3^- + 2H^+ + 2e^-$

Equation 18 Overall reaction $Ni^{+2} + H_2PO_2^- + H_2O \rightarrow Ni + H_2PO_3^- + 2H^+$

The reduction of the nickel ions will continue until all of the hypophosphite ($H_2PO_2^-$) has been oxidised in the solution [126]. A side reaction to the reduction of nickel is the production of hydrogen, which must be monitored as excess hydrogen can affect the quality of the deposited film [126]. When using electroless to deposit onto non-conductive materials a reducing agent such as $SnCl_2$ / HCl or $PdCl_2$ / HCl is used to initiate the reduction reactions within the solution [53; 126]. Buffers are also added to the aqueous solution in order to control pH during electro-deposition [126].

3.2.2.2.1 Electroless experimental process

Electroless is a plating method similar to electroplating but no electrical current is required and the sample need not be conductive prior to plating. The electroless solution used comprised of 100 ml nickel base solution (Ni21330), 200 ml nickel initial additive (Ni21331) and 700 ml deionised water [193]. The electroless solution was maintained at pH 5 and between 88 – 90 ^oC by a water bath heated by a hot plate. The silicon insert was suspended in the solution, which is continuously agitated by a magnetic stirrer, for 1 hour or until an even coating of nickel was observed. The insert was then rinsed in deionised water and left to air dry.

3.2.2.3 Electroplating

There are several journal papers that demonstrate the use of nickel inserts in micro-injection moulding for the replication of structures in the nano range [60; 86; 131; 140; 164]. The use of a nickel insert in micro-injection moulding will allow for

more replication cycles as nickel is more durable than silicon which is liable to break during repetitive replication cycles especially when replicating high-aspect-ratio structures [60].

In the case of nickel electroforming (Figure 3.24) a direct current causes the nickel anode to dissolve in a nickel sulfamate solution. Once in solution the positively charges nickel ions react with the free electrons also in solution and are converted back to metallic nickel at the cathode (silicon insert) surface [40]. The mechanical and physical properties of the final nickel part can be controlled by making alterations to the salt solution and operating conditions i.e. solution concentration and length of time sample is left in the solution. Nickel electroforming can be used to replicate complex surfaces with high accuracy and good surface finish without the need for additional machining of polishing of individual parts [40].

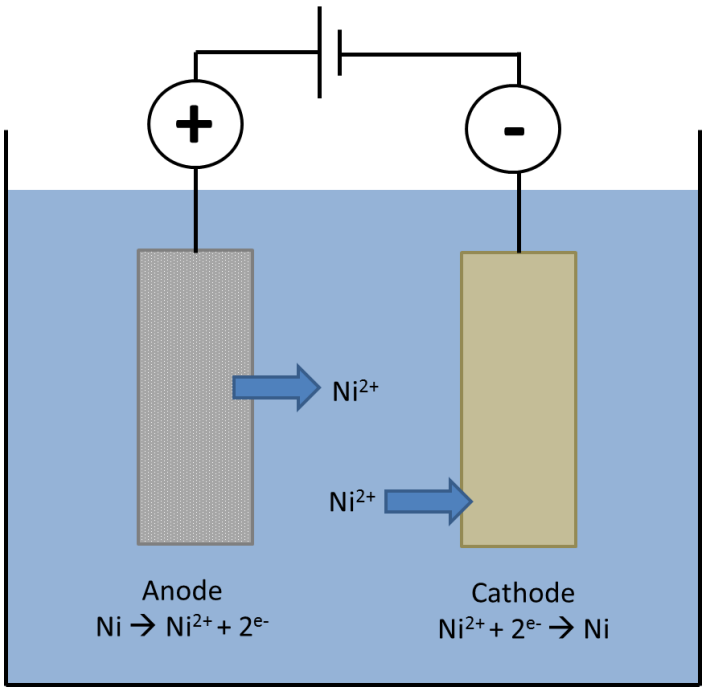

Figure 3.24 Schematic of nickel electroforming set-up

3.2.2.3.1 Nickel electroplating experimental procedure

Prior to electroplating the silicon samples from both sputter-coating and electroless were tested to ensure they are conductive enough using a multimeter. Due to the thickness of the nickel layer required a Watts plating bath was used to fabricate the final nickel electroform. The Watts bath solution was maintained at pH 4, 60 ^{o}C and consists of 330 g/L nickel sulphate ($NiSO_4.6H_2O$), 45 g/L nickel chloride ($NiCl_2.6H_2O$) and 38 g/L boric acid (H_3BO_3). The insert was attached to the cathode and placed in the plating bath until the required thickness had been deposited. The insert was then rinsed in distilled water and left to air dry.

3.2.2.4 Nickel electroform-silicon insert separation

Once a structured silicon insert has undergone electroplating the insert and electroform can be separated and the newly formed metal insert can then be used for further replication processes i.e. injection moulding. However, it should be noted that separation of the silicon and metal insert can result in the destruction of the silicon insert [101]. Therefore, the silicon insert was dissolved thereby leaving the nickel electroform intact.

In order to determine the conditions required to dissolve the silicon two 20 ml 1 molar sodium hydroxide (NaOH) solutions were prepared. One NaOH solution was heated to between 60 – 70 ^{O}C in a water-bath, the other was kept at room temperature. A single Silicon insert was then submerged into each solution and observed for 3 – 4 hours to determine the conditions and time required to dissolve a single silicon insert.

3.3 Micro – injection moulding

Micro-injection moulding, as described in section *2.1.1 Polymer micro-injection moulding*, is a low-cost, high throughput technique for the replication of micro- and nano-scale features onto polymer replicates

The following sub-sections will discuss micro-injection moulding of micro-scale features with high density polyethylene (HDPE), polypropylene (PP) and 316LS stainless steel feedstocks. The design of the mould and mould inserts used and the moulding familiarisation stage will also be outlined. The following sub-sections will also provide a detailed outline of the design of experiment approach used to examine the effect of process factors on preselected responses such as part mass and feature dimensions.

3.3.1 Feedstock selection

During a review of the available literature several polymers were identified for their use as feedstocks in the micro-injection moulding process. A preliminary search of the literature examined sixty-two papers relating to micro-injection moulding. Of these papers the most commonly used polymer feedstock was polycarbonate (PC), which was used in eighteen of the sixty-two papers (Table 3.18). Polypropylene (PP) was found to have been used thirteen times and polymethyl methacrylate (PMMA) was used twelve times. Of the polymer feedstock identified the one which was used least within the scope of the preliminary search was high density polyethylene (HDPE).

Of the sixty-two papers obtained during the preliminary search of the micro-injection moulding literature nineteen were found to examine the production of pillar features. A secondary search of these nineteen papers found that PC was used in seven and PP was used in four. PMMA was used only once, as was Polyoxymethylene (POM), Cyclic olefin copolymer (COC) and Acrylonitrile butadiene styrene (ABS) (Table 3.18).

A further refinement of the literature search (tertiary search) into the use of statistical design in the micro-injection moulding process identified forty-five papers. Within these papers PP was found to have been used ten times, PC used nine times and PMMA was used eight times. HDPE was found to be used in only three of the papers, the same was found of COC (Table 3.18).

Table 3.18 Occurrence of polymer feedstock within review of the literature relating to micro-injection moulding

Feedstock	Primary search	Secondary search	Tertiary search
HDPE	6	0	3
PP	13	4	10
PC	18	7	9
PMMA	12	1	8
POM	7	1	9
PS	7	2	4
COC	6	1	3
ABS	7	1	6

After the review of the available literature it was decided that two polymer feedstocks would be examined. The first polymer selected was polypropylene (PP) which was selected due to its widespread occurrence within the literature. The second polymer selected was high density polyethylene (HDPE). HDPE was selected due to its minimal use within the literature, especially with regards to its use in the replication of pillar features.

316LS stainless steel was selected as the metal powder feedstock to be examined due to it prevalence within the literature. A detailed list of the papers examined during the feedstock literature search can be found in the appendix of this thesis.

3.3.2 Familiarisation of micro-injection moulding process

A Battenfeld Microsystem 50 was used for the injection moulding of HDPE replicates. A silicon insert was mounted into the mould casing (Figure 3.22) and loaded into the Battenfled where heaters and thermocouples were attached to the mould casing. Sixty-two HDPE replicates were produced using a removable silicon mould insert structured with micro-channel insert features. The first factors assessed were the optimum factors used by Morel [144] (Table 3.19). However, the holding pressure, mould temperature and cooling time were then altered as air bubbles were observed on the surface of the replicates. Once it became apparent that the aforementioned factors could no longer be altered to prevent air bubbles the injection speed of the polymer melt was increased in a further attempt to remove the air bubbles. It was finally decided to increase the metering volume (the volume of polymer melt injected into the mould) which did improve the surface of the replicates by removing the air bubbles. Ideally the mould should be evacuated of air prior to melt injection. However, the Battenfeld injection moulding equipment used did not have the capacity to evacuate the moulds prior to injection.

Once the moulding process was complete the HDPE replicates deemed, on visual inspection, to be most accurately replicated were examined using the SFEG-SEM. The larger features were found to have been well replicated by the micro-injection moulding process (Figure 3.25). However, it was also noted that the smaller pillars were not as well replicated (Figure 3.26) and appeared to have been deformed by the process.

Table 3.19 Factor combinations used for silicon insert replication with high density polyethylene

Barrel temp (°C)	Mould temp (°C)	Holding pressure (bars)	Cooling time (sec)	Holding time (sec)	Injection speed (mm/s)	Part volume (mm^3)
200	100	300	12	2	200	655
-	-	400	-	-	-	-
-	-	-	14	-	-	-
-	110	-	-	-	-	-
-	-	-	16	-	-	-
-	-	-	20	-	-	-
-	-	-	24	-	-	-
-	105	-	-	-	-	-
-	-	-	22	4	-	-
-	-	-	20	6	-	-
-	-	-	22	4	-	-
-	-	450	-	-	-	-
-	-	500	-	-	-	-
-	-	-	-	-	250	-
-	-	-	-	-	300	-
-	-	-	-	-	350	-
-	-	-	-	-	400	-
-	-	550	-	-	350	-
-	-	550	-	-	400	-
-	-	500	-	-	350	-
-	-	-	-	-	-	700

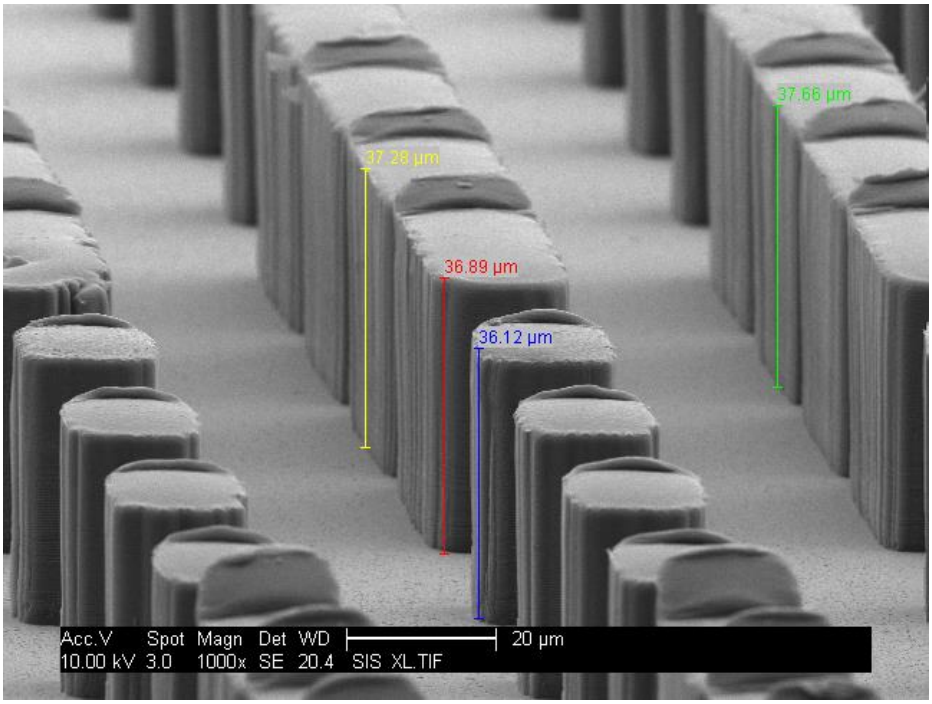

Figure 3.25 High density polyethylene pillar features successfully replicated during micro-injection moulding

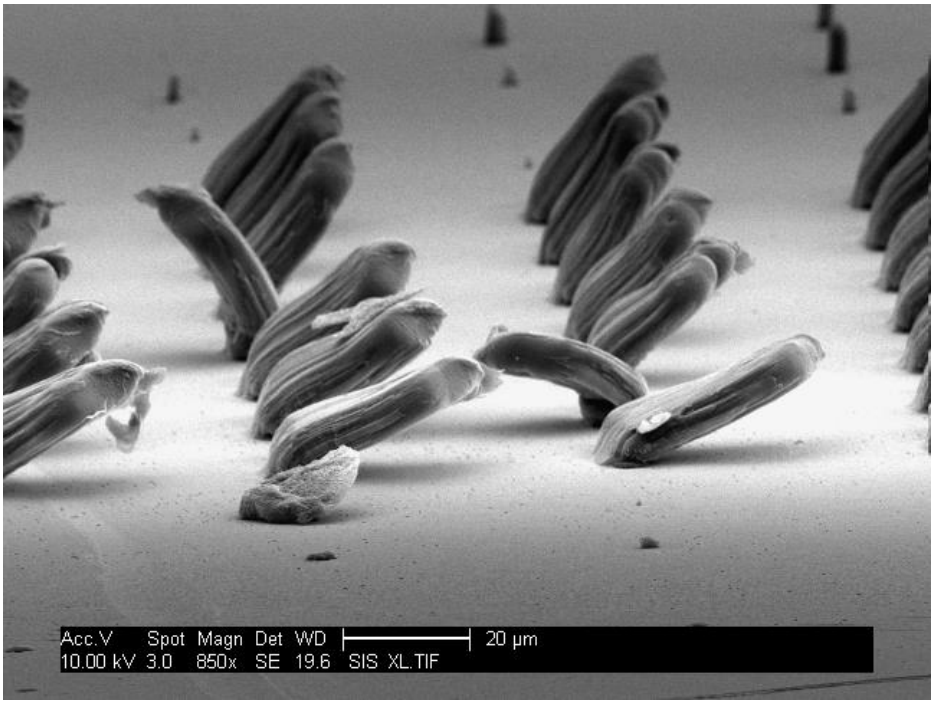

Figure 3.26 High density polyethylene pillar features not successfully replicated during micro-injection moulding

3.3.3 Design of experiment for micro-injection moulding

The significance of selected factors during the process of micro-injection moulding were investigated using a design of experiment approach. After an examination of the literature the factors selected for examination were injection speed [7; 81; 188], holding pressure [3; 7; 59; 160], mould temperature [5; 7; 14; 189] and cooling time [5; 7; 79; 130].

3.3.4 Design of experiment of micro-channel and 10 - 2 µm mould inserts experimental design

The production of polymer and metal powder replicates via micro-injection moulding was examined using a design of experiment approach. A 16 run full

factorial design was utilised to examine the effect of mould temperature, cooling time, holding pressure and injection speed on preselected responses. The responses selected for examination were pillar width and height [14; 59; 160], variation of replicate pillar height and width from the silicon mould insert, part mass and buffer mass [3; 7; 154; 189; 222].

3.3.4.1 Factor levels

The factor levels used for the production of HDPE and PP polymer replicates in the design of experiment processes are displayed in Table 3.20. The same factor levels were used for both silicon mould insert designs: Micro-channel and 10 - 2 µm. The criterion for the selection of the high and low levels is explained in Table 3.21. The melt temperature, injection pressure used and the metering volume of the injected polymers and metal powder are displayed in Table 3.24.

Table 3.20 High and low levels for factors examined with high density polyethylene & polypropylene polymer melts

Factor	Low level	High level
Injection speed (mm/s)	60	150
Holding pressure (bar)	300	500
Mould temperature (^{o}C)	45	80
Cooling time (sec)	12	24

Table 3.21 Criteria for factor level selection

Factor	Low level	High level
Injection speed (mm/s)	Selected via experimentation	Selected via experimentation
Holding pressure (bar)	Selected via experimentation	Value based on material specification from provider
Moulding temperature (^{o}C)	Selected via experimentation	Selected via experimentation
Cooling time (sec)	Experimentation - based on time required for replicate to be cool enough to handle following ejection	Selected as twice the minimum

Factor levels used for the 316LS powder micro-injection moulding are displayed in Table 3.22. The criterion for the selection of the high and low levels is explained in Table 3.23. The melt temperature, injection pressure and the metering volume use for the 316LS melt is displayed in Table 3.24.

Table 3.22 High and low levels for factors examined with 316LS melt

Factor	Low level	High level
Injection speed (mm/s)	150	250
Holding pressure (bar)	200	400
Moulding temperature (^{o}C)	130	140
Cooling time (sec)	12	24

Table 3.23 Criteria for factor level selection with 316LS powder melt

Factor	Low level	High level
Injection speed (mm/s)	Selected via experimentation	Selected via experimentation
Holding pressure (bar)	Selected via experimentation	Selected via experimentation
Moulding temperature (^{o}C)	Selected via experimentation	Selected via experimentation
Cooling time (sec)	Same as those levels selected for HDPE & PP design of experiment	Same as those levels selected for HDPE & PP design of experiment

Table 3.24 Melt temperature, injection pressure and metering volume used during the design of experiment investigation

Factor	High density polyethylene	Polypropylene	316LS
Melt temperature (^{O}C)	170	180	198
Injection pressure (Bar)	900	900	900
Metering volume (ccm)[‡]	700	700	700

3.3.4.2 Design of experiment randomised sequence

The design of experiment scheme used was devised using a full factorial 16 run design, generated using Minitab®15. The order of the design of experiment runs (Table 3.25) was generated using a built-in randomiser function in Minitab15®.

[‡] ccm – Cubic cemtimeter

The same design of experiment sequence was used with both insert designs and all injection feedstock materials.

Table 3.25 Randomised sixteen run full factorial design of experiment sequence

DOE	Mould temp (ºC)	Cooling temp (ºC)	Holding pressure (Bar)	Injection speed (mm / s)
1	-	-	+	+
2	+	+	+	-
3	-	+	+	-
4	+	-	+	+
5	-	-	+	-
6	-	+	+	+
7	-	+	-	+
8	+	-	-	+
9	+	-	+	-
10	+	+	+	+
11	+	-	-	-
12	+	+	-	-
13	-	-	-	-
14	-	-	-	+
15	+	+	-	+
16	-	+	-	-

3.3.5 Experimental procedure for the replication of micro-channel and 10 - 2 µm inserts via a design of experiment approach

A Battenfeld Microsystems 50 micro-injection moulding machine fitted with a removable silicon mould insert was used during the course of this research. The silicon mould insert was fabricated via photolithography and deep reactive ion

etching (Section *3.2.1 Silicon Insert Fabrication*). A sixteen run full factorial design of experiment sequence was carried out for each feedstock material. Ten polymer replicates were produced for each design of experiment run resulting in a total of 160 replicate samples for each polymer. The selected responses to be examined were part and buffer mass, pillar height, pillar width and the variation of pillar height and width of the replicate from the silicon mould (Section *3.4 Metrology and Optical Analysis*).

3.3.6 Debinding and sintering

After micro-injection moulding the replicates produced using 316LS were subjected to debinding and sintering to remove the polyoxymethylene (POM) binder and produce a dense metal part. Debinding was conducted using the BASF process. The samples were heated to 110 ^{o}C with a high concentration of nitric acid (> 98 %) in a purging gas of nitrogen at a flow rate of 100 l/h. The sintering process was conducted in a furnace in an atmosphere of pure hydrogen according to the schedule displayed in Table 3.26.

Table 3.26 Sintering schedule for debound replicates

Stage	Schedule
1	Furnace temperature raised from room temperature to 600 ^{o}C at a rate of 5 ^{o}C/min
2	Hold at 600 ^{o}C for 1 hour
3	Furnace temperature was then raised from 600 ^{o}C to 1350 ^{o}C at a rate of 5 ^{o}C/min
4	Hold at 1350 ^{o}C for 3 hours
5	Furnace cooled to room temperature

3.4 Metrology and optical analysis

The following subsections discuss the various metrological and optical techniques and analysis undertaken. Section *3.4.1 Optical analysis* outlines the optical analysis techniques used to capture images of the various sample surfaces. Section *3.4.2 Metrology* and its related subsections outlines the metrological techniques implemented to determine the values of the responses examined during the various DOE processes. The responses examined cover pillar undercut on silicon mould inserts, part and buffer mass of polymer and metal powder replicates, pillar height and width of polymer and metal powder replicates. The variation of the pillar height and width of the polymer and metal powder replicates from the silicon mould inserts was also examined. The methods used to determine droplet contact angles on 10 - 2 µm sample surfaces (Section *3.4.3 Contact Angle Analysis*), droplet channelling on micro-channel structured samples (Section *3.4.4 Droplet Channelling*) and droplet evaporation on micro-channel structured samples (Section *3.4.5 Droplet Evaporation*) is also discussed.

3.4.1 Optical analysis

The features of interest on all silicon inserts, polymer and metal powder replicates produced were examined using various optical analytical equipment. Optical microscopy was used to obtain 2D images of the sample surfaces. Confocal microscopy was used to obtain 2D surface images and also 3D images of the surface features by use of laser scanning. An SFEG-SEM (scanning electron microscope) was used to tilt the samples to obtain 3D images of the surfaces features.

3.4.2 Metrology

The following subsections discuss the metrological techniques used in gathering the selected responses in the various design of experiment

investigations. These responses include pillar undercut on silicon mould inserts (Section *3.4.2.1*), part mass (Section *3.4.2.2.1*) and buffer mass (Section *3.4.2.2.2*) of polymer and metal powder replicates, pillar height and width of polymer and metal powder replicates (Section *3.4.2.2.3*) and the variation of the pillar height and width of the polymer and metal powder replicates from the silicon mould inserts (Section *3.4.2.2.4*).

3.4.2.1 Design of experiment response examined in the deep reactive ion etching process

The response examined during the design of experiment investigation of the deep reactive ion etching process was the undercut of the pillar features (Figure 3.27) the pillar undercut was calculated using Equation 19. Where W_1 is the width of the pillar apex, W_2 is the width of the pillars base and U is the degree of undercut. For each run five pillars were measured and the average of these was taken as the response value.

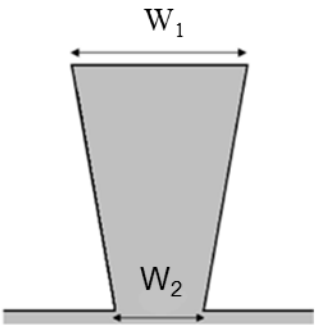

Figure 3.27 Schematic of pillar undercut

Equation 19 $W_1 - W_2 = U$

The experimental data gathered was analysed using main-effects plots and Pareto charts generated using Minitab15®.

3.4.2.2 Design of experiment response examined in the micro-injection moulding process

As part of the design of experiment investigations into the micro-injection moulding process four responses were examined. These were part mass, buffer mass, dimensions of the pillar features and replicate feature variation from silicon mould insert. The part mass was examined for the 316LS replicates fabricated using the silicon inserts structured with micro-channel features. The HDPE and PP replicates fabricated using the silicon inserts structured with 10 - 2 µm insert features were also examined using part mass as a response. The height and width of the pillar features and the variation of the replicate pillar height and width from the silicon mould insert were examined on all replicates produced.

3.4.2.2.1 Part mass

Part mass is defined here as the weight of the complete moulded part. The part mass was determined using a micro-balance. Each of the ten replicates produced per design of experiment run were weighed and a mean average was taken to determine the average part mass.

3.4.2.2.2 Buffer mass

Buffer mass is defined here as the mass of the protruding portion of polymer on the underside of the replicate, created by a portion of the polymer shot which did not fill the mould cavity (Figure 3.28). The buffer mass was obtained using

the dimensions of the buffer and the theoretical density value of the polymer (PP 905 kg/m^3, HDPE 950 kg/m^3) to calculate mass (Equation 20).

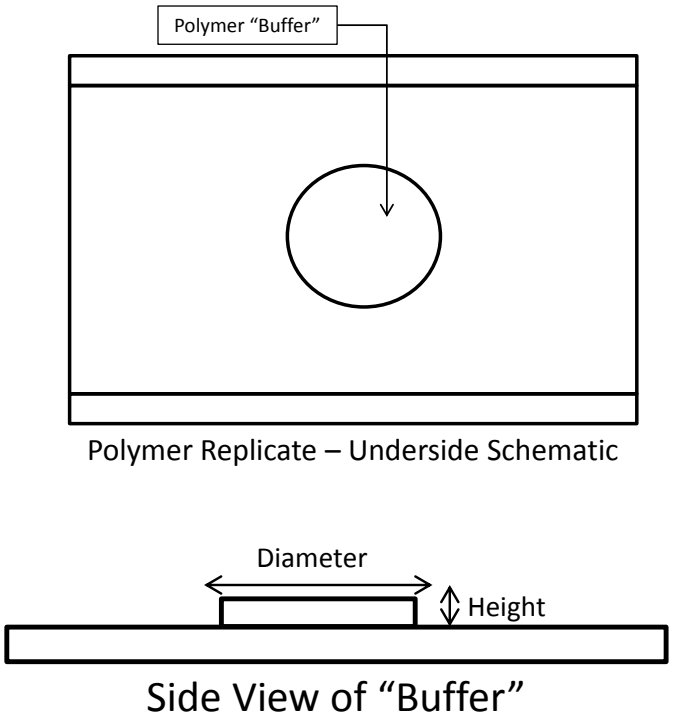

Figure 3.28 Polymer replicate buffer

Equation 20 Mass = Volume x Density

3.4.2.2.3 Part dimensions

The part dimensions measured were height (h) and width (w) (Figure 3.29) the features were measured using an SFEG-SEM. Feature measurements were only taken from one side of the pillar features therefore the area/volume of the pillars could not be determined. The side of the pillar features which varied in size across the replicate were measured during this examination. 5 - 10

measurements were taken for each pillar size and a mean average was calculated.

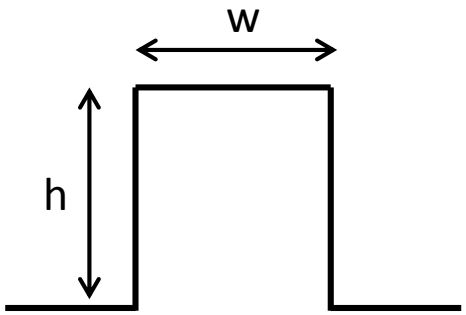

Figure 3.29 Dimensions measured from pillar features

3.4.2.2.4 Replicate feature variation from silicon mould insert

The height and width of the hole features in the silicon mould inserts was also measured. The averages calculated for the pillar features on the replicates was then be compared to the measurements taken from the original silicon mould insert to determine how much the replicate features varied from the silicon mould (Equation 21). The calculated variation from the silicon mould is the measured response used to identify the statistical significance of the factors examined. $Si_{(v)}$ is the measurement value from the silicon mould insert, $Rep_{(v)}$ is the measurement value from the polymer or metal replicate. ±Response is the variation of the replicate from the silicon mould insert.

Equation 21 $Si_{(v)} - Rep_{(v)} = \pm Response$

3.4.3 Contact angle analysis

The following method of image capture was selected due to its ability to capture continuous video footage, as opposed to capturing individual still images. This enabled the examination of the entire 'life cycle' of the droplet from deposition to evaporation.

In order to measure the droplet contact angle on samples structured with 10 - 2 μm insert features digital recordings of the droplets were taken over a specified time. Still images were then extracted from these recording and analysed to determine the droplet contact angles. Prior to recording the sample was first mounted onto a metal block and illuminated using a KL 1500 electronic lamp.

A 3.CCD colour JVC video camera connected to a computer was fitted with a 28 - 70 zoom lens and 40 mm lens extension tube. The camera was then mounted on a tripod and positioned infront of the sample so that the samples image was displayed on the computer monitor.

A digital camera was then mounted on a tripod and positioned infront of the computer monitor in order to digitally capture the video feed displayed.

The camera recording was commenced and a 1 μL droplet was placed on the sample surface using a 10 μL micro-litre syringe. The droplet was recorded for 5 minutes from the time of deposition.

For each video still images of the droplet were obtained at 1 minute intervals over a 5 minute period using 'Windows Live Movie Maker' software. The contact angle of the droplet at each time interval was measured using Image J, a free online software for measuring contact angles.

Five contact angle measurements were taken for each droplet at each time interval and an average for the droplet contact angle was taken at each time interval.

3.4.4 Droplet channelling

The micro-channel insert feature design was initially developed to examine how surface features can affect droplet movement. In order to examine how the movement of a droplet can be affected by these surface features samples structured with the micro-channels were mounted at various angles, ranging from 30 – 90 ^{o} in order to observe what effect the features had on the movement of a 0.2 μL droplet.

Each sample was mounted on a metal block and adjusted until the desired angle was reached. The sample was then secured with moulding putty and illuminated using an electronic lamp.

The same digital video capture set-up as described in section *3.4.3 Contact Angle Analysis* was used when recording droplets on the tilted sample surfaces. The droplets were recorded to the point of complete evaporation.

3.4.5 Droplet evaporation

The evaporation of 0.2 μL droplets on sample surfaces structured with micro-channel insert features was examined. The samples examined were silicon, uncoated HDPE and HDPE coated with a sputtered layer of gold-palladium (AgPd). The sample surfaces were magnified using an optical microscope. The selected area of the sample surface was then displayed on a computer monitor via a video feed.

As with the image capture of droplet contact angles and droplet channelling in sections *3.4.3 Contact angle analysis* and *3.4.4 Droplet channelling* a digital camera was secured to a tripod and placed in-front of the monitor, so a digital recording of the video feed from the optical microscope may be captured.

The digital camera was set to record, and the 0.2 μL droplet was then placed onto the surface of the sample using a 10 μL micro-litre syringe. The droplet was recorded to the point of completely evaporated. Two droplets were

observed on each of the structured areas of the sample surface, resulting in two digital recording per surface area and twelve recordings per sample.

3.5 Summary of methodology

The content of this chapter discusses the various experimental methods used during the course of this research into the micro-texturing of surfaces for fluid control. Section *3.1 Overview of experimental design* outlines the use of experimental design in the optimisation of experimental methods and the reasons for the selection of the design of experiment approach. Section *3.2 Mould design and fabrication* discussed the design and fabrication of micro-channel and 10 - 2 µm silicon inserts using photolithography and Deep reactive ion etching. The use of the design of experiment approach for examining the effect of process factors on the undercut of pillar features was also outlined. Section *3.3 Micro-moulding* outlines the production of HDPE, PP and 316LS replicates by micro-injection moulding using removable silicon mould inserts. The use of the design of experiment approach to determine the effect of process factors on selected responses (part and buffer mass, pillar height and width of replicates and the variation of replicate pillar height and width from the silicon mould insert) is also outlined and discussed. The methods used to obtain optical information of the various sample surfaces and the metrological methods used to obtain response values for the design of experiment examinations is discussed in Section *3.4 Metrology and Optical Analysis*. The measurement of contact angles on 10 - 2 µm structured silicon, HDPE and PP samples, the movement and evaporation of droplets on silicon, HDPE, PP and 316LS micro-channel structured samples is also discussed in this section.

4 Mould design and fabrication results

The following chapter details the results gathered from the mould design and fabrication of mould insert to be used in micro-injection moulding. Section *4.1 Silicon mould inserts* outlines the results gathers from the photolithography and deep reactive ion etching familiarisation stages using micro-channel and 10 – 2 μm insert designs. It also discusses the results from the design of experiment investigation into the effect of deep reactive ion etching process factors on pillar undercut. Section *4.2 Nickel mould insert fabrication* outlines the results from the sputter-coating and electroless coating of silicon inserts to produce a nickel mould insert for use in micro-injection moulding.

4.1 Silicon mould insert fabrication

The fabrication of silicon mould inserts for use in micro-injection moulding was examined and will be discussed in the following chapter. Pillar and hole features (ranging from 5 – 80 μm in diameter) were etched into silicon wafers using a photolithography and deep reactive ion etching process. A design of experiment approach was applied to the production of pillar features ranging from 10 – 5 μm in diameter.

4.1.1 Fabrication of micro-channel insert features

It was found that the features with dimensions above 10 μm were successfully replicated. However, the features with dimensions below 10 μm were not successfully replicated (Figure 4.1).

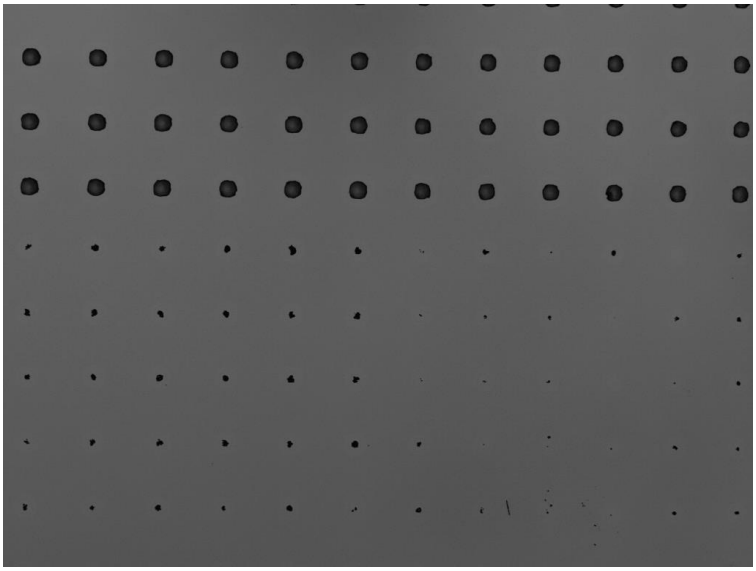

Figure 4.1 Hole features below 10 µm not successfully replicated

The confocal and optical microscopes allowed the measurements of the tops of the pillar features and the entrance to the hole features, enabling any irregularities in the feature shape to be identified (Figure 4.2 and Figure 4.3). The features displayed in Figure 4.2 were originally designed on the photomask to be 80 x 80 µm and 80 x 29 µm, and the features in Figure 4.3 were 20 x 20 µm. Therefore it can be seen that there is a variation between the dimensions on the photomask and the dimensions structured.

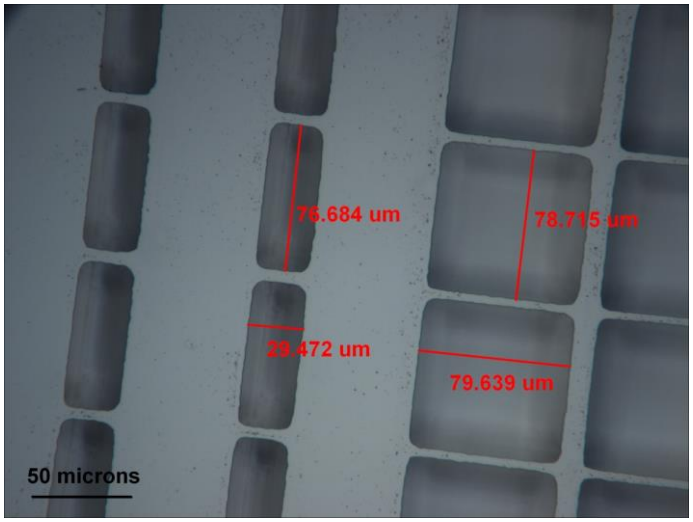

Figure 4.2 Hole feature dimensions measured via optical microscopy

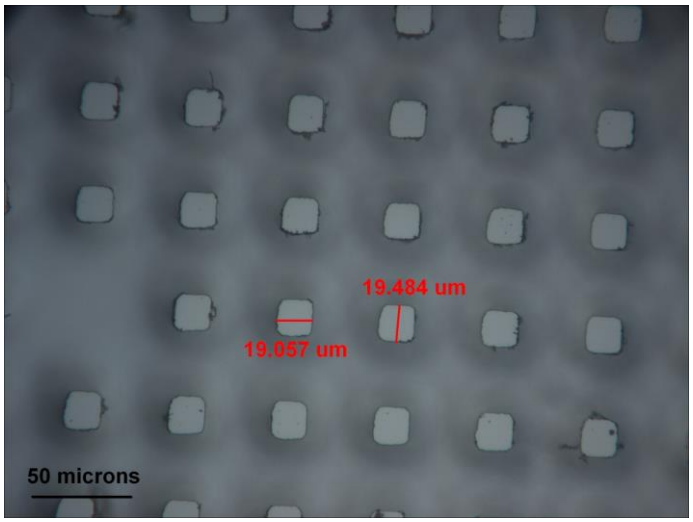

Figure 4.3 Pillar feature dimensions measured via optical microscopy

The SFEG-SEM allowed the examination of the entire depth of the pillar features by examining the inserts at a 45 – 85 ° angle (Figure 4.4 and Figure 4.5).

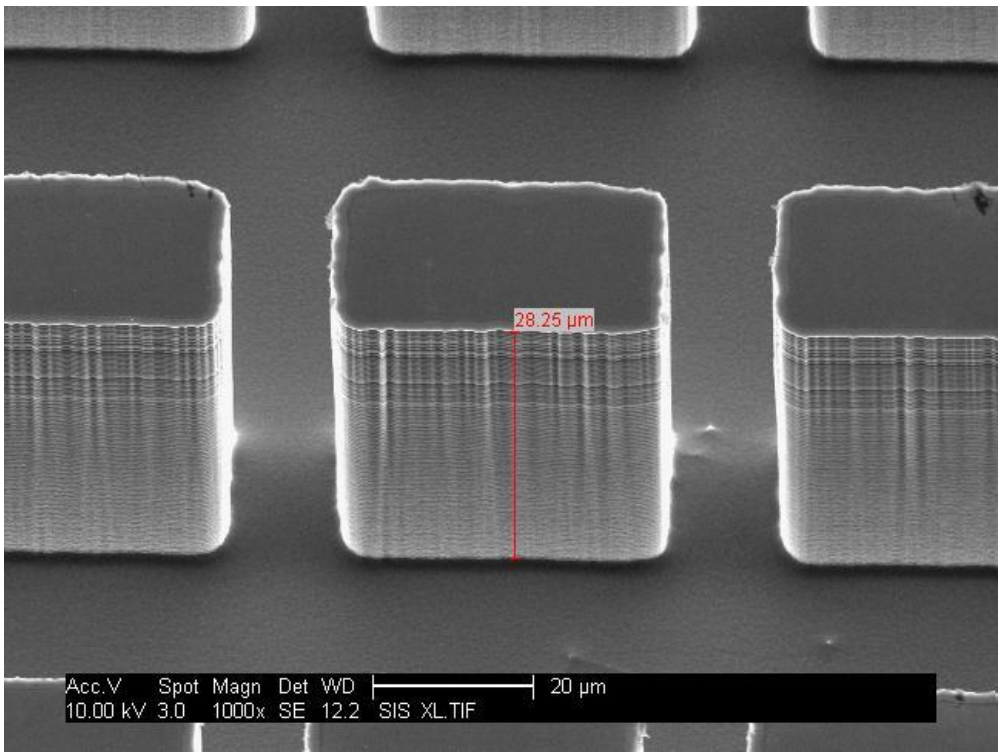

Figure 4.4 Pillar features observed at a 45 º angle

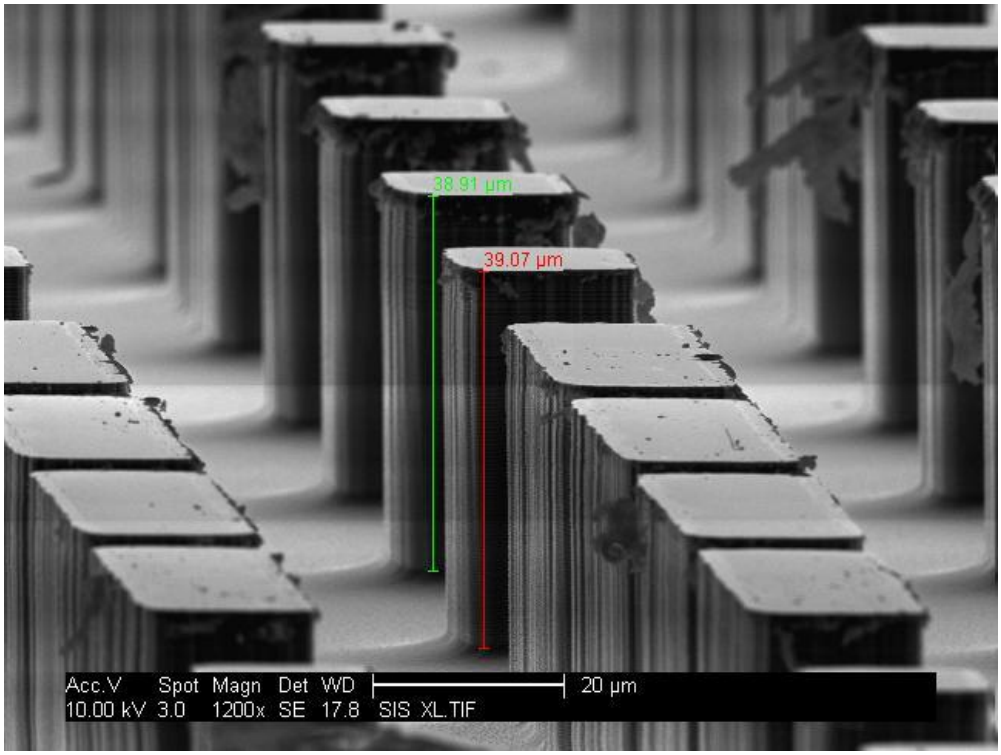

Figure 4.5 Pillar features observed at an 85 º angle

With regards to the hole features it was not possible to measure the depth using the SEFG-SEM as the sample could not be tilted to an angle in which the base of the holes could be seen. Therefore confocal microscopy was used to obtain measurements of the feature depth. Feature depths ranging from 37 – 45 µm were recorded for the micro-channel inserts (Figure 4.6 and Figure 4.7).

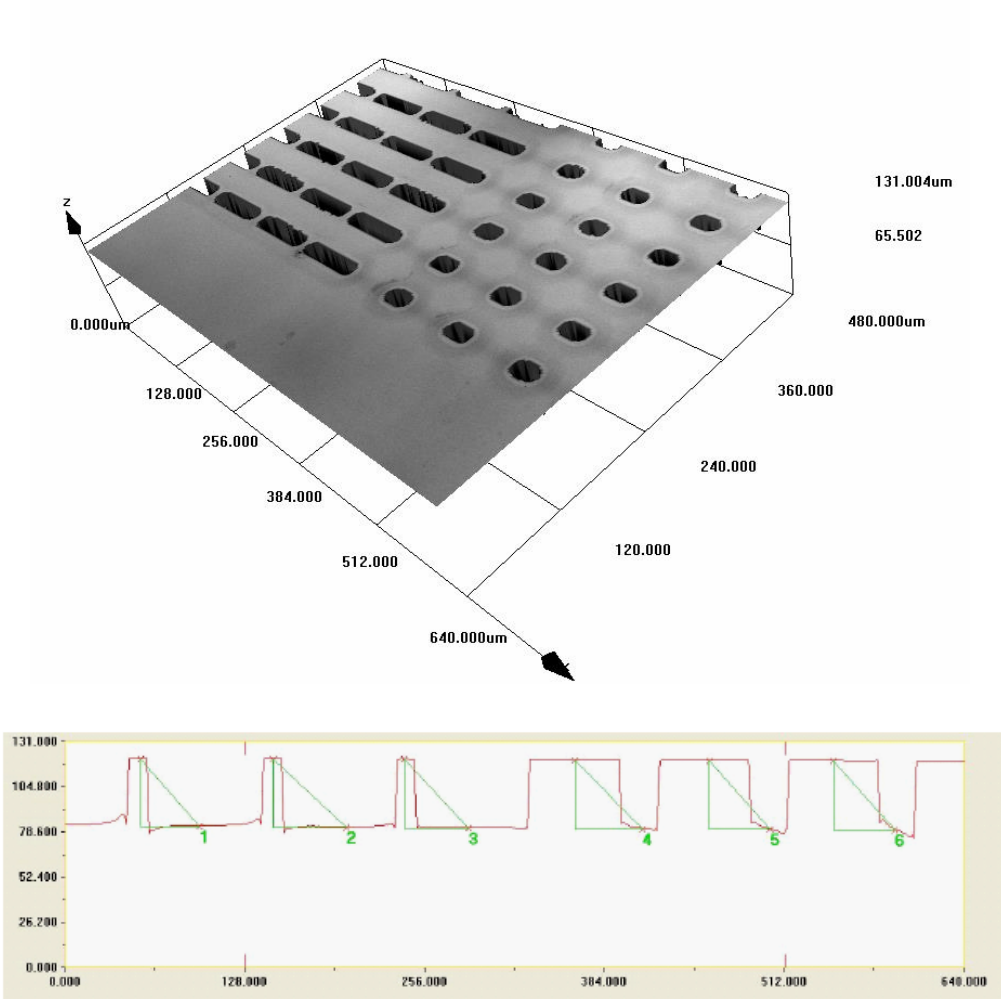

Figure 4.6 Example of confocal microscopy depth analysis of hole features and 3D scan of insert surface

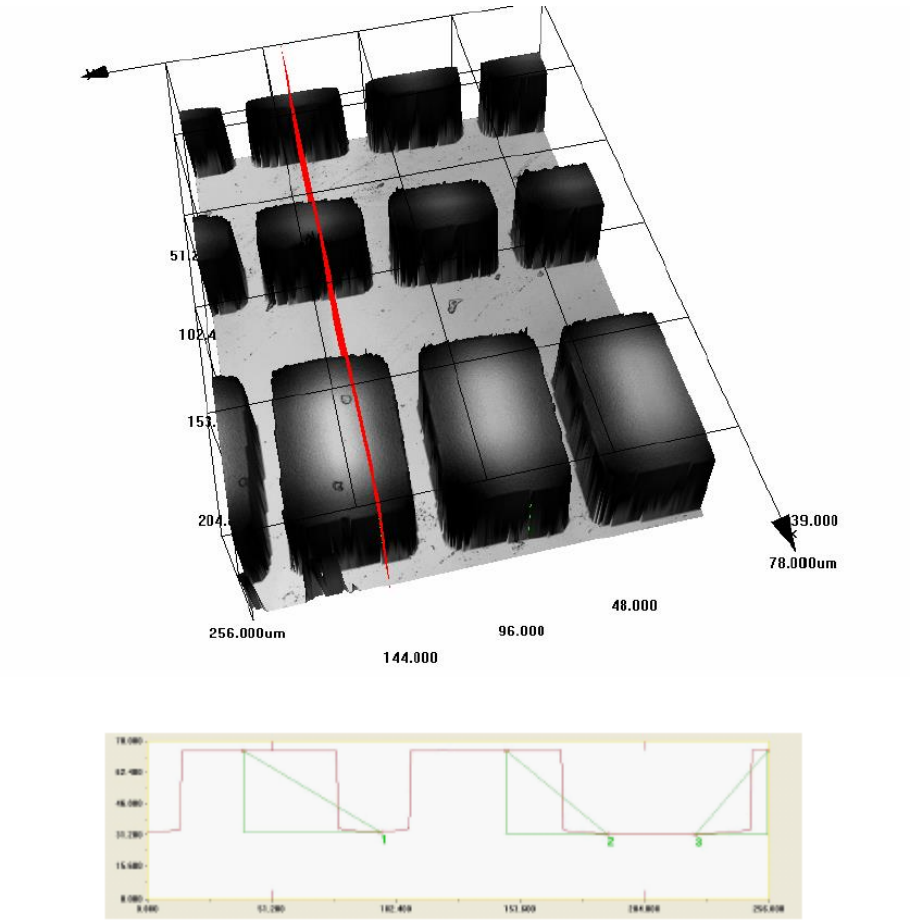

Figure 4.7 Example of confocal microscopy depth analysis of pillar features and 3D scan of insert surface

4.1.2 Familiarisation stage for the fabrication of 10 – 2 μm insert features

As well as micro-channel insert features, 10 – 2 μm insert features were etched onto silicon wafers via deep reactive ion etching. A familiarisation stage was conducted so that the effect of the etching process on pillar dimensions of this size could be determined.

4.1.2.1 Photolithography

The 10 x 10 μm and 5 x 5 μm pillar and hole features and the 2 x 2 μm pillar features were patterned onto the silicon wafer. However, the 2 x 2 μm hole features were not present.

4.1.2.2 Deep reactive ion etching

Both the 10 x 10 μm and 5 x 5 μm pillars and holes appeared to have been successfully replicated. However, the 5 x 5 μm pillars were severely undercut and as a result did not stand up-right but rather lay at an angle across the wafer surface. The 2 x 2 μm features were not present.

Examination revealed that the 5 x 5 μm pillar features observed immediately after deep reactive ion etching were no longer present (Figure 4.8 and Figure 4.9).

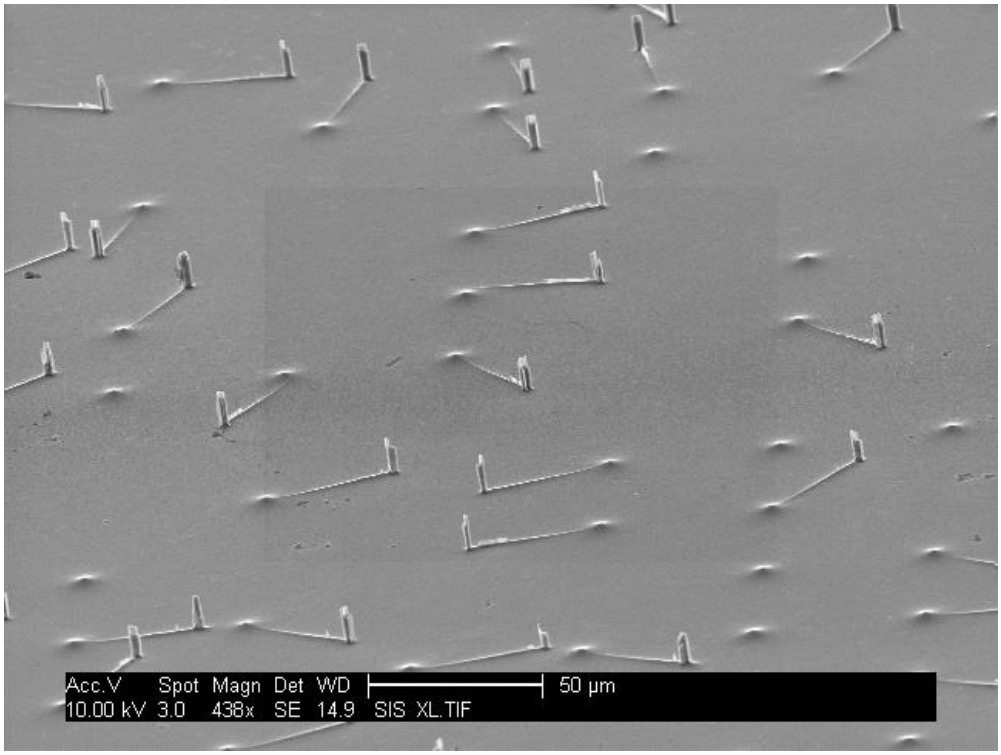

Figure 4.8 5 x 5 µm pillar stumps

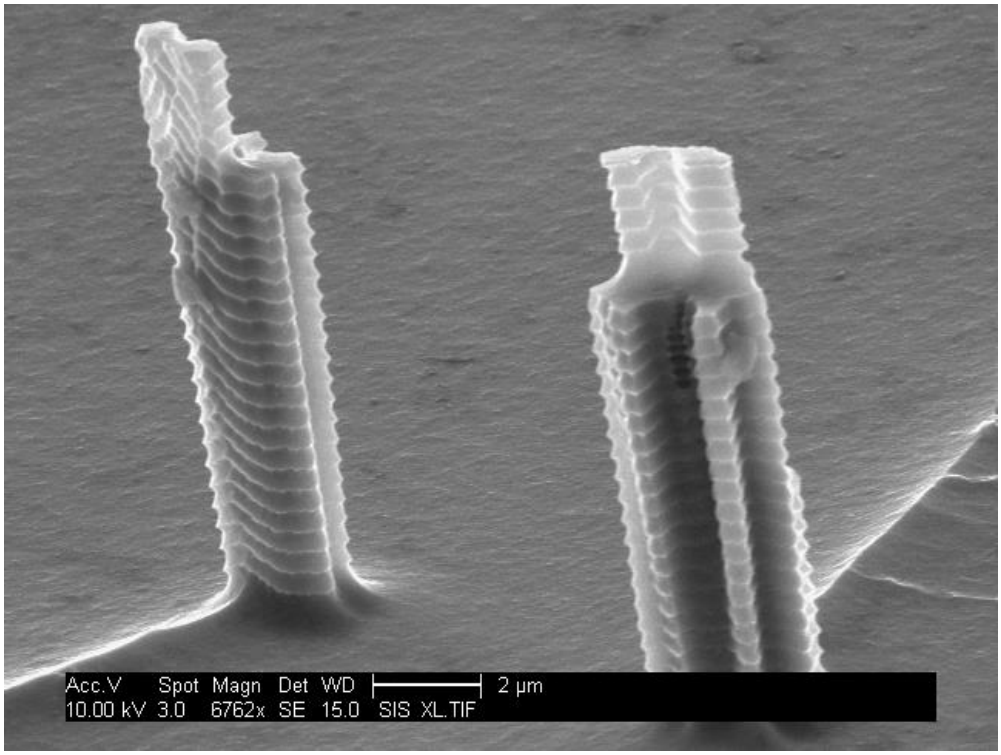

Figure 4.9 5 x 5 µm pillar stumps

It was also noted that the 10 x 10 µm pillar features were undercut (Figure 4.10 and Figure 4.11), and this had resulted in some of the pillars breaking (Figure 4.12).

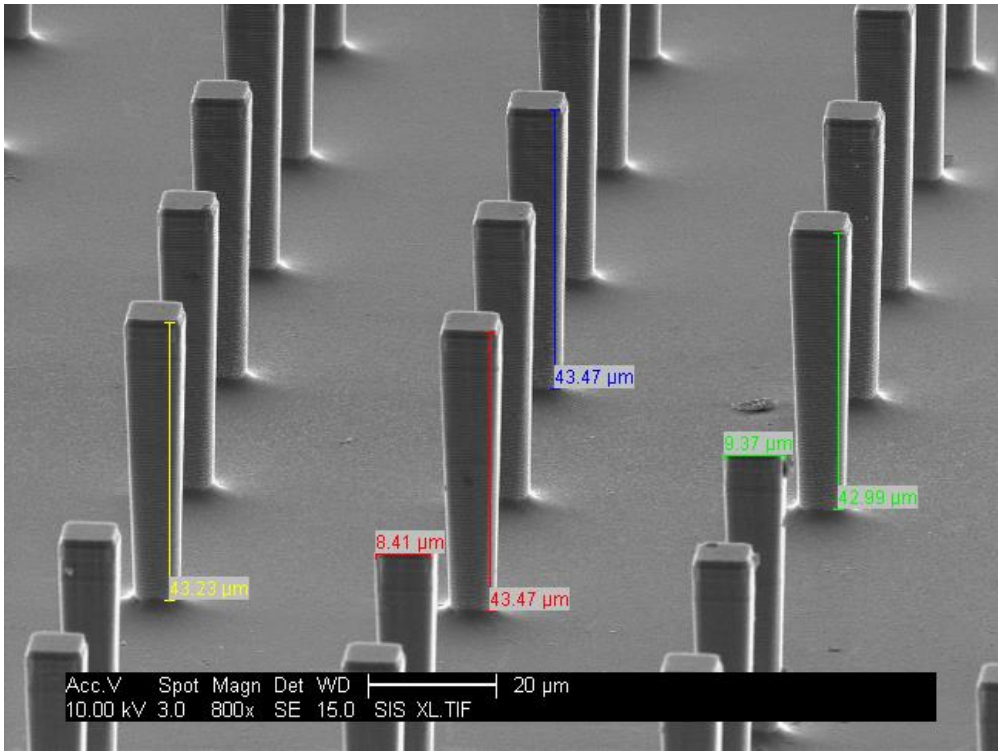

Figure 4.10 Pillar depth of 10 x 10 µm pillar features

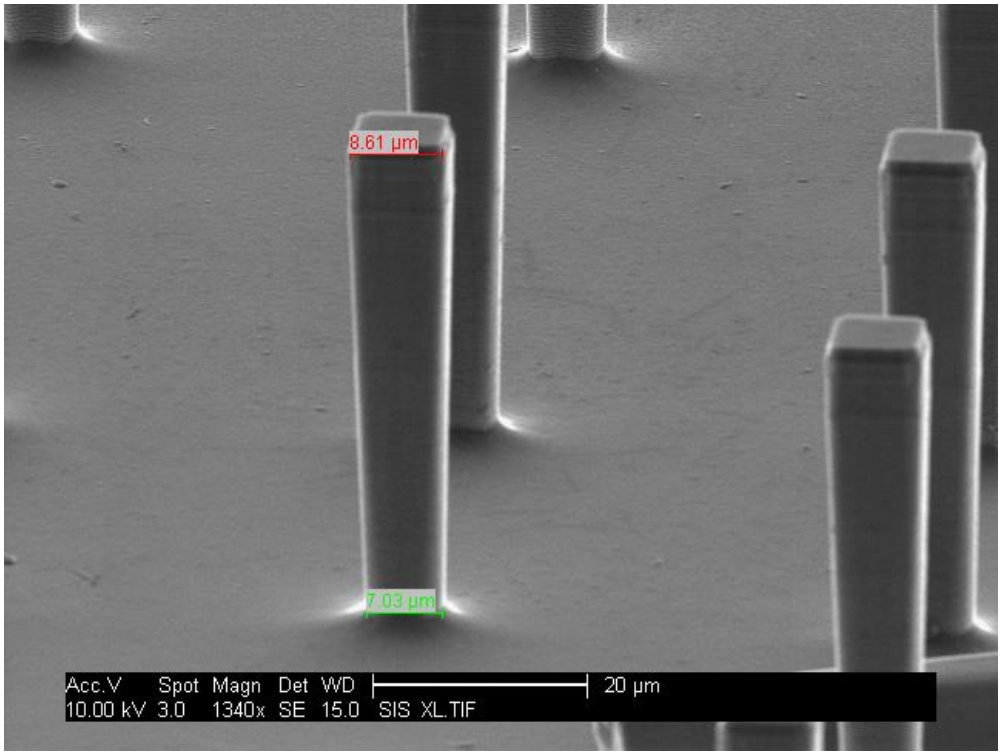

Figure 4.11 Pillar width at base and apex of 10 x 10 µm pillar features

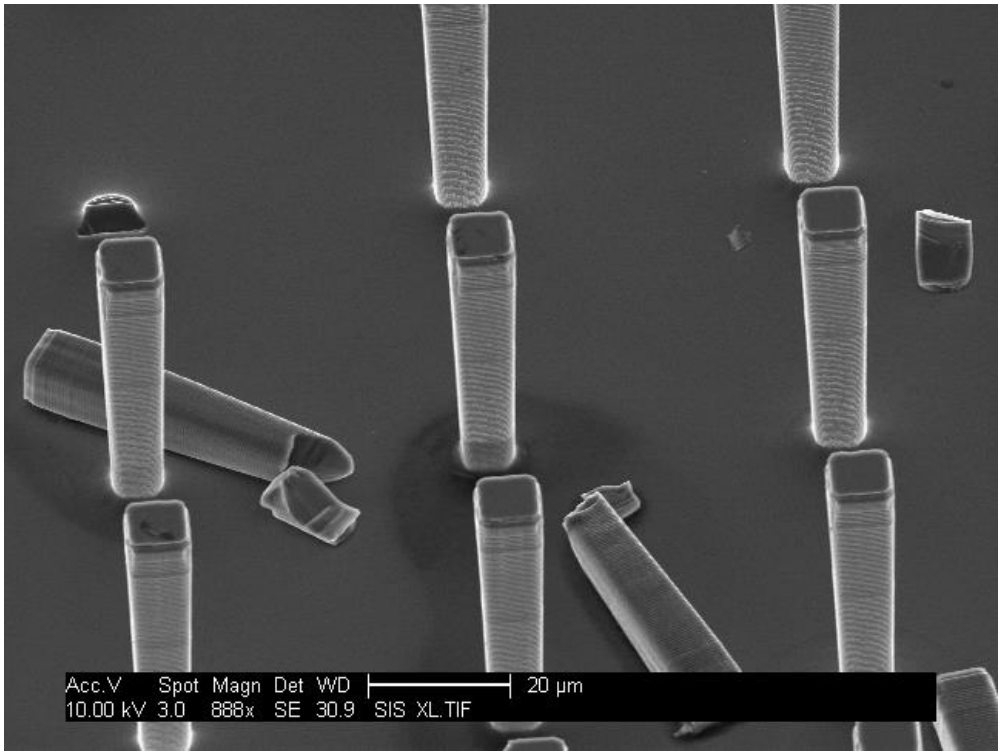

Figure 4.12 10 x 10 µm pillar features broken due to feature undercut

As before, the depth of the hole features could not be measured using the SEFG-SEM as the sample could not be tilted to an angle in which the base of the holes could be seen. Therefore, confocal microscopy was used to obtain measurements of the feature depth. The depths of 35 – 38 µm were found for the 10 x 10 µm hole features on the inserts.

4.1.3 Design of experiments of 10 – 2 µm insert features

The factors examined for their effect on the production of pillar undercuts were platen power, C_4F_8 gas flow in the passivation phase and etching:passivation switching times.

4.1.3.1 Photolithography

Using optical microscopy to ensure the photoresist had been patterned accurately it was noted that the 2 x 2 μm hole features were not present.

4.1.3.2 Appearance of features

The pillar features produced during the various design of experiment runs were compared to identify the effect the different factor levels had on the optical appearance of the features. Pillars from runs 3 and 4 (Figure 4.13a and Figure 4.13b) show examples of severe undercutting achieved on 5 x 5 μm features. The degree of undercut is such that no pillars could be observed standing on these samples. In contrast runs 1 and 2 (Figure 4.14a and Figure 4.14b) show examples where the undercut is either positive or minimal.

Features from runs 2, 1 and 8 (Figure 4.15 and Figure 4.16) display uneven etching, where features are present between the pillars. For contrast, an example of an evenly etched surface is shown in run 7 (Figure 4.16). A potential mechanism for the uneven etching observed for runs 2, 1 and 8 is the incomplete removal of the passivation layer during the etching phase. In extreme cases this can result in the “black silicon” effect, shown in run 8 (Figure 4.16).

a

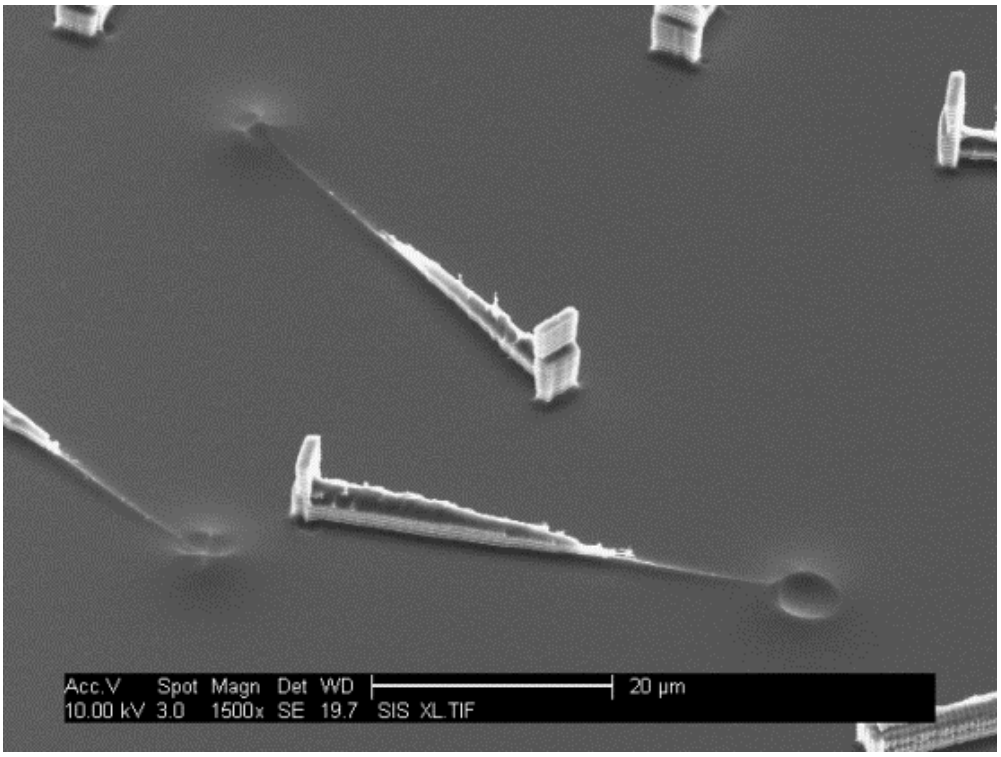

b

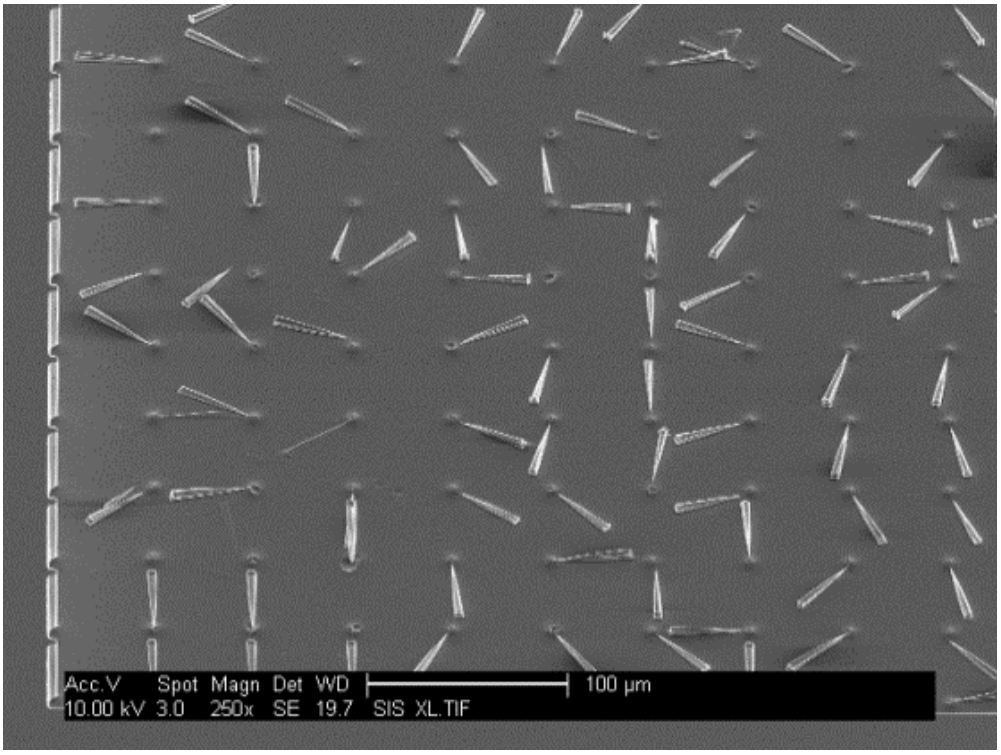

Figure 4.13 5 x 5 µm pillars, a) run 3, b) run 4

a

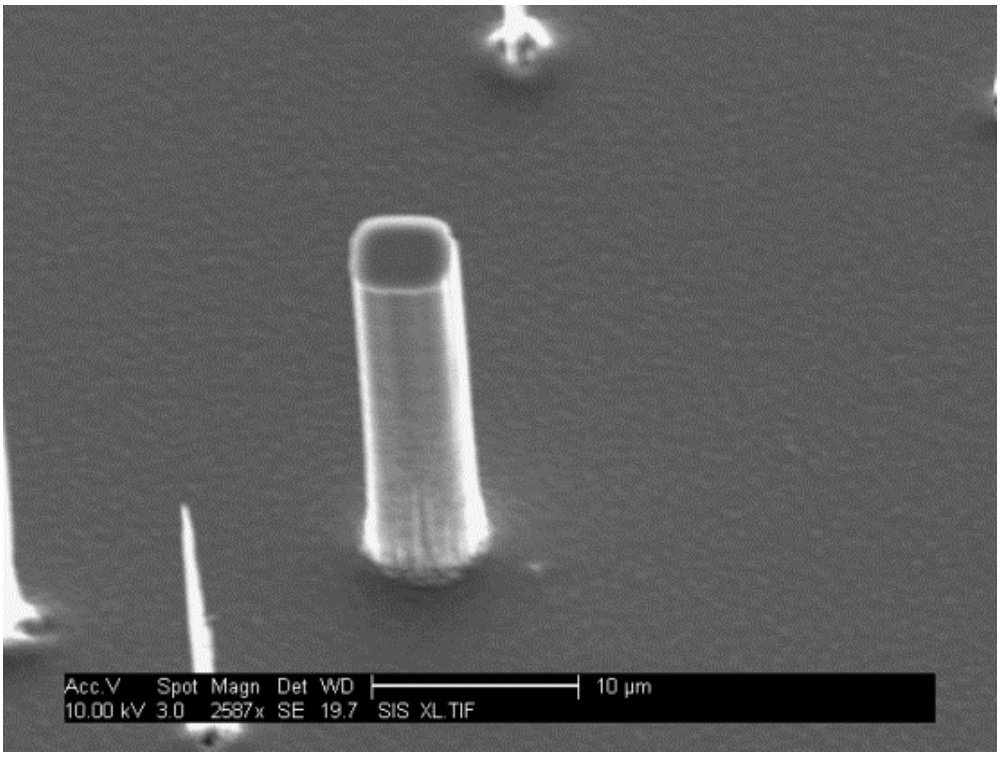

b

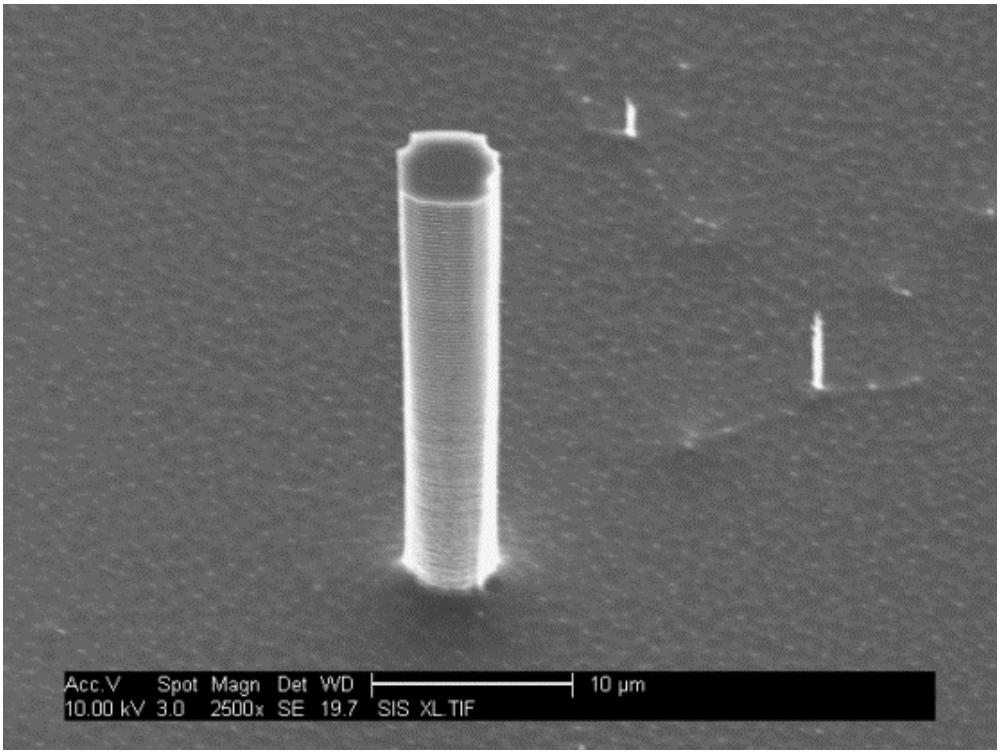

Figure 4.14 5 x 5 μm pillars, a) run 1, b) run 2

a

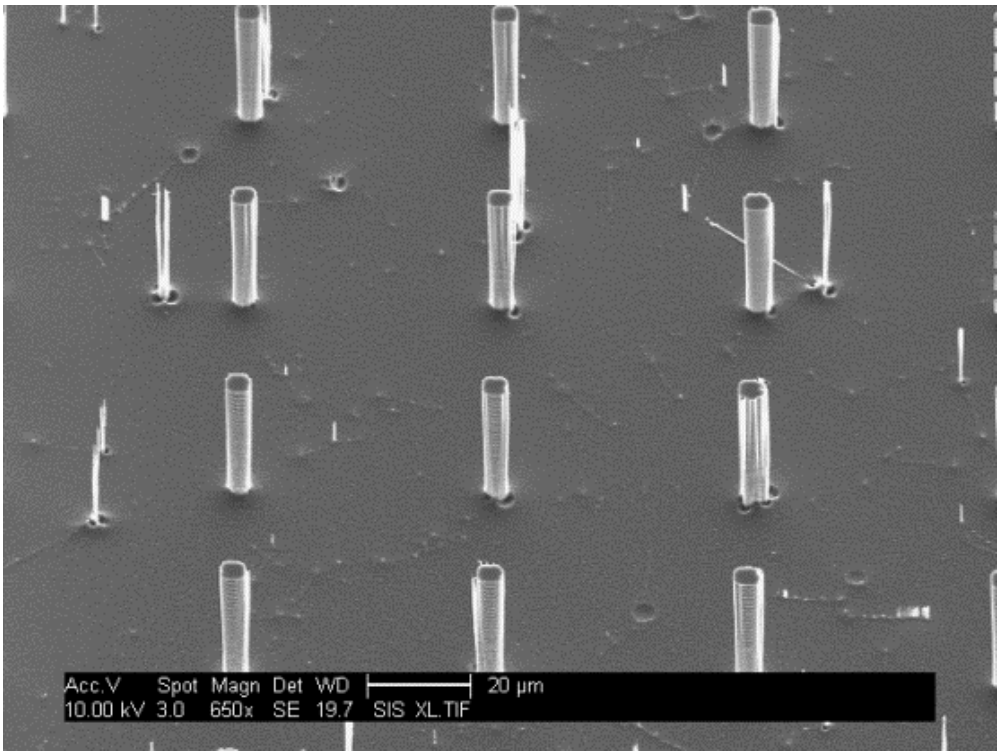

b

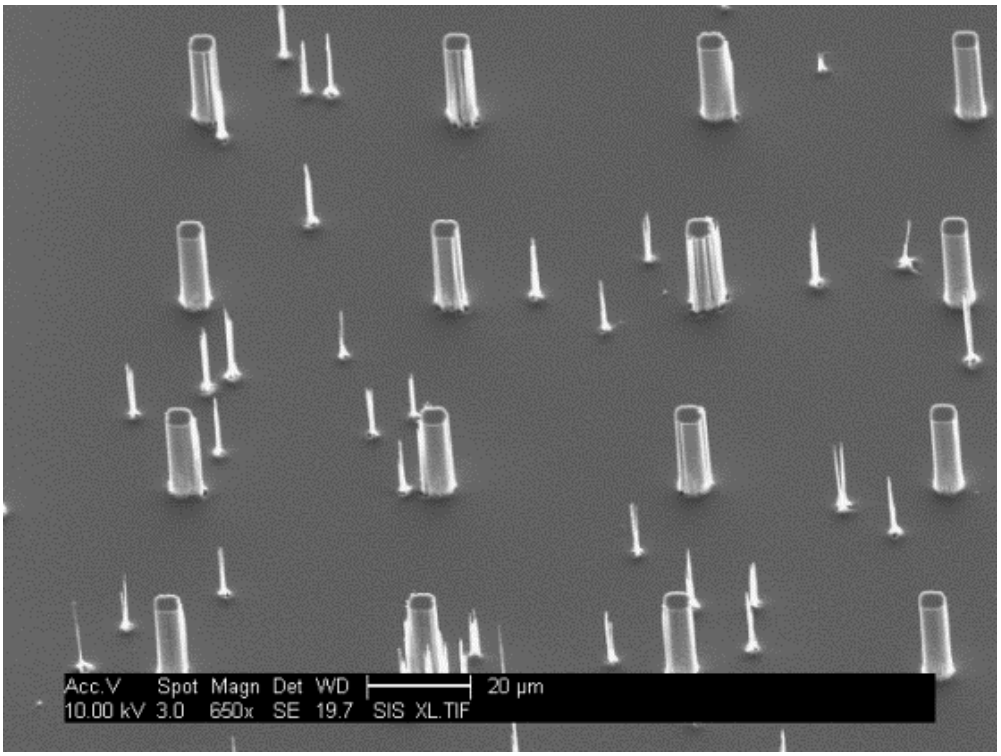

Figure 4.15 5 x 5 μm pillars, a) run 2, b) run 1

a

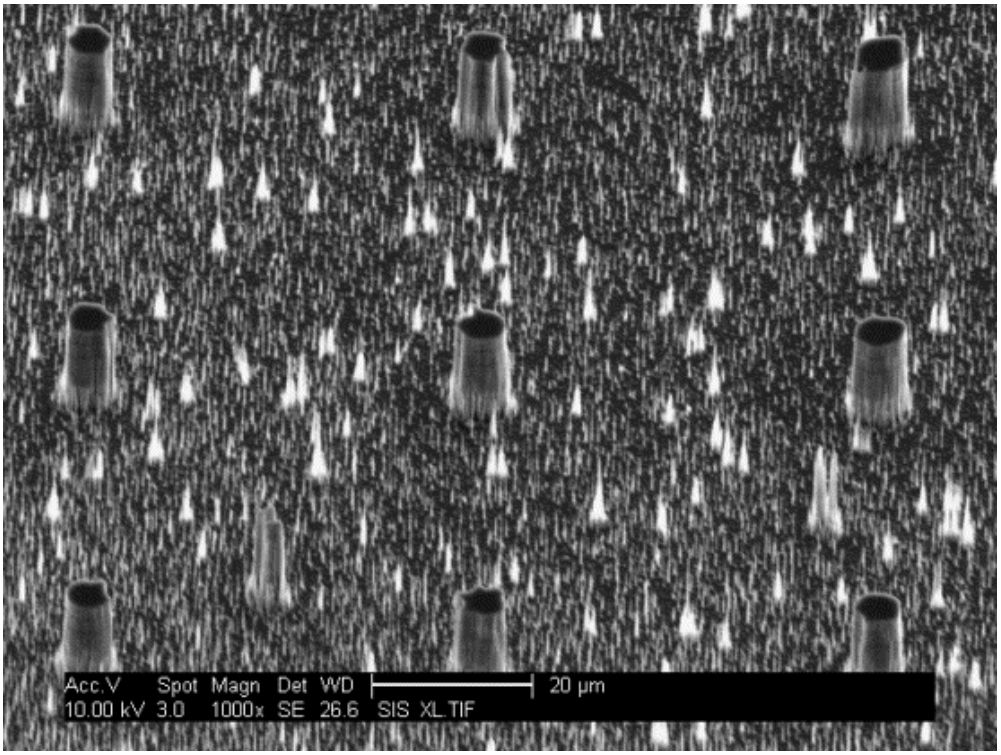

b

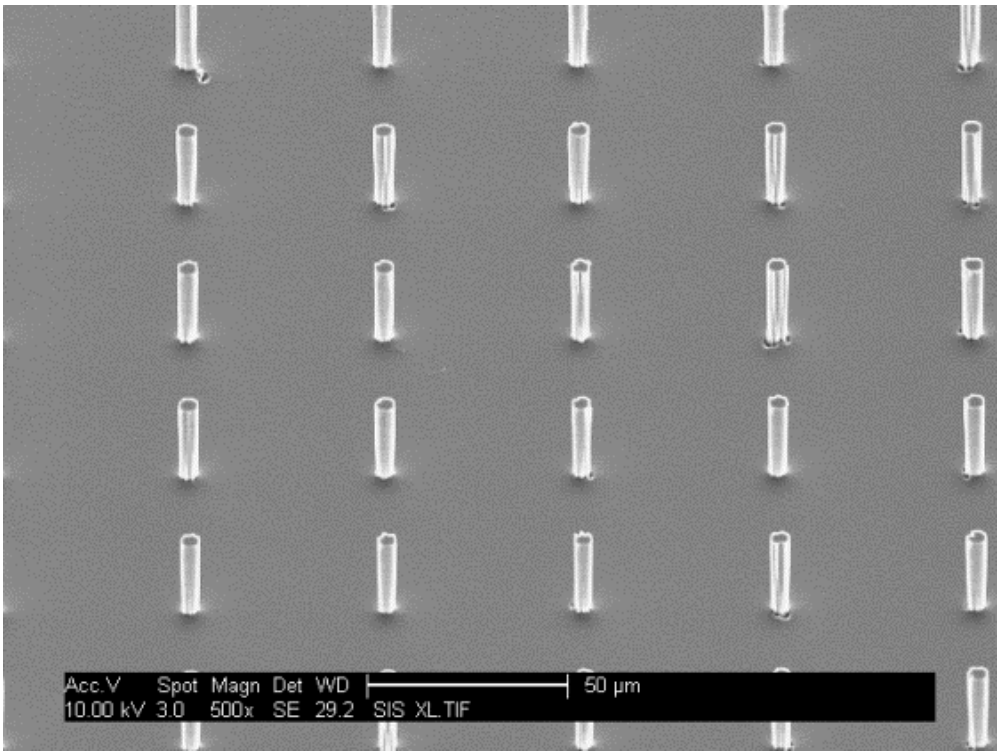

Figure 4.16 5 x 5 μm pillars, a) run 8 b) run 7

Upon examination of the 10 x 10 μm features it was noted that incomplete etching of the wafer surfaces was observed for the same runs as those displayed for the 5 x 5 μm pillars (Figure 4.17 and Figure 4.18). It should also be noted that the runs which resulted in the severely undercut 5 x 5 μm pillars also resulted in 10 x 10 μm pillars with large undercuts. Although all the 10 x 10 μm pillars remained standing (Figure 4.19 and Figure 4.20).

a

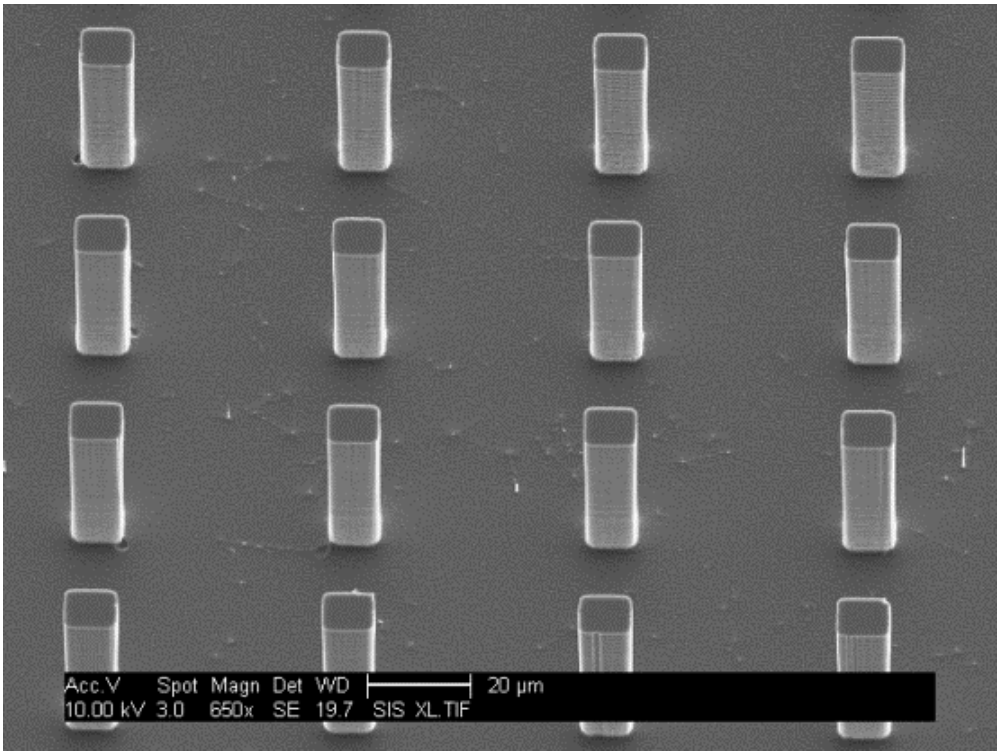

b

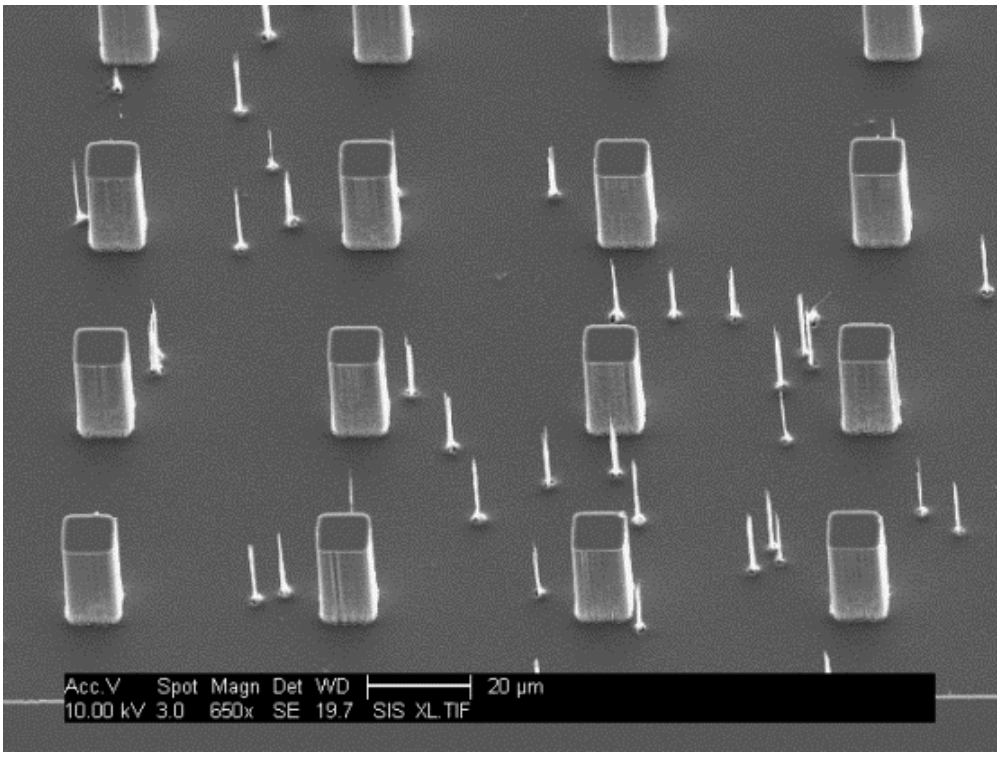

Figure 4.17 10 x 10 μm pillars, a) run 2, b) run 1

a

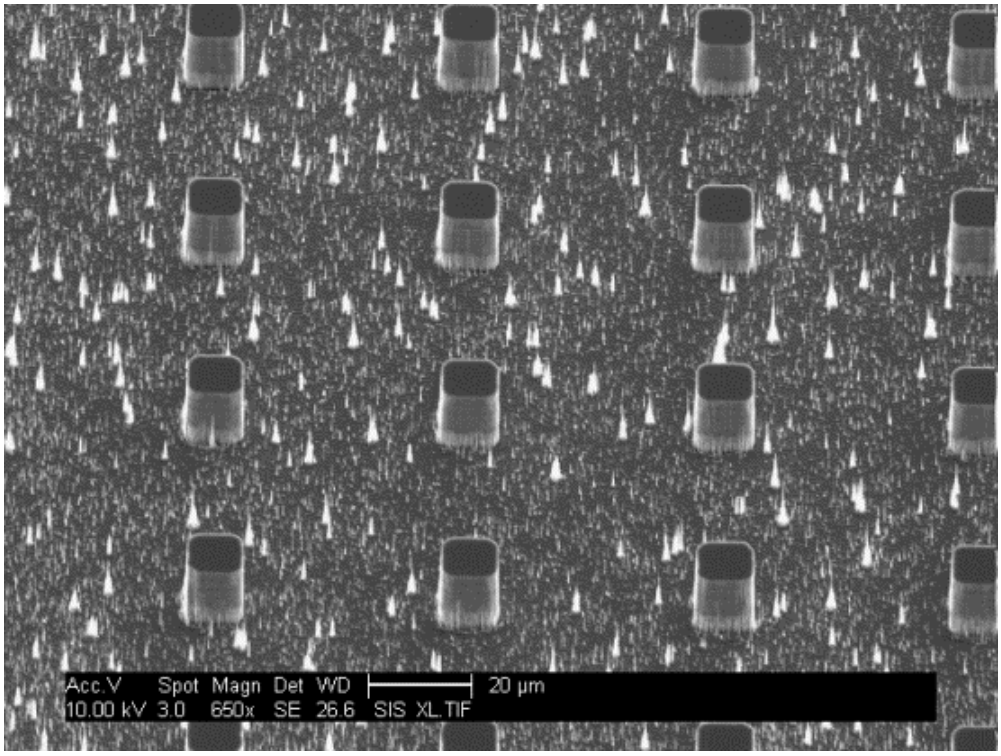

b

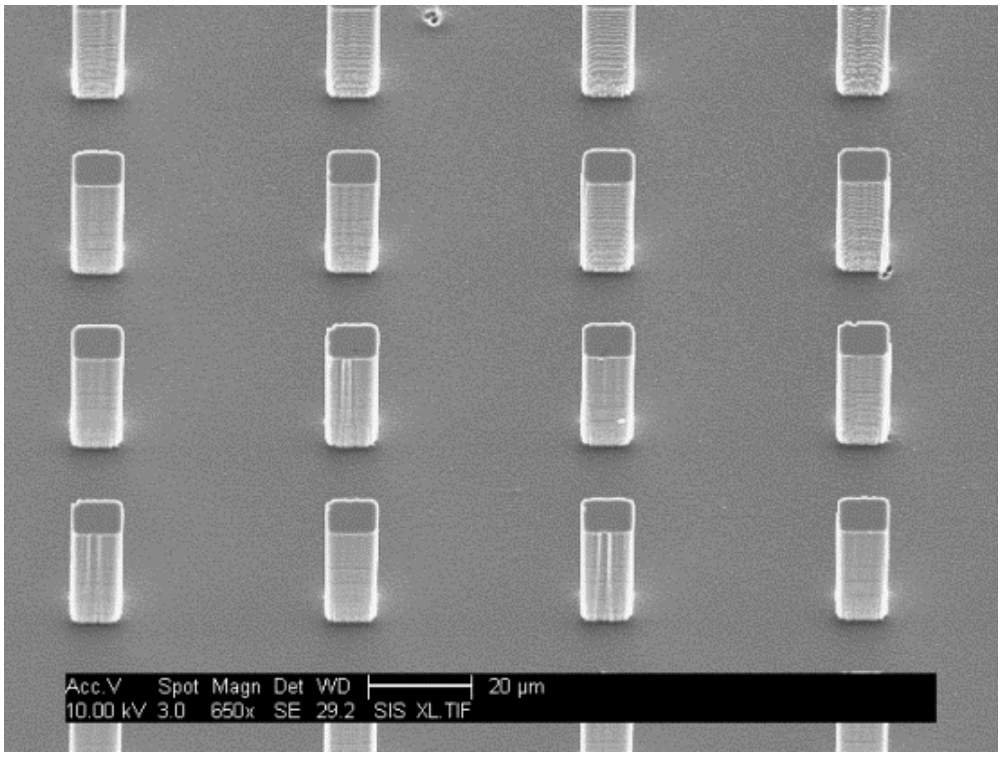

Figure 4.18 10 x 10 μm pillars, a) run 8 b) run 7

a

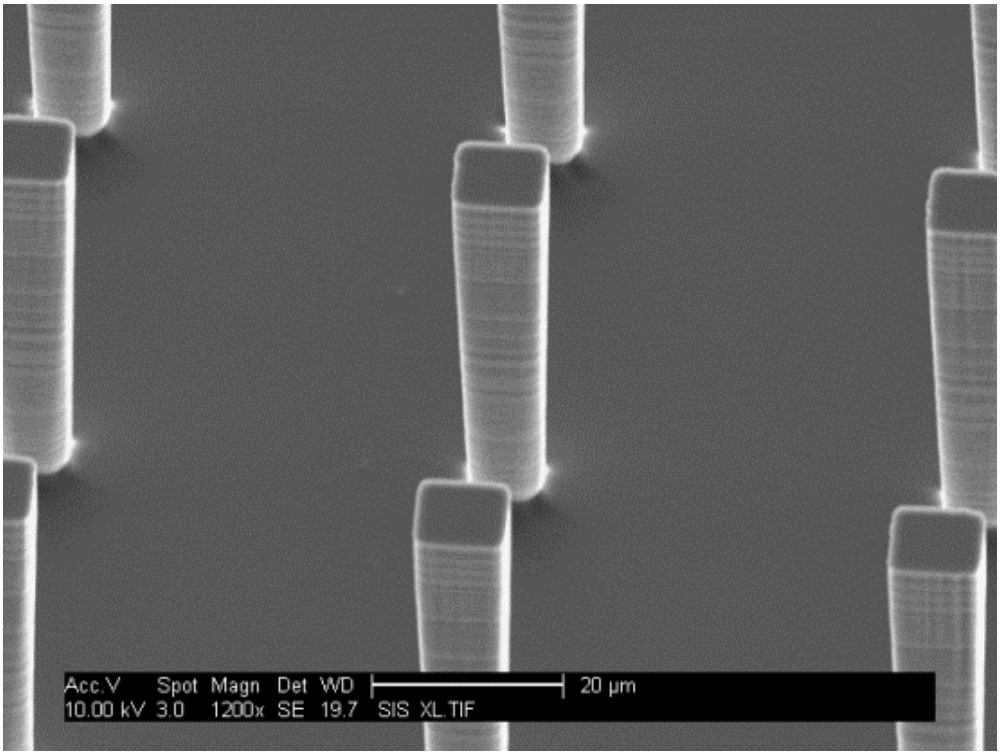

b

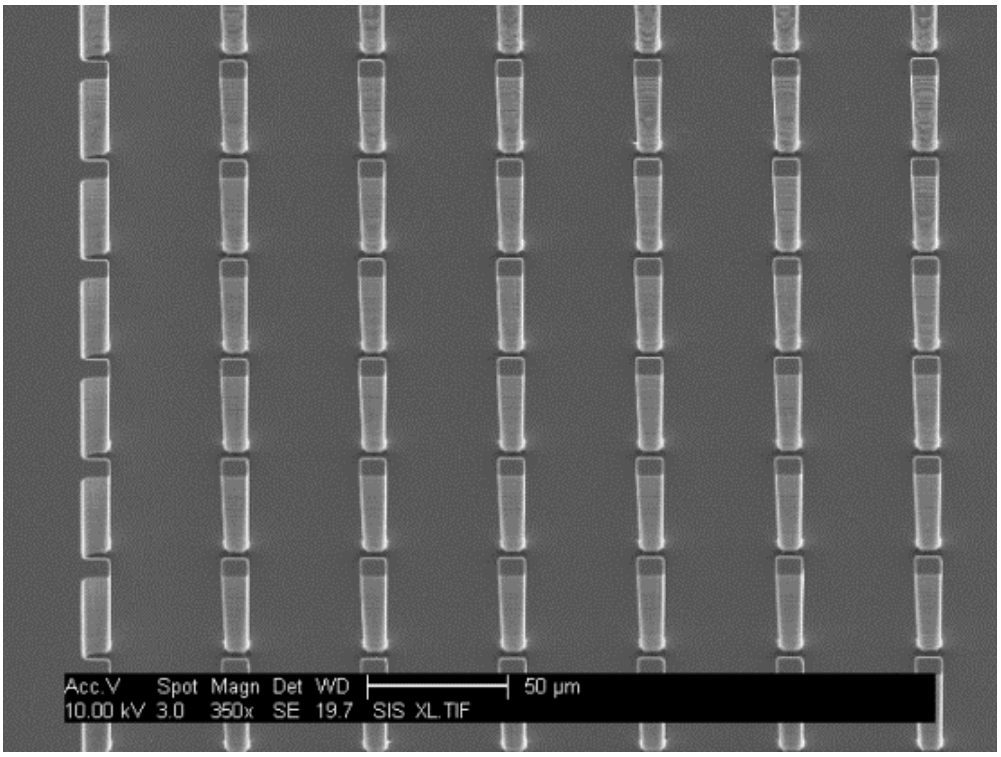

Figure 4.19 10 x 10 μm pillars, a) run 3, b) run 4

a

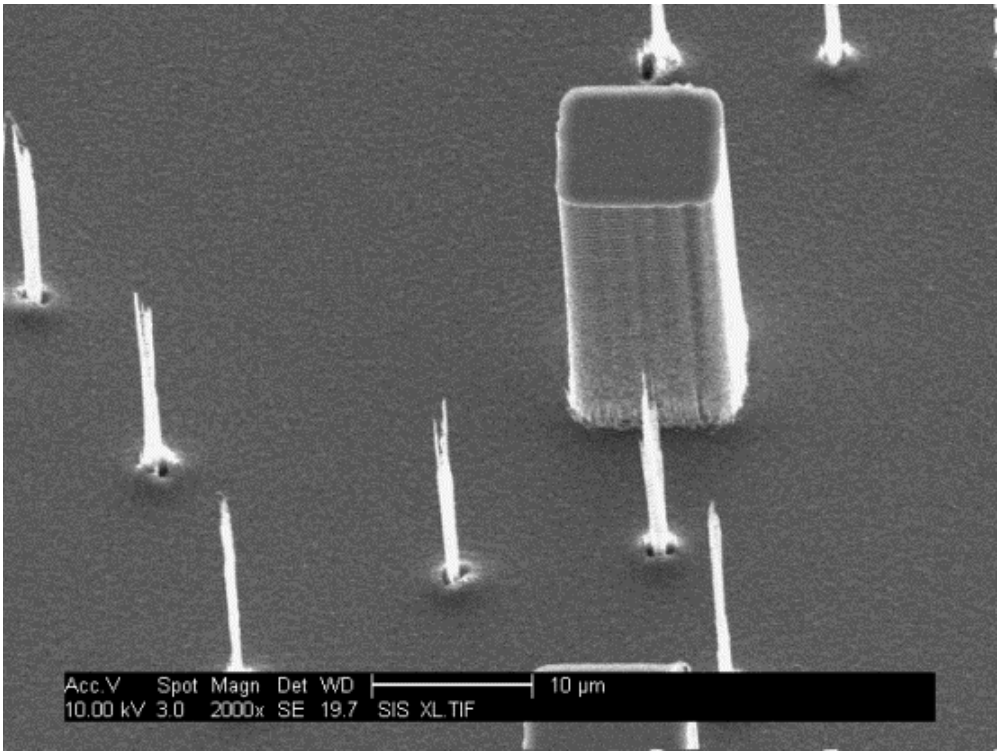

b

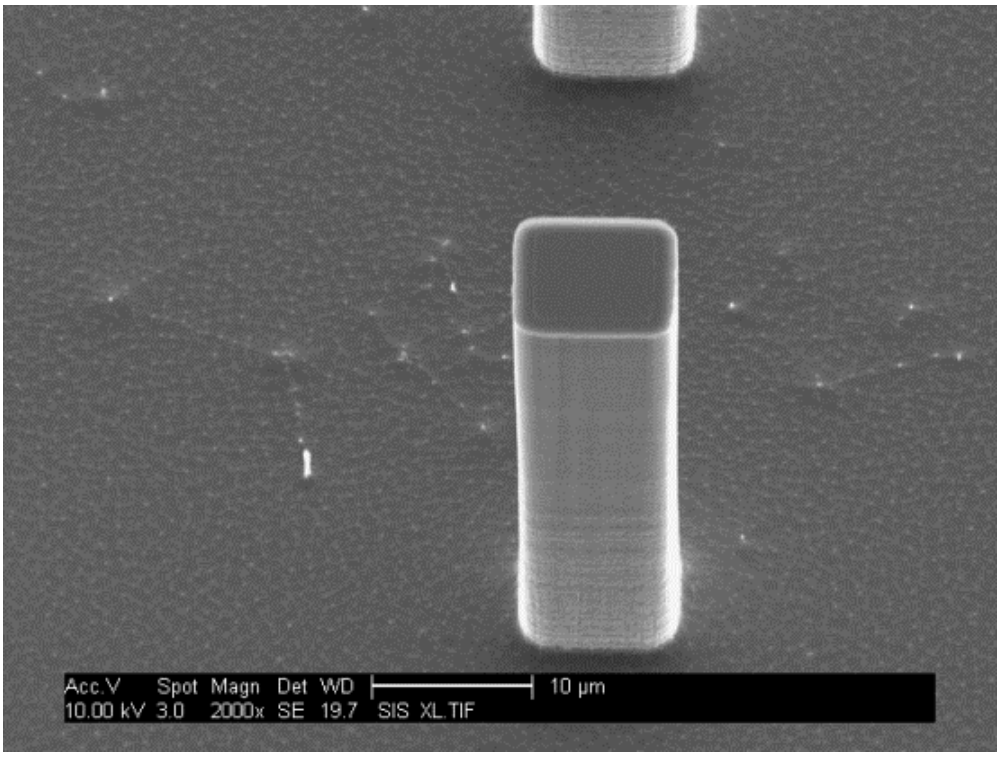

Figure 4.20 10 x 10 μm pillars, a) run 1, b) run 2

4.1.3.3 Measured undercut

The average undercut of the 10 x 10 μm and 5 x 5 μm pillars is displayed in Table 4.1. None of the 2 x 2 μm pillars were successfully etched.

Table 4.1 Average undercut for 10 x 10 μm and 5 x 5 μm pillars

DOE	Platen power (W)	C_4F_8 Gas flow in passivation stage (sccm)	Switching times – etching : passivation (s : s)	Average undercut	
				10 x 10 μm	5 x 5 μm
1	-	+	-	0.028	-0.349
2	+	+	-	0.354	0.441
3	-	+	+	1.271	No Pillars
4	-	-	+	1.572	3.986
5	+	-	+	2.545	No Pillars
6	+	+	+	1.800	No Pillars
7	+	-	-	0.087	0.444
8	-	-	-	-0.729	-1.091

4.1.3.4 Statistical analysis

Examination of the Pareto Charts (Figure 4.21 and Figure 4.23) identified switching times as the most significant factor of those examined for both 10 x 10 and 5 x 5 μm pillars. The main effects plots (Figure 4.22 and Figure 4.24), also identified switching times as the factor with the main effect on pillar undercut for both 10 x 10 and 5 x 5 μm pillars.

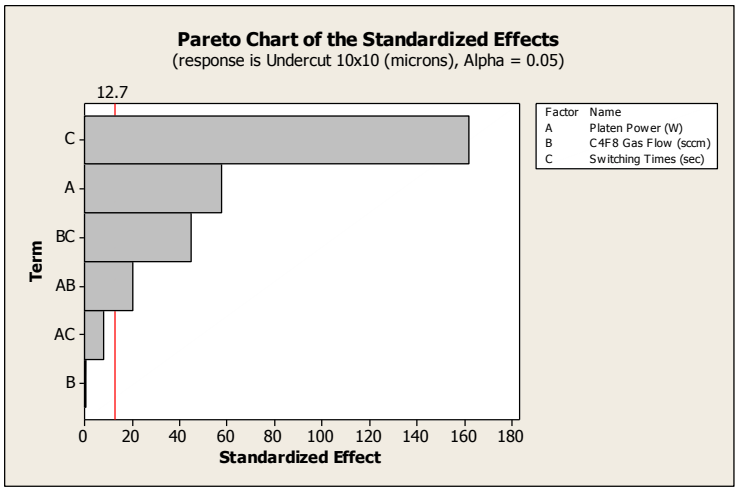

Figure 4.21 Pareto chart for 10 x 10 μm pillars

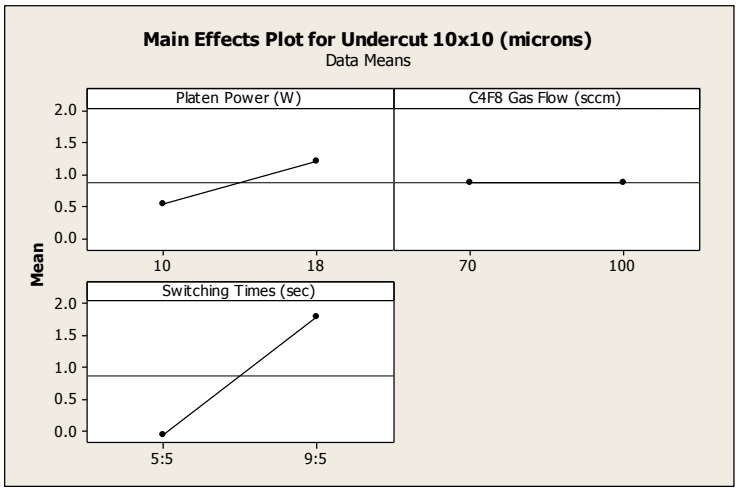

Figure 4.22 Main-effects plot for 10 x 10 μm pillars

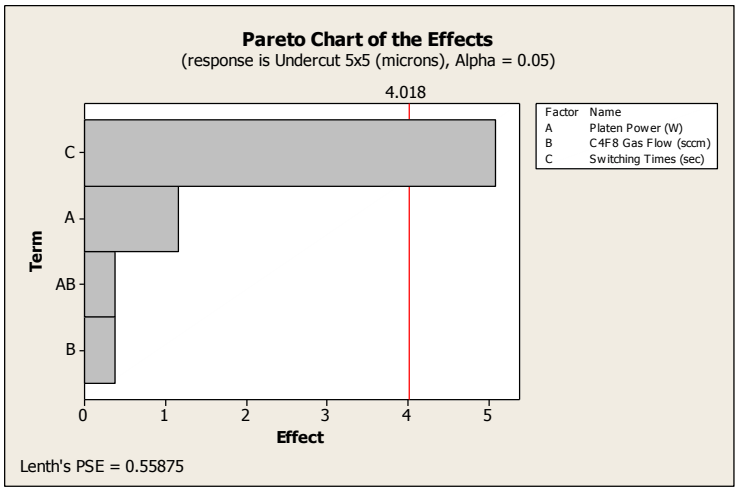

Figure 4.23 Pareto chart for 5 x 5 μm pillars

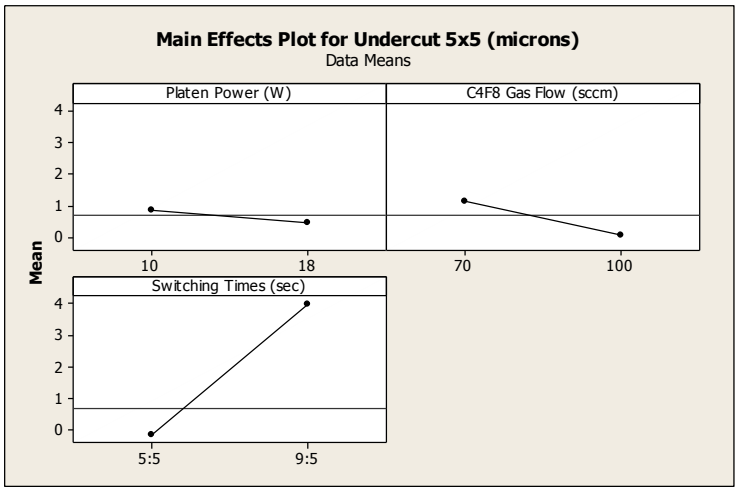

Figure 4.24 Main-effects plot for 5 x 5 μm pillars

4.2 Nickel mould insert fabrication

The fabrication of nickel mould inserts was examined. Two possible fabrication routes were considered, Sputter-coating followed by electroplating or

electroless followed by electroplating. Neither the sputter-coating nor the electroless processes could produce a coating on the silicon samples with a high enough conductivity reading for use in the electroplating process.

4.2.1 Sputter coating

The silicon inserts which were sputtered for 20 minutes were found to not be conductive enough for electroplating. The silicon inserts which were sputtered for 40 minutes did produce a slight conductive reading. However, it was decided that the conductivity of the samples needed to be improved before the nickel electroplating process could take place. Six silicon mould inserts were sputter coated in total (Figure 4.25).

.

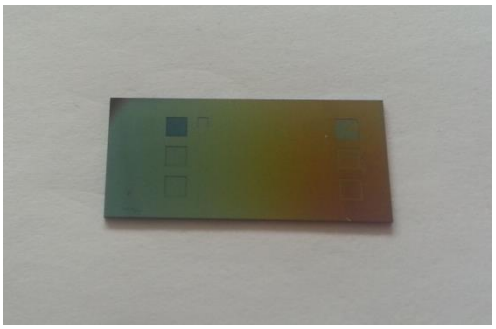

Figure 4.25 Silicon insert coated with nickel via sputter-coating

4.2.2 Electroless coating

It was found that when removed from the electroless bath the nickel deposit began to flake and detach from the sample surface over time (Figure 4.26). No silicon samples were successfully coated with a conductive nickel seed layer via the electroless process.

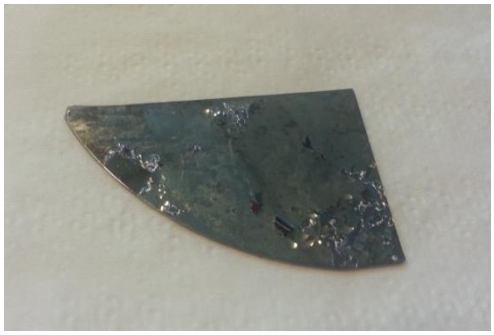

Figure 4.26 Nickel coated silicon coated via electroless

4.2.3 Summary of mould design and fabrication results

Within this chapter the results gathered during the design and fabrication of mould inserts for micro-injection moulding were discussed. A familiarisation stage in which silicon wafers was etched with eight mould inserts containing 10 – 2 μm insert features was undertaken using a chrome-on-glass mask. A design of experiment was undertaken to determine the significant factors affecting pillar undercut in the deep reactive ion etching process. It was found that the most significant factor was switching times. Silicon wafers etched with micro-channel insert features were also fabricated and examined using optical and confocal microscopy and SFEG-SEM imaging.

Silicon mould inserts were then coated in a nickel seed layer by either sputter-coating or electroless coating. Silicon mould inserts coated for 20 minutes via sputter-coating were found to not produce a conductive nickel seed layer. Those coated for 40 minutes did produce a conductive layer. However, it was decided that this nickel layer was not conductive enough for use in electroplating. With regards to electroless coating it was found that the nickel coating began to flake and detach from the silicon mould insert over time. This made the silicon mould insert coated via electroless unsuitable for electroplating. Therefore, no nickel mould inserts were produced for use in micro-injection moulding

5 Polymer micro-injection moulding results

The following chapter discusses the design of experiment approach used during the examination of the fabrication of high density polyethylene and polypropylene replicates via micro-injection moulding. The design of experiment approach used examined the effect of moulding temperature, cooling time, holding pressure and injection speed on the production of polymer pillar features ranging from 80 x 80 μm to 5 x 5 μm. Pareto charts and main effects plots were used to determine the most significant factor for the various responses selected. The responses examined were part mass, buffer mass, pillar width and height and the variation of the replicate features from the silicon mould insert.

Chapter section *5.1 Design of experiments for micro-channel insert features* discusses the identification of significant factors relating to pillar width and height and the variation of the replicate feature dimensions from the silicon mould insert. This is done for high density polyethylene and polypropylene replicates structured with micro-channel features using Pareto charts. Observations regarding the appearance of the replicate surfaces and features are also outlined. In section *5.2 Design of experiment of 10 – 2 μm insert features* the most significant factors and the main-effects on the part and buffer mass of high density polyethylene and polypropylene replicates structures with 10 – 2 μm features are outlined. Section *5.2* also outlines the most significant factor and the main-effect on the pillar dimensions and the variation of replicate feature dimensions from the silicon mould insert for polypropylene and high density polyethylene replicates. The appearance of the replicate features and surfaces is also displayed and observations detailed.

5.1 Design of experiments for micro-channel insert features

A design of experiment approach was used to examine how moulding temperature, cooling time, holding pressure and injection affect the production

of polypropylene and high density polyethylene pillar features ranging from 80 x 80 μm to 5 x 5 μm by micro-injection moulding. The responses examined via statistical analysis were part and buffer mass as well as pillar width and height and the variation of the replicate feature dimensions from the silicon mould insert.

Pillars with twenty-seven different width dimensions were examined. The replicates produced were structured with micro-channel insert features. As explained in *Chapter 3 Methodology*, micro-channel insert features were designed to incorporate three different feature arrangements in both pillar and hole forms (Figure 5.1 and Figure 5.2). Squares 3 and 4 were adapted from the work of Fang et al to produce micro-channels of varying pillar size and spacing across the sample surface to produce a wettability gradient. Squares 5 and 6 used the surface design proposed by Shastry et al, which used the variation of pillar width and gap length to produce a superhydrophobic surface with a surface-energy gradient. Squares 1 and 2 were designed by Morel by combining the design patterns proposed by Shastry et al and Fang et al. The presence of micro-channels was adapted from the work of Fang et al and the pillar gradient used by Shastry et al. The features in squares 1, 3 and 5 resulted in hole features. Whereas features in squares 2, 4 and 6 resulted in pillar features.

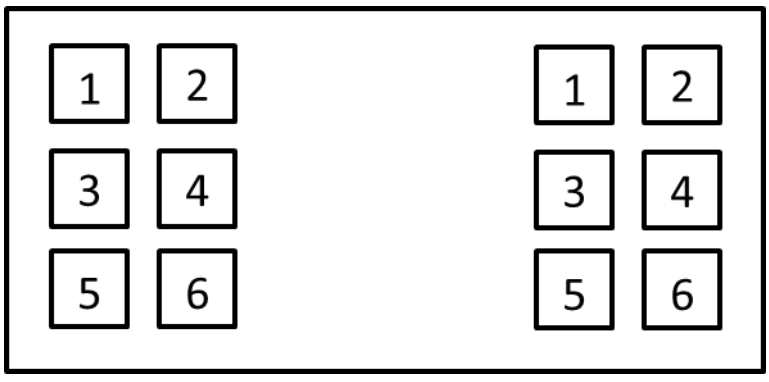

Figure 5.1 Schematic of silicon inserts

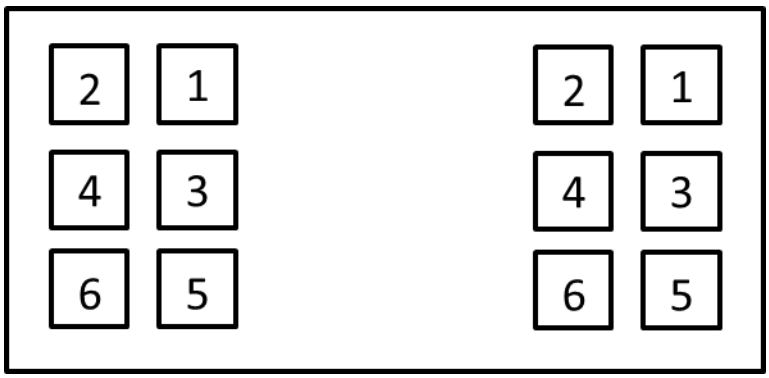

Figure 5.2 Schematic of polymer replicates

The Morel and Fang designs in squares 1, 2, 3 and 4 contained micro-channels. Two different micro-channels with varying feature dimensions were used in each square (Table 5.1).

Table 5.2 Feature dimensions in micro - channels

Square	Micro-channel 1 (μm)	Micro-channel 2 (μm)
1 & 2 (Morel)	30 x 30	30 x 10
	25 x 30	25 x 10
	20 x 30	20 x 10
	15 x 30	15 x 10
	10 x 30	10 x 10
	5 x 30	5 x 10
3 & 4 (Fang)	80 x 80	80 x 29
	53 x 80	53 x 29
	43 x 80	43 x 29
	29 x 80	29 x 29
	19 x 80	19 x 29

In order to simplify analysis the pillars were separated into three groups according to the pillar widths. The width ranges selected were 40 – 80 μm, 20 – 39 μm and 5 – 19 μm (Table 5.3). The following subsections will use these three ranges to present the data collected.

Table 5.3 Pillars included in analysis ranges

Dimension range (μm)	Pillar dimensions (μm)	Surface area/volume ratio
40 – 80	80 x 80	0.100
	53 x 80	0.113
	43 x 80	0.122
	80 x 29	0.144
	53 x 29	0.157
	43 x 29	0.165
20 – 39	30 x 30	0.183
	30 x 30[§]	0.183
	30 x 10	0.317
	29 x 80	0.144
	29 x 29	0.188
	25 x 30	0.197
	25 x 10	0.330
	25 x 25	0.210
	20 x 30	0.217
	20 x 10	0.350
	20 x 20	0.250
5 - 19	19 x 80	0.180
	19 x 29	0.224
	15 x 30	0.250
	15 x 10	0.383
	15 x 15	0.317
	10 x 30	0.317
	10 x 10	0.450
	10 x 10[**]	0.450
	5 x 30	0.517
	5 x 10	0.650
	5 x 5	0.850

[§] 30 x 30 μm features from squares 5 and 6

[**] 10 x 10 μm features from squares 5 and 6

5.1.1 Polypropylene pillar dimensions

The height and width of ten pillars at each pillar size were measured and an average calculated. The average measurements taken and used in statistical analysis are displayed in the appendix of this thesis.

It was noted that the 10 x10 μm, 10 x 10 μm (from square 6), 5 x 30 μm, 5 x 10 μm and 5 x 5 μm features were not replicated.

5.1.1.1 Statistical analysis of 40 – 80 μm polypropylene pillar features

Using the Pareto charts generated injection speed was identified as the most significant factor for the width of 80 x 29 μm pillars (Figure 5.3). Holding pressure was found to be the most significant factor for the height of 53 x 29 μm pillars (Figure 5.4) and the interaction between mould temperature and cooling time was found to be the most significant for the height of 43 x 29 μm pillars (Figure 5.5). Significant factors were not identified for the height of the 80 x 80, 80 x 29, 53 x 80 or the 43 x 80 μm pillars. Significant factors were also not identified for the width of the 80 x 80, 53 x 80, 53 x 29, 43 x 80 and the 43 x 29 μm pillars.

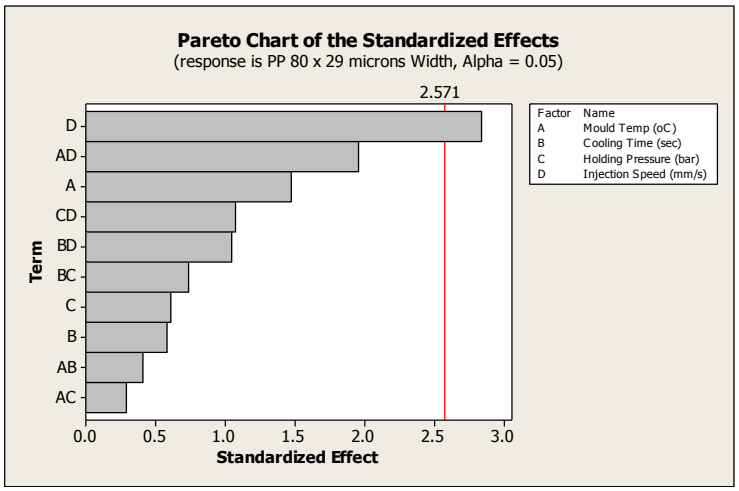

Figure 5.3 Most significant factor for width of 80 x 29 μm polypropylene pillars

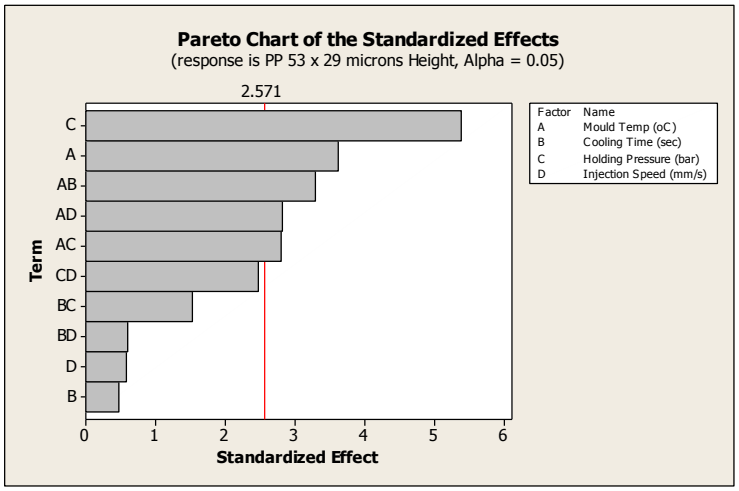

Figure 5.4 Most significant factor for height of 53 x 29 μm polypropylene pillars

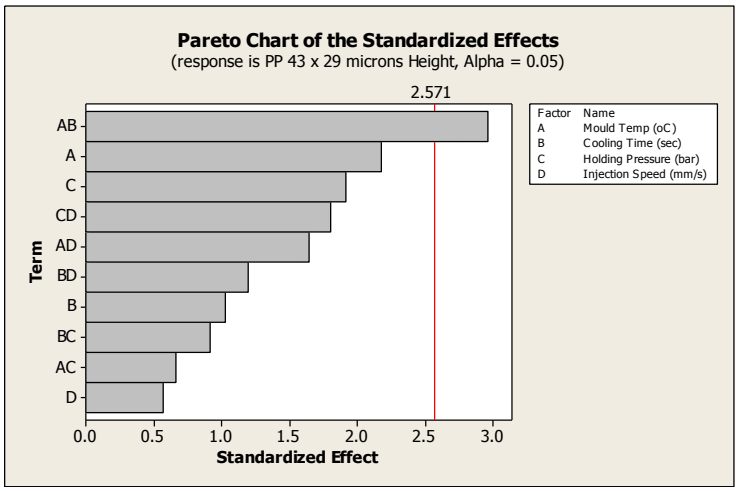

Figure 5.5 Most significant factor for height of 43 x 29 μm polypropylene pillars

5.1.1.2 Statistical analysis of 20 – 39 μm pillar features

Upon examination of the generated Pareto charts cooling time was found to be the most significant factor with regards to the height of the 30 x 10, 25 x 10 and 20 x 10 μm pillars (Figure 5.6, Figure 5.9 and Figure 5.11). The interaction between mould temperature and injection speed was identified as the most significant factor for the height of the 25 x 30 μm pillars (Figure 5.7). Injection speed was found to be the most significant factor for the height of the 25 x 25 μm pillars (Figure 5.8). The mould temperature was found to be most significant with regards to the 20 x 20 μm pillars (Figure 5.10). Significant factors were not identified for the height of the 30 x 30 (from squares 1 and 2), 30 x 30 (from squares 5 and 6), 29 x 80, 29 x 29 and the 20 x 30 μm pillars. Significant factors were also not identified for the width of and of the pillar features.

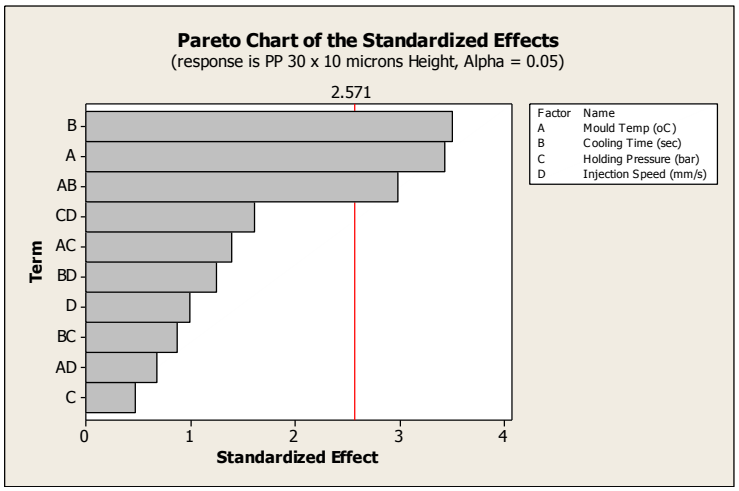

Figure 5.6 Most significant factor for height of 30 x 10 μm polypropylene pillars

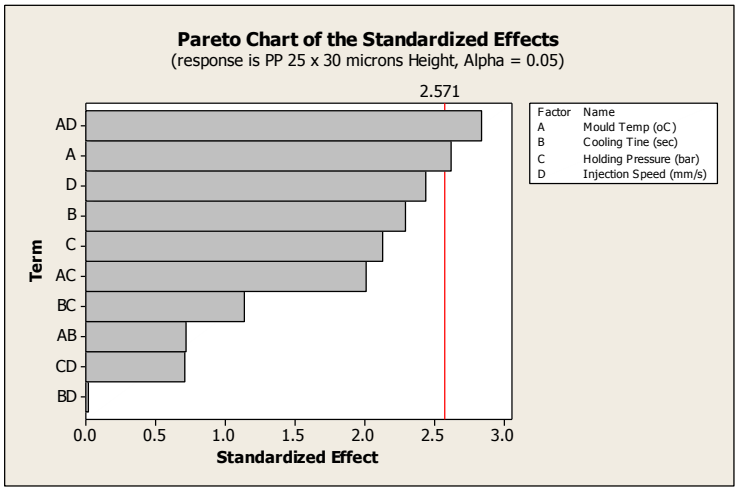

Figure 5.7 Most significant factor for height of 25 x 30 μm polypropylene pillars

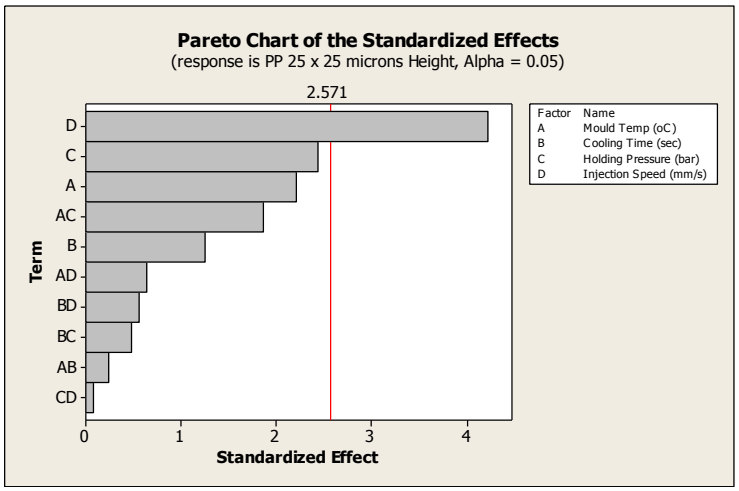

Figure 5.8 Most significant factor for height of 25 x 25 μm polypropylene pillars

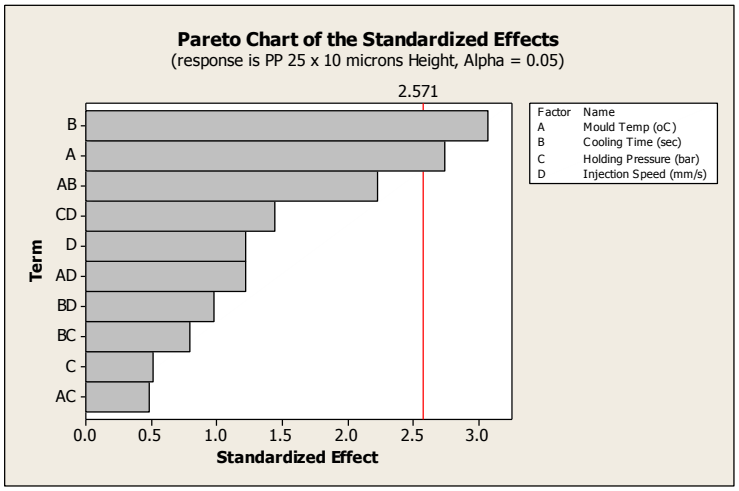

Figure 5.9 Most significant factor for height of 25 x 10 μm polypropylene pillars

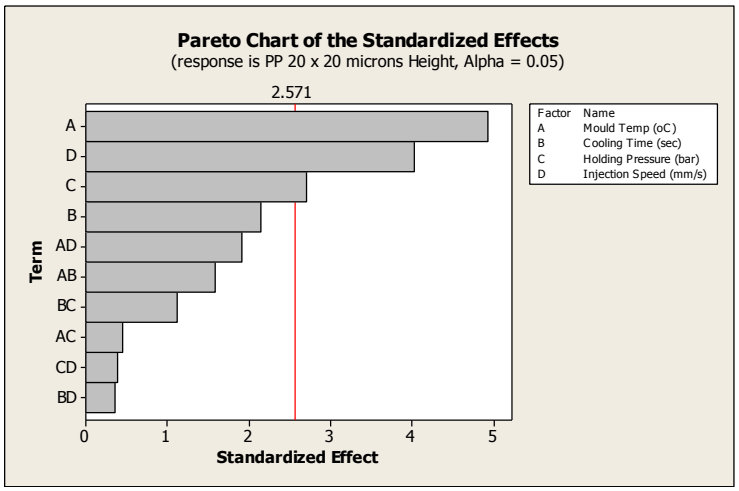

Figure 5.10 Most significant factor for height of 20 x 20 μm polypropylene pillars

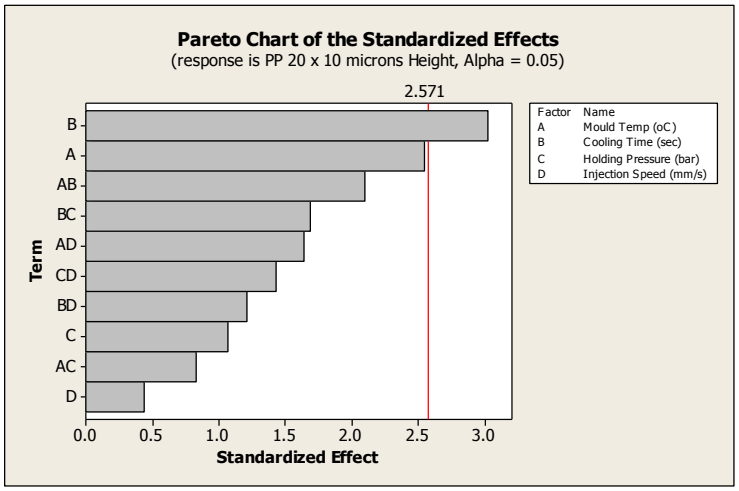

Figure 5.11 Most significant factor for height of 20 x 10 μm polypropylene pillars

5.1.1.3 Statistical analysis of 5 – 19 μm pillar features

Following the examination of the produced Pareto charts holding pressure was found to be the most significant factor regarding the height of the 19 x 80 μm pillars (Figure 5.12). Injection speed was found to be the most significant factor

for the 19 x 29 μm pillars closely followed by mould temperature (Figure 5.13). Mould temperature was identified as the most significant factor regarding the height of the 15 x 15 and the 10 x 30 μm pillars (Figure 5.14 and Figure 5.16). Cooling time was found to be the most significant factor for the 15 x 10 μm pillars (Figure 5.15). A significant factor was not identified for the height of the 15 x 30 μm pillars or for the widths of any of the pillars. As mentioned at the start of this section the 10 x10 μm, 10 x 10 μm (from square 6), 5 x 30 μm, 5 x 10 μm and 5 x 5 μm features were not replicated.

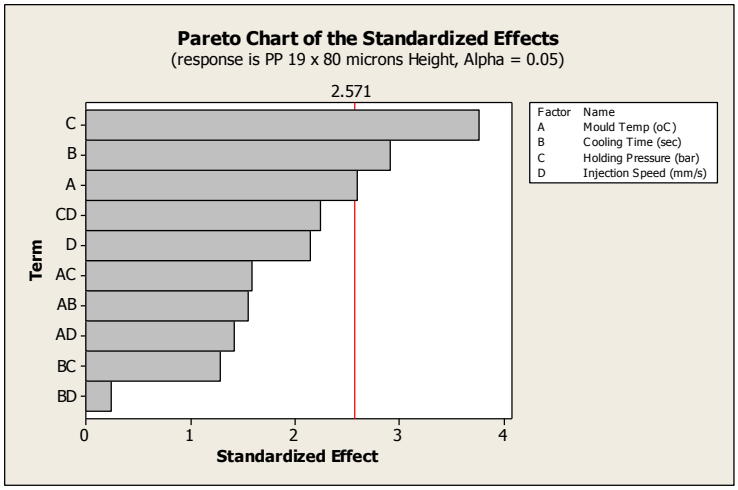

Figure 5.12 Most significant factor for height of 19 x 80 μm polypropylene pillars

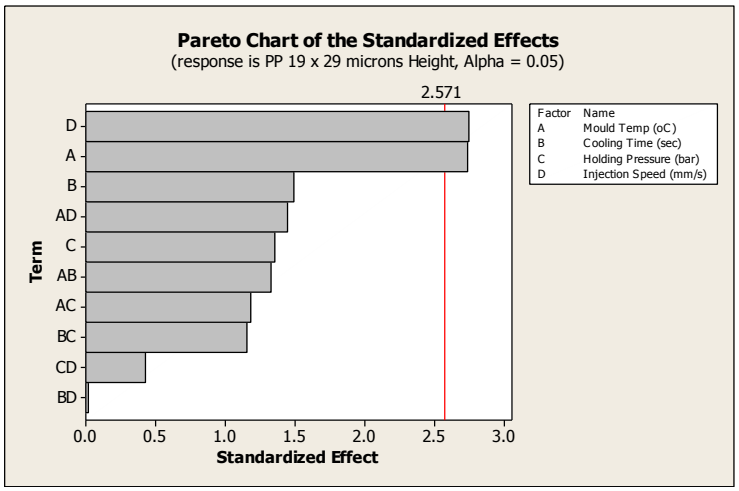

Figure 5.13 Most significant factor for height of 19 x 29 μm polypropylene pillars

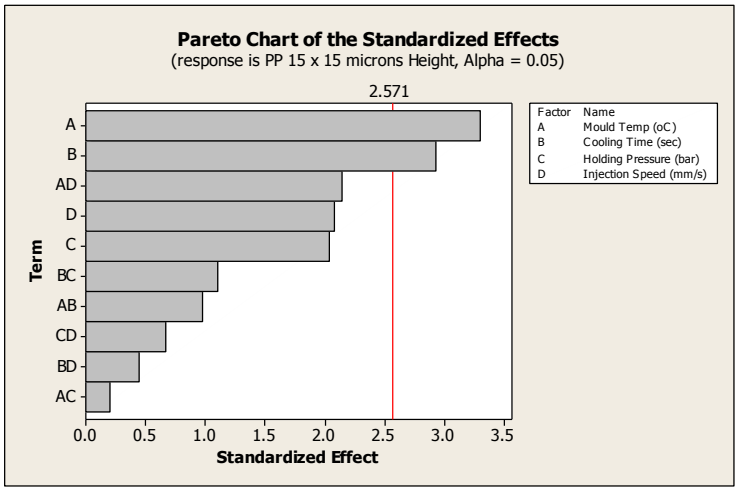

Figure 5.14 Most significant factor for height of 15 x 15 μm polypropylene pillars

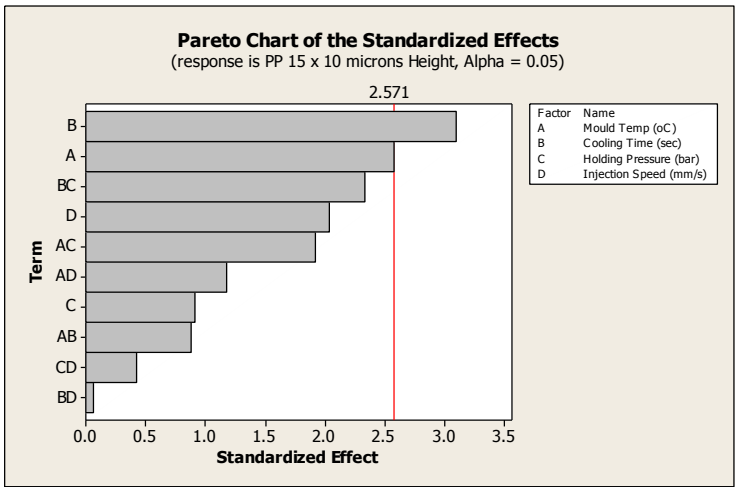

Figure 5.15 Most significant factor for height of 15 x 10 μm polypropylene pillars

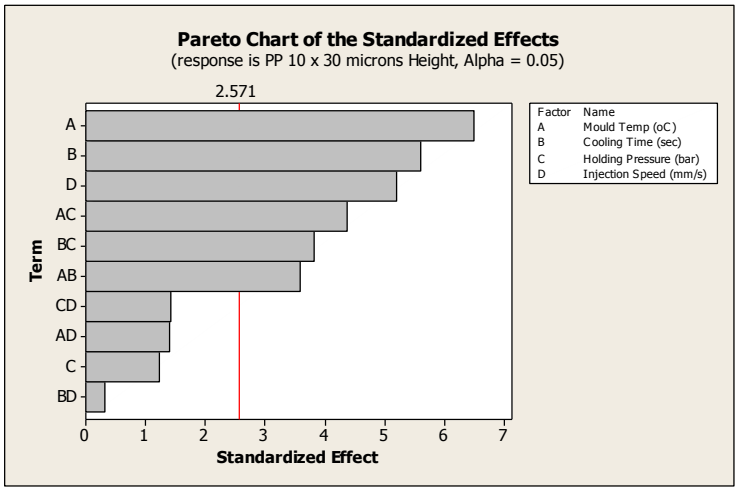

Figure 5.16 Most significant factor for height of 10 x 30 μm polypropylene pillars

5.1.1.4 Comparison of polypropylene pillar heights

A comparison was made between the intended designed height of pillars, the height of pillars on the silicon mould insert and the height of the polypropylene replicated pillars. The results of this comparison were categorised into three

surface area/volume ratio categories and are displayed in Figure 5.17, Figure 5.18 and Figure 5.19.

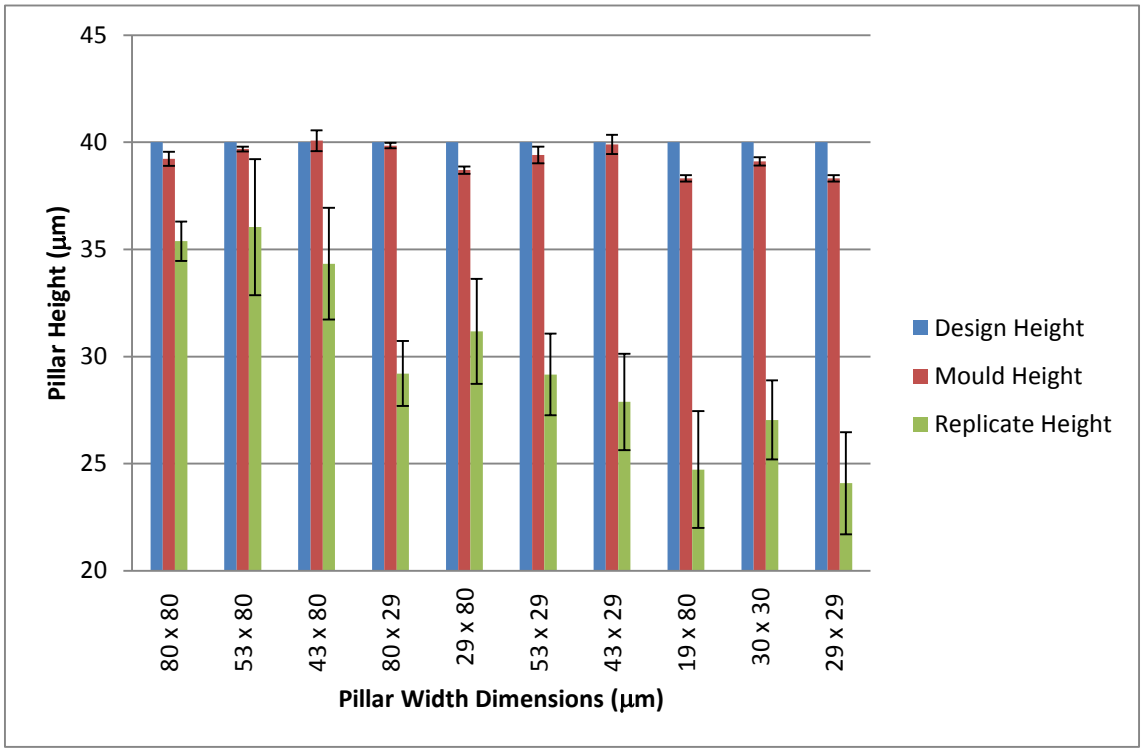

Figure 5.17 Comparison of designed feature height, mould feature height and replicate feature height for polypropylene pillars in the 0.1 – 0.19 surface area/volume range

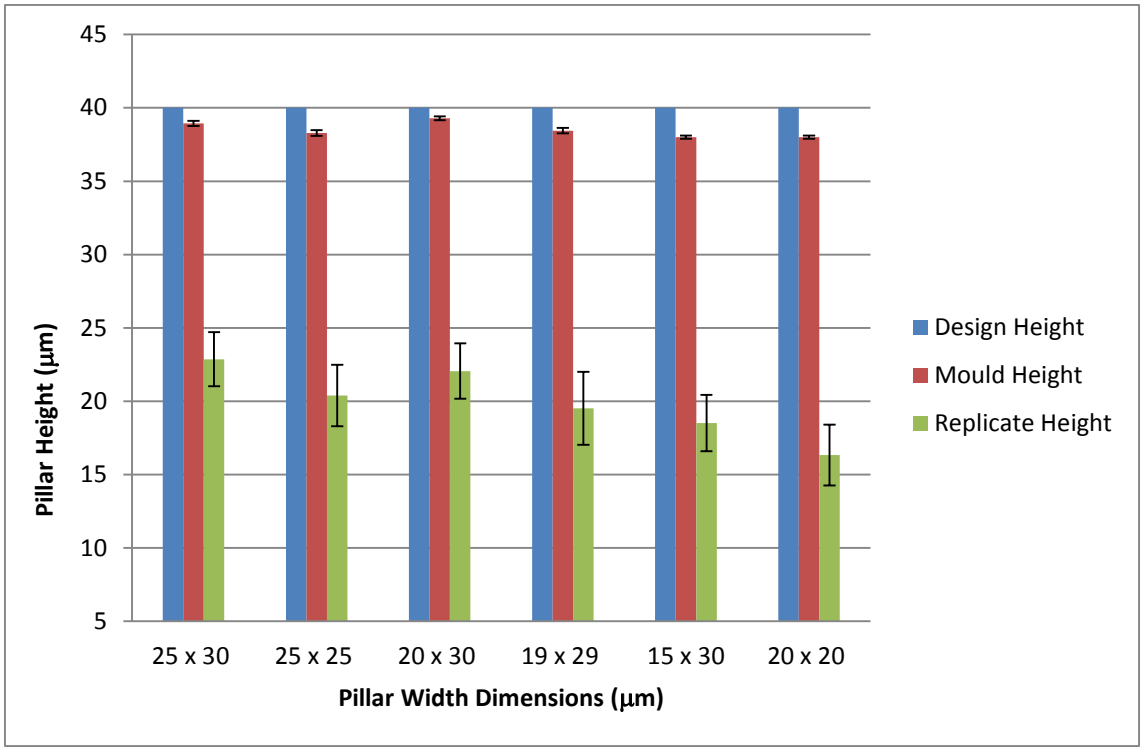

Figure 5.18 Comparison of designed feature height, mould feature height and replicate feature height for polypropylene pillars in the 0.19 – 0.3 surface area/volume ratio range

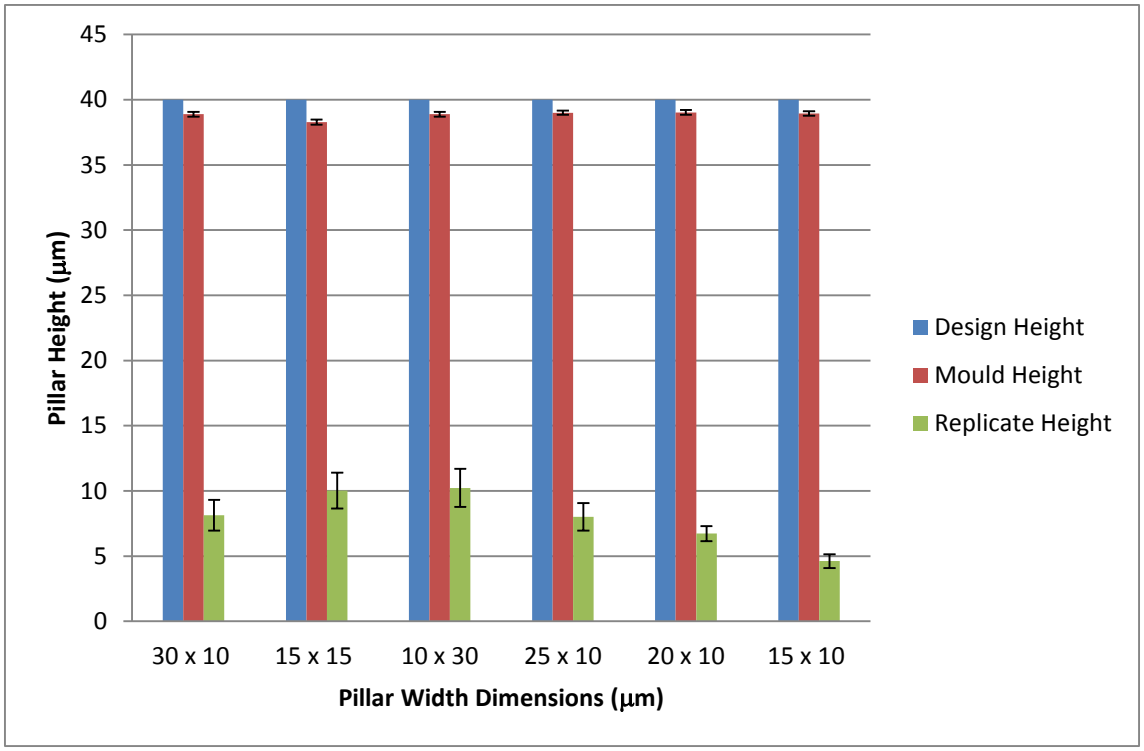

Figure 5.19 Comparison of designed feature height, mould feature height and replicate feature height for polypropylene pillars in the 0.3 – 0.9 surface area/volume ratio range

5.1.2 High density polyethylene pillar dimensions

The height and width of ten pillars at each pillar size were measured and an average calculated. The average measurements taken and used in statistical analysis are displayed in the appendix of this thesis.

It was noted that the 10 x10 μm, 10 x 10 μm (from square 6), 5 x 30 μm, 5 x 10 μm and 5 x 5 μm features were not replicated.

5.1.2.1 Statistical analysis of 40 – 80 μm pillar features

Examination of the generated Pareto charts identified mould temperature as the most significant factor for the height of the 80 x 29, 53 x 29 and 43 x 29 μm pillars (Figure 5.20 - Figure 5.22). No significant factor was identified for the width of any of the pillars or for the height of the 80 x 80, 53 x 80 or the 43 x 80 μm pillars.

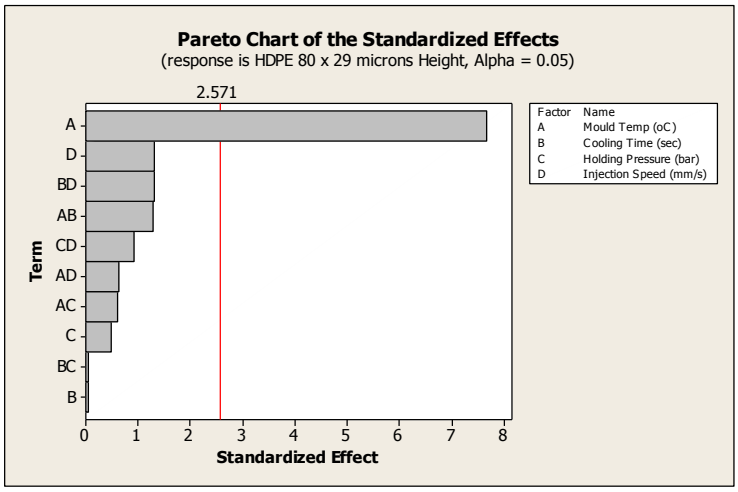

Figure 5.20 Most significant factor for height of 80 x 29 μm high density polyethylene pillars

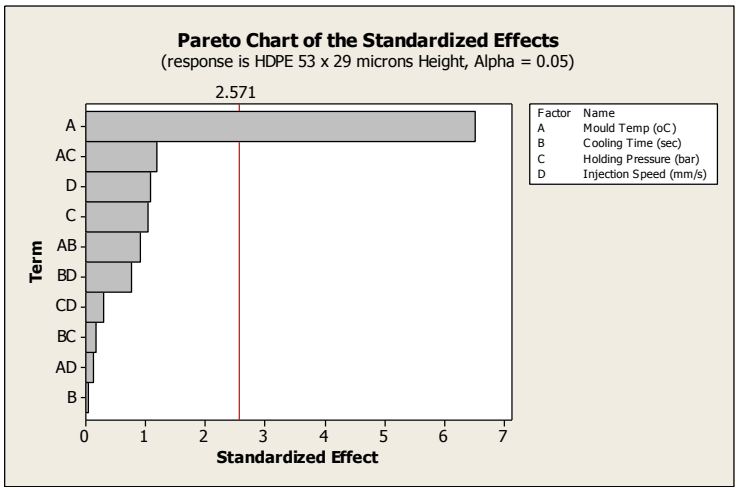

Figure 5.21 Most significant factor for height of 53 x 29 μm high density polyethylene pillars

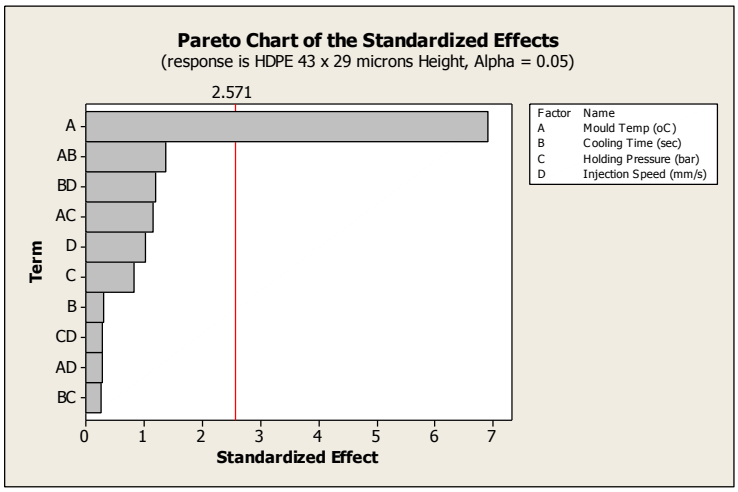

Figure 5.22 Most significant factor for height of 43 x 29 μm high density polyethylene pillars

5.1.2.2 Statistical analysis of 20 – 39 μm pillar features

Examination of the generated Pareto charts identified mould temperature as the most significant factor for the height of all the pillars (Figure 5.23 - Figure 5.25, Figure 5.27 - Figure 5.31 and Figure 5.33 - Figure 5.35). Significant factors for the width of pillars were only identified for the 30 x 10, 25 x 10 and 20 x 10 μm pillars (Figure 5.26, Figure 5.32 and Figure 5.36). For which mould temperature was found to be the most significant factor.

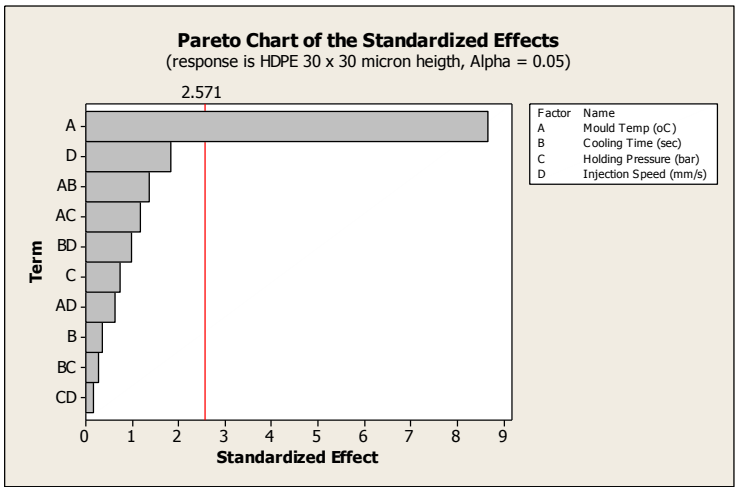

Figure 5.23 Most significant factor for height of 30 x 30 μm high density polyethylene pillars on squares 5 and 6

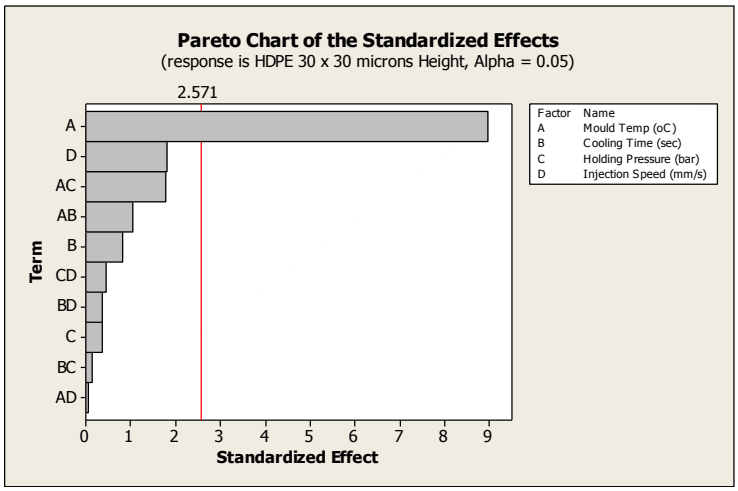

Figure 5.24 Most significant factor for height of 30 x 30 μm high density polyethylene pillars from squares 1 and 2

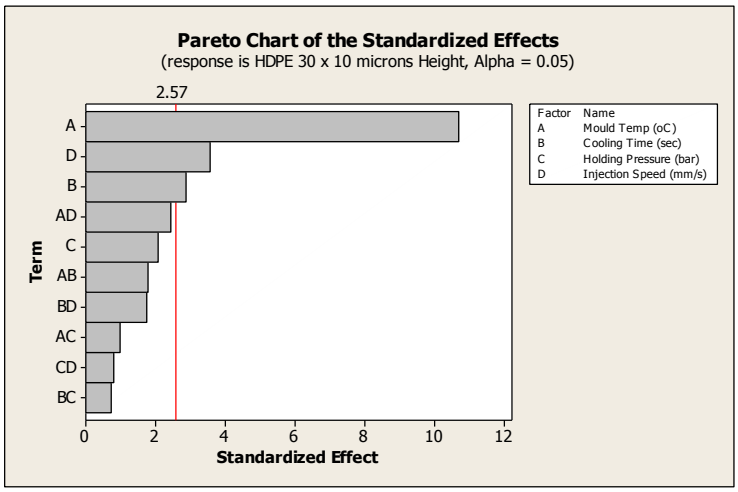

Figure 5.25 Most significant factor for height of 30 x 10 μm high density polyethylene pillars

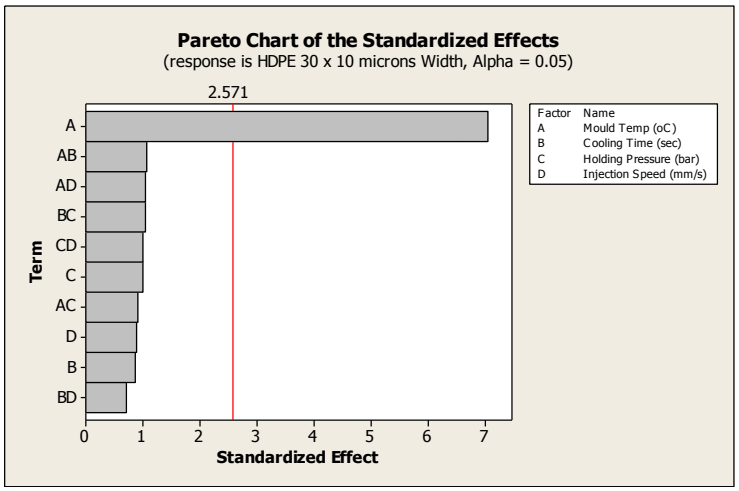

Figure 5.26 Most significant factor for width of 30 x 10 μm high density polyethylene pillars

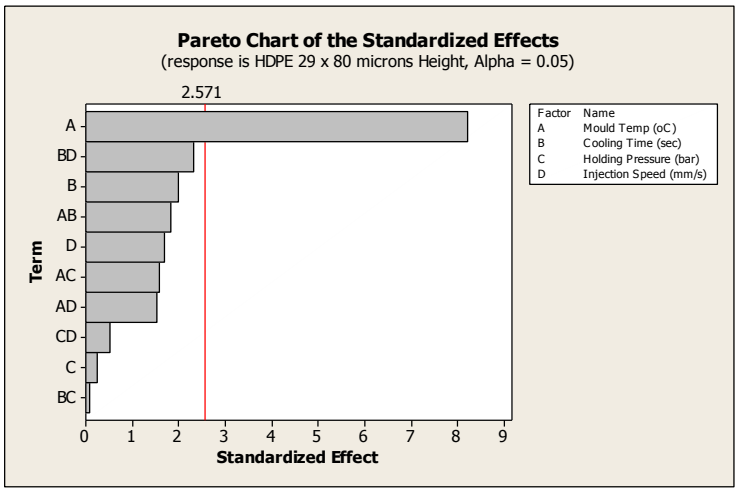

Figure 5.27 Most significant factor for height of 29 x 80 μm high density polyethylene pillars

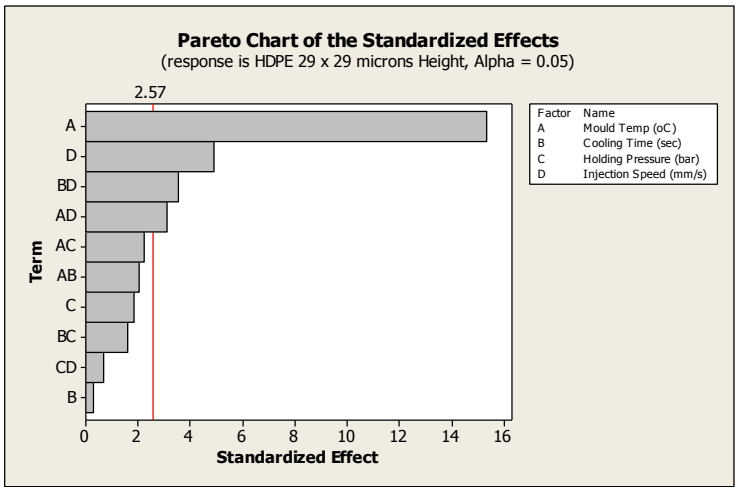

Figure 5.28 Most significant factor for height of 29 x 29 μm high density polyethylene pillars

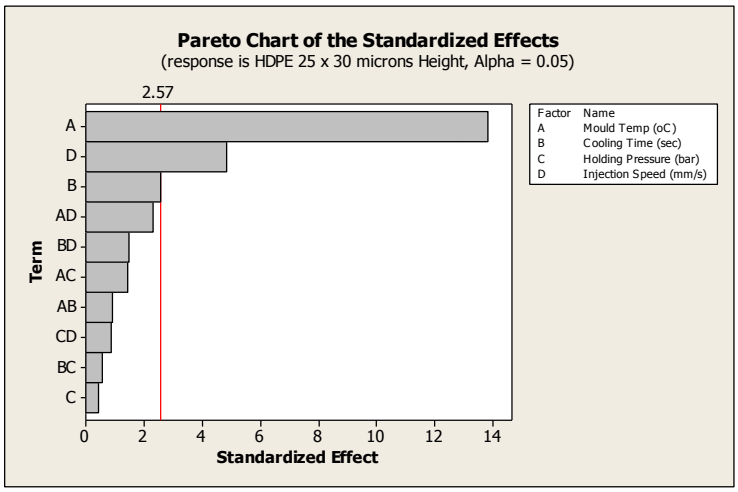

Figure 5.29 Most significant factor for height of 25 x 30 μm high density polyethylene pillars

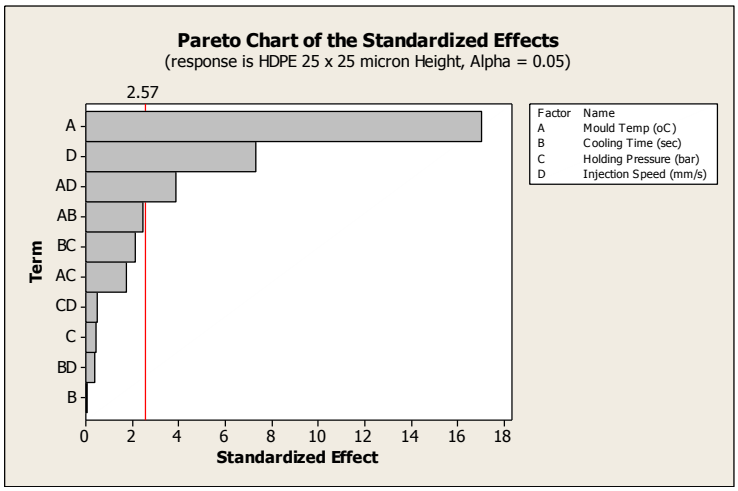

Figure 5.30 Most significant factor for height of 25 x 25 μm high density polyethylene pillars

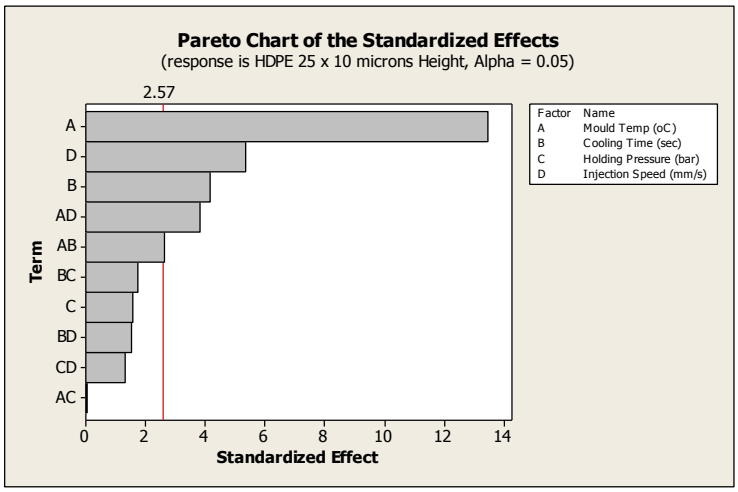

Figure 5.31 Most significant factor for height of 25 x 10 μm high density polyethylene pillars

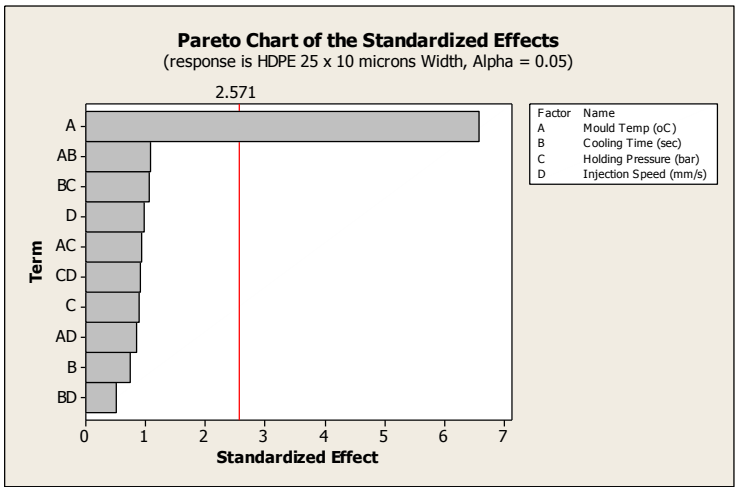

Figure 5.32 Most significant factor for width of 25 x 10 μm high density polyethylene pillars

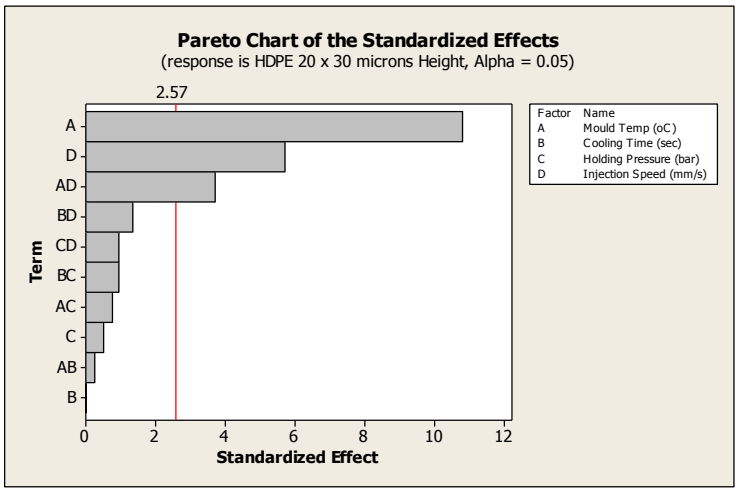

Figure 5.33 Most significant factor for height of 20 x 30 μm high density polyethylene pillars

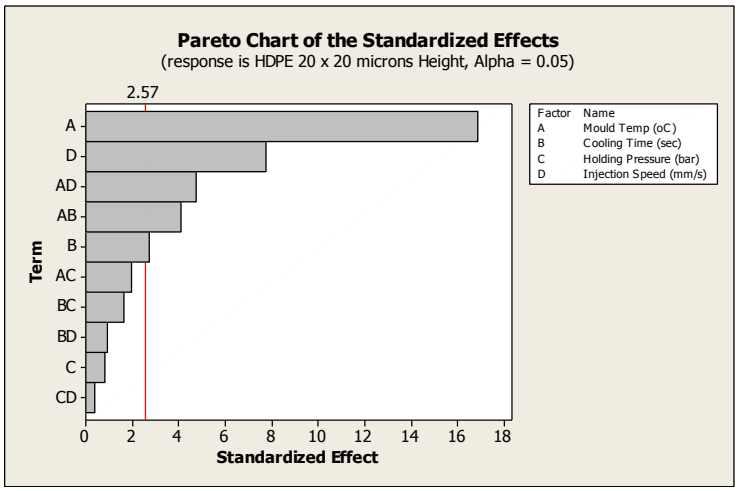

Figure 5.34 Most significant factor for height of 20 x 20 μm high density polyethylene pillars

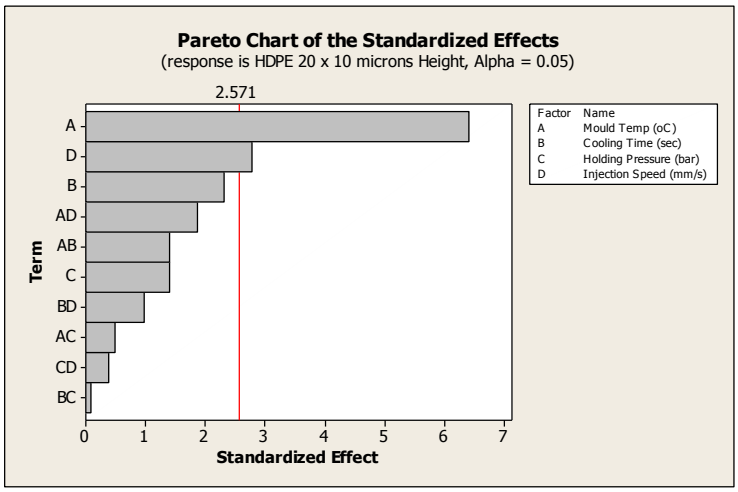

Figure 5.35 Most significant factor for height of 20 x 10 μm high density polyethylene pillars

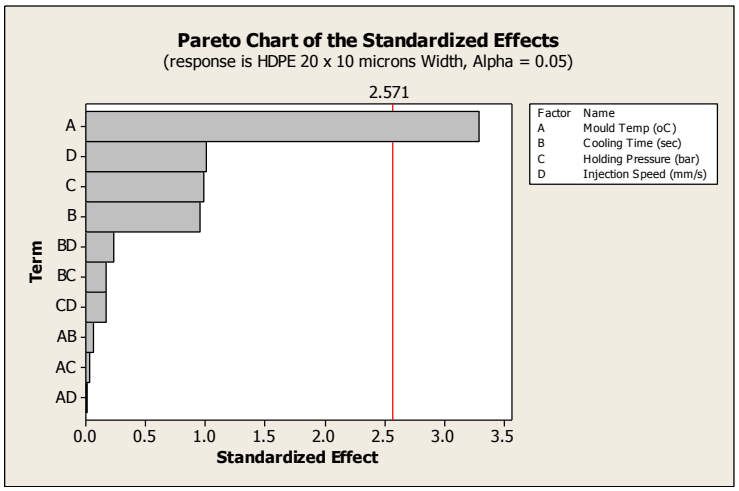

Figure 5.36 Most significant factor for width of 20 x 10 μm high density polyethylene pillars

5.1.2.3 Statistical analysis of 5 – 19 μm pillar features

As mentioned at the start of this section the 10 x10 μm, 10 x 10 μm (from square 6), 5 x 30 μm, 5 x 10 μm and 5 x 5 μm features were not replicated. However, upon examination of the Pareto charts mould temperature was found to be the most significant factor for all of the replicated pillars examined (Figure 5.37-Figure 5.48).

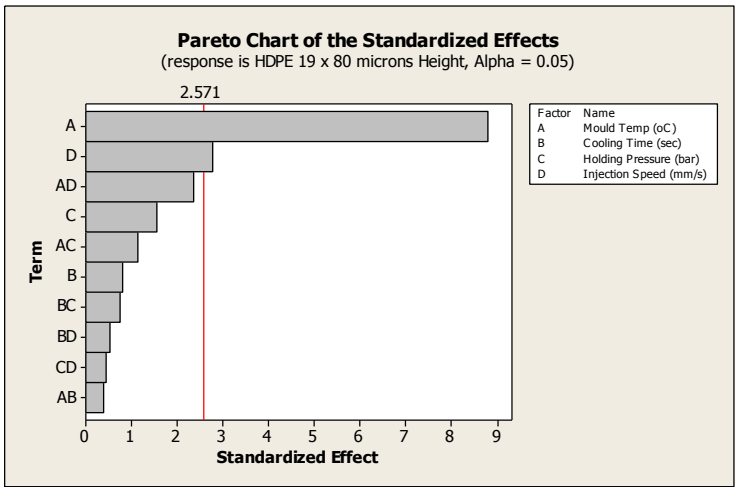

Figure 5.37 Most significant factor for height of 19 x 80 μm high density polyethylene pillars

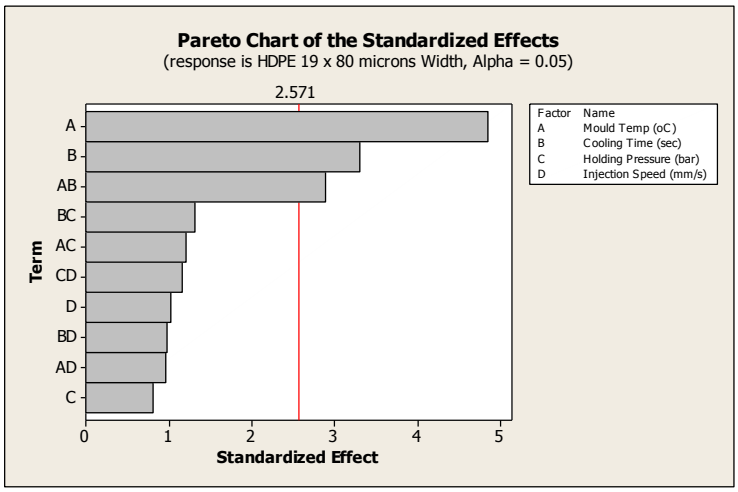

Figure 5.38 Most significant factor for width of 19 x 80 μm high density polyethylene pillars

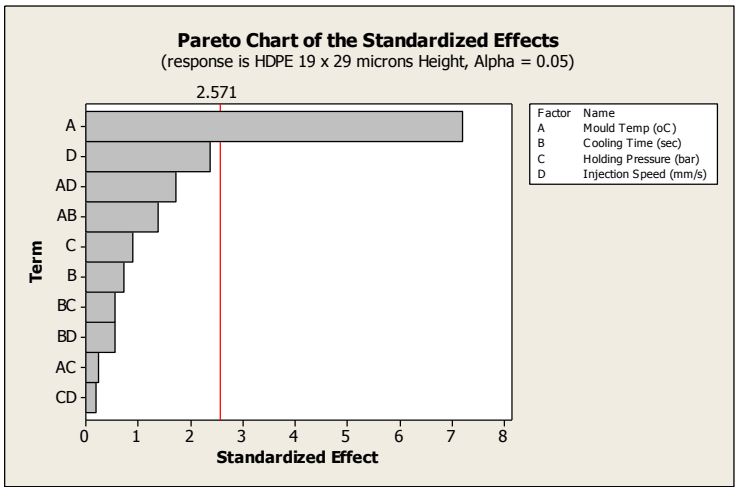

Figure 5.39 Most significant factor for height of 19 x 29 μm high density polyethylene pillars

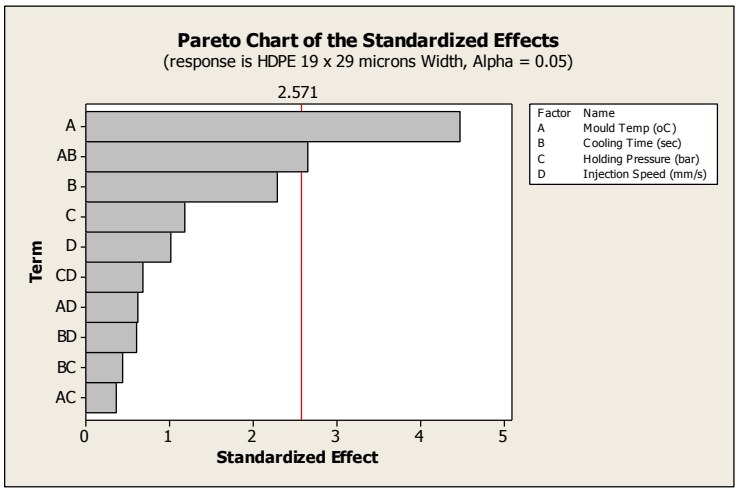

Figure 5.40 Most significant factor for width of 19 x 29 μm high density polyethylene pillars

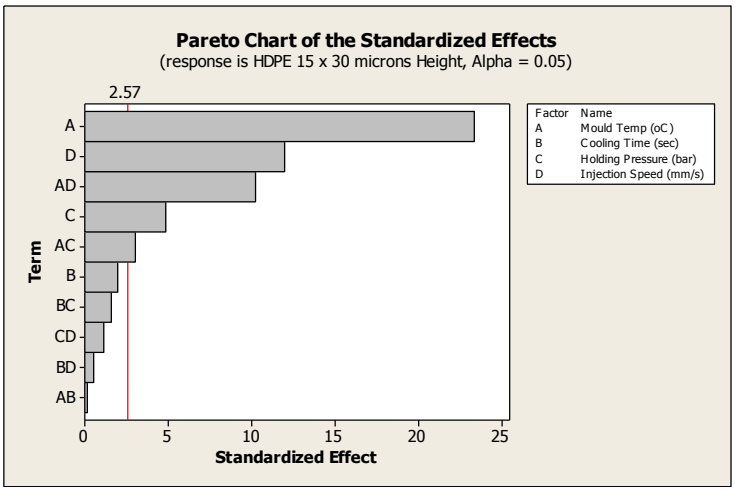

Figure 5.41 Most significant factor for height of 15 x 30 μm high density polyethylene pillars

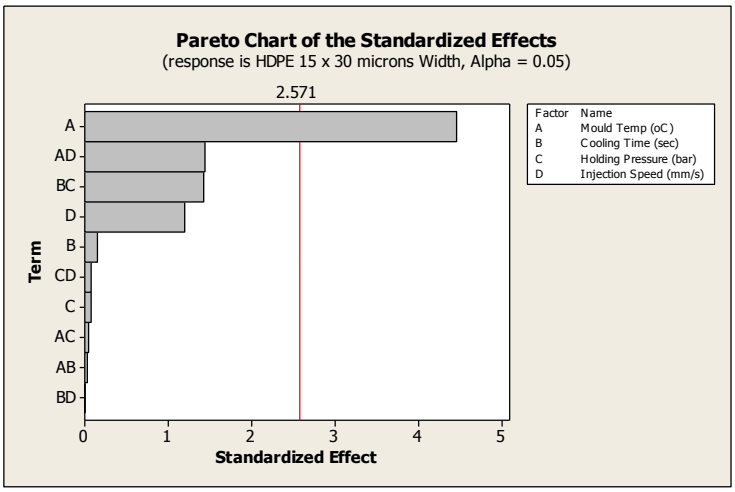

Figure 5.42 Most significant factor for width of 15 x 30 μm high density polyethylene pillars

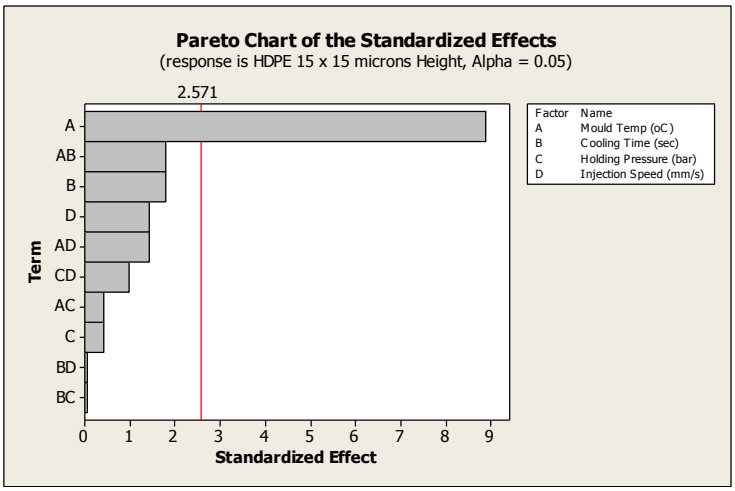

Figure 5.43 Most significant factor for height of 15 x 15 μm high density polyethylene pillars

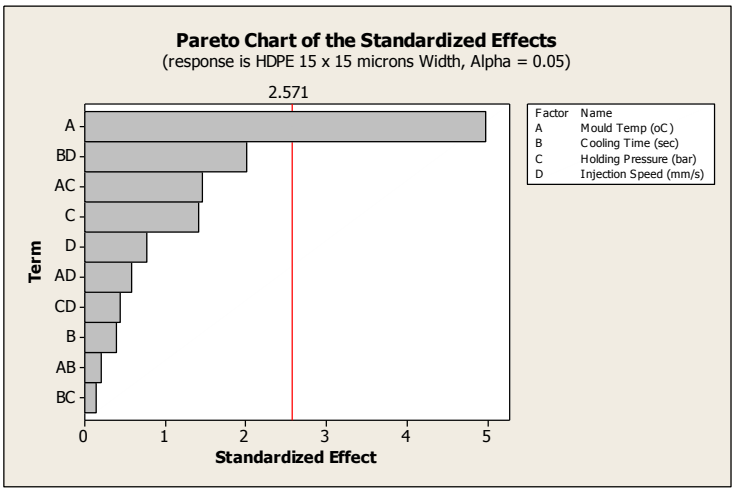

Figure 5.44 Most significant factor for width of 15 x 15 μm high density polyethylene pillars

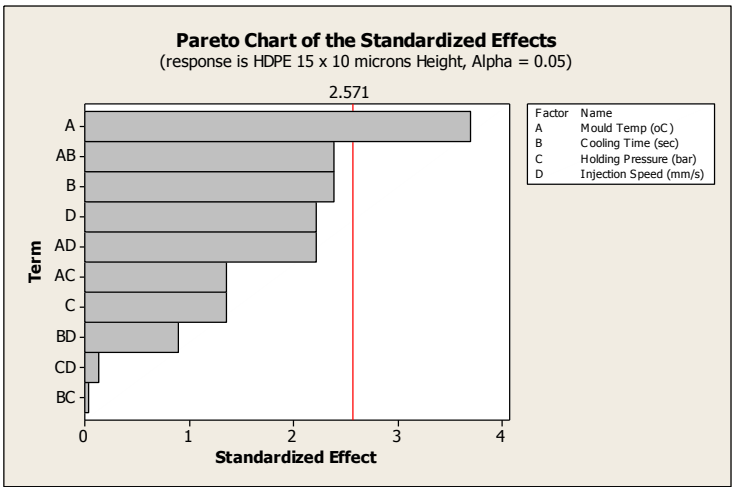

Figure 5.45 Most significant factor for height of 15 x 10 μm high density polyethylene pillars

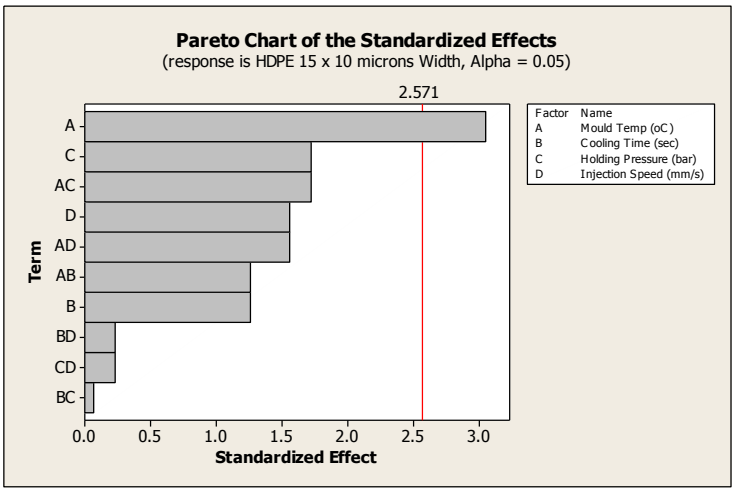

Figure 5.46 Most significant factor for width of 15 x 10 μm high density polyethylene pillars

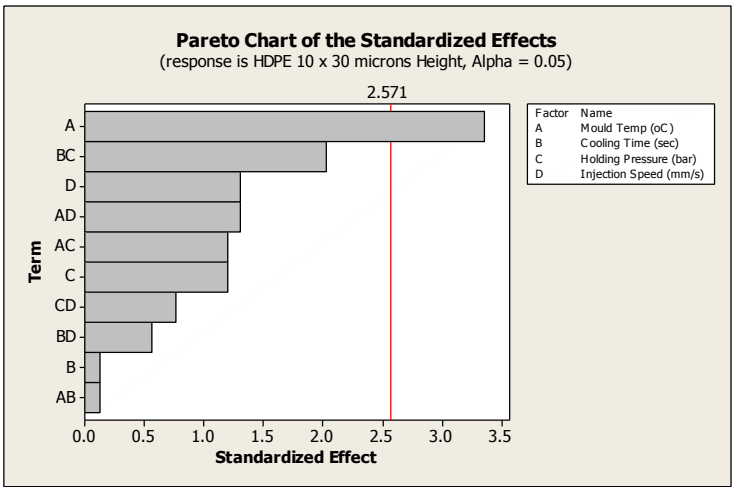

Figure 5.47 Most significant factor for height of 10 x 30 μm high density polyethylene pillars

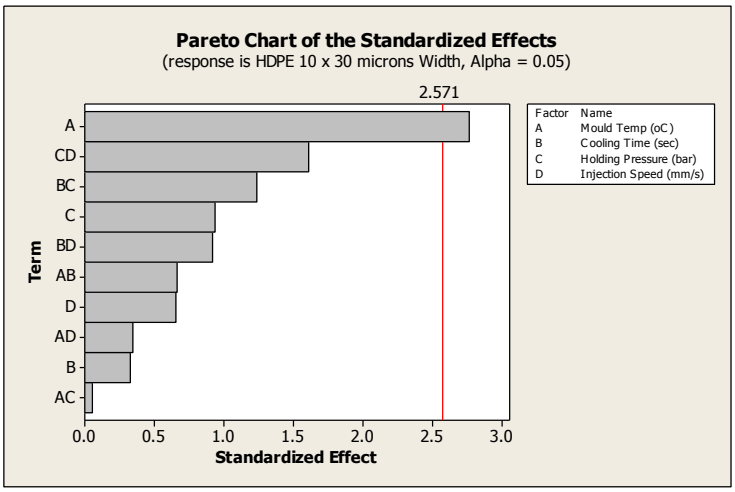

Figure 5.48 Most significant factor for width of 10 x 30 μm high density polyethylene pillars

5.1.3 Polypropylene pillar feature variation from silicon mould insert dimensions

The feature variation between the polypropylene moulded replicate and the silicon mould insert was calculated using the average measurements for height and width obtain in section *5.1.1 Polypropylene pillar dimensions*. The measurements taken and used in statistical analysis are displayed in the appendix of this thesis.

5.1.3.1 Statistical analysis of 40 – 80 μm pillar feature variation from silicon mould insert

After examination of the generated Pareto charts injection speed was identified as the most significant factor regarding the variation of the replicate pillar from the silicon mould insert for the width of the 80 x 29 μm pillars (Figure 5.49). Holding pressure was found to be the most significant factor for the height of the 53 x 29 μm pillars (Figure 5.50). The interaction between mould temperature and cooling time was found to be most significant for the height of the 43 x 29 μm pillars (Figure 5.51). Significant factors were not identified for the replicate pillar height variation from the silicon mould insert for the 80 x 80, 53 x 80, 43 x 80 and the 80 x 29 μm pillars. Significant factor were also not found for the replicate pillar width variation from the silicon mould insert for the 80 x 80, 53 x 80, 53 x 29, 43 x 80 and the 43 x 29 μm pillars.

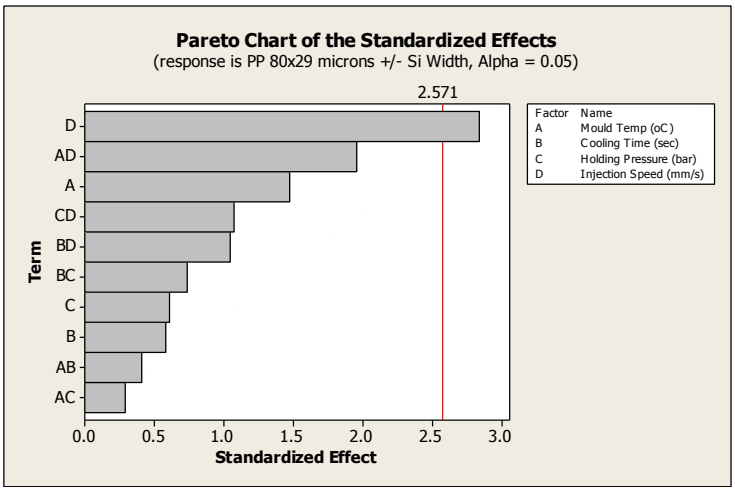

Figure 5.49 Most significant factor for the variation in the width of 80 x 29 μm polypropylene pillars from the silicon mould insert

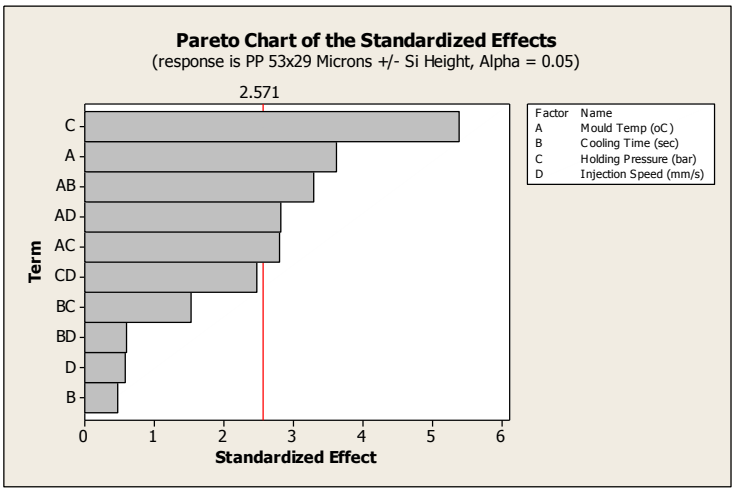

Figure 5.50 Most significant factor for the variation in the height of 53 x 29 μm polypropylene pillars from the silicon mould insert

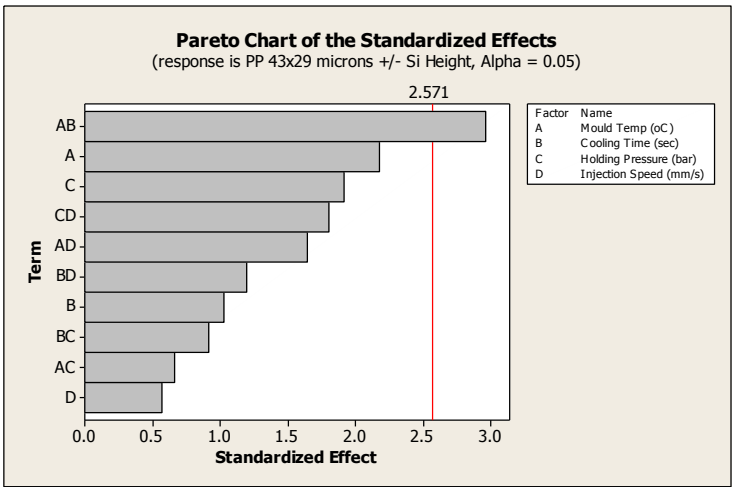

Figure 5.51 Most significant factor for the variation in the height of 43 x 29 μm polypropylene pillars from the silicon mould insert

5.1.3.2 Statistical analysis of 20 – 39 μm pillar feature variation from silicon mould insert

Upon examination of the Pareto charts regarding the variation of the replicate pillar dimensions from the silicon mould insert cooling time was identified as the most significant factor for the height of the 30 x 10, 25 x 10 and 20 x 10 μm pillars (Figure 5.52, Figure 5.55 and Figure 5.57). The interaction between mould temperature and injection speed was found to be the most significant factor for the height of the 25 x 30 μm pillars (Figure 5.53). Injection speed was identified as the most significant factor for the height of the 25 x 25 μm pillars (Figure 5.54). Mould temperature was found to be the most significant factor for the height of the 20 x 20 and 15 x 15 μm pillars (Figure 5.56 and Figure 5.58). Significant factor were not identified for the variation of pillar width from the silicon mould insert for any of the pillars. Significant factors were also not identified for the variation of pillar width from the silicon mould insert for the 30 x 30 (from square 2), 30 x 30 (from square 6), 29 x 80, 29 x 29 or the 20 x 30 μm pillars.

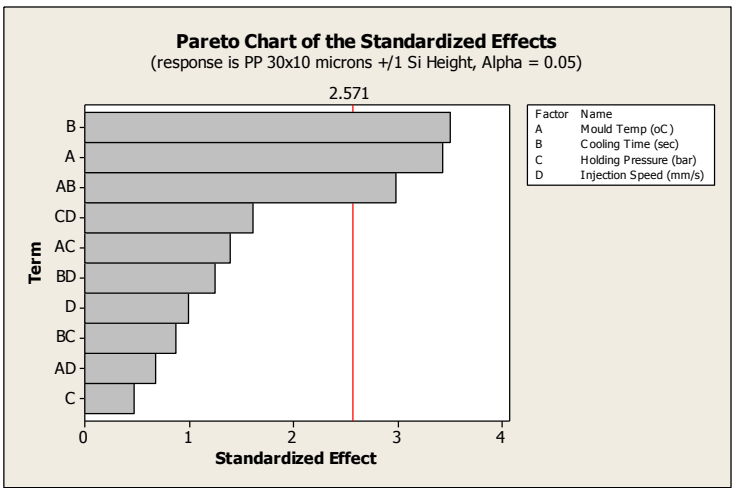

Figure 5.52 Most significant factor for the variation in the height of 30 x 10 μm polypropylene pillars from the silicon mould insert

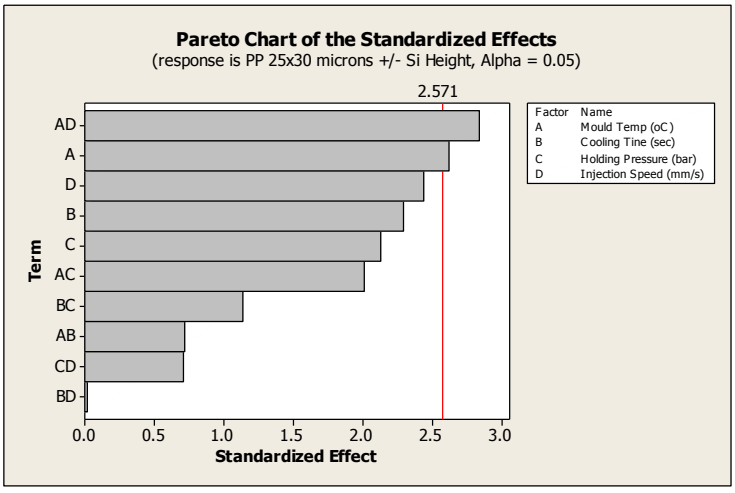

Figure 5.53 Most significant factor for the variation in the height of 25 x 30 μm polypropylene pillars from the silicon mould insert

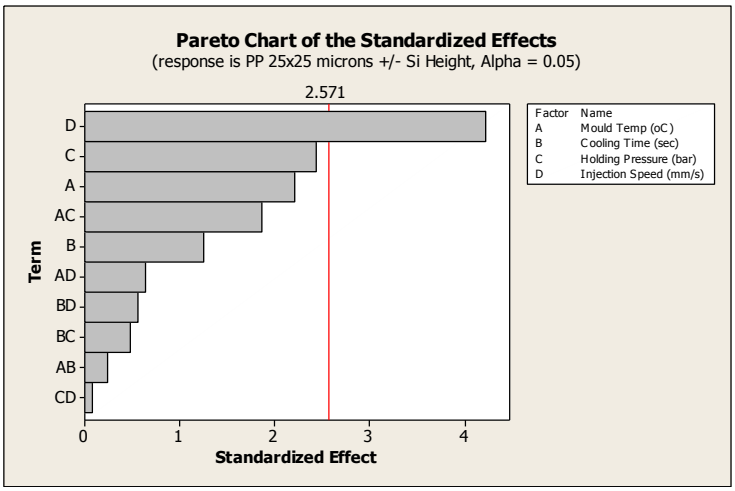

Figure 5.54 Most significant factor for the variation in the height of 25 x 25 μm polypropylene pillars from the silicon mould insert

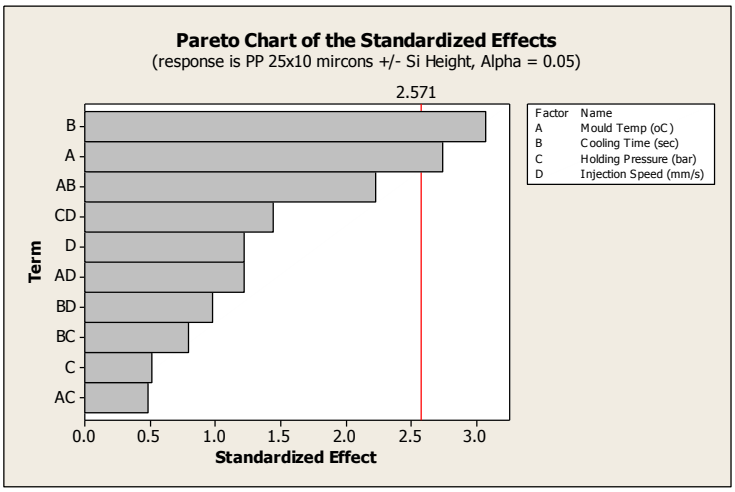

Figure 5.55 Most significant factor for the variation in the height of 25 x 10 μm polypropylene pillars from the silicon mould insert

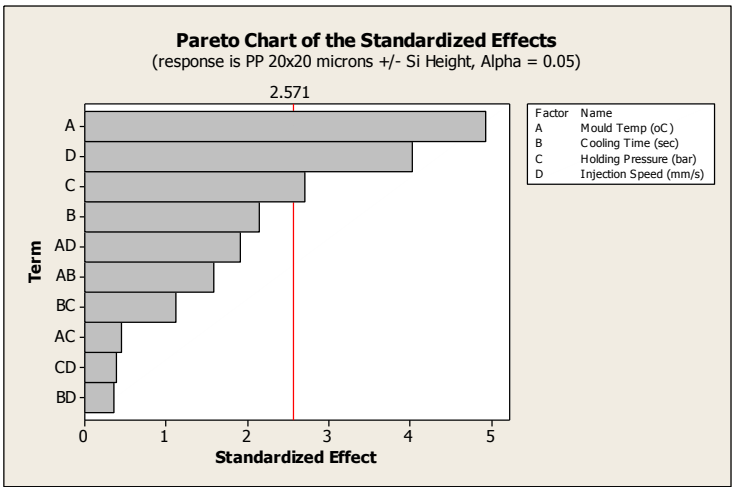

Figure 5.56 Most significant factor for the variation in the height of 20 x 20 μm polypropylene pillars from the silicon mould insert

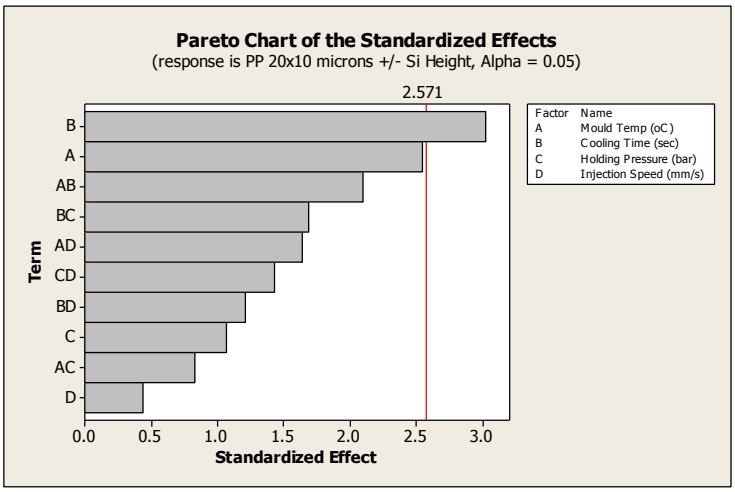

Figure 5.57 Most significant factor for the variation in the height of 20 x 10 μm polypropylene pillars from the silicon mould insert

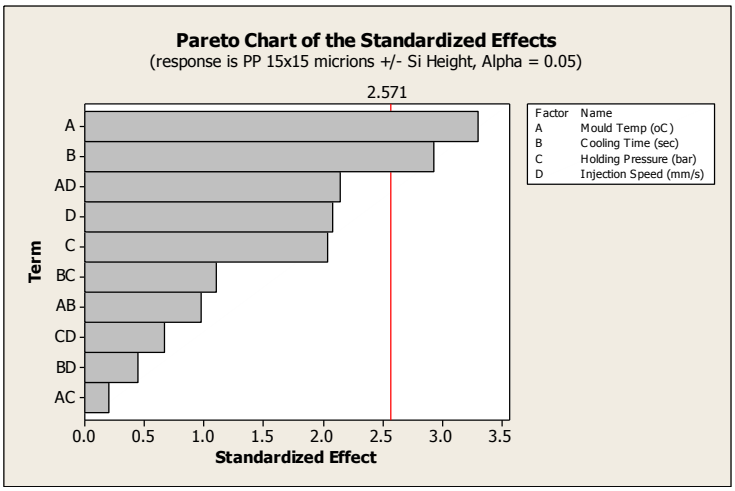

Figure 5.58 Most significant factor for the variation in the height of 15 x 15 μm polypropylene pillars from the silicon mould insert

5.1.3.3 Statistical analysis of 5 – 19 μm pillar feature variation from silicon mould insert

Examination of the generated Pareto charts identified the most significant factors for the variation of pillar dimensions from the silicon mould insert. Holding pressure was found to be the most significant factor regarding the height of the 19 x 80 μm pillars (Figure 5.59). Injection speed was found to be the most significant factor for the height of the 19 x 29 μm pillars closely followed by mould temperature (Figure 5.60). Cooling time was identified as the most significant factor for the height of the 15 x 10 μm pillars (Figure 5.61). With regards to the height of the 10 x 30 μm pillars, mould temperature was found to be the most significant factor (Figure 5.62). Significant factors for the variation of pillar width from the silicon mould insert were not identified for any of the pillars. Also, no factor was found to be significant with regards to the variation of the height of the 15 x 30 μm pillars from the silicon mould insert.

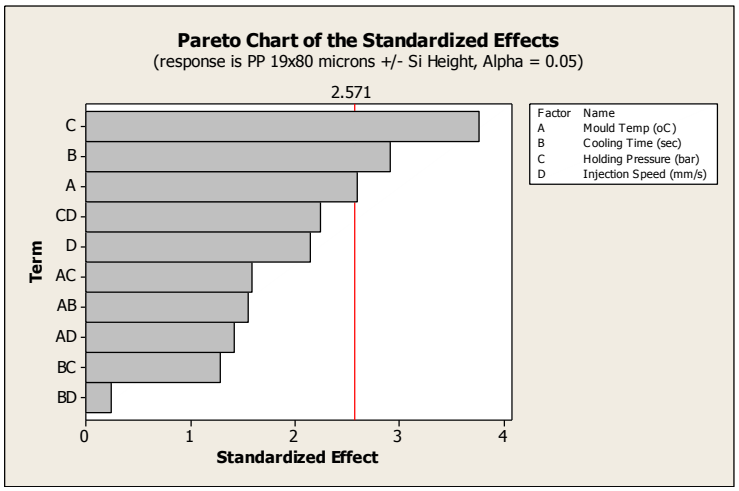

Figure 5.59 Most significant factor for the variation in the height of 19 x 80 μm polypropylene pillars from the silicon mould insert

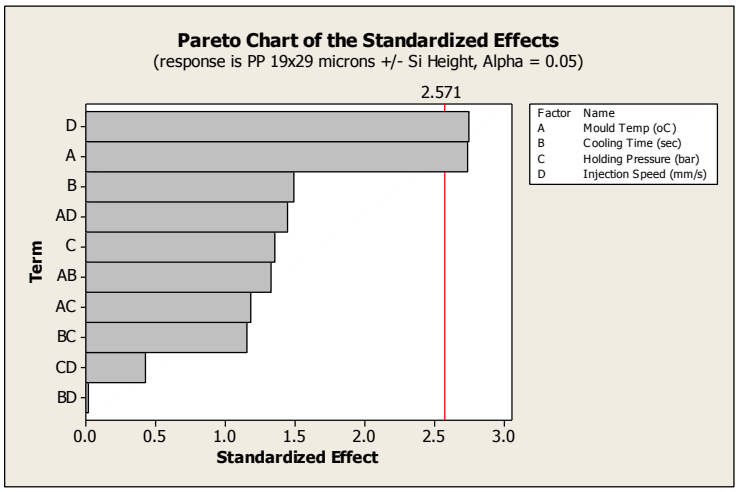

Figure 5.60 Most significant factor for the variation in the height of 19 x 29 μm polypropylene pillars from the silicon mould insert

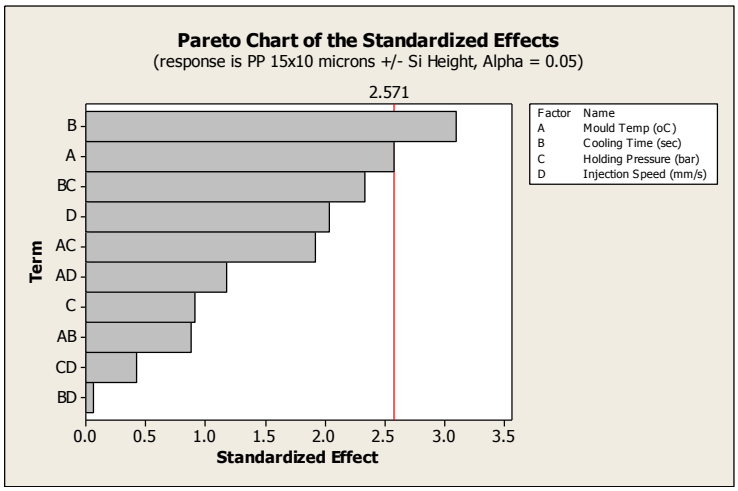

Figure 5.61 Most significant factor for the variation in the height of 15 x 10 μm polypropylene pillars from the silicon mould insert

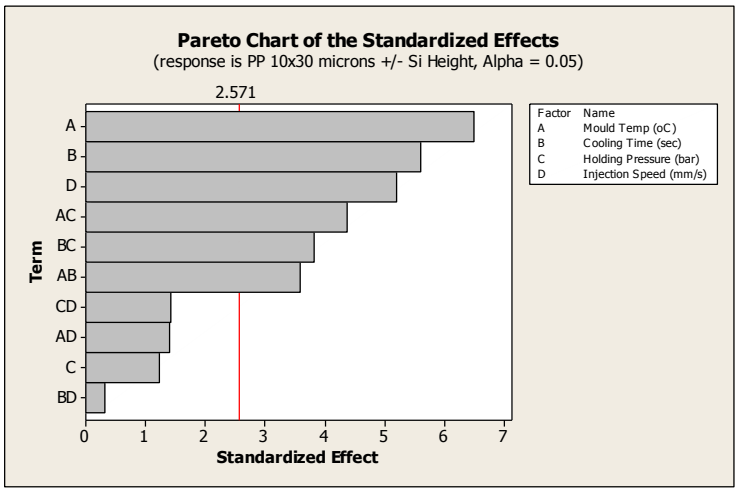

Figure 5.62 Most significant factor for the variation in the height of 10 x 30 μm polypropylene pillars from the silicon mould insert

5.1.4 High density polyethylene pillar feature variation from silicon mould insert dimensions

The feature variation between the high density polyethylene moulded replicate and the silicon mould insert was calculated using the average measurements for height and width obtain in section *5.1.2 High density polyethylene pillar dimensions*. The measurements taken and used in statistical analysis are displayed in the appendix of this thesis.

5.1.4.1 Statistical analysis of 40 – 80 μm pillar feature variation from silicon mould insert

Following the examination of the generated Pareto charts mould temperature was identified as the most significant factor for the height of the 80 x 29, 53 x 29 and the 43 x 29 μm pillars (Figure 5.63 - Figure 5.65). Significant factors were not identified for the variation of replicate pillar width from the silicon mould insert for any of the pillars. Also, significant factors were not identified for the variation of replicate pillar height from the silicon mould insert for the 80 x 80, 53 x 80 or the 43 x 80 μm pillars.

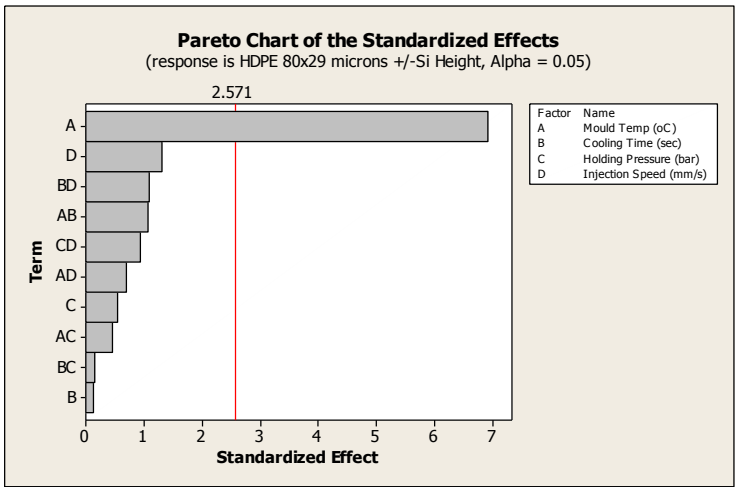

Figure 5.63 Most significant factor for the variation in the height of 80 x 29 μm high density polyethylene pillars from the silicon mould insert

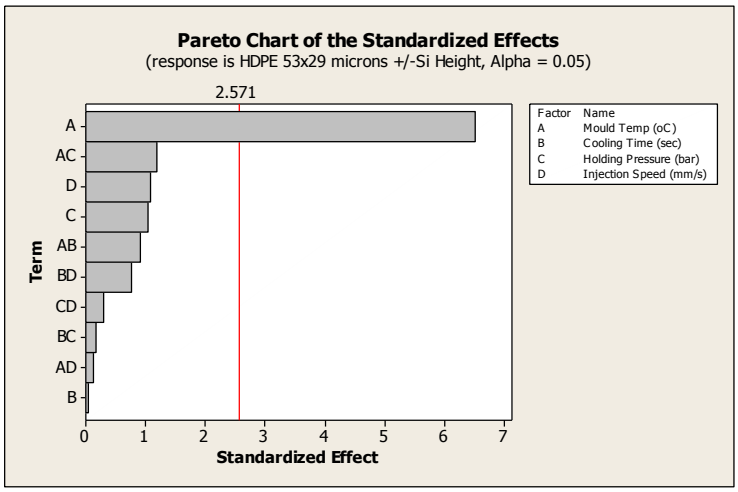

Figure 5.64 Most significant factor for the variation in the height of 53 x 29 μm high density polyethylene pillars from the silicon mould insert

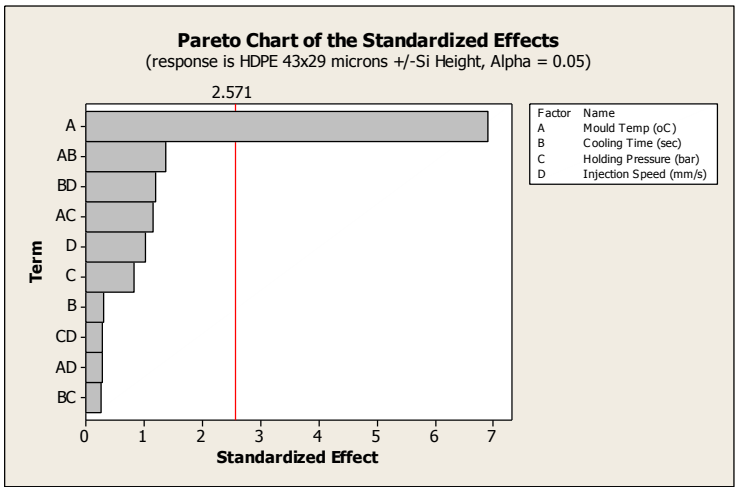

Figure 5.65 Most significant factor for the variation in the height of 43 x 29 μm high density polyethylene pillars from the silicon mould insert

5.1.4.2 Statistical analysis of 20 – 39 μm pillar feature variation from silicon mould insert

Examination of the Pareto charts identified mould temperature as the most significant factor for the variation of replicate pillar height from the silicon mould insert for all the pillars (Figure 5.66 - Figure 5.68, Figure 5.70 - Figure 5.74 and Figure 5.76 - Figure 5.78). Mould temperature was also identified as the most significant factor for the variation of replicate pillar width from the silicon mould insert for the 30 x 10, 25 x 10 and the 20 x 10 μm pillars (Figure 5.69, Figure 5.75 and Figure 5.79). The significant factors for the variation of pillar width from the silicon mould insert were not identified for the 30 x 30 (from square 1), 30 x 30 (from square 6), 29 x 80, 29 x 29, 25 x 30, 25 x 25, 20 x 30 or the 20 x 20 μm pillars.

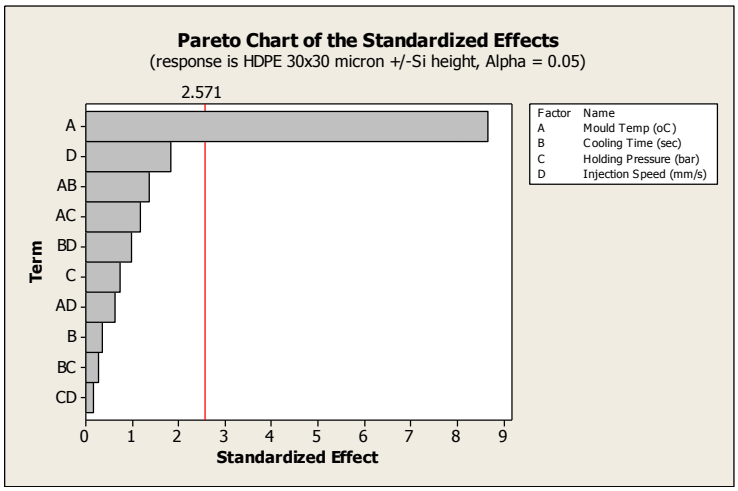

Figure 5.66 Most significant factor for the variation in the height of 30 x 30 μm high density polyethylene pillars from squares 5 and 6 from the silicon mould insert

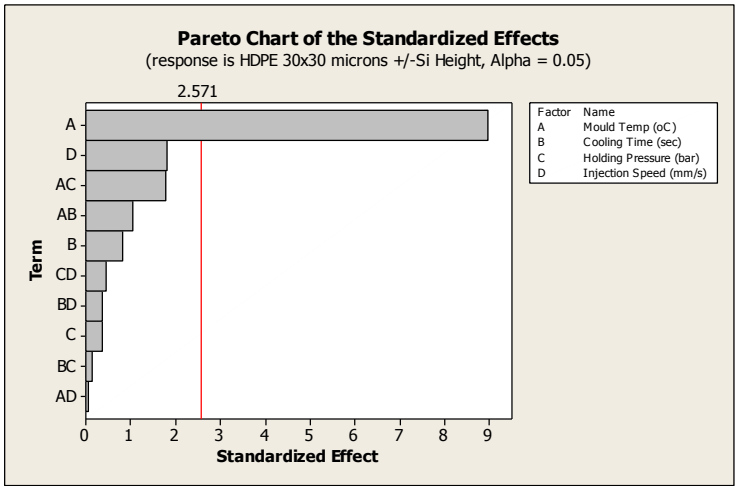

Figure 5.67 Most significant factor for the variation in the height of 30 x 30 μm high density polyethylene pillars from squares 1 and 2 from the silicon mould insert

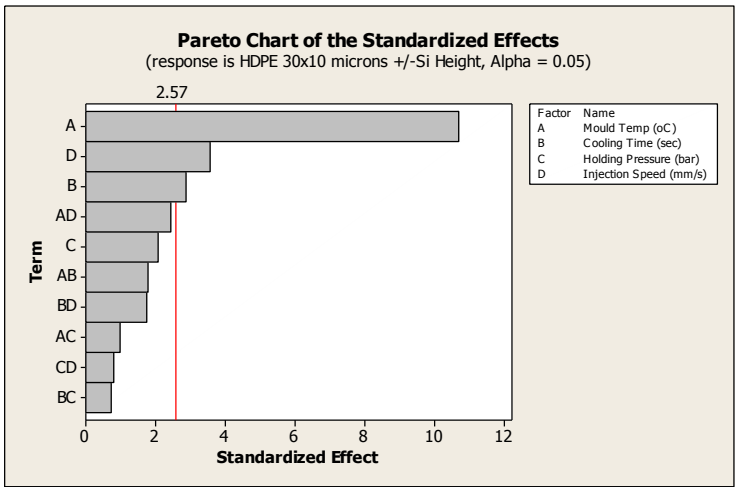

Figure 5.68 Most significant factor for the variation in the height of 30 x 10 μm high density polyethylene pillars from the silicon mould insert

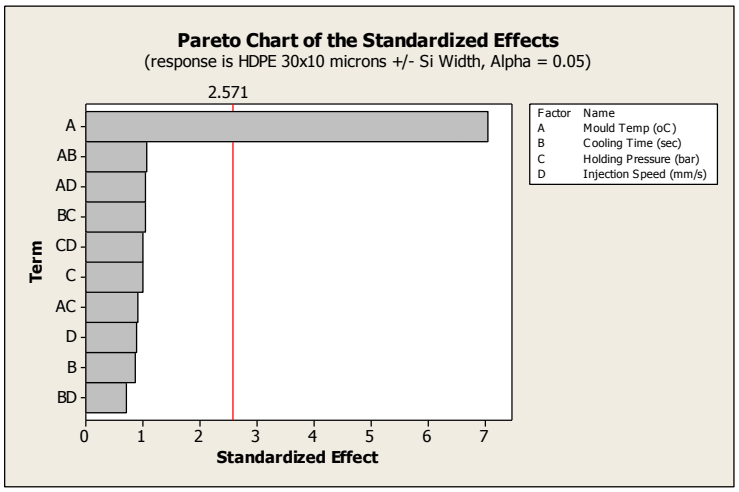

Figure 5.69 Most significant factor for the variation in the width of 30 x 10 μm high density polyethylene pillars from the silicon mould insert

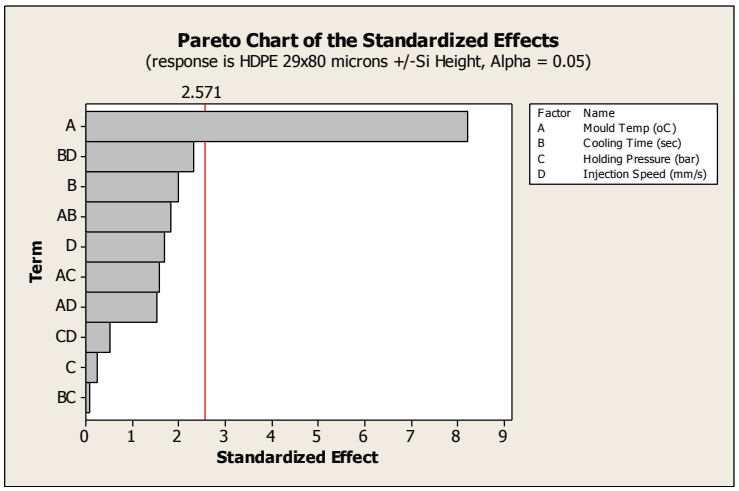

Figure 5.70 Most significant factor for the variation in the height of 29 x 80 μm high density polyethylene pillars from the silicon mould insert

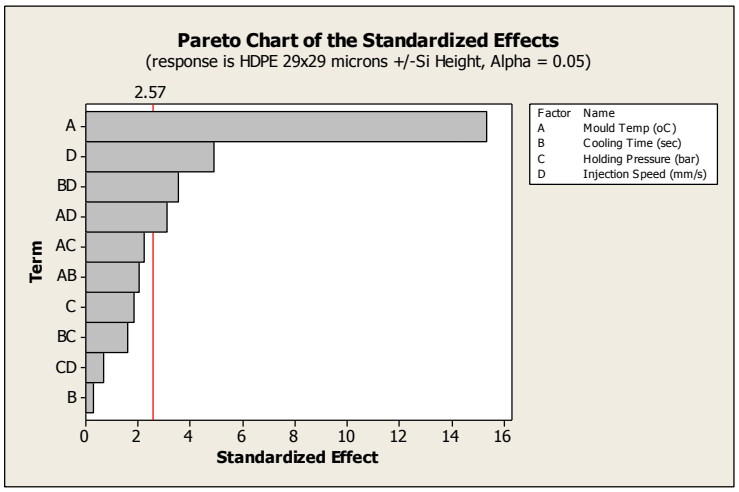

Figure 5.71 Most significant factor for the variation in the height of 29 x 29 μm high density polyethylene pillars from the silicon mould insert

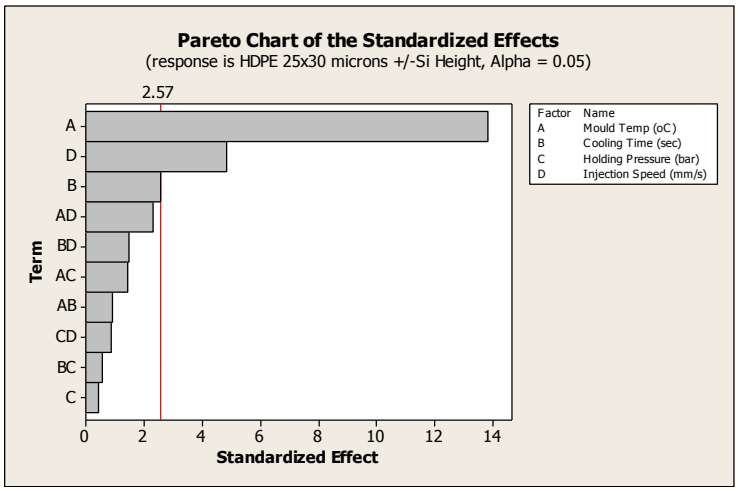

Figure 5.72 Most significant factor for the variation in the height of 25 x 30 μm high density polyethylene pillars from the silicon mould insert

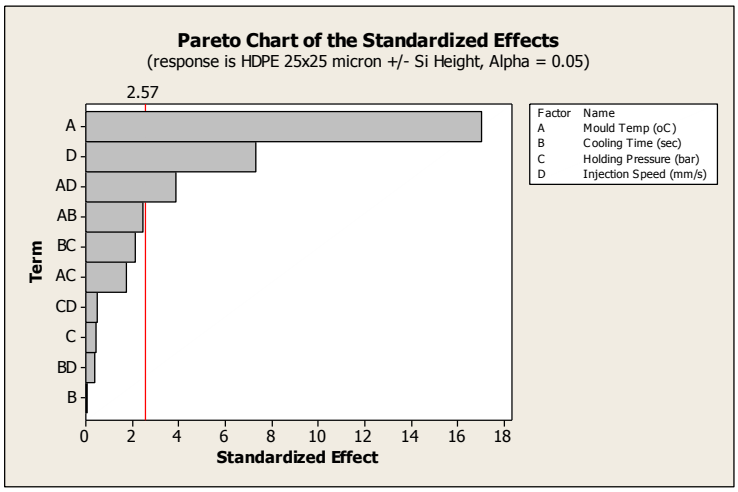

Figure 5.73 Most significant factor for the variation in the height of 25 x 25 μm high density polyethylene pillars from the silicon mould insert

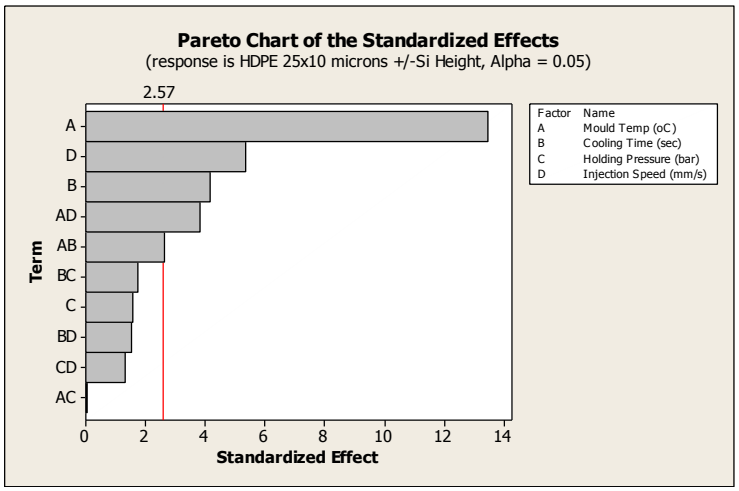

Figure 5.74 Most significant factor for the variation in the height of 25 x 10 μm high density polyethylene pillars from the silicon mould insert

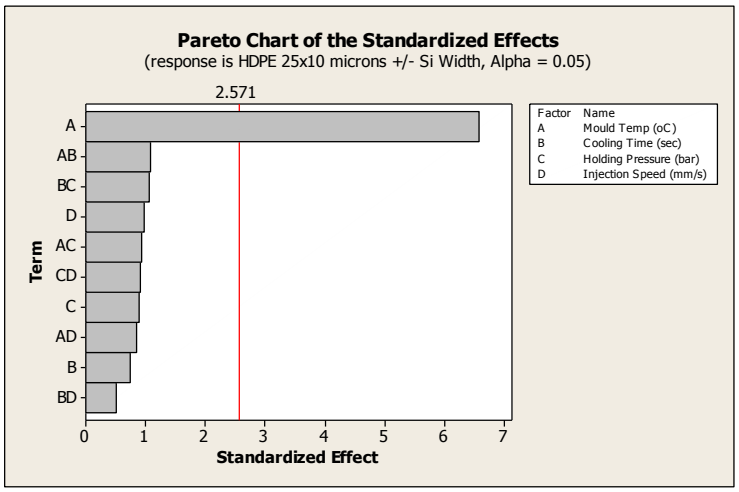

Figure 5.75 Most significant factor for the variation in the width of 25 x 10 μm high density polyethylene pillars from the silicon mould insert

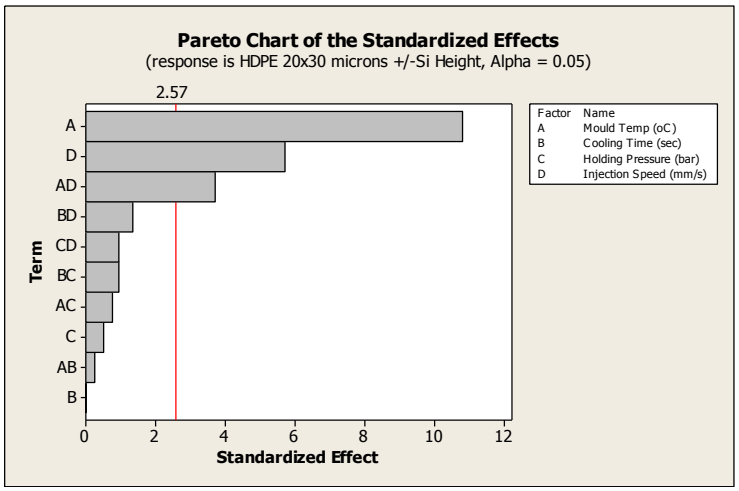

Figure 5.76 Most significant factor for the variation in the height of 20 x 30 μm high density polyethylene pillars from the silicon mould insert

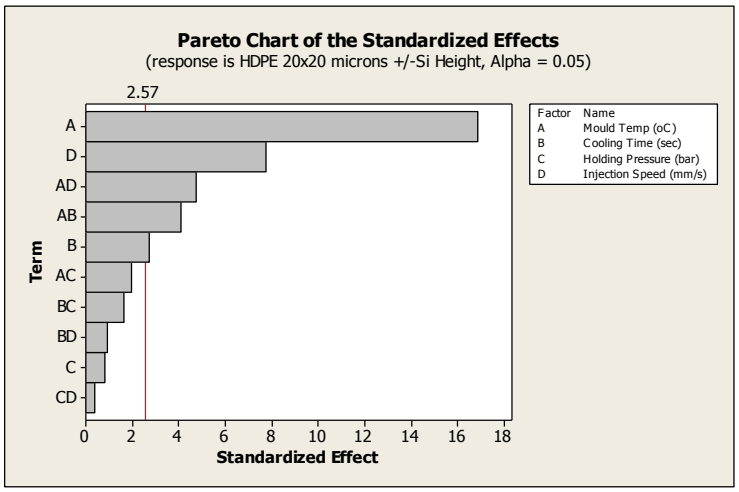

Figure 5.77 Most significant factor for the variation in the height of 20 x 20 μm high density polyethylene pillars from the silicon mould insert

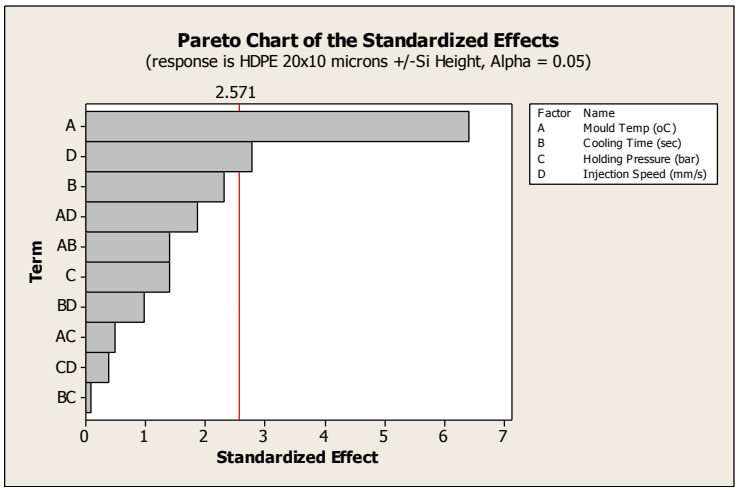

Figure 5.78 Most significant factor for the variation in the height of 20 x 10 μm high density polyethylene pillars from the silicon mould insert

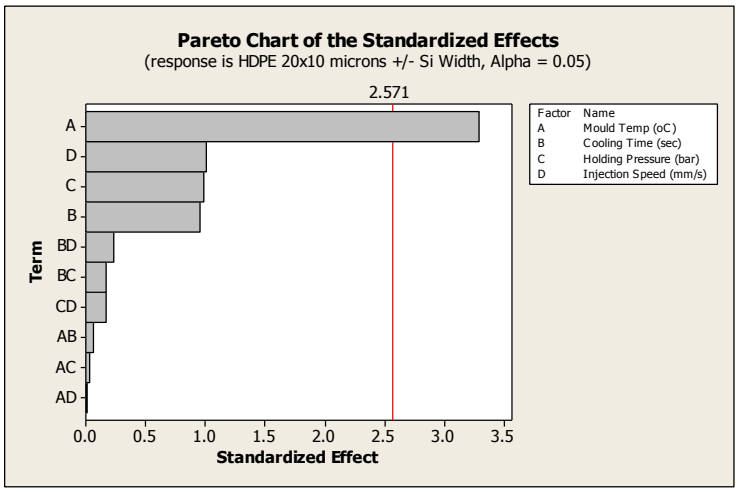

Figure 5.79 Most significant factor for the variation in the width of 20 x 10 μm high density polyethylene pillars from the silicon mould insert

5.1.4.3 Statistical analysis of 5 – 19 μm pillar feature variation from silicon mould insert

After examination of the generated Pareto charts it was found that the mould temperature was identified as the most significant factor for all pillar examined regarding the variation of replicate pillar dimensions from the silicon mould insert (Figure 5.80 - Figure 5.91).

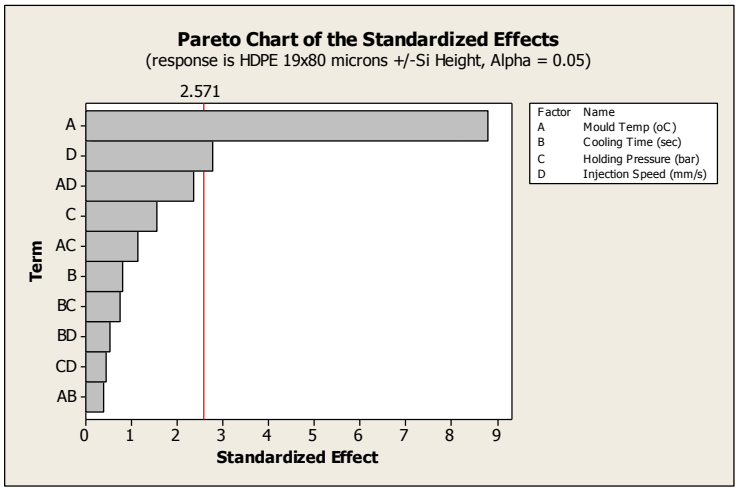

Figure 5.80 Most significant factor for the variation in the height of 19 x 80 μm high density polyethylene pillars from the silicon mould insert

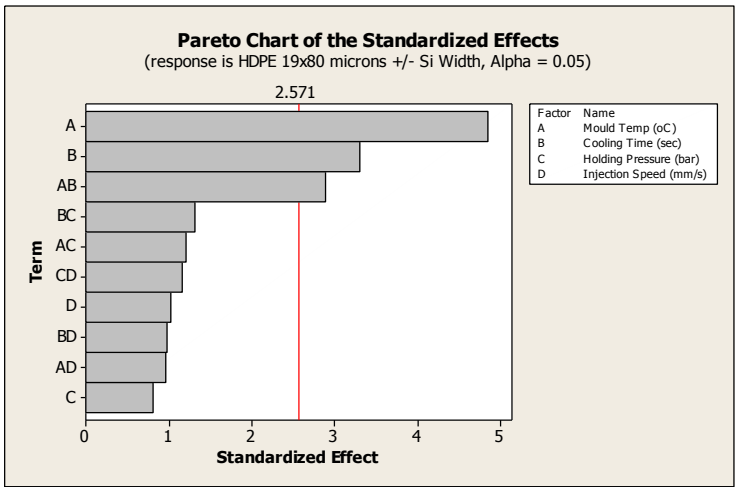

Figure 5.81 Most significant factor for the variation in the width of 19 x 80 μm high density polyethylene pillars from the silicon mould insert

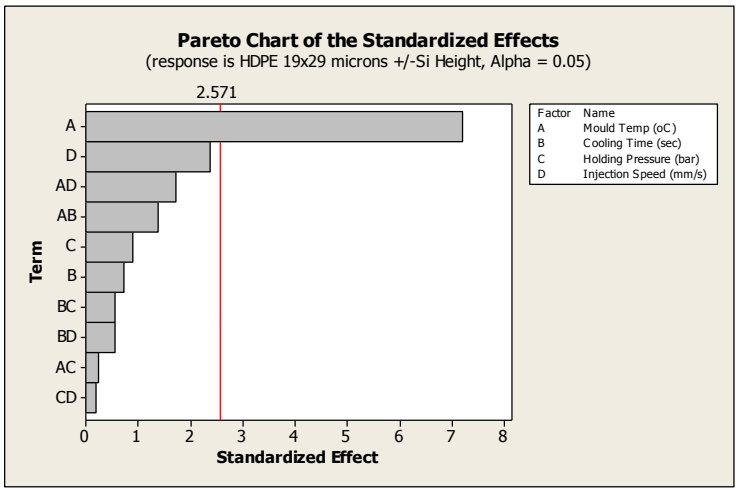

Figure 5.82 Most significant factor for the variation in the height of 19 x 29 μm high density polyethylene pillars from the silicon mould insert

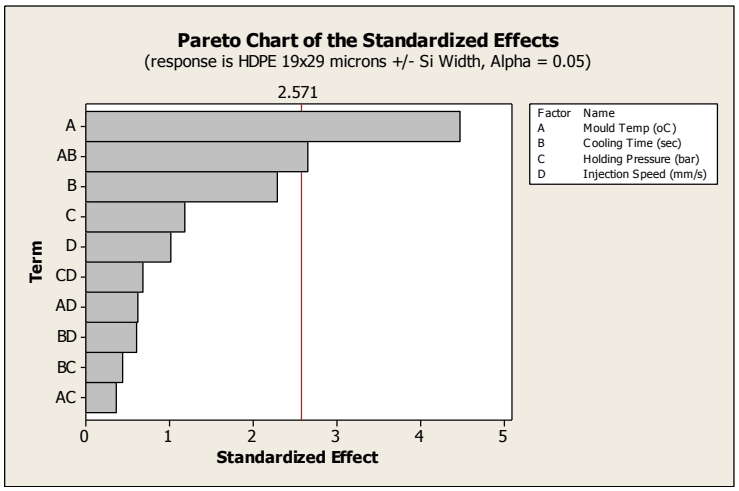

Figure 5.83 Most significant factor for the variation in the width of 19 x 29 μm high density polyethylene pillars from the silicon mould insert

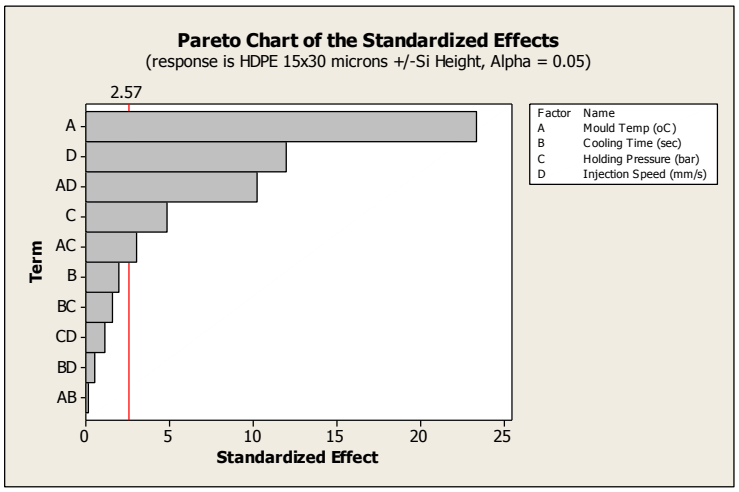

Figure 5.84 Most significant factor for the variation in the height of 15 x 30 μm high density polyethylene pillars from the silicon mould insert

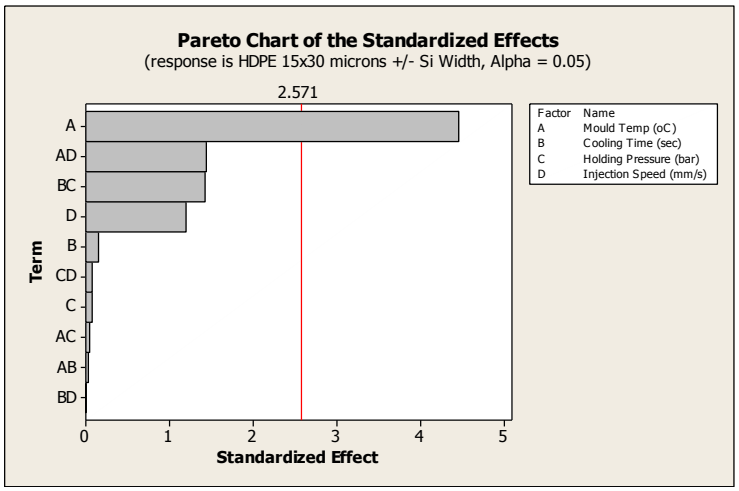

Figure 5.85 Most significant factor for the variation in the width of 15 x 30 μm high density polyethylene pillars from the silicon mould insert

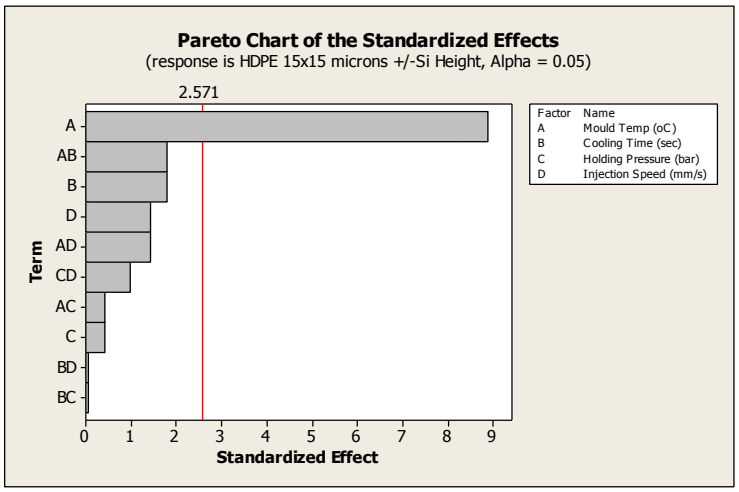

Figure 5.86 Most significant factor for the variation in the height of 15 x 15 μm high density polyethylene pillars from the silicon mould insert

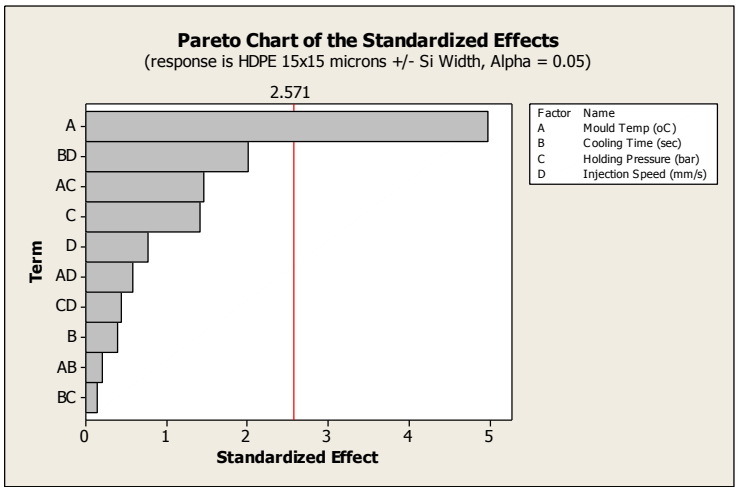

Figure 5.87 Most significant factor for the variation in the width of 15 x 15 μm high density polyethylene pillars from the silicon mould insert

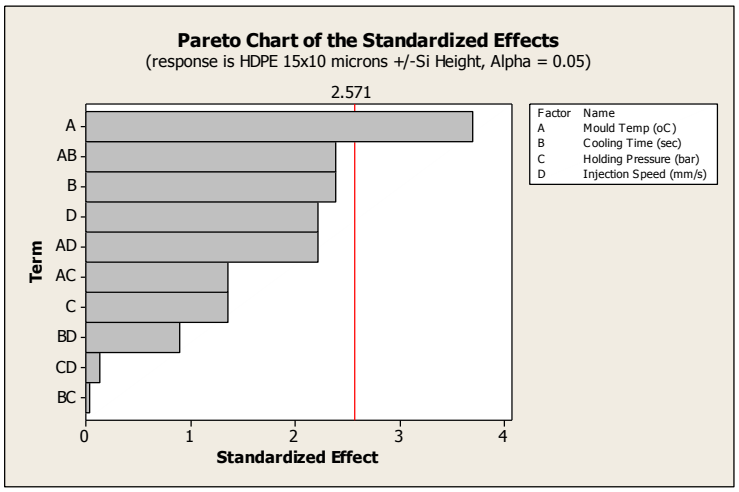

Figure 5.88 Most significant factor for the variation in the height of 15 x 10 μm high density polyethylene pillars from the silicon mould insert

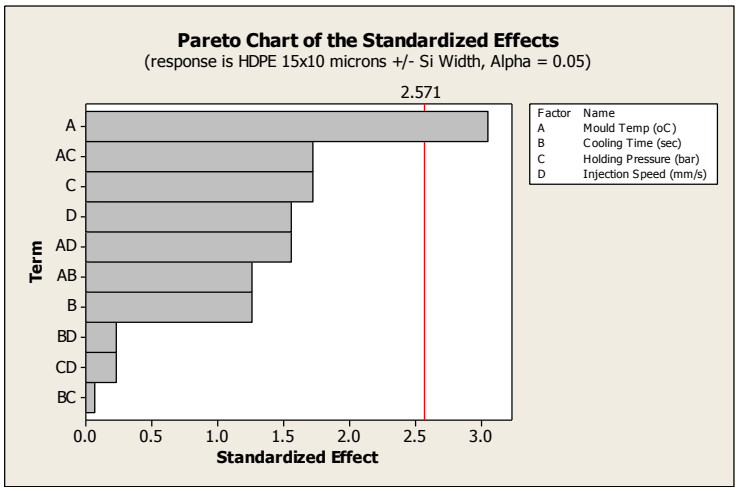

Figure 5.89 Most significant factor for the variation in the width of 15 x 10 μm high density polyethylene pillars from the silicon mould insert

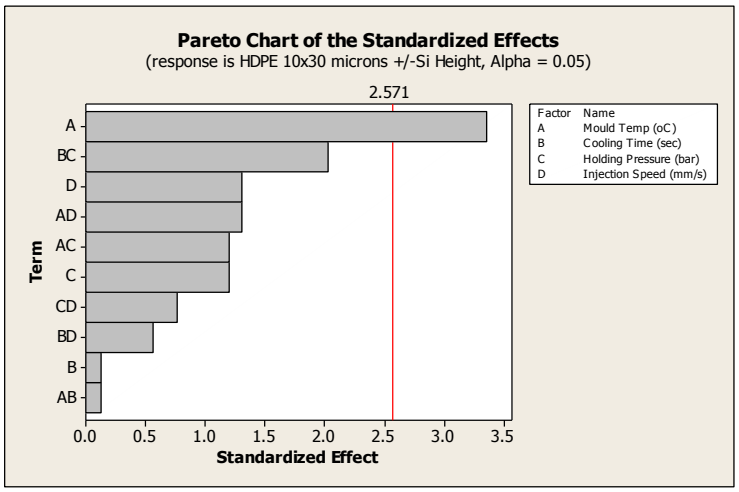

Figure 5.90 Most significant factor for the variation in the height of 10 x 30 μm high density polyethylene pillars from the silicon mould insert

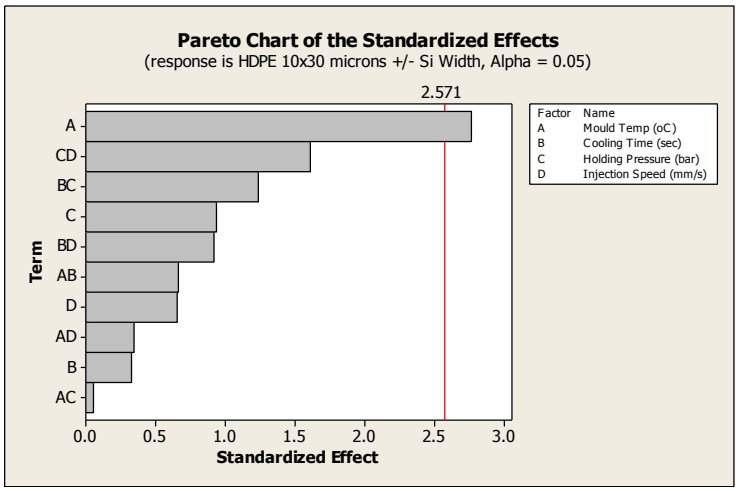

Figure 5.91 Most significant factor for the variation in the width of 10 x 30 μm high density polyethylene pillars from the silicon mould insert

5.1.5 Appearance of polypropylene features

The appearance of pillar features on polypropylene replicates was examined. The following subsections present the various observations made whilst examining the replicate surfaces from all design of experiment runs.

5.1.5.1 Polypropylene 40 – 80 μm pillar features

The 80 x 80 μm pillars were observed on replicates from all design of experiment runs. Those observed to be most successfully replicated were those found on the replicates from DOE runs 4, 8 and 9 (Figure 5.92).

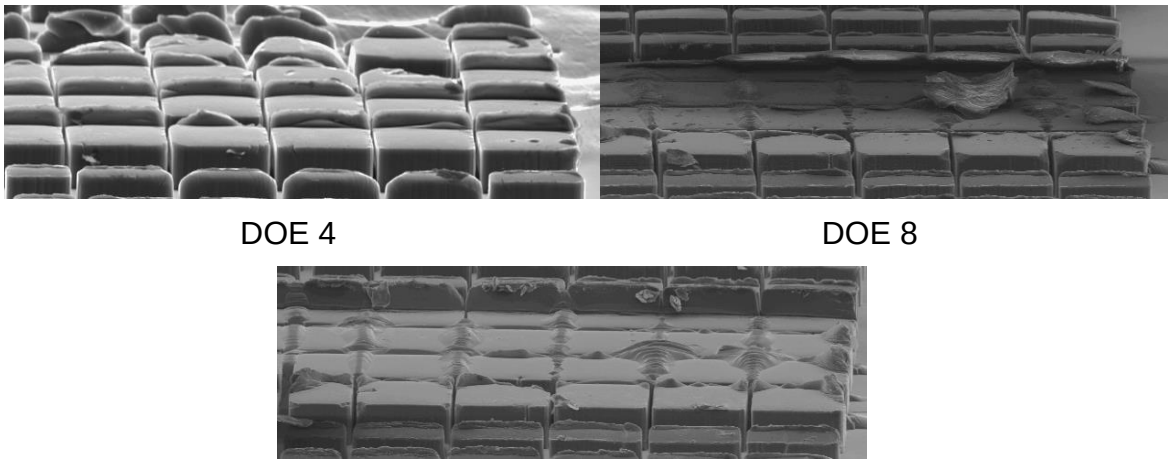

DOE 4 DOE 8

DOE 9

Figure 5.92 Most well replicated polypropylene 80 x 80 μm pillars

The pillars from DOE runs 3, 5 and 6 were observed to be the least well replicated (Figure 5.93).

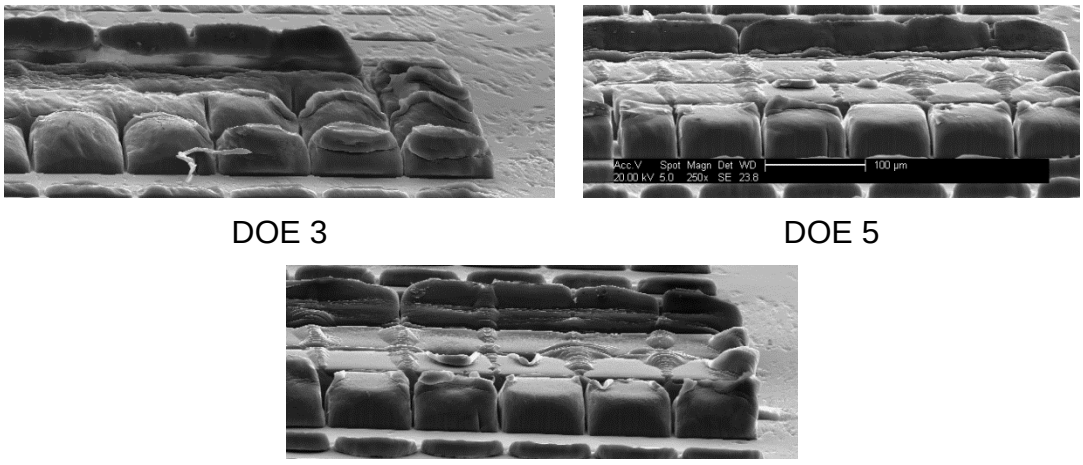

DOE 3 DOE 5

DOE 6

Figure 5.93 Least well replicated polypropylene 80 x 80 μm pillars

The 53 x 80 μm pillars were observed on replicates from all design of experiment runs. Those observed to be most successfully replicated were those found on the replicates from DOE runs 11 and 15 (Figure 5.94).

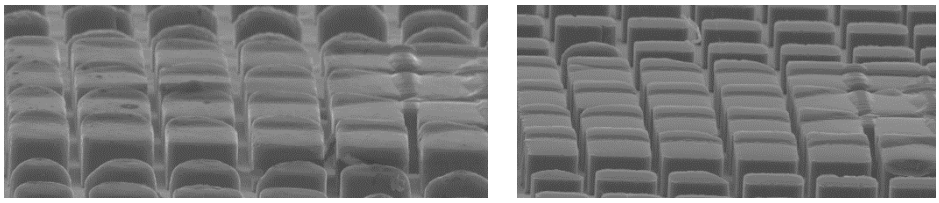

DOE 11 DOE 15

Figure 5.94 Most well replicated polypropylene 53 x 80 μm pillars

The pillars from DOE run 3 were observed to be the least well replicated (Figure 5.95).

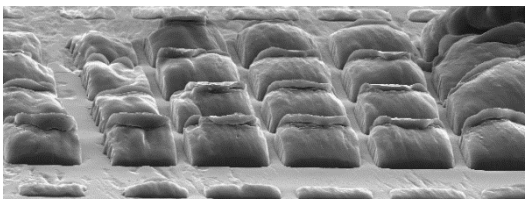

DOE 3

Figure 5.95 Least well replicated polypropylene 53 x 80 μm pillars

The 43 x 80 μm pillars were observed on replicates from all design of experiment runs. Those observed to be most successfully replicated were those found on the replicates from DOE runs 11 and 10 (Figure 5.96).

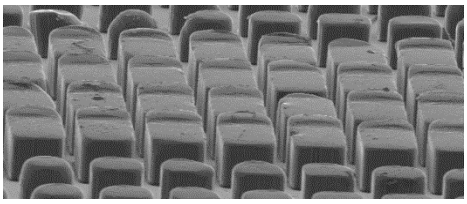

DOE 10

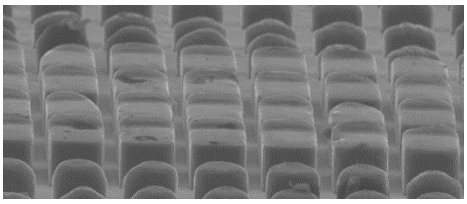

DOE 11

Figure 5.96 Most well replicated polypropylene 43 x 80 μm pillars

The pillars from DOE run 3 were observed to be the least well replicated (Figure 5.97).

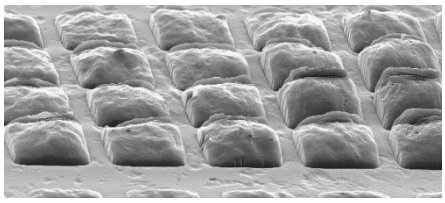

DOE 3

Figure 5.97 Least well replicated polypropylene 43 x 80 μm pillars

The 80 x 29 μm pillars were observed on replicates from all design of experiment runs. Those observed to be well replicated were those found on the replicates from DOE runs 8, 10 and 15 (Figure 5.98).

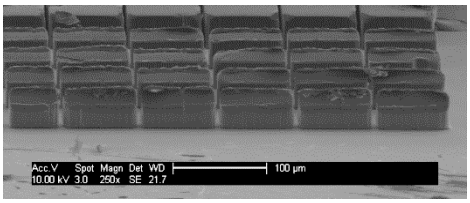

DOE 8

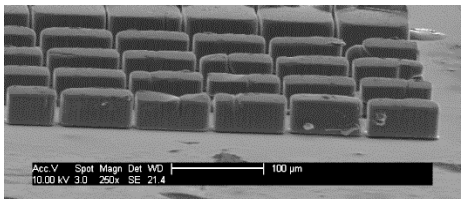

DOE 10

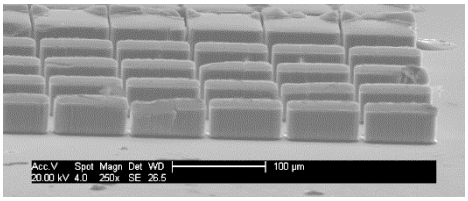

DOE 15

Figure 5.98 Most well replicated polypropylene 80 x 29 μm pillars

The pillars from DOE runs 3 and 6 were observed to be the least well replicated (Figure 5.99).

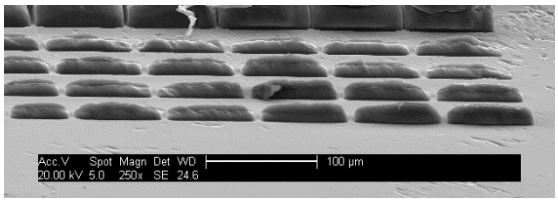

DOE 3

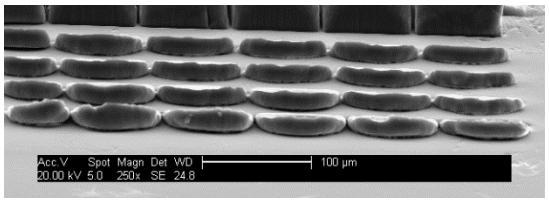

DOE 6

Figure 5.99 Least well replicated polypropylene 80 x 29 μm pillars

The 53 x 29 μm pillars were observed on replicates from all design of experiment runs. Those observed to be well replicated were those found on the replicates from DOE runs 4 and 15 (Figure 5.100).

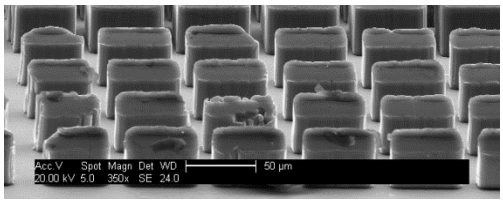

DOE 4

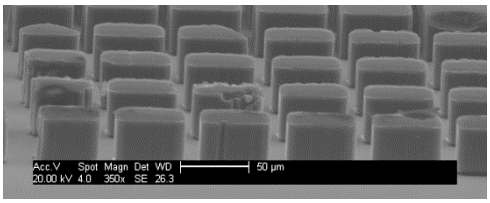

DOE 15

Figure 5.100 Most well replicated polypropylene 53 x 29 μm pillars

The pillars from DOE run 3 were observed to be the least well replicated (Figure 5.101).

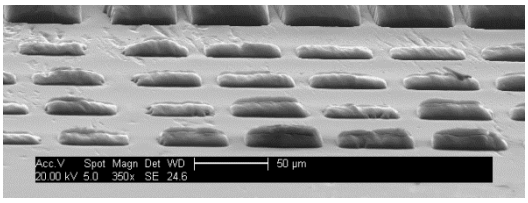

DOE 3

Figure 5.101 Least well replicated polypropylene 53 x 29 μm pillars

The 43 x 29 μm pillars were observed on replicates from all design of experiment runs. Those observed to be well replicated were those found on the replicates from DOE runs 10, 14 and 15 (Figure 5.102).

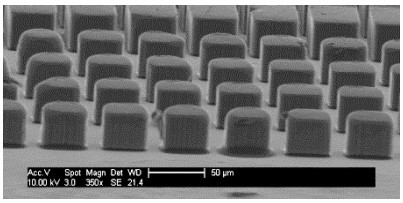

DOE 10

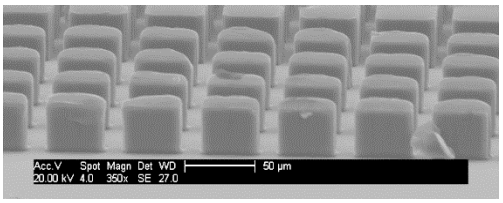

DOE 14

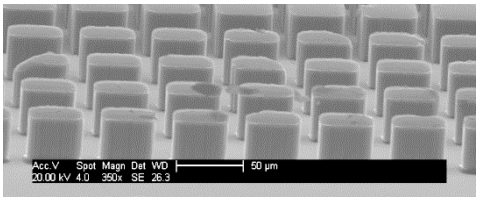

DOE 15

Figure 5.102 Most well replicated polypropylene 43 x 29 μm pillars

The pillars from DOE run 3 were observed to be the least well replicated (Figure 5.103).

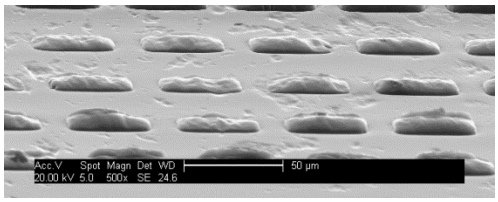

DOE 3

Figure 5.103 Least well replicated polypropylene 43 x 29 μm pillars

5.1.5.2 Polypropylene 20 – 39 μm pillar features

The 30 x 30 μm pillars, located in square 1 of the replicates, were found to be replicated for all design of experiment runs. Those observed to be most

successfully replicated were those found on the replicates from DOE runs 4, 8, 9 and 15 (Figure 5.104).

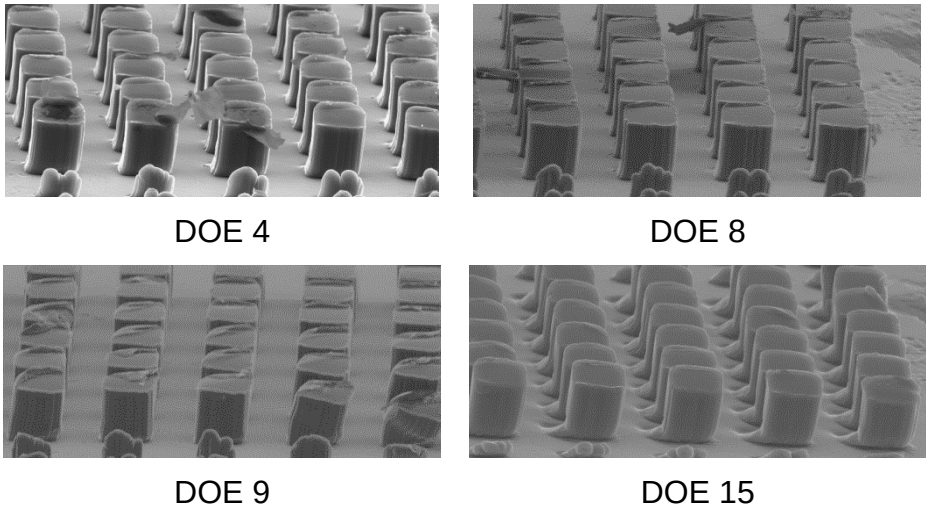

Figure 5.104 Most well replicated polypropylene 30 x 30 μm pillars

The pillars from DOE runs 5 and 6 were observed to be the least well replicated (Figure 5.105).

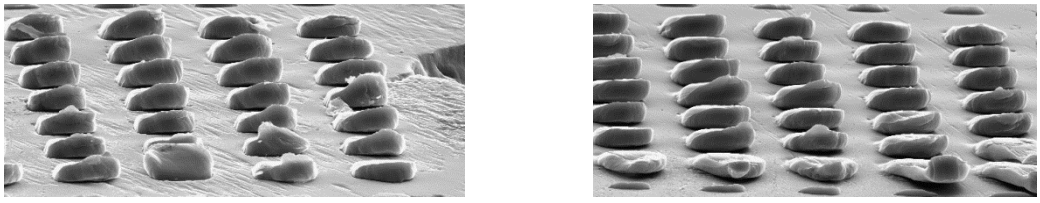

Figure 5.105 Least well replicated polypropylene 30 x 30 μm pillars

The 25 x 30 μm pillars were found to be replicated on replicates from all design of experiment runs. Those observed to be most successfully replicated were those found on the replicates from DOE runs 4, 8 and 9 (Figure 5.106).

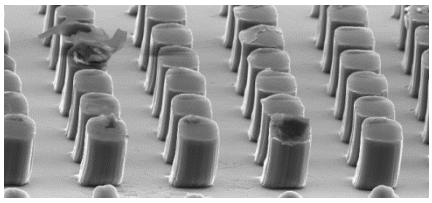

DOE 4

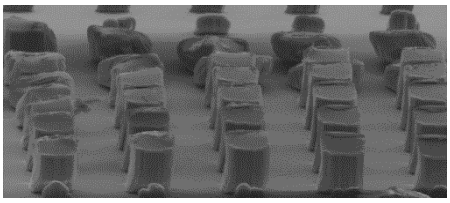

DOE 8

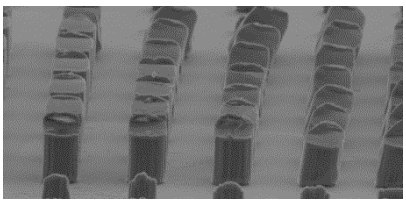

DOE 9

Figure 5.106 Most well replicated polypropylene 25 x 30 μm pillars

The pillars from DOE run 3 were observed to be the least well replicated (Figure 5.107).

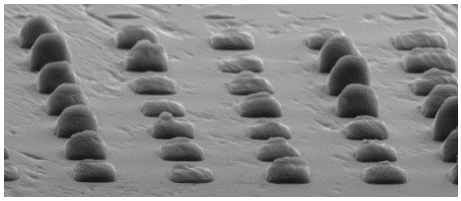

DOE 3

Figure 5.107 Least well replicated polypropylene 25 x 30 μm pillars

The 20 x 30 μm pillars were found to be replicated for all DOE runs. Those observed to be most successfully replicated were those found on the replicates from DOE runs 4, 8 and 9 (Figure 5.108).

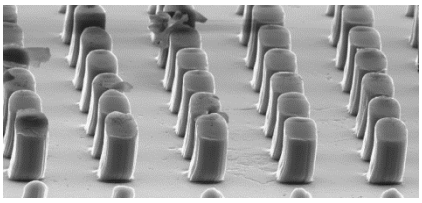

DOE 4

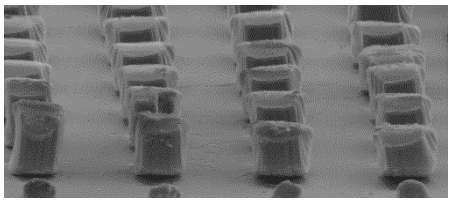

DOE 8

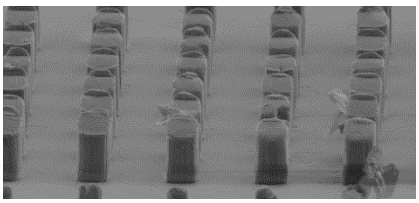

DOE 9

Figure 5.108 Most well replicated polypropylene 20 x 30 μm pillars

The pillars from DOE run 6 were observed to be the least well replicated (Figure 5.109).

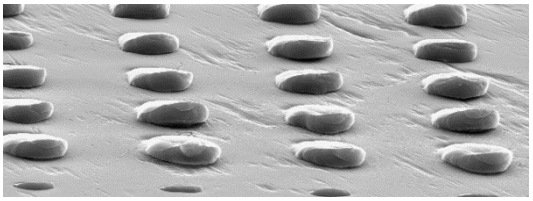

DOE 6

Figure 5.109 Least well replicated polypropylene 20 x 30 μm pillars

The 30 x 10 μm pillars were found on replicates from all design of experiment runs. Those observed to be most successfully replicated were those found on the replicates from DOE runs 4, 8 and 9 (Figure 5.110).

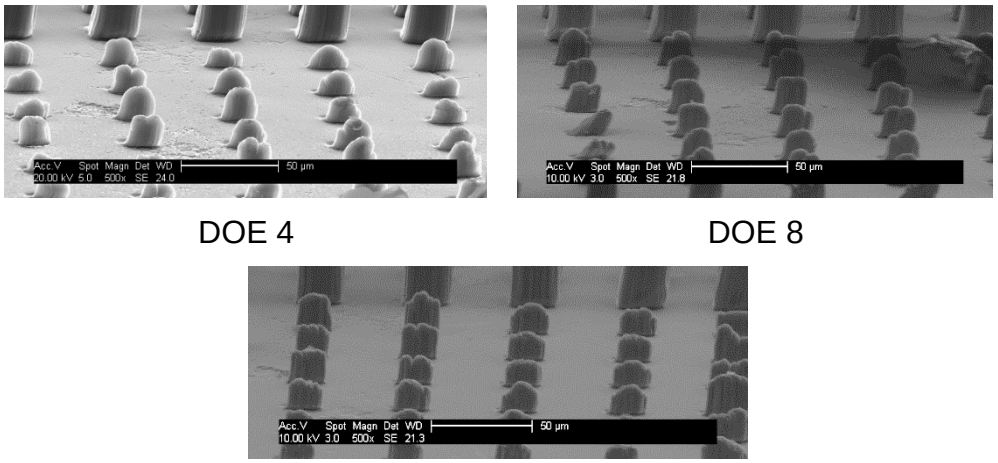

DOE 4 DOE 8

DOE 9

Figure 5.110 Most well replicated polypropylene 30 x 10 μm pillars

The pillars from DOE run 6 were observed to be the least well replicated (Figure 5.111).

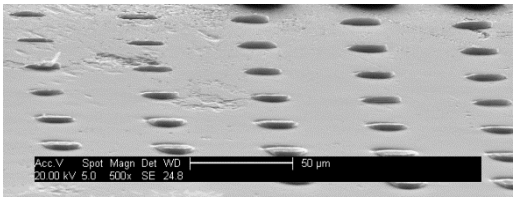

DOE 6

Figure 5.111 Least well replicated polypropylene 30 x 10 μm pillars

The 25 x 10 μm pillars were observed on replicates from all design of experiment runs. Those observed to be most successfully replicated were those found on the replicates from DOE runs 4, 8 and 9 (Figure 5.112).

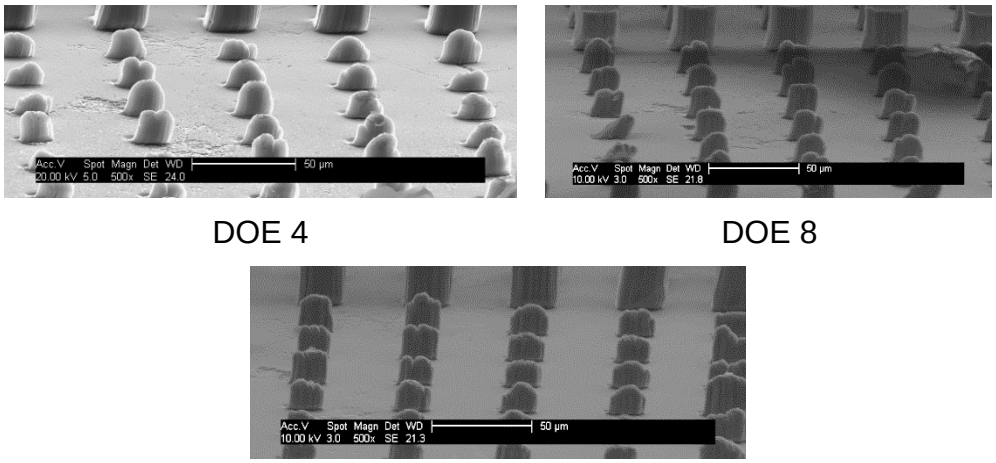

DOE 4 DOE 8

DOE 9

Figure 5.112 Most well replicated polypropylene 25 x 10 μm pillars

The pillars from DOE runs 3 and 6 were observed to be the least well replicated (Figure 5.113).

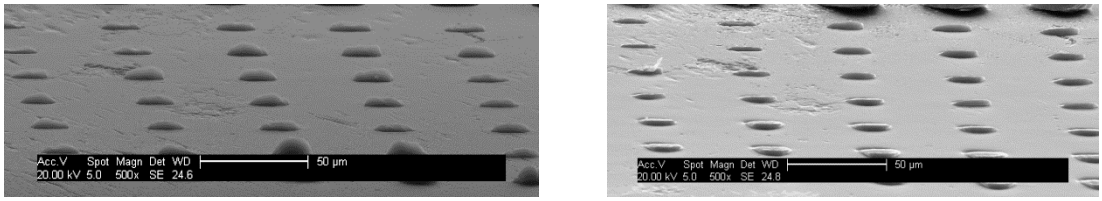

DOE 3 DOE 6

Figure 5.113 Least well replicated polypropylene 25 x 10 μm pillars

The 20 x 10 μm pillars were observed on replicates from all design of experiment runs. Those observed to be most successfully replicated were those found on the replicates from DOE runs 4 and 9 (Figure 5.114).

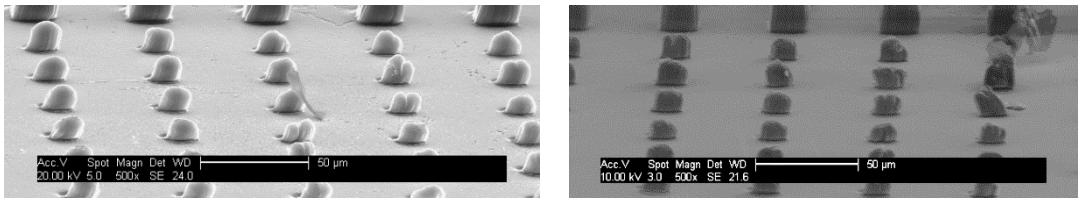

DOE 4 DOE 9

Figure 5.114 Most well replicated polypropylene 20 x 10 μm pillars

The pillars from DOE run 6 were observed to be the least well replicated (Figure 5.115).

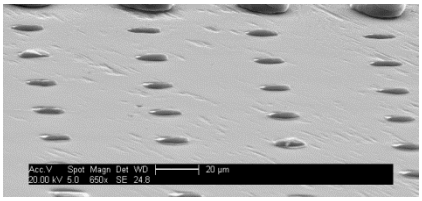

DOE 6

Figure 5.115 Least well replicated polypropylene 20 x 10 μm pillars

The 29 x 80 μm pillars were observed on replicates from all design of experiment runs. Those observed to be most successfully replicated were those found on the replicates from DOE run 15 (Figure 5.116).

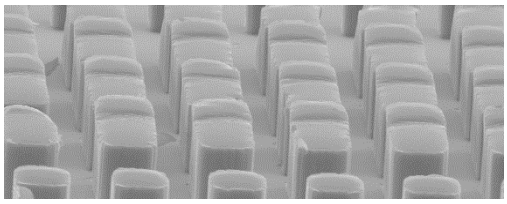

DOE 15

Figure 5.116 Most well replicated polypropylene 29 x 80 μm pillars

The pillars from DOE run 3 were observed to be the least well replicated (Figure 5.117).

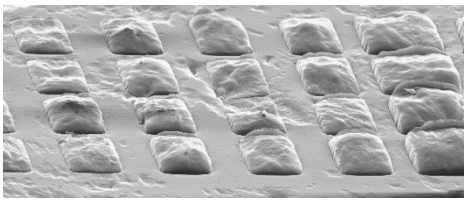

DOE 3

Figure 5.117 Least well replicated polypropylene 29 x 80 μm pillars

The 29 x 29 μm pillars were observed on replicates from all design of experiment runs. Those observed to be well replicated were those found on the replicates from DOE run 15 (Figure 5.118).

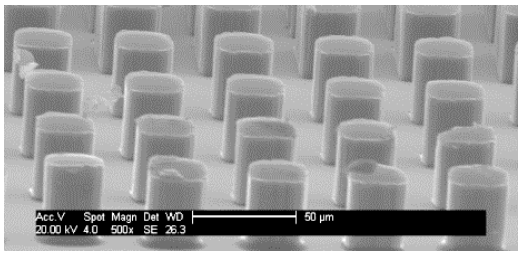

DOE 15

Figure 5.118 Most well replicated polypropylene 29 x 29 μm pillars

The pillars from DOE run 3 were observed to be the least well replicated (Figure 5.119).

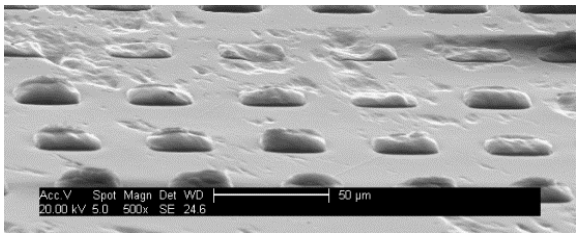

DOE 3

Figure 5.119 Least well replicated polypropylene 29 x 29 μm pillars

The 30 x 30 μm pillars were observed on replicates from all design of experiment runs. Those observed to be most successfully replicated were those found on the replicates from DOE run 15 (Figure 5.120).

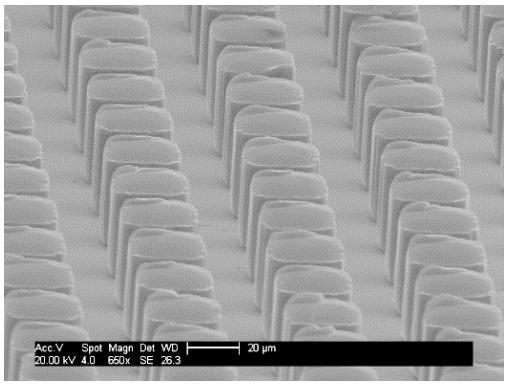

DOE 15

Figure 5.120 Most well replicated polypropylene 30 x 30 μm pillars

The pillars from DOE runs 3, 5, 6 and 13 were observed to be the least well replicated (Figure 5.121).

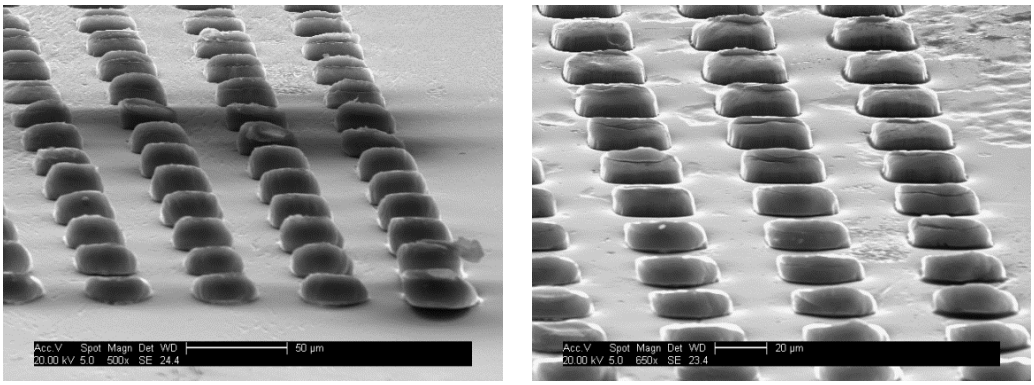

DOE 3 DOE 5

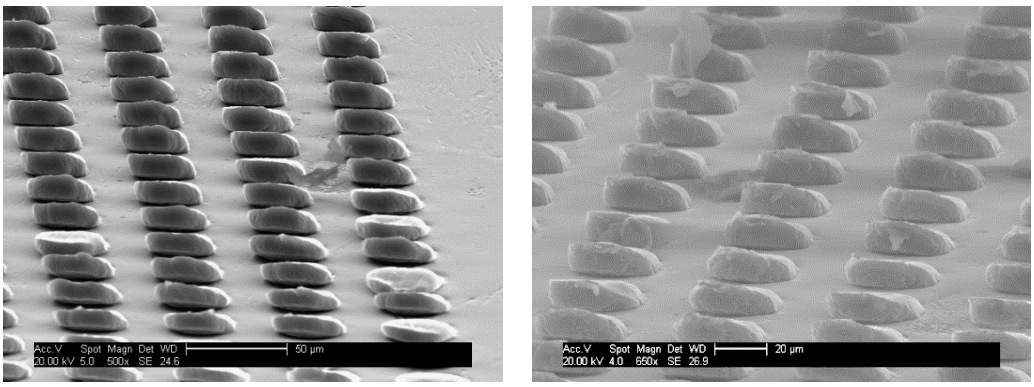

DOE 6 DOE 13

Figure 5.121 Least well replicated polypropylene 30 x 30 μm pillars

The 25 x 25 μm pillars were found to be replicated on replicates from all design of experiment runs. Those observed to be most successfully replicated were those found on the replicates from DOE run 15 (Figure 5.122).

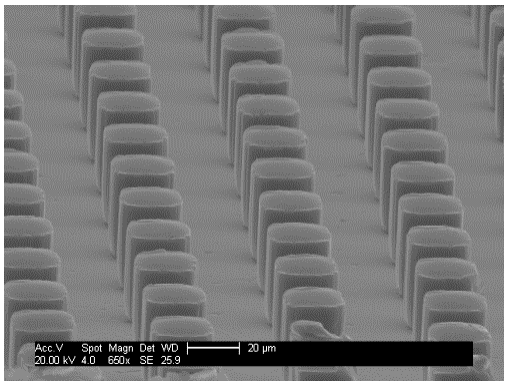

DOE 15

Figure 5.122 Most well replicated polypropylene 25 x 25 μm pillars

The pillars from DOE runs 3 and 5 were observed to be the least well replicated (Figure 5.123).

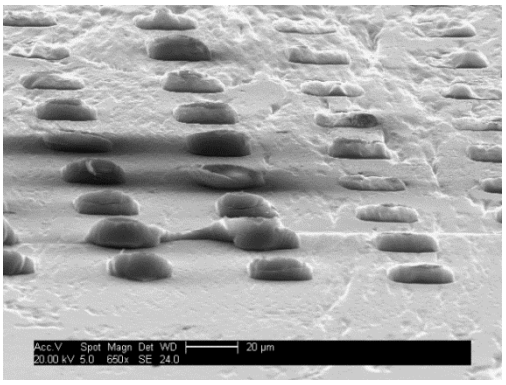

DOE 3

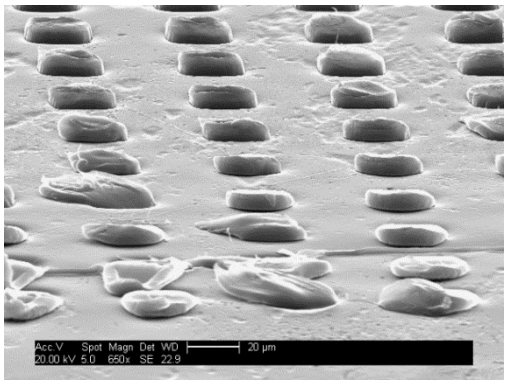

DOE 5

Figure 5.123 Least well replicated polypropylene 25 x 25 μm pillars

The 20 x 20 μm pillars were observed on replicates from all design of experiment runs. Those observed to be most well replicated were those found on the replicates from DOE run 4, 8 and 15 (Figure 5.124).

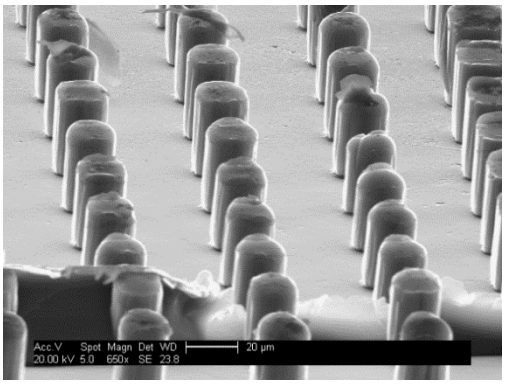

DOE 4

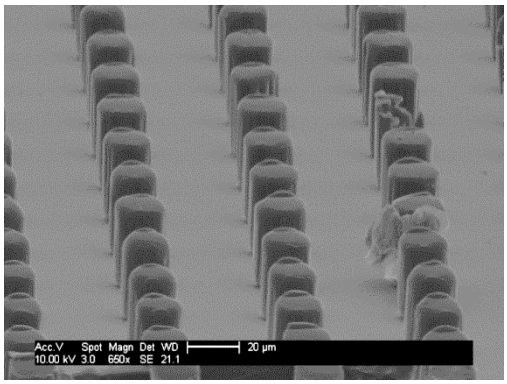

DOE 8

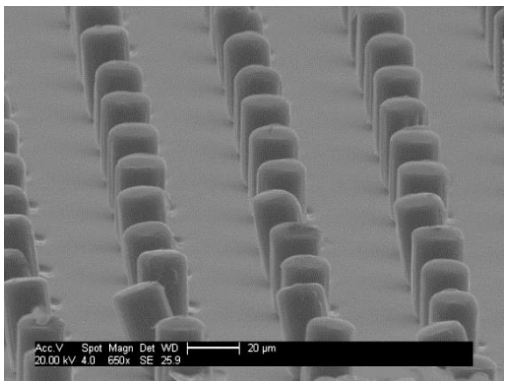

DOE 15

Figure 5.124 Most well replicated polypropylene 20 x 20 μm pillars

The pillars from DOE run 3 were observed to be the least well replicated (Figure 5.125).

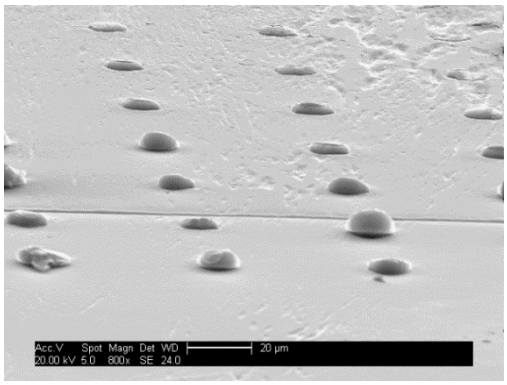

DOE 3

Figure 5.125 Least well replicated polypropylene 20 x 20 μm pillars

5.1.5.3 Polypropylene 2 – 19 μm pillar features

The 15 x 30 μm pillars were found to be replicated on replicates from all design of experiment runs. Those observed to be most successfully replicated were those found on the replicates from DOE runs 4, 8 and 9 (Figure 5.126).

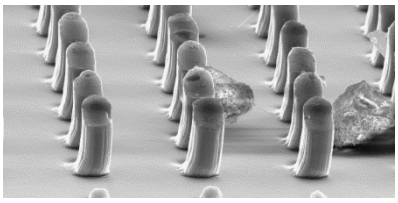

DOE 4

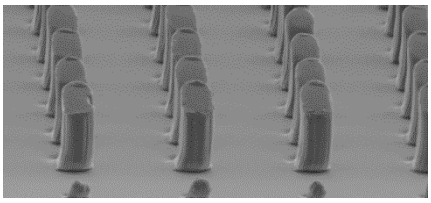

DOE 8

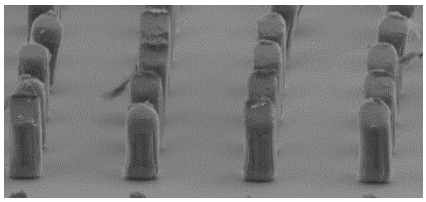

DOE 9

Figure 5.126 Most well replicated polypropylene 15 x 30 μm pillars

The pillars from DOE run 6 were observed to be the least well replicated (Figure 5.127).

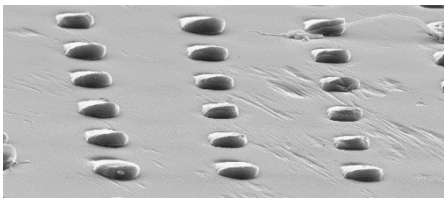

DOE 6

Figure 5.127 Least well replicated polypropylene 15 x 30 μm pillars

The 10 x 30 μm pillars were found to be replicated for all design of experiment runs. Those observed to be most successfully replicated were those found on the replicates from DOE runs 4 and 9 (Figure 5.128).

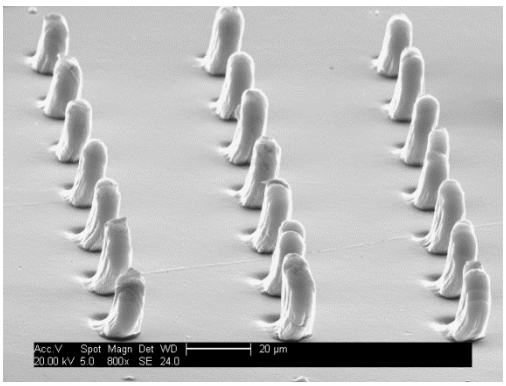

DOE 4

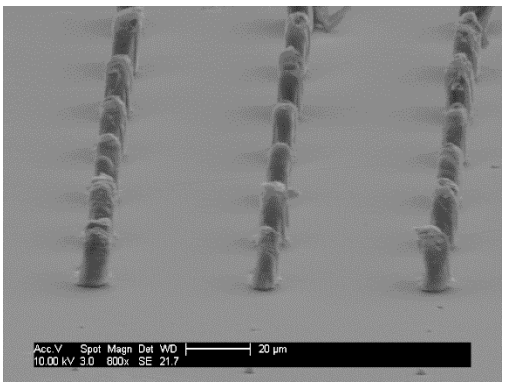

DOE 9

Figure 5.128 Most well replicated polypropylene 10 x 30 μm pillars

The pillars from DOE run 3 were found to have not been replicated. No 5 x 30 μm pillars were observed on replicates from any of the design of experiment runs.

The 15 x 10 μm pillars were observed on replicates from all design of experiment runs. Those observed to be most successfully replicated were those found on the replicates from DOE runs 4, 8 and 9 (Figure 5.129).

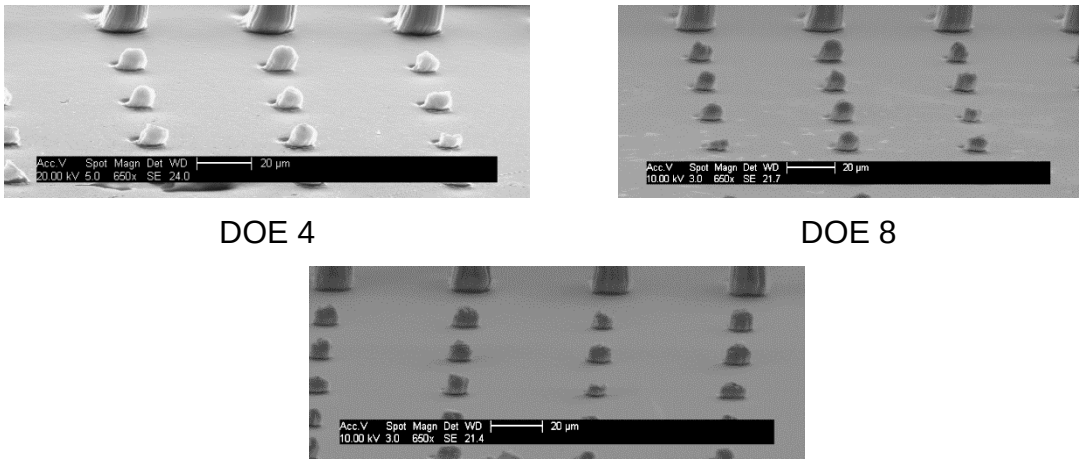

DOE 4 DOE 8

DOE 9

Figure 5.129 Most well replicated polypropylene 15 x 10 μm pillars

The pillars from DOE runs 2, 3 and 6 were observed to be the least well replicated (Figure 5.130).

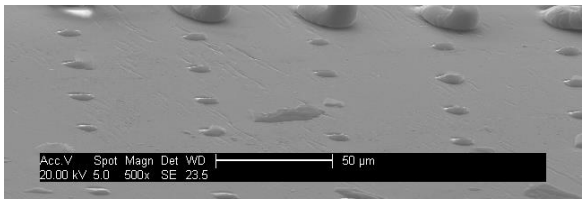

DOE 2

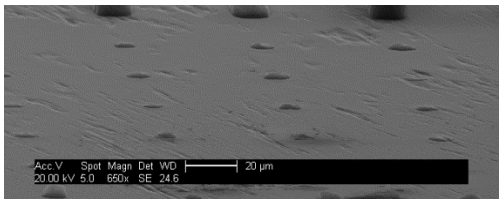

DOE 3

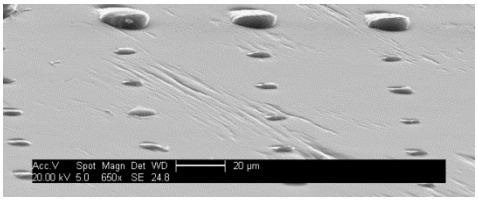

DOE 6

Figure 5.130 Least well replicated polypropylene 15 x 10 μm pillars

No 10 x 10 μm or 5 x 10 μm pillars were observed to have been replicated on any of the design of experiment runs.

The 19 x 80 μm pillars were observed on replicates from all design of experiment runs. Those observed to be most successfully replicated were those found on the replicates from DOE runs 4, 9 and 15 (Figure 5.131).

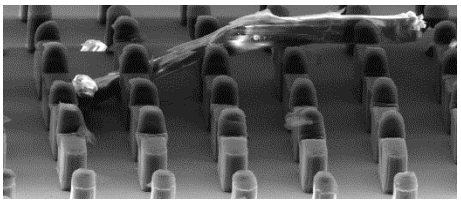

DOE 4

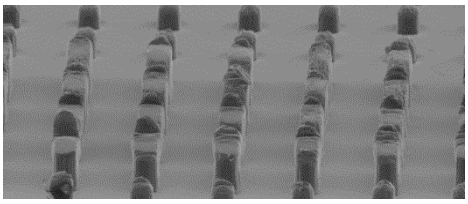

DOE 9

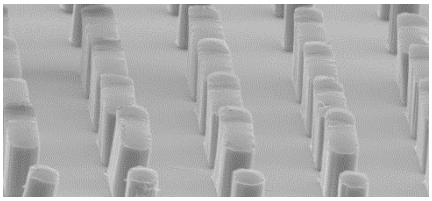

DOE 15

Figure 5.131 Most well replicated polypropylene 19 x 80 μm pillars

The pillars from DOE runs 5 and 6 were observed to be the least well replicated (Figure 5.132).

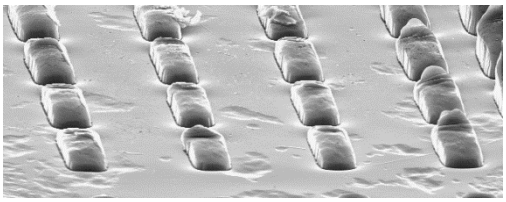

DOE 5

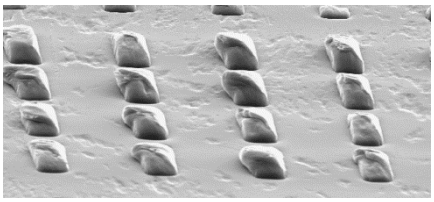

DOE 6

Figure 5.132 Least well replicated polypropylene 19 x 80 μm pillars

It was observed that the 19 x 80 μm were not replicated on samples from DOE run 3.

The 19 x 29 μm pillars were observed on replicates from all design of experiment runs. Those observed to be well replicated were those found on the replicates from DOE runs 4 and 15 (Figure 5.133).

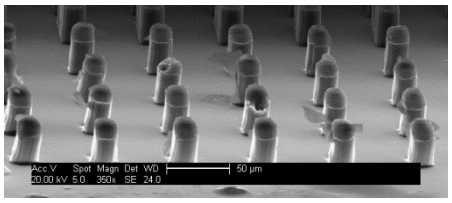

DOE 4

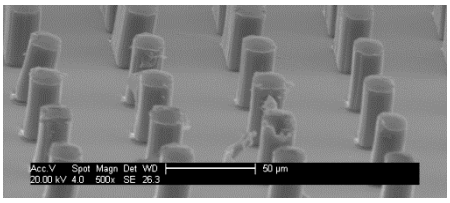

DOE 15

Figure 5.133 Most well replicated polypropylene 19 x 19 μm pillars

The pillars from DOE run 3 were observed to have not been replicated with those from DOE runs 5 and 6 to be the least well replicated of those observed to have been replicated (Figure 5.134).

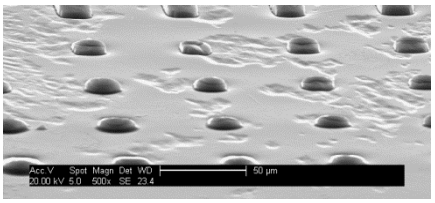

DOE 5

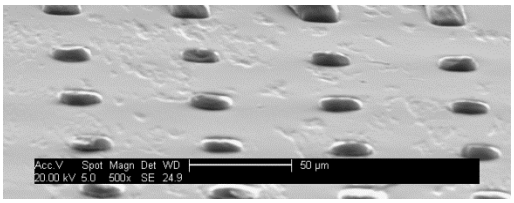

DOE 6

Figure 5.134 Least well replicated polypropylene 19 x 19 μm pillars

The 15 x 15 μm pillars were observed on replicates from all design of experiment runs. Those observed to be most well replicated were those found on the replicates from DOE run 4 and 8 (Figure 5.135).

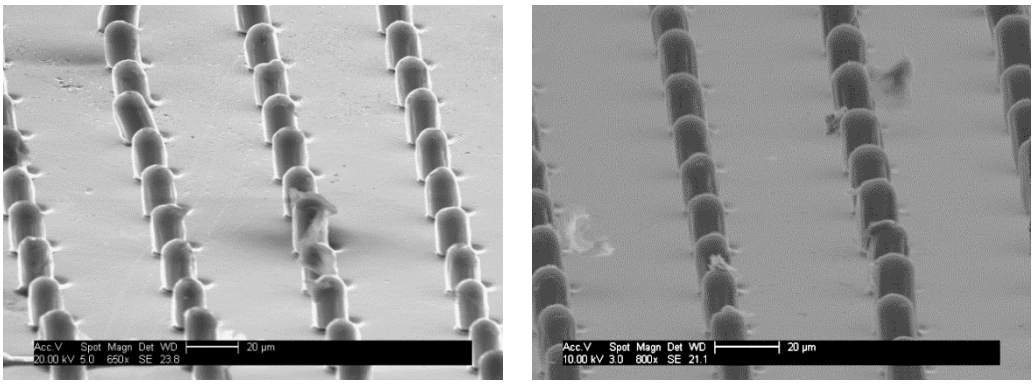

DOE 4 DOE 8

Figure 5.135 Most well replicated polypropylene 15 x 15 μm pillars

The pillars from DOE run 3 were observed to have not been replicated. No 10 x 10 μm or 5 x 5 μm pillars were observed to have been replicated on any of the design of experiment runs.

5.1.6 Appearance of high density polyethylene features

The appearance of pillar features on high density polyethylene replicates was examined. The following subsections present the various observations made whilst examining the replicate surfaces from all design of experiment runs.

5.1.6.1 High density polyethylene 40 – 80 μm pillar features

The 80 x 80 μm pillars were observed on replicates from all design of experiment runs. Those observed to be most successfully replicated were those found on the replicates from DOE runs 4 and 8 (Figure 5.136).

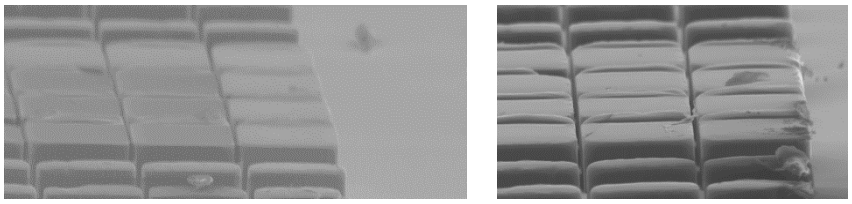

DOE 4 DOE 8

Figure 5.136 Most well replicated 80 x 80 μm high density polyethylene pillars

The pillars from DOE runs 13 and 16 were observed to be the least formed of those replicated (Figure 5.137).

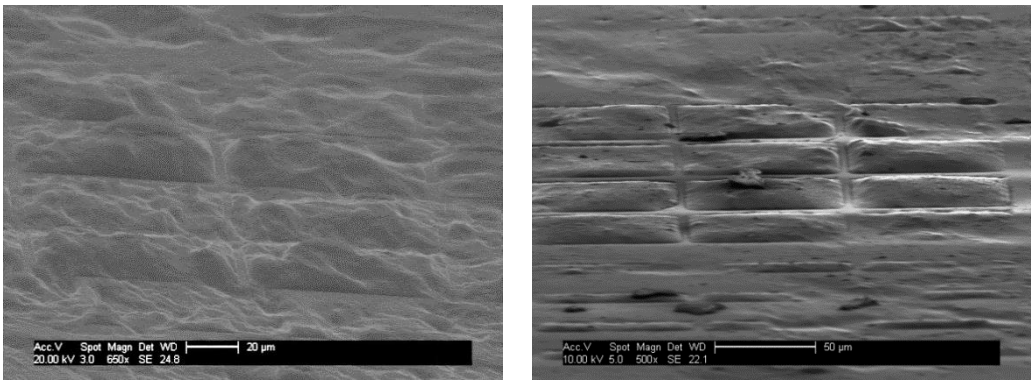

DOE 13 DOE 16

Figure 5.137 Least well replicated 80 x 80 μm high density polyethylene pillars

The 53 x 80 μm pillars were observed on replicates from all design of experiment runs. Those observed to be most successfully replicated were those found on the replicates from DOE runs 4, 8 and 15 (Figure 5.138).

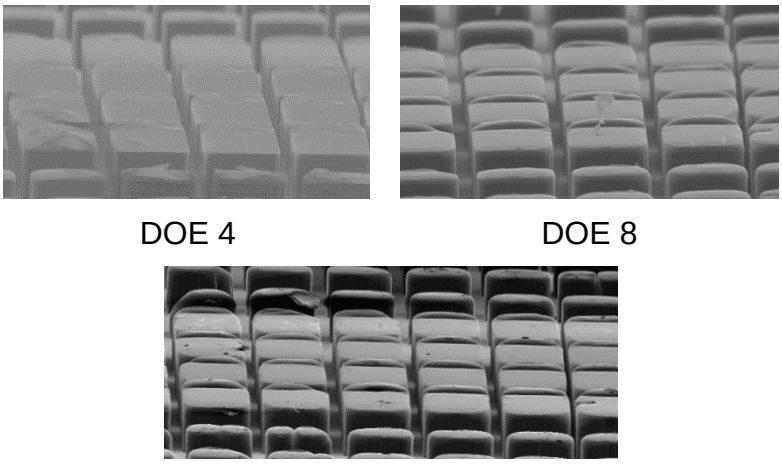

Figure 5.138 Most well replicated 53 x 80 μm high density polyethylene pillars

It was observed that the 53 x 80 μm pillars were not replicated on DOE run 13.

The 43 x 80 μm pillars were observed on replicates from all design of experiment runs. Those observed to be most successfully replicated were those found on the replicates from DOE runs 4, 8 and 15 (Figure 5.139). It was observed that the 43 x 80 μm pillars were not replicated on DOE run 13.

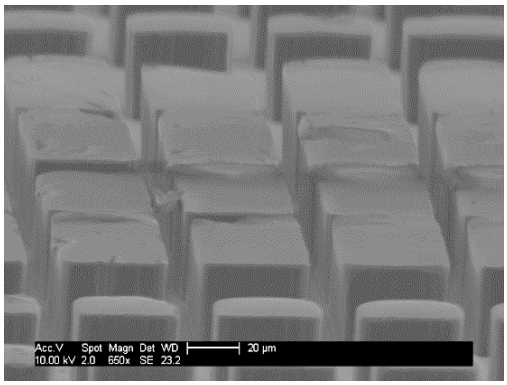

DOE 4

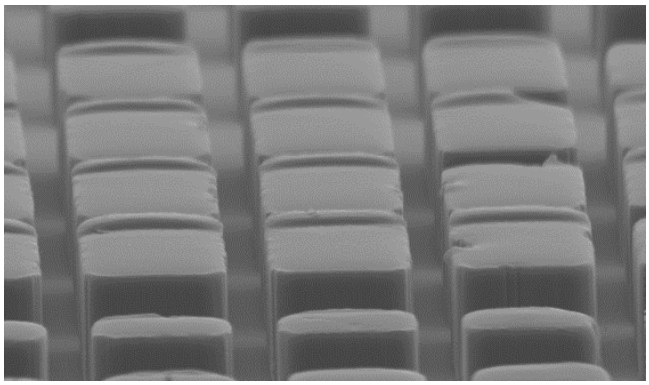

DOE 8

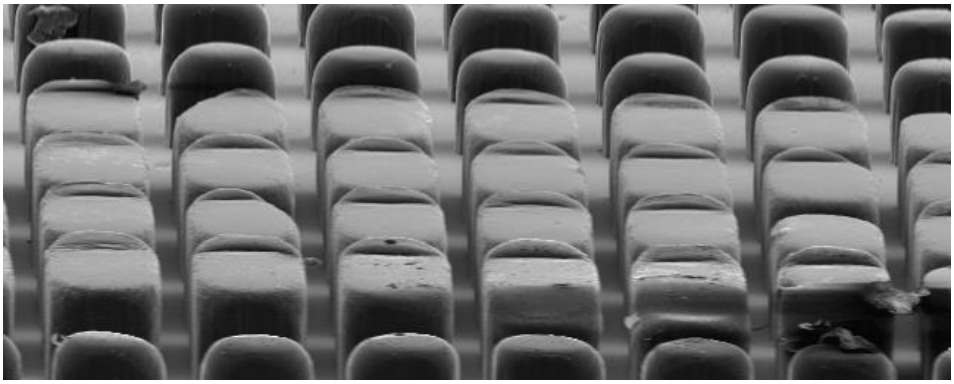

DOE 15

Figure 5.139 Most well replicated 43 x 80 μm high density polyethylene pillars

The 80 x 29 μm pillars were observed on replicates from all design of experiment runs. Those observed to be most successfully replicated were those found on the replicates from DOE runs 4, 8 and 15 (Figure 5.140). It was observed that the 80 x 29 μm pillars were not replicated on DOE run 13.

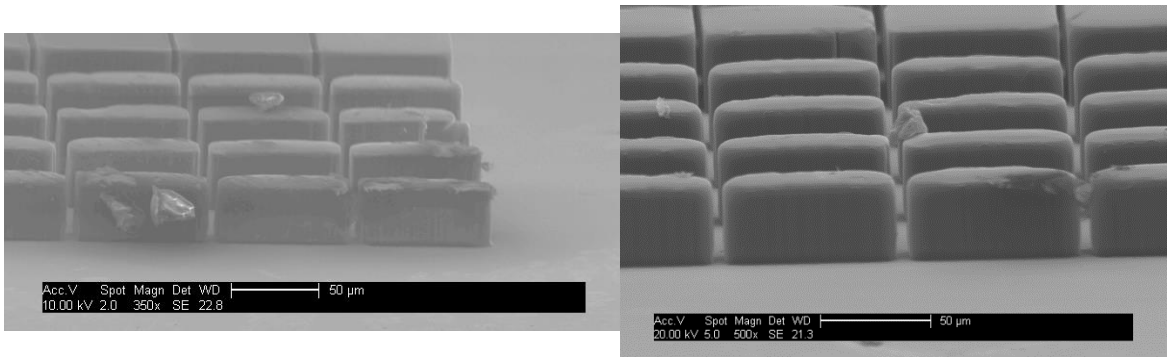

DOE 4 DOE 8

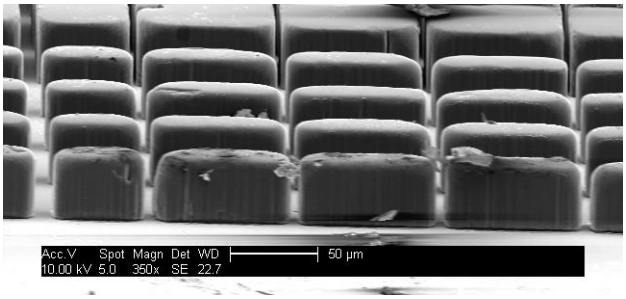

DOE 15

Figure 5.140 Most well replicated 80 x 29 μm high density polyethylene pillars

The 53 x 29 μm pillars were observed on replicates from all design of experiment runs. Those observed to be most successfully replicated were those found on the replicates from DOE runs 4, 8, 10 and 15 (Figure 5.141). It was observed that the 53 x 29 μm pillars were not replicated on DOE run 13.

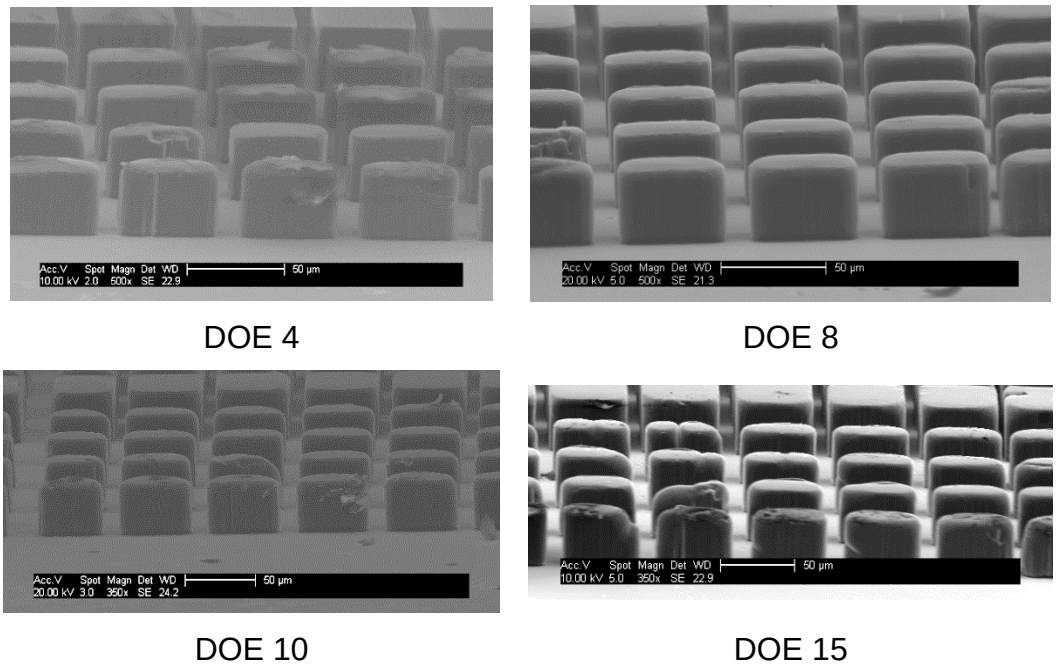

Figure 5.141 Most well replicated 53 x 29 μm high density polyethylene pillars

The 43 x 29 μm pillars were observed on replicates from all design of experiment runs. Those observed to be most successfully replicated were those found on the replicates from DOE runs 4 and 8 (Figure 5.142). It was observed that the 43 x 29 μm pillars were not replicated on DOE run 13.

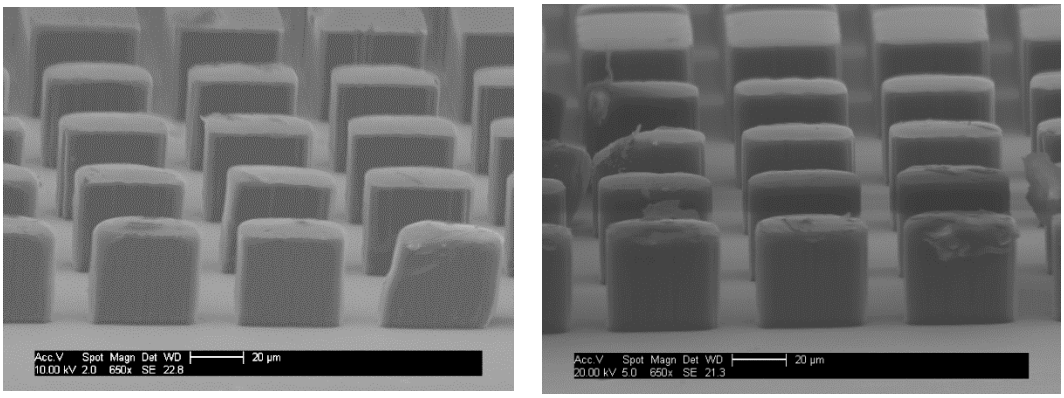

DOE 4 DOE 8

Figure 5.142 Most well replicated 43 x 29 μm high density polyethylene pillars

5.1.6.2 High density polyethylene 20 – 39 μm pillar features

The 30 x 30 μm pillars were observed on replicates from all design of experiment runs. Those observed to be most successfully replicated were those found on the replicates from DOE runs 4, 8 and 15 (Figure 5.143). It was observed that the 30 x 30 μm pillars were not replicated on DOE runs 13 and 16.

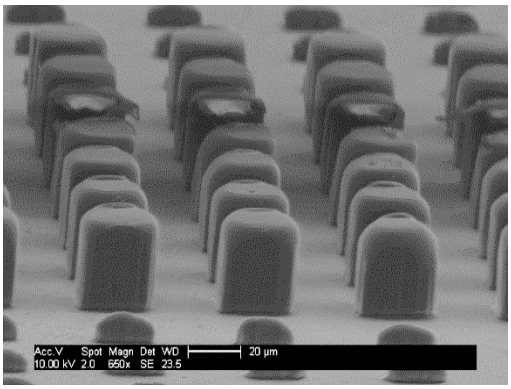

DOE 4

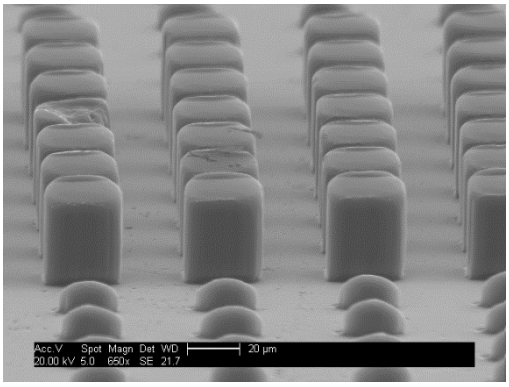

DOE 8

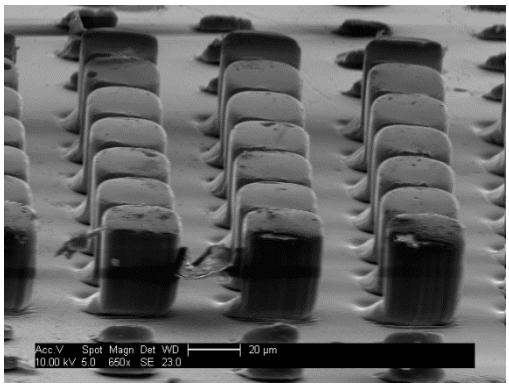

DOE 15

Figure 5.143 Most well replicated 30 x 30 μm high density polyethylene pillars

The 25 x 30 μm pillars were observed on replicates from all design of experiment runs. Those observed to be most successfully replicated were those found on the replicates from DOE runs 4, 8 and 15 (Figure 5.144). It was observed that the 25 x 30 μm pillars were not replicated on DOE runs 13 and 16.

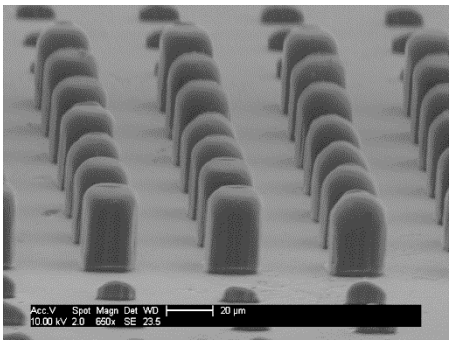

DOE 4

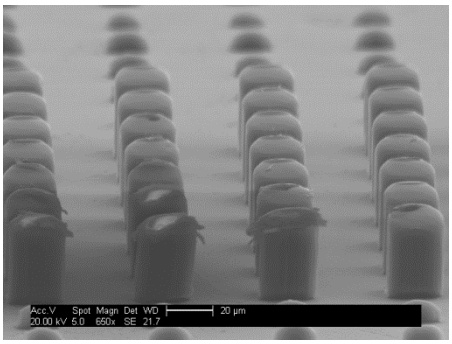

DOE 8

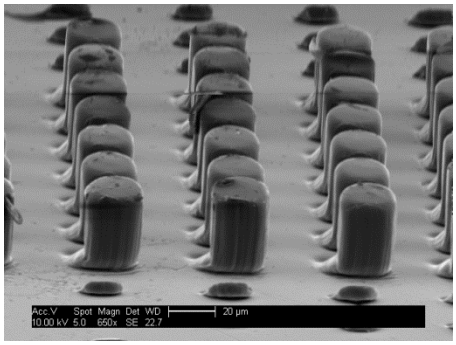

DOE 15

Figure 5.144 Most well replicated 25 x 30 μm high density polyethylene pillars

The 20 x 30 μm pillars were observed on replicates from all design of experiment runs. Those observed to be most successfully replicated were those found on the replicates from DOE runs 4, 8 and 15 (Figure 5.145). It was observed that the 20 x 30 μm pillars were not replicated on DOE runs 13 and 16.

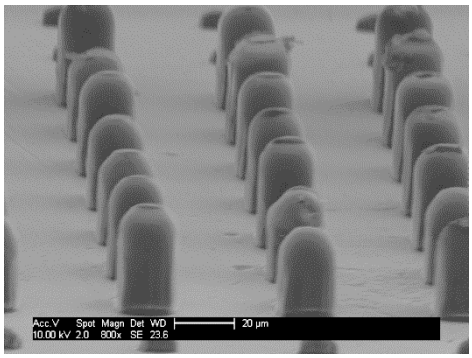

DOE 4

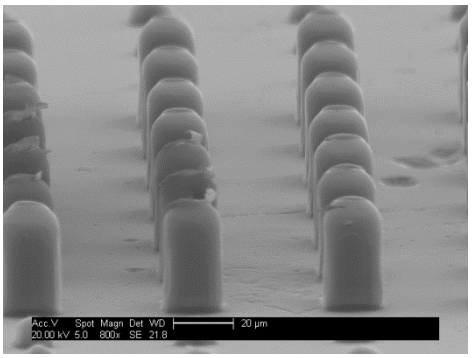

DOE 8

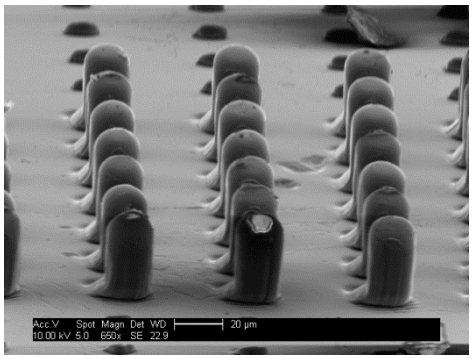

DOE 15

Figure 5.145 Most well replicated 20 x 30 μm high density polyethylene pillars

The 30 x 10 μm pillars were observed on replicates from all design of experiment runs. Those observed to be most successfully replicated were those found on the replicates from DOE runs 4 and 8 (Figure 5.146). It was observed that the 30 x 10 μm pillars were not replicated on DOE runs 5-7, 13 and 16.

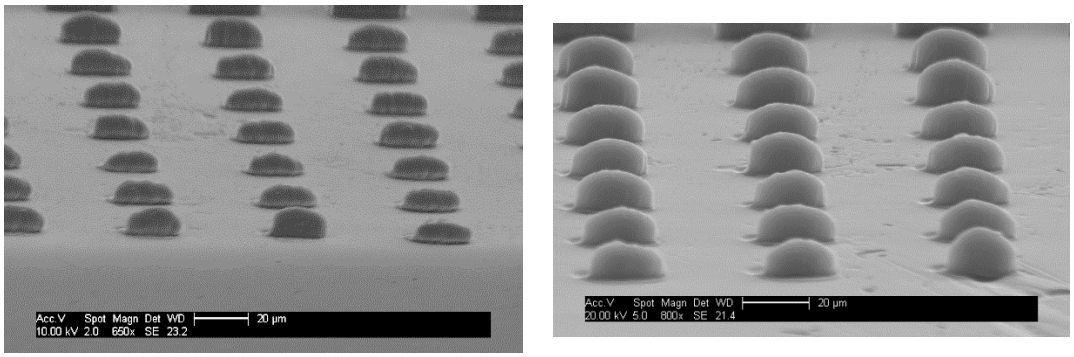

DOE 4 DOE 8

Figure 5.146 Most well replicated 30 x 10 μm high density polyethylene pillars

The 25 x 10 μm pillars were observed on replicates from all design of experiment runs. Those observed to be most successfully replicated were those found on the replicates from DOE runs 4 and 8 (Figure 5.147). It was observed that the 25 x 10 μm pillars were not replicated on DOE runs 1, 3, 5-7, 13 and 16.

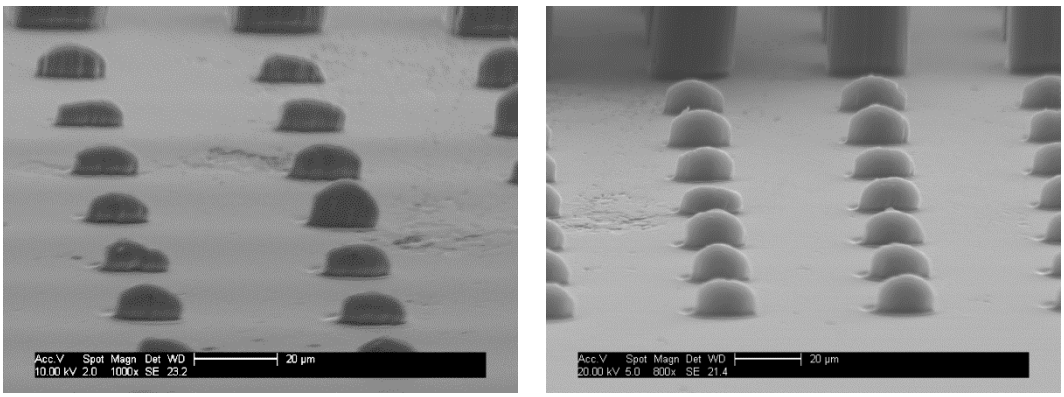

DOE 4 DOE 8

Figure 5.147 Most well replicated 25 x 30 μm high density polyethylene pillars

The 20 x 10 μm pillars were observed on replicates from all design of experiment runs. Those observed to be most successfully replicated were those found on the replicates from DOE runs 4 and 8 (Figure 5.148). It was observed that the 20 x 10 μm pillars were not replicated on DOE runs 1, 3, 5-7, 13 and 16.

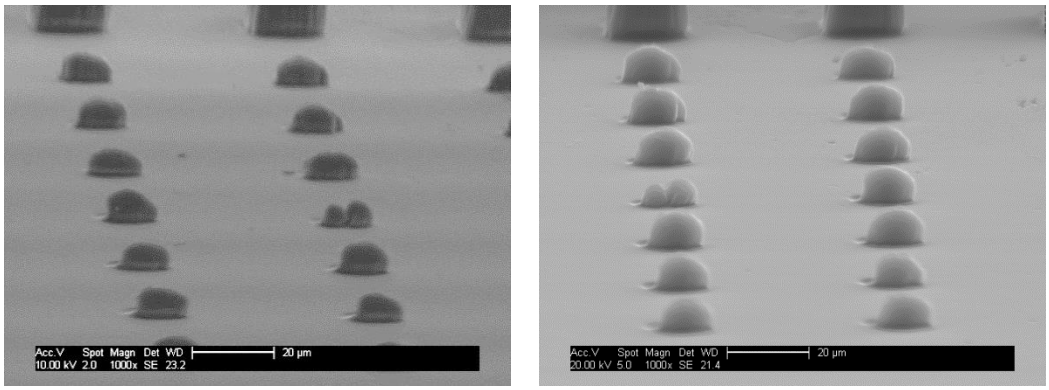

DOE 4 DOE 8

Figure 5.148 Most well replicated 20 x 10 μm high density polyethylene pillars

The 29 x 80 μm pillars were observed on replicates from all design of experiment runs. Those observed to be most successfully replicated were those found on the replicates from DOE runs 4, 8 and 15 (Figure 5.149). It was observed that the 29 x 80 μm pillars were not replicated on DOE runs 13 and 16.

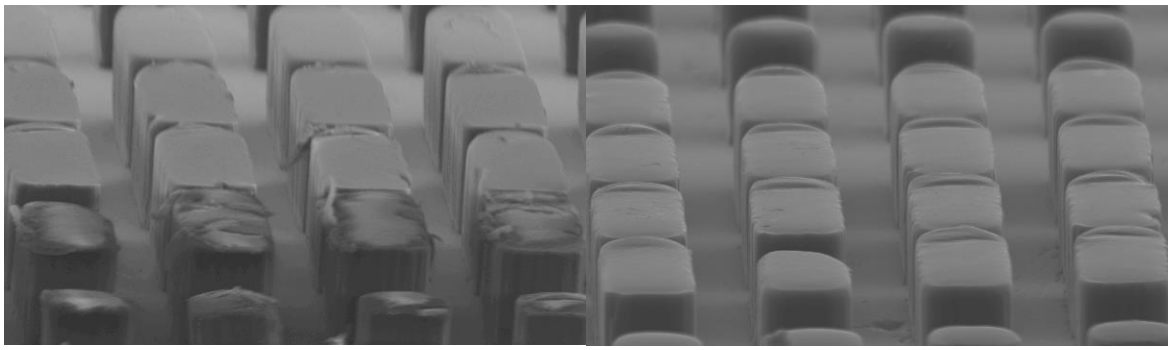

DOE 4 DOE 8

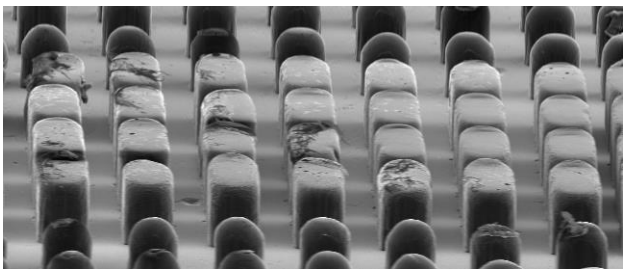

DOE 15

Figure 5.149 Most well replicated 29 x 80 μm high density polyethylene pillars

The 29 x 29 μm pillars were observed on replicates from all design of experiment runs. Those observed to be most successfully replicated were those found on the replicates from DOE runs 4 and 8 (Figure 5.150). It was observed that the 29 x 29 μm pillars were not replicated on DOE runs 13 and 16.

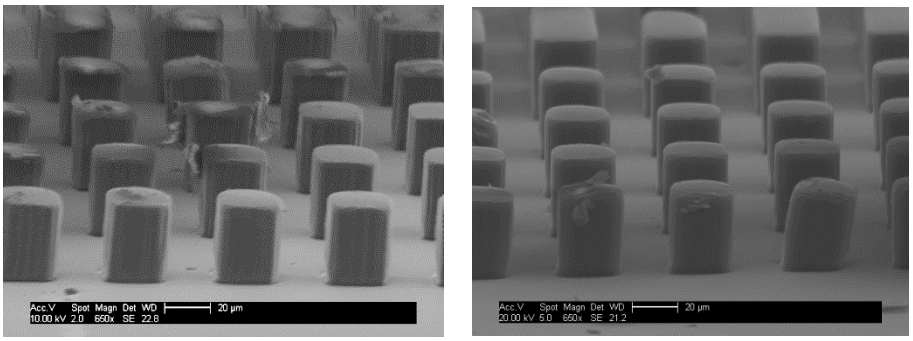

DOE 4 DOE 8

Figure 5.150 Most well replicated 29 x 29 µm high density polyethylene pillars

The 30 x 30 µm pillars were observed on replicates from all design of experiment runs. Those observed to be most successfully replicated were those found on the replicates from DOE runs 4 and 8 (Figure 5.151). It was observed that the 30 x 30 µm pillars were not replicated on DOE run 16.

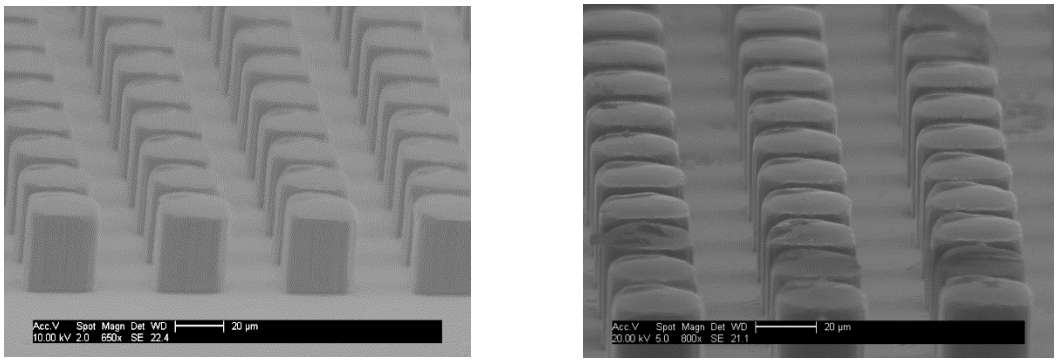

DOE 4 DOE 8

Figure 5.151 Most well replicated 30 x 30 µm high density polyethylene pillars located in square 5

The 25 x 25 μm pillars were observed on replicates from all design of experiment runs. Those observed to be most successfully replicated were those found on the replicates from DOE run 4 (Figure 5.152). It was observed that the 25 x 25 μm pillars were not replicated on DOE runs 13 and 16

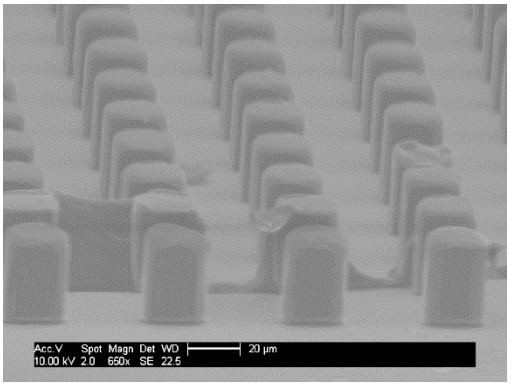

DOE 4

Figure 5.152 Most well replicated 25 x 25 μm high density polyethylene pillars

The 20 x 20 μm pillars were observed on replicates from all design of experiment runs. Those observed to be most successfully replicated were those found on the replicates from DOE runs 8 and 15 (Figure 5.153). It was observed that the 20 x 20 μm pillars were not replicated on DOE runs 13 and 16.

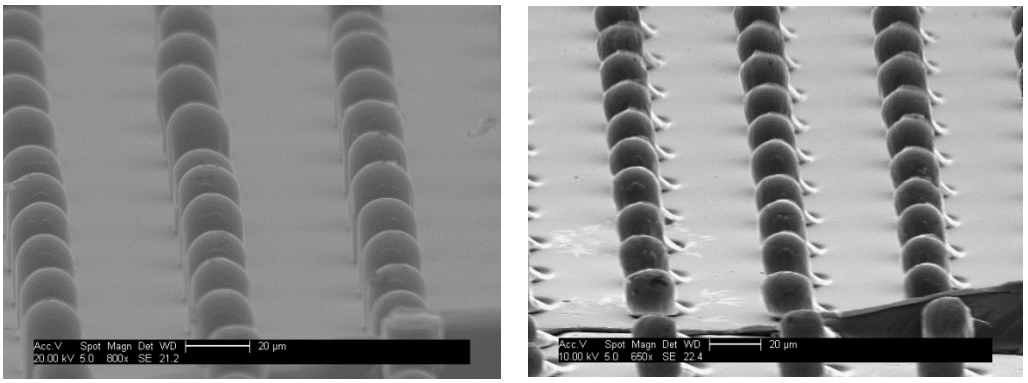

DOE 8 DOE 15

Figure 5.153 Most well replicated 20 x 20 μm high density polyethylene pillars

5.1.6.3 High density polyethylene 2 – 19 μm pillar features

The 15 x 30 μm pillars were observed on replicates from all design of experiment runs. Those observed to be most successfully replicated were those found on the replicates from DOE runs 4 and 8 (Figure 5.154). It was observed that the 15 x 30 μm pillars were not replicated on DOE runs 1, 3, 5, 13 and 16.

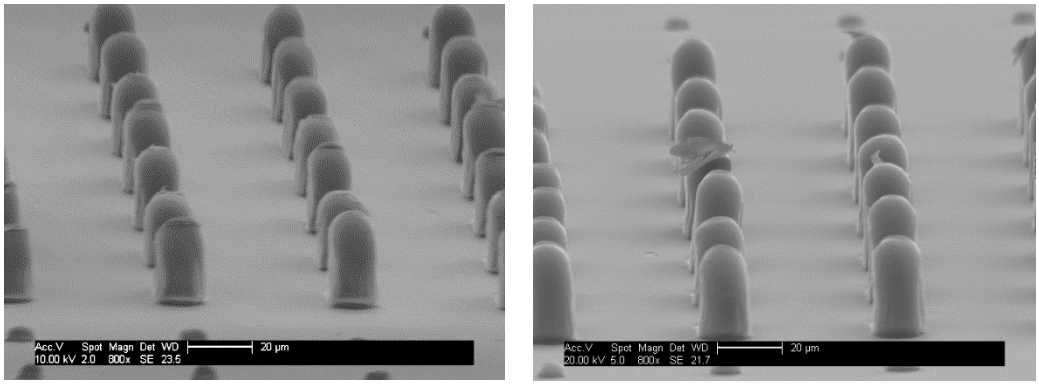

DOE 4 DOE 8

Figure 5.154 Most well replicated 15 x 30 μm high density polyethylene pillars

The 10 x 30 μm pillars were observed on replicates from all design of experiment runs. Those observed to be most successfully replicated were those found on the replicates from DOE runs 4 and 8 (Figure 5.155). It was observed that the 10 x 30 μm pillars were not replicated on DOE runs 1, 3, 5 - 7, 13 and 16.

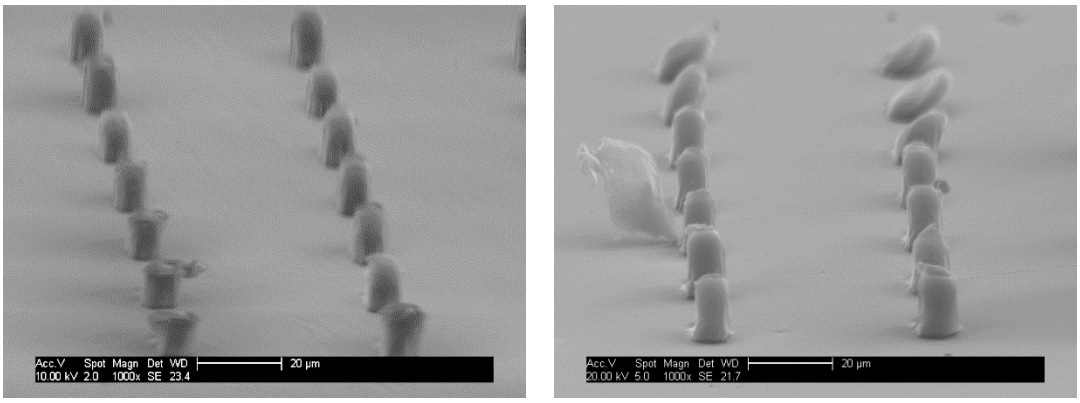

DOE 4 DOE 8

Figure 5.155 Most well replicated 10 x 30 μm high density polyethylene pillars

No 5 x 30 μm pillars were observed to have been replicated on any of the design of experiment runs.

The 15 x 10 μm pillars were observed on replicates from all design of experiment runs. Those observed to be most successfully replicated were those found on the replicates from DOE run 4 (Figure 5.156). It was observed that the 15 x 10 μm pillars were not replicated on DOE runs 1-3, 5-8, 13, 14 and 16.

No 10 x 10 μm or 5 x 5 μm pillars were observed to have been replicated on any of the design of experiment runs

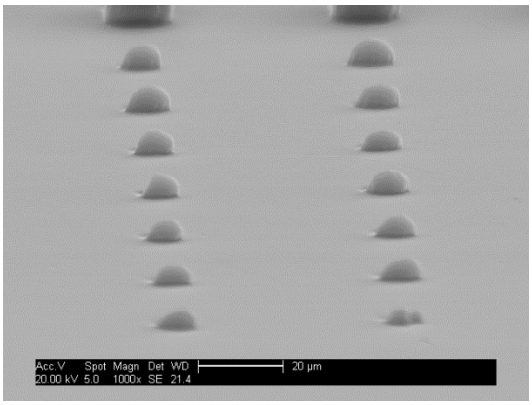

DOE 4

Figure 5.156 Most well replicated 15 x 10 μm high density polyethylene pillars

The 19 x 80 μm pillars were observed on replicates from all design of experiment runs. Those observed to be most successfully replicated were those found on the replicates from DOE runs 4, 8 and 15 (Figure 5.157). It was observed that the 19 x 80 μm pillars were not replicated on DOE runs 1, 3, 5, 13, 14 and 16.

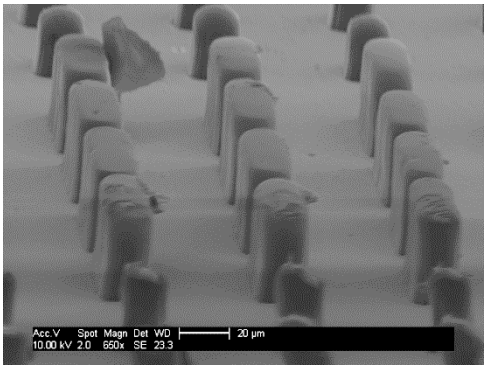

DOE 4

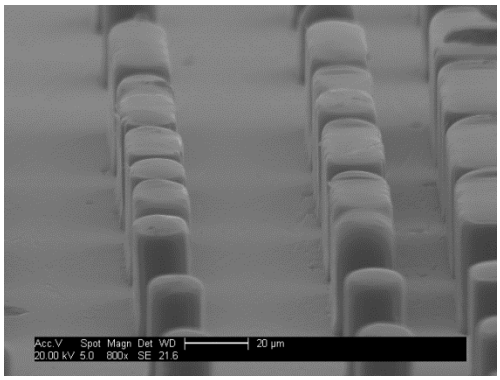

DOE 8

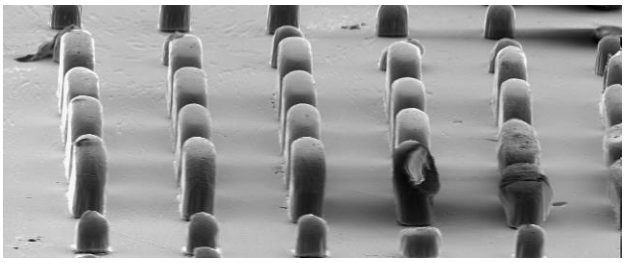

DOE 15

Figure 5.157 Most well replicated 19 x 80 μm high density polyethylene pillars

The 19 x 29 μm pillars were observed on replicates from all design of experiment runs. Those observed to be most successfully replicated were those found on the replicates from DOE run 8 (Figure 5.158). It was observed that the 19 x 29 μm pillars were not replicated on DOE runs 1, 13 and 16.

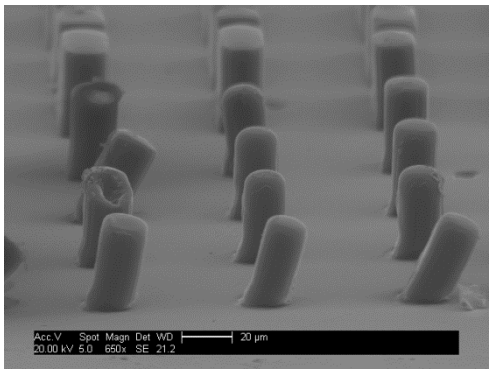

DOE 8

Figure 5.158 Most well replicated 19 x 29 μm high density polyethylene pillars

The 15 x 15 μm pillars were observed on replicates from all design of experiment runs. Those observed to be most successfully replicated were those found on the replicates from DOE run 8 (Figure 5.159). It was observed that the 15 x 15 μm pillars were not replicated on DOE runs 1, 3, 13, 14 and 16.

No 10 x 10 μm or 5 x 5 μm pillars were observed to have been replicated on any of the design of experiment runs.

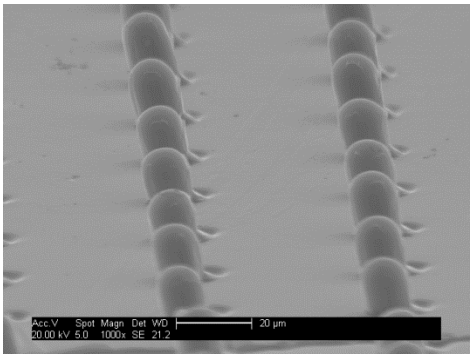

DOE 8

Figure 5.159 Most well replicated 15 x 15 μm high density polyethylene pillars

5.2 Design of experiment of 10 – 2 μm insert features

A design of experiment approach was used to examine how moulding temperature, cooling time, holding pressure and injection affected the production of polypropylene and high density polyethylene 10 x 10 μm, 5 x 5 μm and 2 x 2 μm pillar features by micro-injection moulding. The responses examined via statistical analysis were part and buffer mass as well as pillar width and height and the variation of the replicate features from the silicon mould insert.

No 5 x 5 μm or 2 x 2 μm pillars were found to have been replicated on the polypropylene features. None of the pillar features were found to have been replicated on the high density polyethylene replicates.

5.2.1 Part mass

The mass of ten replicates per design of experiment run was recorded and an average calculated. These averages were then statistically analysed using Pareto charts and main effects plots constructed in Minitab15® to determine the effect of the examined factors on the average part mass. The average part mass values recorded can be found in the appendix.

5.2.1.1 Statistical analysis of part mass of high density polyethylene and polypropylene replicates

Pareto charts generated identified injection speed as the most significant factor for both the polypropylene and high density polyethylene replicates.

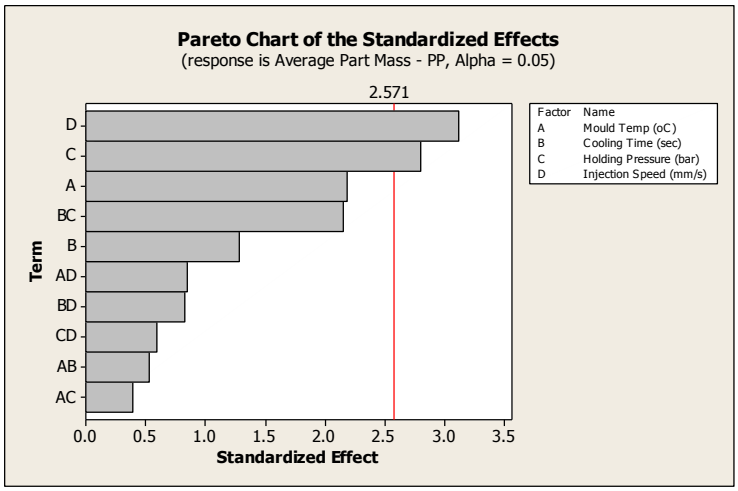

Figure 5.160 Most significant factor for part mass of polypropylene replicates

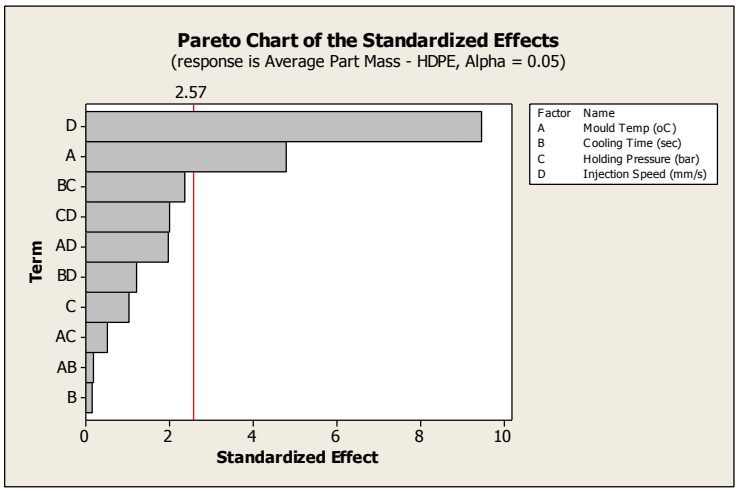

Figure 5.161 Most signficant factor for part mass of high density polyethylene replicates

5.2.2 Buffer mass

The buffer mass of ten replicates per design of experiment run was calculated and an average taken. These averages were then statistically analysed using

Pareto charts and main-effects plots to determine the effect of the examined factors on the average buffer mass. The average buffer mass values recorded can be found in the appendix.

5.2.2.1 Statistical analysis of buffer mass of high density polyethylene and polypropylene replicates

Upon examination of the Pareto Charts and main effects plots no factor was found to be significant to buffer mass for the polypropylene or high density polyethylene replicates. Holding pressure was found to have the main effect on average polypropylene buffer mass (Figure 5.162). While injection speed was found to be the factor with the main effect on the high density polyethylene average buffer mass (Figure 5.163).

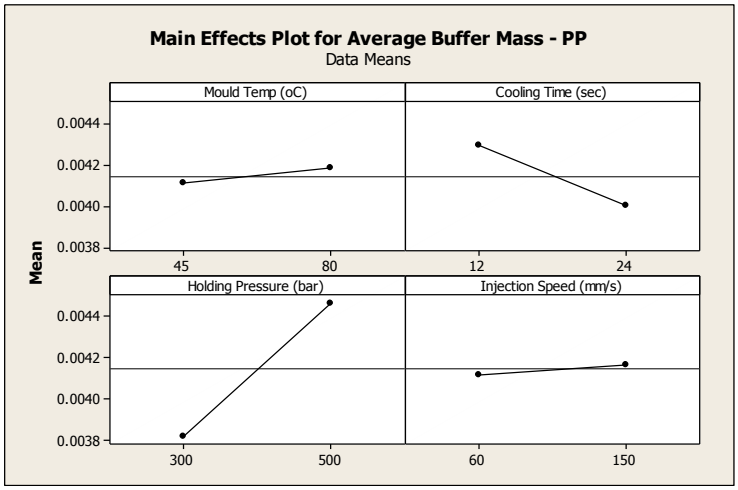

Figure 5.162 Main-effects plot – average buffer mass of polypropylene

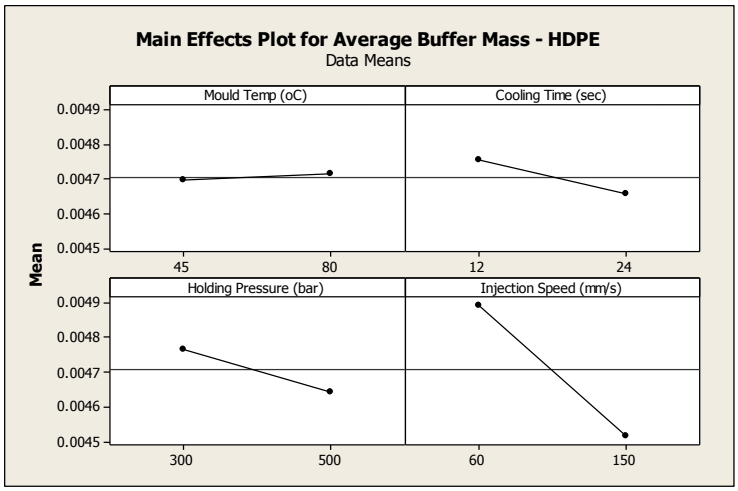

Figure 5.163 Main-effects plot – average buffer mass of high density polyethylene

5.2.3 Part dimensions of polypropylene pillar features

The height and width of ten pillars were measured on one replicated from each design of experiment run and an average calculated. These average values were then used to identify the factors with the most effect on the response and which factor and/or factor interaction was the most significant via statistical analysis. As previously mentioned only the 10 x 10 μm pillars were replicated.

The height and width averages calculated can be found in the appendix of this thesis.

5.2.3.1 Statistical analysis of polypropylene pillar features

Upon examination of the generated Pareto charts mould temperature was identified as the most significant factor regarding the height of the 10 x 10 μm pillars (Figure 5.164). No factor was identified as significant for the width of the 10 x 10 μm pillars.

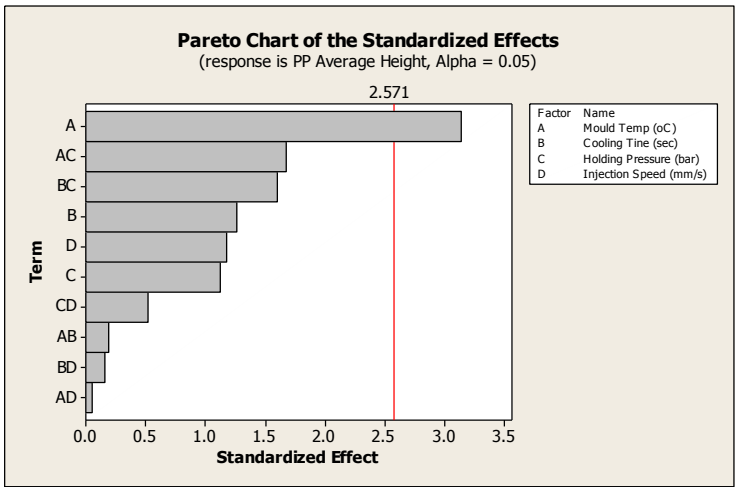

Figure 5.164 Most significant factor for 10 x 10 μm polypropylene pillar height

5.2.4 Polypropylene pillar feature variation from silicon mould insert

The variation of average height and width of pillars on polypropylene replicates from the silicon mould insert were calculated using the average height and width values calculated previously in section 5.2.3 *Dimensions of pillar features*, and measurements taken from the silicon mould insert. The values obtained were then statistically analysed using Pareto charts and main effects plots. The values calculated for replicate pillar variation from the silicon mould insert can be found in the appendix of this thesis.

5.2.4.1 Statistical analysis of polypropylene pillar feature variation from silicon mould insert

Examination of the Pareto charts generated for the variation of replicate pillar dimensions from the silicon mould insert identified mould temperature as the most significant factor for the height of the 10 x 10 μm pillars (Figure 5.165). No factor was identified as significant for the variation of replicate pillar width from the silicon mould insert.

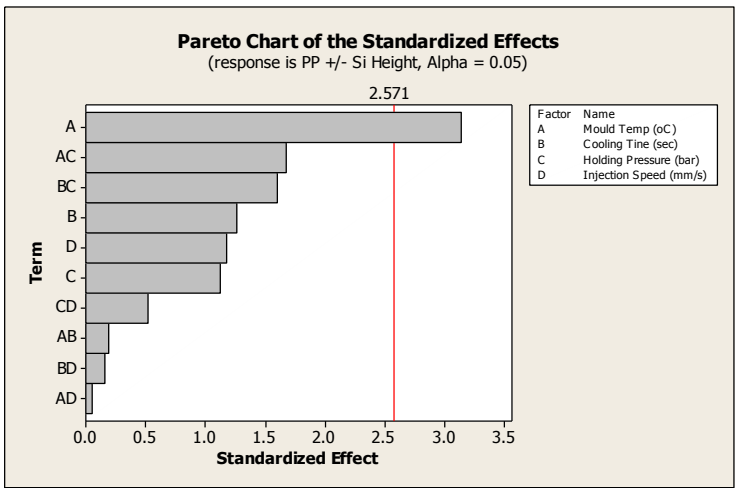

Figure 5.165 Most significant factor for the variation of 10 x 10 μm polypropylene pillar height from the silicon mould insert

5.2.5 Appearance of polypropylene features

None of the 2 x 2 μm features were produced on any of the polypropylene replicates. Slight indentations were found where the 5 x 5 μm pillars should have been replicated (Figure 5.166). But, no 5 x 5 μm pillars were found to be replicated on the polypropylene replicates. 10 x 10 μm pillar features were found to be replicated during all design of experiment runs. Optically the most successful replications were observed for DOE runs 4 and 8 (Figure 5.167) and the least successful were observed for DOE runs 3 and 16 (Figure 5.168).

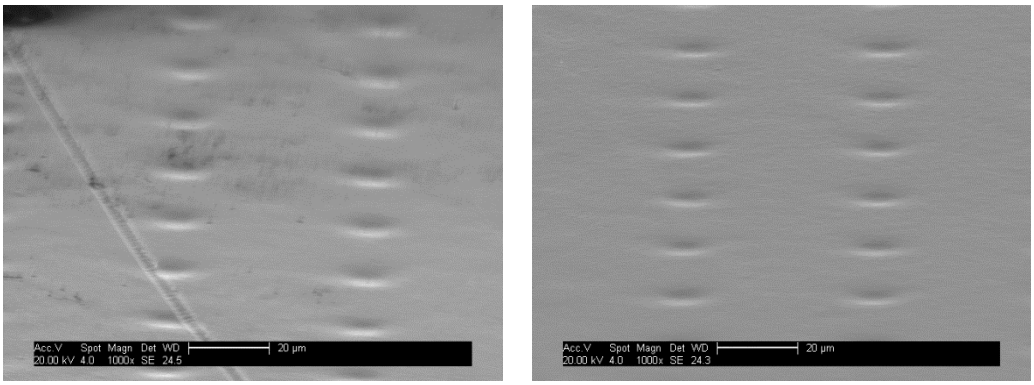

DOE 1 DOE 7

Figure 5.166 Indentations of 5 x 5 μm polypropylene pillars

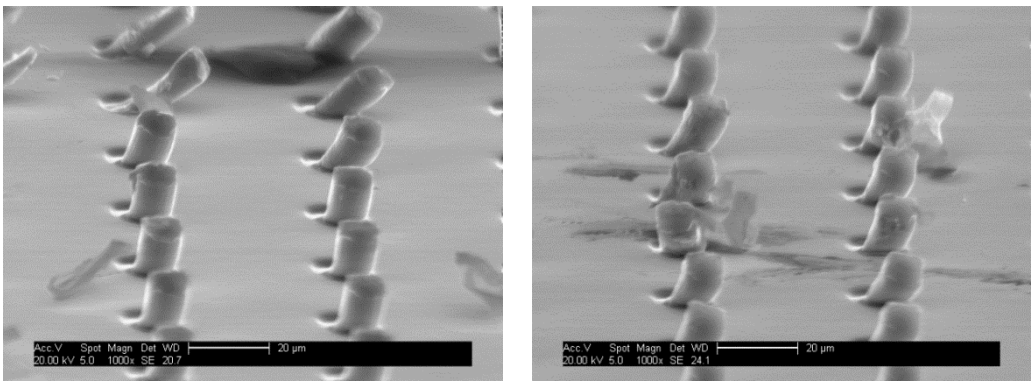

DOE run 4 DOE run 8

Figure 5.167 Most well replicated 10 x 10 μm polypropylene pillars

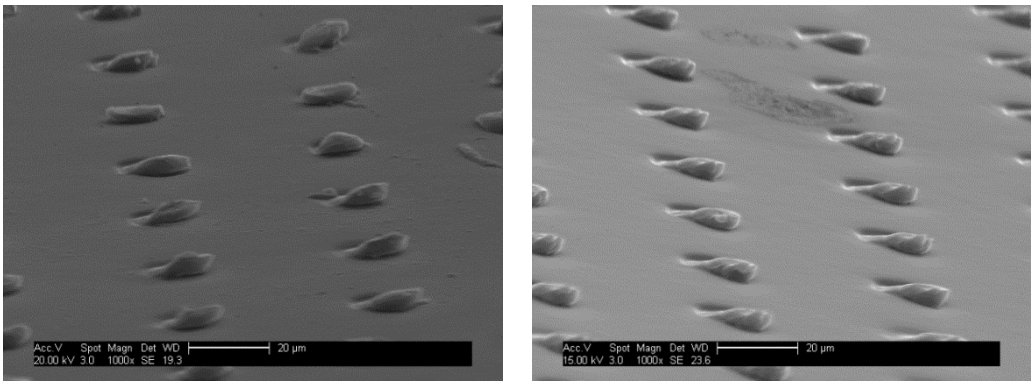

DOE run 3 DOE run 16

Figure 5.168 Least well replicated 10 x 10 μm polypropylene pillars

10 x 10 μm and 5 x 5 μm holes were replicated on all design of experiment run replicates examined. On some of the holes replicated a “lip” was observed at the entrance to the hole (Figure 5.169).

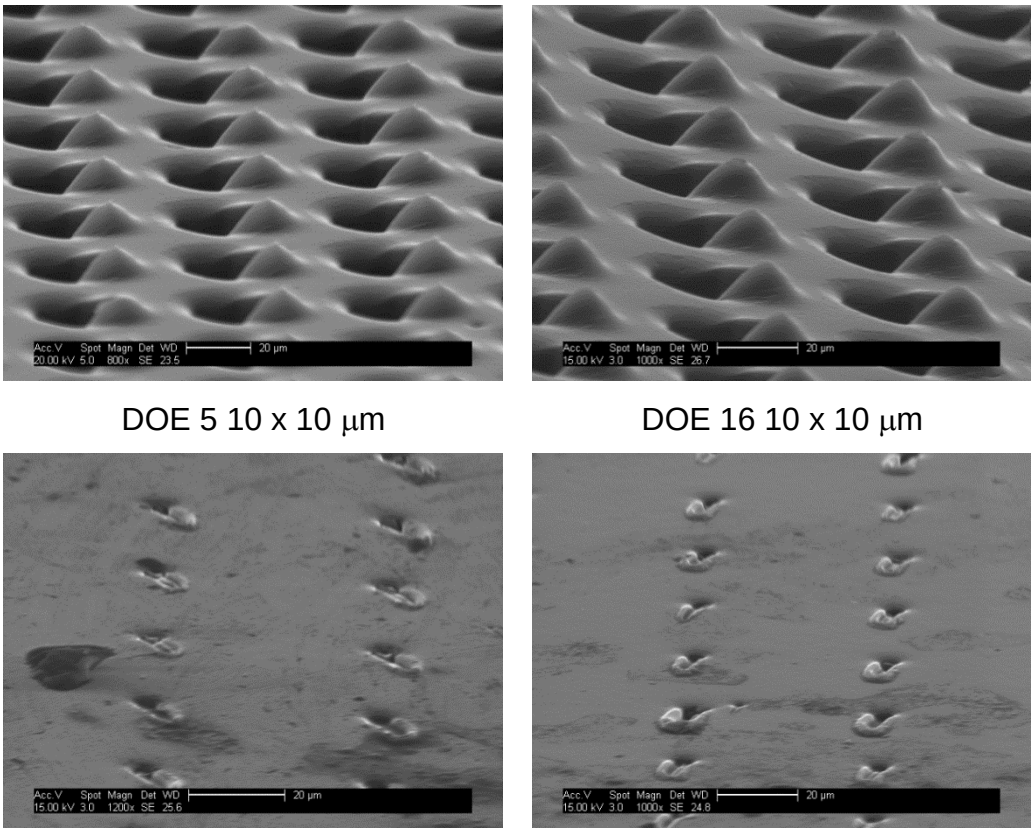

Figure 5.169 Irregularities in 10 x 10 μm and 5 x 5 μm polypropylene holes

5.2.6 Appearance of high density polyethylene features

None of the 2 x 2 μm features were produced on any of the high density polyethylene replicates. Slight indentations were found where the 10 x 10 μm pillars should have been replicated (Figure 5.170). But, no pillars (10 x 10 μm or 5 x 5 μm) were found to be replicated in the high density polyethylene replicates.

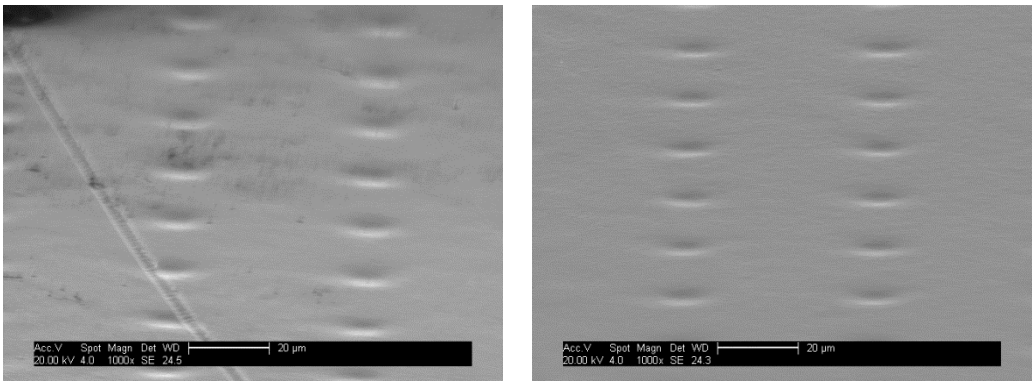

DOE 1 DOE 7

Figure 5.170 Indentations of 10 x 10 μm high density polyethylene pillars

10 x 10 μm and 5 x 5 μm holes were at least partially replicated in all high density polyethylene replicates examined. Some of the holes appeared not as deep as others (Figure 5.171).

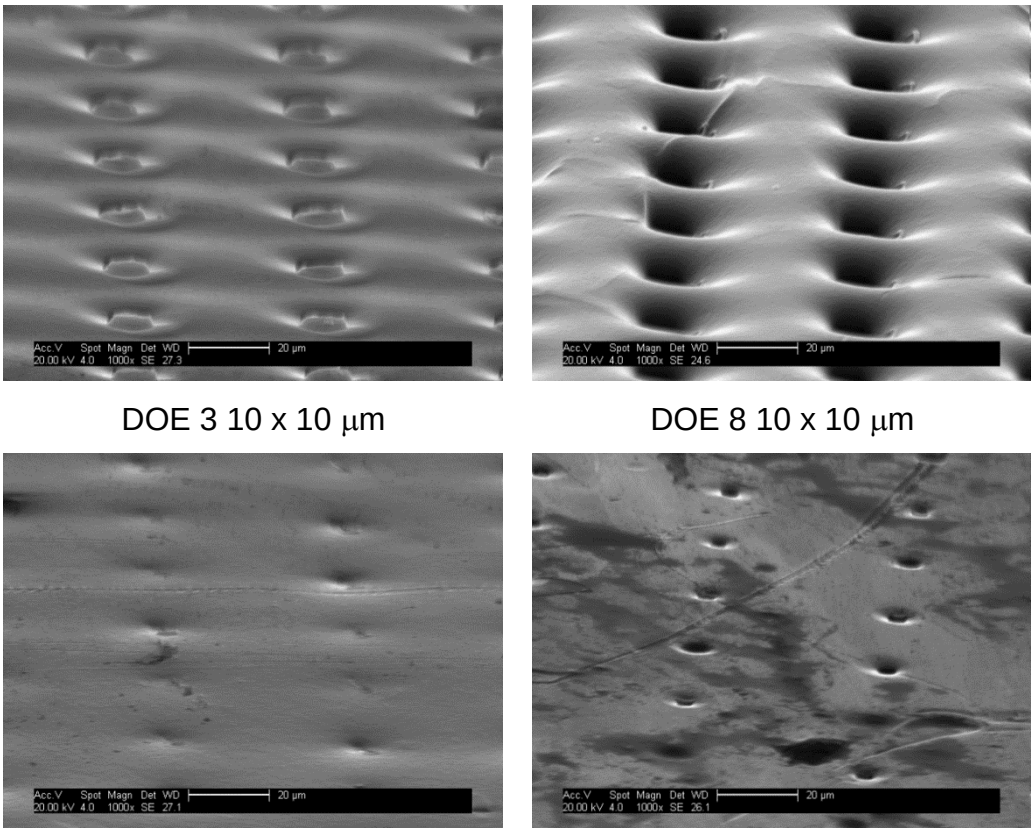

DOE 3 10 x 10 μm

DOE 8 10 x 10 μm

DOE 3 5x5μm

DOE 4 5x5μm

Figure 5.171 10 x 10 μm and 5 x 5 μm high density polyethylene holes

On some of the 10 x 10 μm holes formed a “lip” was observed at the entrance to the hole (Figure 5.172).

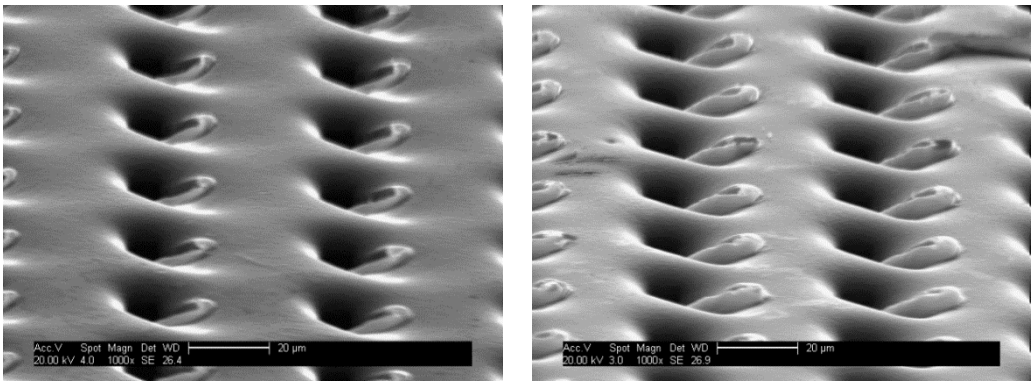

DOE 2 DOE 10

Figure 5.172 Irregularities in 10 x 10 μm high density polyethylene holes

5.3 Process window for polypropylene and high density polyethylene using process-volume-temperature curves

The process windows used during the undertaking of the design of experiments investigations are displayed on the pressure-volume-temperature (PVT) curves in Figure 5.173 and Figure 5.174.

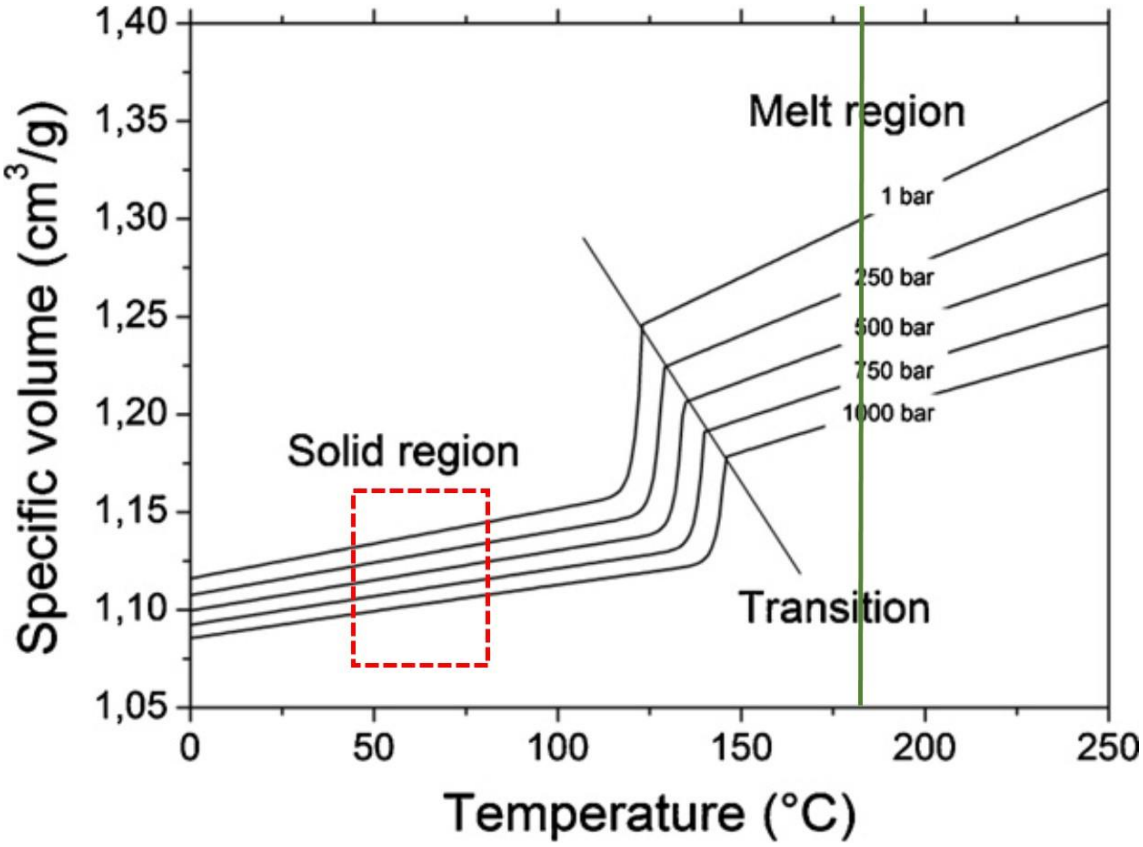

Figure 5.173 Pressure-volume-temperature curve for polypropylene[162], with process window and melt temperature used

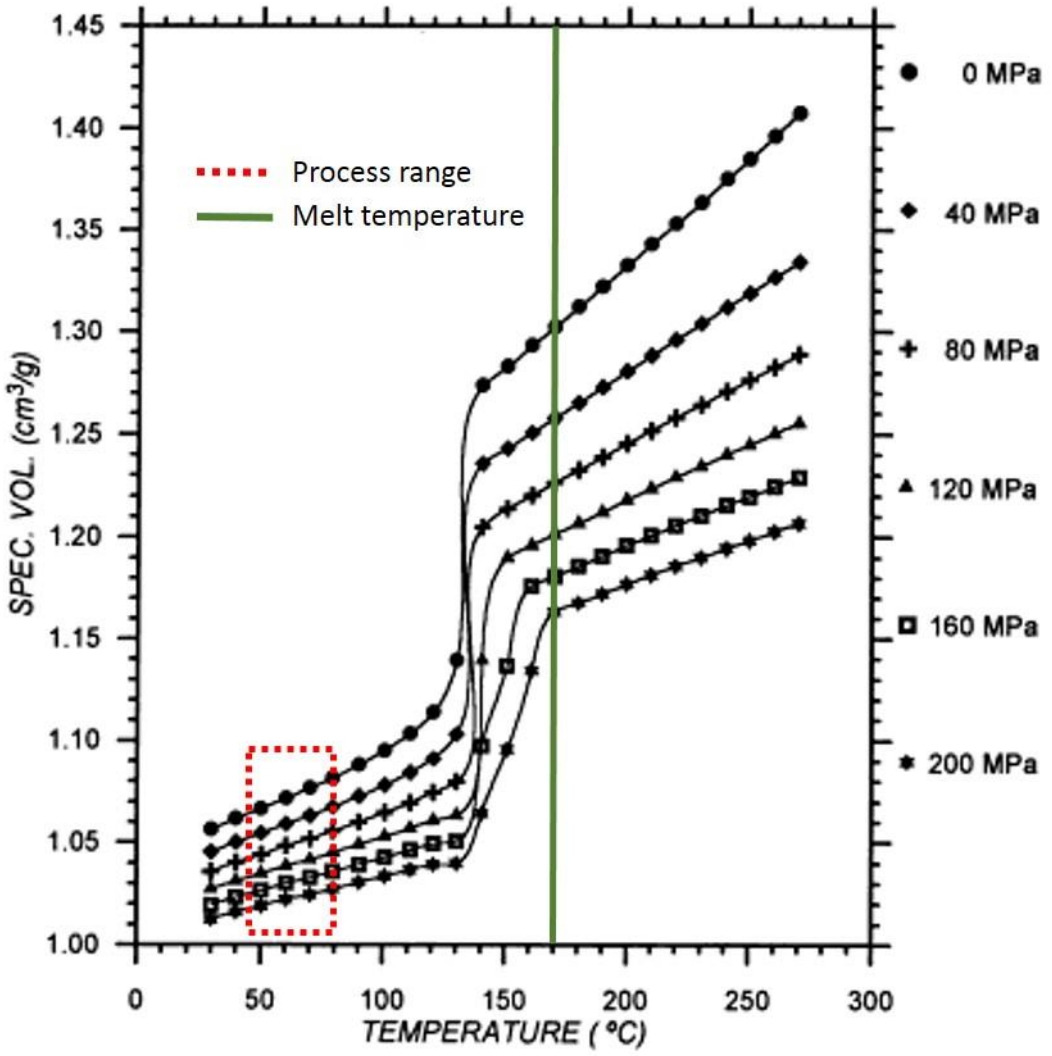

Figure 5.174 Pressure-volume-temperature curve for high density polyethylene[37], with process window and melt temperature used

5.4 Summary of polymer micro-injection moulding results

This chapter has presented the responses gathered through a design of experiment approach examining the fabrication of polymer micro-injection moulded replicates. The fabrication of polypropylene and high density polyethylene replicates using two surface designs, micro-channels and 10 – 2 μm, were examined. The responses of interest were part and buffer mass, pillar

height and width and the variation of the replicate pillar dimensions from the silicon mould insert.

The appearance of the surface of the replicates was also observed and the most and least well replicated pillars were identified at each pillar size. Irregular pillar formations, indentations, and feature deformations were also identified.

6 Metal injection moulding results

The following chapter outlines the design of experiment approach used for the examination of the fabrication of 316LS stainless steel replicates via metal-injection moulding. The design of experiment approach used examined how moulding temperature, cooling time, holding pressure and injection speed affect the production of 316LS pillar features ranging from 80 x 80 μm to 5 x 5 μm. Pareto charts and main effects plots were used to determine the most significant factor for the various responses selected. The responses examined were part mass, pillar width and height and the variation of the replicate pillar width and height from those on the silicon mould insert.

In the following chapter section *6.1 Part mass* will outline the results gathered regarding the average part mass of the 316LS replicates from each design of experiment run. The identification of significant factors and main effects on part mass is also outlined. In section *6.2 Part dimensions* the most significant factors relating to the height and width of the replicate pillars is displayed. Due to the large collection of feature sizes within the data section *6.2* has been divided into three subsections relating to the following three size ranges: 40 – 80 μm, 20 – 39 μm and 5 – 19 μm. In section *6.3 Dimensional variation of 316LS replicate from silicon mould insert* Pareto charts are used to display the most significant factors with regards to the variation of the 316LS features from the original silicon mould insert. As with section *6.2* the data has been divided into three subsections relating to the three size ranges previously mentioned. The recorded values for the pillar height and width as well as the variation of the replicate pillar dimensions from the silicon mould insert are tabulated and displayed within the appendix of this thesis. Section *6.4 Appearance of 316LS replicate features* outlines the variation in the replicate surface appearance across the various design of experiment runs. Once again this section is divided into three subsections relating to the three feature size ranges previously mentioned.

6.1 Part mass

The average part mass of 316LS replicates for the sixteen design of experiment runs is displayed in Table 6.1.

Table 6.1 Average part mass of 316LS replicates

DOE run	Average Part Mass 316LS (g)
1	3.52198
2	3.54684
3	3.53531
4	3.53140
5	3.53715
6	3.50816
7	3.49235
8	3.51144
9	3.54073
10	3.51175
11	3.52308
12	3.52851
13	3.51982
14	3.51828
15	3.49977
16	3.51981

6.1.1 Statistical analysis of part mass of 316LS stainless steel replicates

Upon examination of the Pareto chart it was found that injection speed was the most significant factor when considering part mass, followed by holding pressure and then the interaction between cooling time and injection speed (Figure 6.1). Injection speed was also found to be the factor with the main effect on part mass upon examination of the main effects plot (Figure 6.2).

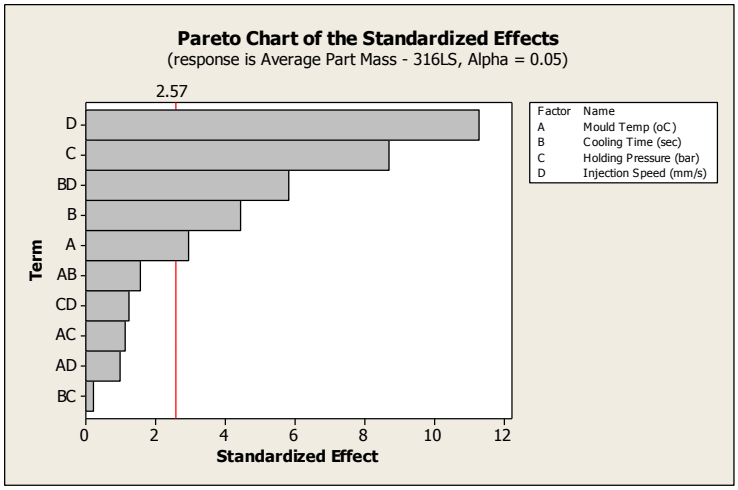

Figure 6.1 Pareto chart – Average part mass of 316LS replicates

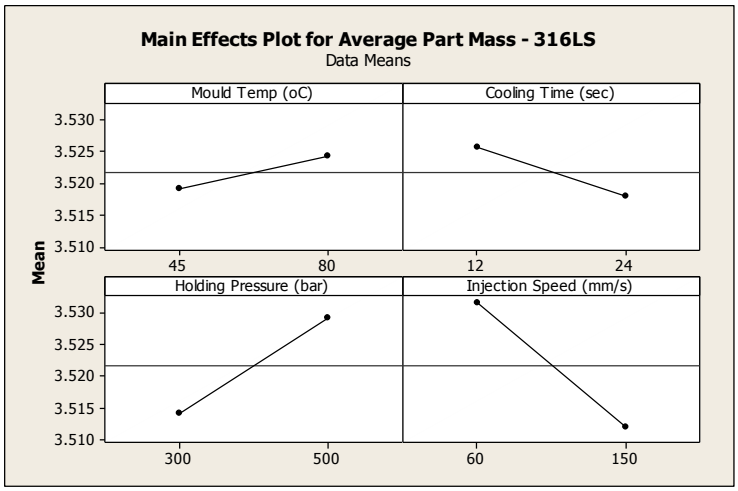

Figure 6.2 Main effects plot – Average part mass of 316LS stainless steel

6.2 Part dimensions

The 316LS replicates were structured with micro-channel insert features. The feature width dimensions ranged from 80 x 80 μm – 5 x 5 μm. In order to simplify analysis the pillars have been separated into three groups according to the pillar widths measured. The width ranges selected were 40 – 80 μm, 20 – 39 μm and 5 – 19 μm (Table 3.5).

Table 6.2 Pillar analysis ranges

Dimension range (μm)	Pillar dimensions (μm)
40 – 80	80 x 80
	53 x 80
	43 x 80
	80 x 29
	53 x 29
	43 x 29
20 – 39	29 x 80
	29 x 29
5 - 19	19 x 80
	19 x 29

6.2.1 Statistical analysis of 40 – 80 μm pillar features

Using Pareto charts mould temperature was found to be the most significant factor with regards to the height and width of 80 x 80 μm pillars (Figure 6.3 and Figure 6.4). Injection speed was found to be the most significant factor for the height of 53 x 80 μm pillars (Figure 6.5). Significant factors were not identified for the height of 40 x 80, 80 x 29, 53 x 29 and 43 x 29 μm pillars or for the width of 53 x 80, 43 x 80, 80 x 29, 53 x 29 and 43 x 29 μm pillars.

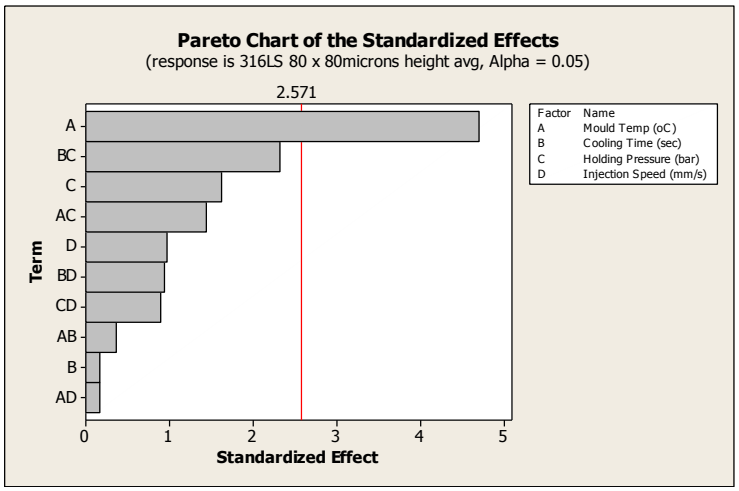

Figure 6.3 Pareto chart – most significant factor for the height of 80 x 80 μm 316LS pillars

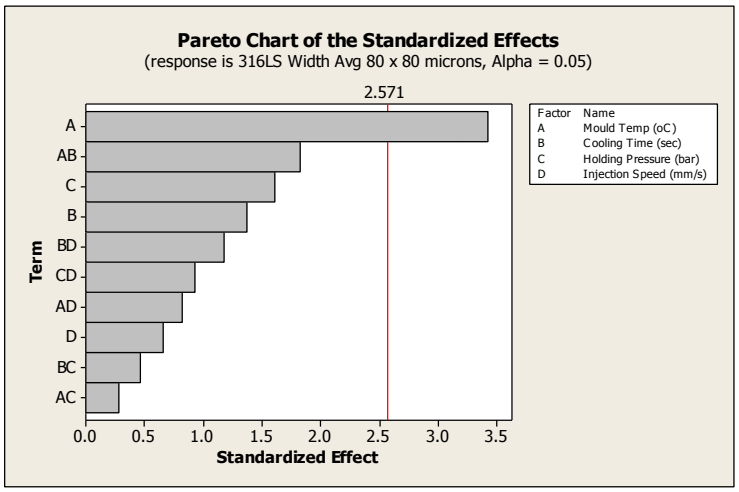

Figure 6.4 Pareto chart – most significant factor for the width of 80 x 80 μm 316LS pillars

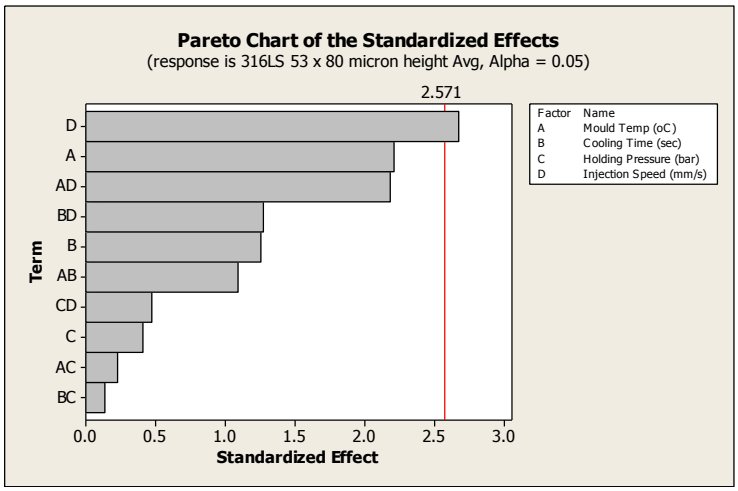

Figure 6.5 Pareto chart – most significant factor for the height of 53 x 80 μm 316LS pillars

6.2.2 Statistical analysis of 20 – 39 μm pillar features

Using Pareto charts holding pressure was found to be the most significant factor with regards to the height and width of 29 x 29 μm pillars (Figure 6.6).Significant factors were not identified for the height of the 29 x 80 mm pillars or the width of the 29 x 80 and the 29 x 29 μm pillars.

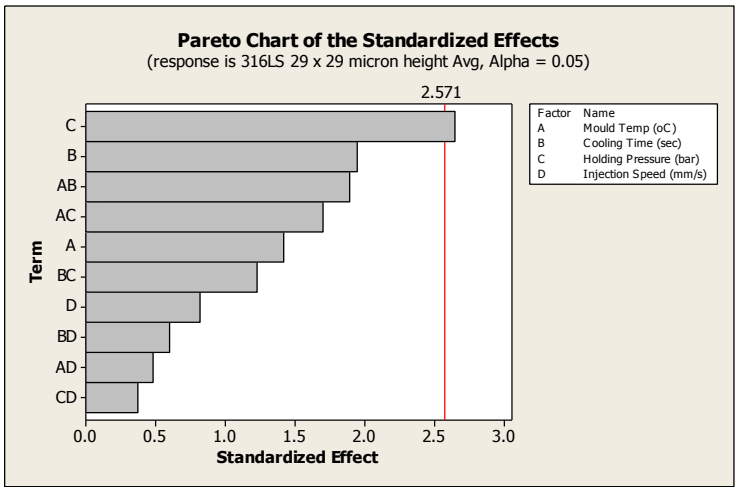

Figure 6.6 Pareto chart – most significant factor for the height of 29 x 29 μm 316LS pillars

6.2.3 Statistical analysis of 5 – 19 μm pillar features

Using Pareto charts moulding temperature was found to be the most significant factor followed by the interactions between mould temperature and cooling time with regards to the height of 19 x 80 μm pillars (Figure 6.7).Significant factors were not identified for the height of the 19 x 29 mm pillars or the width of the 19 x 80 and the 19 x 29 μm pillars

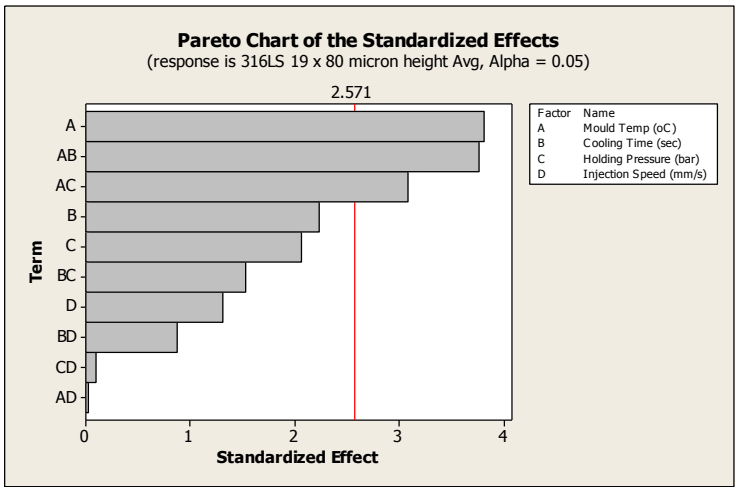

Figure 6.7 Pareto chart – most significant factor for the height of 19 x 80 μm 316LS pillars

6.3 Dimensional variation of 316LS replicate from silicon mould insert

As with the previous section the pillars in this subsection have been separated into three groups according to the pillar widths measured. The width ranges selected were 40 – 80 μm, 20 – 39 μm and 5 – 19 μm (Table 3.5).

6.3.1 Statistical analysis of 40 – 80 μm pillar feature variation from silicon mould insert

Using Pareto charts mould temperature was found to be the most significant factor with regards to the variation in replicate pillar height and width from the silicon mould insert of 80 x 80 μm pillars (Figure 6.8 and Figure 6.9). Injection speed was found to be the most significant factor for the variation in replicate pillar height from the silicon mould insert of the 53 x 80 μm pillars (Figure 6.10). Significant factors were not identified for the replicate pillar dimension variation from the silicon mould insert of the height of 40 x 80, 80 x 29, 53 x 29 and 43 x

29 μm pillars or for the width of 53 x 80, 43 x 80, 80 x 29, 53 x 29 and 43 x 29 μm pillars.

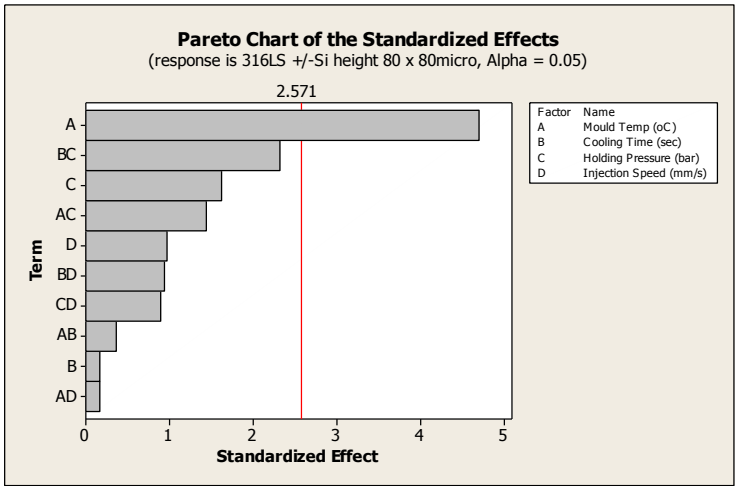

Figure 6.8 Pareto chart – most significant factor for the height of 80 x 80 μm 316LS pillars

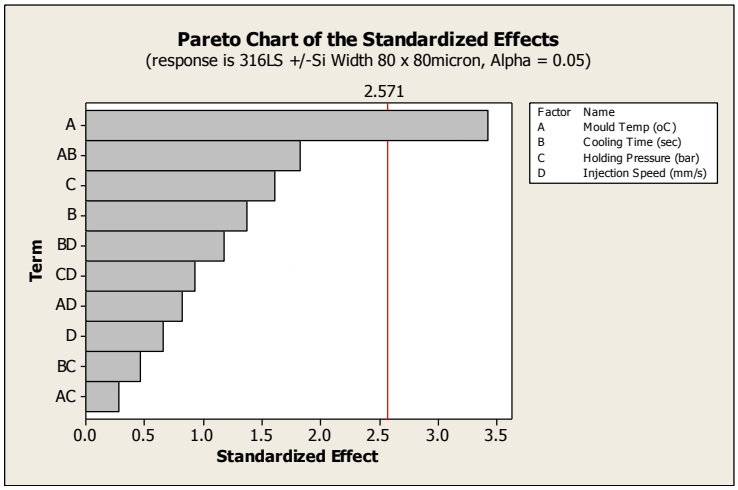

Figure 6.9 Pareto chart – most significant factor for the width of 80 x 80 μm 316LS pillars

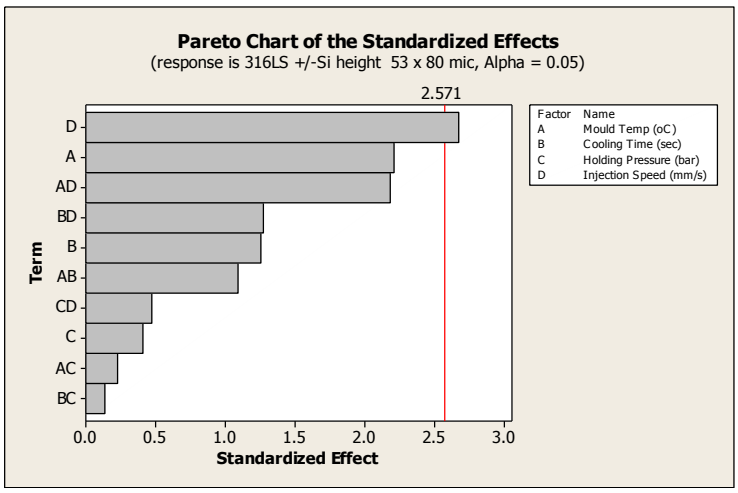

Figure 6.10 Pareto chart – most significant factor for the width of 53 x 80 μm 316LS pillars

6.3.2 Statistical analysis of 20 – 39 μm pillar feature variation from silicon mould insert

Using Pareto charts holding pressure was found to be the most significant factor with regards to the variation in replicate pillar height from the silicon mould insert of 29 x 29 μm pillars (Figure 6.11).Significant factors were not identified for the replicate pillar dimension variation from the silicon mould insert of the height of 29 x 80 μm pillars or for the width of 29 x 80 and 29 x 29 μm pillars.

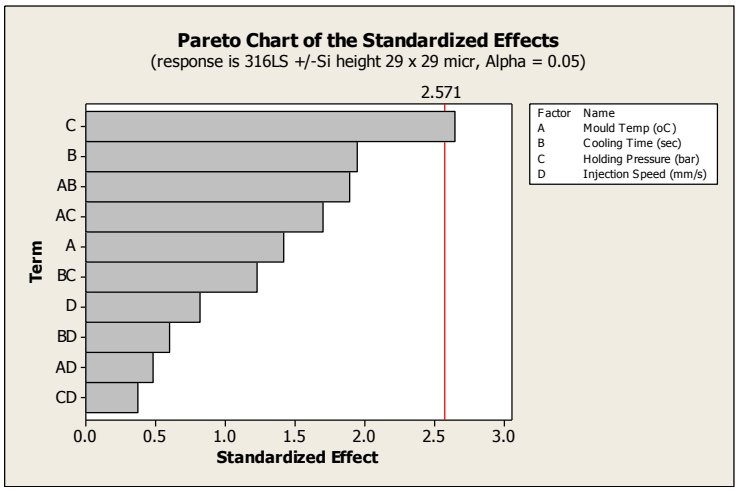

Figure 6.11 Pareto chart – most significant factor for the width of 29 x 29 μm 316LS pillars

6.3.3 Statistical analysis of 5 – 19 μm pillar feature variation from silicon mould insert

Using Pareto charts moulding temperature was found to be the most significant factor followed by the interactions between mould temperature and cooling time with regards to the variation in replicate pillar height from the silicon mould insert of 29 x 29 μm pillars (Figure 6.12).Significant factors were not identified for the replicate pillar dimension variation from the silicon mould insert of the height of 19 x 29 μm pillars or for the width of 19 x 80 and 19 x 29 μm pillars.

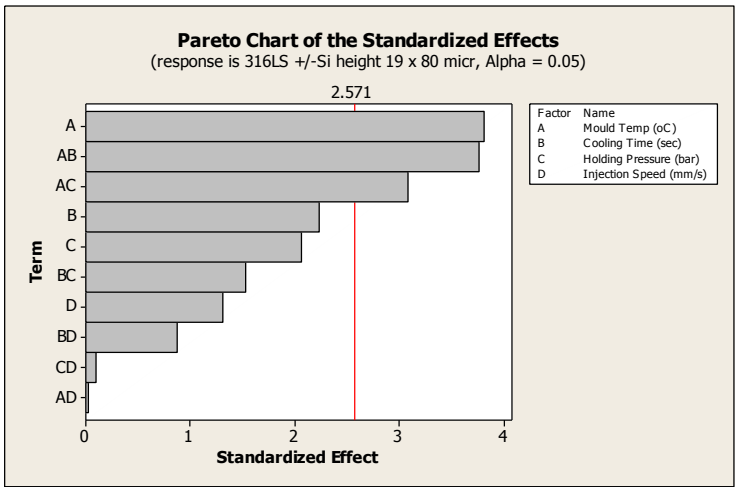

Figure 6.12 Pareto chart – most significant factor for the height of 19 x 80 μm 316LS pillars

6.4 Appearance of 316LS replicate features

The following subsection presents observations of the replicated 316LS pillar features and the surface substrate for the various pillar sizes. Once again the data has been separated into three sections as displayed in Table 3.5.

6.4.1 Appearance of 316LS stainless steel 40 – 80 μm pillar features

The 80 x 80 μm pillars were observed on all DOE runs. Those observed to have been most successfully replicated were found on the replicates from DOE runs 1, 3, 5, 6 and 10 (Figure 6.13).

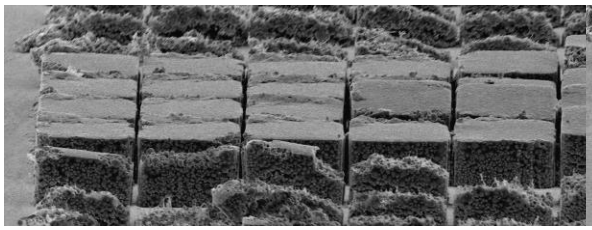

DOE 1

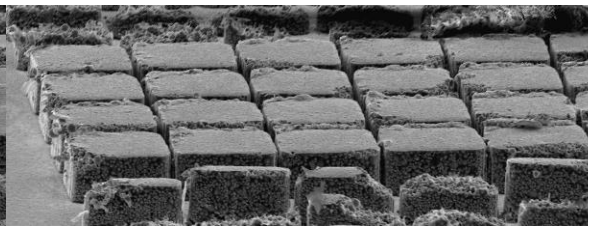

DOE 3

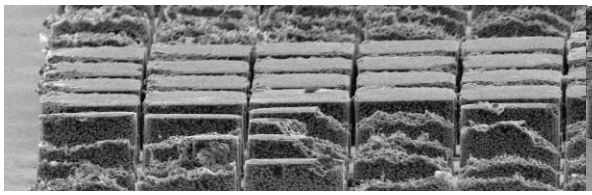

DOE 5

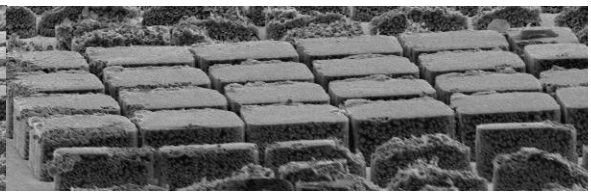

DOE 6

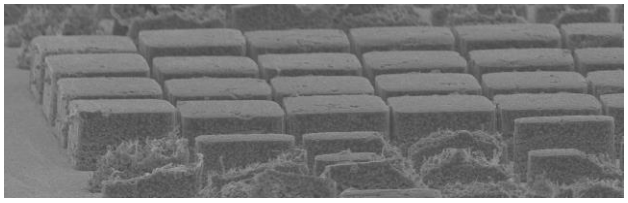

DOE 10

Figure 6.13 Most well replicated 80 x 80 μm 316LS pillars

Pillars observed on DOE run 11 were found to be least well replicated (Figure 6.14).

DOE 11

Figure 6.14 Least well replicated 80 x 80 μm 316LS pillars

The 53 x 80 μm pillars were observed on all DOE runs. Those observed to have been most successfully replicated were found on the replicates from DOE runs 3, 5, 6 and 9 (Figure 6.15).

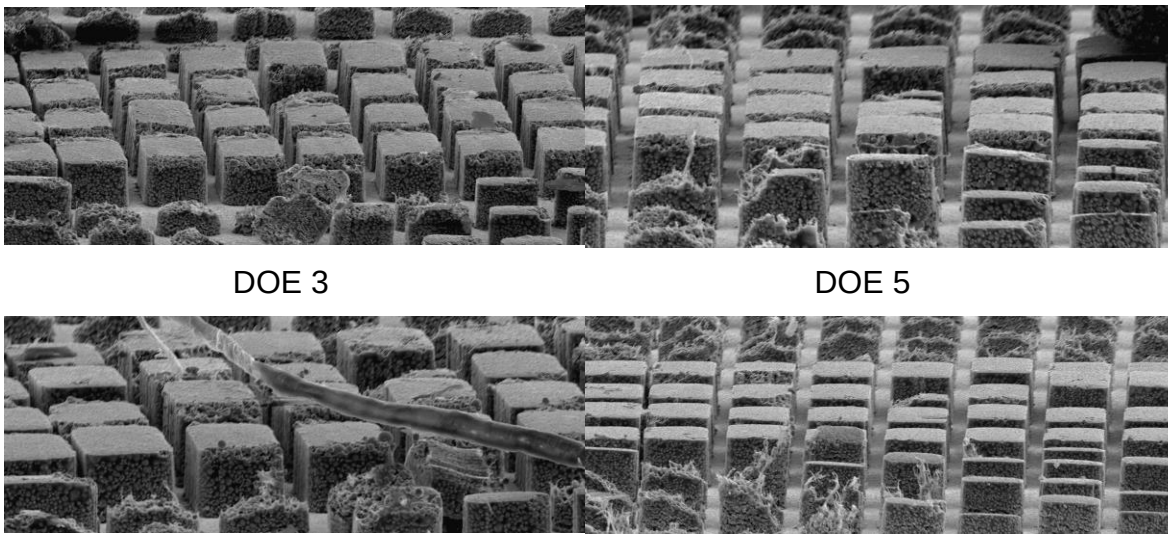

DOE 3 DOE 5

DOE 6 DOE 9

Figure 6.15 Most well replicated 53 x 80 μm 316LS pillars

Pillars observed on DOE runs 11, 12 and 15 were found to be least well replicated (Figure 6.16).

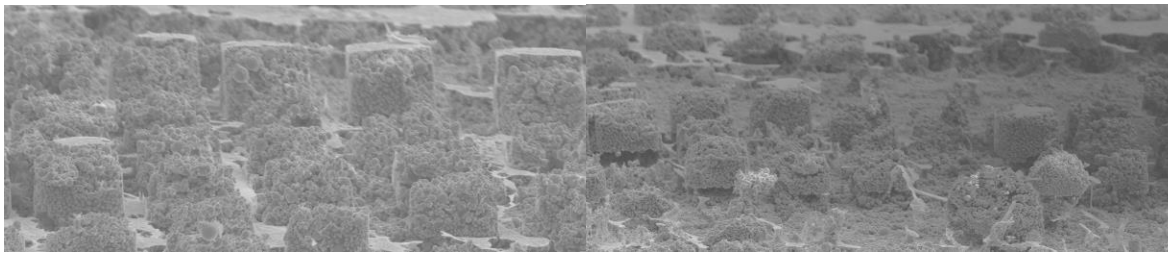

DOE 11 DOE 12

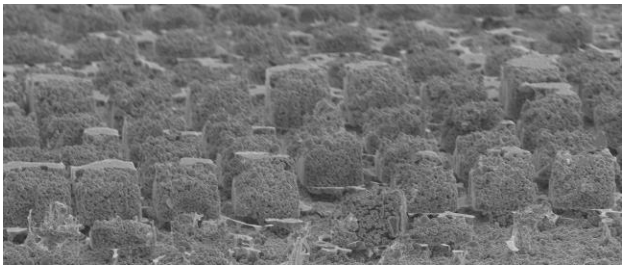

DOE 15

Figure 6.16 Least well replicated 53 x 80 μm 316LS pillars

The 43 x 80 μm pillars were observed on all DOE runs. Those observed to have been most successfully replicated were found on the replicates from DOE runs 9 and 10 (Figure 6.17).

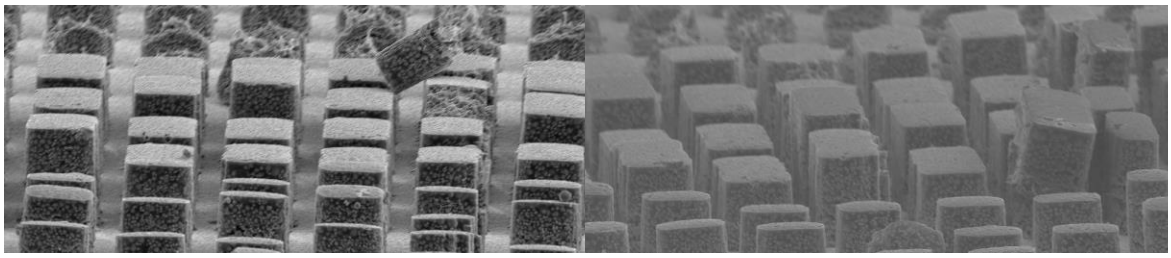

DOE 9 DOE 10

Figure 6.17 Most well replicated 43 x 80 μm 316LS pillars

Pillars observed on DOE runs 12 and 15 were found to be least well replicated (Figure 6.18).

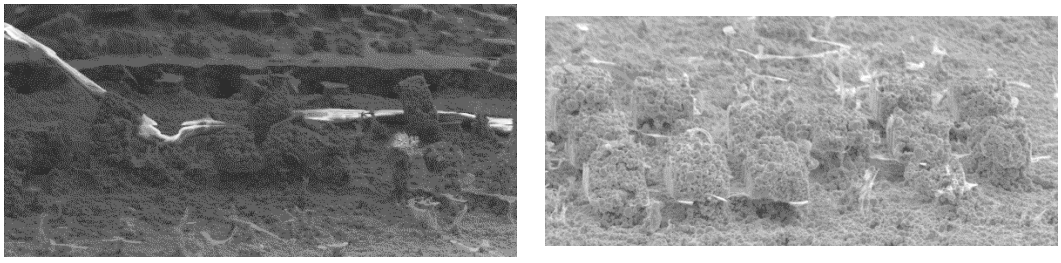

DOE 12 DOE 15

Figure 6.18 Least well replicated 43 x 80 μm 316LS pillars

The 80 x 29 μm pillars were found to have been at least partially replicated on all DOE runs. None of the pillars produced were fully replicated however, of those observed the least formed were those from DOE runs 2, 8, 11 and 15 (Figure 6.19).

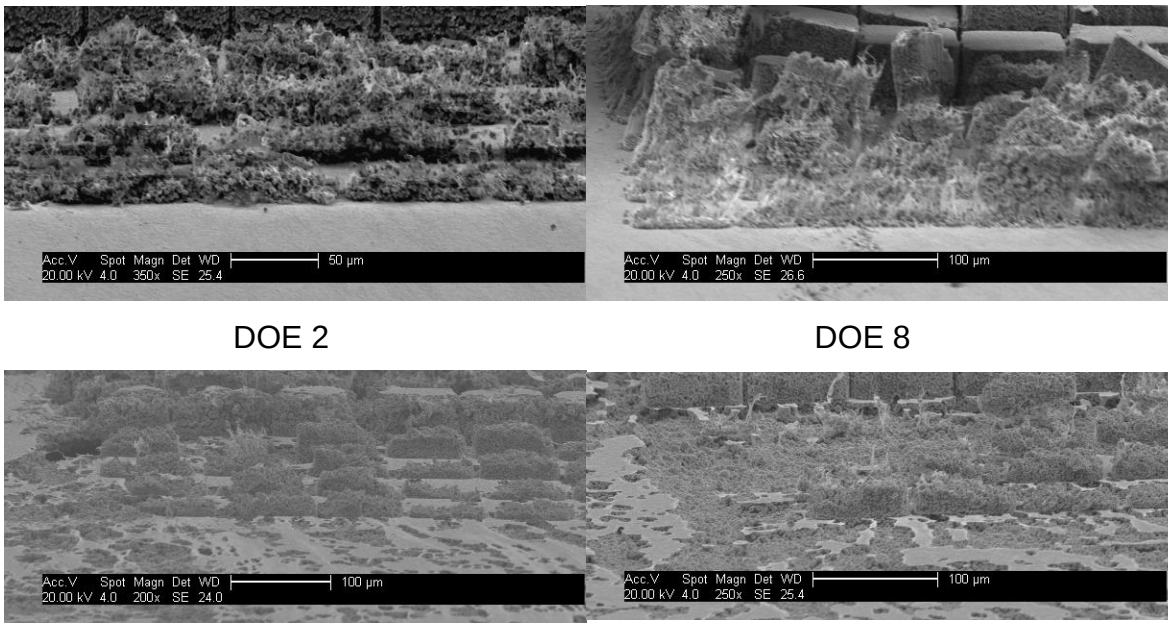

DOE 2 DOE 8

DOE 11 DOE 15

Figure 6.19 Least well replicated 80 x 29 μm 316LS pillars

The 53 x 29 μm pillars were found to have been at least partially replicated on all DOE runs. None of the pillars produced were fully replicated however, of those observed the least formed were those from DOE runs 12 and 15 (Figure 6.20).

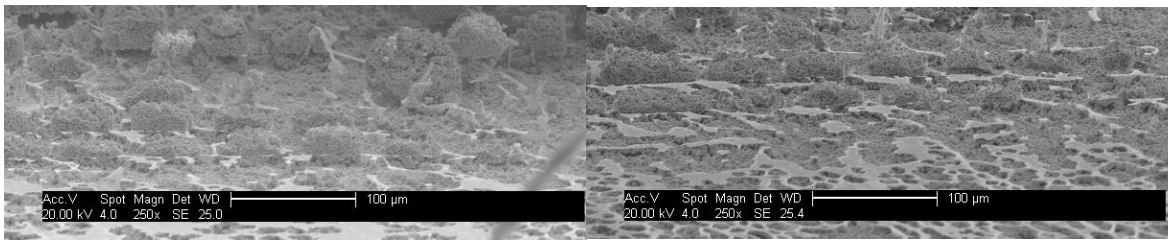

DOE 12 DOE 15

Figure 6.20 Least well replicated 53 x 29 μm 316LS pillars

The 43 x 29 μm pillars were found to have been at least partially replicated on all DOE runs. Of those observed the most well replicated were 9 and 10 (Figure 6.21). The least formed were those from DOE runs 12 and 15 (Figure 6.22).

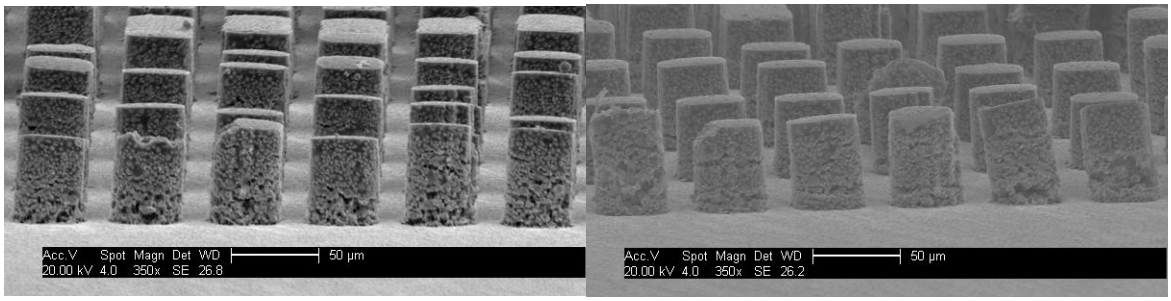

DOE 9 DOE 10

Figure 6.21 Most well replicated 43 x 29 μm 316LS pillars

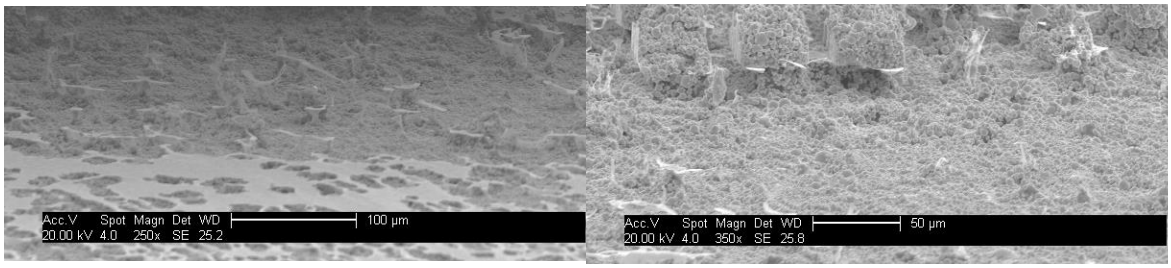

DOE 12 DOE 15

Figure 6.22 Least well replicated 43 x 29 μm 316LS pillars

6.4.2 Appearance of 316LS stainless steel 20 – 39 μm pillar features

The 29 x 80 μm pillars were observed on all DOE runs. Those observed to have been most successfully replicated were found on the replicates from DOE runs 9 and 10 (Figure 6.23).

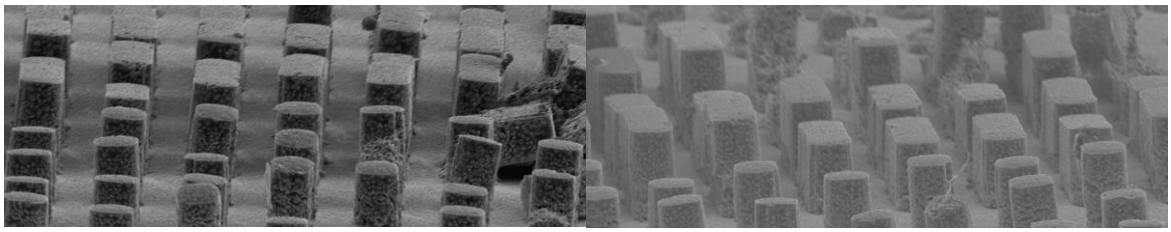

DOE 9 DOE 10

Figure 6.23 Most well replicated 29 x 80 μm 316LS pillars

Pillars observed on DOE runs 2, 4, 8 and 11 were found to be least well replicated (Figure 6.24).

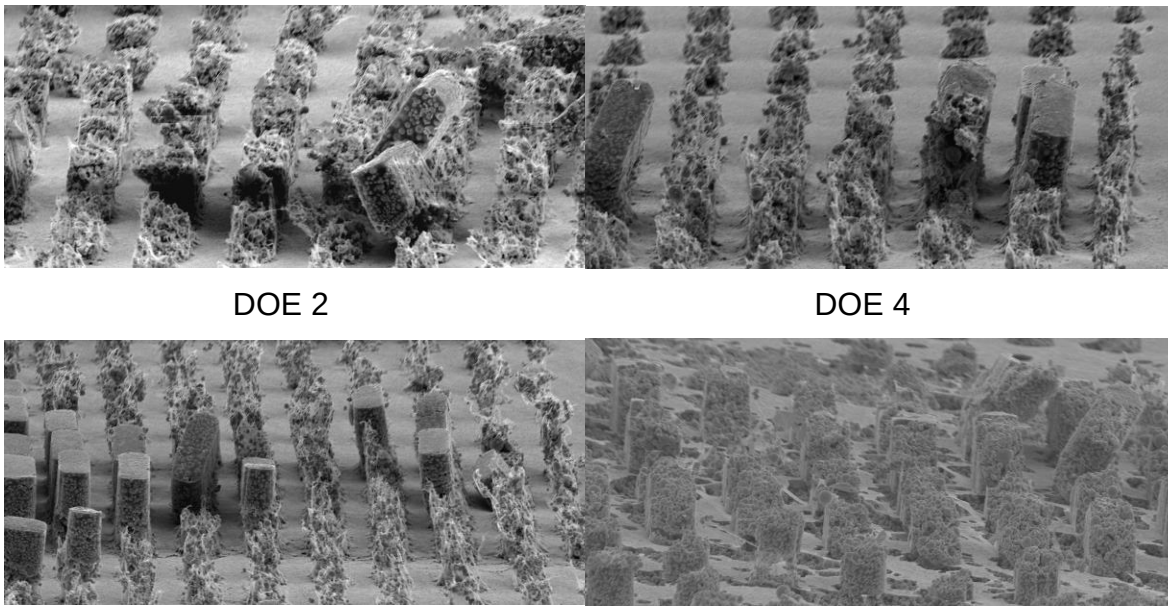

DOE 2 DOE 4

DOE 8 DOE 11

Figure 6.24 Least well replicated 29 x 80 μm 316LS pillars

Of the 29 x 29 μm pillars observed the most well replicated was DOE run 9 (Figure 6.25). Pillars were found to have not been replicated on replicates from DOE runs 12 and 15.

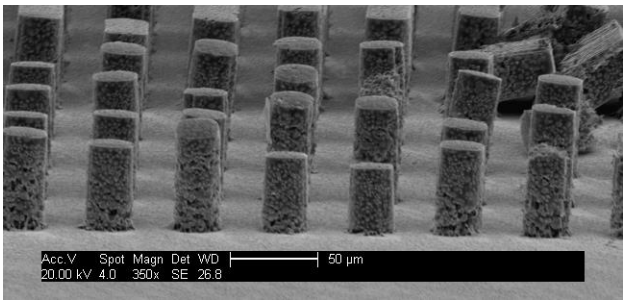

DOE 9

Figure 6.25 Most well replicated 29 x 29 μm 316LS pillars

6.4.3 Appearance of 316LS stainless steel 2 – 19 μm pillar features

The 19 x 80 μm pillars were observed on all DOE runs. Those observed to have been most successfully replicated were found on the replicates from DOE run 5 (Figure 6.26).

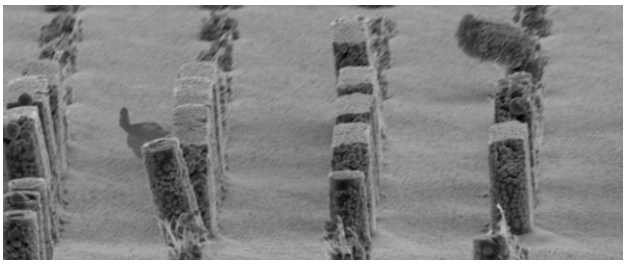

DOE 5

Figure 6.26 Most well replicated 19 x 80 μm 316LS pillars

Pillars observed on DOE runs 2, 8, and 11 were found to be least well replicated (Figure 6.27).

The 19 x 29 μm pillars were found to have been at least partially replicated on all DOE runs except 12 and 15.

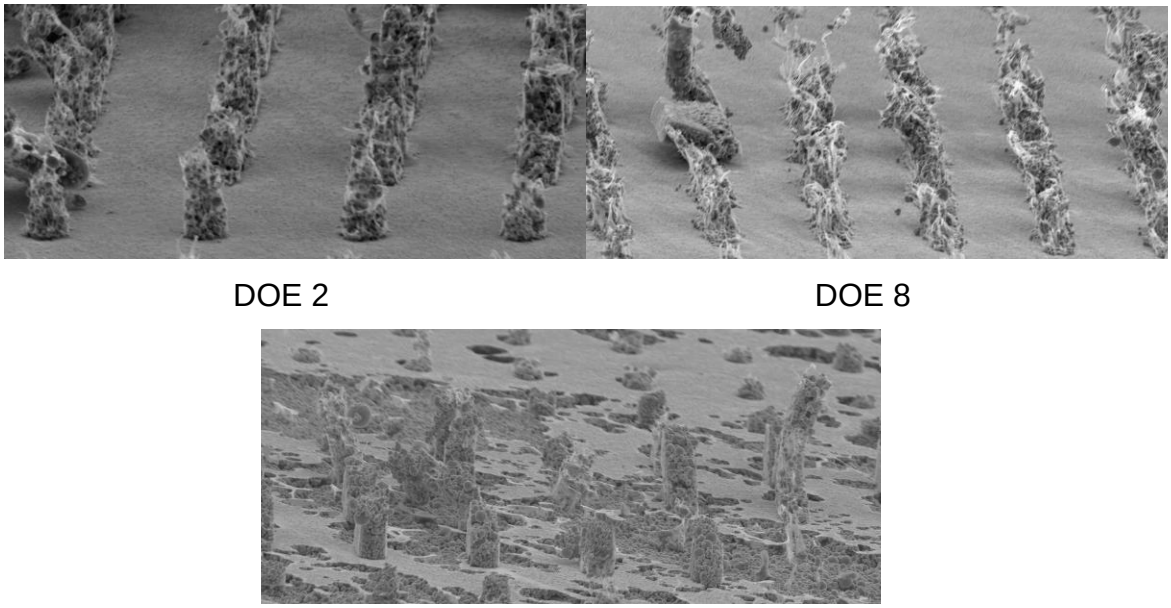

DOE 2 DOE 8

DOE 11

Figure 6.27 Least well replicated 19 x 80 μm 316LS pillars

6.5 Process window for 316LS using process-volume-temperature curves

The process window used during the undertaking of the design of experiments investigation are displayed on the pressure-volume-temperature (PVT) curve in Figure 6.28.

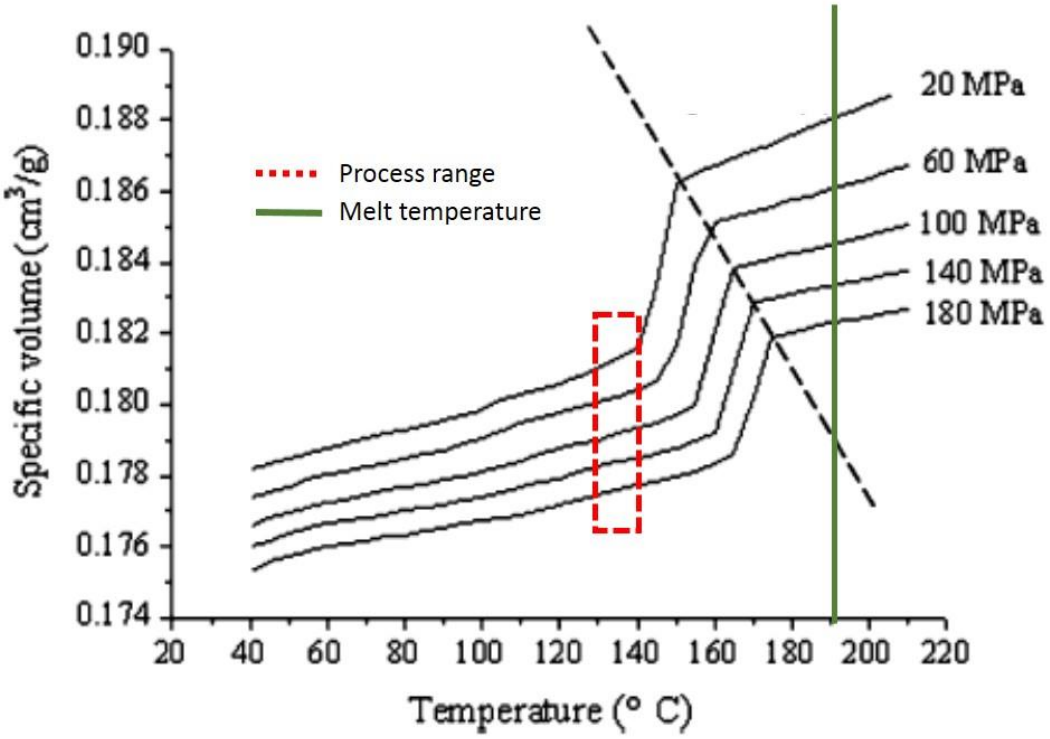

Figure 6.28 Pressure-volume-temperature curve for 316LS[58], with process window and melt temperature used

6.6 Summary of metal injection moulding results

This chapter has described the responses gathered through a design of experiment approach examining the fabrication of metal powder micro-injection moulded replicates. The fabrication of 316LS stainless steel replicates with micro-channels surface features has been presented. The responses of interest were part mass, pillar height and width and the variation of the replicate pillar dimensions from the silicon mould insert.

The appearance of the surface of the replicates was also observed and the most and least well replicated pillars were identified at each pillar size. Irregular pillar formations, indentations, and feature deformations were also identified.

7 Droplet behaviour results

The following chapter discusses the behaviour of water droplets on the various surfaces produced. Section *7.1 Droplet contact angles* discusses the contact angles of droplets observed on 10 - 2 µm surface features. The droplet contact angles were examined on polypropylene and high density polyethylene replicates and silicon mould inserts. Section *7.2 Droplet channelling* examines the movement and "channelling" of 0.2 µL droplets on polyethylene, high density polyethylene and 316LS stainless steel replicates and silicon mould inserts structured with micro-channel surface features. Section *7.3 Droplet evaporation* discusses the behaviour of deionised water droplets during evaporation on polypropylene, high density polyethylene and 316LS stainless steel replicates and silicon mould inserts structured with micro-channel surface features.

7.1 Droplet contact angles

The droplet contact angles of 1 µL deionised water droplets on 10 - 2 µm surface features were examined. The purpose for examining the droplet contact angles was to determine the effect the different surface features had on the wettability of the sample surface. The samples used were polypropylene and high density polyethylene replicates and silicon mould inserts. Each droplet was observed over a 5 minute period and contact measurements were taken at 1 minute intervals.

In the interest of simplicity the following subsections will examine the data according firstly to surface material and secondly to contact angle measurements i.e. highest and lowest contact angles and the largest and smallest contact angle decrease.

7.1.1 Polypropylene 10 - 2 µm inserts

Of the sixteen micro-injection moulding design of experiment runs (*Chapter 3 Methodology*) examined the highest initial contact angle observed for the 10 x 10 µm pillar features was from DOE run 1, on which an average contact angle of 111 ° was recorded (Figure 7.1). The highest contact angle on 10 x 10 µm hole features was also found to be from DOE 1, on which an average contact angle of 107 ° was recorded (Figure 7.1). With regards to the 5 x 5 µm features the highest contact angle observed for the pillar features was on the samples from DOE run 7, 107 ° (Figure 7.2). For the 5 x 5 µm hole features the highest contact angle was observed for DOE run 6 on which an average contact angle of 100 ° was observed (Figure 7.2).

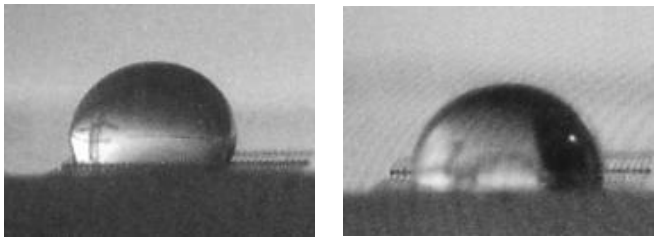

DOE run 1 : 111 ° DOE run 1 : 107 °

Figure 7.1 Highest droplet contact angle on 10 x 10 µm pillars (Left) and 10 x 10 µm hole features (Right)

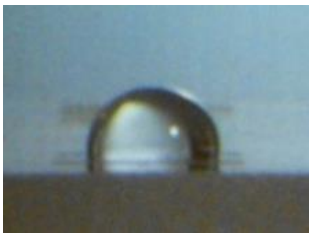
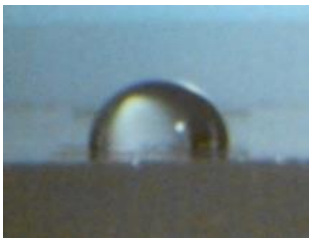

DOE run 7 : 107 ° DOE run 6 : 100 °

Figure 7.2 Highest droplet contact angle on 5 x 5 μm pillars (Left) and 5 x 5 μm hole features (Right)

The lowest initial contact angle examined for the 10 x 10 μm pillar features was found to be 91 ° on samples from DOE run 10 (Figure 7.3). For the 10 x 10 μm hole features the lowest initial contact angle was recorded as 83 ° for DOE run 5 (Figure 7.3). Regarding the 5 x 5 μm features the lowest initial contact angle for the pillar features was found to be 79 ° from DOE run 3 and 74 ° from DOE run 14 for 5 x 5 μm hole features (Figure 7.4).

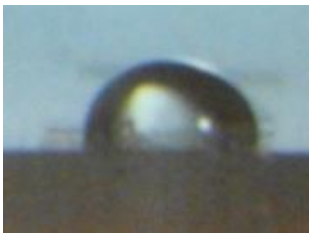
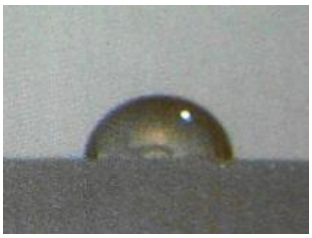

DOE run 10 : 91 ° DOE run 5 : 83 °

Figure 7.3 Lowest droplet contact angle on 10 x 10 μm pillars (Left) and 10 x 10 μm hole features (Right)

DOE run 3 : 79 °

DOE run 14 : 74 °

Figure 7.4 Lowest droplet contact angle on 5 x 5 μm pillars (Left) and 5 x 5 μm hole features (Right)

Of those droplets examined on the 10 x 10 μm pillar features it was observed that the droplet placed on the sample from DOE run 1 decreased the most over a 5 minute period, a decrease of 17 ° from 111 - 94 °. For the 10 x 10 μm holes features the droplet placed on DOE run 15 was found to decrease the most, from 95 - 77 ° (Figure 7.5). A decrease of 15 ° was observed on DOE run 1 for 5 x 5 μm pillar features, from an initial droplet contact angle of 91 ° to 76 °. The contact angle of droplets on 5 x 5 μm holes on DOE run 10 were observed to decrease the most over the 5 minute observation period from an initial contact angle of 83 - 69 °, a decrease of 14 ° (Figure 7.6).

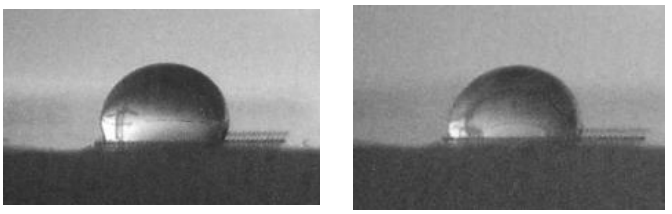

DOE run 1 : 111 - 94 °

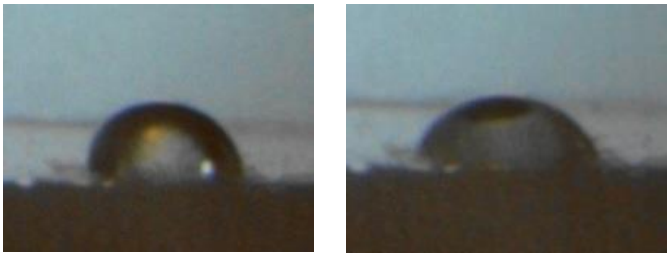

DOE run 15 : 95 - 77 °

Figure 7.5 Largest decrease in droplet contact angle on 10 x 10 μm pillars (Left) and 10 x 10 μm hole features (Right)

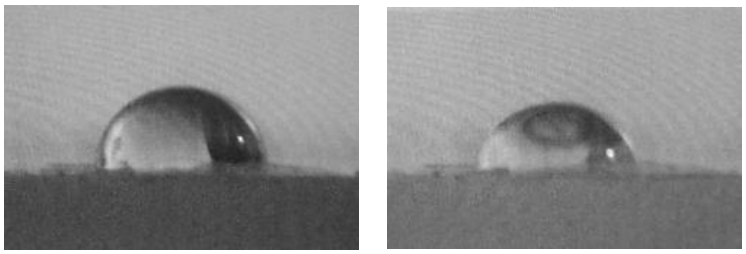

DOE run 1 : 91 - 76 °

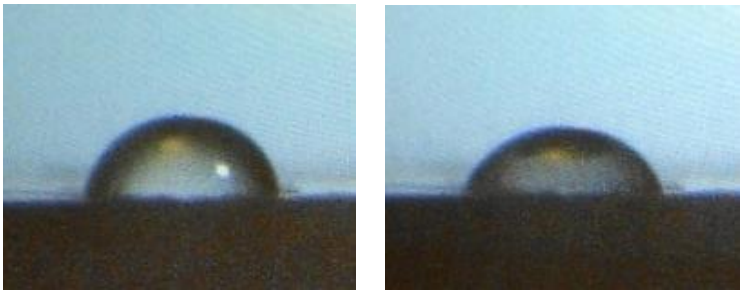

DOE run 10 : 83 – 69 °

Figure 7.6 Largest decrease in droplet contact angle on 5 x 5 μm pillars (Left) and 5 x 5 μm hole features (Right)

The droplets which exhibited the least decrease over time on 10 x 10 μm pillar features were found on DOE run 9. Droplets examined decreased by 6 ° over a 5 minute period from 105 - 99 °. For droplets on 10 x 10 μm hole features a contact angle decrease of 6 ° (105 - 99 °) was calculated for droplets on samples from DOE run 8 (Figure 7.7). On 5 x 5 μm pillar features the droplet which exhibited the least change in contact angle over time was on a sample from DOE run 5. An initial contact angle of 92 ° was seen to decrease to 85 ° over a 5 minute period, resulting in a decrease of 7 °. The lowest decrease in contact angle on 5 x 5 μm hole features was observed on samples from DOE run 16. On which a decrease of 6 ° was recorded from an initial contact angle of 91 ° to a final contact angle of 85 ° (Figure 7.8).

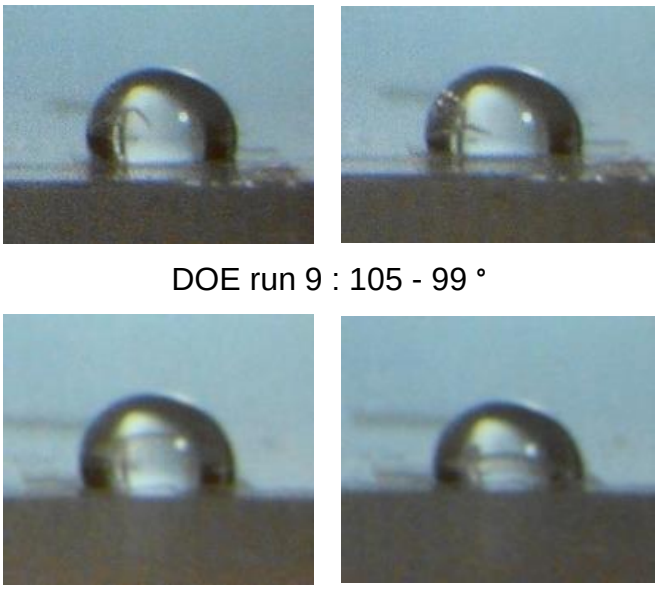

DOE run 9 : 105 - 99 °

DOE run 8 : 105 - 99 °

Figure 7.7 Lowest decrease in droplet contact angle on 10 x 10 μm pillars (Left) and 10 x 10 μm hole features (Right)

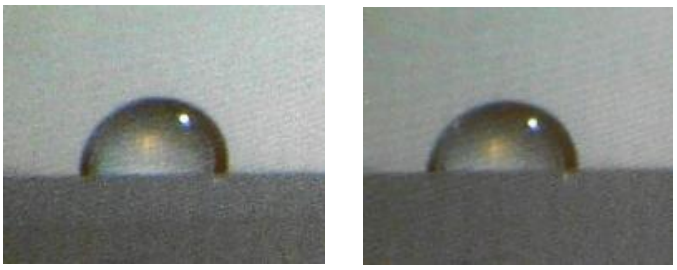

DOE run 5 : 92 - 85 °

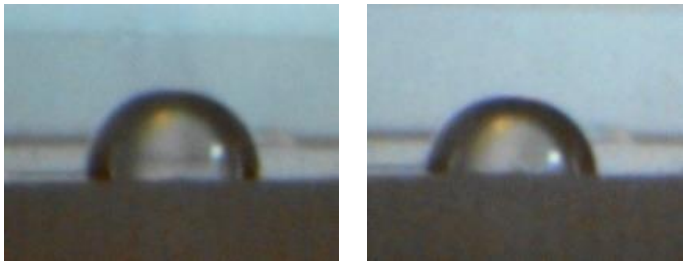

DOE run 16 : 91 - 85 °

Figure 7.8 Lowest decrease in droplet contact angle on 5 x 5 μm pillars (Left) and 5 x 5 μm hole features (Right)

On an unstructured polypropylene surface the contact angle of a 1 μL water droplet was found to decrease from 100 - 90 °. When initial droplet contact angles from all polypropylene design of experiment runs were compared to that of an unstructured PP surface it was noted that the presence of a structured surface underneath the droplet did not always result in an initial contact angle higher than that observed on the unstructured surface (Table 7.1). Ten of the initial contact angles examined on 10 x 10 μm pillar features were higher than the initial contact angle recorded on an unstructured surface. Six of the initial contact angle examined on the 10 x 10 μm hole and 5 x 5 μm pillar features were higher than that observed on the unstructured surface. Only one of the initial contact angles on the 5 x 5 μm hole features was found to be higher than that observed on the unstructured surface.

Table 7.1 Design of experiment runs with initial contact angle higher than that observed on an unstructured polypropylene surface

Features	Design of experiment runs
10 x 10 μm pillars	1, 6, 7, 9, 11, 12, 13, 14, 15, 16
10 x 10 μm holes	1, 6, 8, 9, 11, 12
5 x 5 μm pillars	7, 8, 9, 11, 12, 16
5 x 5 μm holes	6

7.1.2 High density polyethylene 10 – 2 μm Inserts

Contact angles of 1 μL droplets were examined on high density polyethylene samples from all 16 micro-injection moulding design of experiment runs (*Chapter 3 Methodology*). The highest contact angle on the 10 x 10 μm pillar features was observed on the sample from DOE run 6, on which a contact angle of 108 ° was recorded (Figure 7.9). On 10 x 10 μm hole features the highest contact angle was 105 °, observed on samples from DOE run 1 (Figure 7.9). On the 5 x 5 μm pillar features the highest contact angle, 104 °, was found on samples from DOE run 3. A contact angle of 90 °, on samples from DOE 6, was found to be the highest contact angle observed on 5 x 5 μm hole features (Figure 7.10).

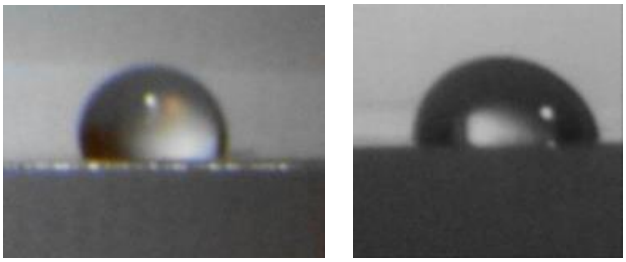

DOE run 6 : 108 ° DOE run 1 : 105 °

Figure 7.9 Highest droplet contact angle on 10 x 10 μm pillars (Left) and 10 x 10 μm hole features (Right)

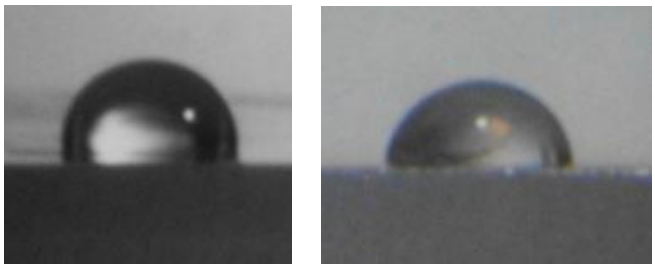

DOE run 3 : 104 ° DOE run 6 : 90 °

Figure 7.10 Highest droplet contact angle on 5 x 5 μm pillars (Left) and 5 x 5 μm hole features (Right)

The lowest contact angle recorded on 10 x 10 μm pillar features was 80 ° from DOE run 13. A contact angle of 76 ° was observed on the sample surface from DOE run 9 for 10 x 10 μm hole features (Figure 7.11). With regards to the 5 x 5 μm pillar features it was found that the lowest contact angle, of 75 °, was observed on the surface of DOE run 11. The 5 x 5 μm hole features on samples from DOE run 13 were found to display the lowest contact angle, 74 ° (Figure 7.12).

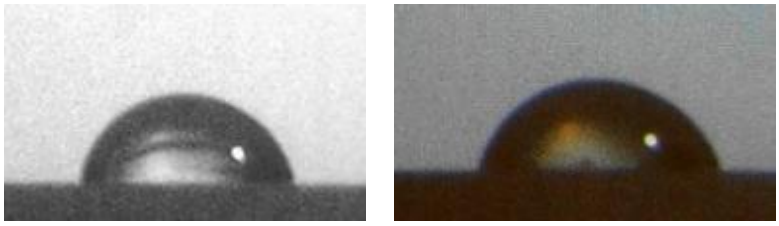

DOE run 13 : 80 ° DOE run 9 : 76 °

Figure 7.11 Lowest droplet contact angle on 10 x 10 μm pillars (Left) and 10 x 10 μm hole features (Right)

DOE run 11 : 75 ° DOE run 13 : 74 °

Figure 7.12 Lowest droplet contact angle on 5x5μm pillars (Left) and 5x5μm hole features (Right)

The change in droplet contact angle was observed over a 5 minute period. The greatest change in droplet contact angle on 10 x 10 μm pillars was observed on the sample from DOE run 2 (Figure 7.13). The contact angle decreased from 102 - 88 °, a decrease of 14 °. The surface on which the smallest change in contact angle was examined for 10 x 10 μm pillar features was DOE run 9 (Figure 7.15). A contact angle decrease of 8 ° was observed, from 85 - 77 °. On 10 x 10 μm hole features the largest decrease in contact angle was observed on the samples from DOE run 10 (Figure 7.13). The contact angle decreased from 104 - 91 °, a total decrease of 13 °. The smallest decrease in contact angle

on 10 x 10 μm hole features was on samples from DOE run 1 on which the contact angle decreased from 105 - 97 °, a total decrease of 8 ° (Figure 7.15). A contact angle decrease of 12 ° from 104 - 91 ° was observed on 5 x 5 μm pillar features on the sample from DOE run 3 (Figure 7.14). The smallest decrease in contact angle on 5 x 5 μm pillars was from 80 - 74 °, a total decrease of 6 °, observed on the sample from DOE run 8 (Figure 7.16). With regards to the 5 x 5 μm hole features the largest decrease in contact angle was observed on the samples from DOE run 4 where a decrease of 19 °, 88 - 69 °, was observed (Figure 7.14). The smallest decrease in contact angle on 5 x 5 μm hole features was observed on the surface from DOE run 2. From an initial contact angle of 86 ° over 5 minutes the droplet contact angle decreased by 7 ° resulting in a final contact angle of 79 ° (Figure 7.16).

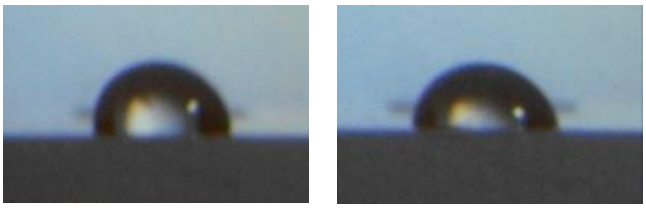

DOE run 2 : 102 - 88 °

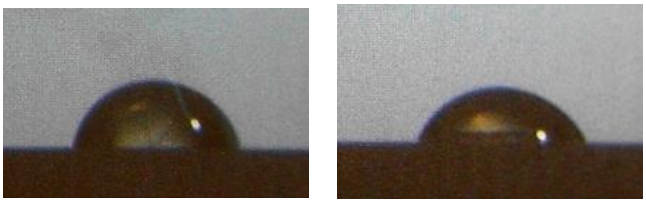

DOE run 10 : 104 - 91 °

Figure 7.13 Largest decrease in droplet contact angle on 10 x 10 μm pillars (Top) and 10 x 10 μm hole features (Bottom)

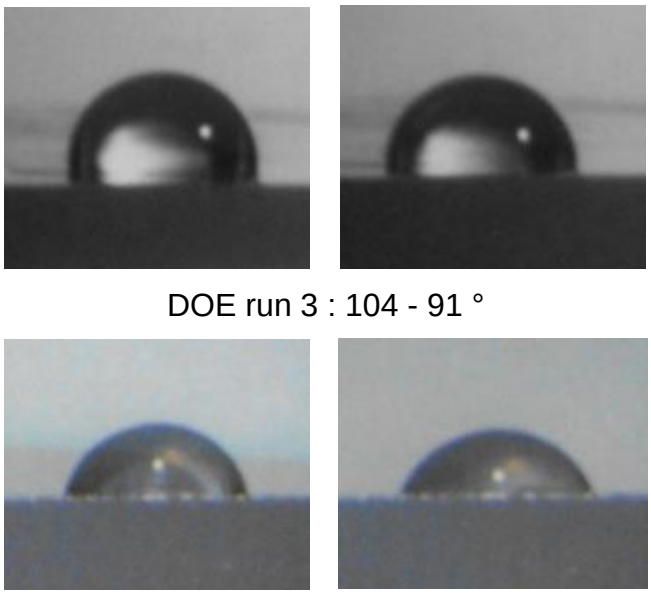

DOE run 3 : 104 - 91 °

DOE run 4 : 88 - 69 °

Figure 7.14 Largest decrease in droplet contact angle on 5 x 5 μm pillars (Left) and 5 x 5 μm hole features (Right)

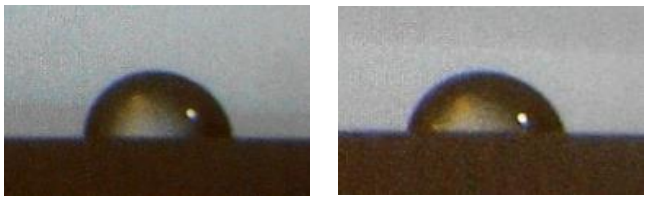

DOE run 9 : 85 - 77 °

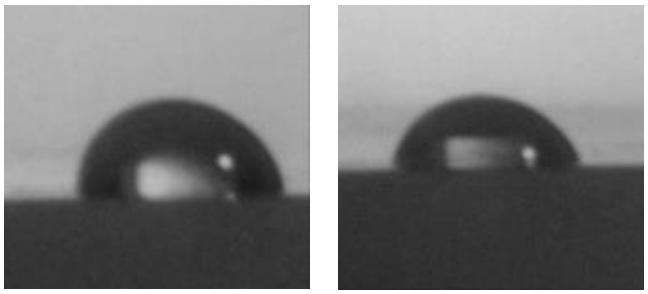

DOE run 1 : 105 - 97 °

Figure 7.15 Lowest decrease in droplet contact angle on 10 x 10 μm pillars (Left) and 10 x 10 μm hole features (Right)

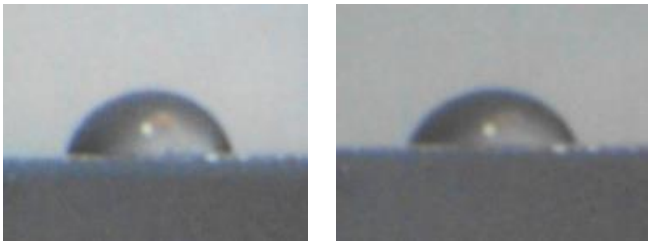

DOE run 8 : 80 - 74 °

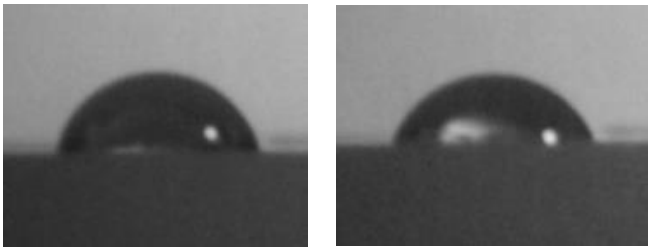

DOE run 2 : 86 - 79 °

Figure 7.16 Lowest decrease in droplet contact angle on 5 x 5 μm pillars (Left) and 5 x 5 μm hole features (Right)

On an unstructured high density polyethylene surface the droplet contact angle was observed to decrease from 96 - 86 °.

Initial contact angles of droplets on surfaces from all design of experiment runs were compared to the initial contact angle on the unstructured high density polyethylene surface. It was noted that the presence of surface roughness induced by the pillar and hole features did not always result in an increased contact angle (Table 7.2). Droplet contact angles on 10 x 10 μm pillar features were observed to be higher than those on the unstructured surface on samples from 7 DOE runs. With regards to the droplets on the 10 x 10 μm hole and 5 x 5 μm pillar features two were found to have an initial contact angle higher than that recorded on the unstructured surface. None of the droplets measured on the 5 x 5 μm hole features were found to have an initial contact angle larger than that of the unstructured surface.

Table 7.2 Design of experiment runs with initial contact angle higher than that observed on an unstructured high density polyethylene surface

Feature	Design of experiment runs
10 x 10 μm pillars	1, 2, 3, 5, 6, 7, 15
10 x 10 μm holes	1, 2
5 x 5 μm pillars	3, 7
5 x 5 μm holes	None

7.1.3 Silicon 10 - 2 μm insert features

The contact angles of 1 μL water droplets were measured on 10 – 2 μm surface features which had been etched onto silicon wafers via deep reactive ion etching. With regards to the 10 x 10 μm pillar features the highest droplet

contact angle (Figure 7.17) was found on the wafer from DOE run 7, 75 °, and the lowest contact angle was found on the wafer from DOE run 4, 33 ° (Figure 7.19). On 10 x 10 μm hole features the largest contact angle (Figure 7.17) was observed on the silicon wafer from DOE run 7, 71 °, and the lowest contact angle was found on the silicon wafer from DOE run 3, 54 ° (Figure 7.19) . The largest droplet contact angle observed on the 5 x 5 μm pillar features was on the silicon wafer from DOE run 7, 61 ° (Figure 7.18) and the lowest contact angle was found on the wafer from DOE run 1, 38 ° (Figure 7.20). With regards to the 5 x 5 μm hole features the largest contact angle was observed on the silicon wafer from DOE run 7, 63 ° (Figure 7.18) and the lowest on the silicon wafer from DOE run 1, 38 ° (Figure 7.20).

DOE run 7 : 75 °

DOE run 7 : 71 °

Figure 7.17 Highest droplet contact angle on 10 x 10 μm pillars (Left) and 10 x 10 μm hole features (Right)

DOE run 7 : 61 °

DOE run 7 : 63 °

Figure 7.18 Highest droplet contact angle on 5 x 5 μm pillars (Left) and 5 x 5 μm hole features (Right)

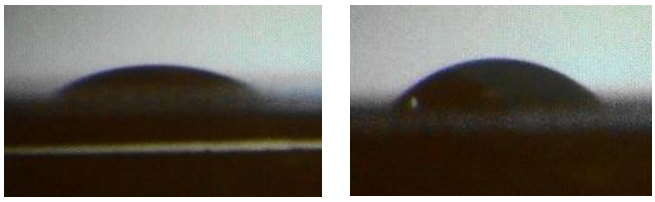

DOE run 4 : 33 ° DOE run 3 : 54 °

Figure 7.19 Lowest droplet contact angle on 10 x 10 μm pillars (Left) and 10 x 10 μm hole features (Right)

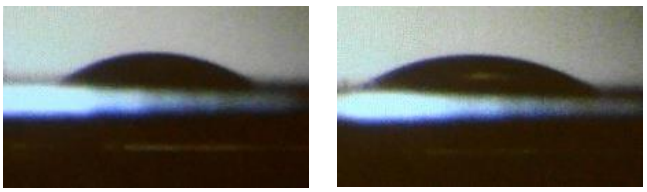

DOE run 1 : 38 ° DOE run 1 : 38 °

Figure 7.20 Lowest droplet contact angle on 5 x 5 μm pillars (Left) and 5 x 5 μm hole features (Right)

Each droplet was observed over a 5 minute period and contact angle measurements made at 1minute intervals. On 10 x 10 μm pillar features the droplet which changes the most over the 5 minute period was observed on the wafer from DOE run 6 which decrease from 53 to 33 ° (Figure 7.21). The droplet which changed the least on 10 x 10 μm pillar features was on the silicon wafer from DOE run 4 which decreased from 33 to 26 ° (Figure 7.23). With regards to the 10 x 10 μm hole features the droplet which displayed the largest contact angle decrease over a 5 minute period was observed on the silicon wafer from DOE run 7 on which the droplet contact angle decreased from 71 - 49 ° (Figure 7.21). The droplet which decreased the least was observed on DOE run 2, on

which the contact angle decreased from 42 - 30 ° (Figure 7.23). Upon observation of droplets on the 5 x 5 μm features it was found that the largest decrease in contact angle was 45 - 28 ° on DOE run 8 for pillar features and 58 - 40 ° on DOE run 8 for hole features (Figure 7.22). The lowest decrease in contact angle on the 5 x 5 μm features was 38 - 30 ° on DOE run 1 for pillar features and 38 – 30 ° on DOE run 1 for hole features (Figure 7.24).

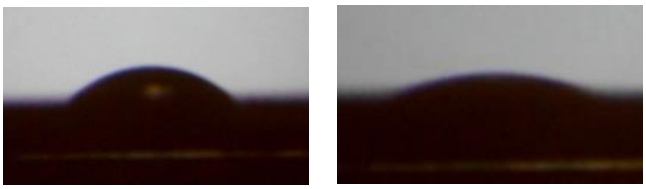

DOE run 6 : 53 - 33 °

DOE run 7 : 71 - 49 °

Figure 7.21 Largest decrease in droplet contact angle on 10 x 10 μm pillars (Left) and 10 x 10 μm hole features (Right)

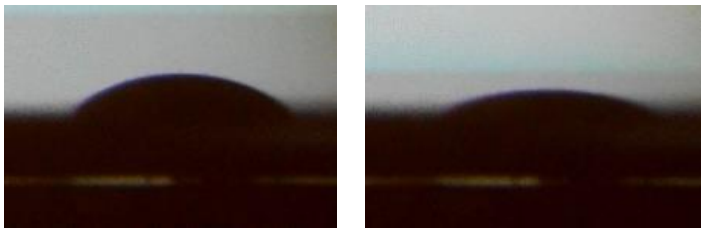

DOE run 8 : 45 - 28 °

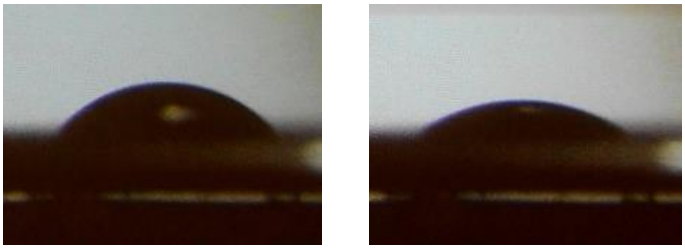

DOE run 8 : 58 - 40 °

Figure 7.22 Largest decrease in droplet contact angle on 5 x 5 μm pillars (Left) and 5 x 5 μm hole features (Right)

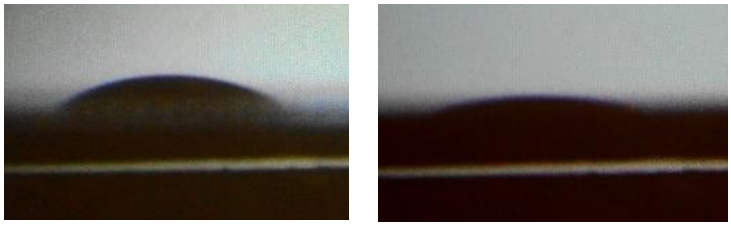

DOE run 4 : 33 - 26 °

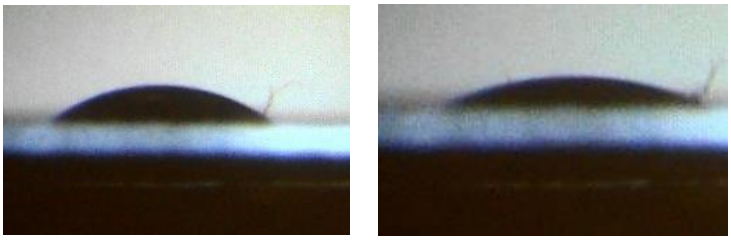

DOE run 2 : 42 - 30 °

Figure 7.23 Lowest decrease in droplet contact angle on 10 x 10 μm pillars (Left) and 10 x 10 μm hole features (Right)

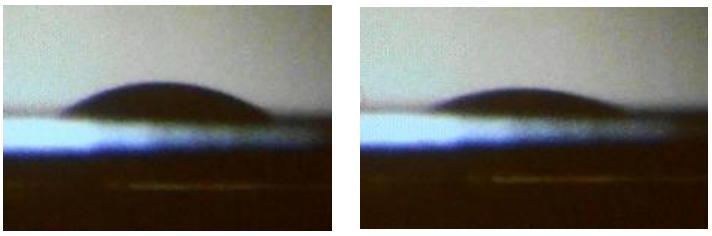

DOE run 1 : 38 - 30 °

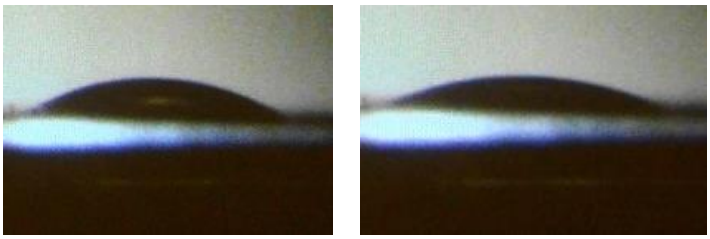

DOE run 1 : 38 - 30 °

Figure 7.24 Lowest decrease in droplet contact angle on 5 x 5 μm pillars (Left) and 5 x 5 μm hole features (Right)

Droplet contact angles were also observed on unstructured silicon, over a 5minute period the droplets contact angle decreased from 64 - 41 °. When comparing the initial contact angle of droplets on silicon wafers from all 8 design of experiment runs it was noted that in only four cases the initial contact angle was higher on a structured surface than on an unstructured surface. These surfaces were 10 x 10 μm hole features on DOE run 4, 10 x 10 μm pillars on DOE run 7, 10 x 10 μm holes on DOE run 7 and 10 x 10 μm holes on DOE run 8.

7.1.4 Droplet contact angle comparisons between sample material

The droplet contact angles were compared to examine the differences in wettability between samples structured with the same surface features. Upon comparison it was noted that the contact angles observed on the polypropylene surfaces were higher than those observed on the corresponding high density

polyethylene surfaces. Also the contact angles on both polypropylene and high density polyethylene surfaces were found to be higher than those on the corresponding silicon features.

7.2 Droplet channelling

The ability to control droplet movement via surface texturing of 0.2 μL droplets was examined. The surfaces used during this examination were silicon mould inserts, high density polyethylene and gold-palladium coated high density polyethylene samples and high density polyethylene, polypropylene and 316LS samples at tilt angles ranging from 30 – 90 °.

The samples used were structured with micro-channel insert features. As explained in *Chapter 3 Methodology* micro-channel insert features were designed to incorporate three different feature arrangements in both pillar and hole forms (Figure 7.25 and Figure 7.26Figure 5.2). Squares 3 and 4 were adapted from the work of Fang et al [48] to produce micro-channels of varying pillar size and spacing across the sample surface to produce a wettability gradient. These features will be hence forth defined as '80 – 19 μm micro-channels' when included in tables and graphs. Squares 5 and 6 used the surface design proposed by Shastry et al [179], which used the variation of pillar width and gap length to produce a superhydrophobic surface with a surface-energy gradient. These features will hence forth be defined as '30 – 5 μm feature gradient' when included in tables and graphs. Squares 1 and 2 were designed by Morel[144] by combining the design patterns proposed by Shastry et al [179] and Fang et al [48]. These features will hence forth be defined as '30 – 5 μm micro-channels' when included in a table or graph. The presence of micro-channels was adapted from the work of Fang et al [48] and the pillar gradient used by Shastry et al [179]. The features in squares 1, 3 and 5 resulted in hole features. Whereas features in squares 2, 4 and 6 resulted in pillar features.

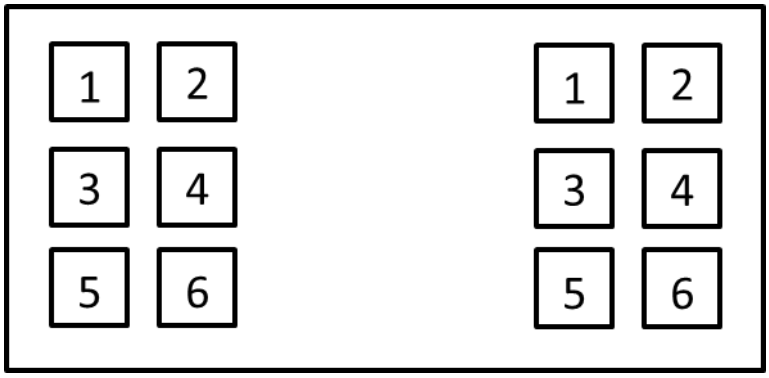

Figure 7.25 Schematic of silicon inserts

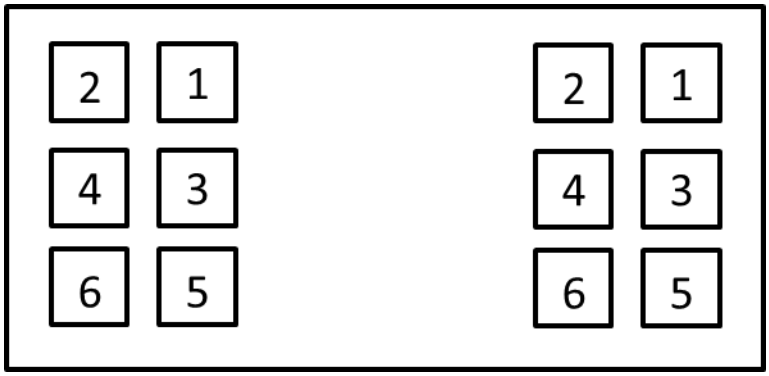

Figure 7.26 Schematic of polymer and metal powder replicates

In the interest of simplicity the following subsections with examine and display the data gathered firstly according to the surface material and secondly the tilt angle of the surface. The data will then be examined according to the design of the surface features i.e. 30 – 5 μm micro-channels, 80 – 19 μm micro-channels, 30 – 5 μm feature gradient or unstructured.

7.2.1 Silicon mould insert

A silicon mould insert was tilted to 30 ° and a 0.2 μL droplet of deionised water was placed on each of the structured areas (Figure 7.27). Each droplet was observed to the point of complete evaporation. No droplet movement was observed at a tilt angle of 30 ° for any of the structured to unstructured areas. The angle of the silicon mould insert was adjusted by 10 ° and the droplet observation was repeated. This process continued until movement of the droplet was observed or the sample tilt angle reached 90 °.

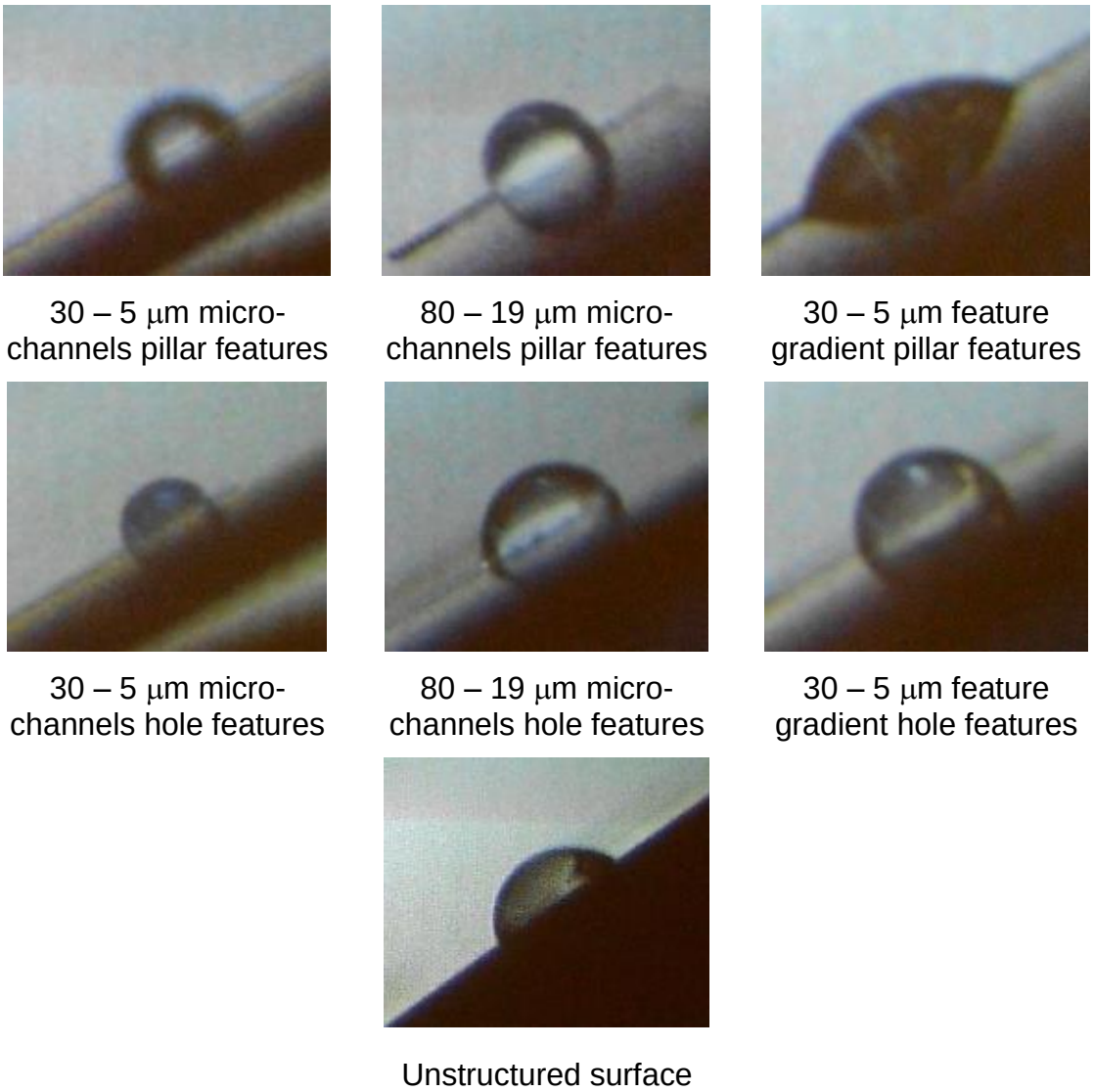

Figure 7.27 Silicon insert tilted to a 30 ° angle

At a tilt angle of 90 ° the droplet was observed to remain stationary until the point of complete evaporation (Figure 7.28). This lack of movement was observed on all structured and unstructured areas.

30 – 5 μm micro-channels pillar features

80 – 19 μm micro-channels pillar features

30 – 5 μm feature gradient pillar features

30 – 5 μm micro-channels hole features

80 – 19 μm micro-channels hole features

30 – 5 μm feature gradient hole features

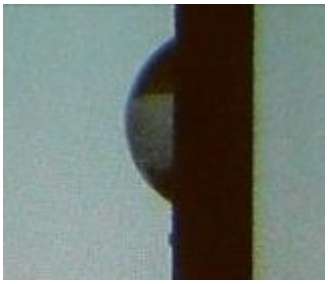

Unstructured surface

Figure 7.28 Silicon insert tilted to a 90 ° angle

7.2.2 Micro-injection moulding polymer replicates

The surfaces of high density polyethylene replicate samples, coated with gold-palladium and uncoated, produced during the micro-injection moulding familiarisation stage (Chapter 5. *Polymer micro-injection moulding results)* were examined for their ability to channel 0.2 μL droplets.

An uncoated high density polyethylene replicate was tilted to 30 ° and a 0.2 μL droplet of deionised water was placed on each of the structured areas (Figure 7.29). Each droplet was observed to the point of complete evaporation. No droplet movement was observed at a tilt angle of 30 ° for any of the structured to unstructured areas. The angle of the sample was adjusted by 10 ° and the droplet observation was repeated. This process continued until movement of the droplet was observed or the sample tilt angle reached 90 °.

30 – 5 μm micro-channels pillar features

80 – 19 μm micro-channels pillar features

30 – 5 μm feature gradient pillar features

30 – 5 μm micro-channels hole features

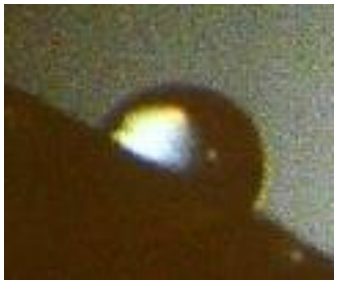

80 – 19 μm micro-channels hole features

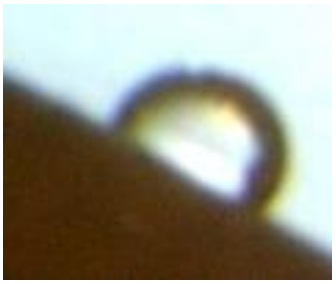

30 – 5 μm feature gradient hole features

Unstructured surface

Figure 7.29 Uncoated high density polyethylene sample tilted to a 30 ° angle

At a tilt angle of 90 ° the droplet was observed to remain stationary on the uncoated high density polyethylene replicate surface until the point of complete evaporation (Figure 7.30). This lack of movement was observed on all structured and unstructured areas.

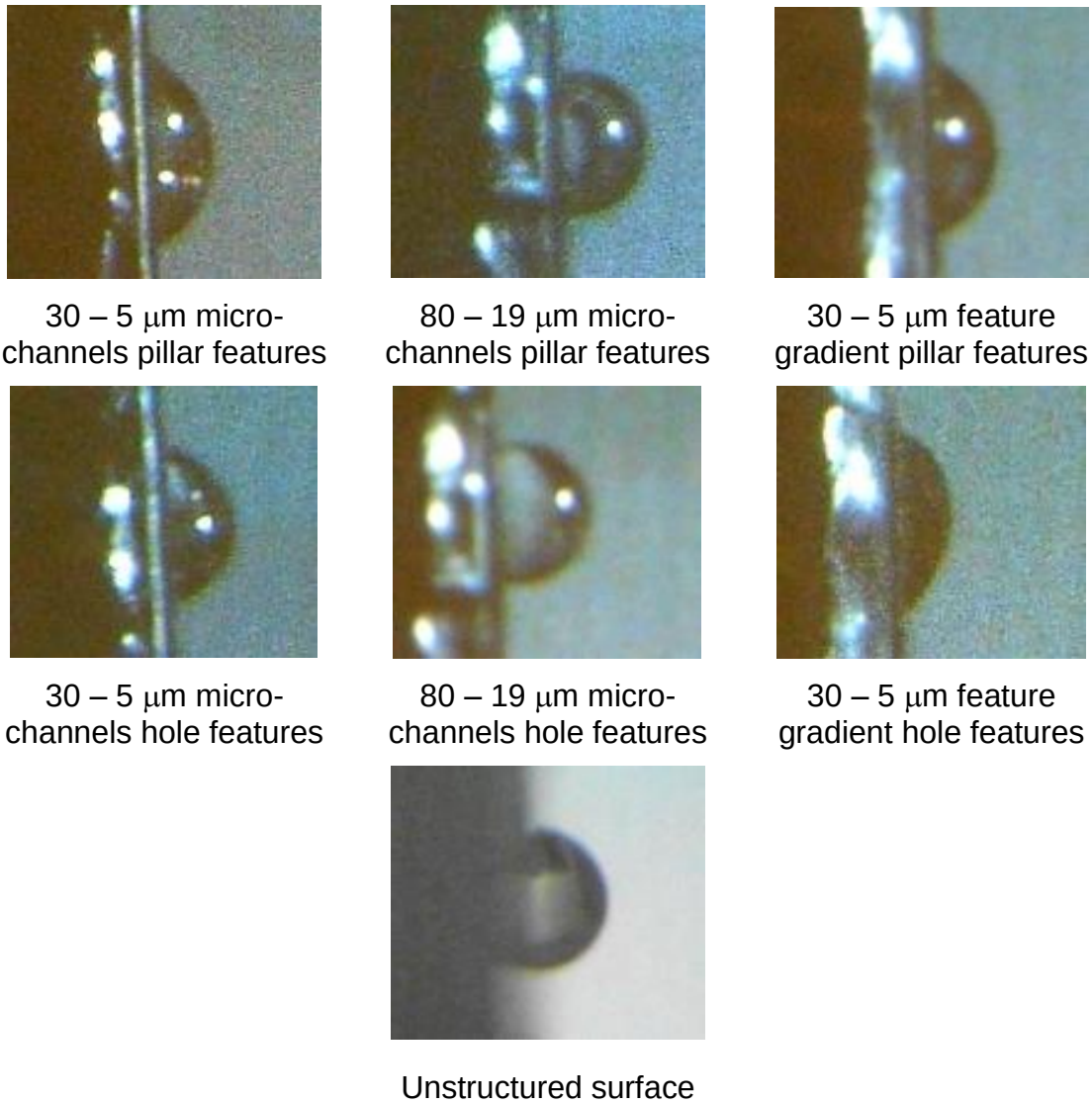

Figure 7.30 Uncoated high density polyethylene sample tilted to a 90 ° angle

As with the uncoated high density polyethylene replicate a high density polyethylene replicate coated with gold-palladium was tilted to 30 ° and a 0.2 μL droplet of deionised water was placed on each of the structured areas (Figure 7.31). Each droplet was observed to the point of complete evaporation. No droplet movement was observed at a tilt angle of 30 ° for any of the structured to unstructured areas. The angle of the coated high density polyethylene

replicate was adjusted by 10 ° and the droplet observation was repeated. This process continued until movement of the droplet was observed or the sample tilt angle reached 90 °.

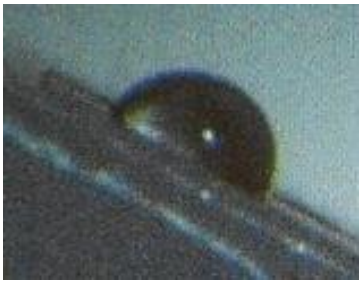

30 – 5 μm micro-channels pillar features

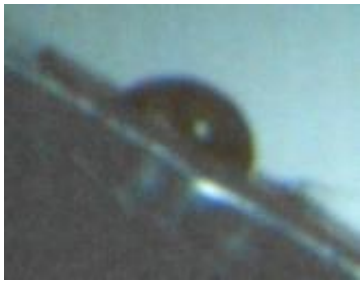

80 – 19 μm micro-channels pillar features

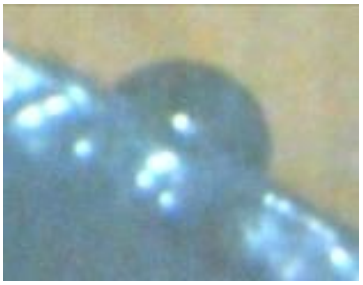

30 – 5 μm feature gradient pillar features

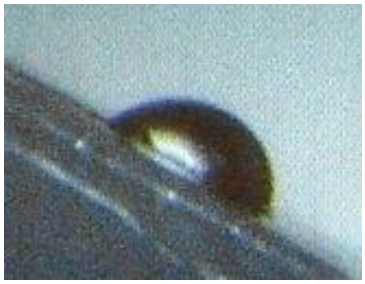

30 – 5 μm micro-channels hole features

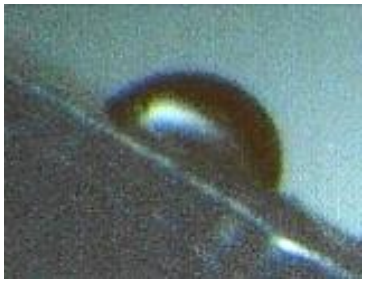

80 – 19 μm micro-channels hole features

30 – 5 μm feature gradient hole features

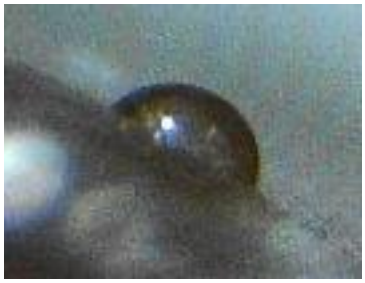

Unstructured surface

Figure 7.31 Gold-palladium coated high density polyethylene sample tilted to a 30 ° angle

At a tilt angle of 90 ° the droplet was observed to remain stationary on the coated high density polyethylene replicate surface until the point of complete evaporation (Figure 7.32). This lack of movement was observed on all structured and unstructured areas.

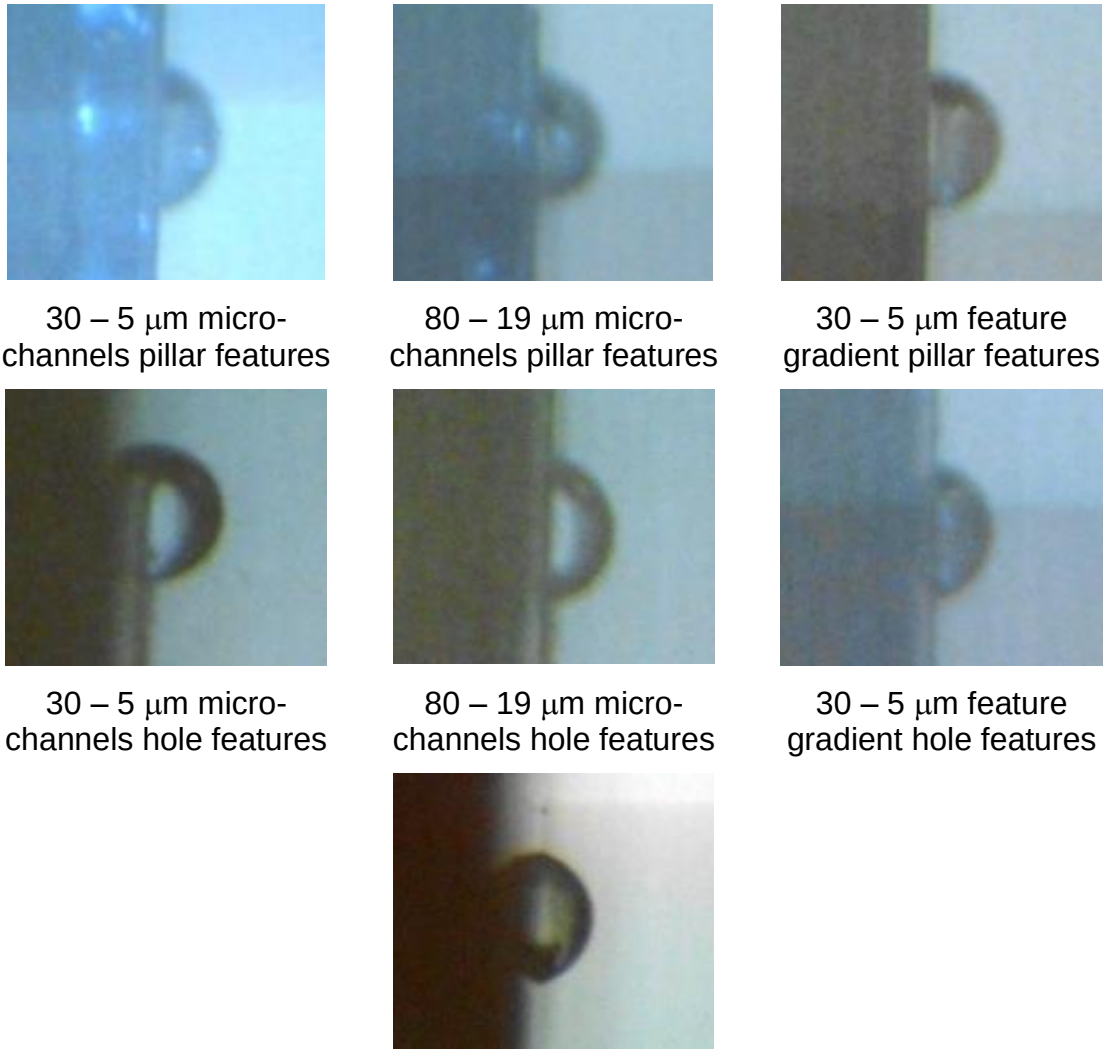

Figure 7.32 Gold-palladium coated high density polyethylene sample tilted to a 90 ° angle

7.2.3 Micro-injection moulding design of experiment replicates

The surfaces of high density polyethylene, polypropylene and 316LS replicate samples, produced during the design of experiment micro-injection moulding examinations (Chapters 5 *Polymer micro-injection moulding results* and *6 Metal injection moulding results)*, were examined for their ability to channel 0.2 μL droplets.

high density polyethylene replicates from DOE run 3 (The least well replicated) and DOE run 4 (The most well replicated) were tilted to 90 ° and a 0.2 μL droplet of deionised water was placed on each of the structured areas (Figure 7.33). Each droplet was observed to the point of complete evaporation. No droplet movement was observed at a tilt angle of 90 ° for any of the structured to unstructured areas.

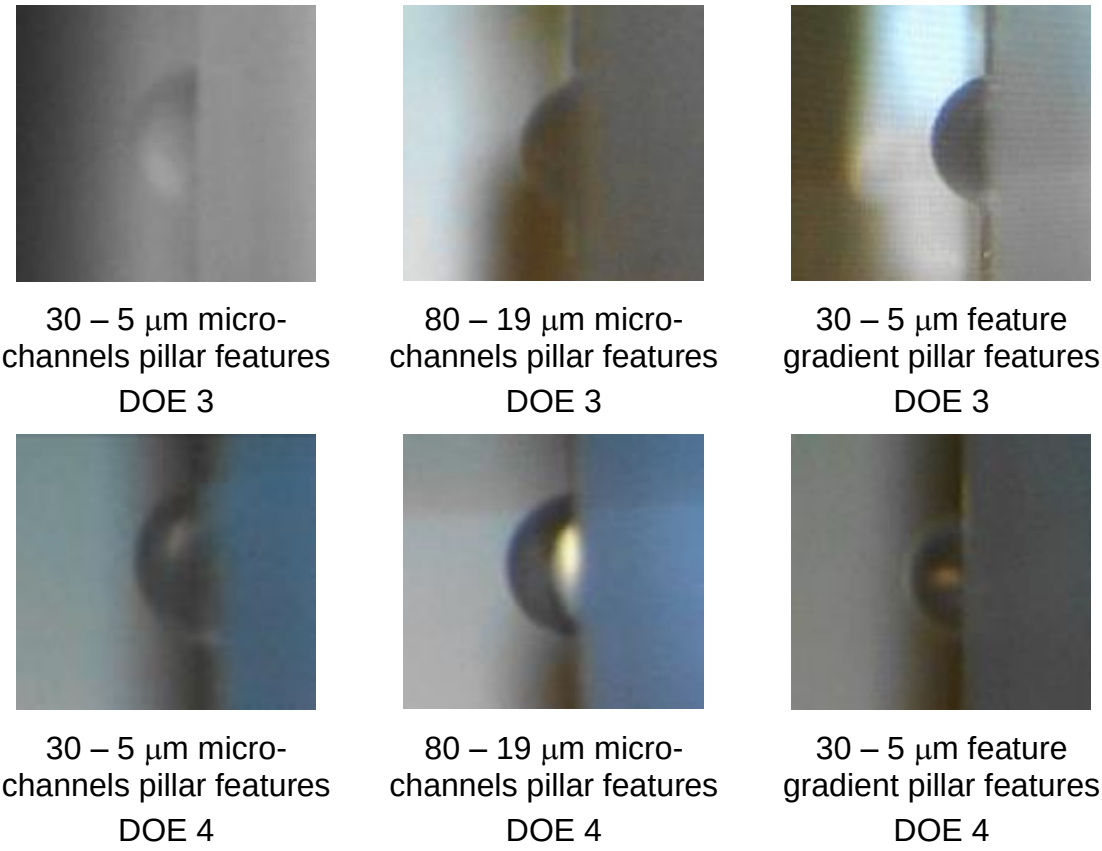

Figure 7.33 High density polyethylene samples from design of experiment run 3 (Left) and design of experiment run 4 (right) tilted to a 90 ° angle

The polypropylene replicates from DOE run 3 (The least well replicated) and DOE run 4 (The most well replicated) were tilted to 90 ° and a 0.2 μL droplet of deionised water was placed on each of the structured areas (Figure 7.34). Each droplet was observed to the point of complete evaporation. No droplet movement was observed at a tilt angle of 90 ° for any of the structured or unstructured areas.

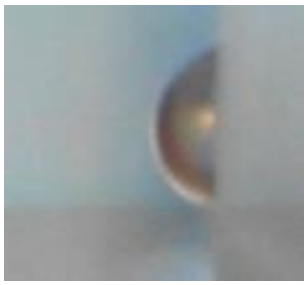

30 – 5 μm micro-channels pillar features DOE 3

80 – 19 μm micro-channels pillar features DOE 3

30 – 5 μm feature gradient pillar features DOE 3

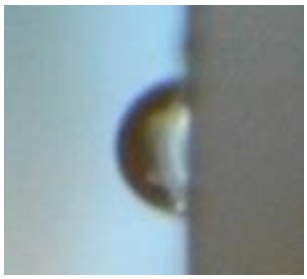

30 – 5 μm micro-channels pillar features DOE 4

80 – 19 μm micro-channels pillar features DOE 4

30 – 5 μm feature gradient pillar features DOE 4

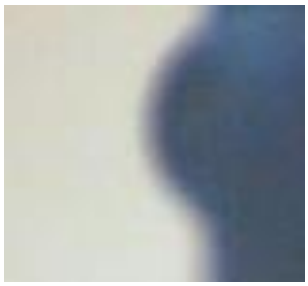

Unstructured surface

Figure 7.34 Polypropylene samples from design of experiment run 3 (left) and design of experiment run 4 (right) tilted to a 90 ° angle

The 316LS replicates from DOE run 12 (The most well replicated) and DOE run 5 (The least well replicated) were tilted to 90 ° and a 0.2 μL droplet of deionised water was placed on each of the structured areas (Figure 7.35). Each droplet

was observed to the point of complete evaporation. No droplet movement was observed at a tilt angle of 90 ° for any of the structured to unstructured areas.

80 – 19 μm micro-channels pillar features DOE 12

80 – 19 μm micro-channels pillar features DOE 5

Unstructured surface

Figure 7.35 316LS samples tilted to a 90 ° angle

7.3 Droplet evaporation

The evaporation of 0.2 μL droplets was examined to determine what effect the micro-channel surface features had on the droplets behaviour during evaporation. The samples used and described in section *7.2 Droplet channelling* were also used to examine droplet evaporation. The 30 – 5 μm micro-channels and 80 – 19 μm micro-channels designs in squares 1, 2, 3 and 4 contained two types of micro-channels. The two different micro-channels with varying feature dimensions were used in each square (Table 3.5).

Table 7.3 Feature dimensions in micro-channels

Square	Micro-channel 1 (μm)	Micro-channel 2 (μm)
30 – 5 μm micro-channels	30 x 30	30 x 10
	25 x 30	25 x 10
	20 x 30	20 x 10
	15 x 30	15 x 10
	10 x 30	10 x 10
	5 x 30	5 x 10
80 – 19 μm micro-channels	80 x 80	80 x 29
	53 x 80	53 x 29
	43 x 80	43 x 29
	29 x 80	29 x 29
	19 x 80	19 x 29

The evaporation of 0.2.μL deionised water droplets was examined on each surface feature design.

In the interest of simplicity the following subsections will each examine firstly a different surface feature and secondly, the “behaviour” of the droplets during evaporation i.e. the change in shape and dimensions of the droplet. The surface designs examined were fabricated in silicon, high density polyethylene, high density polyethylene coated in gold-palladium, polypropylene and 316LS.

7.3.1 Unstructured surfaces

Droplets placed on unstructured polypropylene, gold-palladium coated high density polyethylene and silicon surfaces were observed to evaporate evenly until the last 30 seconds of evaporation with no channelling effects (Figure 7.36). Droplets placed on unstructured 316LS and high density polyethylene surfaces were observed to evaporate more quickly from one side while the other appeared to remain pinned to the surface (Figure 7.37).

6sec	1min 8	2min 6

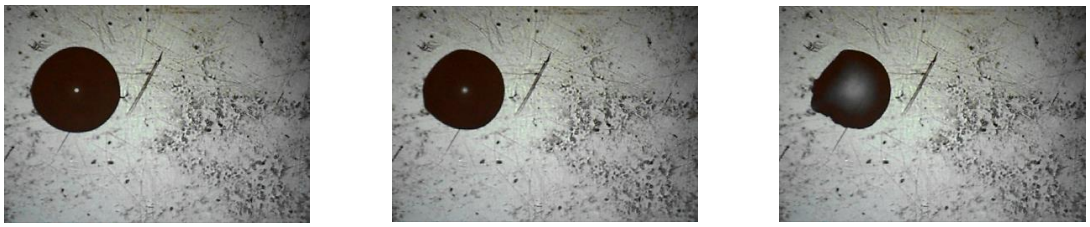

3min 5	4min 13	5min 31

5min 36	5min 39	5min 41

5min 42	5min 43	5min 46

Figure 7.36 Unstructured polypropylene surface

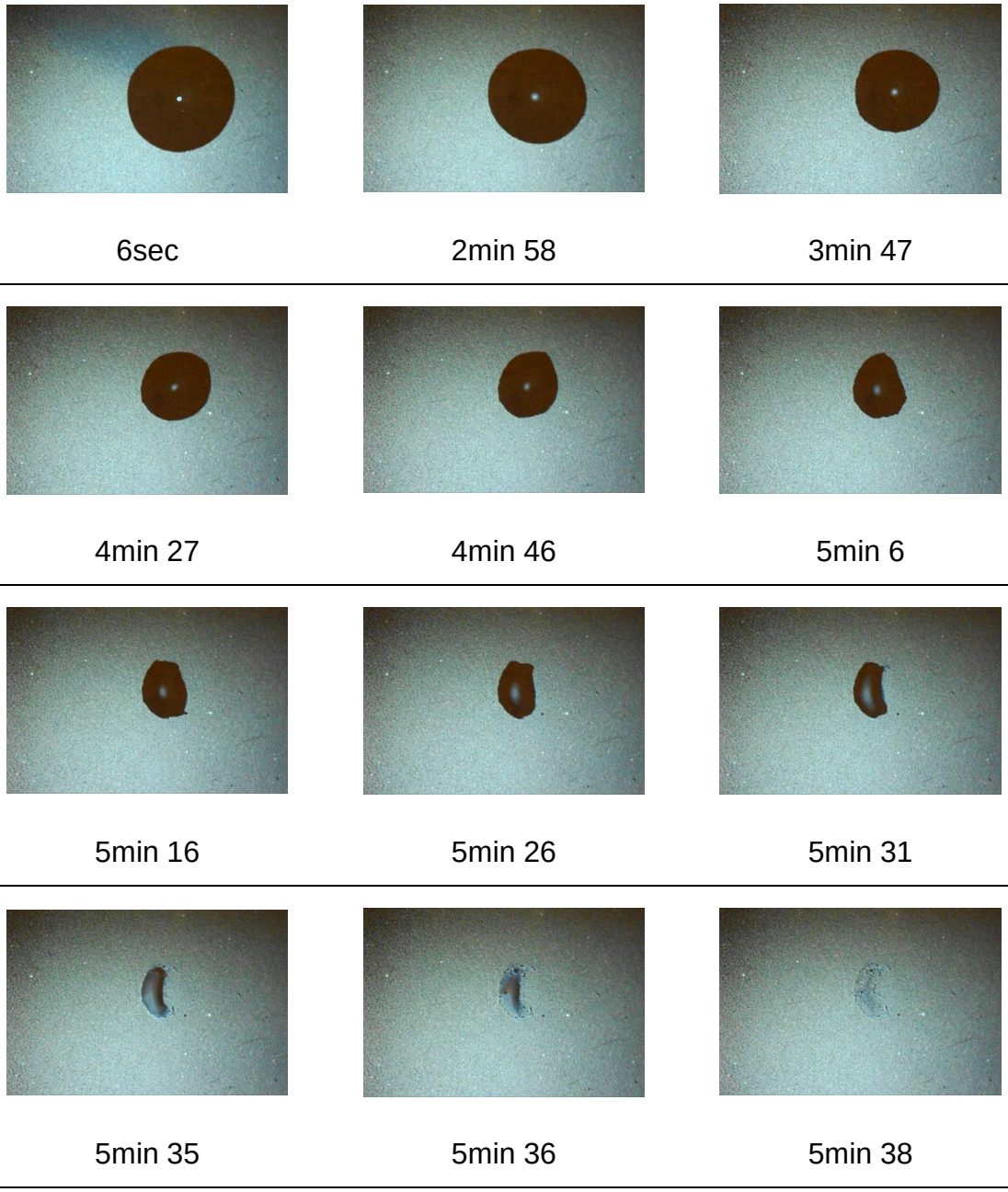

Figure 7.37 Unstructured 316LS surface

7.3.2 30 – 5 μm micro-channels surface design

Droplets observed on surfaces structured with the hole 30 – 5 μm micro-channels feature designs were noted to gradually evaporate without any

channelling of the features being observed (Figure 7.38). However, on the pillar features droplets were seen to evaporate from micro-channel two before micro-channel one (Figure 7.39). The evaporation of the droplet was also observed to occur from the smaller pillars first and then the larger pillars. This resulted in a gradual evaporation across the droplet area. These observations were noted on all samples structured with the 30 – 5 μm micro-channels surface features.

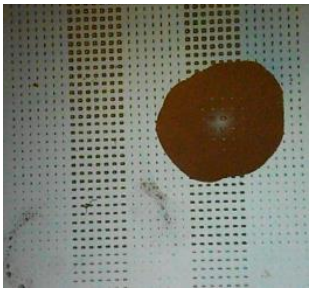

3sec

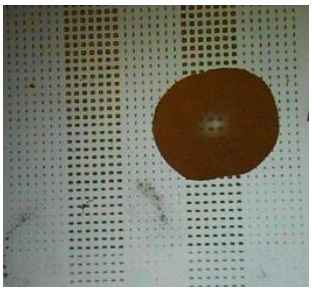

2min 56

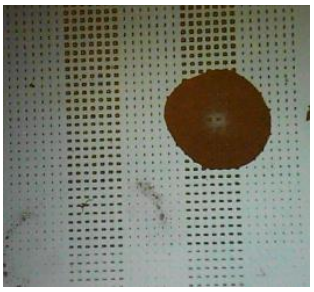

3min 54

4min 53

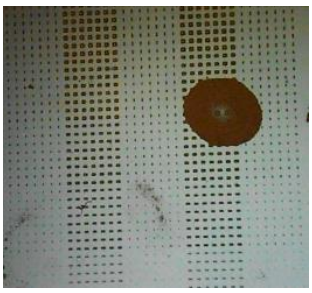

5min 3

5min 22

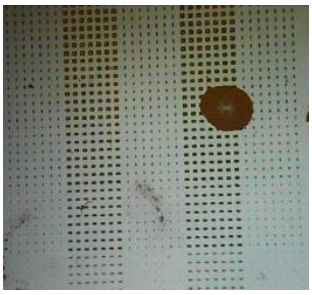

5min 42

5min 52

6min

Figure 7.38 30 – 5 μm micro-channels hole design on silicon mould insert

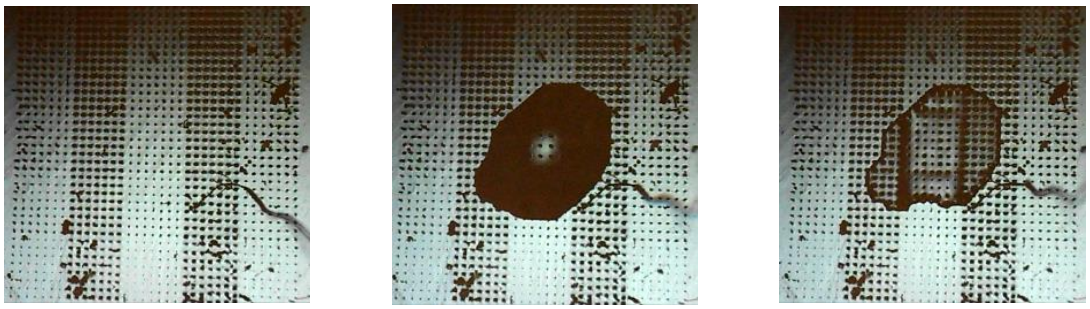

0sec	4sec	3min 51

3min 54	4min 1	4min 9

4min 16	4min 20	4min 22

Figure 7.39 30 – 5 μm micro-channels pillar design on high density polyethylene replicate

7.3.3 80 – 19 μm micro-channels surface design

Droplets on surfaces structured with 80 – 19 μm micro-channels hole features were noted to evaporates evenly with no obvious channelling effects (Figure 7.40). This was also observed on surfaces with unsuccessfully replicated pillar features

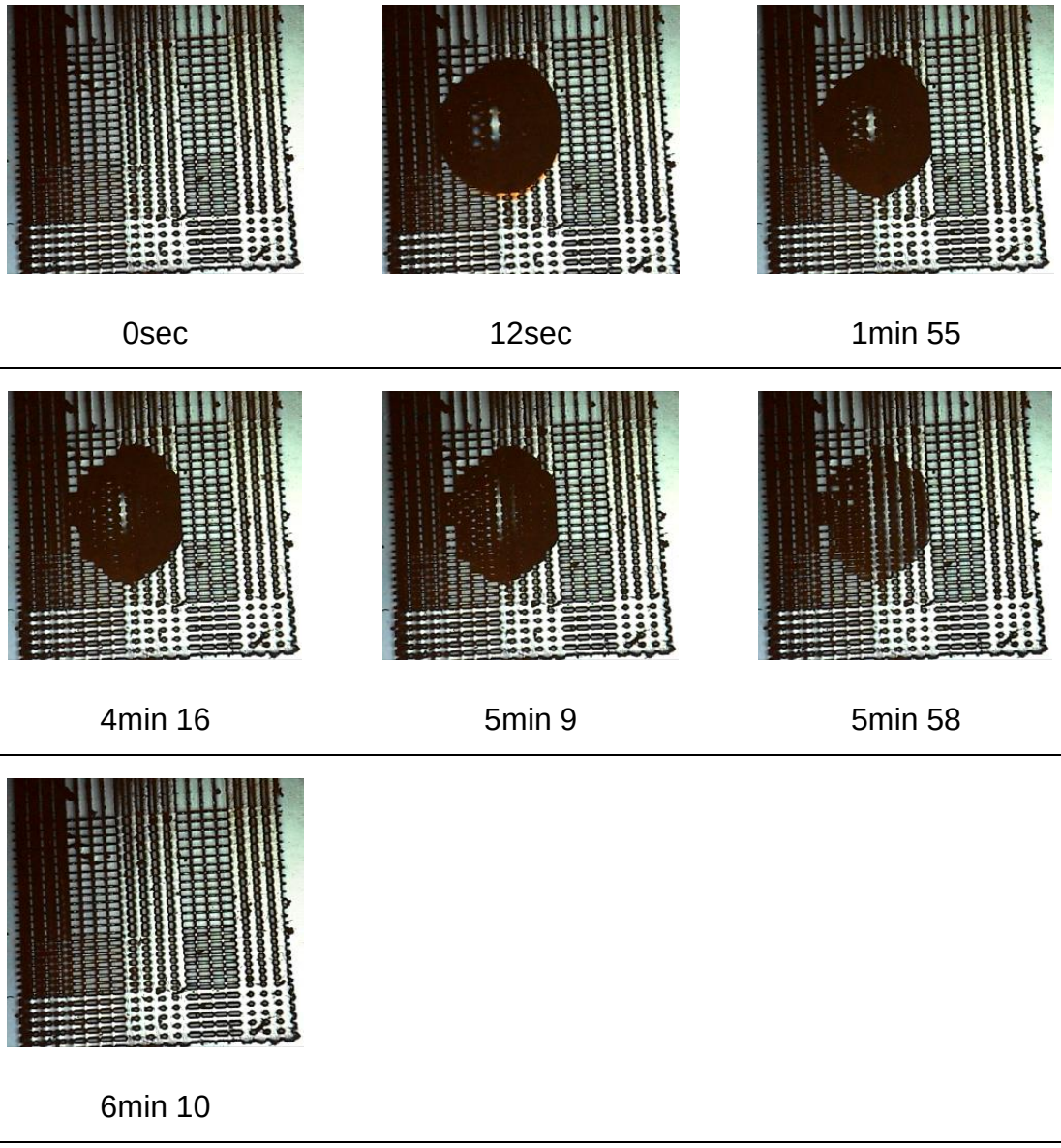

Figure 7.40 80 – 19 μm micro-channels hole design on high density polyethylene

On the pillar features two different droplet behaviours were observed. The first was a squaring of the droplet edges onto micro-channel two, followed by a gradual evaporation of the droplet from the smaller pillars to the larger (Figure 7.41).

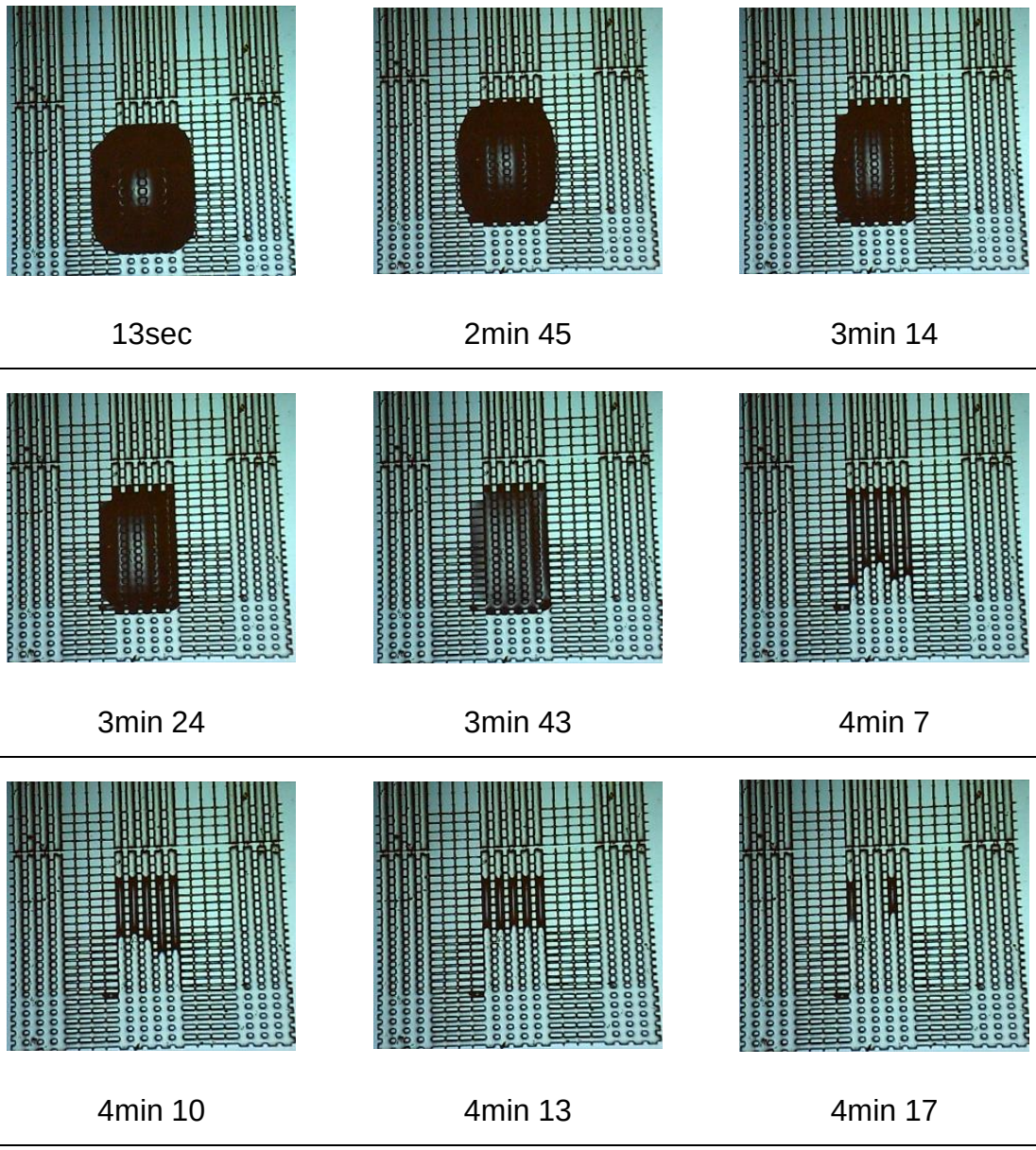

Figure 7.41 80 – 19 μm micro-channels pillar design on silicon mould insert

The second droplet behaviour observed on the pillar features was the directional spreading of the droplet (Figure 7.42). The droplet was observed to square off at the edges and spread along the micro-channels from the largest to the smallest pillars (10 sec – 15 sec). The droplet was then seen to spread

across the micro-channels before it began to evaporate from the smallest pillars to the largest (17 sec – 1 min 4 sec).

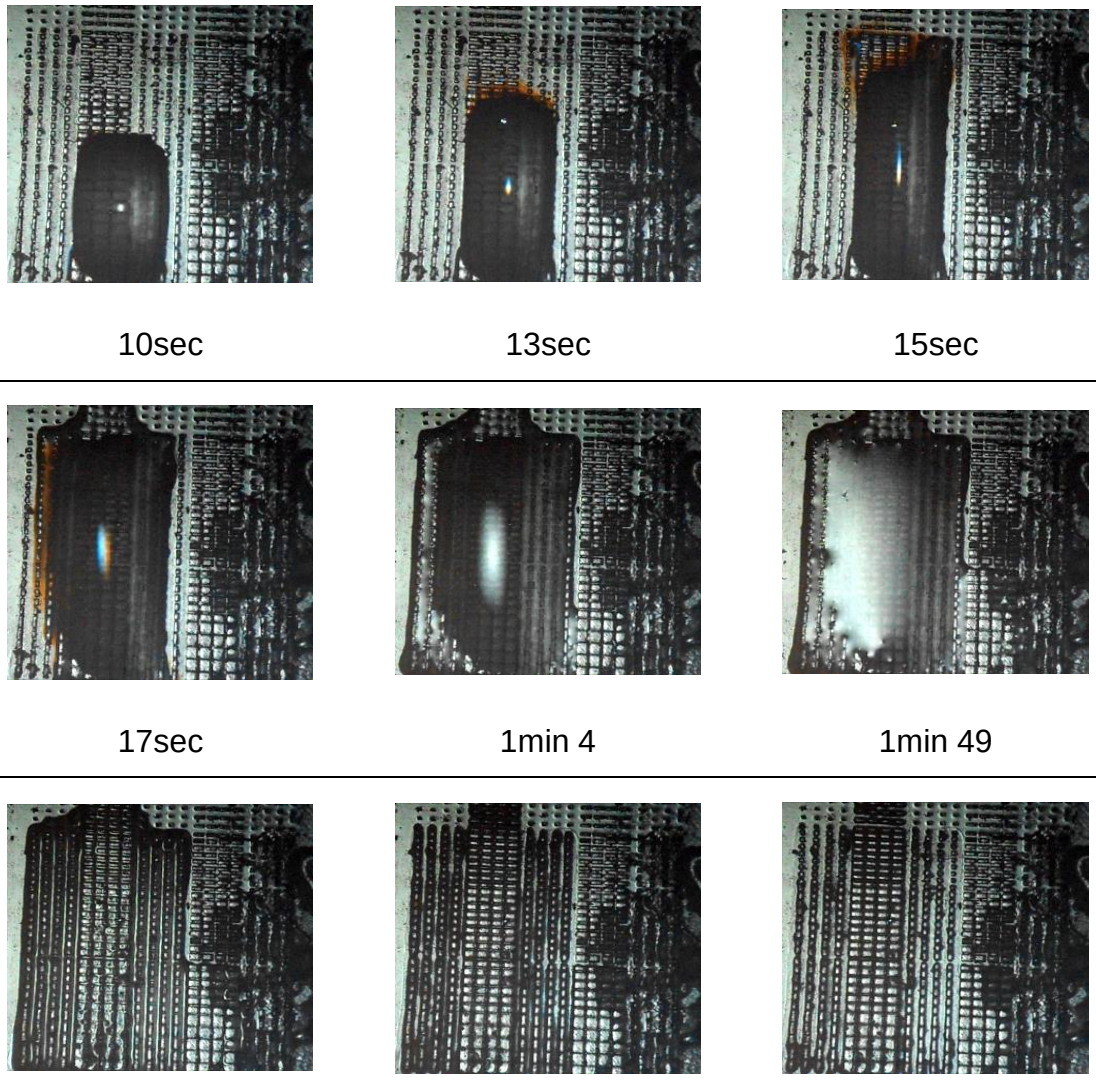

Figure 7.42 80 – 19 μm micro-channels pillar design on high density polyethylene

7.3.4 30 – 5 μm feature gradient surface design

Droplets placed on surfaces structured with 30 – 5 μm feature gradient surfaces hole features were observed to evaporate evenly without any channelling being observed (Figure 7.43). This even evaporation was also observed on unsuccessfully replicated pillar features.

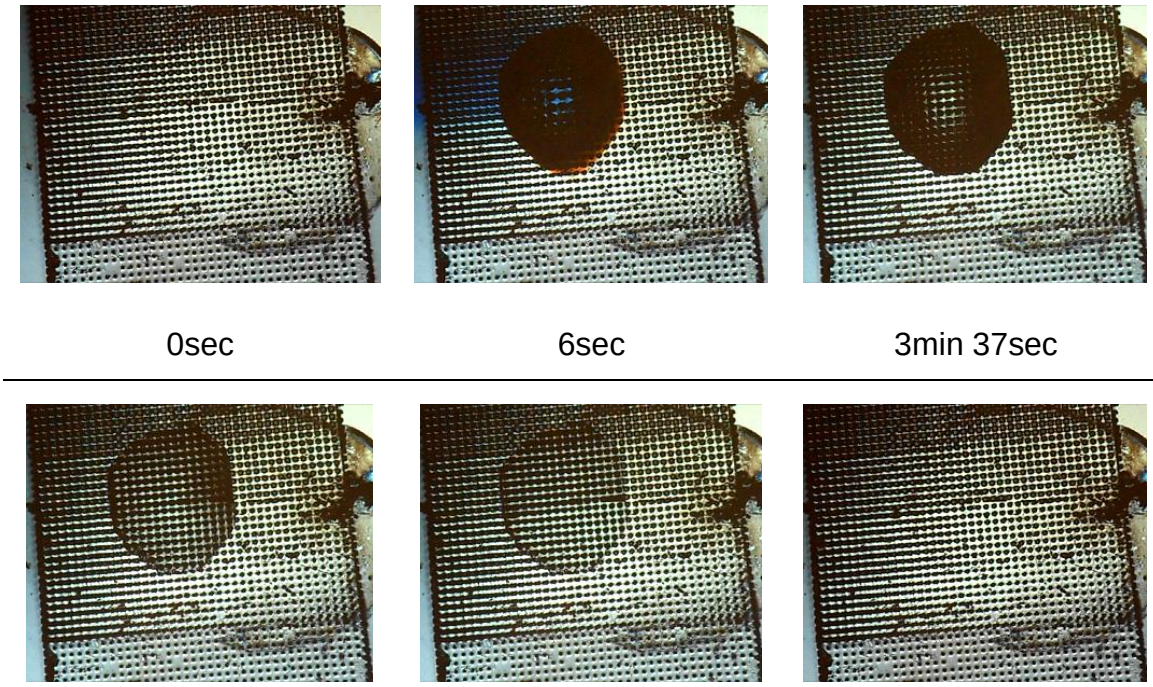

Figure 7.43 30 – 5 μm feature gradient hole design on silicon mould insert

Droplets placed on the pillar features were observed to square off at the edges along the rows of pillars (2 min 8 – 3 min 46). The droplets were then observed to evaporate from the smallest to the largest pillars (Figure 7.44).

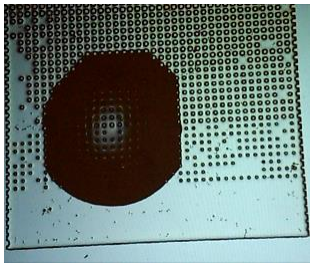	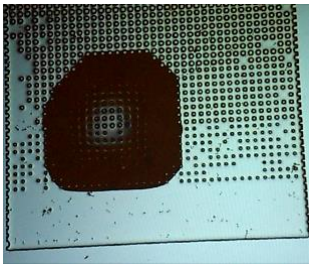	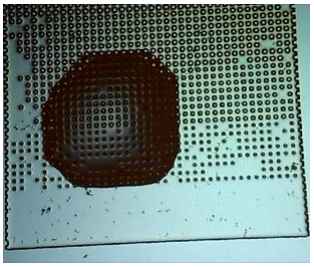
2min 8	2min 47	3min 46
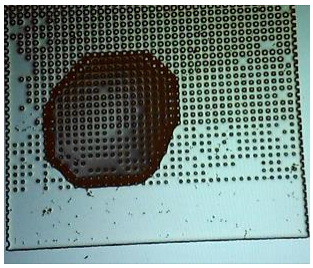	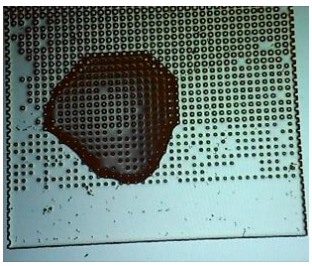	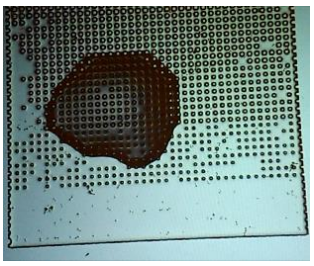
4min 6	4min 16	4min 18
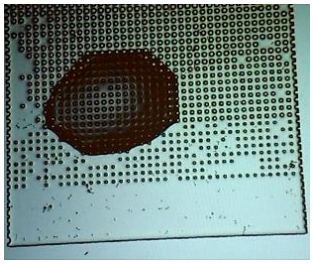	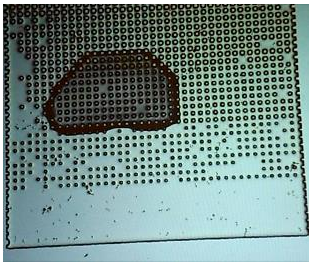	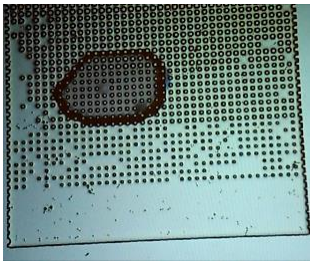
4min 20	4min 45	5min
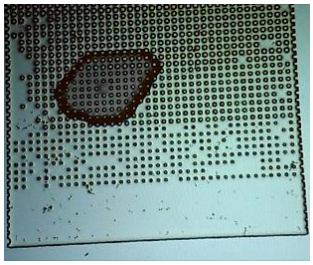	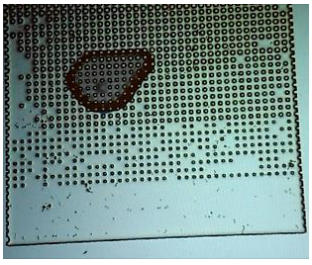	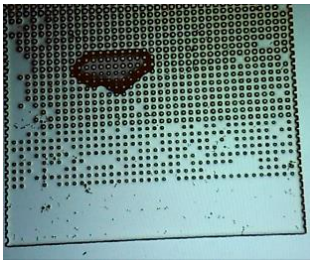
5min 5	5min 15	5min 25

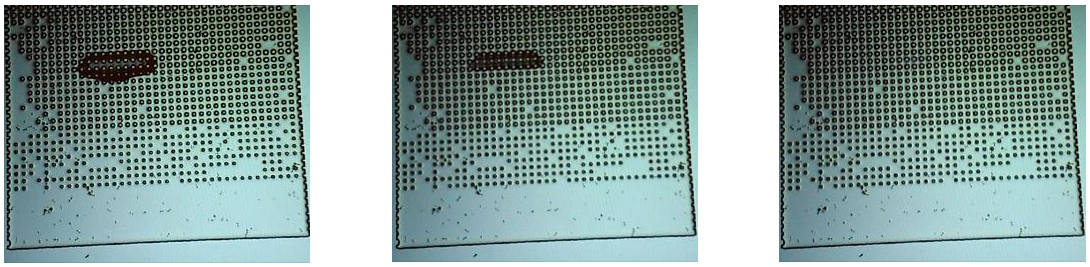

5min 30	5min 40	5min 43

Figure 7.44 30 – 5 μm feature gradient pillar design on silicon mould insert

7.4 Summary of droplet behaviour results

This chapter has presented the results gathered during the examination of droplet behaviour on textured surfaces. Droplet contact angles on silicon, polymer and metal surfaces structures with 10 – 2 μm surfaces were described and the effect of micro-channel surface features on droplet channelling and evaporation was also detailed.

8 Discussion

The following chapter presents a discussion of the results gathered during this research. Section *8.1 Mould design and fabrication* details a discussion of the fabrication processes undertaken into the production of silicon and nickel mould inserts. An examination into the results gathered from the design of experiment investigation into the deep reactive ion etching process is also discussed. Section *8.2 Polymer micro-injection moulding* presents a discussion of the design of experiment investigations into the fabrication of micro-channel and 10 – 2 μm pillar arrays. An examination of the appearance of the surface features is also discussed. Section 8.3 Metal micro-injection moulding discusses the results gathered during the design of experiment investigations into the fabrication of 316LS metal powder replicates and an examination of the appearance of the surface features produced. Finally section *8.4 Droplet behaviour* discusses the effect of the various surface designs on the behaviour of droplet contact angle, channelling and evaporation.

8.1 Mould design and fabrication

8.1.1 Fabrication of micro-channel insert features

Micro-channel pillar and hole features were fabricated onto silicon inserts via photolithography and deep reactive ion etching. The dimensions of the pillar and hole features ranged from 80 x 80 μm to 5 x 5 μm. An emulsion-on-polymer photomask was used during the photolithograph process to pattern the silicon wafers prior to etching. Upon completion of the etching process it was found, through optical microscopy and SFEG-SEM, that the features below 10 x 10 μm were not successfully etching into the silicon substrate. Whereas, those greater than 10 x 10 μm were successfully etched into the substrate surface.

A possible mechanism for the unsuccessful etching of the features below 10 x 10 μm would be the properties of the photomask used during photolithography.

The emulsion-on-polymer mask used does not produce sub-10 μm features with as high a degree of accuracy as other photomasks, such as a chrome-on-glass photomask [95], which may result in less than optimal etching of the features during the deep reactive ion etching process.

Another possible mechanism for the unsuccessful etching of the sub – 10 μm features could be the etch rate of the deep reactive ion etching process. If the etch rate is too high the feature sidewalls could become slanted and eventually produce feature undercuts. These undercuts could in turn cause the features to break and separate from the silicon insert.

8.1.2 Fabrication of 10 – 2 μm insert features

The photolithography and deep reactive ion etching of sub - 10 μm insert features was examined. The sub - 10 μm features chosen for examination were 10 x 10 μm, 5 x 5 μm and 2 x 2 μm. These dimensions were selected as they are in the lower range limitations of both the emulsion-on-polymer and the chrome-on-glass photomasks.

The sub- 10 μm features were patterned onto the silicon wafer using a chrome-on-glass photomask. Prior to etching the silicon wafer was examined using optical microscopy. It was noted that the 2 x 2 μm hole features were not present. A possible mechanism for the absence of these features is the capabilities of the photomask used. The chrome-on-glass photomask used can produce a minimum feature size of 2 x 2 μm. However, as this is at the lower end of the masks capabilities it may not be as accurate as larger features.

During examination of the silicon wafers after etching, using optical microscopy, the 10 x 10 μm and the 5 x 5 μm pillar and hole features appeared to have been successfully replicated. However, the 2 x 2 μm features were not present.

Upon further examination of the etched pillars using SFEG-SEM, it was found that all the pillar features were undercut. In the case of the 5 x 5 μm pillars,

some were so severely undercut that they did not stand up-right but rather lay at an angle across the surface of the wafer.

Due to the unsuccessful etching of the sub - 10 μm features it was decided that a design of experiment approach would be applied. The design of experiment approach was used to determine which process factors had the greatest effect upon the etching of the sub - 10 μm pillar features.

The process factors examined for the deep reactive ion etching process were platen power, C_4F_8 gas flow in the passivation stage and switching times between etching and passivation stage. The factors were selected due to their effect on etch rate and undercut. The factor levels were selected by taking into account the system limits and the minimum / maximum requirements of the feature examined.

A full factorial design was used, which resulted in the completion of eight deep reactive ion etching process runs. Upon examination, using optical microscopy, it was found that the 2 x 2 μm pillar features were not successfully replicated on any of the design of experiment runs. A possible mechanism for the absence of the 2 x 2 μm features would be that the etch rate of the process is still too high and therefore the pillar features are being completely removed during the etched cycles.

Upon examination of the 5 x 5 μm pillar features, using the SFEG-SEM, the degree of feature undercut was found to vary across the design of experiment runs. Some of the pillars suffered such severe undercutting that pillar were no longer observed to be upright on these surfaces. Whereas, the pillars observed on other samples possessed minimal undercuts. A possible mechanism for the difference between the degrees of undercuts observed across the various samples could be the switching times between the etching and passivation stages during the deep reactive ion etching process. The pillars which displayed the higher degrees of undercut underwent a longer etching phase (9 seconds

etching and 5 seconds passivation) compared to those pillars with minimal undercut (5 seconds etching and 5 seconds passivation).

During the examination of the 5 x5 μm pillars the uneven etching of some of the surfaces was also noted, where features are present between the pillars.

A potential mechanism for the uneven etching observed is the incomplete removal of the passivation layer during the etching phase. In extreme cases this can result in the 'black silicon effect'. The 'black silicon effect' occurs when the uneven etching of the sample causes the surface to become gradually rougher during the etching cycles so that 'black silicon' is been formed. 'Black silicon' is a needle-like surface structure comprised of silicon spikes which absorbs light reducing the reflective properties of the silicon surface [94].

Using statistical analysis of the response data gathered during the design of experiment investigation it was determined that the most significant factor with regards to the 5 x 5 μm pillars was the switching times between the etching and passivation phases. A possible mechanism for this is that if the etching cycle is longer than the passivation cycle then there is more time for the passivation layer and underlying substrate to be removed before the next protective layer is applied. Resulting in the eventual undercut of the pillar features.

Upon examination of the 10 x 10 μm features it was found that the runs which resulted in pillar features with undercuts were the same as those observed during the examination of the 5 x 5 μm pillars. Although it was found that none of the 10 x 10 μm pillar were detached from the sample surface due to the undercuts. As with the 5 x 5 μm pillars, the variation in the switching times between the etching and passivation phases is assumed a possible mechanism for the undercutting of the 10 x 10 μm pillar features.

The incomplete etching of the wafer surfaces was also observed for the 10 x 10 μm pillars on the same runs as those found for the 5 x 5 μm pillars. And as with the 5 x 5 mm pillars, the possible mechanism for this uneven etching is thought

to be the partial removal of the passivation layer during etching. Resulting in the roughening of the samples surface and the formation of 'black silicon'.

Once again, the switching times between the etching and passivation phases was found to be the most significant factor with regards to the 10 x 10 μm pillars. And as before, a possible mechanism for this would be the effect of the length of the etching cycle in comparison to the passivation cycle.

8.1.3 Fabrication of micro-channel and 10 – 2 μm pillar insert features in comparison to the literature

As mentioned during chapter *2 Literature review*, the use of the design of experiment approach in the statistical analysis of deep reactive ion etching is not very wide spread. Papers were identified which used statistical experimental design to examine the effects of process factors on the angle of the feature sidewall[19; 137; 150]. Though the features examined in these papers were predominantly trenches and the variation in size between the base and apex of the feature (undercut) was not discussed. The paper identified to examine the fabrication of 2 μm pillar arrays also examined angle of feature sidewall as a response[137]. However, they did not examine a surface containing several varying pillar sizes. During this thesis general factor levels, which were suitable for not just one pillar size but many, were of interest in an attempt to fabricate surface gradient micro-channel features. whereas, factor levels specific to a given feature size are examined within the literature.

8.1.4 Nickel mould insert fabrication

During the fabrication of nickel mould inserts two techniques were used for the application of a conductive seed layer. This seed layer is required when electroplating non-conductive materials. Silicon inserts underwent either sputter-coating or electroless coating to deposit the conductive seed layer.

During the sputter-coating process the silicon inserts were initially subjected to sputter-coating for 20 minutes. This did not produce a conductive enough seed layer, so the process duration was increased to 40 minutes. After 40 minutes the silicon inserts were successfully coated with a conductive seed layer. However, it was decided that the level of conductivity was not high enough for use in the electroplating process. A possible mechanism for obtaining a seed layer which is conductive enough for the silicon insert to undergo electroplating would be to further increase the duration of the sputter-coating process.

During the electroless coating process the silicon inserts were coated with a thin layer of nickel. However, over time it was noted that the nickel deposition began to crack and detach from the silicon surface. A possible reason for this would be that the silicon surface was not sufficiently clean prior to the electroless process. In future the silicon inserts should undergo more thorough cleaning with IPA prior to coating. The seed layer should also be make it thicker as layer produced was not conductive enough for the silicon insert to be used in the electroplating process.

8.1.5 Nickel mould insert fabrication in comparison to the literature

There were many papers identified within the literature, both with and without the use of statistical experimental design, which used a nickel mould insert in the injection-moulding process[88; 89; 108; 140; 160]. However, no papers were identified which examined the fabrication of nickel mould inserts using a statistical experimental design. Of the papers which were identified to use nickel mould inserts it was noted that the information presented regarding the fabrication process was not as in-depth as can be found regarding the photolithographic and deep reactive ion etching processes. Information regarding the factor levels used during the deposition of the conductive seed layer and the electroforming process is not widely found within the literature[101]. Also information regarding how the nickel inserts is separated from the silicon mould after the electroforming process is rarely found within the literature[101].

8.2 Polymer micro-injection moulding

8.2.1 Micro-channel pillar surface features

For each pillar dimension examined it was found that the most significant factor was the same for the pillar dimension (height and width) and the variation of the pillar dimensions from the silicon mould insert (±si). Therefore, to avoid unnecessary repetition of the analysis of the results the following sections (8.2.1.1 and 8.2.1.2) will incorporate a discussion of the results gathered for both pillar dimension (height and width) and the variation of the pillar dimensions from the silicon mould insert (±si) and will be referred to in these sections by the dimension in question i.e. height or width.

8.2.1.1 Polypropylene

Significant factor were not identified for the width of any of the polypropylene pillar features with the exception of the 80 x 29 μm pillars for which injection speed (Is) was found to be the most significant. Injection speed was also found to be most significant to the height of the 25 x 25 and 19 x 29 μm pillars. With regards to the height of the pillar features, cooling time (Ct) was found to be most significant for the 30 x 10, 25 x 10, 20 x 10 and 15 x 10 μm pillars. Mould temperature (Mt) was found to be the most significant factors, with regards to pillar height, for the 20 x 20, 15 x 15 and 10 x 30 μm pillars. Holding pressure (Hp) was found to be the most significant factor for the height of the 53 x 29 and 19 x 80 μm pillars. The interaction between mould temperature and injection speed (Mt/Is) was found to be most significant with regards to the 25 x 30 and 43 x 29 μm pillars. No significant factors were found for the height of the 30 x 30, 29 x 80, 29 x 29, 20 x 30, 80 x 29, 80 x 80, 53 x 80, 43 x 80, 15 x 30 μm pillars. The 10 x 10, 5 x 30, 5 x 10 and 5 x 5 μm pillars were not replicated (NR) on any of the polypropylene replicate surfaces.

Table 8.1 Significant factors for polypropylene pillar height and width and the variation of the replicate features from the silicon mould insert in order of surface area/volume ratio (SA/V)

Pillar dimensions (μm)	Surface area (μm^2)	Volume (μm^2)	SA/V Ratio	Height	±Si Height	Width	±Si Width
80 x 80	25600	256000	0.100	-	-	-	-
53 x 80	19120	169600	0.113	-	-	-	-
43 x 80	16720	137600	0.122	-	-	-	-
80 x 29	13360	92800	0.144	-	-	Is	Is
29 x 80	13360	92800	0.144	-	-	-	-
53 x 29	9634	61480	0.157	Hp	Hp	-	-
43 x 29	8254	49880	0.165	Mt/Is	Mt/Is	-	-
19 x 80	10960	60800	0.180	Hp	Hp	-	-
30 x 30	6600	36000	0.183	-	-	-	-
30 x 30	6600	36000	0.183	-	-	-	-
29 x 29	6322	33640	0.188	-	-	-	-
25 x 30	5900	30000	0.197	Mt/Is	Mt/Is	-	-
25 x 25	5250	25000	0.210	Is	Is	-	-
20 x 30	5200	24000	0.217	-	-	-	-
19 x 29	4942	22040	0.224	Is	Is	-	-
20 x 20	4000	16000	0.250	Mt	Mt	-	-
15 x 30	4500	18000	0.250	-	-	-	-
30 x 10	3800	12000	0.317	Ct	Ct	-	-
15 x 15	2850	9000	0.317	Mt	Mt	-	-
10 x 30	3800	12000	0.317	Mt	Mt	-	-
25 x 10	3300	10000	0.330	Ct	Ct	-	-
20 x 10	2800	8000	0.350	Ct	Ct	-	-
15 x 10	2300	6000	0.383	Ct	Ct	-	-
10 x 10	1800	4000	0.450	NR	NR	NR	NR
5 x 30	3100	6000	0.517	NR	NR	NR	NR
5 x 10	1300	2000	0.650	NR	NR	NR	NR
5 x 5	850	1000	0.850	NR	NR	NR	NR

When ordered according to the surface area/volume ratio (SA/V) (Table 8.1) it can be seen that cooling time is more significant for the pillar features with a higher SA/V. The same can be observed for the significance of mould temperature. However, holding pressure and the interaction between mould temperature and injection speed can be seen to be more significant for pillar features within the lower end of the SA/V range. With this in mind a possible reason for the increase significance of mould temperature and cooling time with regards to the features with higher SA/V is that these features are more likely to experience premature freezing of the polymer at the entrance to the feature cavity. Therefore, altering the mould temperature and cooling time can improve the rate of filling of these smaller cavities.

When comparing the heights of the intended pillar design, the silicon mould insert features and the replicate pillars. It was found that there was little variation between the feature heights of the intended design and the silicon mould insert. However, there was significant variation observed between the replicate pillar height and both the designed and silicon mould insert feature heights. A possible mechanism for this variation is the incomplete filling of the mould features.

8.2.1.2 High density polyethylene

Upon examination of the significant factors identified for height of high density polyethylene pillars mould temperature (Mt) was found to be the most significant for all pillars, with the exception of the 80 x 80, 53 x 80 and 43 x 80 μm pillars. For which no factor was found to be significant. Mould temperature was also identified as the most significant factor with regards to pillar width for the 30 x 10, 25 x 10, 20 x 10, 19 x 80, 19 x 29, 15 x 30, 15 x 10, 15 x 15 and 10 x 30 μm pillars. As discussed in the previous sub-section, a high mould temperature can prevent premature freezing of the polymer at the entrance to high aspect ratio features and improve mould cavity filling. The 10 x 10, 5 x 30, 5 x 10 and 5 x 5

μm pillars were not replicated (NR) on any of the high density polyethylene replicates surfaces.

Table 8.2 Significant factors for high density polyethylene pillar height and width and the variation of the replicate features from the silicon mould in order of surface area/volume ratio (SA/V)

Pillar dimensions (μm)	Surface area (μm^2)	Volume (μm^2)	SA/V Ratio	Height	±Si Height	Width	±Si Width
80 x 80	25600	256000	0.100	-	-	-	-
53 x 80	19120	169600	0.113	-	-	-	-
43 x 80	16720	137600	0.122	-	-	-	-
80 x 29	13360	92800	0.144	Mt	Mt	-	-
29 x 80	13360	92800	0.144	Mt	Mt	-	-
53 x 29	9634	61480	0.157	Mt	Mt	-	-
43 x 29	8254	49880	0.165	Mt	Mt	-	-
19 x 80	10960	60800	0.180	Mt	Mt	Mt	Mt
30 x 30	6600	36000	0.183	Mt	Mt	-	-
29 x 29	6322	33640	0.188	Mt	Mt	-	-
25 x 30	5900	30000	0.197	Mt	Mt	-	-
25 x 25	5250	25000	0.210	Mt	Mt	-	-
20 x 30	5200	24000	0.217	Mt	Mt	-	-
19 x 29	4942	22040	0.224	Mt	Mt	Mt	Mt
20 x 20	4000	16000	0.250	Mt	Mt	-	-
15 x 30	4500	18000	0.250	Mt	Mt	Mt	Mt
30 x 10	3800	12000	0.317	Mt	Mt	Mt	Mt
15 x 15	2850	9000	0.317	Mt	Mt	Mt	Mt
10 x 30	3800	12000	0.317	Mt	Mt	Mt	Mt
25 x 10	3300	10000	0.330	Mt	Mt	Mt	Mt
20 x 10	2800	8000	0.350	Mt	Mt	Mt	Mt
15 x 10	2300	6000	0.383	Mt	Mt	Mt	Mt
10 x 10	1800	4000	0.450	NR	NR	NR	NR
5 x 30	3100	6000	0.517	NR	NR	NR	NR
5 x 10	1300	2000	0.650	NR	NR	NR	NR
5 x 5	850	1000	0.850	NR	NR	NR	NR

When ordered according to the surface area/volume ratio (SA/V) (Table 8.2) it can be seen that mould temperature is the most significant factor regarding height and ±Si height for all factor sizes except those with the lowest SA/V and the highest, which were not successfully replicated. A possible mechanism for this is that altering the mould temperature can influence cavity filling i.e. increasing the mould temperature can prevent premature freezing of the polymer so smaller features can be filled. Regarding width and ±Si width, mould temperature was found to me significant for features in the larger end of the SA/V range. As before, a possible mechanism for this would be the influence mould temperature has on cavity filling.

8.2.1.3 Comparison of pillar features fabricated

The pillars fabricated in both polypropylene and high density polyethylene were compared, in terms of average pillar width and height, and are displayed in Figure 8.1. It can be seen from the distribution of the data points that the pillars fabricated were within the same working range for both polymer melts.

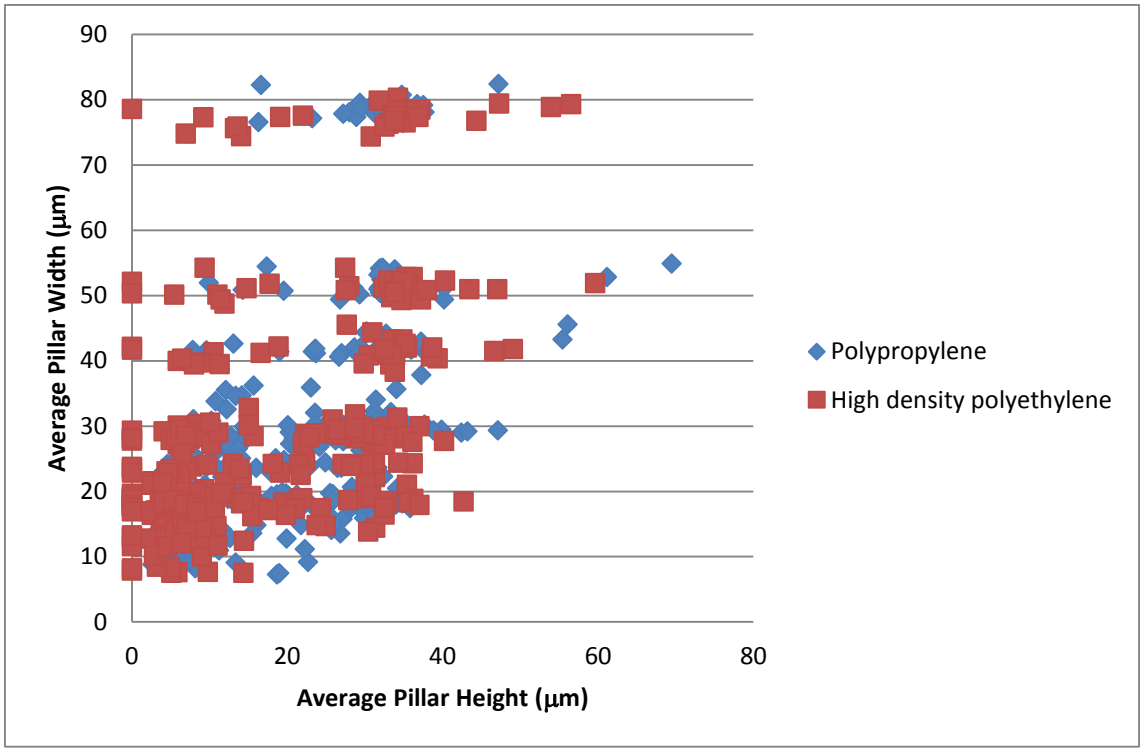

Figure 8.1 Comparison of average pillar height and width for polypropylene and high density polyethylene pillars fabricated

8.2.1.4 Discussion of significant factor for the dimensions and variation from the silicon mould insert of micro-channel surface features

A possible mechanism for the significance of injection speed is that a[177]

[171]

[161,164,162] high injection speed decreases the polymer melt viscosity which results in the improved filling of the mould features cavities. The significance of mould temperature is due to the temperature difference between the polymer melt and the mould. The closer to the melt temperature the mould is the less likely it is that the polymer melt will experience premature freezing at the entrance to the mould cavities and result in improved filling of the cavities. A possible mechanism for the significance of holding pressure would be that it

reduces shrinkage of the polymer and also prevents the back-flow of polymer from the mould, resulting in better mould cavity filling. A possible reason for the significance of the interaction between mould temperature and cooling time is that a higher mould temperature would require a longer cooling time to adequately reduce the temperature of the sample and prevent the deformation of the replicate features. In the cases where significant factors were not identified it is possible that the factor levels selected do not cater closely enough for the specific polymer in question, as the factor levels were chosen to be suitable for both polymer specification. Therefore, if the factor levels were refined to more closely encompass the specifications of the individual polymer more significant factors may be identified.

A possible mechanism for the failure of the 10 x 10, 5 x 30, 5 x 10 and 5 x 5 μm pillars to replicated is the premature freezing of the polymer melt at the entrance to the mould cavity. Another possible mechanism would be the quality of the mould cavities. If the features are not fully formed on the mould then they will not be present in the replicate samples.

8.2.2 Feature dimensions and variation from silicon mould insert micro-channel surface feature replicates in the literature

During the review of the literature undertaken as part of this research it was found that many papers examined the fabrication of pillar arrays via micro-injection moulding[57; 117; 143; 168; 173; 174; 214]. There were also many papers identified to have used statistical experimental analysis, both design of experiment and Taguchi, to examine the effect of process factors on the micro-injection moulding process[5; 7; 59; 79; 88; 155]. However, only one paper[176] was found to have used statistical experimental design, in this case design of experiment, to examine the fabrication of pillar arrays via micro-injection moulding. This paper examined pillar features with diameters of 100 and 150 μm.

A direct dimensional comparison between the replicate sample and the mould used during fabrication was not found within the literature.

8.2.3 Appearance of pillar features on micro-channel surface feature replicates

During the examination of both the polypropylene and high density polyethylene replicate features it was also noted that some pillars were not completely formed and possessed curved edges (Figure 8.2 and Figure 8.3). A possible mechanism for this the incomplete filling of the silicon mould insert due to premature freezing of the polymer during injection.

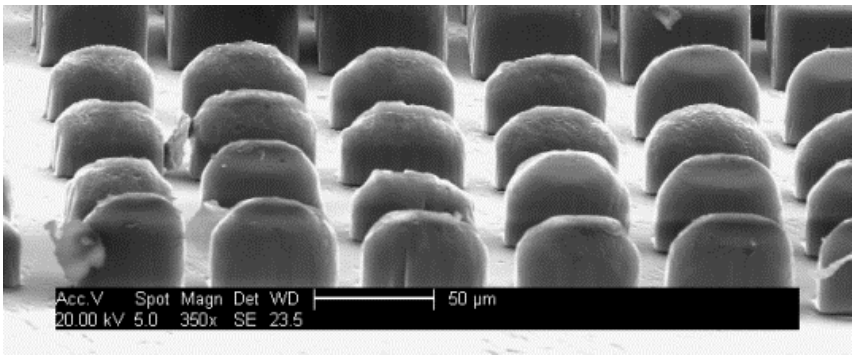

Figure 8.2 Curved polypropylene 53 x 80 µm pillars

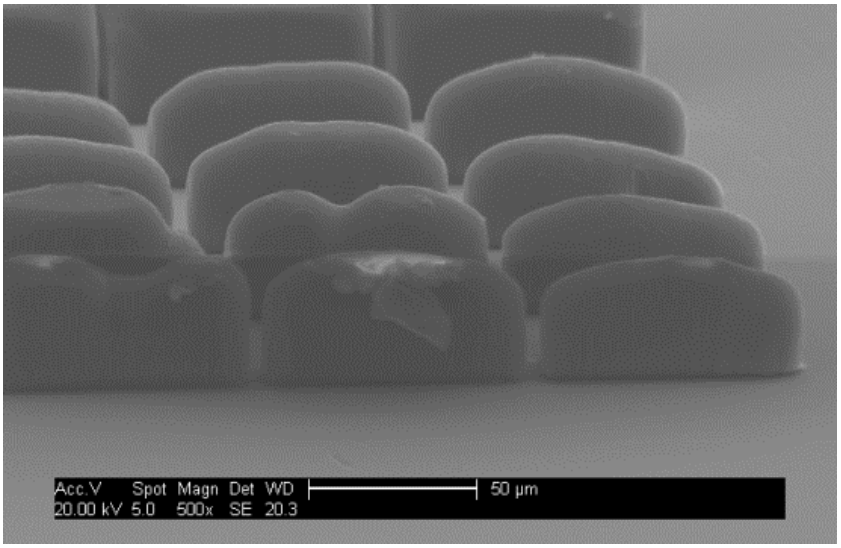

Figure 8.3 Curved 80 x 29 μm high density polyethylene pillars

As well as the incomplete filling of the pillar features, deformities were also observed on some of the pillars. In some cases the pillars were slanted rather than upright (Figure 8.5 and Figure 8.6). A possible mechanism for the occurrence of slanted pillars could be that the polymer wasn't completely cool and set prior to demoulding. However, on comparison of the pillars produced it was found that those pillars which experienced the most pronounced slanting had both the high mould temperature and high cooling time. Whereas the pillars which experienced the least slanting had a high mould temperature but a low cooling time (Figure 8.4). Therefore it can be deduced that the mould temperature alone doesn't influence the formation of slanted pillars.

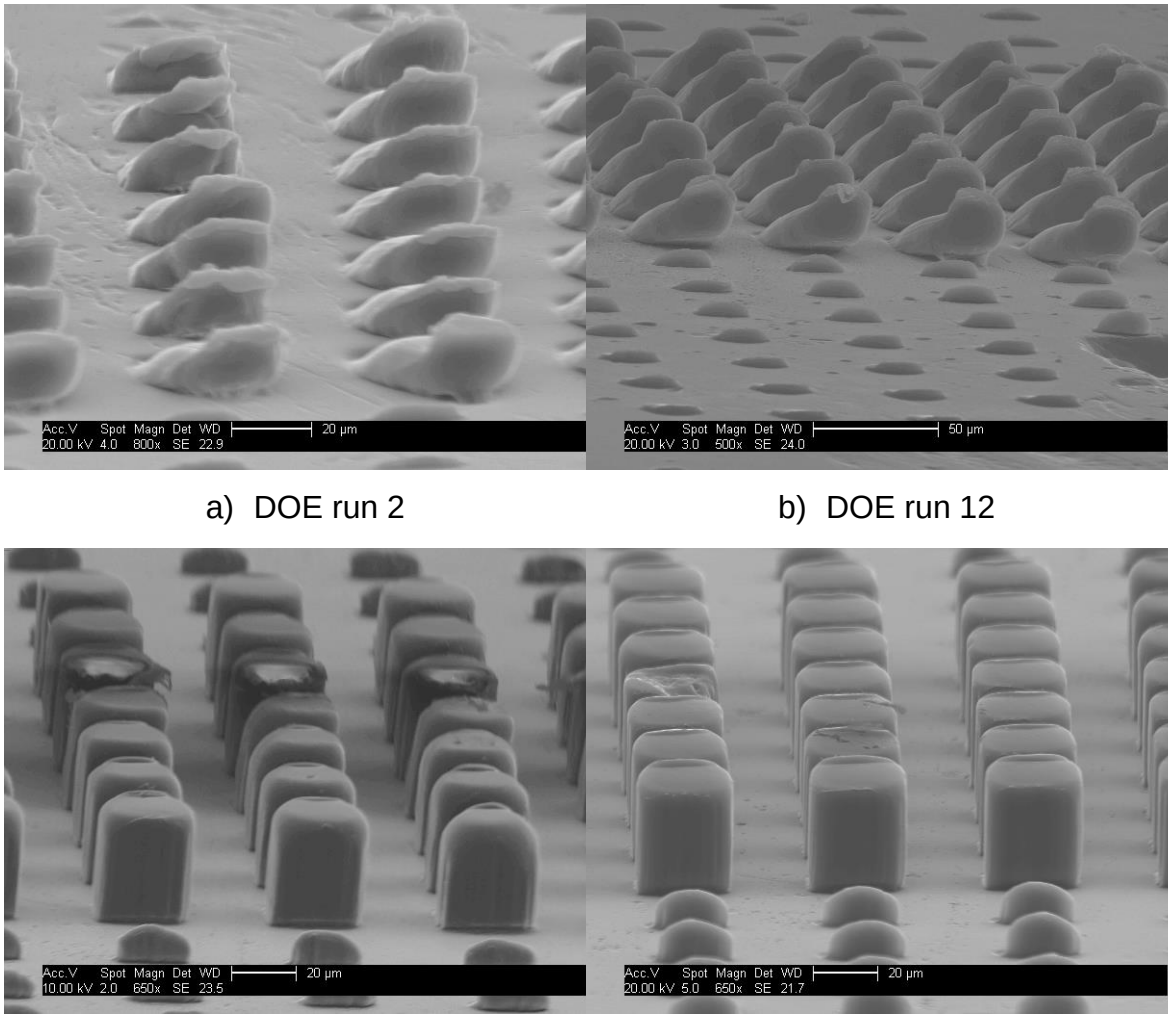

a) DOE run 2

b) DOE run 12

c) DOE run 4

d) DOE run 8

Figure 8.4 High density polyethylene 30 x 30 μm pillars, a and b) High mould temperature and high cooling time, c and d) high mould temperature and low cooling time

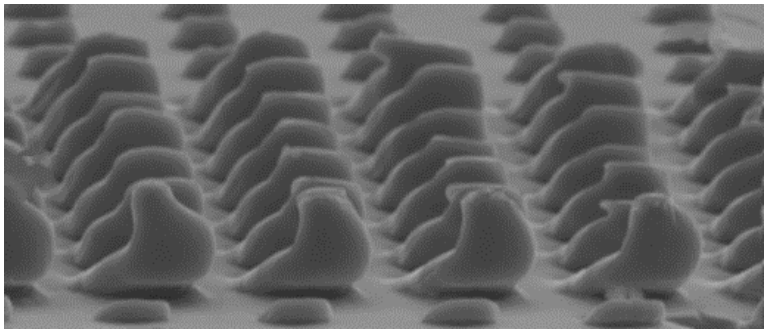

Figure 8.5 Slanted polypropylene 30 x 30 μm pillars

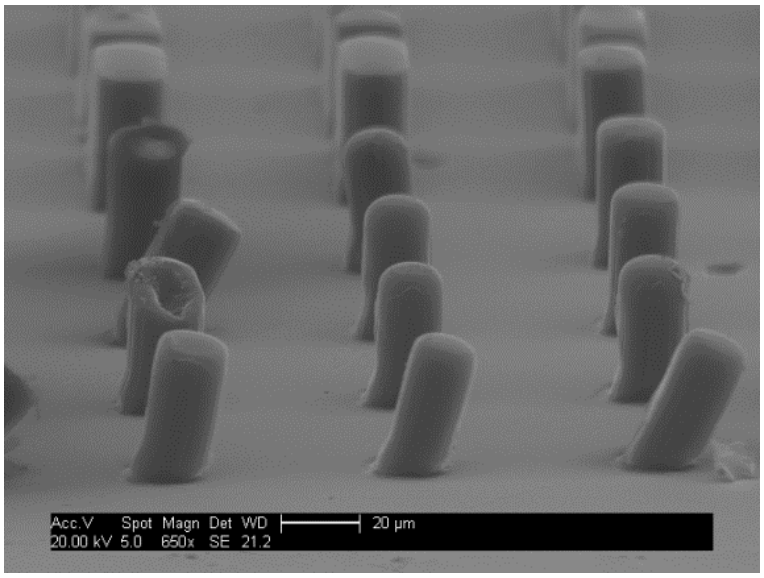

Figure 8.6 Slanted high density polyethylene 19 x 19 μm pillars

In other cases the far side of the pillar top appeared to have been extended, resulting in the pillar edge being taller than the cavity of the silicon mould insert (Figure 8.7 and Figure 8.8). A possible mechanism for these observed deformities is the forces inflicted on the pillar features during the demoulding process. The extension of the pillar is only observed on the replicates with had

a high mould temperature but a low cooling time. If the polymer replicate is still too warm when removed from the mould the pillar features could, momentarily, remain in the mould cavities resulting in the deformations observed.

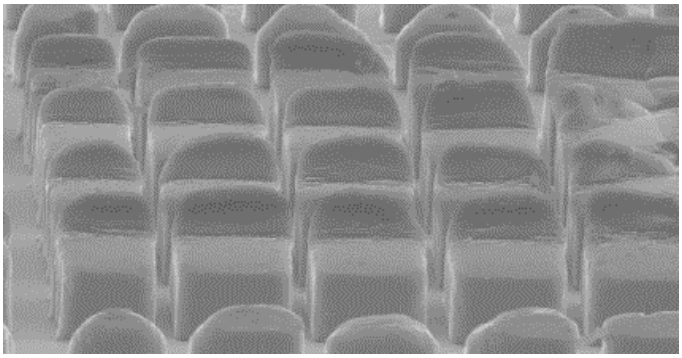

Figure 8.7 Extension at back edge of 53 x 80 μm polypropylene pillars

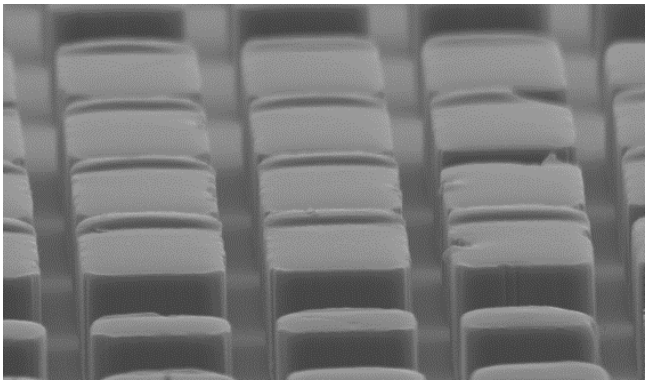

Figure 8.8 Extension at back edge of 43 x 80 μm high density polyethylene pillars

8.2.3.1 Polypropylene

An optical examination of the polypropylene pillars replicated was made. It was found that the features produced using the factor levels from run 4 of the design

of experiment were the most well replicated. While the least well replicated were produced using the factor levels from run 3 (Table 8.3). This was found for both the largest and smallest SA/V ratio pillars (Figure 8.9), despite different process factors being found significant for each. No significant factor was identified for the 80 x 80 μm pillars, while cooling time was identified as the most significant factor for the 15 x 10 μm pillars.

Table 8.3 Design of experiment runs resulting in the most and least well replicated polypropylene pillar features

DOE	Mould temperature	Cooling time	Holding pressure	Injection speed
Run 3	-	+	+	-
Run 4	+	-	+	+

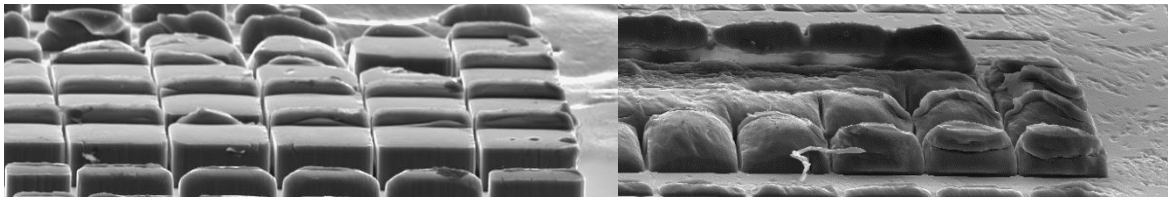

80 x 80 μm DOE run 4

80 x 80 μm DOE run 3

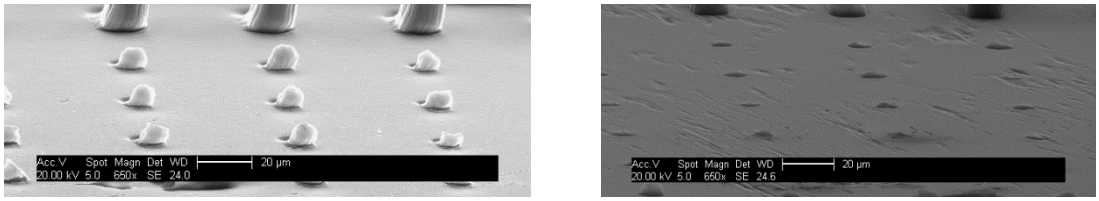

15 x 10 μm DOE run 4

15 x 10 μm DOE run 3

Figure 8.9 Comparison of most and least well replicated polypropylene pillars

Upon examination of the factor levels used in these two runs it was noted that they were different from each other for three of the four factors. From the variations between these two runs it could be assumed that the improved feature replication could be due to (a) a high mould temperature, (b) a low cooling time or (c) a high injection speed, as these are the factors which differ between the two runs. However, when a more general examination of the surface features was made it was noted that the design of experiment runs which produced the most well replicated features all had a high mould temperature. Whereas the runs which results in the production of less accurately replicated pillars had a low mould temperature. Therefore, it can be assumed that a high mould temperature is possible mechanism for obtaining replicate pillar features with a high level of accuracy.

8.2.3.2 High density polyethylene

An optical examination of the high density polyethylene pillars replicated was made. It was found that the features produced using the factor levels from runs 4 and 8 of the design of experiment were the most well replicated. While the least well replicated were produced using the factor levels from run 13 (Table 8.4). It should be noted that of the entire variety of pillar dimensions fabricated only one was produced when using the factor levels from run 13, the others were not fabricated at all.

Table 8.4 Design of experiment runs resulting in the most and least well replicated high density polyethylene pillar features

DOE	Mould temperature	Cooling time	Holding pressure	Injection speed
Run 4	+	-	+	+
Run 8	+	-	-	+
Run 13	-	-	-	-

Upon examination of the factor levels used in these three runs it was noted that the design of experiment runs which produced the most well replicated features all had a high mould temperature and injection speed. Whereas the runs which results in the production of less accurately replicated pillars had a low mould temperature and injection speed. Therefore, it can be assumed that a high mould temperature and injection speed is a possible mechanism for obtaining replicate pillar features with a high level of accuracy.

8.2.3.3 Comparison of appearance of pillar features

When the process factors of the most and least well replicated pillars were examined it was found that the most well replicated pillars were all fabricated using the high mould temperature level. Whereas the least well replicated pillars were fabricated using the low mould temperature level. This was found for both the polypropylene and high density polyethylene replicates. No clear pattern was identified with any of the other process factors. This would indicate that a high mould temperature is preferable to a low mould temperature with regards to the appearance of pillar features.

8.2.4 Appearance of pillar features on micro-channel surface feature replicates within the literature

The occurrence of micro-channel pillar features is not prevalent within the literature[48]. Papers found, which detail the use of a design of experiment approach of other surface features, presented images of the most well replicated features, but not the least well replicated[4; 6; 7; 35; 88; 130; 202; 223]. An optical comparison between the replicates produced was found to have been made.by Sha et al[176]. However, in some cases images of the fabricated samples were not presented[155].

8.2.5 10 – 2 μm pillar surface features

8.2.6 Part and buffer mass of 10 – 2 μm surface feature replicates

Using statistical analysis, of the data gathered during the design of experiment investigation, injection speed was identified as the most significant factor with regards to the part mass of polypropylene and high density polyethylene replicate samples. A possible reason for this would be that a high injection speed aids with the filling of the mould features, thereby filling the mould with a greater portion of the polymer melt shot.

None of the factors examined were found to be significant to the buffer mass. However, holding pressure was found to have the main effect on the buffer mass of polypropylene replicates, using a main effects plot. The holding pressure used during the injection moulding process is meant to prevent polymer flowing out of the mould and increasing the size of the buffer. With regards to the high density polyethylene replicates, injection speed was found to have the main effect on buffer mass. A possible reason for this is that a high injection speed aids with the filling of the mould cavities resulting in more polymer being forced into the mould rather than being in the buffer.

8.2.7 Part and buffer mass of polymer micro-injection moulded replicates within the literature

Within the literature examined part and/or buffer mass were not found to have been examined for surfaces containing pillar arrays. However, when the part and/or buffer mass was measured as a response it was noted that melt temperature, holding pressure and injection speed were all identified as significant factors[3; 5; 8; 154; 222; 223].

8.2.8 Feature dimensions and variation from the silicon mould insert of polymer 10 – 2 μm injection moulded replicates

As previously mentioned the most significant factor was found to the same for both the pillar dimension (height and width) and the variation of the pillar dimensions from the silicon mould insert (±si). Therefore, to avoid unnecessary repetition of the analysis of the results this section will incorporate a discussion of the results gathered for both pillar dimension (height and width) and the variation of the pillar dimensions from the silicon mould insert (±si) and will be referred to in this sections by the dimension in question i.e. height or width.

Significant factors were not identified for the width of the 10 x 10 μm pillars or the variation of these pillars from the silicon mould insert. However, mould temperature was found to be the most significant factor with regards to the height of the 10 x 10 μm pillars and the variation of these pillars from the silicon mould insert. As previously mentioned a high mould temperature can aid the filling of mould cavities. Thereby, producing a more accurate replicate of the mould features.

No pillars were found to have been replicated for the 5 x 5 or 2 x 2 μm pillars. a possible mechanism for this would be the premature freezing of the polymer at the entrance to the mould feature cavities.

No pillars were found to have been replicated in the high density polyethylene replicates. A possible reason for this could again be the premature freezing of

the polymer within the mould. However, it could be that the factor levels examined need to be adjusted to better suit the requirements of the high density polyethylene melt.

8.2.9 Feature dimensions and variation from the mould insert of 10 – 2 μm pillar features within the literature

As previously discussed in section 8.2.2 a direct dimensional comparison between the replicate sample and the mould used during fabrication was not found within the literature. Also, as previously discussed, only one paper was identified within the available literature which used the design of experiment approach to examine the effect of factors on pillar arrays. This paper examined pillars with diameters in 100 and 150 μm[176]. No papers were found within the literature which used a statistical experimental design to examine the fabrication of 10 – 2 μm pillar arrays.

8.2.10 Appearance of pillar features on 10 – 2 μm polymer replicated

During the optical examination of the replicate features it was noted that the most well replicated 10 μm polypropylene pillars were produced using runs 4 and 8 from the design of experiment investigation. While the least well replicated pillars were produced by runs 3 and 6 (Table 8.5).

Table 8.5 Design of experiment runs resulting in the most and least well replicated polypropylene 10 μm pillar features

DOE	Mould temperature	Cooling time	Holding pressure	Injection speed
Run 4	+	-	+	+
Run 8	+	-	-	+
Run 3	-	+	+	-
Run 6	-	+	+	+

Through an examination of the factor levels used during these runs it can be seen that the most well replicated pillars were moulded using a high mould temperature and a low cooling time. A high mould temperature would prevent the premature freezing of the polymer resulting in more accurately replicated pillars.

Examination of the 5 μm polypropylene features found that the pillars had not been replicated on any of the samples. A possible mechanism for this is that the polymer underwent premature freezing during the moulding process and the mould cavities were not filled.

8.2.11 Appearance of pillar features on 10 – 2 μm polymer replicated within the literature

The fabrication of 10 – 2 μm pillar features via a design of experiment approach was not found within the available literature. However, papers discussing the fabrication of sub – 10 μm pillars via micro-injection moulding (but not using a design of experiment approach) were identified. These papers however only display images of the final product and not comparisons between fully and incomplete replicated features[110; 125; 164].

8.2.12 Pressure-Volume-Temperature data

One of the main issue identified from the results gathered regarding the micro-injection moulding of high surface area/volume ratio features is the premature freezing of the polymer melt. In sections 5.3 and 6.5 the process windows used during the micro-injection moulding process were displayed using PVT data curves.

8.3 Metal micro-injection moulding

8.3.1 Part mass of 316LS metal-injection moulded replicates

Using statistical analysis of the data gathered during the design of experiment investigation it was found that the most significant factor affecting the part mass of the 316LS replicate samples was injection speed. A possible reason for this would be that the speed at which the feedstock is forced into the mould effects the filling of the features and therefore the final weight of the sample.

8.3.2 Part mass of 316LS metal-injection moulded replicates comparison to the literature

During the examination of the literature the examination of the papers found which examined part mass of metal powder replicates of other features melt temperature, mould temperature and holding pressure were identified as significant factors[90; 113; 114]. However, analysis of metal powder replicate mass via a statistical experimental analysis approach could not be found for surfaces with pillar arrays.

8.3.3 Feature dimensions of 316LS micro-channel metal-injection moulded replicates

Once again the most significant factor was found to the same for both the pillar dimension (height and width) and the variation of the pillar dimensions from the silicon mould insert (±si). Therefore, this section will discuss the results gathered for both pillar dimension (height and width) and the variation of the pillar dimensions from the silicon mould insert (±si) and will be referred to in this sections by the dimension in question i.e. height or width.

An examination of the 316LS pillars revealed that no significant factors were identified for the majority of the pillars examined. Significant factors were identified for the height of four of the pillars and for the width of one pillar.

Mould temperature (Mt) was identified as the most significant factor for the height and width of the 80 x 80 μm pillars and for the height of the 19 x 80 μm pillars. A possible mechanism for the significance of mould temperature on pillar replication is that the metal powder melt may experience premature freezing at the entrance to the mould cavities if the temperature difference between the mould and metal powder melt is too great.

Injection speed (Is) was found to be the most significant factor with regards to the 53 x 80 μm pillars. A possible reason for the significance of injection speed on the replication of 316LS pillar features is that injection speed can influence the viscosity of the metal powder melt viscosity which can affect the filling of the mould features cavities. With a higher injection speed resulting in improved filling of the mould cavities.

While holding pressure (Hp) was found to be the most significant factor for the 29 x 29 μm pillars. Holding pressure can prevent back flow of the metal powder melt which could be a reason why it is a significant factor to the replication of features and the filling of mould cavities.

The average pillar width and height of the fabricated 316LS were compared and are displayed in Figure 8.10 which outlines the distribution of pillars fabricated.

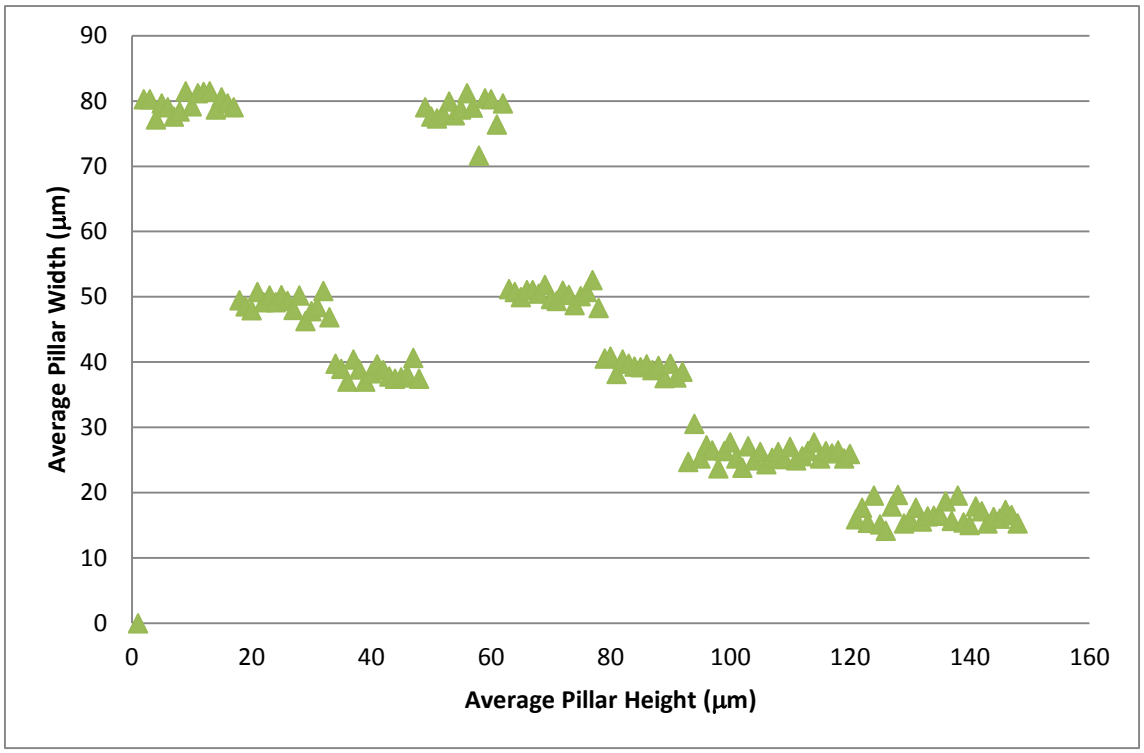

Figure 8.10 Distribution of 316LS pillar fabricated

When ordered according to the surface area /volume ratio (SA/V) (Table 8.6) it can be seen that significant factors were not identified for the pillar features with SA/V within the mid-range. Whereas, holding pressure was found to be significant for features in the higher SA/V range, injection speed was significant in the low SA/V range and mould temperature was found to be significant at both the higher and lower ends of the SA/V range.

Table 8.6 Most significant factor for the height and width and the variation of the replicate features from the silicon mould insert of the 316LS pillar features in order of surface area/volume ratio (SA/V)

Pillar dimensions (μm)	Surface area (μm^2)	Volume (μm^2)	SA/V Ratio	Height	±Si Height	Width	±Si Width
80 x 80	25600	256000	0.100	Mt	Mt	Mt	Mt
53 x 80	19120	169600	0.113	Is	Is	/	/
43 x 80	16720	137600	0.122	/	/	/	/
29 x 80	13360	92800	0.144	/	/	/	/
80 x 29	13360	92800	0.144	/	/	/	/
53 x 29	9634	61480	0.157	/	/	/	/
43 x 29	8254	49880	0.165	/	/	/	/
19 x 80	10960	60800	0.180	Mt	Mt	/	/
29 x 29	6322	33640	0.188	Hp	Hp	/	/
19 x 29	4942	22040	0.224	/	/	/	/

8.3.4 Feature dimensions of 316LS micro-channel metal-injection moulded replicates in comparison to the literature

There were several examples of 316LS pillar arrays being fabricated using metal powder injection moulding noted within the literature examined[56; 57; 123]. However, none examined the fabrication process of pillar arrays using statistical experimental analysis. It was also noted that the smallest pillar size found within the literature to have been fabricated using 316LS was 40 μm[57]. whereas in the course of this research pillars ranging from 19 – 80 μm were fabricated.

8.3.5 Appearance of pillar features on 316LS micro-channel metal-injection moulded replicates

During and optical examination of the 316LS pillars replicated it was found that the most well replicated pillars were produced during run 9 of the design of

experiment. With the least well replicated observed on the replicates produced using run 15 (Table 8.7). However, it should be noted that as many of the 316LS replicate pillars were not fully formed and therefore the 'most well replicated' pillars are still in need of improvement.

Table 8.7 Design of experiment runs resulting in the most and least well replicated 316LS pillar features

DOE	Mould temperature	Cooling time	Holding pressure	Injection speed
Run 9	+	-	+	-
Run 15	+	+	-	+

Upon examination of the factor levels of these two runs it was noted that the same mould temperature was used for both. Therefore, it can be assumed that the mould temperature does not influence the replication quality of metal powder features as much as it does when a polymer feedstock is used. From the difference between these two runs it would also appear that a low cooling time, high holding pressure and low injection speed produce more well replicated pillar features.

The pillar features on the 316LS replicate samples fabricated also appeared to be rough and pitted. A possible reason for the rough appearance of the replicate surface would be the metal particles used in the metal powder feedstock. Unlike a polymer feedstock the metal powder consists of metal particles within a polymer binder. It is possible that these metal particles may be large enough to cause the surface of the features to appear rough and pitted when not sufficiently compacted within the mould (Figure 8.11). Another possible mechanism for the rough appearance and incomplete filling of the 316LS features would be that the separating of the polymer binder from the metal particles resulting in the rough appearance due to the metal particles

filling the feature cavity but not the polymer binder. The mould insert was examined after the completion of replicate production to ensure that the features remained intact. It was confirmed that the surface features were intact after the moulding processes and no metal powder residue was found.

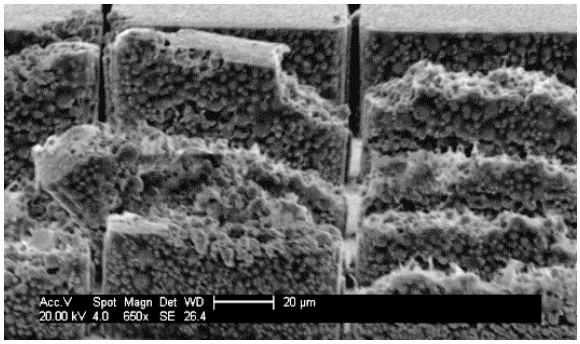

Figure 8.11 Surface roughness of 80 x 29 μm 316LS pillars DOE run 1

The uneven formation of the pillar features was also observed. Where it was found that some pillars varied in height (Figure 8.12).

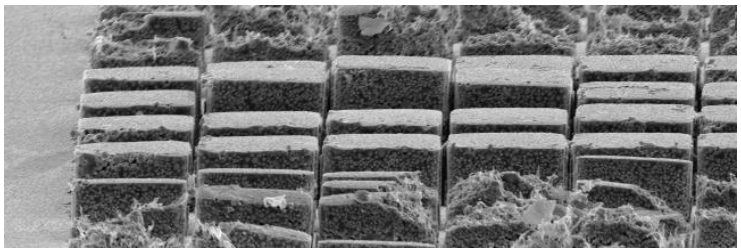

80 x 80 μm

Figure 8.12 Uneven heights of pillars of the same widths

A possible reason for the uneven pillar heights observed could be the incomplete filling of the mould feature. Possibly due to the premature freezing of the feedstock in the mould. Another possible mechanism which could cause the variation in height of the pillars is the demoulding process. If the metal powder was not sufficiently cool prior to ejection from the mould, the features may have been deformed and stretched by the demoulding forces.

Observations of the smaller pillars found that several of the pillars were slanted rather than upright (Figure 8.13).

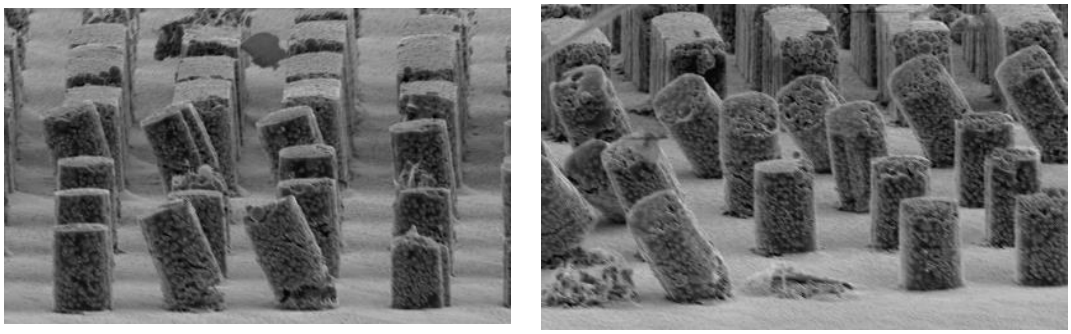

29 x 80 μm 29 x 29 μm

Figure 8.13 Slanting of 316LS pillars

A possible mechanism for the slanting of the pillar features would be the forces exhorted on the features during demoulding. As previously mentioned, if the metal powder wasn't cool enough prior to demoulding the ejection forces could cause the deformation observed.

8.3.6 Appearance of pillar features on 316LS metal-injection moulded replicates within the literature

During a review of the literature, discussed in Chapter *2 Literature review*, two papers were identified which discussed the production of 316LS pillar features via metal injection moulding[56; 57]. In both cases images are presented which display both incompletely filled and completely filled pillar features. Images of the pillar features after the sintering and debinding processes is also presented.

8.4 Droplet behaviour

8.4.1 Droplet contact angles

The contact angles of 1 μL droplets was observed on polypropylene, high density polyethylene and silicon samples structured with 10 – 2 μm pillar and hole surface features. No distinct pattern was observed for the droplet contact angles. However, the highest initial contact angles were observed on the polypropylene surfaces. While the lowest initial contact angles were observed on the silicon surfaces. A possible reason for this would be that of the three surface material examined polypropylene is the most hydrophobic, while silicon is the most hydrophilic.

8.4.2 Droplet contact angles in the literature

The measurement of droplet contact angles has been used extensively throughout the literature to examine the effect of surface texturing on the wettability of the surface. It has been demonstrated that increase surface roughness can increase the contact angle of a droplet making the surface more hydrophobic[42; 49; 62; 169; 226].

8.4.3 Droplet channelling

During an examination of the effect of surface texturing on droplet movement silicon inserts, high density polyethylene and polypropylene replicates were structured with micro-channel features. The effect of structured micro-channels on the directional movement or 'channelling' of droplets was examined on each surface at tilt angles ranging from 30 – 90 ^{o}. It was found that none of the surfaces examined displayed the ability to 'channel' the droplets at any of the tilt angles. A possible mechanism for this lack of movement could that the three-phase-line of the droplet is being pinned to the surface features. Thereby, preventing the droplet from moving across the surface of the sample.

8.4.4 Droplet channelling in the literature

There have been several examples within the literature of surface structuring to aid and manipulate the movement and channelling of droplets[33; 48; 62; 100; 226]. Surface gradients have been used to direct the movement of droplets in a specific direction upon vibration of the surface. One such example is the paper upon which one of the designs used in this research was adapted from[179]. In which the authors succeeded in using vibrational energy to move the droplet along the surface gradient. However, this surface did not assist in the movement of the droplets examined during this research. A possible reason for this would be that no external vibrational energy was exhorted on the sample during this research.

8.4.5 Droplet evaporation

An examination into the effect of surface features on the evaporation behaviour of 0.2 μL deionised water droplets was conducted. Polypropylene, high density polyethylene, Ag-Pd coated high density polyethylene, 316LS stainless steel and silicon surfaces were structured with pillar and hole surface designs: 30 – 5

μm micro-channels, 80 – 19 μm micro-channels and 30 – 5 μm feature gradients.

On unstructured PP, Si and Ag-Pd coated HDPE surfaces the droplets were observed to evaporate evenly with no channelling effects. However, slight pinning of the droplets was observed on 316LS and HDPE unstructured surfaces.

Examination of droplet evaporation on hole 30 – 5 μm micro-channels, 80 – 19 μm micro-channels and 30 – 5 μm feature gradients found that the three-phase-line of the droplets receded gradually. No identifiable pinning effects were observed for any of the sample substrates.

Examination of the 30 – 5 μm micro-channel surface designs found that the droplets evaporation was affected by the underlying surface features. The rate of evaporation of the droplet was found to be higher on the micro-channels containing the smaller pillars. This resulted in the splitting of the droplet during evaporation (Figure 8.14). This splitting of the droplet during evaporation was observed on the 30 – 5 μm micro-channel surface design on all sample substrates.

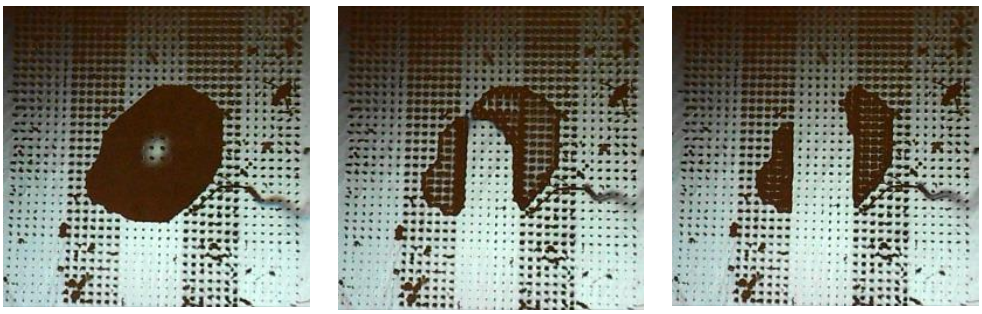

Figure 8.14 Droplet evaporation on 30 – 5 μm micro-channel surfaces

Droplets observed on the 80 – 19 μm micro-channel surface designs were found to become square during evaporation. The droplet edges appeared to recced in-line with the micro-channels so that the orientation of the three-phase-line became parallel to the surface features (Figure 8.15).

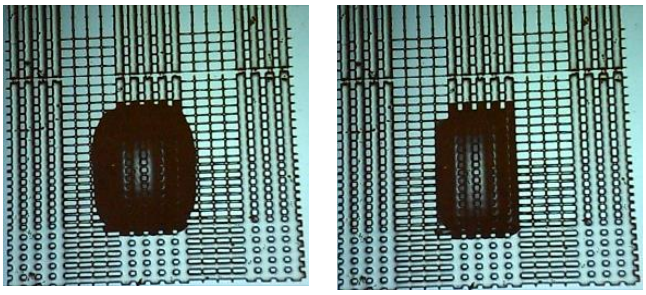

Figure 8.15 Squaring of droplet three-phase-line on 80 – 19 μm micro-channel surface

The droplets were also observed to spread along the micro-channels (from the largest to the smallest pillars) upon placement on the surface. Once the droplet had covered the length of the micro-channel it then began to spread across them until the edge of the structured surface was reached (Figure 8.16). The droplets were then observed to evaporate gradually. With evaporation occurring from the smallest pillar first and the largest pillars last.

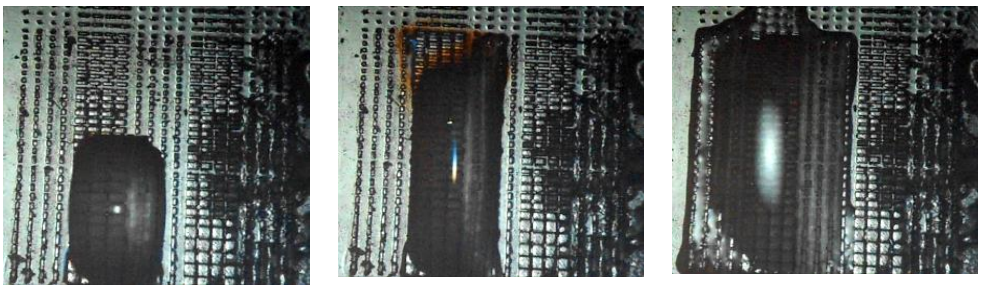

Figure 8.16 Spreading of droplet on 80 – 19 μm micro-channel surface

Droplets on the 30 – 5 μm feature gradient pillar surfaces were displayed an evaporation gradient. The droplets three-phase-line receded from the smaller pillar to the largest (Figure 8.17).

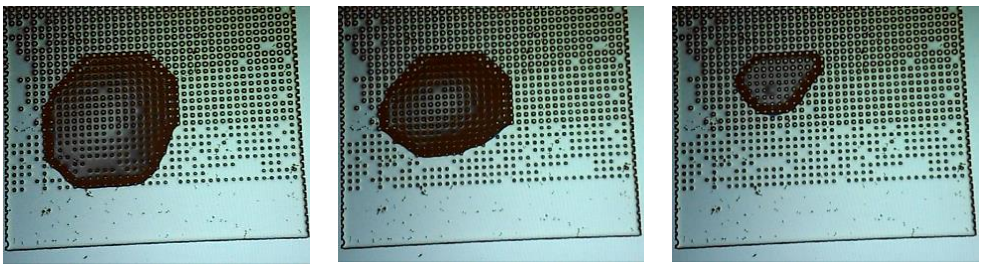

Figure 8.17 Evaporation gradient of 30 – 5 μm feature gradient surfaces

On all pillar surface feature an evaporation gradient was observed. The three-phase-line of the droplets was found to recede from the pillars with the smallest dimensions first. With the point of complete evaporation occurring once the three-phase-line reached the pillars with the largest dimensions.

A possible reason for the droplet pinning and evaporation gradients observed is the effect the surface design is having on the droplets free-energy barriers. In

order for the droplet three-phase-line to move it must possess enough energy to overcome the effect of surface pinning. In altering the structure of the surface at the droplets three-phase-line the energy required for the droplet to move is also changing. When this is considered with the presence of micro-channel/gradient pillars the energy required for a droplet to move will be different for each micro-channel and/or pillar size. This will result in the evaporation of the droplet from one micro-channel and/or pillar size before the other as the droplet will take the path of least resistance during movement of the three-phase-line.

8.4.6 Droplet evaporation in the literature

Many papers within the literature observed droplet evaporation on surfaces structured with pillar arrays where the pillars are all of the same dimensions[43; 147; 206]. The evaporation of droplets on/or straddling micro-channels of pillars was not found within the available literature. The directional evaporation, caused by a surface gradient, of droplets observed during this research was also seen within the literature[220]. Although within the literature the directional evaporation micro-channels are not used and no splitting of the droplet during evaporation due to the surface features is observed.

8.4.7 The Wenzel and Cassie-Baxter debate

As discussed during Chapter *2 Literature review*, Section *2.4 Behaviour of droplets on micro-textured surfaces*, there is an on-going debate regarding the use and application of the Wenzel and Cassie-Baxter equations. There are those who feel that the surface area under a droplet determines droplet contact angle[129; 132; 156], and therefore advocate the use of the Wenzel and Cassie-Baxter equations. There are also those who feel that it is instead the structure of the surface at the three-phase-contact line which influences the contact angle of a droplet[65].

During the course of this thesis it has been noted that the pinning of the three-phase-line appears to have a large effect on droplet shape and contact angle i.e. the observed pinning of the droplets during ‘channelling’. It can also be seen from the examination of droplet evaporation that the surface area under a droplet does have some effect on droplet behaviour. However, with regards to the effect of surface area on the behaviour of droplets during evaporation, it is assumed that the surface structure merely decreases the de-pinning energy required to move the three-phase-line.

Using the observations made during the course of this thesis it would appear that the effect of the three-phase-contact line is greater than the effect of surface area when examining droplet behaviour.

9 Conclusions

The research undertaken within this thesis was done so in an attempt to realise the research aim, “to identify the effects of process factors on the fabrication of micro-textured surfaces and the effect of such surfaces on droplet behaviour”, by addressing four objectives. This chapter presents a realisation of the research aim and the conclusions drawn from the research objectives examined.

9.1 Research objectives compared with research achievements

Objective 1:

‘To understand the state-of-the-art in the statistical experimental analysis of micro-scale pillar fabrication’

A review of the available literature was undertaken to investigate the state-of-the-art in statistical experimental analysis. The literature search focused on the deep reactive ion etching, polymer micro-injection moulding and metal powder micro-moulding techniques.

The following conclusions have been made during the undertaking of this objective

- Limited literature regarding the application of statistical experimental design to deep reactive ion etching process
- Lack of examination statistical experimental design in the production of sub – 100 μm pillar features using deep reactive ion etching – only one paper found
- Examination of feature undercut not examined within literature but sidewall and profile angle are.

- The use of statistical experimental design in the fabrication of pillar arrays via metal powder injection moulding is not found within the available literature
- The production of sub – 40 μm pillar features using a metal powder feedstock were also not present within the literature.

Objective 2:

'To identify the effect of process factors on the design and fabrication of silicon and nickel mould inserts'

The second objective was investigated using the available literature and the results gathered during the course of this research. The results of which are outlined in chapter *4 mould design and fabrication results*. This objective was partially realised as an examination into the effect of process factor on the fabrication of nickel mould inserts could not be undertaken due to issues encountered during the fabrication process.

The following conclusions were drawn from an examination of the fabrication of silicon mould inserts:

- For the fabrication of sub – 10 μm features a chrome-on-glass photomask rather than an emulsion-on-polymer mask as it produces features of this size with a greater accuracy.
- Design of experiment analysis of the deep reactive ion etching process identified switching times as the most significant factor with regards to pillar undercut.

Objective 3:

'To identify the effect of process factors on the micro-moulding of polymer and metal powder feedstocks'

Using the silicon mould inserts, fabricated during the realisation of objective two, the effects of process factors on the micro-injection moulding of polymer and metal powder feedstocks was investigated. The realisation of objective three incorporated examination of the available literature and the results discussed in chapters *5 polymer micro-moulding results* and *6 metal powder micro-moulding results*.

The following conclusions were drawn regarding the effect of process factors on the micro-injection moulding of polymer and metal powder feedstocks:

- Mould temperature was identified as the most significant regarding the high density polyethylene pillar features.
- Mould temperature and cooling time were identified as the most commonly occurring significant factors for the polypropylene pillar features.
- Significant factors were identified for the largest and smallest of the 316LS pillars with regards to the pillar height and ±Si height.
- Mould temperature was found to be the most commonly occurring significant factor for the 316LS pillars.
- Injection speed was found to be the most significant factor affecting the part mass of 316LS replicate samples.
- Injection speed was found to be the most significant factor affecting the part mass of polypropylene and high density polyethylene replicate samples.
- Holding pressure was found to have the main effect on buffer mass for the polypropylene replicate samples.
- Injection speed was found to have the main effect on buffer mass for the high density polyethylene replicate samples.

Objective 4:

'Examine the effect of surface texturing on droplet behaviour'

The investigation into the effect of surface texturing on droplet behaviour was conducted through a review of the literature and an examination of the work undertaken during this research. The findings of which are outlined in chapter *7 droplet behaviour results*.

The following conclusions have been made during the undertaking of this objective

- Highest initial contact angles observed on polypropylene replicates
- Lowest initial contact angles observed on silicon inserts
- No droplet channelling was observed on any of the micro-channelled surfaces even when tilted to a 90 ^{o} angle.
- Droplets were observed to evaporate evenly on all unstructured surfaces and all hole patterned features.
- Droplets on pillar patterned surfaces exhibited an evaporation gradient. Evaporating from the smallest to the largest pillars prior to the point of complete evaporation.
- Droplets were observed to spread along the micro-channels (from the largest to the smallest pillars) when placed on the structured surfaces before spreading across the micro-channels and evaporating.
- Droplets on micro-channel patterned surfaces were observed to evaporate from the micro-channel containing the smallest pillar first, in some cases splitting the droplet in two. The droplets were then observed to follow an evaporation gradient on the remaining micro-channel, evaporating from the smallest to the largest.

10 Future work

Upon completion of this research into the micro-texturing of surfaces for fluid control, via a design of experiment approach, several aspects were identified as possible avenues for future work. This chapter will discuss these avenues in the following four subsections. *10.1 Mould fabrication* discusses the proposed future work with regards to the fabrication of silicon and nickel mould inserts for use in micro-injection moulding. *10.2 Polymer micro-injection moulding* outlines the possible avenues which could explore in the extension of the polymer micro-injection moulding work previously discussed in this thesis. *10.3 Metal injection moulding* discusses aspects of metal powder injection moulding which can be further developed from the work undertaken. *10.4 Droplet behaviour* outlines the future work which can be undertaken in the examination of droplet contact angles, 'channelling' and evaporation.

10.1 Mould fabrication

Upon examination of the work presented during this thesis several points relating to possible extensions in the work undertaken into the fabrication of silicon and nickel mould inserts were identified.

- *Identification of the effects of process factors on the fabrication of 2 x 2 μm pillars via deep reactive ion etching:* it was noted during the present work that 2 x 2 μm pillars were not produced using the factor levels examined. Therefore, further research into the required factor levels for the production of features of this scale is required as they are still not discussed within the available literature.

- *Further development of the processes used to fabricate a nickel mould insert:* The exact details as to how nickel mould inserts for micro-injection moulding are fabricated is scarce within the available literature. The deposition of a conductive seed layer during the present work was unsuccessful and as such a nickel mould insert was not constructed.

Increasing the deposition time during the sputter-coating process and more extensive cleaning of the silicon surface prior to electroless are two possibilities recommended to improve the deposition of a conductive nickel seed layer. Once a successful nickel seed layer has been constructed the production of a nickel electroform for use as a mould insert should be examined.

10.2 Polymer micro-injection moulding

In addition to the work presented during this thesis into polymer micro-injection moulding several opportunities for future work were identified.

- *Identify the effects of process factors on the fabrication of polypropylene replicates via micro-injection moulding:* During the present work significant factors were not identified for the majority of the polypropylene features. Therefore, it is recommended that further research into the factor levels examined should be undertaken to better explore the limitations of the feedstock when used in the moulding of 80 – 2 μm pillar features.

- *Identification of the effect of process factors on the replication of 10 – 2 μm features in both polypropylene and high density polyethylene replicates via micro-injection moulding:* In the present work the replication of sub - 10 μm features was found to be problematic, with some failing to be successfully replicated. It is recommended that in future the factor levels used be altered to focus on the production of these sub - 10 μm features as pillars for this scale are not examined within the literature by a design of experiment approach.

- *Identify the effects of process factors on the fabrication polymer micro-textures surfaces using a nickel mould insert in micro-injection moulding:* The use of a nickel mould inserts in the replication of 80 – 2 μm features

should be examined and the performance of the two types of mould insert (silicon and nickel) compared. The use of nickel inserts in micro-injection moulding design of experiment investigation is limited within the literature and a comparison of the two types of inserts was not found within the literature.

- *Identify the effect of process factors on the fabrication of micro-textured surfaces with a variety of different polymer feedstock:* Further examination of the effect of process factor on the production of pillar and hole features should be undertaken using a variety of other polymers including polymethyl methacrylate (PMMA), cyclic olefin copolymer (COC), polycarbonate (PC), acrylonitrile butadiene styrene (ABS) and polyoxymethylene (POM). By extending the examination to other polymers a more comprehensive and detailed view of the effect of factors on pillar and hole replication at the sub – 80 μm scale can be obtained.

- *Examination of process factor effects using computer simulations:* Undertake an examination of the process factors using simulations software, such as Autodesk® simulation Moldflow® plastic injection moulding simulation software, and compare the simulation data to the experimental data gathered.

- *Utilise conditions monitoring to further analyse the micro-injection moulding process:* Further analysis of the effect of process factors can be undertaken using conditions monitoring. This will enable the natural variations within the moulding cycle to be quantified.

10.3 Metal powder injection moulding

The work presented during this thesis into metal powder injection moulding identified several opportunities for a further extension of the work undertaken.

- *Investigation into the effect of process factor levels on the replication of micro-textured surfaces and the life-span of the mould in the metal powder injection moulding process*: Further examination of the moulding process and the factor levels used is required to improve not only the life-span of the mould insert but also the replication of the features on the mould surface. The use of a nickel mould insert in the fabrication of metal powder replicates should also be examined as nickel mould inserts are more durable than silicon mould inserts. The use of nickel mould inserts in the replication of sub – 80 μm pillars is also not present within the literature.

- *Examine the use of other metal and ceramic powder feedstock in the metal powder injection moulding process*: Further examination of the effect of process factor should be undertaken in order to obtain a more thorough understanding of the effect of factors on replication of sub - 80 μm pillar and hole features using a variety of other metal and ceramic powders as this area is limited within the literature.

- *Examination of process factor effects using computer simulations:* Undertake an examination of the process factors using simulations software, such as Autodesk® simulation Moldflow® plastic injection moulding simulation software, and compare the simulation data to the experimental data gathered.

- *Utilise conditions monitoring to further analyse the micro-injection moulding process:* Further analysis of the effect of process factors can be undertaken using conditions monitoring. This will enable the natural variations within the moulding cycle to be quantified.

10.4 Droplet behaviour

In relation to the work undertaken in this thesis relating to droplet behaviour several points were identified which could be examined further in order to gain a more thorough understanding of the behaviour of micro-scale droplets.

- *Identify the effect on droplet 'channelling' behaviour when the droplet is placed on a single micro-channel rather than straddling two micro-channels*: In the presented work droplet 'channelling' was examined on surfaces on which the droplet spanned more than one micro-channel. Further examination is required to observe the behaviour of the droplet when placed on a single micro-channel to determine if this had any effect on the 'channelling' of the droplet.

- *Identify the effect of a droplet being placed on a single micro-channel rather than straddling two micro-channels on droplet behaviour during evaporation*: As with the examination of droplet 'channelling' in the presented work droplet evaporation was examined on surfaces on which the droplet spanned more than one micro-channel. Further examination is required to observe the effect on droplet evaporation when the droplet is initially placed on a single micro-channel rather than several.

- *Contribute to the Wenzel and Cassie-Baxter debate:* A comparison of the theoretical contact angles, calculated using the Wenzel and Cassie-Baxter equations, and the experimental contact angles should be undertaken to further the understanding of the application of the Wenzel and Cassie-Baxter equations.

REFERENCES

1. Aggarwal, G., Park, S. -., Smid, I. and German, R. M. (2007), "Master decomposition curve for binders used in powder injection molding", *Metallurgical and Materials Transactions A: Physical Metallurgy and Materials Science,* vol. 38, no. 3, pp. 606-614.

2. Anantharaju, N., Pancnagnula, M. V., Vedantam, S., Neti, S. and Tatic-Lucic, S. (2007), "Effect of three-phase contact line topology on dynamic contact angles on heterogeneous surfaces", *Langmuir,* vol. 23, no. 23, pp. 11673-11676.

3. Attia, U. M. and Alcock, J. R. (2009), "An evaluation of process-parameter and part-geometry effects on the quality of filling in micro-injection moulding", *Microsystem Technologies,* vol. 15, no. 12, pp. 1861-1872.

4. Attia, U. M. and Alcock, J. R. (2009), "An evaluation of process-parameter and part-geometry effects on the quality of filling in micro-injection moulding", *Microsystem Technologies,* vol. 15, no. 12, pp. 1861-1872.

5. Attia, U. M. and Alcock, J. R. (2010), "Optimising process conditions for multiple quality criteria in micro-injection moulding", *International Journal of Advanced Manufacturing Technology,* , pp. 1-10.

6. Attia, U. M. and Alcock, J. R. (2010), "Optimising process conditions for multiple quality criteria in micro-injection moulding", *International Journal of Advanced Manufacturing Technology,* vol. 50, no. 5-8, pp. 533-542.

7. Attia, U. M. and Alcock, J. R. (2011), "Evaluating and controlling process variability in micro-injection moulding", *International Journal of Advanced Manufacturing Technology,* vol. 52, no. 1-4, pp. 183-194.

8. Attia, U. M. and Alcock, J. R. (2011), "Evaluating and controlling process variability in micro-injection moulding", *International Journal of Advanced Manufacturing Technology,* vol. 52, no. 1-4, pp. 183-194.

9. Attia, U. M. and Alcock, J. R. (2011), "A review of micro-powder injection moulding as a microfabrication technique", *Journal of Micromechanics and Microengineering,* vol. 21, no. 4.

10. Attia, U. M. and Alcock, J. R. (2011), "A review of micro-powder injection moulding as a microfabrication technique", *Journal of Micromechanics and Microengineering,* vol. 21, no. 4.

11. Attia, U. M. and Alcock, J. R. (2012), "Fabrication of ceramic micro-scale hollow components by micro-powder injection moulding", *Journal of the European Ceramic Society,* vol. 32, no. 6, pp. 1199-1204.

12. Attia, U. M. and Alcock, J. R. (2012), "Fabrication of hollow, 3D, micro-scale metallic structures by micro-powder injection moulding", *Journal of Materials Processing Technology,* vol. 212, no. 10, pp. 2148-2153.

13. Attia, U. M., Marson, S. and Alcock, J. R. (2009), "Micro-injection moulding of polymer microfluidic devices", *Microfluidics and Nanofluidics,* vol. 7, no. 1, pp. 1-28.

14. Aufiero, R. (2005), "The effect of process conditions on part quality in microinjection molding", *Society of Plastics Engineers Annual Technical Conference 2005, ANTEC 2005,* Vol. 10, 1 May 2005 through 5 May 2005, Boston, MA, pp. 36.

15. Ayad, G., Barriere, T., Gelin, J. C., Song, J. and Liu, B. (2007), "Optimal design of material and process parameters in powder injection molding", *10TH ESAFORM CONFERENCE ON MATERIAL FORMING,* Vol. 907, 18 April 2006 through 20 April 2006, Zaragoza, pp. 1518.

16. Ayón, A. A., Braff, R., Lin, C. C., Sawin, H. H. and Schmidt, M. A. (1999), "Characterization of a time multiplexed inductively coupled plasma etcher", *Journal of the Electrochemical Society,* vol. 146, no. 1, pp. 339-349.

17. Baram, A. and Naftali, M. (2006), "Dry etching of deep cavities in Pyrex for MEMS applications using standard lithography", *Journal of Micromechanics and Microengineering,* vol. 16, no. 11, pp. 2287-2291.

18. Barriere, T., Renault, D. and Gelin, J. C. (2001), "Experimental and numerical analysis of the effects of process parameters on the properties of components in metal injection molding", in Aeby-Gautier E., Clavel M. and Dunne D. (eds.), *4th European Mechanics of Materials Conference on Processes, Microstructures and Mechanical Properties EUROMECH-MECAMAT'2000,* Vol. 11, 26 June 2000 through 29 June 2000, Metz, pp. Pr4249.

19. Beheim, G. M. and Evans, L. J. (2006), "Control of trenching and surface roughness in deep reactive ion etched 4H and 6H SiC", *2006 MRS Spring Meeting,* Vol. 911, 18 April 2006 through 20 April 2006, San Francisco, CA, pp. 329.

20. Bellantone, V., Surace, R., Trotta, G. and Fassi, I. (2013), "Replication capability of micro injection moulding process for polymeric parts manufacturing", *International Journal of Advanced Manufacturing Technology,* vol. 67, no. 5-8, pp. 1407-1421.

21. Bhushan, B. and Jung, Y. C. "Natural and biomimetic artificial surfaces for superhydrophobicity, self-cleaning, low adhesion, and drag reduction", *Progress in Materials Science,* .

22. Bico, J., Marzolin, C. and Quéré, D. (1999), "Pearl drops", *Europhysics Letters,* vol. 47, no. 2, pp. 220-226.

23. Bico, J., Thiele, U. and Quéré, D. (2002), "Wetting of textured surfaces", *Colloids and Surfaces A: Physicochemical and Engineering Aspects,* vol. 206, no. 1-3, pp. 41-46.

24. Bormashenko, E. (2008), "Why does the Cassie-Baxter equation apply?", *Colloids and Surfaces A: Physicochemical and Engineering Aspects,* vol. 324, no. 1-3, pp. 47-50.

25. Brousseau, E. B., Krohs, F., Caillaud, E., Dimov, S., Gibaru, O. and Fatikow, S. (2010), "Development of a novel process chain based on atomic force microscopy scratching for small and medium series production of polymer nanostructured components", *Journal of Manufacturing Science and Engineering, Transactions of the ASME,* vol. 132, no. 3, pp. 0309011-0309018.

26. C. Patrick Doncaster and Andrew J.H. Davey. (2007), *Analysis of variance and covariance : how to choose and construct models for the life sciences,* Cambridge University Press, Cambridge.

27. Callies, M. and Quéré, D. (2005), "On water repellency", *Soft Matter,* vol. 1, no. 1, pp. 55-61.

28. Cassie, A. B. D. and Baxter, S. (1944), "Wettability of porous surfaces", *Transactions of the Faraday Society,* vol. 40, pp. 546-551.

29. Chandrasekaran, A. and Packirisamy, M. (2010), "Integrated microfluidic biophotonic chip for laser induced fluorescence detection", *Biomedical Microdevices,* vol. 12, no. 5, pp. 923-933.

30. Chang, P. -. and Hwang, S. -. (2006), "Experimental investigation of infrared rapid surface heating for injection molding", *Journal of Applied Polymer Science,* vol. 102, no. 4, pp. 3704-3713.

31. Chaudhury, M. K. and Whitesides, G. M. (1992), "How to make water run uphill", *Science,* vol. 256, no. 5063, pp. 1539-1544.

32. Chen, S. -., Jong, W. -., Chang, Y. -., Chang, J. -. and Cin, J. -. (2006), "Rapid mold temperature variation for assisting the micro injection of high aspect ratio micro-feature parts using induction heating technology",

Journal of Micromechanics and Microengineering, vol. 16, no. 9, pp. 1783-1791.

33. Chen, W., Fadeev, A. Y., Hsieh, M. C., Öner, D., Youngblood, J. and McCarthy, T. J. (1999), "Ultrahydrophobic and ultralyophobic surfaces: some comments and examples", *Langmuir,* vol. 15, no. 10, pp. 3395-3399.

34. Chen, Z., Yu, Z. and Chen, G. (2010), "Low-cost fabrication of poly(methyl methacrylate) microchips using disposable gelatin gel templates", *Talanta,* vol. 81, no. 4-5, pp. 1325-1330.

35. Chu, J., Kamal, M. R., Derdouri, S. and Hrymak, A. (2010), "Characterization of the microinjection molding process", *Polymer Engineering and Science,* vol. 50, no. 6, pp. 1214-1225.

36. Cortese, B., Riehle, M. O., D'Amone, S. and Gigli, G. (2013), "Influence of variable substrate geometry on wettability and cellular responses", *Journal of colloid and interface science,* vol. 394, no. 1, pp. 582-589.

37. D, W., and P, Z. (1995), *Standard pressure volume temperature data for polymers,* CRC Press.

38. del Campo, A. and Arzt, E. (2008), "Fabrication approaches for generating complex micro- and nanopatterns on polymeric surfaces", *Chemical reviews,* vol. 108, no. 3, pp. 911-945.

39. Dettre, R. H. and Johnson Jr., R. E. (1967), *SCI Monogr.,* vol. 25, pp. 144.

40. Di Bari, G. A. (2000), "Electrodepostion of Nickel", in Schlesinger, M. and Paunovic, M. (eds.) *Modern Electroplating,* Fourth ed, John Wiley & Sons Ltd, New York, pp. 139.

41. Do, J., Zhang, J. Y. and Klapperich, C. M. (2011), "Maskless writing of microfluidics: Rapid prototyping of 3D microfluidics using scratch on a polymer substrate", *Robotics and Computer-Integrated Manufacturing,* vol. 27, no. 2, pp. 245-248.

42. Dorrer, C. and Ruhe, J. (2006), "Advancing and receding motion of droplets on ultrahydrophobic post surfaces", *Langmuir,* vol. 22, no. 18, pp. 7652-7657.

43. Dufour, R., Brunet, P., Harnois, M., Boukherroub, R., Thomy, V. and Senez, V. (2012), "Zipping effect on omniphobic surfaces for controlled deposition of minute amounts of fluid or colloids", *Small,* vol. 8, no. 8, pp. 1229-1236.

44. Erbil, H. Y. (2012), "Evaporation of pure liquid sessile and spherical suspended drops: A review", *Advances in Colloid and Interface Science,* vol. 170, no. 1-2, pp. 67-86.

45. Erbil, H. Y., McHale, G. and Newton, M. I. (2002), "Drop evaporation on solid surfaces: Constant contact angle mode", *Langmuir,* vol. 18, no. 7, pp. 2636-2641.

46. Eriksson, L. (2008), ***Design of experiments : principles and applications****,* 3rd revised and enlarged edition ed, Umetrics Academy, Umeå.

47. Evans, L.J. and Beheim, G.M., (2006), *Deep reactive ion etching (DRIE) of high aspect ratio SiC microstructures using a time-multiplexed etch-passivate process*, Pittsburgh, PA ed.

48. Fang, G., Li, W., Wang, X. and Qiao, G. (2008), "Droplet motion on designed microtextured superhydrophobic surfaces with tunable wettability", *Langmuir,* vol. 24, no. 20, pp. 11651-11660.

49. Feng, L., Li, S., Li, Y., Li, H., Zhang, L., Zhai, J., Song, Y., Liu, B., Jiang, L. and Zhu, D. (2002), "Super-hydrophobic surfaces: From natural to artificial", *Advanced Materials,* vol. 14, no. 24, pp. 1857-1860.

50. Forrest W. Breyfogle III. (1992), *Statistical methods for testing, developing and manufacturing,* John Wiley, New York ; Chichester.

51. Fox, R. T. and Lee, D. (1990), "Optimization of metal injection molding. Experimental design", *International Journal of Powder Metallurgy (Princeton, New Jersey),* vol. 26, no. 3, pp. 233-243.

52. Franssila, S. (2004), *Introduction to Microfabrication,* John Wiley & Sons Ltd, Chichester.

53. Franssila, S. (2004), "Thin-Film Material and Processes", in *Introduction to Microfabrication,* John Wiley & Son Ltd, Chichester, pp. 47.

54. Franssila, S. (2004), "Optical Lithography", in *Introduction to Microfabrication,* John Wiley & Sons Ltd, Chichester, pp. 99.

55. Fu, G., Loh, N. H., Tor, S. B., Murakoshi, Y. and Maeda, R. (2005), "Effects of injection molding parameters on the production of microstructures by micropowder injection molding", *Materials and Manufacturing Processes,* vol. 20, no. 6, pp. 977-985.

56. Fu, G., Loh, N. H., Tor, S. B., Tay, B. Y., Murakoshi, Y. and Maeda, R. (2005), "Injection molding, debinding and sintering of 316L stainless steel

microstructures", *Applied Physics A: Materials Science and Processing,* vol. 81, no. 3, pp. 495-500.

57. Fu, G., Loh, N. H., Tor, S. B., Tay, B. Y., Murakoshi, Y. and Maeda, R. (2005), "A variotherm mold for micro metal injection molding", *Microsystem Technologies,* vol. 11, no. 12, pp. 1267-1271.

58. Fu, G., Loh, N. H., Tor, S. B., Tay, B. Y., Murakoshi, Y. and Maeda, R. (2006), "Analysis of demolding in micro metal injection molding", *Microsystem Technologies,* vol. 12, no. 6, pp. 554-564.

59. Fu, G., Tor, S. B., Hardt, D. E. and Loh, N. H. (2011), "Effects of processing parameters on the micro-channels replication in microfluidic devices fabricated by micro injection molding", *Microsystem Technologies,* vol. 17, no. 12, pp. 1791-1798.

60. Gadegaard, N., Mosler, S. and Larsen, N. B. (2003), "Biomimetic polymer nanostructures by injection molding", *Macromolecular Materials and Engineering,* vol. 288, no. 1, pp. 76-83.

61. Gao, L. and McCarthy, T. J. (2006), ""Artificial lotus leaf" prepared using a 1945 patent and a commercial textile", *Langmuir,* vol. 22, no. 14, pp. 5998-6000.

62. Gao, L. and McCarthy, T. J. (2006), "The "lotus effect" explained: Two reasons why two length scales of topography are important", *Langmuir,* vol. 22, no. 7, pp. 2966-2967.

63. Gao, L. and McCarthy, T. J. (2006), "Contact angle hysteresis explained", *Langmuir,* vol. 22, no. 14, pp. 6234-6237.

64. Gao, L. and McCarthy, T. J. (2006), "A perfectly hydrophobic surface (θ_A/θ_R = 180°/180°)", *Journal of the American Chemical Society,* vol. 128, no. 28, pp. 9052-9053.

65. Gao, L. and McCarthy, T. J. (2007), "How Wenzel and Cassie were wrong", *Langmuir,* vol. 23, no. 7, pp. 3762-3765.

66. Gao, L. and McCarthy, T. J. (2007), "Ionic liquid marbles", *Langmuir,* vol. 23, no. 21, pp. 10445-10447.

67. Gao, L. and McCarthy, T. J. (2007), "Reply to "comment on How Wenzel and Cassie were wrong by Gao and McCarthy"", *Langmuir,* vol. 23, no. 26, pp. 13243.

68. Gao, L. and McCarthy, T. J. (2009), "An attempt to correct the faulty intuition perpetuated by the wenzel and cassie "laws"", *Langmuir,* vol. 25, no. 13, pp. 7249-7255.

69. Gao, L. and McCarthy, T. J. (2009), "Wetting 101°", *Langmuir,* vol. 25, no. 24, pp. 14105-14115.

70. Gao, L., McCarthy, T. J. and Zhang, X. (2009), "Wetting and Superhydrophobicity", *Langmuir,* vol. 25, no. 24, pp. 14100-14104.

71. Garcia-Cordero, J. L., Kurzbuch, D., Benito-Lopez, F., Diamond, D., Lee, L. P. and Ricco, A. J. (2010), "Optically addressable single-use microfluidic valves by laser printer lithography", *Lab on a Chip - Miniaturisation for Chemistry and Biology,* vol. 10, no. 20, pp. 2680-2687.

72. Garino, T. J., Morales, A. M. and Boyce, B. L. (2004), "The mechanical properties, dimensional tolerance and microstructural characterization of micro-molded ceramic and metal components", *Microsystem Technologies,* vol. 10, no. 6-7, pp. 506-509.

73. Gatapova, E. Y., Semenov, A. A., Zaitsev, D. V. and Kabov, O. A. (2013), "Evaporation of a sessile water drop on a heated surface with controlled wettability", *Colloids and Surfaces A: Physicochemical and Engineering Aspects,* .

74. Gelin, J. -., Barriere, T. and Liu, B. (2002), "Improved mould design in metal injection moulding by combination of numerical simulations and experiments", *Proceedings of the Institution of Mechanical Engineers, Part B: Journal of Engineering Manufacture,* vol. 216, no. 12, pp. 1533-1547.

75. Giboz, J., Copponnex, T. and Mélé, P. (2007), "Microinjection molding of thermoplastic polymers: A review", *Journal of Micromechanics and Microengineering,* vol. 17, no. 6.

76. Giboz, J., Copponnex, T. and Mélé, P. (2009), "Microinjection molding of thermoplastic polymers: Morphological comparison with conventional injection molding", *Journal of Micromechanics and Microengineering,* vol. 19, no. 2.

77. Giboz, J., Spoelstra, A. B., Portale, G., Copponnex, T., Meijer, H. E. H., Peters, G. W. M. and Mélé, P. (2011), "On the origin of the "core-free" morphology in microinjection-molded HDPE", *Journal of Polymer Science, Part B: Polymer Physics,* vol. 49, no. 20, pp. 1470-1478.

78. Greco, A., Raphaelson, S., Ehmann, K., Wang, Q. J. and Lin, C. (2009), "Surface texturing of tribological interfaces using the vibromechanical

texturing method", *Journal of Manufacturing Science and Engineering, Transactions of the ASME,* vol. 131, no. 6, pp. 0610051-0610058.

79. Griffiths, C. A., Dimov, S. S., Brousseau, E. B., Chouquet, C., Gavillet, J. and Bigot, S. (2010), "Investigation of surface treatment effects in micro-injection-moulding", *International Journal of Advanced Manufacturing Technology,* vol. 47, no. 1-4, pp. 99-110.

80. Griffiths, C. A., Dimov, S. S., Brousseau, E. B. and Hoyle, R. T. (2007), "The effects of tool surface quality in micro-injection moulding", *Journal of Materials Processing Technology,* vol. 189, no. 1-3, pp. 418-427.

81. Griffiths, C. A., Dimov, S. S., Scholz, S. and Tosello, G. (2011), "Cavity air flow behavior during filling in microinjection molding", *Journal of Manufacturing Science and Engineering, Transactions of the ASME,* vol. 133, no. 1.

82. Griffiths. CA, Dimov. SS, Brousseau.EB, Chouquet. C, Gavillet. J and Bigot. S (2008), "Micro-Injection moulding: surface treatment effects on part demoulding", *Fourth International Conference on Multi-Material Micro Manufacture,* 9th-11th September, Cardiff, UK, pp. 245.

83. Guo, C., Liu, F. H., Wu, X., Liu, H. and Zhang, J. (2012), "Morphological evolution of HDPE parts in the microinjection molding: Comparison with conventional injection molding", *Journal of Applied Polymer Science,* vol. 126, no. 2, pp. 452-462.

84. Guo, Y., Wang, Y., Sun, G. and Zhang, H. (2008), "Parameters extraction for DRIE model", *3rd IEEE International Conference on Nano/Micro Engineered and Molecular Systems, NEMS 2008,* 6 January 2008 through 9 January 2008, Sanya, pp. 544.

85. Hakimian, E. and Sulong, A. B. (2012), "Analysis of warpage and shrinkage properties of injection-molded micro gears polymer composites using numerical simulations assisted by the Taguchi method", *Materials and Design,* vol. 42, pp. 62-71.

86. Hattori, S., Nagato, K., Hamaguchi, T. and Nakao, M. (2010), "Rapid injection molding of high-aspect-ratio nanostructures", *Microelectronic Engineering,* vol. 87, no. 5-8, pp. 1546-1549.

87. Held, J., Gaspar, J., Ruther, P., Hagner, M., Cismak, A., Heilmann, A. and Paul, O. (2008), "Systematic characterization of DRIE-based fabrication process of silicon microneedles", *Microelectromechanical Systems - Materials and Devices,* Vol. 1052, 26 November 2007 through 28 November 2007, Boston, MA, pp. 271.

88. Huang, M. -. and Ku, H. -. (2011), "Microinjection molding of light-guided plates using LIGA-like fabricated stampers", *Journal of Applied Polymer Science,* vol. 122, no. 5, pp. 3446-3455.

89. Huang, M. -., Li, C. -., Yu, J. -., Huang, Y. -. and Hsieh, L. -. (2009), "Robust parameter design of micro-injection molded gears using a LIGA-like fabricated mold insert", *Journal of Materials Processing Technology,* vol. 209, no. 15-16, pp. 5690-5701.

90. Ibrahim, M. H. I., Muhamad, N., Sulong, A. B., Jamaludin, K. R., Nor, N. H. M. and Ahmad, S. (2011), "Optimization of micro metal injection molding with multiple performance characteristics using grey relational grade", *Chiang Mai Journal of Science,* vol. 38, no. 2, pp. 231-241.

91. Inoue, K., Hayashi, K., Kawasaki, Y., Ohno, E., Masuhara, S. and Kaneko, M. (2004), "Study on 100 Gbit/inch2 density molding using double-sided heat insulated mold", *Japanese Journal of Applied Physics, Part 1: Regular Papers and Short Notes and Review Papers,* vol. 43, no. 7 B, pp. 5074-5077.

92. Ito, H., Suzuki, H., Kazama, K. and Kikutani, T. (2009), "Polymer structure and properties in micro- and nanomolding process", *Current Applied Physics,* vol. 9, no. 2 SUPPL.

93. Jamaludin, K. R., Muhamad, N., Ab. Rahman, M. N., Ahmad, S., Ibrahim, M. H. I. and Nor, N. H. M. (2009), "Optimizing the injection parameter of water atomised SS316l powder with design of experiment method for best sintered density", *Chiang Mai Journal of Science,* vol. 36, no. 3, pp. 349-358.

94. Jansen, H., De Boer, M., Legtenberg, R. and Elwenspoek, M. (1995), "The black silicon method: A universal method for determining the parameter setting of a fluorine-based reactive ion etcher in deep silicon trench etching with profile control", *Journal of Micromechanics and Microengineering,* vol. 5, no. 2, pp. 115-120.

95. JD PhotoTools (2013)*, The Photo-Mask Guide*, available at: http://www.jdphoto.co.uk/ (accessed December 2010).

96. Journet, C., Moulinet, S., Ybert, C., Purcell, S. T. and Bocquet, L. (2005), "Contact angle measurements on superhydrophobic carbon nanotube forests: effect of fluid pressure", *Europhysics Letters,* vol. 71, no. 1, pp. 104-109.

97. Jung, W. -., Heo, Y. -., Shin, K. -., Yoon, G. -. and Chang, S. -. (2007), "An experimatal study on micro injection paramaters", *Society of Plastics*

Engineers Annual Technical Conference: Plastics Encounter at ANTEC 2007, Vol. 2, 6 May 2007 through 11 May 2007, Cincinnati, OH, pp. 638.

98. Kamal, M. R., Chu, J., Derdouri, S. and Hrymak, A. (2010), "Morphology of microinjection moulded polyoxymethylene", *Plastics, Rubber and Composites,* vol. 39, no. 7, pp. 332-341.

99. Kang, I. -., Haskard, M. R., Samaan, N. and Orders, P. (1996), "The fabrication of a thick nickel microvalve with truncated pyramid shape", in Aatre V.K., Varadan V.K. and Varadan V.V. (eds.), *Smart Materials, Structures, and MEMS,* Vol. 3321, 11 December 1996 through 14 December 1996, Bangalore, pp. 280.

100. Khoo, H. S. and Tseng, F. -. (2009), "Spontaneous high-speed transport of subnanoliter water droplet on gradient nanotextured surfaces", *Applied Physics Letters,* vol. 95, no. 6.

101. Kim, H., Shin, S. C., Han, J., Han, J. and Kang, S. (2009), "Fabrication of metallic nano stamp to replicate patterned substrate using electron-beam recording, nanoimprinting, and electroforming", *IEEE Transactions on Magnetics,* vol. 45, no. 5, pp. 2304-2307.

102. Kim, M. S., Kim, T., Kong, S. -., Kwon, S., Bae, C. Y., Choi, J., Kim, C. H., Lee, E. S. and Park, J. -. (2010), "Breast cancer diagnosis using a microfluidic multiplexed immunohistochemistry platform", *PLoS ONE,* vol. 5, no. 5.

103. Kim, S., Shiau, C. -., Kim, B. and Yao, D. (2007), "Injection molding nanoscale features with the aid of induction heating", *Polymer - Plastics Technology and Engineering,* vol. 46, no. 11, pp. 1031-1037.

104. Kim, Y., Choi, Y., Kim, Y. -. and Kang, S. (2005), "Construction of injection mold with MEMS RTD sensor and MEMS heater for micro/nano molding process", *Japanese Journal of Applied Physics, Part 1: Regular Papers and Short Notes and Review Papers,* vol. 44, no. 5 B, pp. 3591-3595.

105. Kiyotaka, W. (2004), "Thin Film Process", in *Thin Film Materials Technology: Sputtering of Compound Material,* William Andrew, St Louis, pp. 17.

106. Krupenkin, T. N., Taylor, J. A., Schneider, T. M. and Yang, S. (2004), "From rolling ball to complete wetting: The dynamic tuning of liquids on nanostructured surfaces", *Langmuir,* vol. 20, no. 10, pp. 3824-3827.

107. Larson, C. and Farr, J. P. G. (2010), "Recent advances in pulsed current electrodeposition: A brief review", *Transactions of the Institute of Metal Finishing,* vol. 88, no. 5, pp. 237-242.

108. Lee, B. -., Hwang, C. J., Kim, D. S. and Kwon, T. H. (2008), "Replication quality of flow-through microfilters in microfluidic lab-on-a-chip for blood typing by microinjection molding", *Journal of Manufacturing Science and Engineering, Transactions of the ASME,* vol. 130, no. 2, pp. 0210101-0210108.

109. Lee, K., de Hoyos, M., Ahn, S., Nambiar, R., Gonzalez, M. A., Park, S. J. and German, R. M. (2010), "Gas-assisted powder injection molding: A study on the effect of processing variables on gas penetration", *Powder Technology,* vol. 200, no. 3, pp. 128-135.

110. Lee, N., Han, J., Lim, J., Choi, M., Han, Y., Hong, J. and Kang, S. (2008), "Injection molding of nanopillars for perpendicular patterned magnetic media with metallic nanostamp", *Japanese Journal of Applied Physics,* vol. 47, no. 3 PART 1, pp. 1803-1805.

111. Lee, S. W., Ahn, S., Whang, C. J., Park, S. J., Atre, S. V., Kim, J. and German, R. M. (2011), "Effects of process parameters in plastic, metal, and ceramic injection molding processes", *Korea Australia Rheology Journal,* vol. 23, no. 3, pp. 127-138.

112. Lee, S. W., Ahn, S., Whang, C. J., Park, S. J., Atre, S. V., Kim, J. and German, R. M. (2011), "Effects of process parameters in plastic, metal, and ceramic injection molding processes", *Korea Australia Rheology Journal,* vol. 23, no. 3, pp. 127-138.

113. Li, H.P. and Muhamad, N., (2011), *Determination of optimal microminiature powder injection molding parameters by taguchi approach*, Guilin ed.

114. Li, H.P., Muhamad, N., Sulong, A.B., Yunn, H.S. and Abolhasani, H., (2011), *Application of Taguchi method for parameters optimization in micro metal injection molding*, Phuket ed.

115. Li, J. -., Day, D. and Gu, M. (2010), "Design of a compact microfludic device for controllable cell distribution", *Lab on a Chip - Miniaturisation for Chemistry and Biology,* vol. 10, no. 22, pp. 3054-3057.

116. Li, L., Yang, C., Shi, H., Liao, W. -., Huang, H., Lee, L. J., Castro, J. M. and Yi, A. Y. (2010), "Design and fabrication of an affordable polymer micromixer for medical and biomedical applications", *Polymer Engineering and Science,* vol. 50, no. 8, pp. 1594-1604.

117. Li, S. G., Fu, G., Reading, I., Tor, S. B., Loh, N. H., Chaturvedi, P., Yoon, S. F. and Youcef-Toumi, K. (2007), "Dimensional variation in production of high-aspect-ratio micro-pillars array by micro powder injection molding", *Applied Physics A: Materials Science and Processing,* vol. 89, no. 3, pp. 721-728.

118. Lillehoj, P. B., Wei, F. and Ho, C. -. (2010), "A self-pumping lab-on-a-chip for rapid detection of botulinum toxin", *Lab on a Chip - Miniaturisation for Chemistry and Biology,* vol. 10, no. 17, pp. 2265-2270.

119. Lin, C. -., Tseng, C. -., Huang, C. -., Wang, J. -. and Lee, G. -. (2010), "An integrated microfluidic chip for non-immunological determination of urinary albumin", *Biomedical Microdevices,* vol. 12, no. 5, pp. 887-896.

120. Ling, T. D., Liu, P., Xiong, S., Grzina, D., Cao, J., Wang, Q. J., Xia, Z. C. and Talwar, R. (2013), "Surface texturing of drill bits for adhesion reduction and tool life enhancement", *Tribology Letters,* vol. 52, no. 1, pp. 113-122.

121. Liou, A. -. and Chen, R. -. (2006), "Injection molding of polymer micro- and sub-micron structures with high-aspect ratios", *International Journal of Advanced Manufacturing Technology,* vol. 28, no. 11-12, pp. 1097-1103.

122. Liu, Y., Lin, Z., Moon, K. S. and Wong, C. P. (2011), "Novel ZnO nanowires/silicon hierarchical structures for superhydrophobic, low reflection, and high efficiency solar cells", *2011 61st Electronic Components and Technology Conference, ECTC 2011,* 31 May 2011 through 3 June 2011, Lake Buena Vista, FL, pp. 2114.

123. Liu, Z. Y., Loh, N. H., Tor, S. B., Khor, K. A., Murakoshi, Y., Maeda, R. and Shimizu, T. (2002), "Micro-powder injection molding", *Journal of Materials Processing Technology,* vol. 127, no. 2, pp. 165-168.

124. Lucchetta, G., Fiorotto, M. and Bariani, P. F. (2012), "Influence of rapid mold temperature variation on surface topography replication and appearance of injection-molded parts", *CIRP Annals - Manufacturing Technology,* .

125. Macintyre, D. and Thoms, S. (1998), "The fabrication of high resolution features by mould injection", *Microelectronic Engineering,* vol. 41-42, pp. 211-214.

126. Madou, M. J. (2001), "LIGA and Micromolding", in *Fundamentals of Microfabrication: The Science of Miniaturization,* 2nd ed, CRC Press, UK, pp. 325.

127. Madou, M. J. (2001), "Lithography", in *Fundamentals of Microfabrication: The Science of Miniaturization,* 2nd ed, CRC Press, Boca Raton, pp. 1.

128. Madou, M. J. (2001), "Pattern Transfer with Dry Etching Techniques", in *Fundamentals of Microfabrication: The Science of Miniaturization,* 2nd ed, CRC Press, Boa Raton, pp. 77.

129. Marmur, A. and Bittoun, E. (2009), "When wenzel and cassie are right: Reconciling local and global considerations", *Langmuir,* vol. 25, no. 3, pp. 1277-1281.

130. Marson, S., Attia, U. M., Lucchetta, G., Wilson, A., Alcock, J. R. and Allen, D. M. (2011), "Flatness optimization of micro-injection moulded parts: The case of a PMMA microfluidic component", *Journal of Micromechanics and Microengineering,* vol. 21, no. 11.

131. Matschuk, M., Bruus, H. and Larsen, N. B. (2010), "Nanostructures for all-polymer microfluidic systems", *Microelectronic Engineering,* vol. 87, no. 5-8, pp. 1379-1382.

132. McHale, G. (2007), "Cassie and Wenzel: Were they really so wrong?", *Langmuir,* vol. 23, no. 15, pp. 8200-8205.

133. McHale, G., Aqil, S., Shirtcliffe, N. J., Newton, M. I. and Erbil, H. Y. (2005), "Analysis of droplet evaporation on a superhydrophobic surface", *Langmuir,* vol. 21, no. 24, pp. 11053-11060.

134. Meng, J., Loh, N. H., Fu, G., Tay, B. Y. and Tor, S. B. (2011), "Micro powder injection moulding of alumina micro-channel part", *Journal of the European Ceramic Society,* vol. 31, no. 6, pp. 1049-1056.

135. Meng, J., Loh, N. H., Fu, G., Tor, S. B. and Tay, B. Y. (2010), "Replication and characterization of 316L stainless steel micro-mixer by micro powder injection molding", *Journal of Alloys and Compounds,* vol. 496, no. 1-2, pp. 293-299.

136. MicroChemicals (2008), *Lithography: Theory and Application of Photoresists, Developers, Solvents and Etchants,* 2008/2009 ed, .

137. Miller, K., Li, M., Walsh, K. M. and Fu, X. -. (2013), "The effects of DRIE operational parameters on vertically aligned micropillar arrays", *Journal of Micromechanics and Microengineering,* vol. 23, no. 3.

138. Minitab Inc, *Minitab15*®.

139. Miwa, M., Nakajima, A., Fujishima, A., Hashimoto, K. and Watanabe, T. (2000), "Effects of the surface roughness on sliding angles of water droplets on superhydrophobic surfaces", *Langmuir,* vol. 16, no. 13, pp. 5754-5760.

140. Mnkknen, K., Pakkanen, T. T., Hietala, J., Pkknen, E. J., Pkknen, P., Jskelinen, T. and Kaikuranta, T. (2002), "Replication of sub-micron features using amorphous thermoplastics", *Polymer Engineering and Science,* vol. 42, no. 7, pp. 1600-1608.

141. Montgomery, D. C. (2005), ***Design and Analysis of Experiments****,* 6th ed, John Wiley and Sons Ltd, Chichester.

142. Moosavi, A., Rauscher, M. and Dietrich, S. (2009), "Dynamics of nanodroplets on topographically structured substrates", *Journal of Physics Condensed Matter,* vol. 21, no. 46.

143. Moradi, N., Varnik, F. and Steinbach, I. (2010), "Roughness-gradient-induced spontaneous motion of droplets on hydrophobic surfaces: A lattice Boltzmann study", *Europhysics Letters,* vol. 89, no. 2.

144. Morel, E. (2009), *Lotus-leaf effect process chain for microfluidic devices* (unpublished Msc Advanced Material thesis), Cranfield University, .

145. Nachmias, T., Ohayon, A., Melzer, S. E., Kabla, M., Louzon, E. and Levy, U. (2009), "Shallow Fresnel lens fabrication using grey scale lithography made by high energy beam sensitive mask (HEBS) technology and reactive ion etching", *Advanced Fabrication Technologies for Micro/Nano Optics and Photonics II,* Vol. 7205, 26 January 2009 through 28 January 2009, San Jose, CA, .

146. Neinhuis, C. and Barthlott, W. (1997), "Characterization and distribution of water-repellent, self-cleaning plant surfaces", *Annals of Botany,* vol. 79, no. 6, pp. 667-677.

147. Nguyen, T. A. H., Hampton, M. A. and Nguyen, A. V. (2013), "Evaporation of nanoparticle droplets on smooth hydrophobic surfaces: The inner coffee ring deposits", *Journal of Physical Chemistry C,* vol. 117, no. 9, pp. 4707-4716.

148. Nosonovsky, M. and Bhushan, B. (2005), "Roughness optimization for biomimetic superhydrophobic surfaces", *Microsystem Technologies,* vol. 11, no. 7, pp. 535-549.

149. Nosonovsky, M. and Bhushan, B. (2008), "Roughness-induced superhydrophobicity: A way to design non-adhesive surfaces", *Journal of Physics Condensed Matter,* vol. 20, no. 22.

150. O'Brien, G. J., Monk, D. J. and Najafi, K. (2001), "Sub-micron high aspect ratio silicon beam etch", in Chiao J.C., Faraone L., Barry Harrison H., et al (eds.), *Device and Process Technologies for MEMS and Microelectronics II,* Vol. 4592, 17 December 2001 through 19 December 2001, Adelaide, pp. 315.

151. Ogata, Y. H., Kobayashi, K. and Motoyama, M. (2006), "Electrochemical metal deposition on silicon", *Current Opinion in Solid State and Materials Science,* vol. 10, no. 3-4, pp. 163-172.

152. Oh, S. H., Cho, S. U., Kim, C. S., Han, Y. G., Cho, C. -. and Jeong, M. Y. "Fabrication of nickel stamp with improved sidewall roughness for optical devices", *Microelectronic Engineering,* .

153. Öner, D. and McCarthy, T. J. (2000), "Ultrahydrophobic surfaces. Effects of topography length scales on wettability", *Langmuir,* vol. 16, no. 20, pp. 7777-7782.

154. Ong, N. S. and Koh, Y. H. (2005), "Experimental investigation into micro injection molding of plastic parts", *Materials and Manufacturing Processes,* vol. 20, no. 2, pp. 245-253.

155. Pal, R., Mukhopadhyay, S. and Das, D. (2012), "Optimization of micro-injection molding process with respect to tensile properties of polypropylene", *Indian Journal of Fibre and Textile Research,* vol. 37, no. 1, pp. 11-15.

156. Panchagnula, M. V. and Vedantam, S. (2007), "Comment on how Wenzel and Cassie were wrong by Gao and McCarthy", *Langmuir,* vol. 23, no. 26, pp. 13242.

157. Perry, S. L., Higdon, J. J. L. and Kenis, P. J. A. (2010), "Design rules for pumping and metering of highly viscous fluids in microfluidics", *Lab on a Chip - Miniaturisation for Chemistry and Biology,* vol. 10, no. 22, pp. 3112-3124.

158. Petrie, R. J., Bailey, T., German, C. B. and Genzer, J. (2004), "Fast directed motion of "Fakir" droplets", *Langmuir,* vol. 20, no. 23, pp. 9893-9896.

159. Piotter, V., Bauer, W., Knitter, R., Mueller, M., Mueller, T. and Plewa, K. (2011), "Powder injection moulding of metallic and ceramic micro parts", *Microsystem Technologies,* vol. 17, no. 2, pp. 251-263.

160. Pirskanen, J., Immonen, J., Kalima, V., Pietarinen, J., Siitonen, S., Kuittinen, M., Mönkkönen, K., Pakkanen, T., Suvanto, M. and Pääkkönen, E. J. (2005), "Replication of sub-micrometre features using microsystems

technology", *Plastics, Rubber and Composites,* vol. 34, no. 5-6, pp. 222-226.

161. Pozzato, A., Zilio, S. D., Fois, G., Vendramin, D., Mistura, G., Belotti, M., Chen, Y. and Natali, M. (2006), "Superhydrophobic surfaces fabricated by nanoimprint lithography", *Microelectronic Engineering,* vol. 83, no. 4-9 SPEC. ISS., pp. 884-888.

162. Praher, B., Straka, K. and Steinbichler, G. (2013), "An ultrasound-based system for temperature distribution measurements in injection moulding: System design, simulations and off-line test measurements in water", *Measurement Science and Technology,* vol. 24, no. 8.

163. Prakash, S., Karacor, M. B. and Banerjee, S. (2009), "Surface modification in microsystems and nanosystems", *Surface Science Reports,* vol. 64, no. 7, pp. 233-254.

164. Pranov, H., Rasmussen, H. K., Larsen, N. B. and Gadegaard, N. (2006), "On the injection molding of nanostructured polymer surfaces", *Polymer Engineering and Science,* vol. 46, no. 2, pp. 160-171.

165. Quinard, C., Song, J., Barriere, T. and Gelin, J. C. (2011), "Elaboration of PIM feedstocks with 316L fine stainless steel powders for the processing of micro-components", *Powder Technology,* vol. 208, no. 2, pp. 383-389.

166. Rajabi, J., Muhamad, N. and Sulong, A.B., (2012), *Effect of nano-sized powders on powder injection molding: A review*.

167. Rasilainen, T., Kirveslahti, A., Nevalainen, P., Suvanto, M. and Pakkanen, T. A. (2010), "Modification of polypropylene surfaces with micropits and hierarchical micropits/nanodepressions", *Surface Science,* vol. 604, no. 21-22, pp. 2036-2042.

168. Rasilainen, T., Suvanto, M. and Pakkanen, T. A. (2009), "Anisotropically microstructured and micro/nanostructured polypropylene surfaces", *Surface Science,* vol. 603, no. 14, pp. 2240-2247.

169. Roach, P., Shirtcliffe, N. J. and Newton, M. I. (2008), "Progess in superhydrophobic surface development", *Soft Matter,* vol. 4, no. 2, pp. 224.

170. Ross, P. J. (1995), ***Taguchi techniques for quality engineering : loss function, orthogonal experiments, parameter and tolerance design***, 2nd ed, McGraw-Hill, New York.

171. Roy, R. (1990), *A primer on the Taguchi method,* Van Nostrand Reinhold, New York.

172. Ruh, A., Klimscha, K., Piotter, V., Plewa, K., Ritzhaupt-Kleissl, H. -. and Fleischer, J. (2011), "The development of two-component micro powder injection moulding and sinter joining", *Microsystem Technologies,* vol. 17, no. 10-11, pp. 1547-1556.

173. Saarikoski, I., Joki-Korpela, F., Suvanto, M., Pakkanen, T. T. and Pakkanen, T. A. (2012), "Superhydrophobic elastomer surfaces with nanostructured micronails", *Surface Science,* vol. 606, no. 1-2, pp. 91-98.

174. Saarikoski, I., Suvanto, M. and Pakkanen, T. A. (2009), "Modification of polycarbonate surface properties by nano-, micro-, and hierarchical micro-nanostructuring", *Applied Surface Science,* vol. 255, no. 22, pp. 9000-9005.

175. Schlechtriemen, N., Binder, J. R., Knitter, R. and Haußelt, J. (2010), "Optimization of feedstock properties for reaction-bonded net-shape zircon ceramics by design of experiments", *Ceramics International,* vol. 36, no. 1, pp. 223-229.

176. Sha, B., Dimov, S., Griffiths, C. and Packianather, M. S. (2007), "Investigation of micro-injection moulding: Factors affecting the replication quality", *Journal of Materials Processing Technology,* vol. 183, no. 2-3, pp. 284-296.

177. Sha, B., Dimov, S., Griffiths, C. and Packianather, M. S. (2007), "Micro-injection moulding: Factors affecting the achievable aspect ratios", *International Journal of Advanced Manufacturing Technology,* vol. 33, no. 1-2, pp. 147-156.

178. Sha, B., Dimov, S., Griffiths, C. and Packianather, M. S. (2007), "Micro-injection moulding: Factors affecting the achievable aspect ratios", *International Journal of Advanced Manufacturing Technology,* vol. 33, no. 1-2, pp. 147-156.

179. Shastry, A., Case, M. J. and Böhringer, K. F. (2006), "Directing droplets using microstructured surfaces", *Langmuir,* vol. 22, no. 14, pp. 6161-6167.

180. Shen, Y. -., Chang, C. -., Shen, Y. -. and Yang, S. -. (2006), "A novel fabrication method and optimum tooling design for microlens arrays", *Society of Plastics Engineers Annual Technical Conference 2006, ANTEC 2006,* Vol. 5, 7 May 2006 through 11 May 2006, Charlotte, NC, pp. 2571.

181. Shen, Y. K., Yeh, S. L. and Chen, S. H. (2002), "Three-dimensional non-Newtonian computations of micro-injection molding with the finite element method", *International Communications in Heat and Mass Transfer,* vol. 29, no. 5, pp. 643-652.

182. Sotomayor, M. E., Levenfeld, B. and Várez, A. (2011), "Powder injection moulding of premixed ferritic and austenitic stainless steel powders", *Materials Science and Engineering A,* vol. 528, no. 9, pp. 3480-3488.

183. Surface Technology Systems, *Advanced Silicon Etch*.

184. Tavana, H., Lam, C. N. C., Grundke, K., Friedel, P., Kwok, D. Y., Hair, M. L. and Neumann, A. W. (2004), "Contact angle measurements with liquids consisting of bulky molecules", *Journal of colloid and interface science,* vol. 279, no. 2, pp. 493-502.

185. Taylor, A. M. and Jeon, N. L. (2010), "Micro-scale and microfluidic devices for neurobiology", *Current opinion in neurobiology,* vol. 20, no. 5, pp. 640-647.

186. Theilade, U. A. and Hansen, H. N. (2007), "Surface microstructure replication in injection molding", *International Journal of Advanced Manufacturing Technology,* vol. 33, no. 1-2, pp. 157-166.

187. Tosello, G., Gava, A., Hansen, H. N. and Lucchetta, G. (2007), "Influence of process parameters on the weld lines of a micro injection molded component", *Society of Plastics Engineers Annual Technical Conference: Plastics Encounter at ANTEC 2007,* Vol. 4, 6 May 2007 through 11 May 2007, Cincinnati, OH, pp. 2002.

188. Tosello, G., Gava, A., Hansen, H. N. and Lucchetta, G. (2010), "Study of process parameters effect on the filling phase of micro-injection moulding using weld lines as flow markers", *International Journal of Advanced Manufacturing Technology,* vol. 47, no. 1-4, pp. 81-97.

189. Tosello, G., Hansen, H. N., Dormann, B., Decker, C. and Guerrier, P. (2010), "Process control and product evaluation in micro molding using a screwless/two-plunger injection unit", *68th Annual Technical Conference of the Society of Plastics Engineers 2010, ANTEC 2010,* Vol. 3, 16 May 2010 through 20 May 2010, Orlando, FL, pp. 1947.

190. Tosello, G., Hansen, H. N., Gasparin, S., Albajez, J. A. and Esmoris, J. I. (2012), "Surface wear of TiN coated nickel tool during the injection moulding of polymer micro Fresnel lenses", *CIRP Annals - Manufacturing Technology,* .

191. Tserepi A D, Vlachopoulou M-E and Gogolides E (2006), "Nanotexturing of poly(dimethylsiloxane) in plasmas for creating robust super-hydrophobic surfaces", *Nanotechnology,* vol. 17, pp. 3977-3983.

192. Urval, R., Lee, S., Atre, S. V., Park, S. -. and German, R. M. (2008), "Optimisation of process conditions in powder injection moulding of

microsystem components using a robust design method: Part I. Primary design parameters", *Powder Metallurgy,* vol. 51, no. 2, pp. 133-142.

193. W. Canning Material LTD., *Standard Operating Procedures for Electroless Nickel Plating*.

194. Wang, J., Chen, H., Sui, T., Li, A. and Chen, D. (2009), "Investigation on hydrophobicity of lotus leaf: Experiment and theory", *Plant Science,* vol. 176, no. 5, pp. 687-695.

195. Wang, J. X., Zhang, Y. Z., Zhao, T. Y., Song, Y. L. and Jiang, L. (2010), "Recent research progress in wettability of colloidal crystals", *Science China Chemistry,* vol. 53, no. 2, pp. 318-326.

196. Wang, M. -., Jeng, J. -. and Fu, G. -. (2008), "Optimal molding parameter design of PLA micro lancet needles using Taguchi method", *2008 IEEE International Conference on Service Operations and Logistics, and Informatics, IEEE/SOLI 2008,* Vol. 2, 12 October 2008 through 15 October 2008, Beijing, pp. 2731.

197. Wasilik, M. and Pisano, A. P. (2001), "Low frequency process for silicon on insulator deep reactive ion etching", in Chiao J.C., Faraone L., Barry Harrison H., et al (eds.), *Device and Process Technologies for MEMS and Microelectronics II,* Vol. 4592, 17 December 2001 through 19 December 2001, Adelaide, pp. 462.

198. Wenzel, R. N. (1936), "Resistance of solid surfaces to wetting by water", *Industrial and Engineering Chemistry,* vol. 28, no. 8, pp. 988.

199. Whiteside, B. R., Martyn, M. T., Coates, P. D., Greenway, G., Allen, P. and Hornsby, P. (2004), "Micromoulding: Process measurements, product morphology and properties", *Plastics, Rubber and Composites,* vol. 33, no. 1, pp. 11-17.

200. Woo-Chul Jung, Young-Moo Heo, Kwang-Ho Shin, Gil-Sang Yoon and Sung-Ho Chang (2007), "An Experimental Study on Micro Injection Parameters", *ANTEC 2007 Plastics: Annual Technical Conference Proceedings,* .

201. Xie, L. and Ziegmann, G. (2009), "Influence of processing parameters on micro injection molded weld line mechanical properties of polypropylene (PP)", *Microsystem Technologies,* vol. 15, no. 9, pp. 1427-1435.

202. Xie, L. and Ziegmann, G. (2010), "Effect of gate dimension on micro injection molded weld line strength with polypropylene (PP) and high-density polyethylene (HDPE)", *International Journal of Advanced Manufacturing Technology,* vol. 48, no. 1-4, pp. 71-81.

203. Xin, Z. X., Zhang, Z. X., Pal, K., Byeon, J. U., Lee, S. H. and Kim, J. K. (2010), "Study of microcellular injection-molded polypropylene/waste ground rubber tire powder blend", *Materials and Design,* vol. 31, no. 1, pp. 589-593.

204. Xu, W. and Choi, C. -. (2011), "Experimental studies on evaporation kinetics and wetting dynamics of nanofluid droplets on superhydrophobic surfaces of micro-post patterns", *Journal of Adhesion Science and Technology,* vol. 25, no. 12, pp. 1305-1321.

205. Xu, W. and Choi, C. -. (2012), "Effects of surface topography and colloid particles on the evaporation kinetics of sessile droplets on superhydrophobic surfaces", *Journal of Heat Transfer,* vol. 134, no. 5.

206. Xu, W., Leeladhar, R., Kang, Y. T. and Choi, C. -. (2013), "Evaporation kinetics of sessile water droplets on micropillared superhydrophobic surfaces", *Langmuir,* vol. 29, no. 20, pp. 6032-6041.

207. Yamamoto, K. and Ogata, S. (2008), "3-D thermodynamic analysis of superhydrophobic surfaces", *Journal of colloid and interface science,* vol. 326, no. 2, pp. 471-477.

208. Yang, J. -., Yang, Z. -., Chen, C. -. and Yao, D. -. (2008), "Conversion of surface energy and manipulation of a single droplet across micropatterned surfaces", *Langmuir,* vol. 24, no. 17, pp. 9889-9897.

209. Yang, J. -., Yang, Z. -., Chen, C. -. and Yao, D. -. (2008), "Conversion of surface energy and manipulation of a single droplet across micropatterned surfaces", *Langmuir,* vol. 24, no. 17, pp. 9889-9897.

210. Yao, D., Chen, S. -. and Kim, B. H. (2008), "Rapid thermal cycling of injection molds: An overview on technical approaches and applications", *Advances in Polymer Technology,* vol. 27, no. 4, pp. 233-255.

211. Yeh, K. -., Chen, L. -. and Chang, J. -. (2008), "Contact angle hysteresis on regular pillar-like hydrophobic surfaces", *Langmuir,* vol. 24, no. 1, pp. 245-251.

212. Yildirim Erbil, H. and Elif Cansoy, C. (2009), "Range of applicability of the wenzel and cassie-baxter equations for superhydrophobic surfaces", *Langmuir,* vol. 25, no. 24, pp. 14135-14145.

213. Yoo, Y. E., Kim, T. H., Choi, D. S., Hyun, S. M., Lee, H. J., Lee, K. H., Kim, S. K., Kim, B. H., Seo, Y. H., Lee, H. G. and Lee, J. S. (2009), "Injection molding of a nanostructured plate and measurement of its surface properties", *Current Applied Physics,* vol. 9, no. 2 SUPPL.

214. Yoo, Y.-., Seo, Y.-., Kim, S.-., Je, T.-. and Choi, D.-., (2006), *Injection molding nano and micro pillar arrays*.

215. Yoshimitsu, Z., Nakajima, A., Watanabe, T. and Hashimoto, K. (2002), "Effects of surface structure on the hydrophobicity and sliding behavior of water droplets", *Langmuir,* vol. 18, no. 15, pp. 5818-5822.

216. Young, T. (1805), "An Essay on the Cohesion of Fluids", *Philosophical Transactions: Royal Society: London,* [Online], no. 95, pp. 22/6/10.

217. Youngblood, J. P. and McCarthy, T. J. (1999), "Ultrahydrophobic polymer surfaces prepared by simultaneous ablation of polypropylene and sputtering of poly(tetrafluoroethylene) using radio frequency plasma", *Macromolecules,* vol. 32, no. 20, pp. 6800-6806.

218. Yu, M. -., Young, W. -. and Hsu, P. -. (2007), "Micro-injection molding with the infrared assisted mold heating system", *Materials Science and Engineering A,* vol. 460-461, pp. 288-295.

219. Zema, L., Loreti, G., Melocchi, A., Maroni, A. and Gazzaniga, A. (2012), "Injection Molding and its application to drug delivery", *Journal of Controlled Release,* vol. 159, no. 3, pp. 324-331.

220. Zhang, D., Chen, F., Fang, G., Yang, Q., Xie, D., Qiao, G., Li, W., Si, J. and Hou, X. (2010), "Wetting characteristics on hierarchical structures patterned by a femtosecond laser", *Journal of Micromechanics and Microengineering,* vol. 20, no. 7.

221. Zhao, H. and Law, K. -. (2012), "Directional self-cleaning superoleophobic surface", *Langmuir,* vol. 28, no. 32, pp. 11812-11818.

222. Zhao, J., Mayes, R. H., Chen, G., Chan, P. S. and Xiong, Z. J. (2003), "Polymer micromould design and micromoulding process", *Plastics, Rubber and Composites,* vol. 32, no. 6, pp. 240-247.

223. Zhao, J., Mayes, R. H., Chen, G., Xie, H. and Chan, P. S. (2003), "Effects of Process Parameters on the Micro Molding Process", *Polymer Engineering and Science,* vol. 43, no. 9, pp. 1542-1554.

224. Zheng, Z., Xia, W. and Wu, Y., (2009), *The optimal structure design of mold in powder injection molding based on the numerical simulation*, Shenyang ed.

225. Zhiltsova, T. V., Oliveira, M. S. A. and Ferreira, J. A. (2013), "Integral approach for production of thermoplastics microparts by injection moulding", *Journal of Materials Science,* vol. 48, no. 1, pp. 81-94.

226. Zhu, L., Feng, Y., Ye, X. and Zhou, Z. (2006), "Tuning wettability and getting superhydrophobic surface by controlling surface roughness with well-designed microstructures", *Sensors and Actuators, A: Physical,* vol. 130-131, no. SPEC. ISS., pp. 595-600.

227. Zhu, X., Wang, H., Liao, Q., Ding, Y. D. and Gu, Y. B. (2009), "Experiments and analysis on self-motion behaviors of liquid droplets on gradient surfaces", *Experimental Thermal and Fluid Science,* vol. 33, no. 6, pp. 947-954.

APPENDICES

Appendix A – Feedstock selection literature

Table A 1 Feedstock selection Literature Search Papers

Morphological evolution of HDPE parts in the MIM: comparison with conventional injection molding, Chao Guo et al, Journal of applied Polymer Science	2012	83
Surface wear of TiN coated nickel tool during the injection moulding of polymer micro Fresnel lenses, G Tosello et al, CIRP Annuals - Manufacturing Technology	2012	190
Influence of rapid mold temperature variation on surface topography replication and appearance of injection-molded parts, G Lucchetta et al, CIRP Annuals - Manufacturing Technology	2012	124
Fabrcation of ceramic micro-scale hollow components by micro-powder injection moulding, U M Attia & JR Alcock, Journal of European Ceramic Society	2012	11
Superhydrophobic elastomer surfaces with nanostructured micronails, I Saarikoski et al, Surface Science	2012	173
Effects of processing parmeters on the micro-channels replication in microfluidic devices fabricated by micro injection molding, G Fu et al, Microsyst Technol	2011	59
Flatness optimisation of micro-injection moulded parts: the case of a PMMA microfluidic component, S Marson et al, J micromech microeng	2011	130
Cavity air flow behaviour during filling in MIM, CA Griffiths et al, Journal of manufacturing sci and eng	2011	81

Evaluation and controlling process variability in micro-injection moulding, UM Attia & JR Alcock, Int J Adv Manuf Technol	2011	7
Micro powder injection moulding of alumina micro-channel part, J Meng et al, Journal of European Cermaic Society	2011	134
On the origin of the "core-free" morphology in microinjection-molded HDPE, J Giboz et al, J polymer science part B	2011	77
Microinjection molding of light-guided plates using LIGA-like fabricated stampers, Ming-Shyan Huang & Hong-Hua Ku, Journal of Applied Polymer Science	2011	88
Rapid injection molding of high-aspect-ratio nanostructures, S Hattori et al, Microelectronic Engineering	2010	86
Roughness-gradient-induced spontaneous motion of droplets on hydrophobic surfaces: a lattice boltzmann study, A Letters Journal Exploring The Frontiers of Physics, N Moradi et al	2010	143
Modification of polypropylene surfaces with micropits and hierarchial micropits/nanodepressions, T Rasilainen et al, Surface Science	2010	167
Process control and product evaluation in micro molding using a screwless/two-plunger injection unit, G Tosselle et al, ANTEC	2010	189
Design and fabrication of an affordable polymer micromixer for medical and biomedical applications, Lei Li et al, Polymer engineering and science	2010	116
Characterization of the microinjection molding process, Jingsong Chu et al, Polymer engineering and science	2010	35
Development of a novel process chain based on atomic force microscopy scratching for small and medium series	2010	25

production of polymer nanostructured components, EB Brousseau et al, Journal of manufacturing science and engineering		
Study of process parameters effect on the filing phase of micro-injection moulding using weld lines as flow markers, G Tosello et al, Int J Adv Manuf Technol	2010	188
Investigation of surface treatment effects in micro-injection-moulding, CA Griffiths et al, Int J Adv Manuf Technol	2010	79
Effect of gate dimension on micro injection molded weld line strength with PP and HDPE, Lei Xie & G Ziegmann, Int J Adv Manuf Technol	2010	202
Optimising process conditions for multiple quality criteria in MIM, UM Attia & JR Alcock, Int J Adv Manuf Technol	2010	5
Nanostructures for all-polymer microfluidic systems, M Matschuk et al, Microelectronic engineering	2009	131
Polymer structure and properties in micro- and nanomolding process, Hiroshi Ito et al, Current Applied Physics	2009	92
Injection molding of a nanostructured plate and measurement of its surface properties, YE Yoo et al, Current Applied Physics	2009	213
Anisotropically microstructured and micro/nanostructured polypropylene surfaces, T Rasilainen et al, Surface Science	2009	168
Modification of polycarbonate surface properties by nano-, micro-, and hierarchical micro-nanostructureing, I Saarikoski et al, Applied Surface Science	2009	174
Robust parameter design of micro-injection molded gears using LIGA-like fabricated mold insert, Ming-Shyan Huang et al, Journal of materials processing technology	2009	89

Influence of processing parameters on micro injection molded weld line mechanical properties of PP, Lei Xie & G Ziegmann, Microsyst technol	2009	201
Microinjection molding of thermoplastic polymers: morphological comparison with conventional injection molding, J Giboz et al, J micromech microeng	2009	76
An evaluation of process-parameter and part-geometry effects on the quality of filling in micro-injection moulding, UM Attia &JR Alcock, Microsyst Technol	2009	3
Injection molding of nanopillars for perpendicular patterned magnetic media with metallic nanostamp, Namseok Lee et al, Japanese journal of applied physics	2008	110
Micro-injection moulding: surface treatment effects on part demoulding, CA Griffiths et al, Multi-Material Micro Manufacture	2008	82
Optimal molding parameter design of PLA micro lancet needles using taguchi method, Min-Wen Wang et al, IEEE	2008	196
Replication quality of flow-through microfilters in microfluidic lab-on-a-chip for blood typing by microinjection molding, Bong-Kee Lee et al, Journal of manufacturing science and engineering	2008	108
Micro-injection molding with infrared assisted mold heating system, Ming-Ching Yu et al, Materials Science and engineering A	2007	218
Injecion molding nanoscale features with the aid of induction heating, S Kim et al, polymer-plastic technology and engineering	2007	103
Dimensional variation in production of high-aspect-ratio micro-pillars array by micro powder injection molding, S.G. Li et al, Applied Physics A	2007	117
An experimental study on micro injection parameters, Woo-Chul Jung et al, ANTEC	2007	97

Influence of process parameters on the weld lines of a micro injection molded component, G Tosello et al, ANTEC	2007	187
Investigation of micro-injection moulding: factors affecting the replication quality, B Sha et al, Journal of materials processing technology	2007	176
Micro-injection moulding: factors affecting the achievable aspect ratios, B Sha et al, Int J Adv Manuf Technol	2007	178
The effects of tool surface quality in micro-injection moulding, CA Griffiths et al, Journal of materials processing technology	2007	80
On the injection molding of nanostructured polymer surfaces, H Pranov et al, Polymer engineering and science	2006	164
Rapid mold temperature variation for assisting the micro injection of high aspect ratio micro-feature parts using induction heating technology, Shia-Chung Chen et al, J Micromech Microeng	2006	32
Experimental investigation of infrared rapid surface heating for injection molding, Pei-Chi Chang et al, Journal of applied polymer science	2006	30
Injection molding nano and micro pillar arrays, Yeong-Eun Yoo et al, key engineering materials	2006	214
Injection molding of polymer micro- and sub-micron structures with high-aspect ratios, A-C Liou & R-H Chen, Int J Adv Manuf Technol	2006	121
A variotherm mold for micro metal injection molding, G Fu et al, Microsyst technol	2005	57
Replication of sub-micrometer features using microsystems technology, J Pirskanen et al, Plastics, rubber and composites	2005	160
The effect of process conditions on part	2005	14

quality in microinjection molding, R Aufiero, ANTEC		
Injection molding, debinding and sintering of 316L stainless steel microstructures, G Fu et al, Appl Phys A	2005	56
Experimental investigation into micro injection molding of plastic parts, Nan Shing Ong & Yeow Hwee Koh, Materials and manufacturing processes	2005	154
Construction of injection mold with MEMS RTD sensor and MEMS heater for micro/nano molding process, Y Kim et al, japanese journal of applied physics	2005	104
Polymer micromould design and micromoulding process, J Zhao et al, Plastics, rubber and composites	2003	222
Effects of process parameters on the micro molding process, J Zhao et al, Polymer engineering and Science	2003	223
Study on 40Gbit/inch^2 density molding using heat insulated mold, K Inoue et al, jap j appl phys	2004	91
Micro-powder injection molding, Z.Y. Liu et al, J materials processing technology	2002	123
Three-dimensional non-newtonian computations of micro-injection molding with the finite element method, YK Shen et al, Int Comm Heat Mass Transfer	2002	181
Replication of sub-micron features using amorphous thermoplastics, K Monkkonen et al, Polymer engineering and science	2002	140
The fabrication of high resolution features by mould injection, D Macintyre & S Thoms, Microelectronic Engineering	1998	125

Table A 2 Feedstock Selection Statistical Experimental Design Literature Search

Optimization of micro-injection molding process with respect to tensile properties of polypropylene, R Pal et al, Indian Journal of Fibre & Textile Research	2012	155
Application of taguchi method for parameter optimization in micro metal injection molding, Haw Pei Li et al, Applied mechanics and materials	2011	114
Determination of optimal microminiature powder injection molding parameters by taguchi approach, Haw Pei Li & Norhamidi Muhamad, advanced materials research	2011	113
Optimization of Micro Metal Injection Molding with Multiple Performance Characteristics using Grey Relational Grade, MHI Ibrahim et al, Chiang Mai J Sci	2011	90
Effects of process parameters in plastic, metal, and ceramics injection molding processes, Shi W Lee et al, Korea-Australia Rheology Jorunal	2011	112
Effects of processing parameters on the micro-channels replication in microfluidic devices fabricated by micro injection molding, G Fu et al, Microsyst Technol	2011	59
Flatness optimisation of micro-injection moulded parts: the case of a PMMA microfluidic component, S Marson et al, J micromech microeng	2011	130
Cavity air flow behaviour during filling in MIM, CA Griffiths et al, Journal of manufacturing sci and eng	2011	81
Evaluation and controlling process variability in micro-injection moulding, UM Attia & JR Alcock, Int J Adv Manuf Technol	2011	7
Microinjection molding of light-guided plates using LIGA-like fabricated stampers, Ming-Shyan Huang & Hong-Hua Ku, Journal of Applied Polymer Science	2011	88

Gas-assisted powder injection molding: a study on the effect of processing variables on gas penetration, K Lee et al, Powder Technology	2010	109
Study of microcellular injection-molded polypropylene/waste ground rubbler tire powder blend, Zhen Xiang Xin et al, Materials and Design	2010	203
Morphology of microinjection moulded polyoxymethylene, MR Kamal et al, plastics rubber and composites	2010	98
Optimization of feedstock properties for reaction-bonded net-shape zircon ceramics by design of experiments, N Schlechtriemen et al, Ceramics International	2010	175
Process control and product evaluation in micro molding using a screwless/two-plunger injection unit, G Tosselle et al, ANTEC	2010	189
Design and fabrication of an affordable polymer micromixer for medical and biomedical applications, Lei Li et al, Polymer engineering and science	2010	116
Characterization of the microinjection molding process, Jingsong Chu et al, Polymer engineering and science	2010	35
Development of a novel process chain based on atomic force microscopy scratching for small and medium series production of polymer nanostructured components, EB Brousseau et al, Journal of manufacturing science and engineering	2010	25
Study of process parameters effect on the filing phase of micro-injection moulding using weld lines as flow markers, G Tosello et al, Int J Adv Manuf Technol	2010	188
Investigation of surface treatment effects in micro-injection-moulding, CA Griffiths et al, Int J Adv Manuf Technol	2010	79
Effect of gate dimension on micro injection molded weld line strength with PP and HDPE, Lei Xie & G Ziegmann, Int J Adv Manuf Technol	2010	202

Optimising process conditions for multiple quality criteria in MIM, UM Attia & JR Alcock, Int J Adv Manuf Technol	2010	5
The optimal structure design of mold in powder injection molding based on the numerical simulation, ZhenXing Zheng et al, Applied mechanics and materials	2009	224
Optimizing the injection parameter of water atomised SS316L powder with design of experiment method for bst sintered density, K R Jamaludin et al, Chiang Mai J Sci	2009	90
Robust parameter design of micro-injection molded gears using LIGA-like fabricated mold insert, Ming-Shyan Huang et al, Journal of materials processing technology	2009	89
Influence of processing parameters on micro injection molded weld line mechanical properties of PP, Lei Xie & G Ziegmann, Microsyst technol	2009	201
An evaluation of process-parameter and part-geometry effects on the quality of filling in micro-injection moulding, UM Attia &JR Alcock, Microsyst Technol	2009	3
Optimisation of process conditions in powder injection moulding of microsystem components using a robust design method: part I. primary design parameters, R Urval et al, powder metallurgy	2008	192
Micro-injection moulding: surface treatment effects on part demoulding, CA Griffiths et al, Multi-Material Micro Manufacture	2008	82
Optimal molding parameter design of PLA micro lancet needles using taguchi method, Min-Wen Wang et al, IEEE	2008	196
Replication quality of flow-through microfilters in microfluidic lab-on-a-chip for blood typing by microinjection molding, Bong-Kee Lee et al, Journal of manufacturing science and engineering	2008	108
Optimal design of material and process parameters in powder injection molding, G Ayad et al, 10th ESAFORM Conference on	2007	15

material forming

An experimental study on micro injection parameters, Woo-Chul Jung et al, ANTEC	2007	200
Influence of process parameters on the weld lines of a micro injection molded component, G Tosello et al, ANTEC	2007	187
Investigation of micro-injection moulding: factors affecting the replication quality, B Sha et al, Journal of materials processing technology	2007	176
Micro-injection moulding: factors affecting the achievable aspect ratios, B Sha et al, Int J Adv Manuf Technol	2007	178
The effects of tool surface quality in micro-injection moulding, CA Griffiths et al, Journal of materials processing technology	2007	80
Replication of sub-micrometer features using microsystems technology, J Pirskanen et al, Plastics, rubber and composites	2005	160
The effect of process conditions on part quality in microinjection molding, R Aufiero, ANTEC	2005	14
Experimental investigation into micro injection molding of plastic parts, Nan Shing Ong & Yeow Hwee Koh, Materials and manufacturing processes	2005	154
Polymer micromould design and micromoulding process, J Zhao et al, Plastics, rubber and composites	2003	222
Effects of process parameters on the micro molding process, J Zhao et al, Polymer engineering and Science	2003	223
Three-dimensional non-newtonian computations of micro-injection molding with the finite element method, YK Shen et al, Int Comm Heat Mass Transfer	2002	181
Replication of sub-micron features using amorphous thermoplastics, K Monkkonen et al, Polymer engineering and science	2002	140

Optimization of metal injection molding: experimental design, R T Fox & Daeyong Lee, The international Journal of powder metallurgy	1990	[51]

Table A 3 Powder feedstock selection literature

Fabrication of hollow, 3D, micro-scale metallic structured by micro-powder injection moulding, Usama M Attia, Jeffrey R Alcock, Journal of Materials Processing Technology	2012	12
Powder injection moulding of metallic and ceramic micro parts, V. Piotter et al, Microsyst Technol	2011	159
A review of micro-powder injection moulding as a fabrication technique, Usama M Attia, Jeffrey R Alcock, J. Micromech Microeng	2011	9
Elaboration of PIM feedstock with 316LS fine stainless steel powders for the processing of micro-components, C. Quinard et al, Powder Technology	2011	165
Powder injection moulding of premixed ferritic and austenitic stainless steel powders, M.E. Sotomayor et al, Materials Science and Engineering	2011	182
Replication and characterization of 316LS stainless steel micro-mixer by micro powder injection moulding, Junhu Meng et al, Journal of Alloys and Compounds	2010	135
Master Decomposition Curve for Binders Used in Powder Injection Molding, Gaurav Aggarwal et al, Metallurgical and Material Transactions A	2007	1
Effects of injection molding parameters on the production of microstructures by micropowder injection molding, G. Fu et al, Materials and Manufacturing Porcesses	2005	55
The mechanical properties, dimensional tolerance and microstructural characterization of micro-molded ceramic and metal comonents, T.J.Garino et al, Microsystem technologies	2004	72
Improved mould design in metal injection moulding by combination of numerical	2002	74

simulations and experiments, J-C Gelin et al, J Engineering Manufacture		
Experimental and numerical analysis of the effects of process parameters on the properties of components in metal injection molding, Th. Barriere et al, J. Phys IV France	2001	[18]

Appendix B – Design of experiment response data

Table B-1 Average part and buffer mass of high density polyethylene, polypropylene and 316LS replicates

DOE	Average Part Mass 316LS (g)	Average Buffer Mass HDPE (g)	Average Buffer Mass PP (g)	Average Part Mass HDPE (g)	Average Part Mass PP (g)
1	3.52198	0.00371	0.00355	0.5288	0.5408
2	3.54684	0.00383	0.00381	0.5348	0.5510
3	3.53531	0.00649	0.00373	0.5328	0.5452
4	3.53140	0.0044	0.00464	0.5332	0.5424
5	3.53715	0.00491	0.00565	0.5337	0.5464
6	3.50816	0.00391	0.00524	0.5278	0.5479
7	3.49235	0.00416	0.00341	0.5261	0.5459
8	3.51144	0.00562	0.00424	0.5291	0.5497
9	3.54073	0.00405	0.00408	0.5344	0.5471
10	3.51175	0.00586	0.00502	0.5299	0.5476
11	3.52308	0.00581	0.00464	0.5351	0.5542
12	3.52851	0.00407	0.00373	0.5355	0.5514
13	3.51982	0.00513	0.00355	0.5321	0.5484
14	3.51828	0.0044	0.00396	0.5265	0.546
15	3.49977	0.00409	0.00330	0.5315	0.5467
16	3.51981	0.00485	0.00378	0.5351	0.5505

Table B-2 Average height and width of pillar on polypropylene replicates and variation between polypropylene replicate and silicon mould insert with Type B insert features

DOE	± Si Pitch	± Si Width	Type B Features Height	Type B Features Width
1	-5.61	0.783	8.84	10.783
2	1.809	3.661	16.259	13.661
3	-8.742	2.226	5.708	12.226
4	-0.538	0.8	13.912	10.8
5	-8.206	0.494	6.244	10.494
6	-5.689	1.225	8.761	11.225
7	-7.225	3.819	7.225	13.819
8	-0.75	1.129	13.7	11.129
9	-2.633	1.204	11.817	11.204
10	-2.631	1.302	11.819	11.302
11	-4.422	2.378	10.028	12.378
12	-8.916	1.686	5.534	11.686
13	-3.882	0.878	10.568	10.878
14	-5.516	1.667	8.934	11.667
15	-4.016	1.493	10.434	11.493
16	-8.858	2.05	5.592	12.05

Table B-3 Height of 40 – 80 μm polypropylene pillar feature on Type A inserts

DOE	80 x 80 μm	53 x 80 μm	43 x 80 μm	80 x 29 μm	53 x 29 μm	43 x 29 μm
1	34.258	32.06	30.192	31.074	31.73	42.39
2	30.854	34.366	34.036	31.18	33.158	35.026
3	47.192	14.268	9.608	16.296	9.88	7.838
4	34.28	33.818	31.95	27.978	27.67	27.01
5	36.74	61.156	55.448	28.9	19.542	18.996
6	37.51	69.502	56.106	16.602	17.348	13.066
7	37.662	28.548	29.426	29.36	33.598	23.716
8	33.974	31.95	30.194	27.208	29.316	26.682
9	34.28	32.28	32.72	23.214	26.79	23.278
10	34.126	33.82	34.898	34.126	32.39	31.84
11	35.51	33.598	33.71	35.354	35.462	36.014
12	34.742	31.84	32.28	37.292	40.188	37.222
13	36.122	32.126	35.906	29.514	32.588	28.658
14	31.514	33.93	32.17	31.972	33.27	32.61
15	33.818	33.16	32.72	32.282	31.73	32.72
16	33.512	40.188	37.968	34.894	31.95	29.024

Table B-4 Width of 40 – 80 μm polypropylene pillar features on Type A inserts

DOE	80 x 80 μm	53 x 80 μm	43 x 80 μm	80 x 29 μm	53 x 29 μm	43 x 29 μm
1	79.848	53.928	44.26	79.406	53.16	28.986
2	79.188	52.72	35.686	77.98	51.62	41.842
3	82.414	50.852	41.592	76.572	51.95	41.672
4	79.344	54.034	43.93	78.112	51.73	41.186
5	79.34	52.83	43.272	77.342	50.74	41.404
6	79.188	54.916	45.58	82.262	54.4764	42.612
7	78.112	51.18	42.062	79.496	51.51	41.186
8	77.804	54.148	44.48	77.85	50.19	40.6366
9	78.42	54.254	44.15	77.188	49.424	41.408
10	78.572	51.73	41.624	78.266	49.972	40.966
11	78.882	51.73	42.282	76.88	51.29	41.734
12	80.724	51.29	42.72	78.112	51.18	42.94
13	77.342	52.432	41.736	78.728	51.356	42.062
14	79.802	51.84	42.172	78.878	51.84	41.952
15	79.034	52.388	41.516	77.958	50.96	41.076
16	79.188	49.422	41.054	76.418	50.41	41.134

Table B-5 Height of 40-80-μm high density plyethylene pillar feature on Type A inserts

DOE	80 x 80 μm	53 x 80 μm	43 x 80 μm	80 x 29 μm	53 x 29 μm	43 x 29 μm
1	22.004	17.722	16.57	0	0	0
2	37.134	36.126	33.628	19.068	14.746	10.522
3	34.256	27.44	27.67	9.178	9.376	8.762
4	33.05	32.358	33.878	30.74	33.38	33.27
5	56.546	47.04	39.352	6.92	5.456	5.916
6	47.27	43.426	49.036	13.294	10.99	7.992
7	53.954	59.642	46.652	14.064	11.914	11.296
8	34.972	33.004	35.414	33.588	33.816	32.754
9	35.51	36.044	38.504	36.896	27.514	30.514
10	35.244	34.696	34.806	33.05	34.696	33.82
11	31.782	35.356	30.964	34.038	40.296	38.65
12	33.598	37.222	34.918	32.5	37.99	33.376
13	0	0	0	0	0	0
14	44.358	28	18.884	13.616	11.416	6.48
15	34.148	34.918	35.248	33.71	33.82	32.5
16	0	0	0	0	0	0

Table B-6 Width of 40 – 80 μm high density polyethylene pillar feature on Type A inserts

DOE	80 x 80 μm	53 x 80 μm	43 x 80 μm	80 x 29 μm	53 x 29 μm	43 x 29 μm
1	77.552	51.796	41.224	0	0	0
2	78.512	52.856	43.294	77.36	51.122	41.32
3	80.284	54.276	45.514	77.312	54.276	39.754
4	76.33	51.204	40.866	74.354	49.75	39.43
5	79.298	50.972	40.36	74.79	50.128	39.976
6	79.404	50.974	41.822	75.65	50.124	39.442
7	78.88	51.892	41.5	74.42	48.742	39.518
8	78.492	52.278	42.046	77.492	50.664	40.984
9	78.188	51.356	40.668	77.342	50.818	40.826
10	76.55	52.17	43.272	76.44	49.312	38.33
11	79.862	52.828	44.37	77.54	52.28	42.064
12	77.648	49.42	42.066	75.892	50.85	40.968
13	0	0	0	0	0	0
14	76.77	51.4	42.174	75.89	49.422	40.308
15	78.31	52.17	42.61	76.77	50.52	41.736
16	78.572	52.1	42.168	0	50.326	41.692

Table B-7 Height of 40 – 80 μm 316LS pillar feature on Type A inserts

DOE	80 x 80 μm	53 x 80 μm	43 x 80 μm	80 x 29 μm	53 x 29 μm	43 x 29 μm
1	36.892	42.602	37.444	30.13	26.13	30.414
2	47.804	42.052	42.382	*	23.934	19.122
3	37.508	38.276	38.43	35.664	27.67	39.854
4	41.196	53.142	40.116	35.356	26.462	30.304
5	35.356	37.99	39.528	28.746	35.686	42.054
6	40.274	42.162	38.32	27.364	30.524	38.21
7	37.352	36.892	47.19	27.514	33.51	37.662
8	53.332	55.648	62.108	*	53.326	49.496
9	38.89	41.812	43.702	40.736	43.812	52.374
10	41.656	41.064	45.788	44.578	35.356	52.814
11	45.922	36.782	34.698	20.174	19.434	23.498
12	42.736	35.816	*	27.36	22.136	*
13	38.278	39.662	39.198	28.9	24.288	37.112
14	38.43	38.758	38.1	29.822	30.304	34.146
15	45.96	48.268	41.724	25.978	19.366	*
16	37.044	40.276	42.162	33.972	28.9	31.18

Table B-8 Width of 40 – 80 μm 316LS pillar features on Type A inserts

DOE	80 x 80 μm	53 x 80 μm	43 x 80 μm	80 x 29 μm	53 x 29 μm	43 x 29 μm
1	80.262	49.454	39.758	79.032	51.18	40.53
2	80.262	48.566	38.988	*	50.74	40.856
3	77.19	47.972	37.01	77.65	49.97	38.22
4	79.648	50.742	40.418	77.342	51.07	40.418
5	79.032	49.2	38.88	77.956	51.07	39.76
6	77.646	50.19	37.012	79.958	50.52	39.318
7	78.42	49.202	38.286	77.804	51.818	39.21
8	81.492	50.278	39.672	*	49.664	39.672
9	79.186	49.356	38.77	78.724	49.356	38.77
10	81.23	47.996	37.782	81.186	50.96	39.43
11	81.416	50.19	37.452	78.994	50.302	37.56
12	81.492	46.28	*	71.652	48.74	*
13	78.726	47.818	37.672	80.416	50.124	39.76
14	80.57	48.432	38.11	80.262	50.74	37.67
15	79.648	50.896	40.636	76.418	52.588	*
16	79.032	46.898	37.45	79.65	48.278	38.55

Table B-9 Height of 20 – 39 μm polypropylene pillar features on Type A inserts

DOE	30 x 30 μm	25 x 30 μm 2	20 x 30 μm	30 x 10 μm	25 x 10 μm	20 x 10 μm
1	33.356	29.054	21.282	6.456	7.918	7.034
2	31.402	23.596	22.212	6.37	6.148	4.996
3	28.742	9.606	19.83	5.996	5.84	7.532
4	29.284	26.946	25.902	15.986	14.372	11.068
5	14.14	12.22	12.374	4.536	6.302	5.84
6	12.066	10.762	8.1	3.842	4.306	3.016
7	40.076	31.82	29.44	6.15	6.072	5.61
8	30.36	24.902	19.57	17.756	18.676	10.17
9	27.966	29.012	27.902	18.522	15.834	11.606
10	25.472	22.95	34.124	5.82	6.26	5.888
11	25.36	29.13	25.518	6.81	5.916	5.532
12	31.184	23.056	13.682	5.49	4.998	5.456
13	32.06	20.366	19.096	6.04	6.454	5.972
14	27.23	31.592	33.972	7.684	5.996	5.61
15	28.284	26.47	25.824	6.608	7.38	6.688
16	15.676	14.372	14.122	5.918	5.686	5.52

Table B-10 Height of 20 – 39 μm polypropylene pillar features on Type A inserts

DOE	29 x 80 μm	29 x 29 μm	30 x 30 μm	25 x 25 μm	20 x 20 μm
1	29.974	39.858	35.356	21.446	13.716
2	30.964	23.604	20.338	12.414	9.404
3	5.918	5.304	15.296	8.394	4.56
4	31.18	25.472	29.976	29.59	27.73
5	12.758	6.84	7.922	7.51	6.584
6	37.276	10.222	12.22	10.644	8.218
7	35.586	26.67	35.046	24.122	13.598
8	30.976	27.21	31.284	29.208	31.336
9	31.62	22.508	26.21	19.332	19.51
10	32.5	34.256	27.516	28.616	19.392
11	33.744	27.668	37.65	22.466	21.24
12	31.206	30.358	20.058	13.656	11.174
13	47.104	23.608	13.362	14.07	9.034
14	32.59	30.978	38.814	32.358	18.564
15	32.128	29.972	31.514	30.51	30.154
16	43.196	20.83	27.138	21.816	17.05

Table B-11 Width of 20 – 39 μm polypropylene pillar features on Type A inserts

DOE	30 x 30 μm	25 x 30 μm 2	20 x 30 μm	30 x 10 μm	25 x 10 μm	20 x 10 μm
1	32.136	30.522	24.09	21.606	17.606	14.252
2	34.048	32.06	27.37	23.614	18.758	14.994
3	29.524	23.68	19.68	22.374	17.452	13.07
4	29.29	23.6	19.068	23.598	18.144	14.226
5	34.672	27.292	21.988	24.14	19.296	14.376
6	35.518	33.826	24.544	22.756	19.602	13.6
7	28.01	28.442	26.294	21.308	18.682	12.608
8	29.37	24.448	24.782	23.064	19.528	14.666
9	30.06	24.834	19.222	25.062	19.066	14.144
10	28.446	23.94	20.448	25.15	19.55	15.76
11	30.752	24.448	19.756	25.042	19.684	15.682
12	41.404	35.9	27.908	23.282	19.3	14.146
13	31.084	27.292	24.248	24.16	18.834	13.896
14	30.202	23.678	17.99	25.92	19.526	15.146
15	28.908	23.6	19.604	26.756	23.91	17.99
16	36.21	29.908	27.34	24.446	21.296	15.09

Table B-12 Width of 20 – 39 μm polypropylene pillar features on Type A inserts

DOE	29 x 80 μm	29 x 29 μm	30 x 30 μm	25 x 25 μm	20 x 20 μm
1	29.32	29.432	29.828	26.214	21.17
2	28.884	41.842	29.06	26.768	21.054
3	28.524	28.37	29.52	24.956	12.874
4	32.29	29.654	28.446	24.526	19.338
5	28.444	28.446	31.046	25.546	19.988
6	37.824	30.83	32.596	25.844	20.564
7	29.136	29.138	30.678	26.85	23.894
8	31.368	27.676	28.83	24.128	19.22
9	30.862	27.02	27.832	23.418	18.51
10	28.334	28.556	28.138	23.952	18.926
11	29.368	28.984	30.22	24.07	19.508
12	28.678	29.214	30.136	26.554	23.362
13	29.324	30.31	34.654	25.074	18.74
14	28.756	29.37	29.368	22.296	18.806
15	28.752	28.674	28.978	24.13	18.982
16	29.212	28.062	28.192	24.78	18.164

Table B-13 Height of 20 – 39 μm high density polypropylene pillar features on Type A inserts

DOE	30 x 30 μm	25 x 30 μm 2	20 x 30 μm	30 x 10 μm	25 x 10 μm	20 x 10 μm
1	7.498	6.26	*	*	*	*
2	15.034	12.97	9.3	2.64	2.544	*
3	8.938	*	*	*	*	*
4	32.72	31.29	32.568	8.234	7.686	7.264
5	5.908	4.992	*	*	*	*
6	8.506	7.738	9.13	*	*	*
7	7.392	*	*	*	*	*
8	30.984	31.278	30.212	12.01	10.666	8.34
9	25.838	22.292	13.498	5.28	4.944	3.728
10	29.666	31.218	35.414	5.974	6.244	4.992
11	34.148	27.14	20.692	5.38	4.848	4.196
12	29.82	15.678	14.128	5.452	3.074	4.316
13	*	*	*	*	*	*
14	9.082	7.018	7.112	2.536	2.448	2.46
15	30.154	29.914	36.242	6.244	5.474	4.192
16	*	*	*	*	*	*

Table B-14 Height of 20 – 39 μm high density polypropylene pillar features on Type A inserts

DOE	29 x 80 μm	29 x 29 μm	30 x 30 μm	25 x 25 μm	20 x 20 μm
1	0	0	4.992	4.464	3.6
2	25.892	8.794	15.034	13.834	7.69
3	4.078	0	11.146	6.436	4.496
4	31.808	32.39	31.16	30.096	24.3
5	6.384	5.912	5.616	0	0
6	28.734	6.8	10.042	9.706	4.176
7	22.288	10.23	6.198	4.992	3.936
8	34.352	32.932	26.948	36.132	30.79
9	30.804	21.992	26.544	19.098	14.074
10	34.696	32.612	31.284	34.278	21.522
11	37	28.768	29.864	21.52	16.37
12	40.2	23.75	22.82	18.152	11.468
13	0	0	0	0	0
14	0	0	6.976	4.61	4.038
15	35.134	36.12	28.668	28.208	19.452
16	0	0	0	0	0

Table B-15 Width of 20 – 39 μm high density polyethylene pillar features on Type A inserts

DOE	30 x 30 μm	25 x 30 μm 2	20 x 30 μm	30 x 10 μm	25 x 10 μm	20 x 10 μm
1	28.062	21.418	17.684	*	*	*
2	32.77	24.266	20.298	21.524	16.388	*
3	29.454	23.444	18.98	*	*	*
4	29.872	22.186	18.26	19.88	15.16	12.266
5	30.078	23.156	19.62	*	*	*
6	30.264	23.782	19.268	*	*	*
7	29.154	23.736	19.144	*	*	*
8	29.51	24.248	18.932	21.38	17.204	12.724
9	30.988	24.7	19.124	22.58	18.212	13.376
10	29.904	24.838	20.992	22.828	19.988	15.818
11	31.3	24.188	18.122	22.402	17.328	14.666
12	39.594	28.446	22.474	21.682	17.068	13.186
13	*	*	*	*	*	*
14	28.398	23.3	18.164	20.99	16.916	12.764
15	28.564	24.128	18.866	22.294	17.78	12.84
16	*	*	*	*	*	*

Table B-16 Width of 20 – 39 μm high density polyethylene pillar features on Type A inserts

DOE	29 x 80 μm	29 x 29 μm	30 x 30 μm	25 x 25 μm	20 x 20 μm
1	27.774	0	27.87	23.06	19.124
2	28.782	28.302	30.174	23.446	18.164
3	29.214	28.14	29.022	25.806	20.604
4	27.44	27.13	28.508	21.232	17.446
5	27.262	27.202	28.388	22.886	18.39
6	31.816	27.44	30.51	24.12	18.02
7	28.8	27.264	29.502	23.398	21.316
8	28.21	28.27	28.638	24.272	19.268
9	27.736	27.44	29.452	22.886	18.164
10	28.116	27.24	28.598	24.372	18.836
11	29.98	28.118	28.884	24.16	17.53
12	27.708	28.906	28.268	24.188	19.754
13	0	0	0	0	0
14	29.292	28.138	28.562	22.864	18.334
15	28.446	27.57	29.754	23.912	18.274
16	0	0	0	0	0

Table B-17 Height and Width of 20 – 39 μm 316LS pillar features on Type A inserts

DOE	Height 29 x 80 μm	Height 29 x 29 μm	Width 29 x 80 μm	Width 29 x 29 μm
1	49.518	39.75	24.712	25.37
2	43.26	21.41	30.532	26.248
3	40.186	37.222	25.26	25.15
4	45.59	38.758	27.238	27.02
5	38.87	37.002	26.47	24.93
6	39.418	37.332	23.722	25.59
7	46.776	33.16	26.36	26.36
8	52.418	35.968	27.678	27.678
9	40.846	46.224	25.26	25.26
10	43.262	50.728	23.83	26.36
11	38.102	30.964	27.13	26.03
12	*	*	*	*
13	39.088	30.522	24.93	26.468
14	43.482	34.806	26.25	25.26
15	*	*	*	*
16	43.04	33.268	24.38	25.92

Table B-18 Height of 5 – 19 μm polypropylene pillar features on Type A inserts

DOE	15 x 30 μm	10 x 30 μm	5 x 30 μm	15 x 10 μm	10 x 10 μm	5 x 10 μm
1	19.332	7.878	/	4.376	/	/
2	11.606	6.856	/	3.304	/	/
3	16.02	/	/	*	/	/
4	24.712	22.676	/	8.16	/	/
5	8.988	6.1	/	4.314	/	/
6	6.03	5.184	/	2.66	/	/
7	17.974	11.338	/	4.612	/	/
8	26.84	18.688	/	8.16	/	/
9	25.66	18.976	/	7.508	/	/
10	27.132	9.706	/	4.168	/	/
11	21.756	8.746	/	3.192	/	/
12	11.352	6.148	/	3.606	/	/
13	12.358	7.254	/	4.73	/	/
14	25.954	11.646	/	4.552	/	/
15	29.898	13.354	/	5.534	/	/
16	10.618	9.082	/	4.896	/	/

Table B-19 Height of 5 – 19 μm polypropylene pillar features on Type A inserts

DOE	19 x 80 μm	19 x 29 μm	15 x 15 μm	10 x 10 μm	5 x 5 μm
1	34.82	28.132	9.082	/	/
2	13.142	15.142	6.146	/	/
3	*	*	*	/	/
4	28.33	21.52	19.924	/	/
5	9.07	5.994	6.608	/	/
6	8.686	7.302	5.714	/	/
7	25.828	20.058	6.766	/	/
8	28.59	25.286	22.244	/	/
9	29.204	31.4	11.194	/	/
10	30.742	27.78	7.786	/	/
11	35.816	20.06	11.002	/	/
12	31.67	21.444	8.646	/	/
13	30.668	11.836	12.634	/	/
14	35.202	32.666	7.21	/	/
15	30.592	31.514	15.492	/	/
16	23.212	12.142	9.914	/	/

Table B-20 Width of 5 – 19 μm polypropylene pillar features on Type A inserts

DOE	15 x 30 μm	10 x 30 μm	5 x 30 μm	15 x 10 μm	10 x 10 μm	5 x 10 μm
1	19.872	8.802	/	8.692	/	/
2	22.216	12.95	/	10.072	/	/
3	14.842	/	/	*	/	/
4	15.908	9.166	/	9.346	/	/
5	16.262	9.562	/	10.052	/	/
6	16.56	11.05	/	8.814	/	/
7	19.28	13.212	/	8.576	/	/
8	13.544	7.258	/	8.22	/	/
9	14.074	7.45	/	9.284	/	/
10	15.762	18.308	/	13.3	/	/
11	14.842	10.762	/	9.878	/	/
12	18.572	8.17	/	9.698	/	/
13	18.864	11.194	/	10.286	/	/
14	15.14	13.494	/	9.758	/	/
15	15.914	9.082	/	14.84	/	/
16	17.924	11.914	/	9.994	/	/

Table B-21 Width of 5 – 19 μm polypropylene pillar features on Type A inserts

DOE	19 x 80 μm	19 x 29 μm	15 x 15 μm	10 x 10 μm	5 x 5 μm
1	18.144	17.374	14.128	/	/
2	18.374	19.604	13.21	/	/
3	*	*	*	/	/
4	20.65	18.23	12.772	/	/
5	18.448	18.912	13.416	/	/
6	19.298	20.298	12.538	/	/
7	18.53	19.374	14.374	/	/
8	19.45	16.452	11.146	/	/
9	17.572	16.364	10.954	/	/
10	18.12	17.9	18.02	/	/
11	17.45	17.914	13.644	/	/
12	17.99	17.066	13.282	/	/
13	20.526	23.446	12.876	/	/
14	20.51	17.99	13.684	/	/
15	17.374	18.066	13.602	/	/
16	17.836	19.22	13.072	/	/

Table B-22 Height of 5 – 19 μm high density polyethylene pillar features on Type A inserts

DOE	15 x 30 μm	10 x 30 μm	5 x 30 μm	15 x 10 μm	10 x 10 μm	5 x 10 μm
1	*	0	/	0	/	/
2	7.418	5.858	/	0	/	/
3	*	0	/	0	/	/
4	24.932	0	/	5.07	/	/
5	*	0	/	0	/	/
6	*	0	/	0	/	/
7	*	0	/	0	/	/
8	31.32	14.334	/	4.88	/	/
9	7.304	0	/	0	/	/
10	23.78	9.764	/	0	/	/
11	15.514	8.994	/	3.216	/	/
12	10.878	0	/	0	/	/
13	*	0	/	0	/	/
14	5.574	0	/	0	/	/
15	30.406	9.608	/	2.844	/	/
16	*	0	/	0	/	/

Table B-23 Height of 5 – 19 μm high density polyethylene pillar features on Type A inserts

DOE	19 x 80 μm	19 x 29 μm	15 x 15 μm	10 x 10 μm	5 x 5 μm
1	0	0	0	/	/
2	21.908	7.45	4.56	/	/
3	0	0	0	/	/
4	32.516	21.738	9.032	/	/
5	0	0	0	/	/
6	0	0	0	/	/
7	5.382	6.858	0	/	/
8	35.646	32.46	14.41	/	/
9	6.486	15.322	11.002	/	/
10	37.002	27.854	8.314	/	/
11	32.99	19.83	7.066	/	/
12	20.982	14.374	6.342	/	/
13	0	0	0	/	/
14	0	0	0	/	/
15	42.712	17.566	8.338	/	/
16	0	0	0	/	/

Table B-24 Width of 5 – 19 μm high density polyethylene pillar features on Type A inserts

DOE	15 x 30 μm	10 x 30 μm	5 x 30 μm	15 x 10 μm	10 x 10 μm	5 x 10 μm
1	*	0	/	0	/	/
2	14.646	7.642	/	0	/	/
3	*	0	/	0	/	/
4	14.66	0	/	7.536	/	/
5	*	0	/	0	/	/
6	12.876	0	/	0	/	/
7	*	0	/	0	/	/
8	14.416	7.534	/	8.418	/	/
9	14.684	7.88	/	0	/	/
10	14.85	7.686	/	0	/	/
11	16.192	10.032	/	8.458	/	/
12	14.664	0	/	0	/	/
13	*	0	/	0	/	/
14	14.106	8.19	/	0	/	/
15	13.836	12.88	/	10.148	/	/
16	*	0	/	0	/	/

Table B-25 Width of 5 – 19 μm high density polyethylene pillar features on Type A inserts

DOE	19 x 80 μm	19 x 29 μm	15 x 15 μm	10 x 10 μm	5 x 5 μm
1	0	0	0	/	/
2	18.932	17.684	11.578	/	/
3	18.762	17.53	0	/	/
4	16.44	22.514	14.452	/	/
5	0	0	11.578	/	/
6	17.862	16.912	13.26	/	/
7	18.628	18.038	0	/	/
8	18.308	17.506	12.416	/	/
9	15.81	19.268	11.674	/	/
10	17.9	18.67	17.54	/	/
11	18.528	16.376	14.366	/	/
12	17.37	18.3	12.058	/	/
13	0	0	0	/	/
14	0	0	0	/	/
15	18.45	17.132	16.914	/	/
16	0	0	0	/	/

Table B-26 Height and width of 5 – 19 μm 316LS pillar features on Type A inserts

DOE	Height 19 x 80 μm	Height 19 x 29 μm	Width 19 x 80 μm	Width 19 x 29 μm
1	38.122	17.444	15.914	16.558
2	23.058	13.758	17.682	18.682
3	42.712	24.156	15.378	15.706
4	42.492	13.284	19.55	19.55
5	37.582	21.364	15.144	15.452
6	44.03	26.9	14.17	15.048
7	54.79	25.804	17.9	17.9
8	37.112	12.078	19.66	17.132
9	44.028	27.778	15.268	15.268
10	41.616	32.94	15.926	16.256
11	34.146	34.148	17.682	16.034
12	*	0	*	0
13	38.978	16.91	15.598	17.352
14	43.81	19.214	16.364	16.584
15	*	0	*	0
16	40.736	21.632	16.474	15.268

Table B-27 Variation of pillar height from silicon mould insert of 40 – 80 μm polypropylene replicates on Type A inserts

DOE	80 x 80 μm	53 x 80 μm	43 x 80 μm	80 x 29 μm	53 x 29 μm	43 x 29 μm
1	-6.7224	-9.0264	-10.82	-9.9064	-9.3564	1.378
2	-10.1264	-6.7204	-6.976	-9.8004	-7.9284	-5.986
3	6.2116	-26.8184	-31.404	-24.6844	-31.2064	-33.174
4	-6.7004	-7.2684	-9.062	-13.0024	-13.4164	-14.002
5	-4.2404	20.0696	14.436	-12.0804	-21.5444	-22.016
6	-3.4704	28.4156	15.094	-24.3784	-23.7384	-27.946
7	-3.3184	-12.5384	-11.586	-11.6204	-7.4884	-17.296
8	-7.0064	-9.1364	-10.818	-13.7724	-11.7704	-14.33
9	-6.7004	-8.8064	-8.292	-17.7664	-14.2964	-17.734
10	-6.8544	-7.2664	-6.114	-6.8544	-8.6964	-9.172
11	-5.4704	-7.4884	-7.302	-5.6264	-5.6244	-4.998
12	-6.2384	-9.2464	-8.732	-3.6884	-0.8984	-3.79
13	-4.8584	-8.9604	-5.106	-11.4664	-8.4984	-12.354
14	-9.4664	-7.1564	-8.842	-9.0084	-7.8164	-8.402
15	-7.1624	-7.9264	-8.292	-8.6984	-9.3564	-8.292
16	-7.4684	-0.8984	-3.044	-6.0864	-9.1364	-11.988

Table B-28 Variation of pillar width from silicon mould insert of 40 – 80 μm polypropylene replicates on Type A inserts

DOE	80 x 80 μm	53 x 80 μm	43 x 80 μm	80 x 29 μm	53 x 29 μm	43 x 29 μm
1	-0.152	0.928	1.26	-0.594	0.16	-14.014
2	-0.812	-0.28	-7.314	-2.02	-1.38	-1.158
3	2.414	-2.148	-1.408	-3.428	-1.05	-1.328
4	-0.656	1.034	0.93	-1.888	-1.27	-1.814
5	-0.66	-0.17	0.272	-2.658	-2.26	-1.596
6	-0.812	1.916	2.58	2.262	1.4764	-0.388
7	-1.888	-1.82	-0.938	-0.504	-1.49	-1.814
8	-2.196	1.148	1.48	-2.15	-2.81	-2.3634
9	-1.58	1.254	1.15	-2.812	-3.576	-1.592
10	-1.428	-1.27	-1.376	-1.734	-3.028	-2.034
11	-1.118	-1.27	-0.718	-3.12	-1.71	-1.266
12	0.724	-1.71	-0.28	-1.888	-1.82	-0.06
13	-2.658	-0.568	-1.264	-1.272	-1.644	-0.938
14	-0.198	-1.16	-0.828	-1.122	-1.16	-1.048
15	-0.966	-0.612	-1.484	-2.042	-2.04	-1.924
16	-0.812	-3.578	-1.946	-3.582	-2.59	-1.866

Table B-29 Variation of pillar height of 20 – 39 μm pillars from silicon mould inserts for polypropylene replicates on Type A inserts

DOE	30 x 30 μm	25 x 30 μm	20 x 30 μm	30 x 10 μm	25 x 10 μm	20 x 10 μm
1	-6.285	-10.548	-18.535	-33.1852	-31.7232	-32.7828
2	-8.239	-16.006	-17.605	-33.2712	-33.4932	-34.8208
3	-10.899	-29.996	-19.987	-33.6452	-33.8012	-32.2848
4	-10.357	-12.656	-13.915	-23.6552	-25.2692	-28.7488
5	-25.501	-27.382	-27.443	-35.1052	-33.3392	-33.9768
6	-27.575	-28.84	-31.717	-35.7992	-35.3352	-36.8008
7	0.435	-7.782	-10.377	-33.4912	-33.5692	-34.2068
8	-9.281	-14.7	-20.247	-21.8852	-20.9652	-29.6468
9	-11.675	-10.59	-11.915	-21.1192	-23.8072	-28.2108
10	-14.169	-16.652	-5.693	-33.8212	-33.3812	-33.9288
11	-14.281	-10.472	-14.299	-32.8312	-33.7252	-34.2848
12	-8.457	-16.546	-26.135	-34.1512	-34.6432	-34.3608
13	-7.581	-19.236	-20.721	-33.6012	-33.1872	-33.8448
14	-12.411	-8.01	-5.845	-31.9572	-33.6452	-34.2068
15	-11.357	-13.132	-13.993	-33.0332	-32.2612	-33.1288
16	-23.965	-25.23	-25.695	-33.7232	-33.9552	-34.2968

Table B-30 Variation of pillar height of 20 – 39 μm pillars from silicon mould inserts for polypropylene replicates on Type A inserts

DOE	29 x 80 μm	29 x 29 μm	30x 30 μm	25 x 25 μm	20 x 20 μm
1	-10.4032	-0.5192	18.9556	5.1032	0.0392
2	-9.4132	-16.7732	3.9376	-3.9288	-4.2728
3	-34.4592	-35.0732	-1.1044	-7.9488	-9.1168
4	-9.1972	-14.9052	13.5756	13.2472	14.0532
5	-27.6192	-33.5372	-8.4784	-8.8328	-7.0928
6	-3.1012	-30.1552	-4.1804	-5.6988	-5.4588
7	-4.7912	-13.7072	18.6456	7.7792	-0.0788
8	-9.4012	-13.1672	14.8836	12.8652	17.6592
9	-8.7572	-17.8692	9.8096	2.9892	5.8332
10	-7.8772	-6.1212	11.1156	12.2732	5.7152
11	-6.6332	-12.7092	21.2496	6.1232	7.5632
12	-9.1712	-10.0192	3.6576	-2.6868	-2.5028
13	6.7268	-16.7692	-3.0384	-2.2728	-4.6428
14	-7.7872	-9.3992	22.4136	16.0152	4.8872
15	-8.2492	-10.4052	15.1136	14.1672	16.4772
16	2.8188	-19.5472	10.7376	5.4732	3.3732

Table B-31 Variation of pillar width of 20 – 39 μm pillars from silicon mould inserts for polypropylene replicates on Type A inserts

DOE	30 x 30 μm	25 x 30 μm	20 x 30 μm	30 x 10 μm	25 x 10 μm	20 x 10 μm
1	2.136	5.522	2.09	-8.394	-7.394	-5.748
2	4.048	7.06	7.37	-6.386	-6.242	-5.006
3	-0.476	-1.32	-0.32	-7.626	-7.548	-6.93
4	-0.71	-1.4	-0.932	-6.402	-6.856	-5.774
5	4.672	2.292	1.988	-5.86	-5.704	-5.624
6	5.518	8.826	4.544	-7.244	-5.398	-6.4
7	-1.99	3.442	6.294	-8.692	-6.318	-7.392
8	-0.63	-0.552	4.782	-6.936	-5.472	-5.334
9	0.06	-0.166	-0.778	-4.938	-5.934	-5.856
10	-1.554	-1.06	0.448	-4.85	-5.45	-4.24
11	0.752	-0.552	-0.244	-4.958	-5.316	-4.318
12	11.404	10.9	7.908	-6.718	-5.7	-5.854
13	1.084	2.292	4.248	-5.84	-6.166	-6.104
14	0.202	-1.322	-2.01	-4.08	-5.474	-4.854
15	-1.092	-1.4	-0.396	-3.244	-1.09	-2.01
16	6.21	4.908	7.34	-5.554	-3.704	-4.91

Table B-32 Variation of pillar width of 20 – 39 μm pillars from silicon mould inserts for polypropylene replicates on Type A inserts

DOE	29 x 80 μm	29 x 29 μm	30x 30 μm	25 x 25 μm	20 x 20 μm
1	0.32	0.432	-0.172	1.214	1.17
2	-0.116	12.842	-0.94	1.768	1.054
3	-0.476	-0.63	-0.48	-0.044	-7.126
4	3.29	0.654	-1.554	-0.474	-0.662
5	-0.556	-0.554	1.046	0.546	-0.012
6	8.824	1.83	2.596	0.844	0.564
7	0.136	0.138	0.678	1.85	-3.894
8	2.368	-1.324	-1.17	-0.872	-0.78
9	1.862	-1.98	-2.168	-1.582	-1.49
10	-0.666	-0.444	-1.862	-1.048	-1.074
11	0.368	-0.016	0.22	-0.93	-0.492
12	-0.322	0.214	0.136	1.554	3.362
13	0.324	1.31	4.654	0.074	-1.26
14	-0.244	0.37	-0.632	-2.704	-1.194
15	-0.248	-0.326	-1.022	-0.87	-1.018
16	0.212	-0.938	-1.808	-0.22	-1.836

Table B-33 Variation of pillar height from silicon mould insert of 5 – 19 μm pillar features on polypropylene replicates on Type A inserts

DOE	15 x 30 μm	10 x 30 μm	5 x 30 μm	15 x 10 μm	10 x 10 μm	5 x 10 μm
1	-18.713	-28.727	/	-33.6688	/	/
2	-26.439	-29.749	/	-34.7408	/	/
3	-22.025	-36.6048	/	-38.0448	/	/
4	-13.333	-13.929	/	-29.8848	/	/
5	-29.057	-30.5048	/	-33.7308	/	/
6	-32.015	-31.4208	/	-35.3848	/	/
7	-20.071	-25.2668	/	-33.4328	/	/
8	-11.205	-17.9168	/	-29.8848	/	/
9	-12.385	-17.6288	/	-30.5368	/	/
10	-10.913	-26.8988	/	-33.8768	/	/
11	-16.289	-27.8588	/	-34.8528	/	/
12	-26.693	-30.4568	/	-34.4388	/	/
13	-25.687	-29.3508	/	-33.3148	/	/
14	-12.091	-24.9588	/	-33.4928	/	/
15	-8.147	-23.2508	/	-32.5108	/	/
16	-27.427	-27.5228	/	-33.1488	/	/

Table B-34 Variation of pillar height from silicon mould insert of 5 – 19 μm pillar features on polypropylene replicates on Type A inserts

DOE	19 x 80 μm	19 x 29 μm	15 x 15 μm	10 x 10 μm	5 x 5 μm
1	-4.434	-11.122	-1.2098	/	/
2	-26.112	-24.112	-4.1458	/	/
3	-39.254	-39.254	-10.2918	/	/
4	-10.924	-17.734	9.6322	/	/
5	-30.184	-33.26	-3.6838	/	/
6	-30.568	-31.952	-4.5778	/	/
7	-13.426	-19.196	-3.5258	/	/
8	-10.664	-13.968	11.9522	/	/
9	-10.05	-7.854	0.9022	/	/
10	-8.512	-11.474	-2.5058	/	/
11	-3.438	-19.194	0.7102	/	/
12	-7.584	-17.81	-1.6458	/	/
13	-8.586	-27.418	2.3422	/	/
14	-4.052	-6.588	-3.0818	/	/
15	-8.662	-7.74	5.2002	/	/
16	-16.042	-27.112	-0.3778	/	/

Table B-35 Variation of pillar width from Silicon mould insert of 5 – 19 μm pillar features for polypropylene replicates of Type A inserts

DOE	15 x 30 μm	10 x 30 μm	5 x 30 μm	15 x 10 μm	10 x 10 μm	5 x 10 μm
1	4.872	-1.198	/	-6.308	/	/
2	7.216	2.95	/	-4.928	/	/
3	-0.158	-10	/	-15	/	/
4	0.908	-0.834	/	-5.654	/	/
5	1.262	-0.438	/	-4.948	/	/
6	1.56	1.05	/	-6.186	/	/
7	4.28	3.212	/	-6.424	/	/
8	-1.456	-2.742	/	-6.78	/	/
9	-0.926	-2.55	/	-5.716	/	/
10	0.762	8.308	/	-1.7	/	/
11	-0.158	0.762	/	-5.122	/	/
12	3.572	-1.83	/	-5.302	/	/
13	3.864	1.194	/	-4.714	/	/
14	0.14	3.494	/	-5.242	/	/
15	0.914	-0.918	/	-0.16	/	/
16	2.924	1.914	/	-5.006	/	/

Table B-36 Variation of pillar width from silicon mould insert of 5 – 19 μm pillar features for polypropylene replicates of Type A inserts

DOE	19 x 80 μm	19 x 29 μm	15 x 15 μm	10 x 10 μm	5 x 5 μm
1	-0.856	-1.626	-0.872	/	/
2	-0.626	0.604	-1.79	/	/
3	-19	-19	-15	/	/
4	1.65	-0.77	-2.228	/	/
5	-0.552	-0.088	-1.584	/	/
6	0.298	1.298	-2.462	/	/
7	-0.47	0.374	-0.626	/	/
8	0.45	-2.548	-3.854	/	/
9	-1.428	-2.636	-4.046	/	/
10	-0.88	-1.1	3.02	/	/
11	-1.55	-1.086	-1.356	/	/
12	-1.01	-1.934	-1.718	/	/
13	1.526	4.446	-2.124	/	/
14	1.51	-1.01	-1.316	/	/
15	-1.626	-0.934	-1.398	/	/
16	-1.164	0.22	-1.928	/	/

Table B-37 Variation of pillar height from silicon mould insert of 40 – 80 μm pillar features on high density polyethylene replicates of Type A inserts

DOE	80 x 80 μm	53 x 80 μm	43 x 80 μm	80 x 29 μm	53 x 29 μm	43 x 29 μm
1	-18.9764	-23.3644	-24.442	-40.9804	-41.0864	-41.012
2	-3.8464	-4.9604	-7.384	-21.9124	-26.3404	-30.49
3	-6.7244	-13.6464	-13.342	-31.8024	-31.7104	-32.25
4	-7.9304	-8.7284	-7.134	-10.2404	-7.7064	-7.74
5	15.5656	5.9536	-1.66	-34.0604	-35.6304	-35.096
6	6.2896	2.3396	8.024	-27.6864	-30.0964	-33.02
7	12.9736	18.5556	5.64	-26.9164	-29.1724	-29.716
8	-6.0084	-8.0824	-5.598	-7.3924	-7.2704	-8.258
9	-5.4704	-5.0424	-2.508	-4.0844	-13.5724	-10.498
10	-5.7364	-6.3904	-6.206	-7.9304	-6.3904	-7.192
11	-9.1984	-5.7304	-10.048	-6.9424	-0.7904	-2.362
12	-7.3824	-3.8644	-6.094	-8.4804	-3.0964	-7.636
13	-40.9804	-41.0864	-41.012	-40.9804	-41.0864	-41.012
14	3.3776	-13.0864	-22.128	-24.3644	-29.6704	-34.532
15	-6.8324	-6.1684	-5.764	-7.2704	-7.2664	-8.512
16	-40.9804	-41.0864	-41.012	-40.9804	-41.0864	-41.012

Table B-38 Variation of pillar width from silicon mould inserts of 40 - 80μm pillar features for high density polyethylene replicates of Type A inserts

DOE	80 x 80 μm	53 x 80 μm	43 x 80 μm	80 x 29 μm	53 x 29 μm	43 x 29 μm
1	-2.448	-1.204	-1.776	-80	-53	-43
2	-1.488	-0.144	0.294	-2.64	-1.878	-1.68
3	0.284	1.276	2.514	-2.688	1.276	-3.246
4	-3.67	-1.796	-2.134	-5.646	-3.25	-3.57
5	-0.702	-2.028	-2.64	-5.21	-2.872	-3.024
6	-0.596	-2.026	-1.178	-4.35	-2.876	-3.558
7	-1.12	-1.108	-1.5	-5.58	-4.258	-3.482
8	-1.508	-0.722	-0.954	-2.508	-2.336	-2.016
9	-1.812	-1.644	-2.332	-2.658	-2.182	-2.174
10	-3.45	-0.83	0.272	-3.56	-3.688	-4.67
11	-0.138	-0.172	1.37	-2.46	-0.72	-0.936
12	-2.352	-3.58	-0.934	-4.108	-2.15	-2.032
13	-80	-53	-43	-80	-53	-43
14	-3.23	-1.6	-0.826	-4.11	-3.578	-2.692
15	-1.69	-0.83	-0.39	-3.23	-2.48	-1.264
16	-1.428	-0.9	-0.832	-80	-2.674	-1.308

Table B-39 variation of pillar height from silicon mould insert of 20 – 39 μm pillar features for high density polyethylene replicates of Type A inserts

DOE	30 x 30 μm	25 x 30 μm	20 x 30 μm	30 x 10 μm	25 x 10 μm	20 x 10 μm
1	-32.1432	-33.3812	-39.8168	-39.6412	-39.6412	-39.8168
2	-24.6072	-26.6712	-30.5168	-37.0012	-37.0972	-39.8168
3	-30.7032	-39.6412	-39.8168	-39.6412	-39.6412	-39.8168
4	-6.9212	-8.3512	-7.2488	-31.4072	-31.9552	-32.5528
5	-33.7332	-34.6492	-39.8168	-39.6412	-39.6412	-39.8168
6	-31.1352	-31.9032	-30.6868	-39.6412	-39.6412	-39.8168
7	-32.2492	-39.6412	-39.8168	-39.6412	-39.6412	-39.8168
8	-8.6572	-8.3632	-9.6048	-27.6312	-28.9752	-31.4768
9	-13.8032	-17.3492	-26.3188	-34.3612	-34.6972	-36.0888
10	-9.9752	-8.4232	-4.4028	-33.6672	-33.3972	-34.8248
11	-5.4932	-12.5012	-19.1248	-34.2612	-34.7932	-35.6208
12	-9.8212	-23.9632	-25.6888	-34.1892	-36.5672	-35.5008
13	-39.6412	-39.6412	-39.8168	-39.6412	-39.6412	-39.8168
14	-30.5592	-32.6232	-32.7048	-37.1052	-37.1932	-37.3568
15	-9.4872	-9.7272	-3.5748	-33.3972	-34.1672	-35.6248
16	-39.6412	-39.6412	-39.8168	-39.6412	-39.6412	-39.8168

Variation of Pillar height from silicon mould insert of 20 – 39 μm pillar features for high density polyethylene replicates of Type A inserts

DOE	29 x 80 μm	29 x 29 μm	30 x 30 μm	25 x 25 μm	20 x 20 μm
1	-40.3772	-40.3772	-11.4084	-11.8788	-10.0768
2	-14.4852	-31.5832	-1.3664	-2.5088	-5.9868
3	-36.2992	-40.3772	-5.2544	-9.9068	-9.1808
4	-8.5692	-7.9872	14.7596	13.7532	10.6232
5	-33.9932	-34.4652	-10.7844	-16.3428	-13.6768
6	-11.6432	-33.5772	-6.3584	-6.6368	-9.5008
7	-18.0892	-30.1472	-10.2024	-11.3508	-9.7408
8	-6.0252	-7.4452	10.5476	19.7892	17.1132
9	-9.5732	-18.3852	10.1436	2.7552	0.3972
10	-5.6812	-7.7652	14.8836	17.9352	7.8452
11	-3.3772	-11.6092	13.4636	5.1772	2.6932
12	-0.1772	-16.6272	6.4196	1.8092	-2.2088
13	-40.3772	-40.3772	-16.4004	-16.3428	-13.6768
14	-40.3772	-40.3772	-9.4244	-11.7328	-9.6388
15	-5.2432	-4.2572	12.2676	11.8652	5.7752
16	-40.3772	-40.3772	-16.4004	-16.3428	-13.6768

Table B-40 Variation of pillar width from silicon mould inserts of 20 – 39 μm pillar features for high density polyethylene replicates of Type A inserts

DOE	30 x 30 μm	25 x 30 μm	20 x 30 μm	30 x 10 μm	25 x 10 μm	20 x 10 μm
1	-1.938	-3.582	-2.316	-30	-25	-20
2	2.77	-0.734	0.298	-8.476	-8.612	-20
3	-0.546	-1.556	-1.02	-30	-25	-20
4	-0.128	-2.814	-1.74	-10.12	-9.84	-7.734
5	0.078	-1.844	-0.38	-30	-25	-20
6	0.264	-1.218	-0.732	-30	-25	-20
7	-0.846	-1.264	-0.856	-30	-25	-20
8	-0.49	-0.752	-1.068	-8.62	-7.796	-7.276
9	0.988	-0.3	-0.876	-7.42	-6.788	-6.624
10	-0.096	-0.162	0.992	-7.172	-5.012	-4.182
11	1.3	-0.812	-1.878	-7.598	-7.672	-5.334
12	9.594	3.446	2.474	-8.318	-7.932	-6.814
13	-30	-25	-20	-30	-25	-20
14	-1.602	-1.7	-1.836	-9.01	-8.084	-7.236
15	-1.436	-0.872	-1.134	-7.706	-7.22	-7.16
16	-30	-25	-20	-30	-25	-20

Table B-41 Variation of pillar width from silicon mould inserts of 20 – 39 μm pillar features for high density polyethylene replicates of Type A inserts

DOE	29 x 80 μm	29 x 29 μm	30 x 30 μm	25 x 25 μm	20 x 20 μm
1	-1.226	-29	-2.13	-1.94	-0.876
2	-0.218	-0.698	0.174	-1.554	-1.836
3	0.214	-0.86	-0.978	0.806	0.604
4	-1.56	-1.87	-1.492	-3.768	-2.554
5	-1.738	-1.798	-1.612	-2.114	-1.61
6	2.816	-1.56	0.51	-0.88	-1.98
7	-0.2	-1.736	-0.498	-1.602	1.316
8	-0.79	-0.73	-1.362	-0.728	-0.732
9	-1.264	-1.56	-0.548	-2.114	-1.836
10	-0.884	-1.76	-1.402	-0.628	-1.164
11	0.98	-0.882	-1.116	-0.84	-2.47
12	-1.292	-0.094	-1.732	-0.812	-0.246
13	-29	-29	-30	-25	-20
14	0.292	-0.862	-1.438	-2.136	-1.666
15	-0.554	-1.43	-0.246	-1.088	-1.726
16	-29	-29	-30	-25	-20

Table B-42 Variation of pillar height from silicon mould insert of 5 – 19 μm pillar features for high density polyethylene replicates of Type A inserts

DOE	15 x 30 μm	10 x 30 μm	5 x 30 μm	15 x 10 μm	10 x 10 μm	5 x 10 μm
1	-38.0448	-33.5996	/	-38.0448	/	/
2	-30.6268	-27.7416	/	-38.0448	/	/
3	-38.0448	-33.5996	/	-38.0448	/	/
4	-13.1128	-33.5996	/	-32.9748	/	/
5	-38.0448	-33.5996	/	-38.0448	/	/
6	-38.0448	-33.5996	/	-38.0448	/	/
7	-38.0448	-33.5996	/	-38.0448	/	/
8	-6.7248	-19.2656	/	-33.1648	/	/
9	-30.7408	-33.5996	/	-38.0448	/	/
10	-14.2648	-23.8356	/	-38.0448	/	/
11	-22.5308	-24.6056	/	-34.8288	/	/
12	-27.1668	-33.5996	/	-38.0448	/	/
13	-38.0448	-33.5996	/	-38.0448	/	/
14	-32.4708	-33.5996	/	-38.0448	/	/
15	-7.6388	-23.9916	/	-35.2008	/	/
16	-38.0448	-33.5996	/	-38.0448	/	/

Table B-43 Variation of pillar height from silicon mould insert of 5 – 19 μm pillar features for high density polyethylene replicates of Type A inserts

DOE	19 x 80 μm	19 x 29 μm	15 x 15 μm	10 x 10 μm	5 x 5 μm
1	-39.254	-39.254	-10.2918	/	/
2	-17.346	-31.804	-5.7318	/	/
3	-39.254	-39.254	-10.2918	/	/
4	-6.738	-17.516	-1.2598	/	/
5	-39.254	-39.254	-10.2918	/	/
6	-39.254	-39.254	-10.2918	/	/
7	-33.872	-32.396	-10.2918	/	/
8	-3.608	-6.794	4.1182	/	/
9	-32.768	-23.932	0.7102	/	/
10	-2.252	-11.4	-1.9778	/	/
11	-6.264	-19.424	-3.2258	/	/
12	-18.272	-24.88	-3.9498	/	/
13	-39.254	-39.254	-10.2918	/	/
14	-39.254	-39.254	-10.2918	/	/
15	3.458	-21.688	-1.9538	/	/
16	-39.254	-39.254	-10.2918	/	/

Table B-44 variation of pillar width from silicon mould insert of 5 – 19 μm pillar features for high density polyethylene replicates of Type A insert

DOE	15 x 30 μm	10 x 30 μm	5 x 30 μm	15 x 10 μm	10 x 10 μm	5 x 10 μm
1	-15	-10	/	-15	/	/
2	-0.354	-2.358	/	-15	/	/
3	-15	-10	/	-15	/	/
4	-0.34	-10	/	-7.464	/	/
5	-15	-10	/	-15	/	/
6	-2.124	-10	/	-15	/	/
7	-15	-10	/	-15	/	/
8	-0.584	-2.466	/	-6.582	/	/
9	-0.316	-2.12	/	-15	/	/
10	-0.15	-2.314	/	-15	/	/
11	1.192	0.032	/	-6.542	/	/
12	-0.336	-10	/	-15	/	/
13	-15	-10	/	-15	/	/
14	-0.894	-1.81	/	-15	/	/
15	-1.164	2.88	/	-4.852	/	/
16	-15	-10	/	-15	/	/

Table B-45 Variation of pillar width from silicon mould insert of 5 – 19 μm pillar features for high density polyethylene replicates of Type A insert

DOE	19 x 80 μm	19 x 29 μm	15 x 15 μm	10 x 10 μm	5 x 5 μm
1	-19	-19	-15	/	/
2	-0.068	-1.316	-3.422	/	/
3	-0.238	-1.47	-15	/	/
4	-2.56	3.514	-0.548	/	/
5	-19	-19	-3.422	/	/
6	-1.138	-2.088	-1.74	/	/
7	-0.372	-0.962	-15	/	/
8	-0.692	-1.494	-2.584	/	/
9	-3.19	0.268	-3.326	/	/
10	-1.1	-0.33	2.54	/	/
11	-0.472	-2.624	-0.634	/	/
12	-1.63	-0.7	-2.942	/	/
13	-19	-19	-15	/	/
14	-19	-19	-15	/	/
15	-0.55	-1.868	1.914	/	/
16	-19	-19	-15	/	/

Table B-46 Variation of pillar height from silicon mould insert of 40 – 80 μm pillar features for 316LS replicates of Type A inserts

DOE	80 x 80 μm	53 x 80 μm	43 x 80 μm	80 x 29 μm	53 x 29 μm	43 x 29 μm
1	-4.0884	1.5156	-3.568	-10.8504	-14.9564	-10.598
2	6.8236	0.9656	1.37	-40.9804	-17.1524	-21.89
3	-3.4724	-2.8104	-2.582	-5.3164	-13.4164	-1.158
4	0.2156	12.0556	-0.896	-5.6244	-14.6244	-10.708
5	-5.6244	-3.0964	-1.484	-12.2344	-5.4004	1.042
6	-0.7064	1.0756	-2.692	-13.6164	-10.5624	-2.802
7	-3.6284	-4.1944	6.178	-13.4664	-7.5764	-3.35
8	12.3516	14.5616	21.096	-40.9804	12.2396	8.484
9	-2.0904	0.7256	2.69	-0.2444	2.7256	11.362
10	0.6756	-0.0224	4.776	3.5976	-5.7304	11.802
11	4.9416	-4.3044	-6.314	-20.8064	-21.6524	-17.514
12	1.7556	-5.2704	-41.012	-13.6204	-18.9504	-41.012
13	-2.7024	-1.4244	-1.814	-12.0804	-16.7984	-3.9
14	-2.5504	-2.3284	-2.912	-11.1584	-10.7824	-6.866
15	4.9796	7.1816	0.712	-15.0024	-21.7204	-41.012
16	-3.9364	-0.8104	1.15	-7.0084	-12.1864	-9.832

Table B-47 Variation of pillar width from silicon mould insert of 40 – 80 μm pillar features for 316LS replicates of Type A inserts

DOE	80 x 80 μm	53 x 80 μm	43 x 80 μm	80 x 29 μm	53 x 29 μm	43 x 29 μm
1	0.262	-3.546	-3.242	-0.968	-1.82	-2.47
2	0.262	-4.434	-4.012	-80	-2.26	-2.144
3	-2.81	-5.028	-5.99	-2.35	-3.03	-4.78
4	-0.352	-2.258	-2.582	-2.658	-1.93	-2.582
5	-0.968	-3.8	-4.12	-2.044	-1.93	-3.24
6	-2.354	-2.81	-5.988	-0.042	-2.48	-3.682
7	-1.58	-3.798	-4.714	-2.196	-1.182	-3.79
8	1.492	-2.722	-3.328	-80	-3.336	-3.328
9	-0.814	-3.644	-4.23	-1.276	-3.644	-4.23
10	1.23	-5.004	-5.218	1.186	-2.04	-3.57
11	1.416	-2.81	-5.548	-1.006	-2.698	-5.44
12	1.492	-6.72	-43	-8.348	-4.26	-43
13	-1.274	-5.182	-5.328	0.416	-2.876	-3.24
14	0.57	-4.568	-4.89	0.262	-2.26	-5.33
15	-0.352	-2.104	-2.364	-3.582	-0.412	-43
16	-0.968	-6.102	-5.55	-0.35	-4.722	-4.45

Table B-48 Variation of pillar heigh and width from silicon mould insert of 20 – 39 μm pillar features for 316LS replicates of Type A insert

DOE	Height 29 x 80 μm	Height 29 x 29 μm	Width 29 x 80 μm	Width 29 x 29 μm
1	9.1408	-0.6272	-4.288	-3.63
2	2.8828	-18.9672	1.532	-2.752
3	-0.1912	-3.1552	-3.74	-3.85
4	5.2128	-1.6192	-1.762	-1.98
5	-1.5072	-3.3752	-2.53	-4.07
6	-0.9592	-3.0452	-5.278	-3.41
7	6.3988	-7.2172	-2.64	-2.64
8	12.0408	-4.4092	-1.322	-1.322
9	0.4688	5.8468	-3.74	-3.74
10	2.8848	10.3508	-5.17	-2.64
11	-2.2752	-9.4132	-1.87	-2.97
12	-40.3772	-40.3772	-29	-29
13	-1.2892	-9.8552	-4.07	-2.532
14	3.1048	-5.5712	-2.75	-3.74
15	-40.3772	-40.3772	-29	-29
16	2.6628	-7.1092	-4.62	-3.08

Table B-49 Variation of pillar height and width from silicon mould insert of 5 – 19 μm pillar features 316LS replicates of Type A inserts

DOE	Height 19 x 80 μm	Height 19 x 29 μm	Width 19 x 80 μm	Width 19 x 29 μm
1	-1.132	-21.81	-3.086	-2.442
2	-16.196	-25.496	-1.318	-0.318
3	3.458	-15.098	-3.622	-3.294
4	3.238	-25.97	0.55	0.55
5	-1.672	-17.89	-3.856	-3.548
6	4.776	-12.354	-4.83	-3.952
7	15.536	-13.45	-1.1	-1.1
8	-2.142	-27.176	0.66	-1.868
9	4.774	-11.476	-3.732	-3.732
10	2.362	-6.314	-3.074	-2.744
11	-5.108	-5.106	-1.318	-2.966
12	-39.254	-39.254	-19	-19
13	-0.276	-22.344	-3.402	-1.648
14	4.556	-20.04	-2.636	-2.416
15	-39.254	-39.254	-19	-19
16	1.482	-17.622	-2.526	-3.732